14th Symposium on

High-Performance Marine Vehicles

HIPER'22

Cortona, 29-31 August 2022

14th Symposium on

High-Performance Marine Vehicles

HIPER'22

Cortona, 29-31 August 2022

Edited by Volker Bertram

2

Sponsored by

Index

The Decarbonizing Quest for Future Bulk Carriers

Morten Løvstad, DNV, Høvik/Norway, morten.lovstad@dnv.com
Volker Bertram, DNV, Hamburg/Germany, volker.bertram@dnv.com

Abstract

This paper discusses options in decarbonizing bulk carrier shipping from now to 2050. The discussion is structured into two phases, short-term to 2030, with tried-and-proven energy efficiency options, and long-term to 2050 using more 'exotic' energy efficiency options and alternative fuels. Design studies from joint industry projects give a glimpse of future bulk carrier designs and bulk shipping.

1. The CO_2 challenge

"Decarbonization" is not just a recent buzzword, it is on many political agendas, including (most notably for us) IMO's agenda. The larger goals as such are clear, but what exactly do we have to achieve in the short and medium term and how do we collectively achieve this best is still very much subject to debate in scientific, business, and political circles.

IMO is set to cut the carbon footprint of shipping. The Big Zero is the long-term goal for the second half of the century, but the next big milestone in the longer journey is coming up on 1.1.2023 with the EEXI and CII becoming mandatory. The EEXI is the Energy Efficiency Existing Ship (Design) Index, akin to the EEDI (Energy Efficiency Design Index) for newbuildings, Fig.1, expressing the theoretically achievable energy efficiency for the ship as designed, in prime condition as in initial sea trials. The CII (Carbon Intensity Indicator) is calculated based on IMO's fuel oil DCS (Data Collection System), where the requirement to just monitor is now enhanced by grading the performance each year from A to E. Poor operational performance (E once or three consecutive years D) will entail mandatory action to improve performance, planned, documented, tracked, and audited in a SEEMP (Ship Energy Efficiency Management Plan). The CII will be subject to increasingly stricter thresholds over time, driving the industry towards decarbonization.
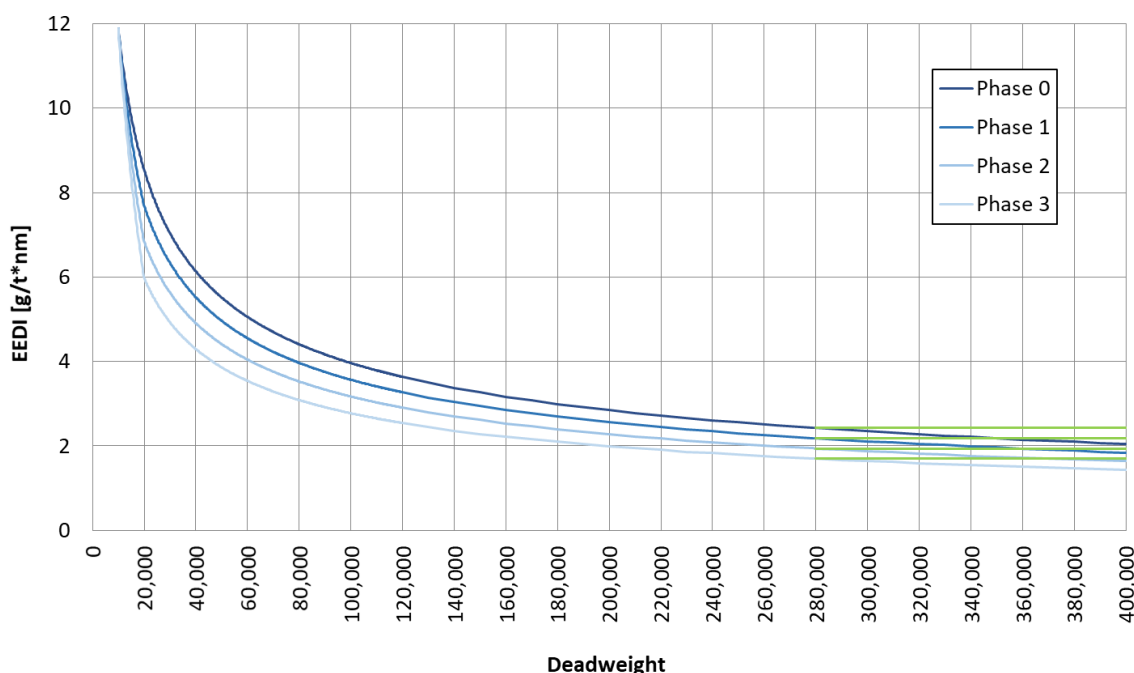
Fig.1: EEDI baseline curves for bulk carriers. From the 2013 baseline (average over the bulker fleet then), in 3 phases to 2025, the EEDI threshold will be lowered by 10% in each step. New bulk carriers in 2025 will be on average 30% more energy efficient designs than the 2013 average.

The impact of the EEXI on the world bulk carrier fleet will be modest, Fig.2. Most modern vessels less than 5 years old will be able to comply with the EEXI requirements without major changes. EPL (engine power limitation) may be needed, but this will reduce maximum speed by only 0.5-1.0 kn, Fig.3. Most vessels older than 5 years will also be able to comply with EEXI requirements by using EPL, but for these older vessels, the measure may reduce the maximum speed by 1.5-2.0 kn, and in some cases even more. The older Handysize (<35000 dwt) and Capesize (100000-200000 dwt) fleet may be most impacted, Fig.2.
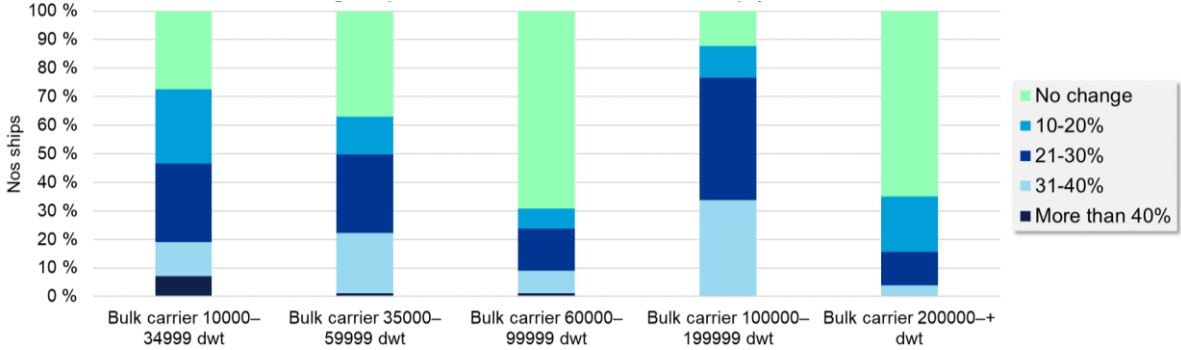
Fig.2: Engine power limitation needed to comply with EEXI
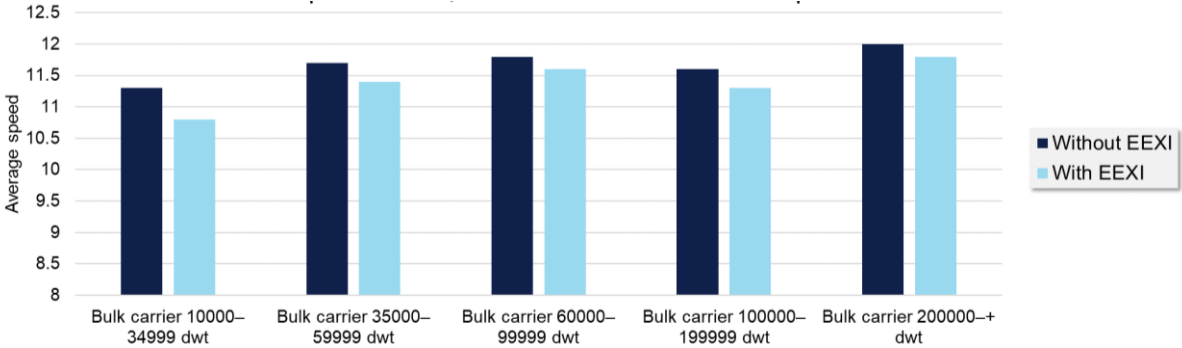
Fig.3: Impact of EEXI, simulated on 2019 fleet and operations
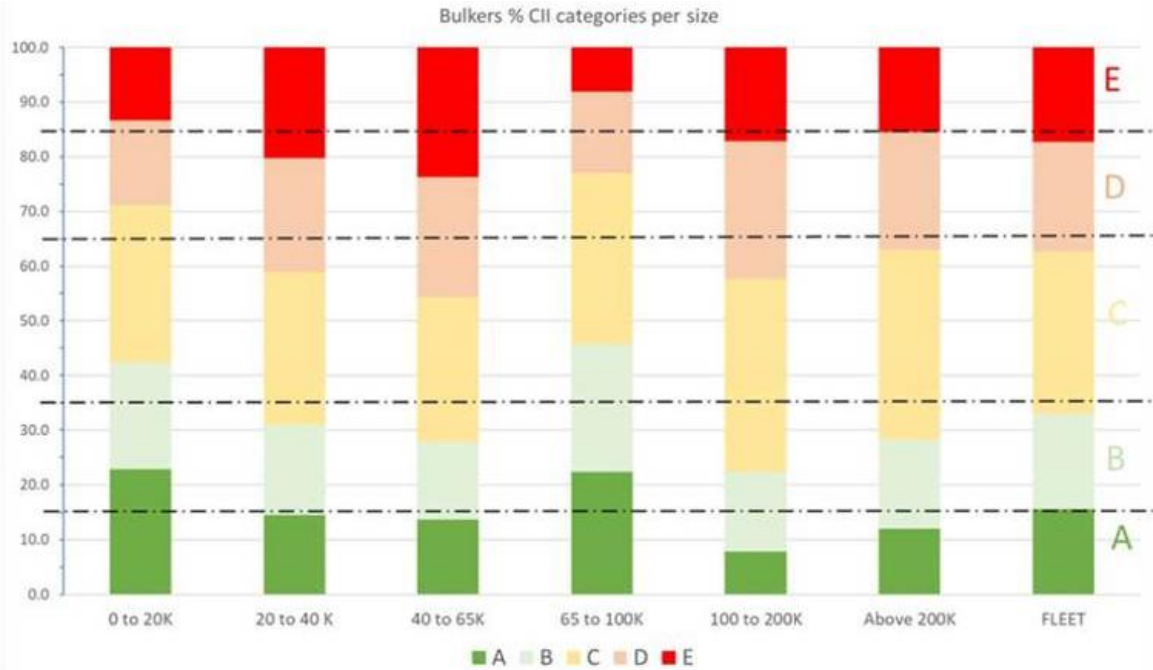
Fig.4: CII 2023 estimates for bulk carrier fleet

The Carbon Intensity Indicator (CII) will have a more profound impact, driving design and operational changes both for the existing fleet in service and future newbuildings, Fig.4. Most modern vessels (< 5 years old) will be able to comply with CII requirements at least up until 2026, without major changes in design or operational procedures. EPL may be enough, and the ensuing reduction of maximum speed by 0.5-1.5 kn is unlikely to have a significant effect, as recorded operational profiles show that vessels already operate very rarely at speeds near maximum speed. Beyond 2026, it may get more challenging. Very few vessels older than 5 years will be able to comply with CII requirements without either reducing speed significantly (maximum speed may need to be as low as 8-9 kn in order to stay compliant beyond 2026) or by blending in biofuels (where there are only limited bunkers available and those at very high price). Thus, within 5 years, a large part of the bulk carrier fleet will face decarbonization challenges requiring action, i.e. retrofits or changes in operational procedures.

In addition to IMO's EEXI and CII requirements, there is increasing pressure from various stakeholders to minimize the carbon footprint:

- Poseidon Principles - The Poseidon Principles, https://www.poseidonprinciples.org/, mean that banks will finance only ships with a good energy efficiency rating.
- Sea Cargo Charter - The Sea Cargo Charter, https://www.seacargocharter.org/, means that major charterers will only opt for ships with low carbon footprint.

The goal of reducing carbon footprint is clear for everyone, and so is the prospect of increasing regulatory and market pressure. But how will we get there? In essence, there are four levers to progress toward lower carbon footprints for ships, or in our case bulk carriers:

- Low/no-carbon fuels – "Decarbonization" makes most people think first of alternative fuels, such as biofuels, ammonia, or hydrogen, *Bertram (2021), Comer et al. (2022).* The problem is that these fuels generally will be significantly more expensive than Heavy Fuel Oil (HFO), the standard shipping fuel of pre-2020 times. Alternative fuels will certainly play a role, but more at a later stage, post 2030.
- Market-based measures - Economic frameworks, such as CO_2 compensation schemes or taxes/surcharges for CO_2 emissions respectively carbon-content of fuels – These will make traditional carbon-based fuels more expensive.
- Wind-assisted ship propulsion (WASP) – The idea of using renewable energy sources directly for ship propulsion is not new, but has been enjoyed exponential growth in installations over the past few years after decades of being rather dormant, *Hochkirch and Bertram (2022), Comer et al. (2022).* Business cases are difficult to establish due to the highly nonlinear nature of exploitable wind conditions. Harnessing the wind is also an option which we will invoke on a wider and larger scale at a later stage, post 2030.
- Energy efficiency – With increasing fuel prices, there will be renewed scrutiny of energy-saving measures in design and operation, https://glomeep.imo.org/. This lever is likely to be the dominant contributor to decarbonizing shipping in the short term (i.e. next decade), not least because many energy saving measures pay for themselves.

In the following, we will discuss the likely measures for bulk carriers, both for the short term (up until around 2030) and the long term (up until 2050).

2. Towards zero-carbon footprint in bulk carriers

2.1. Short-term perspective (towards 2030)

The first phase of marching towards decarbonizing bulk carrier shipping will focus on levers that allow us to stay – technically and economically speaking – in our comfort zone, implementing measures which have not yet been fully exploited in the past. The industry will adopt tried and

proven, technically mature solutions with low risk and low cost, to improve design (EEDI) and operation (CII).

2.1.1. Design measures

Likely measures adopted for bulk carriers on a wider scale will include:

- Hull optimization - One option will be to squeeze everything out of hull design, optimizing automatically for minimum yearly fuel consumption using CFD (Computational Fluid Dynamics), parametric hull modelling and optimization algorithms such a Genetic Algorithms, *Henrichs et al. (2015), Bertram and Campana (2020)*. Typically, 20000 – 30000 designs are analysed in such a project. 95% of these designs will be worse than a good conventional design, 3-4% will be comparable, and 1-2% will be better. For bulk carriers, recent projects have yielded 5% improvement, Fig.5. Especially for fleets of bulkers, the initial investment of such an optimization yields very good return on investment.
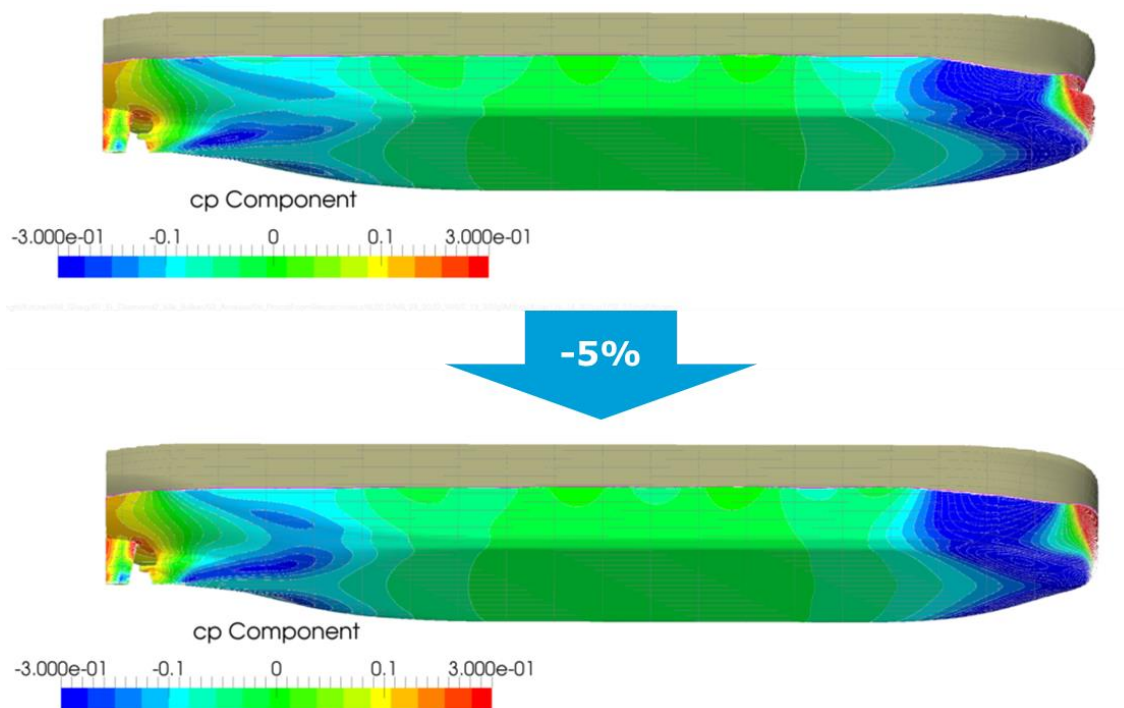
Fig.5: Example of bulk carrier hull optimization (Ultramax project)

- Propulsion Improving Devices (PIDs) – These are also known as ESDs (Energy Saving Devices). The term collectively denotes fins and nozzles in the vicinity of the propeller, intended to improve the propeller efficiency, often through partial recuperation of rotational losses, https://glomeep.imo.org/technology/propulsion-improving-devices-pids/. Among the PIDs, a combination of pre-swirl fins with wake equalizing duct (such as the "Mewis duct", Fig.6, https://friedrich-mewis.de/mewis-duct.html) appears to be the most likely option, as it has proven to give the highest savings in independent analyses of PIDs, *Gatin and Kalajdžić (2022)*. It is best suited for full hull forms, such as bulk carriers and tankers. If the aftbody is well designed, the duct does not improve energy efficiency; but often the aftbody is not optimized for energy efficiency and then overall savings of 2-4% seem realistic for yearly fuel consumption. Retrofits are straightforward, making such PIDs a likely option to be adopted in phase 1.

Fig.6: Mewis duct as example for a PID, source: Oldendorff Carriers

2.1.2. Operational measures

Typical operational measures implemented in the first phase include:

- Improved hull management - Better hull management has been listed as an attractive lever by various sources, including *CSC (2011)*, *OCIMF (2011)*, and https://glomeep.imo.org/. The idea is to have hull coatings and cleaning jointly adjusted, e.g. using easy to clean coatings and soft frequent cleaning, so-called grooming. One example for such coatings would be nano-coatings, Fig.7, *Bertram (2020)*. For niche areas, ultrasonic protection is an attractive complementary technology, Fig.8, *Kelling and Mayorga (2020)*.

Fig.7: Nano-coating, source: Ultra-Ever Dry

Fig.8: Ultrasonic transducer, source: Hasytec

- Trim optimization - Trim optimization works also for bulk carriers. For example, DNV's ECO Assistant was installed on a Supramax bulker; then crew best practice was compared to the trim optimization recommendations. Over a year, a 3% gain for the optimization was calculated. As trim optimization software is easily applied to fleets of sister vessels, it is frequently an energy efficiency measure with very good return on investment.

- Speed profile - Fuel consumption per hour goes roughly with the third power of speed. (This is a crude approximation valid only for small variations around a given point on a speed-

power curve of a ship.) Thus higher speeds cost above proportion fuel, and lower speeds save below proportion speed. Going 10% faster half of the time, and 10% slower half of the time lets a vessel arrive at same time as going at constant speed, but costs ~3% more fuel. A more even speed profile in voyage planning is then a simple option to save fuel. Crew practice may be monitored via continuous monitoring systems or AIS data.

2.1.3. Demonstrator project

Can we achieve 30% energy efficiency improvement over the 2013 baseline, i.e. can we achieve the IMO targets for the EEDI, just by consequently exploiting existing, mature technology? Yes, we can, as the "Diamond 2" project proves, *Larsson (2018), Sørhaug (2018)*.

Fig.9: "Diamond 2" bulk carrier design, 63200 dwt
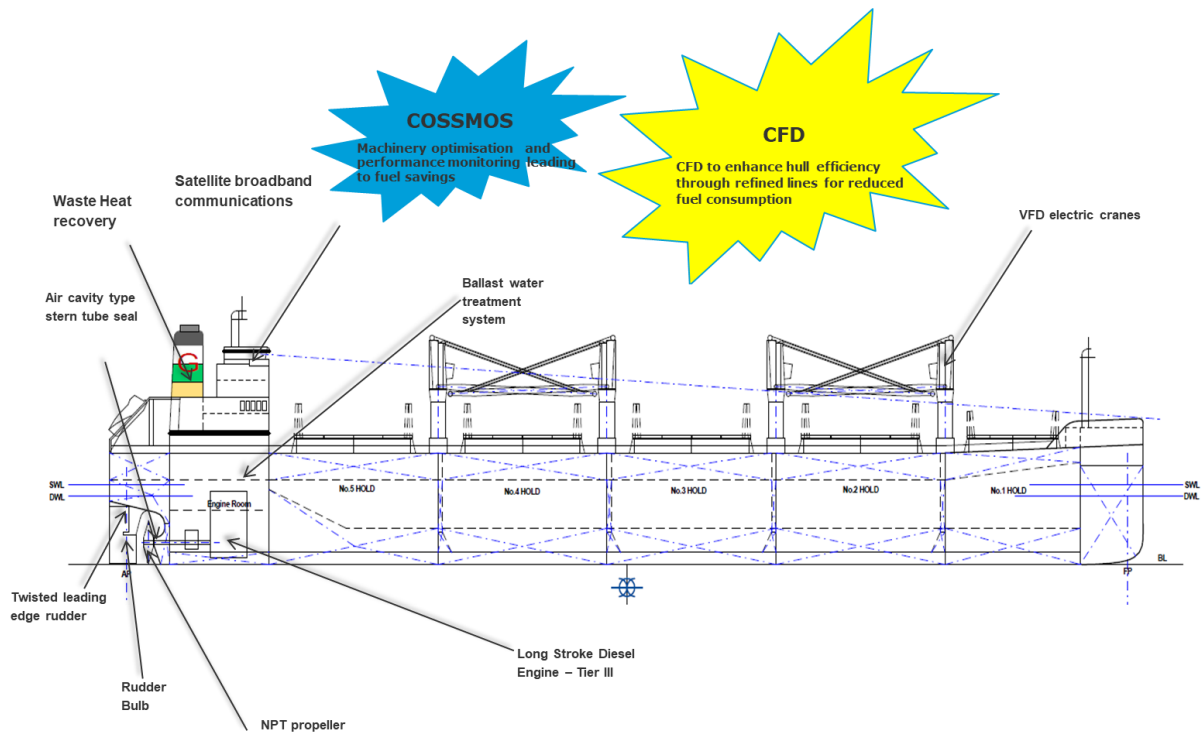
Fig.10: Ultramax "Diamond 2" key features

Continuing a long-standing partnership, the Graig Shipping Group and DNV joined forces to develop the next generation of Ultramax bulk carriers, with focus on fuel efficiency. Assorted measures added up to achieve the objective of being at least 30% below EEDI baseline (= reaching the 2030 target), Figs.9 and 10:

- State-of-the-art hull optimization (ECO Lines) for realistic operational profiles, Fig.11. The optimization allowed an asymmetric aftbody for better inflow to the propeller, Fig.12, which in itself added 2-3% to the fuel efficiency, *Hochkirch and Krebber (2017)*.
- The vertical bow design improves performance across a wide range of weather conditions.
- An energy-efficient twisted rudder with a bulb works with a tip-modified NPT propeller to improve propulsive efficiency further.
- The main engine is a highly fuel-efficient, reliable MAN two-stroke diesel main engine, which is already NO_x Tier III compliant.
- DNV's COSSMOS (Complex Ship Systems Modelling and Simulation), Fig.13, *Kakalis et al. (2014)*, *Georgopoulou et al. (2022),* fine-tuned the auxiliary machinery and all on-board power-dependent systems to avoid excess capacity and maximize efficiency.
- Waste heat recovery from two auxiliary engines and exhaust gas economizer power a section of the boiler.
- LED lighting, frequency-controlled seawater cooling pumps and engine room fans, as well as variable frequency drive (VFD) cranes reduce the electrical load in operation.
- Advanced measuring and data capturing equipment installed will supply continuous performance monitoring to support energy efficient (CII relevant) operation.
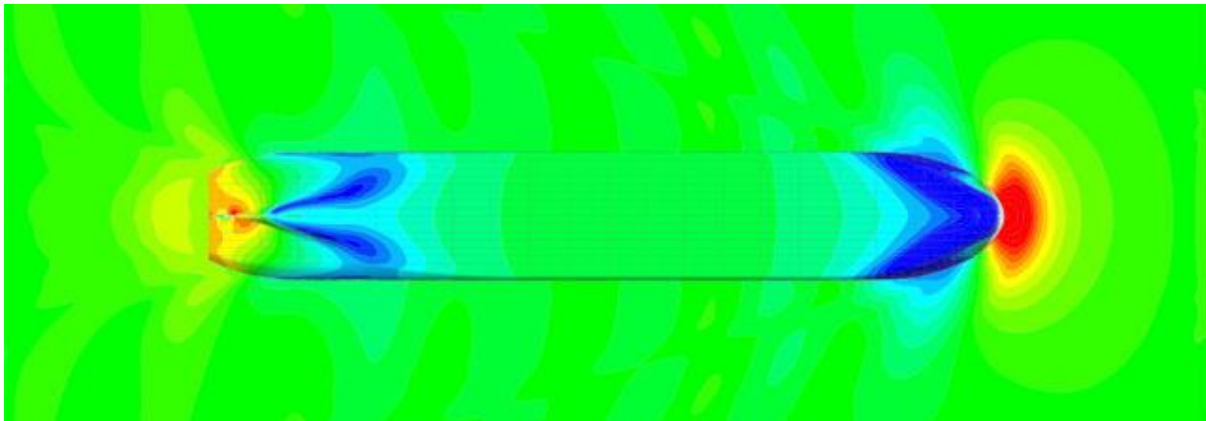
Fig.11: Hull optimization of "Diamond 2" using DNV's ECO Lines service
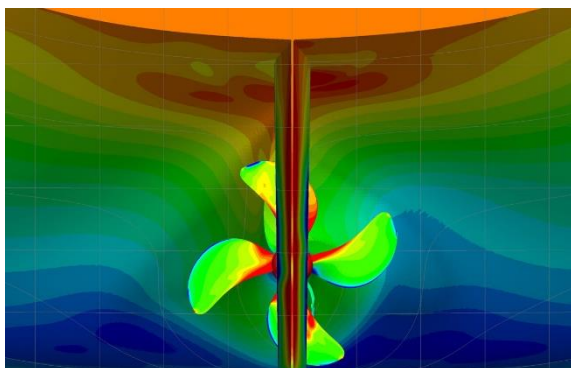
Fig.12: Asymmetric stern as robust PID
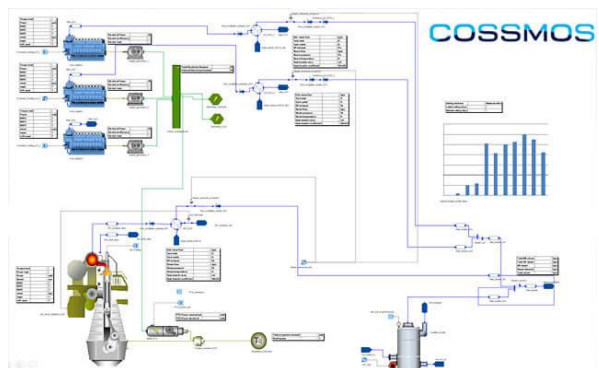
Fig.13: COSSMOS fine-tuned machinery systems

2.2. Long-term perspective (beyond 2030 towards 2050)

To progress further in decarbonizing bulk carrier shipping, we will have to leave – technically and economically speaking – our comfort zones. We will have to adopt technologies that are now in the

R&D stage or "exotic", and in many cases we will have to accept longer payback times or even generally higher costs in shipping.

2.2.1. Design measures

Among the ideas floating around for wider adoption after 2030 are:

- <u>Asymmetric sterns</u>, Fig.12, and other PIDs (Propulsion improving Devices) are expected to become the norm rather than the exception.

- <u>Air lubrication</u>, Fig.14, *Silberschmidt et al. (2016)*, is one of the "exotic" technologies about to take off. Shell Shipping had one of the first installations worldwide on a tanker, where long-term performance monitoring by an external provider showed net savings slightly above 5%. For a bulk carrier, we may expect a bit less, as tankers spend half their times in ballast condition where the air pumps need less energy due to the lower hydrostatic bottom pressure at ballast draft.

- <u>Advanced antifouling solutions</u> will affect mainly the CII, to a much lesser degree the EEDI, *Tan et al. (2022)*. The EU project CHEK, https://www.projectchek.eu/, is developing phase-2 technology for future cruise ships and bulk carriers, Fig.15, *Kelling (2021)*. One of the elements is replacing conventional biocidal paints by ultrasonic protection gluing arrays of transducers on the steel hull. Expanding ultrasonic technology from niche areas to full-hull protection of large cargo vessels is ground-breaking. The project partners target for 10-15% savings in fuel and emissions.

- <u>Tip-modified propellers</u> – Another example are propellers that do not have the traditional straight blades, but are modified at the end, similar to wings on modern airplanes. One example is the Kappel propeller, https://www.mek.dtu.dk/english/Research/Feature_Articles/KAPPEL_Propeller, which is curved 3D in space. While performance monitoring revealed that it requires more fuel in manoeuvring, such a propeller may save 4-6% in design condition, and for a bulker trade 2-4% in overall yearly fuel consumption.

- <u>Wind-assisted Ship Propulsion (WASP)</u> – There is no shortage of concepts harnessing wind energy, including rigid sails, Flettner rotors, and kites, *Hollenbach et al. (2020)*. All concepts have their pros and cons, but we see generally a rapid increase in projects and installations, Fig.16. With expected lower operational speeds, the business case for WASP systems will improve. With more installations and mature system providers, we are likely to see a progressively wider take-up.

Fig.14: Air lubrication system, source: Silver-stream Technologies
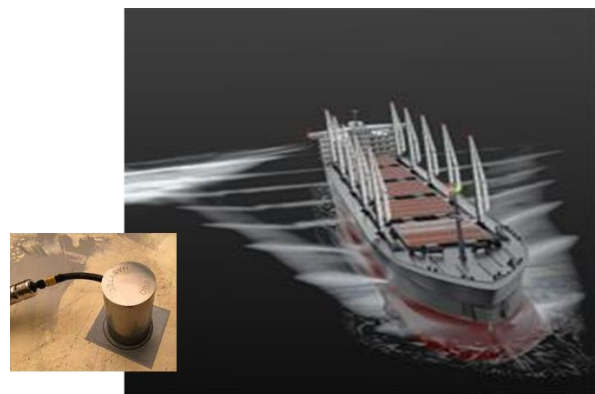
Fig.15: CHEK project with ultrasonic antifouling to protect bulk carrier hull, source: Hasytec

Fig.16: WASP installations on bulk carriers

- Alternative fuels – The 2020 sulphur cap of IMO initiated already a fading out of heavy fuel oil (HFO) in shipping. For the next 1-2 decades, LNG (Liquefied Natural Gas) is likely to be a popular choice; beyond that, a mix of fuels with decidedly lower carbon footprint is likely to be used by the industry, *DNV (2019,2021)*:

  o LNG – LNG effectively improves key parameters such as the EEDI through the c_f factor reflecting the carbon content of a fuel by ~25% compared to HFO. LNG as a fuel is most mature and has been adopted by several bulk carriers already, Fig.17. As IMO considers only tank-to-propeller carbon footprint and not the carbon footprint from well to tank, nor the greenhouse gas (GHG) effect from some unavoidable methane slip, net savings on GHG emissions are debatable.

  o (Bio-)Methanol - Methanol has been advocated as a future low-carbon, or even carbon-neutral fuel (depending on how it is produced), particularly in Scandinavia where a suitable maritime bunker infrastructure is already in place. With growing production facilities and growing worldwide bunkering infrastructure, bio-methanol is certainly a realistic contender in the current quest for alternative fuels. There are several projects for methanol fuelled cargo ships, including some for bulk carriers.

  o Ammonia - Ammonia as a fuel will require more R&D to become a mature and more widely adopted alternative. Ammonia contains much hydrogen, but is much easier to handle in storage and transport than liquid hydrogen, requiring essentially known technology from LPG (Liquid Petrol Gas). We have already large-scale ammonia production facilities world-wide, albeit so far mainly 'brown' ammonia, i.e. using high carbon footprint technology to produce. Envisioned e-ammonia produced using clean electricity, e.g. from hydropower, will be more expensive. There are several projects for ammonia fuelled cargo ships, including some for bulk carriers as the Viridis bulk carrier project, Fig.18, receiving public funding.

Fig.17: LNG as fuel installation on bulk carrier "HL Green"

Fig.18: Ammonia-fuelled bulk carrier project, Source: Viridis Bulk Carriers

2.2.2. Demonstrator projects "Ultramax 2030" and "210000 tdw Newcastlemax"

Various R&D projects with DNV involvement are supporting the process from strategic concepts to industry-mature implementation.

Oshima Shipbuilding and DNV signed a long-term strategic cooperation agreement to conduct R&D together on new bulk carrier designs. The first design, developed together with Wärtsilä, the "Oshima Ultramax 2030", Fig.19, reduces the energy EEDI by 50%. The design maximizes operational performance while minimizing emissions by utilizing LNG as fuel, with an optimized hull shape and a hard sail to generate extra propulsion. In addition, the design uses solar panels and batteries to cover the hotel load during waiting and port operations. The array of options introduced in the new design includes a shaft generator with a battery pack and two different main engine alternatives. The first engine option is a high-pressure, two-stroke dual-fuel engine, while the second option is a four-stroke dual-fuel engine. The 2000 m^3 LNG tank gives a range of 13600 nm, enough to cover the main global trading pattern of a round trip from Singapore to South Africa.

Particular attention was paid to reducing emissions while waiting and in port, in order to shrink the overall environmental footprint, not just while sailing. Solar panels with total area ~1500 m^2, installed on top of the hatch covers, will generate up to 88 kWh during sunlight hours, with the remaining 42 kWh supplied by battery. This covers the expected consumption of the highly optimized hotel load of only 130 kWe in "Eco mode" during waiting times. At night, battery power can be used for three hours before the battery is discharged. Whenever charging is required, diesel fuel gensets will run at optimum engine load to charge the batteries and cover the hotel load. About one hour is required to fully charge the battery.

The 60 m high hard sail generates additional thrust to supplement propulsion power. The sail automatically rotates to the optimal angle of attack to maximize thrust in response to changing wind conditions. The sail will be folded in unfavourable wind conditions and during loading and unloading. For North Pacific, expected fuel savings from sail use is up to 10%.
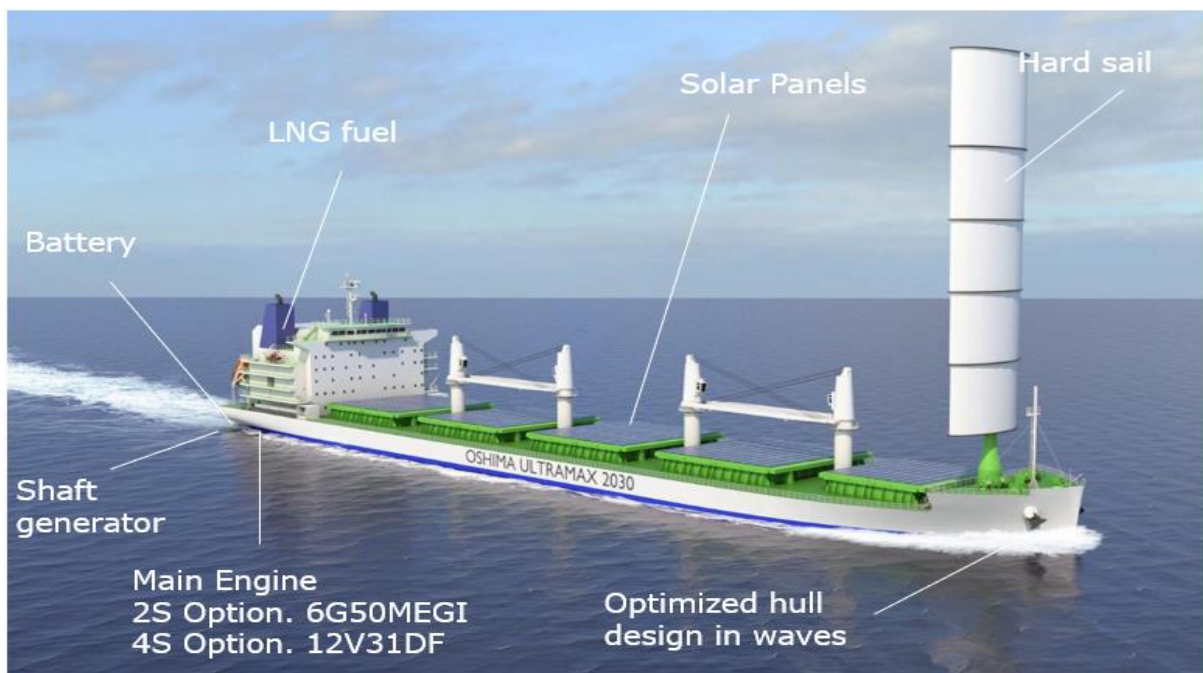
Fig.19: Oshima Ultramax 2030 project

DNV looked into the effect of future alternative fuels on the design of a case study vessel, namely a newbuild 210000 tdw Newcastlemax bulk carrier, Fig.20. The cruising range was assumed to be 16000 nm. Tank capacity was designed to have one bunkering per round trip. The case study covered

various fuels that can be used for each of seven rationally selected design options, either in a newbuild or after a possible future conversion, Fig.21. The study looked into such a large variety of fuel options, because long-term predictions for predominant marine fuels are invariably afflicted by high uncertainty, where it is best to investigate various scenarios or trajectories, particularly for fuel prices, *Eide et al. (2011), DNV (2021)*. E.g. future low-cost renewable energy my become available, making synthetic ammonia commercially more attractive than biofuels. Full details of the Newcastlemax bulk carrier case study findings are available in Maritime Forecast to 2050, *DNV (2021),* but three key ones for the chosen scenario and assumptions are:

- The conventional mono-fuel (MF) ship has the highest total discounted cost beyond 2030. It incurs the lowest capital expenditure (CAPEX), but the highest fuel expenditure (FuelEX) over its lifetime. This is because the study assumes a high price for carbon-neutral marine gas oil (MGO), which would be the only fuel option available for meeting the chosen GHG target trajectory.
- The ammonia-ready design solutions would have a higher CAPEX but comparatively lower FuelEX than the conventional option in their lifetimes.
- The two design options with lowest discounted costs are MF Fuel Ready (ammonia) and dual-fuel (DF) LNG Fuel Ready (ammonia). The study also identifies DF LPG Fuel Ready (ammonia) as a low-cost option but does not investigate it further.
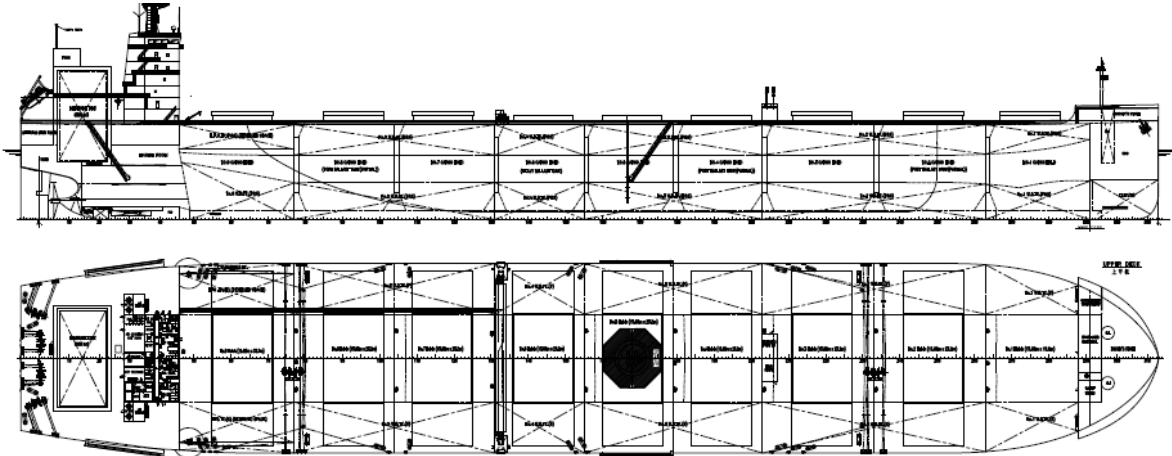
Fig.20: 210000 tdw Newcastlemax bulk carrier concept study, source: SDARI/GTT

Design options related to fuel, investigated for a Newcastlemax bulk carrier					
				■ Mono-fuel	■ Dual-fuel
Design option at newbuild*	**Fuel flexibility at newbuild**		**Fuel flexibility after conversion**		
	Fossil fuels	Carbon-neutral fuels	Fossil fuels	Carbon-neutral fuels	
MF	VLSFO MGO	(bio-/e-)MGO	—		
MF Fuel Ready (methanol)			VLSFO MGO	(bio-/e-)methanol (bio-/e-)MGO	
MF Fuel Ready (ammonia)			VLSFO MGO	e-ammonia (bio-/e-)MGO	
DF LNG	LNG MGO	(bio-/e-)LNG (bio-/e-)MGO	—		
DF LNG Fuel Ready (methanol)			MGO	(bio-/e-)methanol (bio-/e-)MGO	
DF LNG Fuel Ready (ammonia)			MGO	e-ammonia (bio-/e-)MGO	
DF LPG Fuel Ready (ammonia)	LPG MGO	(bio-/e-)MGO	MGO	e-ammonia (bio-/e-)MGO	

*All design options use internal combustion engines as the choice of energy-converter
Key: Mono-fuel (MF); dual-fuel (DF); very low sulphur fuel oil (VLSFO); marine gas oil (MGO); liquefied natural gas (LNG); liquefied petroleum gas (LPG)

Source: DNV 2021

Fig.21: Design options related to fuel, investigated for a Newcastlemax bulk carrier. Fuel flexibility at newbuild and after conversion (if applicable) are shown for each design option.

Fig.21: Vision of unmanned bulk carrier shipping using autonomous technology

And more ideas are waiting in the wings. The vision of the EU project MUNIN, Fig.21, http://www.unmanned-ship.org/munin/wp-content/uploads/2016/02/MUNIN-final-brochure.pdf, may become reality as we progress on autonomous ship technology. Maybe the future lies in very slow bulk carriers without crews, using remote control and autonomous technology. Remember that fuel consumption for a given voyage depends roughly on the square of speed, so half the speed would need only a quarter of the fuel, plus wind power becomes more effective at such low speeds.

3. Conclusions

Decarbonizing shipping is one of the greatest challenges for our industry. The next decade should be devoted to exploiting systematically the existing tried and proven technology. At the same time, we need to increase R&D activities to lay the foundation for the post-2030 phase, where alternative fuels and wind-assisted ship propulsion are expected to carry the decarbonization process to the next level.

Acknowledgements

References

BERTRAM, V. (2020), *Biofouling Management at the Dawn of a Mechanical Era*, 1st PortPIC Conf., pp.87-92, http://data.hullpic.info/PortPIC2020_Hamburg.pdf

BERTRAM, V. (2021), *Fuel Options for Decarbonizing Shipping*, 13th HIPER Conf., Tullamore, pp.12-20, data.hiper-conf.info/Hiper2021_Tullamore.pdf

BERTRAM, V.; CAMPANA, E.F. (2020), *Ship Hull Optimization – An Attempt to Determine Position and Course of the State of the Art*, 19th COMPIT Conf., Pontignano, pp.271-279, http://data.hiper-conf.info/compit2020_pontignano.pdf

COMER, B.; GEORGEFF, E.; STOLZ, D.; MAO, X.L.; OSIPOVA, L. (2022), *Decarbonizing Bulk Carriers with Hydrogen Fuel Cells and Wind-Assisted Propulsion: A Modeled Case Study Analysis*, Int. Council on Clean Transportation, https://theicct.org/sites/default/files/publications/Hydrogen-and-propulsion-ships-jan22.pdf

CSC (2011), *A transparent and reliable hull and propeller performance standard*, Clean Shipping Coalition submission to MEPC 63/4/8, https://jotunimages.azureedge.net/images/images/mepc-63-4-8_tcm214-10265.pdf

DNV (2019), *Assessment of selected alternative fuels and technologies*, DNV, Høvik, https://www.dnv.com/maritime/publications/alternative-fuel-assessment-download.html

DNV (2021), *Maritime Forecast to 2050 – Energy Transition Outlook,* DNV, Høvik, https://eto.dnv.com/2021/maritime-forecast-2050/about

EIDE, M.; LONGVA, T.; HOFFMANN, P.; ENDRESEN, Ø.; DALSØREN, S. (2011), *Future cost scenarios for reduction of ship CO2 emissions*, Maritime Policy & Management 38, pp.11-37, https://www.researchgate.net/publication/241717370_Future_cost_scenarios_for_reduction_of_ship_CO2_emissions

GATIN, I.; KALAJDŽIĆ, M. (2022), *Energy Saving Devices Performance Assessment Using CFD*, 7th HullPIC Conf., Tullamore, pp.30-35, http://data.hullpic.info/HullPIC2022_Tullamore.pdf

GEORGOPOULOU, C.; KOUKOULOPOULOS, L.; DIMOPOULOS, G.; OVRUM, E.; NIKOLO-POULOS, L.; BOUGIOURIS, K. (2021), *Model-Based Assessment of a Fuel Cell Driven Very Large Crude Carrier Concept,* 13th HIPER, Conf., Tullamore, pp.209-217, http://data.hiper-conf.info/Hiper2021_Tullamore.pdf

HENRICHS, J.; HEIMANN, J.; HOCHKIRCH, K.; BERTRAM, V.; KOWALEWSKI, U. (2015), *Design Optimization for Operational Profile – What can be Achieved For Bulky Hulls?*, Conf. Energy Efficient Ship, Rotterdam

HOCHKIRCH, K.; BERTRAM, V. (2022), *Wind Assisted Propulsion – Economic and Ecological Considerations*, Maritime Technology and Research 4(3), https://www.researchgate.net/profile/Karsten-Hochkirch/publication/357362304_Wind_assisted_propulsion_Economic_and_ecological_considerations/links/61dd851c034dda1b9eeda1b5/Wind-assisted-propulsion-Economic-and-ecological-considerations.pdf

HOCHKIRCH, K.; KREBBER, B. (2017), *Optimization of Ships with Asymmetric Aftbodies*, White Paper, DNV, https://www.dnv.com/maritime/publications/optimization-of-ships-with-asymmetric-aftbodies.html

HOLLENBACH, U.; HANSEN, H.; HYMPENDAHL, O.; RECHE, M.; RUIZ CARRIO, E. (2020), *Wind Assisted Propulsion Systems as Key to Ultra Energy Efficient Ships*, 12th HIPER Conf., Cortona, pp.278-296, http://data.hiper-conf.info/Hiper2020_Cortona.pdf

KAKALIS, N.M.P.; DIMOPOULOS, G.G.; STEFANATOS, I.C. (2014), *A Novel Framework for Dynamic Modelling of Integrated Machinery Systems*, 13th COMPIT Conf., Redworth, pp.137-149, http://data.hiper-conf.info/compit2014_redworth.pdf

KELLING, J. (2021), *EU Project CHEK – Ultrasonic Antifouling and other Measures to Meet the CII Challenge*, 13th HIPER Conf., Tullamore, pp.132-139, data.hiper-conf.info/Hiper2021_Tullamore.pdf

KELLING, J.; MAYORGA, X. (2020), *The Silent Revolution in Biocide-Free Antifouling*, 12th HIPER Conf., Cortona, pp.70-73, http://data.hiper-conf.info/Hiper2020_Cortona.pdf

LARSSON, A. (2018), *Reinventing Ultramax*, Bulk Carrier Update, DNV, https://www.iims.org.uk/wp-content/uploads/2018/06/DNV-GL-Bulk-Carrier-Update.pdf

OCIMF (2011), *GHG emission-mitigating measures for oil tankers, Part A: Review of reduction*

potential, Oil Companies International Marine Forum, London, https://www.ocimf.org/document-libary/128-ghg-emission-mitigating-measures-for-oil-tankers-part-a-review-of-reduction-potential/file

SILBERSCHMIDT, N.; TASKER, D.; PAPPAS, T.; JOHANNESSON, J. (2016), *Silverstream System - Air Lubrication Performance Verification and Design Development*, 10th HIPER Conf., Cortona, pp.236-246, http://data.hiper-conf.info/Hiper2016_Cortona.pdf

SØRHAUG, E.M. (2018), *Reinventing Ultramax*, Maritime Impact, DNV, https://www.dnv.com/expert-story/maritime-impact/Reinventing-Ultramax-Diamond-II.html

TAN, K.K.; PAERELI, S.; BRINK, A. (2022), *Impact of hull coating on EEXI and CII*, 7th HullPIC Conf., Tullamore, pp.190-197, http://data.hullpic.info/HullPIC2022_Tullamore.pdf

The Future of Biometrical Measurements on the Ship's Bridge: The Marine Pilots' Biometrical Response During Simulated Port Approach Navigation

Dejan Žagar, University of Ljubljana, FPP Portorož/Slovenia, dejan.zagar@fpp.edu
Franc Dimc, University of Ljubljana, FPP Portorož/Slovenia, franc.dimc@fpp.uni-lj.si

Abstract

This paper introduces the experimental study of marine pilots' biometrical readings during port approach simulation to determine the correlation between the demanding cognitive phase of port approaching and the participants' body responses, including their state of awareness. The findings reveal the reasons for the potential hot spots of the channel entrance where the participants' average body response was high, which support the shore-based services (vessel traffic system). The safety and integrity of navigation are higher when several devices or systems detect that the vessel remains on the desired course, including the integrity and awareness of navigators on the ship's bridge.

1. Introduction

This paper aims to study a navigator's biometric response during a simulated navigation task measured with wristband bio-sensors. The participants' repeated and specific body reactions correlate with the demanding cognitive phase of the simulated port approach, indicating a density of the process in the working memory. In order to increase maritime safety from a coastal services perspective, exchanging such biometric information, e.g., through the AIS data, would help coastal operators be alert to ships where navigators' biometric responses may deviate from the average values.

With increasing computing power performances and measuring technologies, human-computer interactions, *Tkalčič et al. (2016)*, have been developing rapidly in the maritime industry to decrease the number of incidents and ships lost. However, the number of incidents, including the human factor, has remained unchanged for the last seven years, *EMSA (2021), Barnett (2005)*. According to collision reports, including human error, despite all modern navigational aids and instruments on the ship's bridge, incidents/accidents mainly occur due to a high cognitive load on navigators and/or lack of situational awareness. Thus by human-computer interaction, using radar, ECDIS, and AIS increases the navigators' situational awareness, which was a goal; however, the inevitable consequence is that the navigators' cognitive processes in the working memory increase, which affect the erroneous action and human factor error, *Haberlandt (1997)*. For this reason, in the last five years, several types of research and experiments have been conducted to measure the biometric response of navigators during both a real and a simulated navigation task, *Miklody et al. (2017), Di Nocera et al. (2015)*.

After careful preparation, the presented case study is conducted in a full-mission simulator. The scope of marine pilots' biometric readings during a port-approaching task determines the correlation between the challenging cognitive task and the factors affecting participants' physical responses, e.g., ships' approaching speed, objective danger, or potential disturbing factor. The results implicate their state of awareness, including the reasons for possible hotspots at the channel entrance.

The processed and analysed data support e-solutions in smart navigation, which are becoming increasingly important in navigation and modern shipping.

2. Background and Methodology

The primary task of the ship's Officer on Watch is to throughout the ship's navigation, monitor the bridge instruments, and compare the apparent position with the desired ship's route. The task becomes cognitively demanding in dense traffic areas, where, due to situational awareness, the processes in the working memory increase, resulting in specific human body responses. The efficiency of the cognitive

processes during training depends on the number of repetitions and correlates with the participants' prior experience, resulting in a specific response. The scope of the present research is the response due to demanding cognitive tasks to highlight the potential safety issues while entering the narrow channel. The Faculty of Maritime Studies and Transport experimented with the Wärtsilä's full mission nautical simulator to measure such a response. The participants' BVP was recorded during a narrow channel entrance sequence simulation. The scope of the experiment is to analyse the rate of change in participants' body response in the demanding cognitive phase, including 15 s before narrow channel entrance and 15 s after entering the channel. Time "zero" is at the moment when the ship is between two buoys at the channel entrance, Fig.1.

Fig.1: Port of Koper-approach to the container terminal. The ship entered the canal at an undesirable angle due to wind gusts and the participant's late reaction. Two tugs assisted the 14 m draft container ship stay on course within the dredged channel.

The task involves approaching the Port of Koper with a large container ship with a 14 m draft. The channel depth is dredged to 15m, and the NE wind gusts pushed the large ship downwards, so there is not much space for errors. The six marine pilots who participated in the experiment, Table I, were locals familiar with local environmental conditions, including the port approach. The participants may perform the exact port approach in reality with the exact container ship as in the simulation.

Data are recorded with Empatica's E4 wrist-band biometrical sensor, https://www.empatica.com/research/e4/. This approach results in low false readings and noise ratio due to non-invasive sensors. Thus the post-processing is theoretically less complex. The weakness is the low sampling frequency – 64 Hz. As the main observable, the blood volume pulse (BVP) sensor indicates that the more the blood vessels dilate (vasodilation), the greater the signal amplitude, indirectly indicating the reaction process during simulated navigational tasks. The recorded data is synchronized and statistically analysed by moving mean, creating a series of averages of different subsets of the data set.

Table I: Participants' data

Participant	Gender	Age [yrs]	Sea service [yrs]
1	M	37	8
2	M	49	18
3	M	54	7
4	M	41	15
5	M	45	16
6	M	41	6
Average		44.5	11.7
STD		5.65	4.78

The position data was extracted from simulated ships' dynamic files (AIS data) during the experiment, consists of time, latitude, longitude, speed, and several other ships' parameters. The ship's dynamics sampling rate during the experiment is 10Hz. A virtual reference line is set between two buoys marking the entrance of the dredged channel. When the ship passes the virtual line between the buoys, the exact crossing time is recorded and, through Python script, synchronized with biometrical recordings. The participants perform the port approaching two times. The first is adapting session, including familiarisation. The second is the experimental session, where biometrical data is recorded. The results are shown in the next section.

3. Results and Discussion

The interval of interest is chosen from fifteen seconds before entering the channel to fifteen seconds after entering the channel, assuming the cognitively demanding task will induce the biometry. The visualization of the results is seen in Fig.2, where participants' normalized BVP readings (vertical axis) implicate the state of body response. The sampling rate was set to 64 Hz, meaning 1920 samples in the observing interval. For the time series moving average, 120 samples are used. Although each participant's different signal amplitudes and response rate depend on personality traits, the results are similar and comparable.
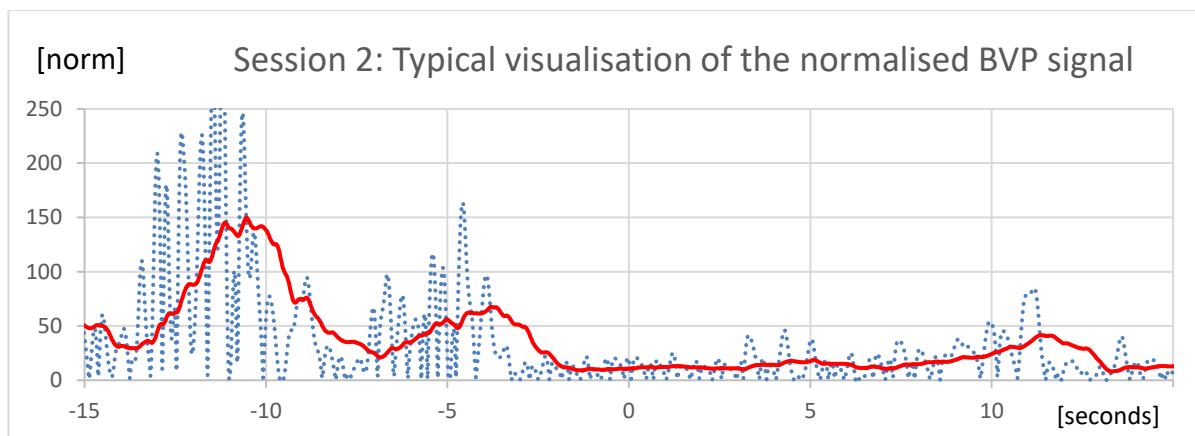
Fig.2: Participant's normalized BVP readings during Session 2: The interval of interest is channel entrance, including + - 15 seconds around time "zero" (horizontal axis). The blue line represents the normalized BVP signal amplitude, and the red line moving average time series. Averagely 10.8 s before time zero, the response becomes higher, indicating the increased density of the cognitive processes in the participants' working memory.

The scope of the research is to find similarities in the participants' body responses induced by the demanding cognitive phase of the task. From that point of view, the time series is applied over the BVP interval using the discrete-time sequence. The normalized BVP signal average amplitude of all participants is 24 (the number has no significant units), and the peak amplitude average is 205 (vertical axis). The interesting part is that, on average, 10.8 s before time zero, the participants' body responses become excited, indicating the increased density of the processes in the working memory. At the point of channel entering, the participants closely monitor both the outside situation and the navigational instruments and give the specific orders to the helm and tugs. The quick assumption from gained results would be that (mental) effort during a demanding cognitive task affects the BVP signal. More importantly, the response is measurable and comparable by all six participants. The algorithm was developed to quantify the participants' response state based on the BVP data to validate the assumption. The variables included in the calculation are presented in Table II. The values were extracted from raw BVP signal for all six participants individually. Furthermore, the average and std values for the population were excerpt. The high state in columns 7-8 represents body response above 400% of the average arousal.

Table II: Variables extracted from raw BVP signal – session 2

Participant	Average value	median	std	Average amplitude	Peak amplitude	high state [%]	high state [s]
1	-1.21	2.13	28.7	14.5	80.2	11.7	6.8
2	-0.18	1.07	45.8	24.3	256.6	15.6	9.3
3	0.12	5.8	98.9	46.2	321.2	7.1	4.8
4	0.93	0.99	51.1	18.5	300.9	2.8	1.8
5	0.084	-0.046	8.87	7.6	24.3	0.2	0.4
6	0.16	0.74	59.5	35	246.3	23.9	13.8
average	0.0	1.8	48.8	24.4	204.9	10.2	6.2
std	0.6	1.9	27.8	12.9	112.0	8.0	4.5

The variables were standardized, including the navigational experiences, type of simulation, average amplitude, high state response, and neuroticism as personal traits. The aim of using one of the personality dimensions in the scope is to neutralize the individual (personality-driven) body response compromising the wrist sensors' measuring data. Fig.3 represents the participants' response index to the task. The value "zero" represents the population's average (expected) response. The positive values represent increased arousal, and the negative values represent body response below expected average arousal.
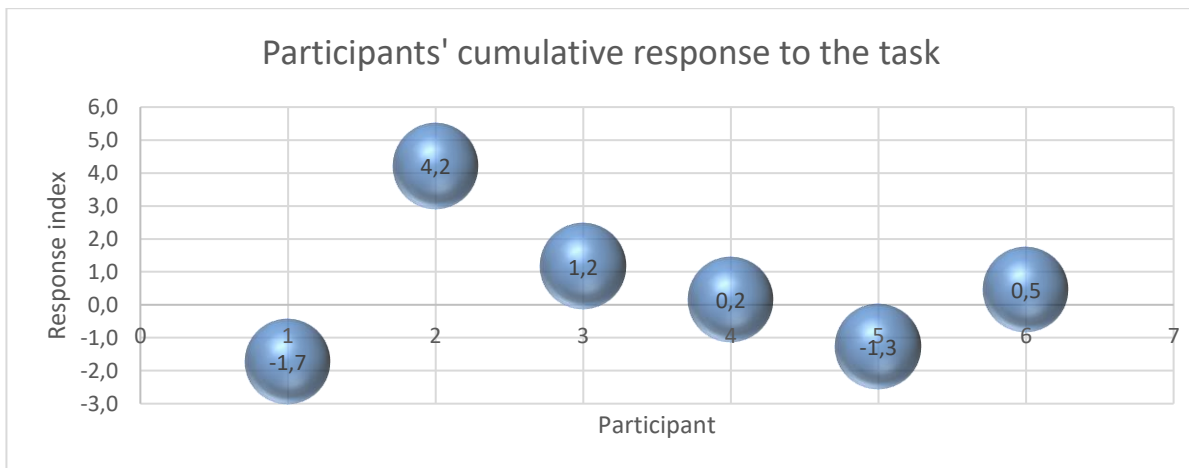
Fig.3: The response index represents the cumulative value of the variables, including navigational experiences, type of simulation, average amplitude, high state response, and personality traits

Interestingly, the response index was unreasonably high when approaching speed was unlimited. After limiting the ships' speed to 6 kn, the index also decreased to average values. The advantage and opportunity of the index are in monitoring the navigators' response in the potentially dangerous areas, e.g., traffic separation zones, narrow channels, and port approaches. The measuring signal could be easily added as a part of NMEA strings of the AIS signal, so the authorities and coastal stations could be informed in real-time and prepared or perhaps give additional assistance to ships where the response index is found to increase.

4. Conclusion

The leading thought of the research was to highlight the potential hotspots during the port approach based on the BVP response. Although the small sample (N=6) and the algorithm are simplified, the valuable indices were excerpted and linked to real-world circumstances. During the research, several proposals to the Port of Koper port authorities were made, already being implemented. The speeds in the ports were found too high; now, the speed limit is 6 kn when approaching the port and 5 kn inside the basins. The maneuvers with these ships start a mile earlier, so pilots can prepare for entry, reducing

stress and increasing safety. Additionally, for maneuvering with large ships, e.g., very large container carriers, navigational devices (Independent Pilot Navigation Systems) are now available to pilots.

Despite the legal issues of accessing and sharing personal biometrical data, we assume that in one way or another, the biometry on the ship's bridge will be, in the near future, part of navigational instruments, including the integrity and awareness of navigators. On the other hand, the safety of navigation is higher when several devices or systems detect that the vessel remains on the desired course, so we expect that such a system, when fully operational, will prevent and foreseen the potential incidents involving the so-called human factor error.

Acknowledgements

References

BARNETT, M.L. (2005), *Searching for the Root Causes of the Maritime Casualties*, WMU J. Maritime Affairs, pp. 131-145

DI NOCERA, F.; MASTRANGELO, S.; BALDAUF, M.; STEINHAGE, A.; KATARIA, A.; PROIETTA, S. (2015), *Mental workload assessment using eye-tracking glasses in a simulated maritime scenario*, Proc. Human Factors and Ergonomics Society Europe (HFESE), Groningen, pp.235-248

EMSA (2021), *Annual overview and accident investigation report 2021*, EMSA, https://www.emsa.europa.eu/accident-investigation-publications/annual-overview.html

HABERLANDT, K. (1997), *Cognitive Psychology*, Allyn and Bacon, Boston

MIKLODY, D.; UITTERHOEVE, W.; VAN HEEL, D.; KLINKENBERG, K.; BLANKERTZ, B. (2017), *Maritime Cognitive Workload Assessment*, 6th Int. Workshop Symbiotic Interaction, Eindhoven, pp.102-114

TKALČIČ, M.; DE CAROLIS, B.; DE GEMMIS, M.; ODIĆ, A.; KOŠIR, A. (2016), *Introduction to Emotions and Personality in Personalized Systems. Emotions and Personality in Personalized Services*, Human–Computer Interaction Series, Springer

Hey Porter, Hey Porter:
Strategic Analysis for Naval Architectural Training in the 21st Century

Volker Bertram, DNV, Hamburg/Germany, volker.bertram@dnv.com

Abstract

The paper applies the Porter framework for strategic management to teaching maritime technologies, with particular focus on post-graduate and professional training. Several factors drive the developments: changes in students, changes in technology, changes in expectations from industry and governments. These factors determine what we need to teach and how we need to teach. A different teaching infrastructure with possibly different providers is expected to evolve. The paper discusses both market and technological aspects, highlighting challenges and pitfalls of new technologies commonly referred to as "e-learning". The paper argues that e-learning may come in many forms, and pedagogical goals need to be defined first to determine the best suited technical implementation.

1. Introduction

A new optimization method combining 3D CFD simulations and new data structures for an Arctic cruise vessel is a safe topic for any conference. An estimated three colleagues may be interested to start with. A suitable mixture of complex equations, daunting diagrams and colourful displays will evoke admiration, little interest, and no aggression. In comparison, education in engineering is a dangerous topic. We all have been exposed to the topic (as students). It is a bit like football:

- It used to be better in the past.
- The players (students) today just do not want to work anymore. Shame on them!
- The coaches (professors/trainers) are incompetent. Shame on them! We could do a better job.
- It is still great fun to talk about…

Teaching environments and techniques have changed over time, Fig. 1. In Germany in the early 1980s, when I studied naval architecture, all professors used blackboard and chalk. Today, a mixture of PowerPoint and blackboard (or whiteboard) prevails. Discussions about future teaching employ terms like "web-based teaching", "e-learning" or "m-learning" (e-learning describes learning (or teaching) using assorted technologies, mainly Internet or computer-based. Students rarely, if ever, are face-to-face with each other or teachers. m-learning describes learning using mobile devices, particularly smartphones.) This comes typically with reorganization of departments and curricula, introduction of further quality management procedures and reduction of budgets. One must be a politician or university president to understand how this will result in better engineers for our industries.

Fig.1: Teaching over time (from left to right: around 1940, 1975 and 2010)

Much of the new teaching technology has been driven by mass markets like language teaching. Here the financial incentives are higher due to much higher numbers of students. In addition, there is traditionally a higher focus on pedagogy and openness to multi-media teaching. Much of what is now discussed for

maritime training has been tested in other fields like language teaching, law, and medicine. Highly specialized engineering (such as graduate and post-graduate training in maritime technologies) is different from these fields in required skills, available market size, and other aspects. Some approaches that work for example in English language teaching do not work for teaching naval architecture.

Despite changes in technologies and students (generations X, Y, Z, etc.), there are some constants in our fundamental guidelines to teaching:

- You learn by doing and face-to-face time with teachers is expensive. So, we need to encourage students to work outside class time.
- Students should use tools that they are familiar with. For my generation, that meant books. For the new generation of students, this may increasingly mean computers and even smartphones.
- Communication with peers should be encouraged. This happened too little in classical engineering training, where frontal teaching has ruled supreme. Internet technology allows virtual meeting spaces for students. While popular in pedagogy theory, in my observation these spaces have been used more for "networking" (gossiping) than real studying. However, traditional teamwork continues to work well, and team communication is then automatically based on internet and mobile phones.
- Modern teaching approaches advocate the mantra: Make teaching competitive, make it fun! We are supposed to move from education to edutainment, where students are entertained while learning quasi without noticing it. This is easier in language education than in engineering. Material science was no fun 30 years ago, still is no fun, and is unlikely to ever be fun. No pain, no gain.

2. Porter model analysis

The introduction has already mentioned several of the driving factors shaping our teaching: budgets, technology, and politics. The demographic and political changes are fairly universal. They will be discussed in the following subsections. The Porter model helps us to bring structure into this analysis. Porter sees five driving factors to consider in a strategic analysis, Fig.2.
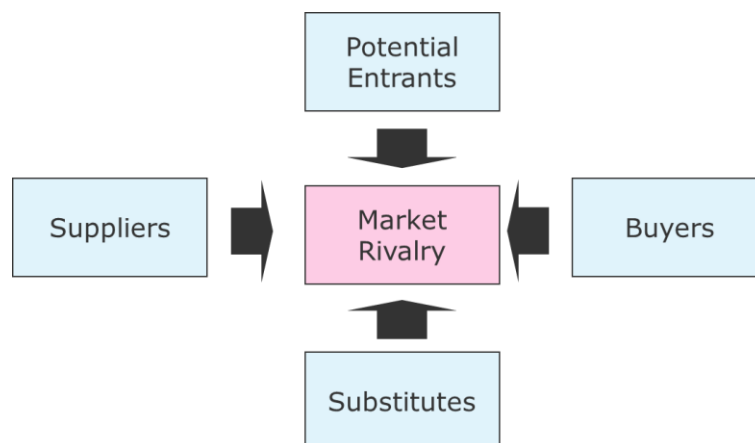
Fig.2: Porter model

2.1. Market rivalry – The status quo

The maritime education landscape was relatively simple in the last century. The universities offering post-graduate degrees were organized in Europe under the umbrella of WEGEMT, http://www.wegemt.com/. In Germany, the engineering education was clearly divided into two worlds apart:

- "Fachhochschulen" ("polytechnics") offered degrees equivalent to a bachelor's degree, with no straightforward continuation to higher degrees. For naval architecture and marine engineering (NAME), such education was offered in Kiel and Bremen.

- Technical universities offered a Dipl.-Ing. (Diplom-Ingenieur) degree, with 5 years' prescribed period of study, and doctoral degrees. For NAME, such education was offered in Hamburg, Berlin, Rostock and Duisburg.

"Market shares" (expressed in number of graduates per year) and curricula were stable. The market was transparent; in the small NAME community, strengths and weaknesses of each academic institution were well known. Post-graduate professional development in Germany has been informally obtained until today via reading of specialized journals and attending conferences. Until the mid-1990s, there were summer schools organised through the German society of Naval Architects and Marine Engineers, the STG (www.stg-online.de). These activities faded out with the retirement of key leaders in the community, as nobody in the new generation of professors was willing to take on the burden of organising such events.

2.2. Potential entrants – New national and international competitors

Then came disruption in the form of the Bologna declaration, https://en.wikipedia.org/wiki/Bologna_declaration, signed in 1999 in Bologna and giving European institutions of higher education a decade to harmonize academic curricula, aiming at a system of comparable degrees to facilitate mobility within Europe, both for academia and labour market. A key Bologna element was a standardization of academic degrees and prescribed durations to obtain these. The future was following the 3-2-3 rule: 3 years to obtain a Bachelor, 2 years to obtain a Master, and another 3 years to get your PhD. In essence, the traditional Anglo-Saxon way of education was imposed Europe-wide. In countries with strong home markets in student base and industry perception, the universities reacted reluctantly and slowly. Typical examples were Germany, France, and Italy. There seemed to be no need for action for 10 years, and a mix of nostalgia and defiance questioned the right of some remote politicians to impose such measures on the universities. But in any disruptive change, there are winners and losers; and the winners saw their chance and grabbed it. The Fachhochschulen, hitherto looked down upon by the universities, rebranded their names to "universities of applied science" and obtained quickly the right to educate to Master level. In Germany, in NAME, we now had 6 academic institutions offering education to Master level, and the standardization of educational degrees meant that a high-school graduate could go e.g. to Kiel, get his Master, and then continue to a PhD at another university anywhere in Europe.

The level of competition in NAME education had increased in Germany, but it was more than that: the market competing for students had opened much wider. More than 30 members of WEGEMT could be seen as "new entries" in the Porter model, increasing competition vying for students. Contrary to some statements from traditional German universities, industry embraced candidates with the "new" degrees, especially if they had studied outside Germany and improved their foreign language proficiency. The market adjusted to the new political frameworks:

- Undergraduate education was mainly a local market, with curricula offered in the home language. For the traditional universities with a 5-year curriculum for a Dipl.-Ing., changing to a 5-year curriculum for a master was easy, but having a "minor-league" degree after 3 years was a challenge. In any case, in the modern job market graduates require retraining (or continuous professional development) in their professional career.
- Postgraduate education has become a much more international market, where good students often actively strive to change not only universities, but also countries of education, adding language and intercultural skills to their portfolio. This requires a working knowledge of the language of the curriculum, creating a dilemma for countries that were already reluctant to change to the Bologna landscape: offer a Master-level education in imperfect English or face brain-drain. Eventually, it was in the cards that small players would withdraw from the market (= discontinue education in NAME, e.g. by disguising the process as changing to a degree in Mechanical Engineering with specialization in NAME). The conditions favoured countries that already had a high affinity to the Anglo-Saxon system and English proficiency: UK, Scandinavia, and The Netherlands.

The larger trends for maritime education are then:

- Increasing demand for life-long training, with upgrades on new developments in legislation and technology. Industry engineers looking for continuous professional development are a new or at least much larger market in Germany. The new customers are willing to spend more money, but less time and will favour on-site training rather than on-campus training. Consequently, the demand for distance learning will increase.
- Increased international competition for students favouring Anglophone graduate education. The transition towards a unified bachelor-master-PhD system in Europe has reduced thresholds between the various states in making university degrees compatible. This means that students will have more choice in where they can study. The winners of the resulting competition between universities are likely to be large Anglophone universities. Post-Brexit uncertainty and thresholds towards the EU handicap UK universities.
- Reduced funding for education in most countries. There is a trend to "privatize" state universities, cutting budgets and encouraging them to generate more own income. This may lead long-term to the starvation of small curricula, such as NAME curricula, after a vicious circle of reducing faculty, thinner and less prestigious curricula, and reduced attraction of students.

2.3. Suppliers – The students

"Students these days are not what they used to be." We heard this sentence when we were students from our professors. We hear it today, and it is the same the world over:

- They do not want to study as much as we did.
- They cannot write properly even in their mother tongue.
- They only want to play with computers; they are not interested in "real" science (i.e. the mathematics involved in fluid or structural analyses).

These are not senile professors ranting, with a selective memory of their past. There are real changes, due to changes in the way of life and upbringing of children. Today's children are exposed to computers before they go to school. *Prensky (2001,2011)* calls them "digital natives": "Today's average college grads [in the USA] have spent less than 5,000 hours of their lives reading, but over 10,000 playing video games […] It is very likely that our students' brains have physically changed […]." These digital natives are our raw material - and they are different from us, with strengths and weaknesses:

- They are used to getting information fast. They google rather than open 20 books in a library.
- They prefer graphics to texts.
- They prefer random access to information (like hypertext links).
- They function best when networked.
- They thrive on instant gratification.
- They prefer games to serious work.

Does any of this sound familiar? My generation is called "digital immigrants" by *Prensky (2001)*. We are always one generation behind in the latest technology tools. Digital Immigrants must teach Digital Natives.

We cannot change the students or course participants we get. Instead, we should work on understanding them better and try to adapt our teaching to them, without sacrificing our goal to teach them what we know (or believe) to be important in their professional careers.

2.4. Substitutes – New forms and providers of maritime education

2.4.1. General considerations

New forms of training invariably involve computer technology. Technology develops and new terms come and go. The elementary learning techniques to teach NAME topics are (largely) media independent and should migrate naturally from traditional to digital training forms, Table I.

Table I: Traditional training techniques and digital equivalents

	Traditional	Digital
watching	Blackboard	PowerPoint Videos
reading	Books Lecture notes	Books Online texts
doing	Exercises Assigned homework/projects Laboratory work	Exercises (web-based) Assigned homework/projects Virtual lab visits
testing/evaluating	In class	On-line, mostly multiple choice Homework submission

In principle, all traditional elements in our curricula could migrate to digital form, except for laboratories and visits to industry sites. The vast majority of the "digital immigrants" defend traditional laboratory time, but personal experience is that they are expensive and ineffective in teaching. If you really want to learn experimental techniques, make an internship or project in a professional testing facility. If you just want some hands-on feeling on some physical behaviour, then a virtual (numerical) lab could serve a similar purpose. Positive examples of virtual laboratories for maritime applications are found in *Fernandes and Van Niekerk (2017)* for ship engine room equipment, *Renganayagalu (2021)* for nautical simulators in Virtual Reality, and *Koelman and Moussault (2021)* for naval architectural training.

So, in principle, migration to e-learning should be feasible in most cases. Then, why don't we see widespread e-learning activities in the maritime world and why do many efforts fall well short of their targets? Partly, because after initial hype and large investments, universities and other adult training institutes frequently have experienced a sobering disillusion with respect to new digital forms of training.

2.4.2. Self-access centres (SAC)

An example may illustrate the problems encountered: "Self-access centres" are educational facilities designed for student learning that are at least partially, if not fully self-directed. Several websites promote SACs claiming that self-access learning gives you the opportunity to develop initiative, responsibility, self-awareness, confidence, and independence in learning. It is about making choices and having flexibility in learning, e.g. https://englishplacementblog.wordpress.com/2016/04/05/cillc-library/. These claims sound too good to be true. And indeed, reality often does not live up to these expectations, for a variety of reasons:

- It is expensive to set up a good SAC. Learning institutes like to boast having an SAC, but do not want to pay much. Token efforts are a waste of money when it comes to SACs.
- SACs are frequently poorly staffed. Existing staff gets tasked with running the new multi-media lab. There is no budget for hiring a dedicated expert or even for training the person responsible.
- Equipment gets stolen or vandalized.
- SACs are set up as a once-off prestige object, often with external once-off funding. There is no budget for maintenance and upgrades. Once impressive hardware and software may quickly become obsolete.
- Students have no time or no motivation to use SACs, at least not for studying.

2.4.3. Web-based teaching

Two years after Covid-19, there is little need to explain how teaching may be based on online self-paced e-learning or live video conferencing. For maritime training, key options in our own experience at DNV are discussed with pros and cons in *Bertram and Plowman (2017,2019), Plowman and Bertram (2020)*.

Things do not automatically get better by converting from analogue to digital. The e-book version of a boring book will still be boring. The e-learning version of a boring classroom training will still be boring. And moving from familiar classroom training to less familiar digital training options comes naturally with risks of exceeding budgets and not reaching expectations. Time and cost budgets for developing digital training are often unrealistically low. As an order of magnitude, one should budget 60-120 h of development time for 1 h of e-learning, *Bertram and Plowman (2019),* both for subject matter experts and e-learning developers. Budgets get even higher, by 1-2 orders of magnitude, for the development of professional Virtual Reality based training in maritime applications, *Bertram and Plowman (2018), Bertram et al. (2020).*

Digitally delivered training has its advantages:

- It is easily distributed via the web. This is particularly attractive if you want to train people in many different locations.
- It offers generally higher flexibility than classroom teaching, especially when using information-on-demand techniques and self-study elements

But it also has inherent disadvantages:

- Subject matter experts (professors/trainers) may struggle with online tools (e.g. MS Teams) or online pedagogy
- There is no or little non-verbal feedback for the learners. ("You no longer see the look in their eyes and know they are lost.")
- Digital training requires more self-discipline from the learners to stay focussed on the training.
- There is more strain on eyes and ears, leading to earlier fatigue.

2.5. Buyers – Industry expectations

Let's say that the "buyers" in the Porter model in our case are the employers of trained professionals. What do they expect from the "products" of our training machines? OK, industry needs naval architects (or XYZ engineers), but what should a naval architect (or XYZ engineer) know? What is a must, what is nice to have? Elucidation of what employers want is not a trivial task; often, the buyer has difficulties in explicitly expressing what he wants and is realistically achievable. This "design elucidation" requires generally a dialogue between provider and buyer, possibly showing a number of candidates and learning likes and dislikes of the buyer. It is the same for buying a house, a car, or hiring an employee.

For naval architects, there has been one such dialogue, namely an ONR Workshop on "Teaching Future Ship Designers", *Rusling et al. (2005)*. The workshop brought academia (university representatives from the USA and Europe) and employers (industry representatives from the USA) together.

There were examples of "design elucidation" for training requirements through longer dialogues. Industry stated initially: "We want creative people." One might be tempted to recruit then from art and design colleges. But after 10 minutes of challenging this request, it emerged that industry meant: "We want engineers who can use first-principles methods," able to tackle non-standard ship design tasks using simulation tools. The lesson learnt was that defining the training objectives can be time-consuming task. If one does not take the time for a proper definition of training objectives, chances are much more time and money will be spent in re-designing curricula to produce something the buyer doesn't want.

The workshop showed large consensus between industry and academia, but also revealed some interesting differences on what should be taught (see also Appendix):

- There was consensus on the importance of a good base in naval architecture/engineering principles (strength and structural design; ship production; ship hydrostatics/stability; ship design (rules, layout, estimations); ship hydrodynamics, marine engineering). Scope and level of detail was not discussed.
- Industry wanted a higher level of computer literacy, especially a basic familiarity with CAD and simulation software. The general discussion may be summed up as "more IT, less theoretical mechanics".
- Industry wanted more hands-on experience (as worker, at sea or in shipyard, as engineer), essentially advocating more internship time.
- Industry advocated to keep more specialized knowledge and mathematics for (elective) courses on post-graduate level. More specialized and "exotic" topics may be taught at lower frequency, e.g. only every second year.
- Industry advocated academia to (more) actively address soft skills in engineering students (e.g. the ability to study independently; team capability; technical and business English; basics of work and business law; basics of business administration and project management; communication and presentation skills)

While it is easy to write down a wish list for what one (industry) would like to have, the dialogue also brought more awareness for constraints:

- For some topics, universities cannot have permanent staff. If industry is unwilling or unable to delegate suitable guest lecturers, these topics will not be taught.
- For training on specific software used in industry, licences and trained instructors are needed. Neither universities nor students usually have the funds to pay for this.
- Some skills are better acquired outside the university or formal training environment, e.g. in training on the job.

3. Conclusions

Industry requirements, learner expectations and technical possibilities should be considered in how we teach:

- More teaching will have to be based on e-learning and short courses. At DNV, we have observed training course times moving from 1 week to one day, with demand increasing for nano-learning offerings of 5 to 45 minutes.
- Teachers will continue with some traditional tasks (definition of learning objectives (what is really needed), selection/creation of appropriate teaching material, assessment of learning success (tests), question/answer discussion of unclear points), even if based on different media.

In selecting suitable forms of training, pedagogy comes first. First, we must decide what to teach. Then we can decide how best to teach it. Poor pedagogy results in poor training, regardless what media is employed.

Content is more important than means of transmission. Flashy e-learning portals do not substitute qualified teachers. E-learning is particularly interesting for commodity subjects (English, business administration, mathematics, etc.). Webinars and live virtual conferencing often offer more flexible and cost-efficient options for global maritime training needs than e-learning courses.

The private training market is expected to gain in importance with life-long learning in incremental steps on latest industry developments. DNV's Academy will continue to play an important role in this regard.

References

BERTRAM, V.; PLOWMAN, T. (2017), *Maritime Training in the 21st Century*, 16th COMPIT Conf., Cardiff, pp.8-17, http://data.hiper-conf.info/compit2017_cardiff.pdf

BERTRAM, V.; PLOWMAN, T. (2018), *Virtual Reality for Maritime Training – A Survey*, 17th COMPIT Conf., Pavone, pp.7-21, http://data.hiper-conf.info/compit2018_pavone.pdf

BERTRAM, V.; PLOWMAN, T. (2019), *A Hitchhiker's Guide to the Galaxy of Maritime e-Learning*, 18th COMPIT Conf., Tullamore, pp.7-23, http://data.hiper-conf.info/compit2019_tullamore.pdf

BERTRAM, V.; PLOWMAN, T.; FEINER, P. (2020), *Survey Simulator – A Virtual Reality Training Tool for Ship Surveys*, 19th COMPIT Conf., Pontignano, pp.7-17, http://data.hiper-conf.info/compit2020_pontignano.pdf

FERNANDES, F.; VAN NIEKERK, T. (2017), *Totally Integrated Automation for Ships: A Step Closer to Industry 4.0 Realization*, 11th Symp. on High-Performance Marine Vehicles, Zevenwacht, pp.202-211, http://data.hiper-conf.info/Hiper2017_Zevenwacht.pdf

KOELMAN, H.J.; MOUSSAULT, S.R.A. (2021), *School's in*, 20th COMPIT Conf., Mülheim, pp.36-42, http://data.hiper-conf.info/compit2021_muelheim.pdf

PLOWMAN, T., BERTRAM, V. (2020), *Digital Maritime Training in Covid-19 Times*, 19th COMPIT Conf., Pontignano, pp.304-315, http://data.hiper-conf.info/compit2020_pontignano.pdf

PORTER, M.E. (2004), *Competitive Strategy: Techniques for Analyzing Industries and Competitors*, Free Press

PRENSKY, M. (2001), *Digital natives, digital immigrants*, On the Horizon, MCB University Press, Vol. 9/5, http://www.marcprensky.com/writing/

PRENSKY, M. (2011), *From digital natives to digital wisdom*, http://marcprensky.com/writing/Prensky-Intro_to_From_DN_to_DW.pdf

RENGANAYAGALU, S.R. (2021*), Eye-tracking in Maritime Training: New Performance Measures for Immersive Virtual Reality Training Applications*, 20th COMPIT Conf., Mülheim, pp.265-271, http://data.hiper-conf.info/compit2021_muelheim.pdf

RUSLING, S.; BUCKNALL, R.; FELLOWS, D.; GREIG, A. (2005), *Teaching future warship designers*, Summary Report of the ONR/ONR Global International Workshop held at UCL, University College London

Appendix: Requirements for Naval Architects

The following is based on an ONR workshop on Future Warship Designers, *Rusling et al. (2005)*. In discussion between (mostly US American) representatives of industry and academia, the following items were listed as guidelines for future curricula for naval architecture:

- Good base in naval architecture/engineering principles
    - strength analyses, structural design, and ship production
    - hydrostatics/stability and ship design (rules, layout, estimation methods)
    - hydrodynamics
    - marine engineering

- Computer literate
    - CAD proficiency seen as main gap
    - Level of competence (hours spent with specific software) should be recorded
    - Naval architecture is increasingly applied computer science and less mechanical engineering

- Hands-on experience
    - as worker and as engineer
    - at sea/at shipyard

- more specialized knowledge/mathematics at post-grad level

- soft skills
    - ability to study independently
    - creative with feel for viability of solutions
    - enthusiastic
    - team capability

- management skills
    - project management
    - communication
    - basic legal frameworks for contract/work laws
    - motivation

- engineering/maritime English
    - vocabulary (incl. mathematical expressions)
    - technical/scientific communication in English

Using Machine Learning for Rapid Propeller Design Tools based on Numerical Series

Sven Albert, NUMECA Ingenieurbüro, Altdorf/Germany, sven.albert@numeca.de
Thomas Hildebrandt, NUMECA Ingenieurbüro, Altdorf/Germany, thomas.hildebrandt@numeca.de
Maurits van den Boogaard, NUMECA-Cadence, Brussels/Belgium, boogaard@cadence.com
Giacomo Alessi, NUMECA-Cadence, Brussels/Belgium
Benoit Mallol, NUMECA-Cadence, Brussels/Belgium
Dirk Wunsch, NUMECA-Cadence, Brussels/Belgium
Nathan Clero, NUMECA-Cadence, Brussels/Belgium
Dario Amadori, NUMECA-Cadence, Brussels/Belgium
Charles Hirsch, NUMECA-Cadence, Brussels/Belgium
Luca Zampieri, Neural Concept, Lausanne/Switzerland

Abstract

This paper presents a machine learning approach to accelerate the design of marine propellers. For open-water propeller characteristics, neural nets are trained to predict both integral quantities of open-water performance curves and local field values of velocities and pressures on two-dimensional planes for Wageningen B-Series propellers. The average difference between the predicted and CFD-obtained values remained below 1.5% for integrated quantities (thrust, torque, efficiency). The quasi-instantaneous response of a trained neural net may accelerate propeller design significantly.

1. Introduction

With the increase in computational power, machine learning offers new opportunities for accelerating the marine engineer's workflow during the initial design phases. Taking the example of open-water calculations, which tend to have high relative computational costs, the application of a machine learning algorithm like a Geodesic Convolutional Neural Network (GCNN) to such computations is shown in this paper to be promising and could allow increasing productivity in the initial design process by orders of magnitude. The goal of this study is therefore to describe the approach and discuss the results of applying a GCNN to open-water computations using geometries following the design of the Wageningen B-series propeller family and explore the productivity gains that can be achieved by applying artificial intelligence to marine CFD results.

2. Methodology

2.1. Geometry generation and verification using CFD

The Wageningen B-series propeller series was chosen as the 'parent' series for the design of experiments (DoE). Propellers in this series are described by four parameters: the diameter D, the expanded area ratio EAR, the number of blades Z, and the propeller pitch P. If the diameter is kept constant ($D = 1$ m), the geometry is fully described by EAR, Z and P. The propellers were modelled using Rhino 3D in combination with Grasshopper along with a proprietary Python code containing the sectional geometry description based on the definitions described in *Kuiper (1992)*. The two-dimensional sections were developed into three-dimensional blades using NURBS.

Van Oossanen and Oosterveld (1975) developed the description of open-water performance curves valid for any Wageningen B-series propeller based on regression analysis of earlier model tests performed at the Maritime Research Institute in the Netherlands (MARIN). The original description of the thrust and torque coefficient curves is valid at a Reynolds number of 2,000,000. These regression curves were subsequently compared to CFD (Computational Fluid Dynamics) results for a selected number of propellers and operating conditions to verify that the created propeller geometries yielded the expected results corresponding to the Wageningen B-series.

34

The results indicated that thrust and torque predictions coming from CFD were within 5% of the regression-based prediction for a wide range of advance ratios J.

Very high advance ratios, where propellers generate close to zero thrust, showed lower accuracy which was already expected based on previous experience. At low values of J, the propeller is acting in bollard pull conditions and this was identified as a less interesting condition to include as most ships only spend very little amount of time operating in these conditions. Therefore, the allowed range of J values was determined by first calculating the theoretical range of positive thrust (first quadrant propeller operation) for each propeller in the design set. Subsequently, the bottom 10% was discarded to avoid bollard pull conditions and the maximum allowed J value was chosen halfway between the point of maximum efficiency and the J value corresponding to thrust breakdown, to avoid inaccuracies of the CFD solver close to the point where $K_t = 0$. This is visualized in Fig.1.
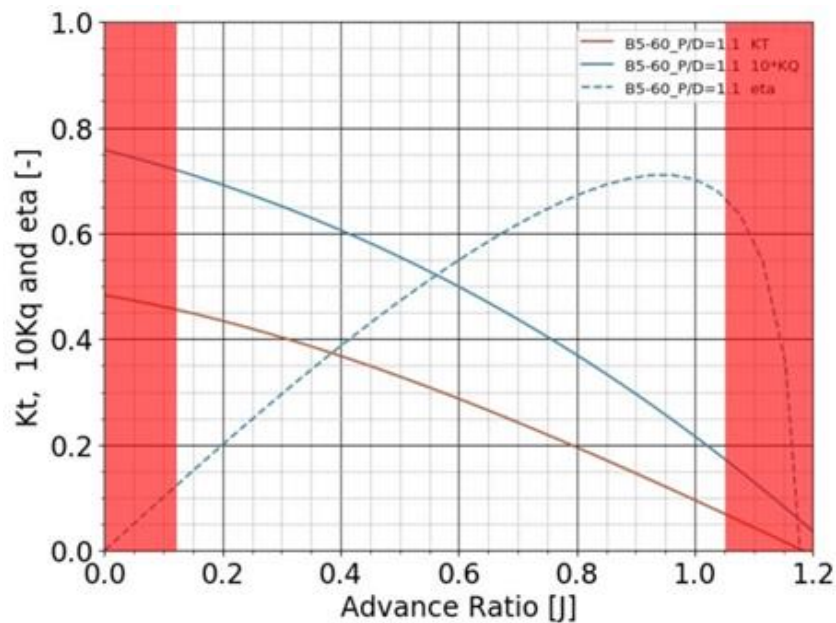
Fig.1: Indication of excluded values of J (in red) in the open-water performance curve for the Wageningen B5-60 propeller with P/D=1.1.

2.2. Design of Experiments (DoE)

The nature of machine learning requires the generation of large amounts of data obtained, in this case, from many similar propellers and operating conditions. The propeller geometries (parametrized as the Wageningen B-Series) and operating conditions must be chosen randomly by what is called the design of experiments (DoE). The DoE was managed using FINE™/Design3D. The CAD files of the propellers were generated using Rhino 3D in combination with Grasshopper, followed by an export as STL using a proprietary tool. As the process needed to be fully automated, the different patches (e.g. leading edge) were identified automatically with this tool if the number of blades was maintained equal. This created a constraint for the creation of the DoE: the design space had to be created for each blade number separately.

The design space for each blade number could therefore be defined by the geometrical parameters *EAR* and *P* (as *D* and *Z* are fixed) and by the operational parameter: the advance ratio *J*. The parametric ranges of the Wageningen B-Series were used for *EAR* and *P* (through the pitch-diameter ratio). The number of blades was varied between 2 and 7. Given the *J* value limits described in Fig.1, the *J* value in the DoE was a normalized range with values between 0 and 1, corresponding to the minimum and maximum of the propeller-specific allowed range, respectively. The normalized values were converted to the actual *J* values when setting up the computations. The Latinized CVT and Inherited LHS (for additional samples) methods were used to sample randomly across the design

space for each blade number. A total of 271 STL files was created, each corresponding to a single propeller operating at a specific advance ratio J.

2.3. Mesh generation

The meshes were generated with OMNIS™/Hexpress using the surface-to-volume (S2V) technique. This methodology ensures superior mesh quality on curved surfaces like propeller blades, but also a more constant viscous layer height enveloping the blades, compared to the more common volume-to-surface approach. Leading and trailing edges as well as the area around the blade tip were more finely discretized compared to the blade surface. This can be seen in the mesh close-ups in Figs.2 and 3.
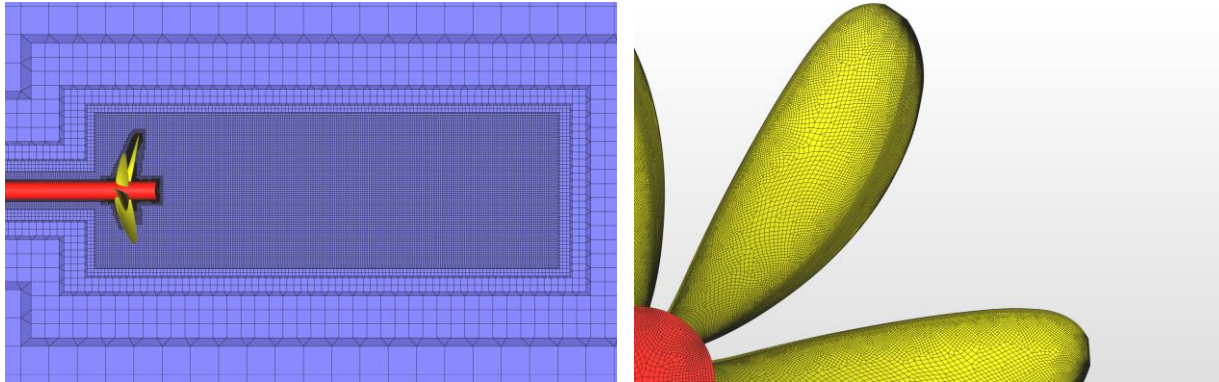
Fig.2: Mesh far field (left) and blade surfaces (right) for Wageningen B7-59 and *P/D*=1.25
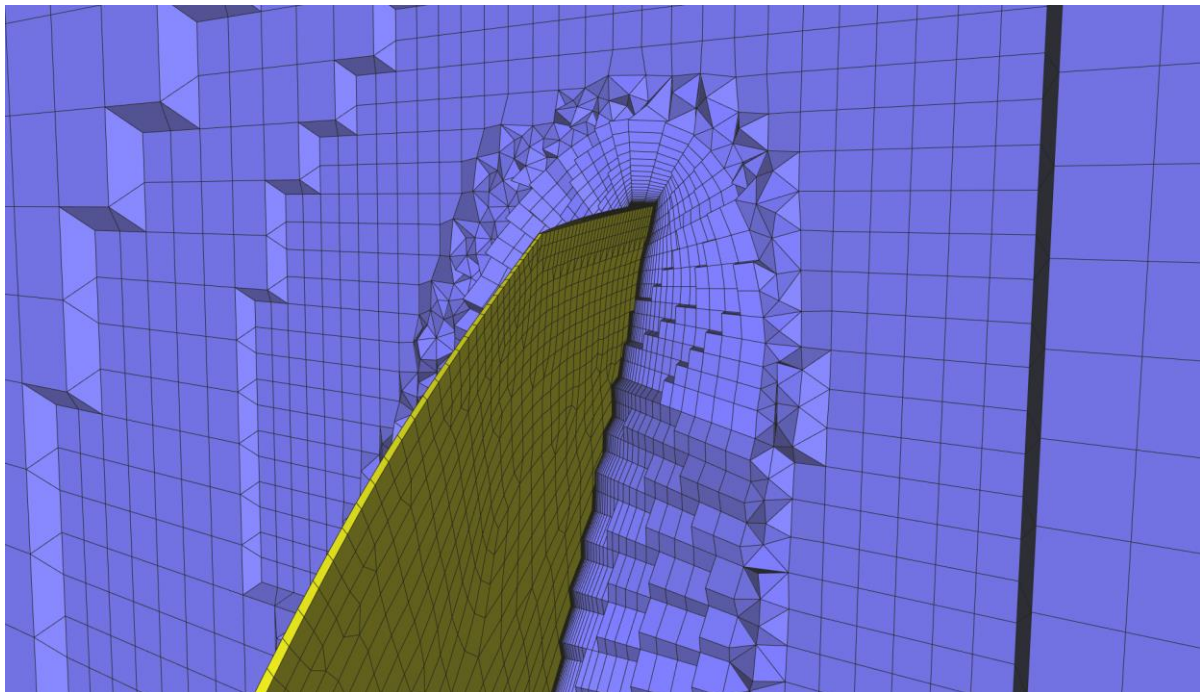
Fig.3: Mesh close-up with viscous layers for Wageningen B7-59 and *P/D*=1.25

Viscous layers were inserted with a first layer thickness defined by $y^+=1$ (and Reynolds number of 2,000,000), Fig.3. Preliminary results were compared between using a y^+ value of 1 and 0.1, but no significant differences were found in the prediction of thrust and torque between both approaches. Given the lower cell count using $y^+=1$, this higher value was used for all meshes. The wake behind the propeller was additionally refined until 4 diameters behind the propeller location to enable an accurate calculation of the flow behind the propeller. The total number of cells for all different propellers ranged from 25 to 35 million cells. The meshing procedure was completely automated with the use of Python.

2.4. Computational details

As the model tests at the basis of the regression curves were performed at Reynolds number of 2,000,000, all computations were set up such that the Reynolds number (based on reference velocity and propeller radius) was kept as close as possible to this value. The reference velocity u_{ref} for propeller was defined as:

$$u_{ref} = \sqrt{u_{x,\infty}^2 + (0.7R\omega)^2},$$ (1)

where $u_{x,\infty}$ is the inflow velocity in the far field in [m/s], R is the propeller radius in [m], and ω is the propeller rotational speed in [rad/s]. Additionally, the advance ratio of the propeller J is defined as:

$$J = {u_{x,\infty}}/{2nR},$$ (2)

where n is the rotational speed in [rps]. n can be converted to ω as $\omega = 2\pi n$.

The goal was to obtain a fixed value of propeller rotation rate n across computations so that only the inflow velocity needed to be varied to simulate different values of J, as the Reynolds number is much more sensitive to changes in the propeller rotation speed than to the inflow velocity (as $\omega^2 \gg u_{x,\infty}^2$) through Eq.(1).

After initially fixing the rotational speed $n = 1.97418$ rps (by fixing ω, see below) and the Reynolds number $Re = 2e6$, the value of $u_{x,\infty}$ could be determined for a target J value using:

$$u_{x,\infty} = J \cdot (2nR)$$ (3)

The value of ω was determined from the definitions of Re and u_{ref} as:

$$\omega = {\nu Re}/{R} \cdot \sqrt{1 \Big/ {R^2 \left(\frac{J_0^2}{\pi^2} + 0.7^2\right)}},$$ (4)

where $J_0 = 0.7$, but this can be set to any realistic value.

The k-ω SST model, *Menter (1994)*, was used as a turbulence model. The model was chosen after comparison with the SSG EARSM model of *Speziale et al. (1991)* and the SST 2003 formulation by *Menter et al. (2003)*, with and without transition modeling (using the γ-model of *Menter et al. (2015)*). The original SST model showed the best agreement with the regression-based predictions. The propeller was accelerated from stand-still in an unsteady simulation and the rotating-frame method (also known as multiple reference frame method) was used to reduce the computational cost. Second-order discretization methods were used for the time, momentum, and turbulence equations. All computations were set up using the C-Wizard and run using FINE™/Marine version 10.1 on a Linux-based HPC cluster using 96 CPU cores (2x Intel Xeon Platinum CLX-9242 48C). As the total number of time steps was fixed and equal for every computation, the total runtime of each computation was between 2 and 3 h (clock time) depending on the mesh density. Only propellers for which thrust convergence was reached within a 1% tolerance of the average were included in the training sets for the neural network. The average was calculated over the last 30% of time steps.

2.5. Machine learning algorithm

For the presented study, a deep learning approach was used, implemented in the form of a geodesic convolutional neural network (GCNN). Such a neural network is trained on a large amount of training

data obtained from CFD computations. The data can be in the form of integral values or field data plotted on two-diemnsional and three-dimensional surfaces. Using a geodesic convolutional neural network is ideal for CFD computations because it does not require equidistant data points in the original data (i.e. CFD output) and accepts surface manifolds as input data. A thorough description of the underlying theory can be found in *Baqué et al. (2018)*.

Of the initial number of 271 computations, 239 yielded converged results based on the previously defined criteria. The computations were subsequently divided into two sets using a 90-10 split; 90% of the computation formed the training set, while 10% of the computations were designated as the validation set to test the model.

Two sets of inputs for the neural network can be distinguished. First, data needs to be provided only for the training data set, consisting of the converged values of the thrust coefficient K_t, torque coefficient K_q and open-water efficiency η (the "integrated quantities") as well as the field quantities. The field quantities consist of the nondimensional axial velocity u'_x in the propeller wake and the pressure coefficient C_p on the propeller blades. Both are defined as:

$$u'_x = {u_x}/{u_{x,\infty}} \quad \text{and} \quad C_p = {p}/{\frac{1}{2}\rho u_{ref}^2} \tag{5}$$

The field quantities were saved as surface CGNS data, while the integrated quantities were saved in comma-separated value files. A support grid needed to be constructed to represent the field quantities for the GCNN.

The second set of data needs to be provided for both the training and the exploitation of the model, and consisted of the STL definition of the blade geometry and the advance ratio *J*. For the research described in this paper, the geometry parameters pitch *P*, number of blades *Z* and the expanded area ratio *EAR* were explicitly provided to the neural network. However, the GCNN can learn straight from the provided STL without this explicit input, which can be exploited in future applications.

The GCNN was trained for approximately 240 thousand iterations, whereby at each iteration, the model is trained on results from a single propeller geometry. This means that the model training enters a new epoch every 239 iterations (i.e. equal to the number of propellers in the training set). The total training time of the neural network is 65 h on a single GPU (Nvidia Tesla V100). Once the model has been trained, it takes roughly 0.3 s to interrogate the model and another 19.7 seconds to represent the data visually. This brings the total to 20 s that are needed to obtain a full performance curve and corresponding velocity and pressure fields for a new propeller geometry.

3. Results

The results for the integrated quantities and field quantities can be discussed using, on the one hand, the R^2-metric and on the other by checking differences between the AI prediction and the CFD result using the L_1-norm. The former relates to an entire set of samples (i.e. the training and the validation set), while the latter can be done on a sample-by-sample basis. The R^2-metric of the training and validation sets is the main indicator for conclusions regarding predictability and generality of the trained model. The R^2- and L_1-norms are defined as:

$$R^2 = 1 - {\Sigma(\phi_{CFD} - \phi_{AI})^2}/{\Sigma(\phi_{CFD} - \overline{\phi_{CFD}})^2} \quad \text{and } L_1 = \phi_{CFD} - \phi_{AI} , \tag{6}$$

where $\overline{\phi_{CFD}}$ indicates the average of all CFD values and ϕ_{CFD} and ϕ_{AI} denote respectively the CFD value and prediction by the GCNN. From Eq.(6) follows that if R^2=1, the predicted result exactly equals the CFD result for the entire set, while if L_1=0, there are no differences for a specific sample between the AI prediction and the CFD result.

3.1. Integrated quantities

The values of R^2 in Fig.3 are very close to 1, indicating very good predictability of the model. The line of the validation set is very close to the line of the training set, indicating that the model generalizes well, i.e. it not only predicts K_t, K_q and η well on already seen data (training set), but also on unseen data (validation set). Table I shows the averaged sample-by-sample error (the difference between the AI prediction and the CFD result) for all three integrated quantities. The averaged error is at most 1.5% for all three quantities, and as such of the same order of magnitude of the modeling error usually accepted in CFD.
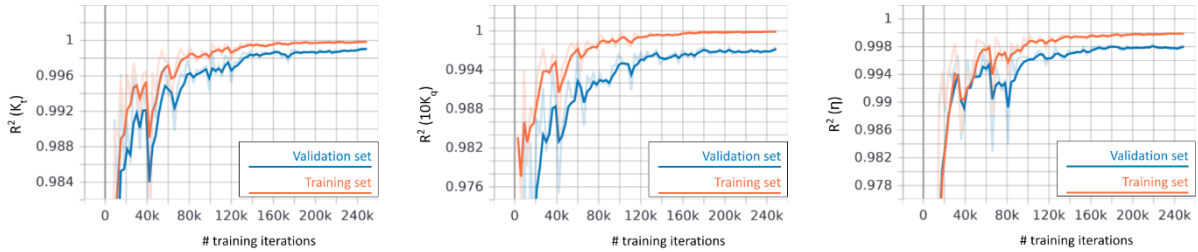
Fig.3: Evolution of R^2 in function of the number of training iterations for K_t, $10K_q$ and η

Table I: Averaged sample-by sample error for integrated quantities

Quantity	Error $\mid\phi\_AI\text{-}\phi\_CFD\mid$
K_t	1.21%
$10K_q$	1.48%
η	1.50%

3.2. Field quantities

The R^2 value for the field quantities u'_x and C_p is slightly lower than for the integrated quantities, as visualized in Fig.4. The R^2 value of the velocity field prediction on the validation set stagnates after the first 80,000 iterations around $R^2 = 0.94$. The value is slightly higher at $R^2 = 0.98$ for the pressure. Given the proximity to $R^2 = 1$ for both quantities and for both sets, it can be concluded that also for the field quantities, the currently trained model generalizes and predicts the solution well. The stagnation of the R^2 value in the case of u'_x indicates that there may be an input-data related issue. This issue is addressed in more detail below.
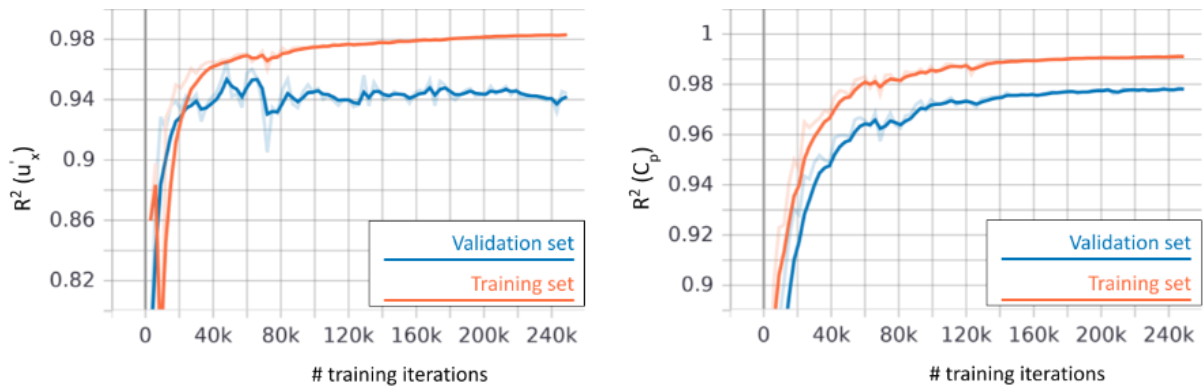
Fig.4: Evolution of R^2 in function of the number of training iterations for u'_x and C_p

Fig.5 shows the best samples for the pressure coefficient of the 7-bladed and 3-bladed Wageningen B-Series propellers that were tested. These were selected from the validation set and represented thus unseen data for the model. While the overall value of L_1 is very low, especially on the blade surfaces, particularly the 7-bladed propeller displays slightly larger differences of around 5-8% between CFD and AI results closer to the tip.
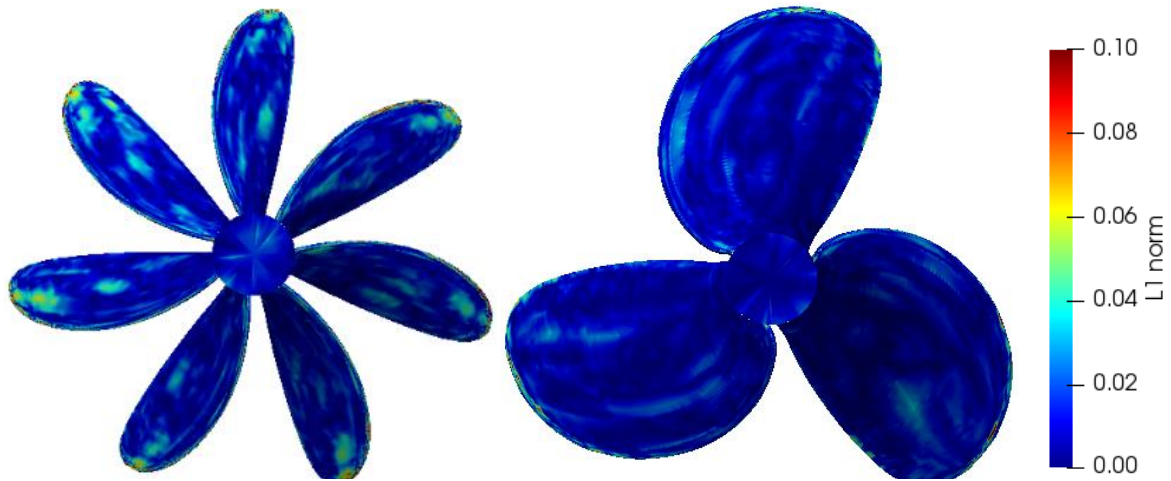
Fig.5: Value of L_1 norm on best samples of 7-bladed and 3-bladed Wageningen B-Series propellers

The plots in Fig.6 comparing the axial velocity field at the different indicated stations A through E also show local differences in the order of a few percent. Results are given for the same 7-bladed propeller as in Fig.5. Differences are largest around the radial location of maximal thrust (i.e. 0.7R). This difference may be due to unsteadiness of the flow field, present for some of the samples. It is probable that this is connected to the stagnating and relatively lower value of the R^2 metric for the u'_x velocity field.
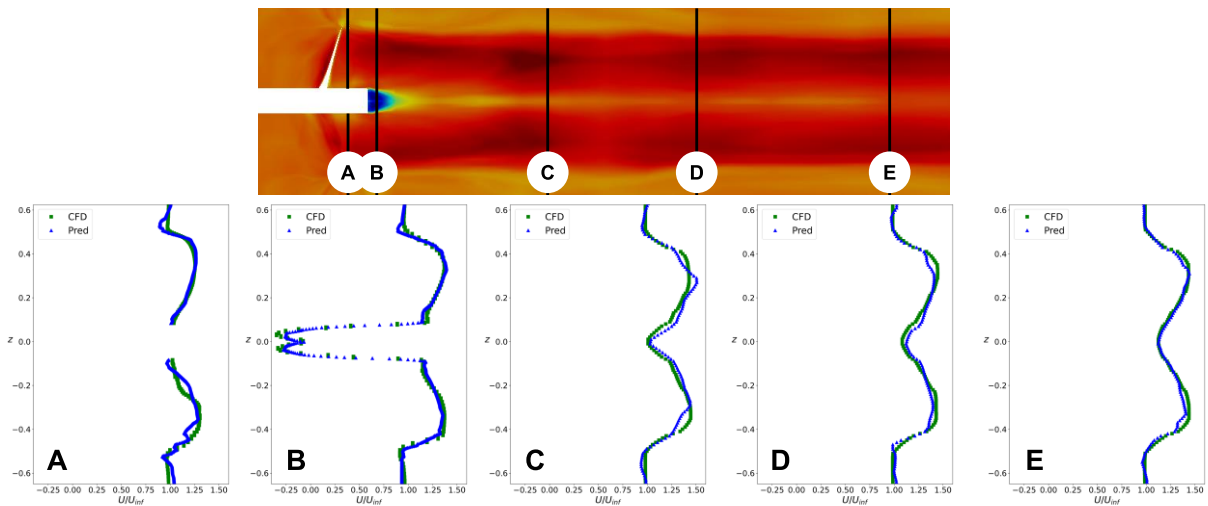
Fig.6: Nondimensional axial velocity field u'_x compared at different stations indicated above
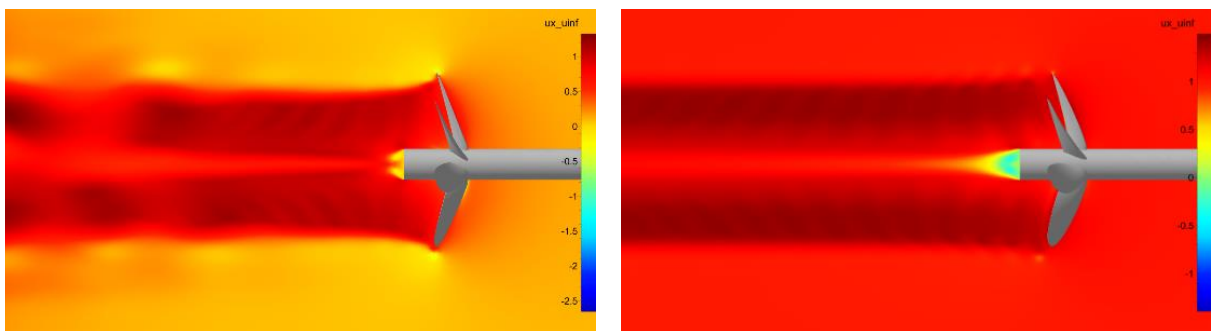
Fig.7: Unsteadiness in wake for low J values (left) compared to expected steady wake result (right)

The earlier mentioned unsteadiness relates to the nature of the input for the machine learning algorithm. Given that the GCNN is trained based on field values, ideally those field values should represent a steady solution. If some of the results are unsteady, this perturbs the training of the

GCNN. Unsteadiness in the wake of the propeller was found for some of the samples used to train the model, see Fig.7. The unsteadiness was found for low values of J and follows from the longer time needed for the flow to stabilize at low inflow speeds. Given that the unsteadiness is linked to the transient solution, the computations should have run approximately twice as long in order to obtain only fully steady fields for all propellers and operating conditions.

4. Conclusion

A working application of machine learning to a marine propeller has been demonstrated, where a geodesic convolutional neural network (GCNN) has been trained to predict both the integral quantities of an open-water performance curve and local field values of velocity and pressure on two-dimensional planes for Wageningen B-Series propellers. The GCNN was trained on 239 samples, of which 90% constituted the training set and the remainder the validation set.

The values of the R^2 metric were almost equal to 1 for the integrated quantities K_t, K_q and η on both training and validation sets, indicating a very good prediction and generalization capability of the trained model for propellers in the Wageningen B-Series regarding integrated quantities. The average difference between the predicted and CFD-obtained value remained below 1.5% for all three integrated quantities. The local field quantities of nondimensional wake velocity u'_x and C_p showed slightly lower R^2 values of respectively 0.94 and 0.98 for the validation set. While capabilities of the model to predict the local flow fields and its generalizability can be qualified as good, improvement is possible.

Unsteadiness in the flow field was identified for several cases with low advance ratios, perturbing the training of the GCNN and reducing the accuracy of the prediction for the u'_x field values. This underlines the importance of careful data selection prior to feeding the data to the GCNN as well as the requirement of understanding the present limitations of neural networks in dealing with unsteady data.

It was shown that when proper care is taken in data selection and computation parameters, machine learning can, in fact, enhance productivity for marine engineers in the initial design process of propellers by orders of magnitude. This is possible due to a drastic reduction in interrogation time from more than 200 CPU-hours per operating point in CFD to 20 s for an entire performance curve using a machine learning approach.

A logical next step is testing the presented concept on resistance and self-propulsion applications.

References

BAQUÉ, P. ; REMELLI, E. ; FLEURET, F. ; FUA, P. (2018), *Geodesic convolutional shape optimization*, 35th Int. Conf. Machine Learning, Stockholm, pp.472-481, https://fleuret.org/papers/baque-et-al-icml2018.pdf

KUIPER, G. (1992), *The Wageningen propeller series*, MARIN, Wageningen, https://www.scribd.com/document/402540817/The-Wageningen-Propeller-Series-G-Kuiper

MENTER, F.R. (1994), *Two-equation eddy-viscosity turbulence models for engineering applications,* AIAA Journal 32(8), pp.1598-1605, https://pdfs.semanticscholar.org/7671/2e2e2063bf33133f10fad4d3ff648b3acd6e.pdf

MENTER, F.R.; KUNTZ, M.; LANGTRY, R. (2003), *Ten years of industrial experience with the SST turbulence model*, Turbulence, Heat and Mass Transfer 4(1), pp.625-632, https://www.researchgate.net/profile/Florian-Menter/publication/228742295_Ten_years_of_industrial_experience_with_the_SST_turbulence_model/links/0046353c6330b1c0a4000000/Ten-years-of-industrial-experience-with-the-SST-turbulence-model.pdf

MENTER, F.R.; SMIRNOV, P.E.; LIU, T.; AVANCHA, R. (2015), *A one-equation local correlation-based transition model*, Flow, Turbulence and Combustion 95(4), pp.583-619

OOSTERVELD, M.W.C.; VAN OOSSANEN, P. (1975), *Further computer-analyzed data of the Wageningen B-screw series*, Int. Shipbuilding Progress 22(251), pp.251-262, http://citeseerx.ist.psu.edu/viewdoc/download?doi=10.1.1.460.2869&rep=rep1&type=pdf

SPEZIALE, C.G.; SARKAR, S.; GATSKI, T.B. (1991), *Modelling the pressure–strain correlation of turbulence: an invariant dynamical systems approach*, J. Fluid Mech. 227, pp.245-272, https://www.researchgate.net/profile/T-Gatski/publication/23820839_Modelling_the_pressure-strain_correlation_of_turbulence_-_An_invariant_dynamical_systems_approach/links/55db599608aed6a199ac5e32/Modelling-the-pressure-strain-correlation-of-turbulence-An-invariant-dynamical-systems-approach.pdf

Effective Digital Training Solutions to Support the Maritime Digital and Decarbonization Transitions

Tracy Plowman, DNV, Hamburg/Germany, tracy.plowman@dnv.com
Ulrich Bernhardt, DNV, Hamburg/Germany, ulrich.bernhardt@dnv.com

Abstract

The paper describes DNV's maritime training department's activities in creating blended training courses to support key strategic developments in maritime digitalization and decarbonizing shipping. The courses combine Virtual Classroom (live online delivery via MS Teams), self-paced e-learning via Rise 360, and libraries of texts and videos from internal and external experts for selective drill-down on topics.

1. Introduction

1.1. General trend towards digital training accelerated by COVID-19

Teaching environments and techniques have always evolved in time, *Bertram and Plowman (2017),* but this evolution has been particularly accelerated with the COVID-19 pandemic, *Plowman and Bertram (2020),* Fig.1. Whether we liked it or not, we had to embrace digital, remote forms of training rapidly, both in academia and in industry.

The first response to the lock-down of physical classrooms was employing ad-hoc measures such as presenting PowerPoint lectures in videoconferences. But at the same time, a more fundamental re-engineering of our training portfolio started, which evolved to the current status of how we do training and how we develop it, *Bernhardt and Plowman (2020),* looking both at training effectiveness and efficiency of the development process. In hindsight, the COVID-19 disruption turned into an opportunity to redesign and modernize our training portfolio for more agile and cost-effective delivery modes.
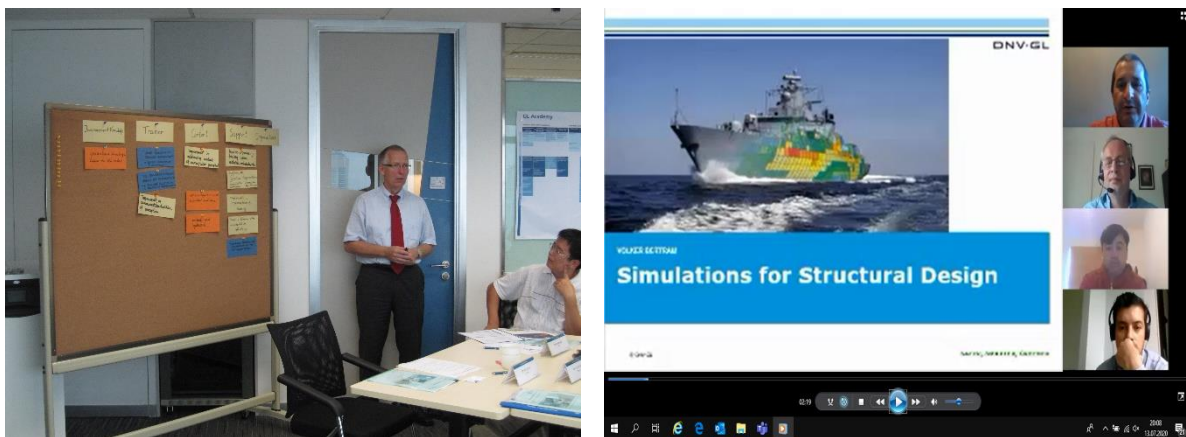
Fig.1: From traditional classroom (left) to ad-hoc video conference training (right)

1.2. Key vehicles to implement digital training at DNV

Digital training has a lot more options or tools than 'clickety-di-click' e-learning, ranging from plain pdf files to Virtual Reality based training, Fig.2. We considered most of them in the course of our work, even wrote a hitchhiker's guide for our community, *Bertram and Plowman (2019).* In view of both required development effort and training effect, Fig.3, live online training via videoconferencing and self-paced e-learning evolved as the 'standard' options for our training courses. Most of courses now employ a blend of these two key options.
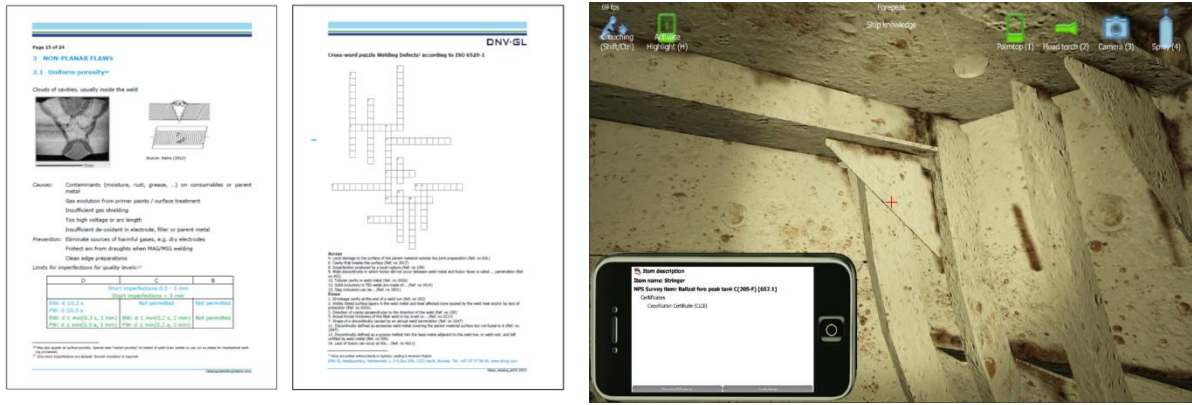
Fig.2: Digital training options range from plain pdf files to Virtual Reality based training
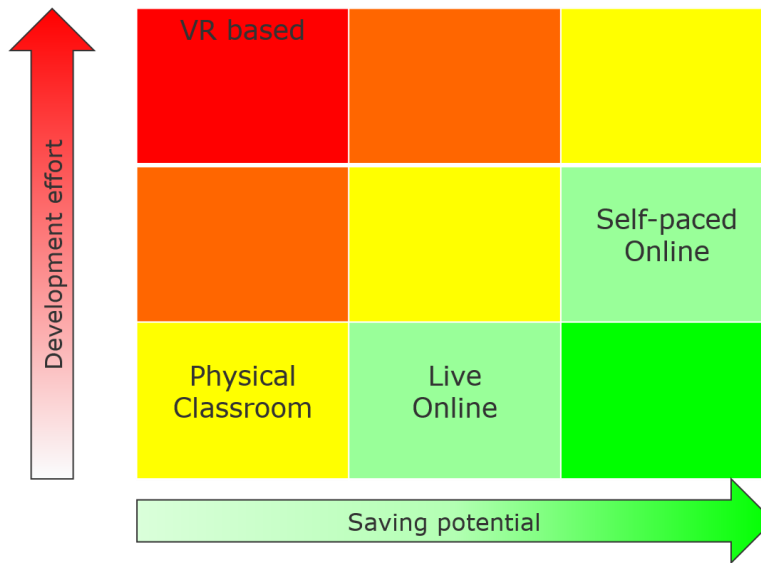
Fig.3: Live online training and self-paced e-learning were the natural standard options for us

Software solutions for developing self-paced online training had been improved as well since DNV started with digital training development. During the COVID-19 pandemic, the move from Articulate's Storyline, https://articulate.com/360/storyline, to Rise, https://articulate.com/360/rise, brought down development times and costs significantly, while at the same time improving trainee satisfaction with the "look and feel" of the training products.

We use self-paced online training based on Rise predominantly for the following applications:

- resource libraries with reading material (pdf files or hyperlinks), Fig.4, and videos, often referencing to publicly available sources, such as IMO websites
- assessment, mainly in the form of multiple-choice tests, Fig.5, for self-assessment as well as formal assessment for compliance purposes
- secondary topics, such as fringe applications or historical background knowledge

We use live online training for the following purposes:

- Kick-off and closure of trainings
- Question & Answer sessions
- Short group activities
- Material that needs live commentary of trainers and is most likely to spark interactivity such as questions from trainees with fast response from trainer
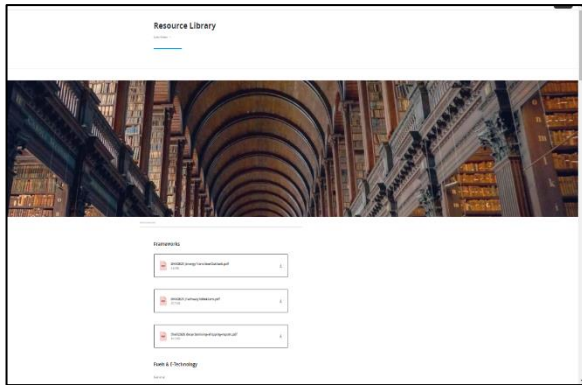
Fig.4: Typical library function for pdf files
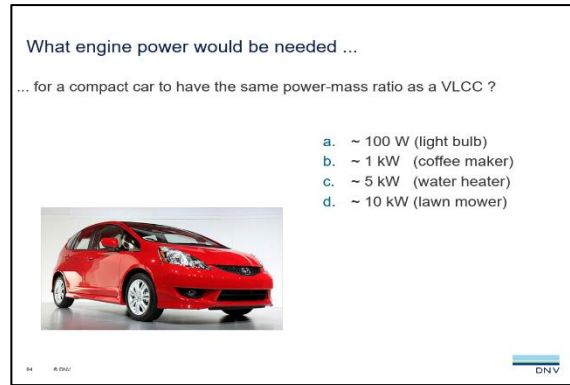
Fig.5: Typical multiple-choice assessment

The first task in (re-)designing a training to digital formats is generally a critical review of the content, identifying

- reference material which cannot be memorized during the training and will be used later for reference, such as extensive tables, lists, complex diagrams, detailed rules, etc. This material is best made available for future reference in the form of pdf files ('lecture notes', check lists, etc.) or hyperlinks).
- background and specialized information which is not of prime focus and typically only of interest for a subset of the audience. This material is best offered as information on demand, e.g. in the form of self-paced, mainly text-based e-learning or video lectures.

Such 'decluttering' of content material allows focussing on the core material of the training. In blended learning, this core material is typically presented live by a trainer, while reference and background/ specialized material is accessed on demand. This reduces fatigue both for trainers and audience.

1.2.1. Virtual classroom (VC) via videoconferencing

In the training community, we refer to live online training via videoconferencing as "Virtual Classroom", Fig.1 (right). As with classroom trainings, there are good Virtual Classroom trainings and bad ones. Bad ones are of the format "you look at PowerPoint slides while the expert drones on". Participants often zone out, doing other things like checking their emails, passively absorbing the audio and tuning back into the training occasionally. The good ones are relatively focused on what the audience really needs to know with clear take-home messages and strong user interaction.

Presentation material should be

- strongly visual, reducing text to a few keywords, Fig.6. The keywords serve as a reminder for the trainer, but do not distract from his narrative. For the live online part, the trainer should be the key focus of attention; the slides should be visual aids to support this narrative, not substitute it. Otherwise, the content could just be given as reading material.
- contain relatively frequent interactive elements, e.g. asking questions to participants instead of stating facts to them ("What do you estimate to be…" or "Who of you has already used…"), Fig.7. The interactive elements stimulate the audience to refocus on the topic, reducing the temptation to multi-task (e.g. read incoming emails).

Generally, Virtual Classroom training is more tiring than traditional classroom training, possibly due to reduced audio and visual resolution. To address this issue, we generally limit online face-to-face time in Virtual Classrooms to half days. Shorter face-to-face time, interspersed with breaks and interactive elements, helps with audience concentration, allows coping with large differences in time zones (e.g. Germany and Singapore), and helps also with ensuring focus on training as half a day is available for urgent tasks of daily business.
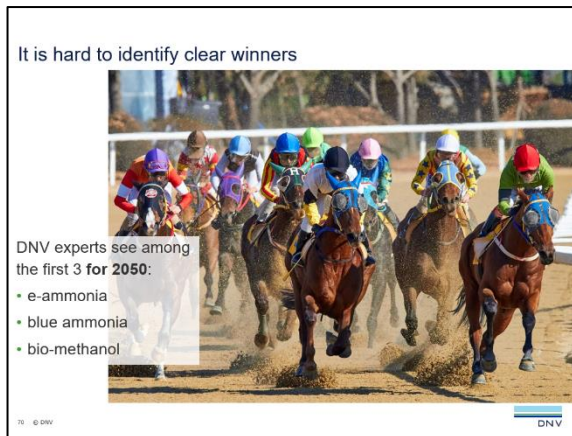
Fig.6: Typical slide with minimum text

Fig.7: Dedicated audience involvement

1.2.2. Self-paced e-learning

E-learning is just one of our tools, albeit a powerful and useful one if properly employed. A key risk with any self-paced learning is that the audience does not study. And self-paced learning generally has less impact than classroom training where individual feedback is possible and where the audience generally has a higher attention rate.
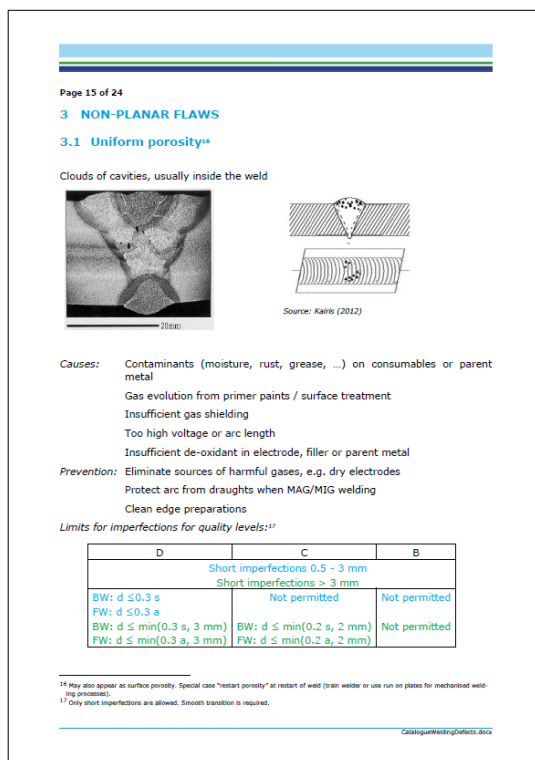
Fig.8: reference knowledge in pdf lecture notes
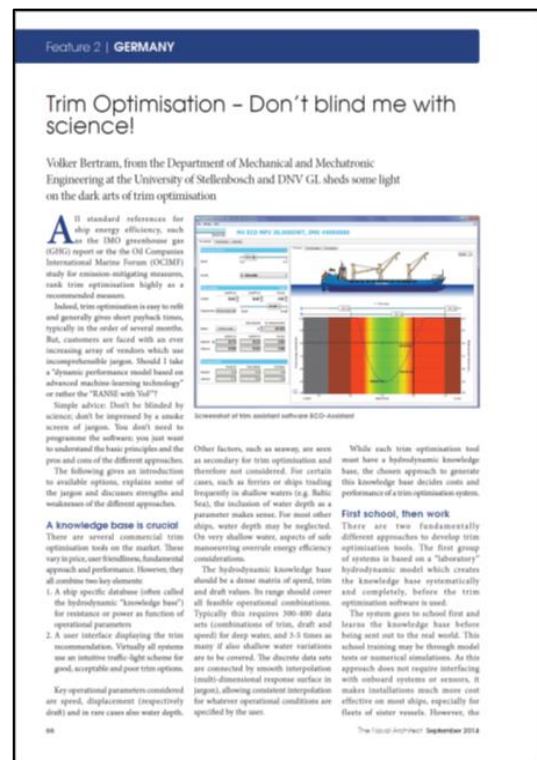
Fig.9: Drill-down referenced publications

E-learning courses employ a wide range of training elements to avoid fatigue:

- text, directly in the e-learning or attached as pdf files (for lecture notes, Fig.8, further recommended reading, Fig.9, reference material, case study instructions, etc.)
- images,
- videos, ranging from small add-on videos embedded in a flow of the training's storyline to longer recorded presentations kept in video libraries

46

- Hyperlinks (to text or videos, e.g. Wikipedia or YouTube),
- interactive elements (click, drag-and drop, mouse-over pop-ups, etc.),
- assessments (usually in the form of multiple-choice quiz),
- …

In principle, all good advice for designing PowerPoint presentations for classroom training also applies to designing e-learnings. The typical e-learning feature of supplying information on demand allows de-cluttering slides with faster progress for those who don't need higher information detail.

2. Decarbonizing and Digitalization courses

2.1. Guiding principles

Our strategy at DNV has been focussing on two key areas, namely digitalization and decarbonization, https://annualreport.dnv.com/2018/research-innovation: "DNV […] continues to invest 5% of its revenues in strategic research, technology development and innovation efforts. Digitalization and decarbonization are the two megatrends defining this era of speed and complexity. Together, they are driving a relentless quest for efficiencies, and that in turn creates a growing need to ensure that efficiency gains do not compromise safety." Training is an important flanking measure in supporting these megatrends both within our company and for our customers. Consequently, corresponding blended training courses have been developed since late 2020. These are described in subchapters 2.2. and 2.3.

The guiding principle was to have 'edutaining', brain-friendly training material, that used a variety of media and training techniques to avoid fatigue for both trainers and audience. The courses were designed to address a broad, heterogeneous audience without specific prerequisites for technical or engineering competence. The courses were to offer value and be accessible for everyone in the hierarchy, (almost) "from cleaning woman to CEO".

2.2. Understanding Digital Transformation

"Digital transformation" or "digitalization" have become very popular marketing terms or buzzwords in the maritime world. We perceived a wide-spread need in the industry (including our own company) to come to terms with the "digital new-age" jargon, focusing on the capabilities, but even more so limits of the key technologies, including Artificial Intelligence, Virtual & Augmented Reality, Digital Twins, and Autonomous Ships.

Fig.13: Slide in Virtual Classroom
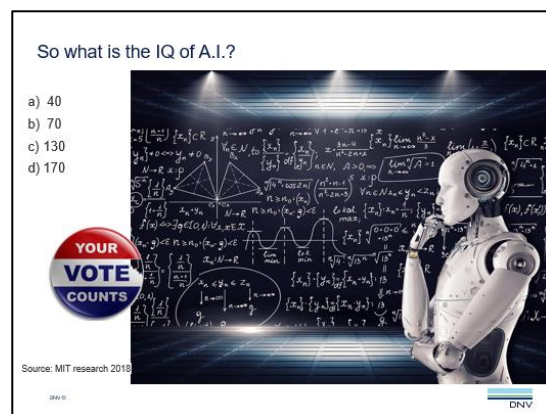
Fig.14: Poll in Virtual Classroom

The answer was developing a blended course, with 2 half-days of Virtual Classroom, Figs.13 and 14, and approximately a day's worth of four e-learning modules plus a library of pdf reading material and videos, Fig.15, where colleagues from DNV and external experts offered drill-down lectures on selected

topics, e.g. hull optimization using high-fidelity Digital Twins in High-Performance Computing, Fig.16. Appendix 1 lists the drill-down lecture videos as to date.
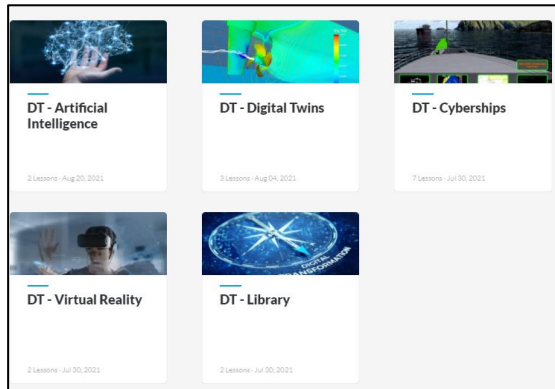
Fig.15: Menu of e-learning modules incl. library
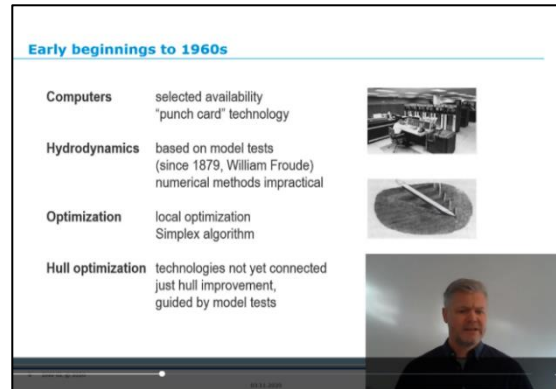
Fig.16: Guest lecture video from library

2.3. Decarbonizing Shipping

With the IMO 2030 and 2050 targets for CO_2 reduction, and rising fuel prices in the wake of the 2020 Global sulphur cap, decarbonization is at the top of the agenda also for shipping worldwide. The short-term focus in decarbonization lies on energy efficiency. Technologies for no/low carbon fuels will require longer for adoption, both for technology and business reasons. However, many of the required long-term developments have already started. Decarbonization is a megatrend that affects DNV on many levels and in many business segments. Both internally and externally, we perceived a demand for an introductory course giving a basic understanding of the issue, the possible (and realistic) pathways and the key terminology.
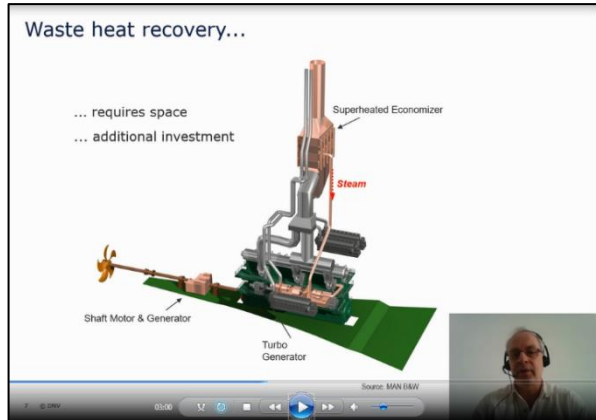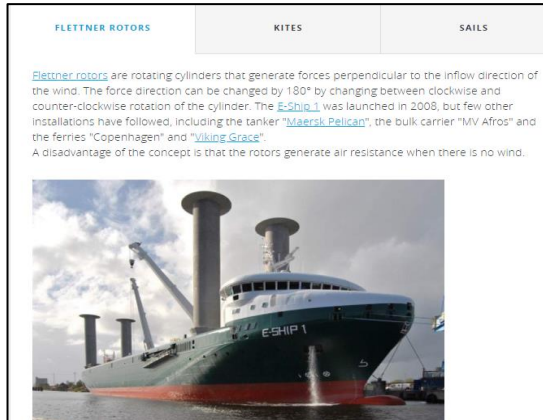
Fig.17: Parts of e-learning; material presented (left) and recorded video (right)
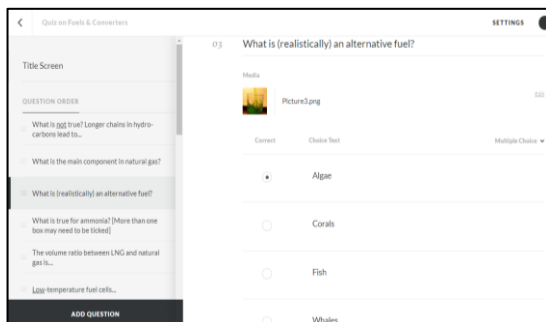
Fig.18: Quiz question in e-learning

Fig.16: Guest lecture video from library

The answer was again developing a blended course, with 2 half-days of Virtual Classroom and approximately a day's worth of e-learning modules plus text and video libraries for selective drill-down. Figs.17-19 show typical components of the e-learning material: reading material, Fig.17 (left), embedded short video, Fig.17 (right), assessment quiz, Fig.19, and guest lecture from an external expert (Diego M. Yebra of Hempel), Fig.19. Appendix 2 lists the drill-down lecture videos as to date.

3. Conclusion

Digitalization is not a goal, it is a process, also in training applications. We learn along the way and adapt, improving continuously our solutions. Over the past two or three years, we have learnt some lessons and we keep learning. Focussing on key elements and doing them well is one of those lessons for successful digital training development.

Using the experience of accelerated evolution during COVID-19, we developed two key courses to flank strategic developments in our industry and in our company. The development of the first prototypes took only three months, using a lean developer team and decluttering the course material before starting with the material development. However, it lies the nature of both courses that they need continuous updating as the topics evolve rapidly in time, as reflected for example in the COMPIT conference, www.compit.info, and the HIPER conference, www.hiper-conf.info.

The basic format has worked very successfully, based on the audience feedback from some 10 deliveries for each course. The key to success is the same as for traditional training: Make it relevant, make it short, make it fun.

Acknowledgements

References

BERTRAM, V.; PLOWMAN, T. (2017), *Maritime Training in the 21st Century*, 16th COMPIT Conf., Cardiff, pp.8-17, http://data.hiper-conf.info/compit2017_cardiff.pdf

BERTRAM, V.; PLOWMAN, T. (2019), *A Hitchhiker's Guide to the Galaxy of Maritime e-Learning*, 18th COMPIT Conf., Tullamore, pp.7-23, http://data.hiper-conf.info/compit2019_tullamore.pdf

PLOWMAN, T.; BERTRAM, V. (2020), *Digital Maritime Training in COVID-19 Times*, 19th COMPIT Conf., Pontignano, pp.304-315, http://data.hiper-conf.info/compit2020_pontignano.pdf

PLOWMAN, T.; BERNHARDT, U. (2022), *Digital Transformation in Maritime Trainings in COVID-19 Times,* 21st COMPIT Conf., Pontignano, pp.16-23, http://data.hiper-conf.info/compit2022_pontignano.pdf

Appendix 1: Video library for Understanding Digital Transformation

The video library is being continuously extended. The entries given below reflect the status in March 2022.

Presenter	Company	Title
Videos for **Module 1 – AI**		
Emilio Campana	CNR	*New IT Technologies for a Sustainable Blue Growth*
Rodrigo Perez	Sener	*The Impact of A.I. in Shipbuilding*
Pierre Sames	DNV	*Developing and Assuring new A.I. Solutions*
Qian Wei	DNV	*An AI-Powered Corrosion Detection Solution*
Videos for **Module 2 – Cyberships**		
Marco Bibuli	CNR	*Smart & Cooperative Marine Robotics*
Robert Hekkenberg	TU Delft	*Rationalising Autonomous Ships*
Jialun Liu	WUT	*Virtual-Real Interaction Testing for Intelligent Ships*
Steinar Laag	DNV	*Ship Connectivity*
Videos for **Module 3 – Digital Twin**		
Stefan Harries	FS Systems	*Simulation-Driven Design*
Karsten Hochkirch	DNV	*Short History of Ship Hull Optimization*
Herbert Koelman	SARC	*Don't let me be misunderstood*
Videos for **Module 4 – Virtual Reality**		
Jose J. Garcia Agis	Ulstein	*The Potential of VR in Conceptual Ship Design*
David Thomson	AVEVA	*Marine Digital Twins in XR*

Appendix 2: Video library for Decarbonizing Shipping

The video library is being continuously extended. The entries given below reflect the status in March 2022.

Presenter	Company	Title	
Videos for Module 1 – Frameworks			
Knut Ørbeck-Nilssen	DNV	*Tackling Global Transformations*	
Volker Bertram	DNV	*Energy Efficiency Options - Fairy Tales?*	
Videos for Module 2 – Fuels & Converters			
Kjeld Aabo	MAN	*Two-stroke dual-fuel engines and transition from LNG to other cleaner fuels as Ammonia*	
Monica Alvarez	DNV	*Hydrogen-fuelled ships – Regulatory framework and challenges*	
Hendrik Brinks	DNV	*Ammonia as a marine fuel*	
Tore Longva	DNV	*Maritime Forecast [on fuels] 2050*	
Per C. Lund	Innovation Norway	*Norwegian Government's Hydrogen Strategy*	
Pierre Sames	DNV	*Ammonia as Ship Fuel*	
Tomas Tronstad	Hyon	*Industrialization of hydrogen as a fuel for maritime*	
Alca Yalcin	Methanex	*Experience with Methanol as a Fuel*	
Videos for Module 3 – Fuel Saving Options in Design & Retrofit			
Stefan Harries	Friendship Systems	*Simulation-driven design*	
Stefan Harries	Friendship Systems	*Quick Guide to Geometric Modeling of Ships*	
Karsten Hochkirch	DNV	*Short History of Ship Hull Optimization*	
Guus van der Bles	eConowind	*WASP Enabling Zero Emission Shipping*	
Hasso Hoffmeister	DNV	*Wind-assisted propulsion systems*	
Heikki Hansen	DNV	*WAPS as key to Ultra Energy Efficient Ships*	
Maxime Garenaux	MARIN	*Numerical Analysis of Flettner Rotors Performances on the MARIN Hybrid Transition Coaster*	
Videos for Module 4 – Fuel Saving Options in Operation			
Ulf Siwe	Swed. Mar. Adm.	*Information Fuel Saving Tool*	
Andre Kauffeldt	DNV	*Trim optimization for improved energy efficiency*	
Nils Hagemeister	Fraunhofer	*Performance Prediction and Weather Routing of Wind Assisted Ships*	
Volker Bertram	DNV	*Options for the Post-Biocide Era of Antifouling*	
Diego M. Yebra	Hempel	*Low Friction Hulls and Propellers*	
Simon Doran	HullWiper	*A Short History of Hull Cleaning and What's Next*	

Aeolus Bag - Consequences of Device-specific Wind Selection on the EEDI Contribution of WASP Devices

Francesco Stella, Computed Wing Sail, Paris/France, francesco.stella@computedwingsail.com
Julien Morel, Computed Wing Sail, Paris/France, julien.morel@computedwingsail.com

Abstract

This paper highlights important drawbacks of the recently adopted MEPC.1-Circ.896(77) EEDI Guidelines for Wind Assisted Ship Propulsion (WASP) devices. The new, device-specific selection of wind conditions allows to improve EEDI performance of WASP devices, but it appears to be based on unrealistic representations of global winds. New EEDI scores seem to be skewed in favour of some WASP technologies, and not commensurate to expected, real fuel savings delivered by wind propulsion. This can favour the development of WASP devices that offer great EEDI improvements based on the regulatory selection of favourable winds, rather than on real fuel savings.

1. Introduction

The Marine Environment Protection Committee (MEPC) of the International Maritime Organization (IMO) has recently adopted circular *MEPC.1-Circ.896(77)* (also referred to as 2021 Guidelines in what follows). This circular contains a review of the Guidelines for calculating the contribution of innovative fuel efficiency technologies to the Energy Efficiency Design Index (EEDI). Among approved changes, this paper focuses on those concerning Wind Assisted Ship Propulsion (WASP) devices, which are among the most promising fuel efficiency technologies available on the market. The 2021 Guidelines improve the EEDI contribution of all WASP devices, by allowing to compute it on a selection of device-specific, best performing wind conditions, among those defined in the IMO Global Wind Standard (see *MEPC 62/INF34*). This new method, however, seems questionable. For instance, selecting winds based on device performance is likely to have paradoxical effects on the representation of global winds, that remind those of the magic bag gifted by Aeolus to Ulysses. As Aeolus bag trapped all winds but those favourable to a safe passage to the Homeric hero's homeland of Ithaca, the 2021 Guidelines simply suppress all wind conditions that are less favourable to one device, and this at a global level! Weather routing is sometimes invoked to justify such an extensive modification of global winds, but the existence of a commercially sustainable weather routing strategy allowing to achieve such radical wind selection should be demonstrated. More importantly, gains relative to the previous version of the Guidelines (*MEPC.1-Circ.815(65)* also referred to as Legacy Guidelines hereafter) appear not to be homogeneous across the market. Indeed, it is quite intuitive that the relative bonus awarded by wind selection becomes higher as the contribution of the neglected wind conditions gets worse. In addition, devices designed to maximize their availability (i.e., as to produce useful thrust in a maximum of different wind condition) lose their competitive advantage over other devices, for example those designed to maximize their peak thrust on a subset of available winds, due to the fixed fraction of wind conditions that is now taken into account. These biases induced by device-specific wind selection might skew the competition between WASP technologies, at least as far as EEDI/EEXI requirements are concerned. They might also open a backdoor for EEDI/EEXI optimization strategies based on devices that are designed as to maximize their EEDI scores via a wise selection of winds, rather than via real CO_2 savings.

In the light of these considerations, this paper aims at rising awareness on the drawbacks of the 2021 EEDI Guidelines for WASP devices, by means of very simple arguments and visualizations.

2. Background

For further reference, this section introduces the EEDI/EEXI and the IMO Global Wind Standard.

2.1. The Energy Efficiency Design Index

The EEDI (for newbuilds, EEXI for existing ships) is one of the ship performance indices adopted by the 72nd MEPC Meeting (MEPC 72, April 2018), as part of the Initial Strategy for the Reduction of Green House Gasses (GHGs) from international shipping (*MEPC.304(72)*). The EEDI/EEXI assesses CO2 emissions of a vessel per unit transport work (measured in [gCO2/T/NM]) based on its design (main particulars, resistance curve) and on the layout of its powerplant, according to the following formulation:

$$\frac{\left(\prod_{j=1}^{n} f_j\right)\left(\sum_{i=1}^{nME} P_{ME(i)} \cdot C_{FME(i)} \cdot SFC_{ME(i)}\right) + \left(P_{AE} \cdot C_{FAE} \cdot SFC_{AE}*\right) + \left(\left(\prod_{j=1}^{n} f_j \cdot \sum_{i=1}^{nPTI} P_{PTI(i)} - \sum_{i=1}^{neff} f_{eff(i)} \cdot P_{AEeff(i)}\right) C_{FAE} \cdot SFC_{AE}\right) - \left(\sum_{i=1}^{neff} f_{eff(i)} \cdot P_{eff(i)} \cdot C_{FME} \cdot SFC_{ME}**\right)}{f_i \cdot f_c \cdot f_l \cdot Capacity \cdot f_w \cdot V_{ref} \cdot f_m}$$

The reader is referred to *MEPC.308(73)* for a thorough discussion of each term of the above expression. The EEDI/EEXI is used to define emission reduction trajectories, tuned as to contribute to cut CO2 emissions of international shipping by at least 70%, relative to 2008, by 2050 (*MEPC.304(72)*). Such trajectories prescribe increasingly stringent EEDI thresholds, relative to baseline emission levels of the 2008 fleets of different ship types (see *MEPC.328(76)*). Newbuilds are required to achieve a EEDI score lower than a threshold, which is periodically reduced. For example, a 100000 DWT bulk carrier has a EEDI historical baseline of 3.96 gCO2/T/NM. A newbuild will have to attain a EEDI score of 3.17 gCO2/T/NM (a 20% reduction with respect to 2008) if its construction is launched before Jan 1st 2025, but of 2.77 gCO2/T/NM (a 30% reduction) if launched afterwards. Existing ships must comply with similar EEXI constraints, on a comparable time frame. Unlike other CO2 emission regulatory tools, the EEDI/EEXI regulation is now fully enforced. Compliance is verified by the administrative authorities (or, more commonly, by delegate organizations such as Class Societies) before the vessel is put into service, and/or reviewed in case of major conversion of the ship. Year-to-year operations (e.g., bunker consumption and total distance travelled, as reported by the IMO Data Collection System, see *MEPC.336(76)*)) do not change the EEDI/EEXI score of a vessel.

A sizeable reduction of the EEDI/EEXI score is one of the selling arguments of all providers of WASP technologies, in particular for the retrofit market. In the above expression, power (and hence CO2) savings delivered by WASP devices are taken into account by the term $f_{eff} P_{eff}$, which is more generally dedicated to innovative energy efficiency devices. In broad strokes, $f_{eff} P_{eff}$ is the product of the power produced by the WASP device (P_{eff}), with its availability factor f_{eff}, that is the fraction of time during which the device can actually deliver its power output. In the case of WASP technologies, f_{eff} should reflect the intermittent nature of wind, in a way that guarantees fairness of treatment among devices that exploit wind according to very different strategies. In addition, since the EEDI/EEXI is fixed for one ship and does not contain any reference to operations and specific trades, the definition of f_{eff} must necessarily be at a global level. Up until adoption of the 2021 Guidelines, the Legacy Guidelines within *MEPC.1-Circ.815(65)* fulfilled all these requirements by adopting the IMO Global Wind Standard, which is introduced in the following paragraph.

2.2. The IMO Global Wind Standard

The IMO Global Wind Standard is defined in *MEPC 62/INF34*. It describes the probability of encountering a set of wind conditions, based on an extensive survey of winds encountered on the main world trades (see Fig.1.a). Probability is expressed as a matrix, in function of the speed of wind with respect to the ground (True Wind Speed or TWS), considered at 10 m above mean sea level; and in function of the origin of wind with respect to the bow of the ship (True Wind Angle or TWA). Encountered winds are distributed on 25 bins of TWS of width 1m/s, and 72 bins of TWA of width 5°. Fig.1.b reports the usual representation of the IMO Standard, as found in most MEPC Resolutions dealing with WASP.
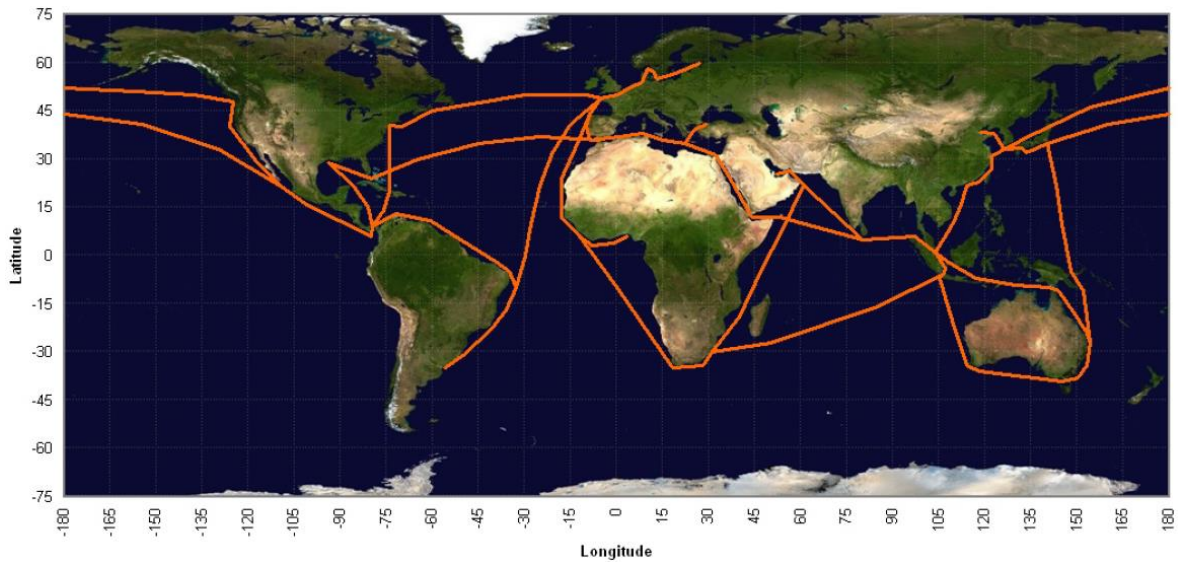
Fig.1.a: Map of surveyed world routes on which the IMO Global Wind Standard is defined, as reported in *MEPC 62/INF34*
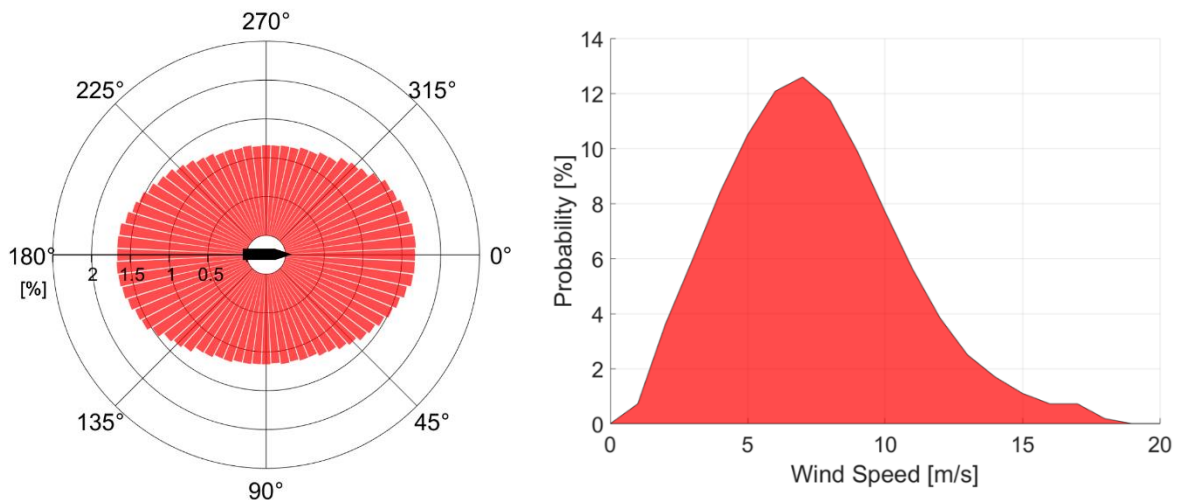
Fig.1.b: The IMO Global Wind Standard. The wind probability distribution is represented in function of TWA (left) and TWS (right)

Although a practical tool to compute EEDI/EEXI, the IMO Standard is not immune to criticism. In particular, trades included in the IMO Standard were picked based on the high frequency they are travelled on, rather than based on the quality of their wind resource (think, for example, to the Suez Canal route in Fig.1.a). As so, the IMO Standard probability matrix was fed with wind resources that are not as favourable to wind propulsion as those on which WASP is likely to be deployed first, such as routes that are exposed to trade winds. Then, the IMO Standard is probably skewed towards low values of TWS and unfavorable TWAs (head and tail winds), with respect to a hypothetical wind probability distribution better tuned on WASP needs. This led to the commonly held view that the IMO Standard provides a conservative estimation of WASP availability. Crucially, a low estimation of availability hinders the potential of WASP with respect to other fuel efficiency technologies, whose availability only depends on factors that the crew can control. In this respect, some contributions have been presented that show that EEDI/EEXI, as defined by the Legacy Guidelines, gives conservative predictions of WASP power that is available on specific routes. For instance, *MEPC.74/INF39* compared EEDI predictions obtained with the IMO Global Wind Standard to estimations of available effective power obtained with the wind resource on a Middle East-Far East route, for a VLCC with two rigid wingsails. It was found that the rigid wingsails provided a 16% improvement of the EEDI score of the vessel when on-route winds were used, but only 1.6% when assessed on the IMO Standard. More

54

recently, contribution *MEPC.77-6-6*, reported predictions at design stage as well as first operational feedback from SC Connector, a Ro-Ro travelling on a North Sea route, which was retrofitted with 2 rotors of height 35 m and diameter 5 m. According to *MEPC.77-6-6*, both design prediction and operational feedback suggest that available power as computed on the IMO Standard greatly underpredicts the on-route yield of the rotors. To a large extent, these reported underestimated savings are just perceived ones, since they are based on questionable comparisons between the IMO Global Standard with the wind resource of specific (and sometimes notoriously favourable) routes. Nevertheless, *MEPC.77-6-6* proposed a new method for computing the EEDI contribution of WASP devices, based on selecting a favourable subset of winds within the IMO Standard. Such proposition was accepted during MEPC 77, and integrated in the 2021 Guidelines. Each device is now allowed to present EEDI contributions computed on those IMO Standard wind conditions that are most favorable to its performances, provided that selected winds account for a cumulative IMO Standard probability of 0.5 (although 0.3 was initially put forward, for an even more aggressive wind selection).

Since wind selection is device-specific, in the next chapter we will introduce models of the Flettner rotor and of the CWS wingsail, which will help us investigating the consequences of this new approach. We stress that we are not interested in providing a benchmark of these two devices in themselves. We will rather consider them as representatives of different families of WASP technologies, active and passive WASP devices respectively, and try to comparatively understand how wind selection affect regulatory performance of these two families of devices.

3. Modelling WASP devices

In this work, we will always consider a wind power plant composed of a single device. We disregard any influence of the interaction of apparent wind with the ship, which is not a specific vessel. The root chord of the device is placed at 25 m above mean sea level. According to *MEPC.1-Circ.896(77)* and ITTC recommendations within, the atmospheric boundary layer is modeled as follows:

$$TWS_z = TWS_{10m}\left(\frac{z}{10}\right)^{1/9}$$

where TWS_z is the true wind speed at height z, and TWS_{10m} is the reference true wind speed at 10 m above mean sea level, as defined in the IMO Global Wind Standard. For simplicity, a single sample point approach is adopted: wind speed is considered at the heigh of the center of effort (coe), which for both devices is roughly placed at mid-span. Apparent Wind Speed (AWS) and Apparent Wind Angle (AWA) are computed at the same height, as the vector sum of TWS_{coe} and of ship reference velocity (V_{ref}). For any condition ($SV,\ TWS_{coe}, TWA_{coe}$), thrust is given by the following general relationship:

$$F(V_{ref}) = 0.5\rho AWS_{coe}^2 S(C_L \sin AWA_{coe} - C_D \cos AWA_{coe})$$

where S is the reference surface of the device and C_L and C_D are its 3D lift and 3D drag coefficients, respectively. In the framework set by the 2021 Guidelines, side forces are neglected. Specifics on modeling of the Flettner rotor and of the wingsail are provided in the following paragraphs.

3.1. Active device: Flettner rotor

The Flettner rotor is a rotating cylinder, which produces high lift coefficients by exploiting the Magnus effect, *Van der Kolk et al. (2019)*. Lift and drag developed by the Flettner rotor are determined by its spin ratio, defined as:

$$V_R = U_{tan}/AWS$$

In this expression, $U_{tan} = \Omega D/2$ is the tangential velocity on the surface of the rotor, D its diameter and Ω is its rotation rate. In this study, we consider a rotor having D = 5 m and height H = 35 m, as the one described in *MEPC77-6-6*. Lift and drag polars, relative to V_R, are obtained from available literature

(see *De Marco et al. (2016)* and *Bordogna et al. (2019)*, among others). The cylinder is put in rotation by an electric engine. Following *Bordogna et al. (2019)*, necessary engine power is computed as:

$$P_{eng} = 0.5\rho\pi DHC_f U_{tan}^3/\eta_{el}$$

where $C_f = 0.007$ is a skin friction coefficient, insensitive to AWS and Utan, and $\eta_{el}= 0.95$ is the efficiency of the electric engine. Rotor performance is computed by optimizing the value of VR as to maximize thrust, on each TWS and TWA defined in the IMO Standard. VR is constrained as to have $P_{eng} < 143$ kW and $\Omega < 180$ RPM, as declared by rotor manufacturers.

3.2. Passive device: CWS rigid wingsail

CWS develops a rigid wingsail having chord c = 9 m and H = 36 m. CWS wingsail uses a cambered, slotted aerofoil, which grants to the 3D wingsail an excellent trade-off between a high maximum lift coefficient and high lift-to-drag ratios at low aerodynamic incidence. The wingsail has an inversion mechanism that allows to flip the camber and equally exploit port and starboard winds. In addition, in case of very strong winds or unfavourable ones, CWS wingsail can be folded in a symmetric configuration, which minimizes structural efforts and drag. Wingsail thrust is computed based on experimental 3D lift and drag coefficients, measured in one of the wind tunnels at Institut Aérotechnique (IAT), Saint-Cyr-l'Ecole, France. In addition of a scale 1:20 lifting surface, the experimental model (see Fig.2) included a pedestal, representative of aerodynamic losses generated by real ship installations. Measurements were run at $Re = AWS\ c/\nu = 1 \cdot 10^6$, as prescribed by *MEPC.1-Circ.896(77)*. CWS wingsail absorbs power only to change its trim, which is expected to be a relatively rare and slow operation. Then, it is assumed that, in average, P_{eng} will be negligible.

Fig.2: Scale 1:4 model of the asymmetric CWS wingsail in the IAT wind tunnel

4. Review of EEDI Guidelines for WASP devices

As far as WASP devices are concerned, reviews of EEDI Guidelines differ in the choice of winds that are to be considered to assess power savings. This chapter gives a closer look to these differences, and to their consequences on EEDI contributions of WASP devices.

4.1. Legacy EEDI Guidelines

MEPC.1-Circ.815(65) require to take into account the complete IMO Global Wind Standard, as defined in *MEPC 62/INF34* (also see Chapter 2). Available effective power is defined with a simple matrix expression, as follows:

$$\left(f_{eff}\, P_{eff}\right) = \left(\frac{0.5144 V_{ref}}{\eta_T} \sum_{i=1}^{m} \sum_{j=1}^{n} F\left(V_{ref}\right)_{i,j} W_{i,j}\right) - \left(\sum_{i=1}^{m} \sum_{j=1}^{n} P\left(V_{ref}\right)_{i,j} W_{i,j}\right)$$

Here $F\left(V_{ref}\right)_{i,j}$ and $P\left(V_{ref}\right)_{i,j}$ are the thrust matrix and the power intake matrix of the WASP device, respectively, at (V_{ref}, TWA_i, TWS_j), where TWA_i and TWS_j are defined as per *MEPC 62/INF34*. The reference ship velocity V_{ref} is determined as described in *MEPC.308(73)*. Both matrices have the same dimensions as $W_{i,j}$, that is the IMO global probability matrix. The term η_T is the total efficiency of the main drive, at reference ship velocity. Since this study does not consider a specific vessel, we set $\eta_T = 0.7$, in accordance with *MEPC.1-Circ.815(65)*. Fig.3 shows values of available effective power (also indicated as EEDI contributions) relative to V_{ref}, obtained with legacy guidelines, for both the active device and the passive one. The two systems offer similar EEDI contributions at low V_{ref}, while at higher velocity the passive device provides more power, due to its higher lift-to-drag ratio and to its negligible power intake.

4.2. 2021 EEDI Guidelines

MEPC.1-Circ.896(77) defines the available effective power as follows:

$$\left(f_{eff}\, P_{eff}\right) = \left(\frac{1}{\sum_{k=1}^{q} W_k}\right)\left(\frac{0.5144 V_{ref}}{\eta_T} \sum_{k=1}^{q} F\left(V_{ref}\right)_k W_k\right) - \sum_{k=1}^{q} P\left(V_{ref}\right)_k W_k$$

The product of net effective power with wind probability is now computed based on *vectors* $F\left(V_{ref}\right)_k$, $P\left(V_{ref}\right)_k$ and W_k. Such vectors contain the same elements as matrices $F\left(V_{ref}\right)_{i,j}$, $P\left(V_{ref}\right)_{i,j}$ and $W_{i,j}$, respectively. However, vectors are now sorted according to the descending order of all the elements of $F\left(V_{ref}\right)_{i,j}$. In addition, only a number of elements $q < i \cdot j$ is included in the computation of available effective power, where q is chosen as to have:

$$\sum_{k=1}^{q-1} W_k < 0.5 \wedge \sum_{k=1}^{q} W_k \geq 0.5$$

Fig.3 also reports EEDI contributions computed with the 2021 Guidelines. The new definition increases the WASP regulatory available effective power of both devices, of a very significant factor of the order of 2. Anyway, the active device appears to be rewarded with a greater bonus, since it now shows a better EEDI performance than the passive device for most considered V_{ref} values. This effect of device-specific selection of winds suggests that the 2021 Guidelines might contribute to skew the playfield in favour of some WASP technologies. This will be discussed in greater detail in Chapter 5.
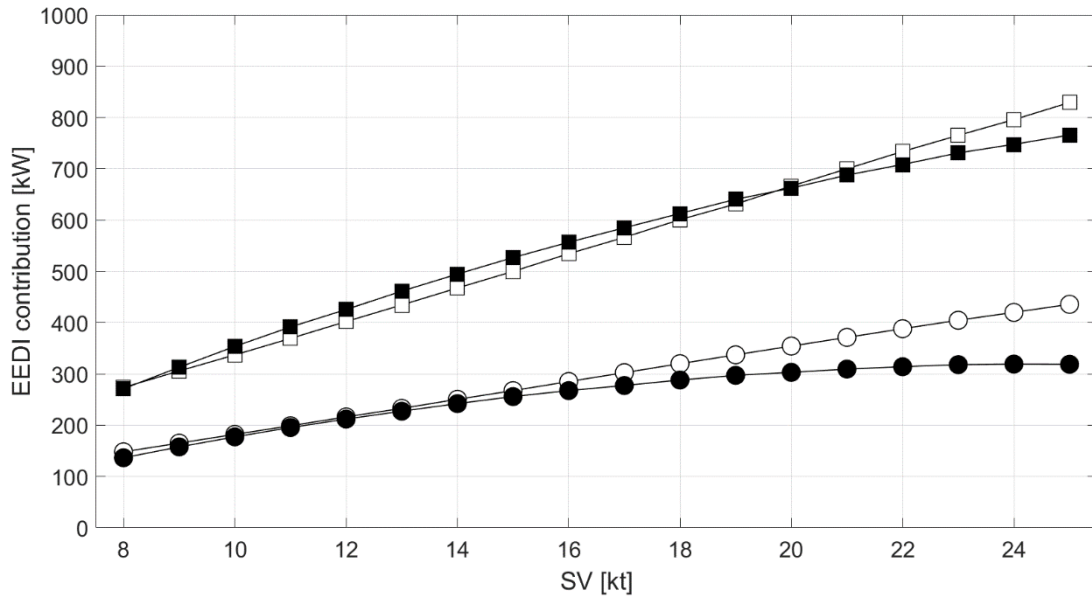
Fig.3: EEDI contributions relative to V_{ref}, for both the active and the passive WASP device. Symbols: ○ passive device, Legacy Guidelines; ● active device, Legacy Guidelines; □ passive device, 2021 Guidelines; ■ active device, 2021 Guidelines.

5. Discussion

This chapter aims at analysing the effects of the 2021 Guidelines highlighted in Fig.3: the EEDI contribution of both devices is improved, relative to Legacy Guidelines, but not to an equal extent.

5.1. Aeolus bag: favourable winds only

To begin with, it is important to graphically visualise how the vector operations described in §4.2 transform the IMO Global Wind Standard. We will focus on the active device, which is better documented in literature, but messages of this section also apply to the passive device. We set V_{ref}= 16 kt, which is at the centre of the V_{ref} range considered above.
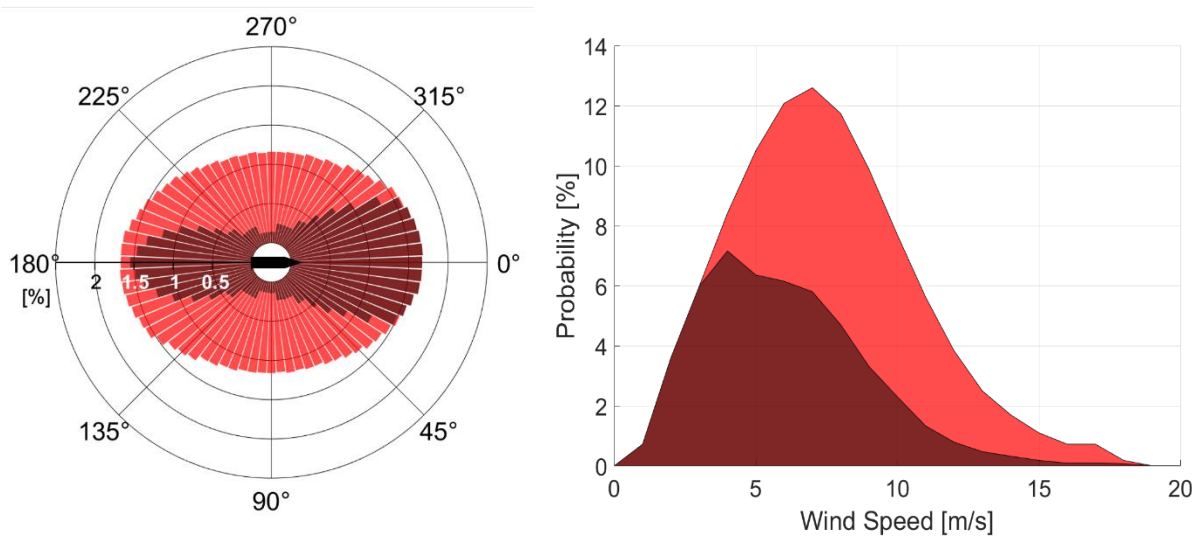
Fig.4.a: Selection of IMO wind conditions for the active device, according to *MEPC.1-Circ.896(77)*. Wind conditions no longer included in the EEDI computation are shaded in black.

58
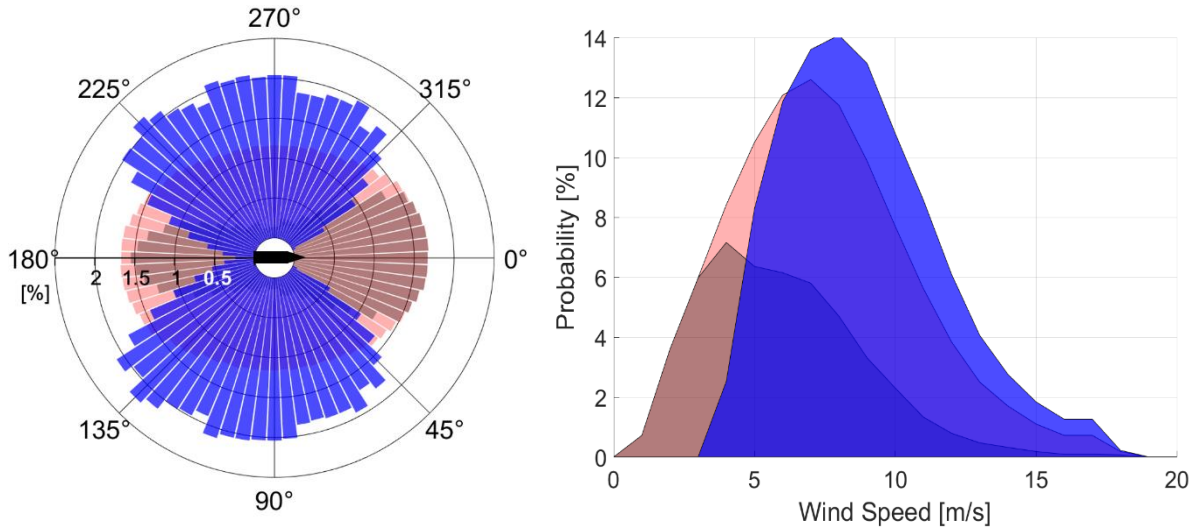
Fig.4.b: blue areas show the actual wind conditions used for computing the EEDI contribution of the active device as 16 kt, according to *MEPC.1-Circ.896(77)*. The full IMO wind probability distribution is also reported for comparison.

In Fig 4.a, IMO wind conditions that are neglected by the 2021 Guidelines have been shaded in black. Quite tellingly, shaded areas encompass all head winds, most trailing winds and a very significant fraction of winds at low TWS. Let us remember that at $V_{ref} = 16$ kt, most low TWS and trailing winds will also give close-hauled apparent winds. These are indeed the least performing wind conditions for the active device, due to its relatively low lift-to-drag ratio. Like a modern-day version of the mythological Aeolus bag, then, the 2021 Guidelines are effective at suppressing low-performance winds. Fig 4.b further shows the wind distribution that is actually used to compute available effective power, after selecting winds and normalizing their probability on $\sum_{k=1}^{q} W_k$. Unsurprisingly, this new distribution only contains strong winds, coming from favourable directions: Aeolus bag has changed the wind matrix as to pump up WASP contributions to EEDI.

Table I: Power savings on three specific legs, favourable to wind propulsion. Power values are computed in a similar way as with the legacy Guidelines (see §4.1), by replacing the IMO global wind matrix with ERA-5 wind statistic along each leg. Values relative to guidelines are on-route power savings, normalized on regulatory available effective power values, as per §4.1 and §4.2.

	North Sea (NLD – NOR)	North Atlantic (US – EU)	South Pacific (PAN – NZL)
Using wind on leg	520 kW	579 kW	423 kW
Relative to Legacy Guidelines	194%	216%	158%
Relative to 2021 Guidelines	93%	104%	76%

5.2. Overestimated wind yield at a global level

Fig.4.b naturally raises the question of whether the high EEDI contributions obtained with such wind distributions are faithful predictions of real power yields, as claimed by promoters of device-specific wind selection. On favourable legs, the device-specific wind matrix might indeed better approximate available effective power than the IMO wind matrix. For instance, this will be the case (by design) on a North Sea route comparable to the one considered in *MEPC.77-6-6*, or on legs that can take advantage

of trade winds, such as in the North Atlantic Ocean or in the South Pacific Ocean (see Table I). Anyway, the EEDI must necessarily be assessed at a global level, if it is to keep its value as a *design* index for the entire world fleet. A containership or a bulk-carrier, for example, will most likely sail on a network of trades, offering disparate wind conditions. On such ships, it does not seem reasonable to assess WASP available power based on the windiest legs exclusively. Then, let us compute the EEDI contribution of the active device on a small network of common commercial trades, composed of the following round-trips: A) Northern Europe to Quebec; B) US East coast to Australia, via Panama and New Zealand; C) Japan to South Africa, via South China Sea and Malacca; D) New Zealand – Hong Kong – Japan; E) Southern Europe to West Africa; F) Southern Europe to Abu Dhabi, via Suez. All trades are shown in Fig.5. It is noteworthy that trades A and B respectively include the North Atlantic leg and the South Pacific leg for which available effective power is given in Table I. Wind statistics are based on 30 (1989-2019) years of ERA-5 data, as extracted from the *Blue Route* online tool edited by the Marin Institute.
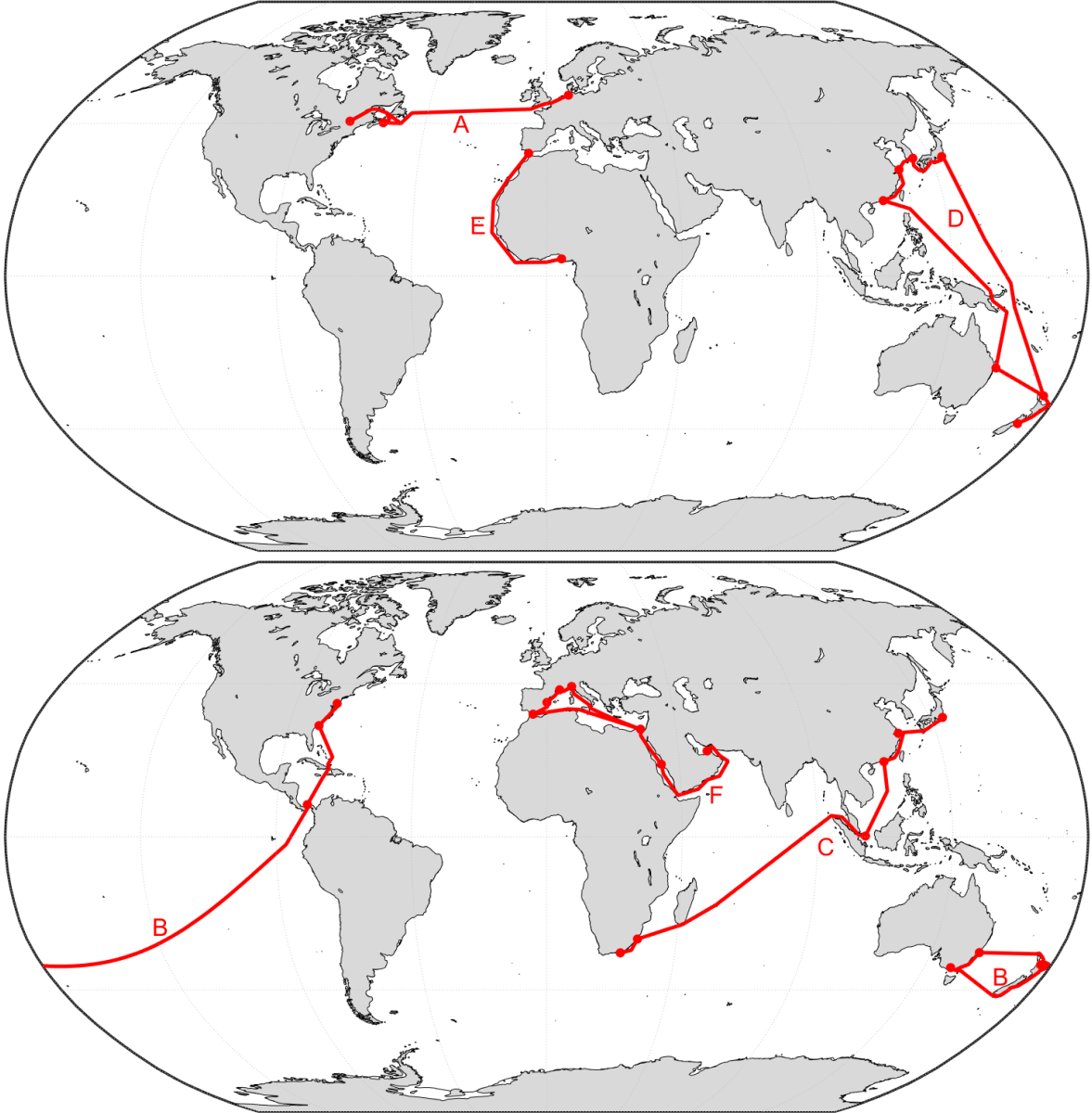
Fig.5: Global network of trades on which available effective power is assesses. Routes are distributed on two maps for greater clarity, as follows. Top: Route A) North Europe to Quebec; Route D) New Zealand – Hong Kong – Japan; Route E) Southern Europe to West Africa. Bottom: Route B) US East coast to Australia, via Panama and New Zealand; Route C) Japan to South Africa, via South China Sea and Malacca; Route F) Southern Europe to Abu Dhabi, via Suez.

Table II presents available effective power computed along each trade of the network. It appears that in most cases, the IMO Global Wind Standard provides a better approximation of the available effective power than the device-specific wind matrix. It is also evident that the IMO Standard is much more accurate in predicting the mean performance of the active device at a network level, in particular if the less favourable trades are discarded under the acceptable (but possibly not inconsequential) hypothesis that WASP will not be deployed on these trades.

Table II: Available effective power on a network of 6 trades for the active device. Mean available effective power on the entire network (Mean A to F) and on the most favourable 4 trades (Mean A to D) are also reported.

	Trade A	Trade B	Trade C	Trade D	Trade E	Trade F	Mean A to F	Mean A to D
Using wind on leg	383 kW	325 kW	212 kW	281 kW	45 kW	98 kW	224 kW	300 kW
Relative to Legacy Guidelines	143%	122%	79%	105%	17%	37%	84%	112%
Relative to 2021 Guidelines	67%	58%	38%	50%	8%	17%	40%	54%

All in all, device-specific wind distributions such as the one displayed in Fig 4.b appear to acceptably approximate wind conditions on specific, favourable legs. However, when available wind resource is considered at a global level, device-specific wind distributions tend to largely overestimate wind yield, and to be less accurate than the full IMO wind matrix. In contradiction with the premises that led to the adoption of the 2021 Guidelines, this result suggests that the IMO Global Wind Standard might be one of the most appropriate representations of the wind resource at a global level.

5.3. EEDI: an unfair bonus to active, high-lift devices

We found at §4.2. that the 2021 Guidelines appear to improve the EEDI score of the active device more than the score of the passive one, relative to the Legacy Guidelines. Fig.6 allows to better visualize this bias, by showing the gain factors brought by the 2021 Guidelines for the two devices, in function of V_{ref}. Such gain factor is defined as:

$$GF = \left(f_{eff}P_{eff}\right)_{2021} / \left(f_{eff}P_{eff}\right)_{Legacy}$$

Values of GF are always higher for the active device, and increasingly so with V_{ref}. This bias stems from the device-specific selection of a fixed fraction of wind conditions, as follows. In the spirit of the Legacy Guidelines (see §4.1), good EEDI contributions could be achieved either by maximizing the peak values of $F(V_{ref})_{i,j}$, or by making sure that $F(V_{ref})_{i,j} > 0$ for the largest possible fraction of the IMO global probability matrix (i.e., by maximizing availability). The 2021 Guidelines suppress all incentive to the latter strategy, by imposing to consider a fixed, high performance 50% fraction of the IMO matrix. In broad aerodynamic terms, high availability requires high lift-to-drag ratios, to exploit close-hauled winds; high peak thrust, instead, requires high lift coefficients. This being so, the 2021 Guidelines systematically exclude part of the performance of the passive device under study, to the extent in which it creates some available power in more than 50% of IMO wind conditions, and in particular for close-hauled winds. On the contrary, the 2021 Guidelines greatly reward the active device, for those wind conditions in which it is able to fully exploit its high lift coefficients.
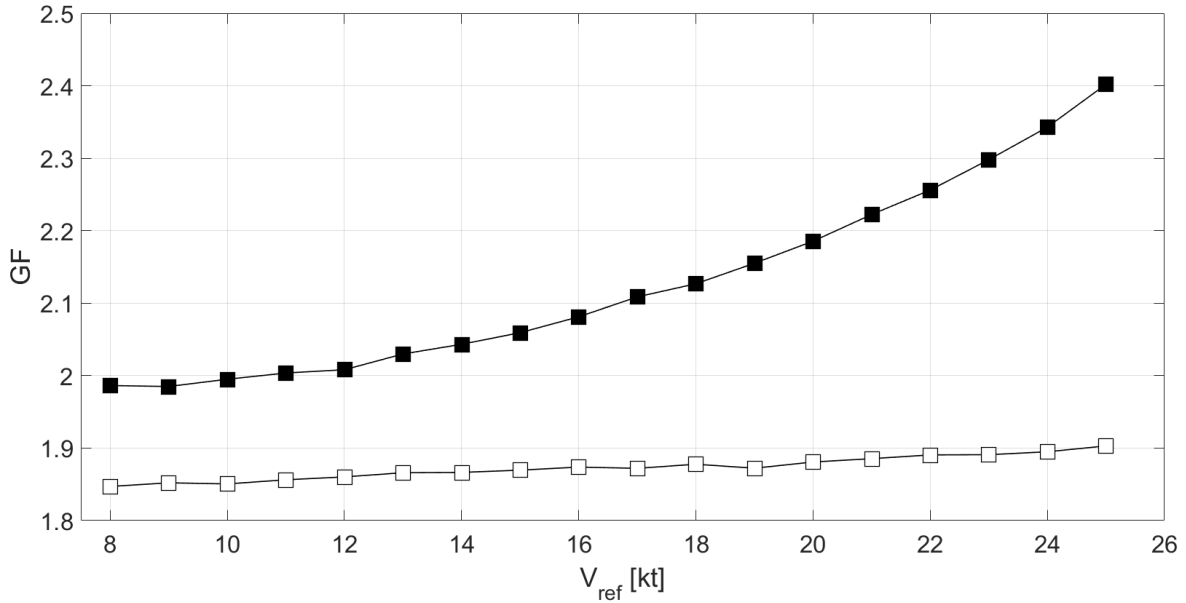
Fig.6: Gain factor (*GF*) brought by the 2021 Guidelines, in function of V_{ref}, for both the active and the passive WASP device. Symbols: □ passive device; ■ active device.

Comparing the force matrices $F\left(V_{ref}\right)_{i,j}$ of the two devices gives further insight into this outcome. Once again, we set V_{ref} = 16 kt: at this velocity, the 2021 Guidelines improve the score of the active device of a factor 2.08, against a factor 1.85 for the passive one. For simplicity, we begin by discriminating which IMO wind conditions produce useful, positive thrust, and which ones only give detrimental, negative thrust. To this end, Fig.7 presents one IMO wind probability matrix, relative to TWA, for each of the two devices under analysis. For a given TWA, probability is accumulated so that more external layers of the distribution represent the probability of winds having higher TWS. For each device, then, probability layers are colored in green if $F\left(V_{ref}\right)_{i,j} > 0$ for the corresponding TWA_i and TWS_j; they are colored in red otherwise. In addition, wind conditions that are excluded from the EEDI computation by the 2021 Guidelines are hashed in black.

As expected, the two devices exclude different (although overlapping) sets of wind conditions. However, it is more important to remark that excluded points mostly give negative thrust in the case of the active device, but they mostly give positive thrust in the case of the passive one. Such difference is due to the aerodynamic efficiency of the two devices, with the smaller, red no-sail cone of the passive device being testimony of a higher lift-to-drag ratio. This qualitative observation can be confirmed by computing the average thrust of each device, weighted on the probability of *excluded* wind conditions. It is found that the device-specific selection of winds frees the active devices of a net negative thrust contribution of about -0.3kN, but it penalizes the passive device of a net positive thrust contribution as high as 4 kN! After normalization, this difference accounts for the higher gain awarded to the active device at V_{ref} = 16 kt.

This finding can be extended to the entire trend of *GF* shown in Fig.6. As V_{ref} grows, more and more true winds give close-hauled apparent winds. In addition, winds within the no-sail cone produce more negative thrust, due to higher apparent wind speeds. To keep providing substantial thrust even at higher V_{ref}, it is then important to have as smaller a no-sail cone as possible, which is achieved by high lift-to-drag ratio devices. On the contrary, due to usually lower aerodynamic efficiencies, high lift devices lose thrust at higher V_{ref}, which in turn hampers available effective power (for example, see the active device in Fig.3). It follows that, in the case of the active device, the contribution of winds neglected by the 2021 Guidelines is increasingly negative as V_{ref} grows. Paradoxically, this translates into growing values of *GF* (see Fig.6). As shown in Fig.3, this bonus can almost fully compensate for the advantage given by a high lift-to-drag ratios at higher V_{ref}, at least for what concerns EEDI considerations, even

if the passive device will still deliver higher fuel and CO2 savings. It seems then that regulation can change the comparative perception of the two devices being analyzed, and skew the competition in favour of the active one.
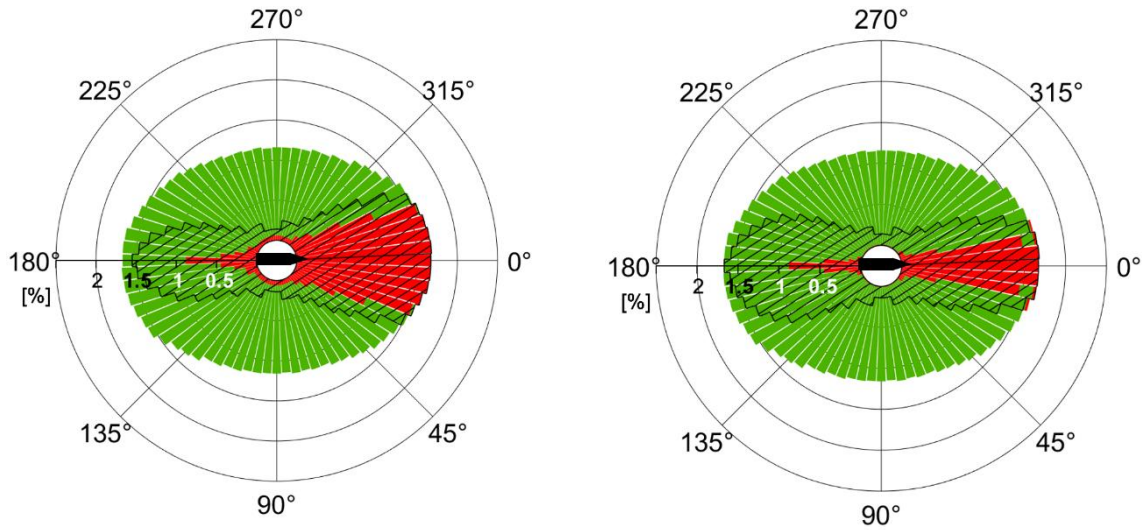
Fig.7: Sign of $F\left(V_{ref}\right)_{i,j}$ for the active device (left) and the passive one (right), at $V_{ref} = 16$ kt. Green indicates wind conditions for which $F\left(V_{ref}\right)_{i,j} > 0$, red otherwise. Wind conditions that are excluded by the 2021 Guidelines are hashed in black.

Anyway, it should be stressed that the 2021 Guidelines do not encourage the adoption of active devices in themselves. They rather reward any kind of device designed as to maximize its thrust on up to 50% of the IMO wind matrix. As such, the 2021 Guidelines could pave the way to unexpected EEDI reduction strategies, based on specially crafted WASP devices. A paradoxical example of one such device is introduced in the next section.

5.4. High EEDI contributions, low CO2 savings: a thought experiment

Let us introduce a new, fictitious wingsail, designed to minimize CAPEX and OPEX. This wingsail has the same lifting surface and the same cambered, slotted aerofoil as the device presented in §3.2. Anyway, significant trade-offs were made to reduce engineering and maintenance costs. Firstly, the new wingsail is not equipped with the patented CWS inversion mechanism. Then, it has a different aerodynamic response for port winds than for starboard ones. For this asymmetric behaviour, we will call it the *Janus sail*. Secondly, Janus has no rotation mechanism and it cannot be trimmed according to wind direction. Encountered aerodynamic angles of attack depend on the direction of apparent wind and they encompass the entire [-180°, 180°) span. This gives a surprising, irregular pattern to thrust developed by Janus. Fig.8 reports the sign of thrust on the IMO wind matrix, with the same colour convention as in Fig.7. For port winds, patches of positive thrust alternate with regions of negative thrust, as the sign of lift changes for strongly negative incidence angles. For starboard winds, the green region hides large ranges of TWA for which Janus is stalled. All in all, it is clear that Janus is not a high-performance device. Its available effective power at $V_{ref} = 16$ kt is of only 47 kW, when assessed according to the Legacy Guidelines, that is 16.5% of the legacy EEDI contribution of the full CWS wingsail.

Let us now adopt the 2021 Guidelines. Fig.8 shows that device-specific wind selection precisely carves out unfavourable wind conditions, leaving a puzzling wind distribution composed of 3 unconnected regions. In consequence, the EEDI contribution of Janus jumps to 160 kW, with a staggering gain factor of 3.40. This result suggests that the 2021 Guidelines give rewards that are not commensurate to the real fuel and CO2 savings delivered by a WASP device. In the case of Janus, for example, the 2021 Guidelines appear to make an unperforming but CAPEX and OPEX inexpensive device competitive

with respect to both the active and the passive device considered in previous sections, at least as far as compliance with EEDI requirements is concerned. It seems then that the 2021 Guidelines open the door to strong market distortions, and possibly to poor EEDI minimization practices.
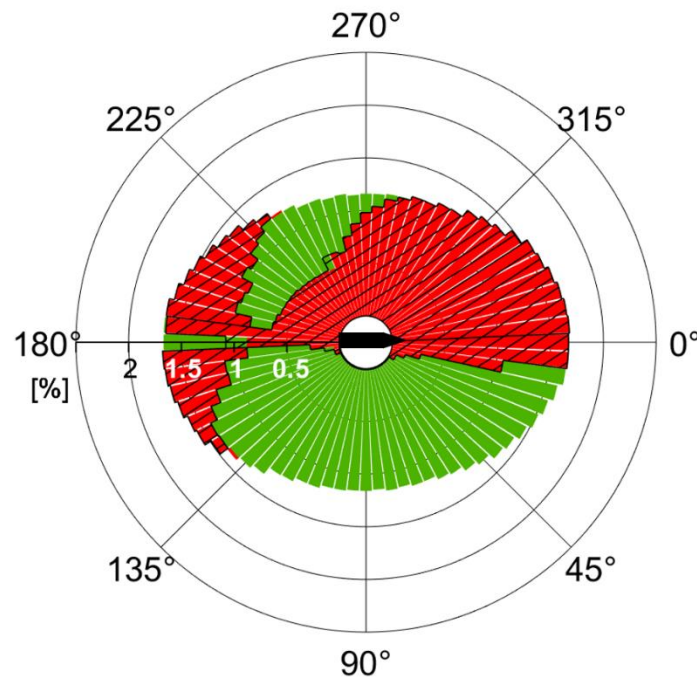
Fig.8: Sign of $F(V_{ref})_{i,j}$ for the Janus sail. Colours are as in Fig.7.

6. Conclusions and ways forward

In this paper, we used simple arguments and graphical visualizations to highlight some of the less visible, but most important, drawbacks of *MEPC.1-Circ.896(77)* EEDI Guidelines for WASP devices. In particular, we have shown that:

1) as a sort of modern-day Aeolus bag, device-specific wind selection transforms the IMO wind matrix into a set of favourable wind distributions, which are unrealistic at a global level;
2) device-specific wind selection is biased in favour of devices that privilege high peak lift coefficients (typically, but not exclusively, active devices), over systems which have more efficient aerodynamics. For the time being, however, there appears to be no compelling reason to skew competition toward one particular kind of WASP device;
3) device-specific wind selection might reward even unperforming devices, to a degree that is not commensurate with real fuel and CO2 saving potential. This could cause strong market distortions and even encourage EEDI compliance strategies unconnected to real CO2 savings.

Nevertheless, modifying the IMO wind matrix might be a promising way to improve the regulatory available effective power delivered by WASP devices, provided that any new definition of such matrix contains all possible winds (including head and trailing winds) and is equally applied to all WASP devices. A possible way forward could consist in recomputing the IMO wind matrix, after the exclusion of those less favourable routes on which wind-assisted propulsion is less likely to be deployed. Reasonable weather routing could also be invoked to improve the global wind resource, provided that one routing strategy is found that benefits to all WASP devices to a comparable extent. We also suggest that sensitivity studies and feedback from ship designers and yards should be used to thoroughly assess the impact of the 2021 Guidelines on design of new vessels, and on installation of WASP devices. In addition, we encourage the shipping industry to study if any correlation exists between EEDI/EEXI and the operational Carbon Intensity Index (CII). If so, it should be verified whether CII could effectively

highlight design choices and EEDI optimization strategies that, once in operation, do not deliver the promised reductions of CO2 emissions.

References

BORDOGNA, G.; MUGGIASCA, S.; GIAPPINO, S.; BELLOLI, M.; KEUNING, J.; HUIJSMANS, R.; VAN'T VEER, A (2019), *Experiments on a Flettner rotor at critical and supercritical Reynolds numbers*, J. Wind Eng. & Industrial Aerodynamics, pp.19-29

DE MARCO, A.; MANCINI, S.; PENSA, C.; CALISE, G.; DE LUCA, F. (2016), *Flettner rotor concept for marine applications: A systematic study,* Int. J. Rotating Machinery

IMO MEPC62 (2011), *MEPC 62/INF34. Global Wind Specification along the Main Global Shipping Routes to be applied in the EEDI Calculation of Wind Propulsion Systems*

IMO MEPC65 (2013), *MEPC.1-Circ.815(65). 2013 Guidance on Treatment of Innovative Energy Efficiency Technologies for Calculation and Verification of the Attained EEDI.*

IMO MEPC72 (2018), *Resolution MEPC.304(72). Initial IMO Strategy on Reduction of GHG Emissions from Ships*

IMO MEPC73 (2018), *Resolution MEPC.308(73). 2018 Guidelines on the Method of Calculation of the Attained Energy Efficiency Design Index (EEDI) for New Ships*

IMO MEPC74 (2019), *MEPC.74/INF39. Air Pollution and Energy Efficiency. Findings on the EEDI Assessment Framework for Wind Propulsion Systems*

IMO MEPC76 (2021), *MEPC.77-6-6. Energy Efficiency of Ships. Additional Draft Amendments to MEPC.1/Circ.815 for Verification of the Wind Propulsion System.*

IMO MEPC76 (2021), *Resolution MEPC.328(76). Amendments to the Annex of the Protocol of 1997 to Amend the International Convention for the Prevention of Pollution from Ships, 1973, as Modified by the Protocol of 1978 Relating Thereto. 2021 Revised MARPOL Annex VI*

IMO MEPC76 (2021), *Resolution MEPC.336(72). 2021 Guidelines on Operational Carbon Intensity Indicators and the Calculation Methods (CII Guidelines, G1)*

IMO MEPC77 (2021), *MEPC.1-Circ.896(77). 2021 Guidance on Treatment of Innovative Energy Efficiency Technologies for Calculation and Verification of the Attained EEDI and EEXI*

VAN DER KOLK, N.; BORDOGNA, G.; MASON, J.C.; DESPRAIRIES, P.; VRIJDAG, A. (2019), *Case study: wind-assisted ship propulsion performance prediction, routing, and economic modelling,* Int. Conf. Power & Propulsion Alternatives for Ships, RINA, London

Applying ANNs to Derive Empirical Design Formulas for Harbor Tugs

Volker Bertram, DNV, Hamburg/Germany, volker.bertram@dnv.com
Marcus Bentin, HS Emden/Leer, Leer/Germany, marcus.bentin@hs-emden-leer.de

Abstract

This paper describes how a database of harbor tugs was used to derive simple design formulas for conceptual design. The approach used artificial neural nets to predict power and displacement based on speed and bollard pull, using length as additional parameter that may be estimated using conventional design formulas for tugs. The agreement of predictions with an independent validation data set is very good.

1. Introduction

Tugs are work boats which differ in many aspects from normal cargo ships, Fig.1, *Allan (2003)*. The main design specification concerns manoeuvrability and ability to assist escort vessels in manoeuvring. Design experience and empirical design formulas for conventional cargo ships or fast pleasure craft are not applicable to tugs. This was the motivation for us to develop corresponding semi-empirical formulas for harbour tug design, *Bentin and Bertram (2000), Bertram and Bentin (2001)*.
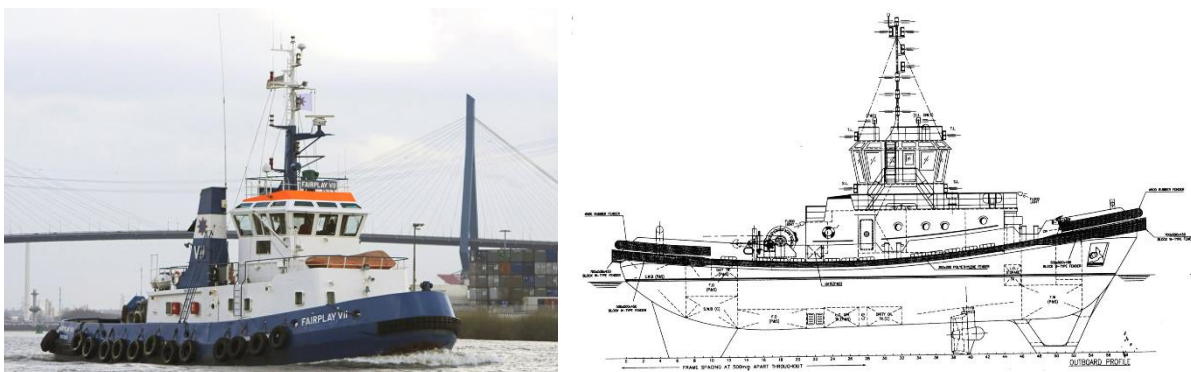
Fig.1: Typical harbor tug

Conventional regression analysis has been extensively used in naval architecture in system identification to provide required factors and coefficients. Based on databases of existing designs, coefficients are then interpolated or even extrapolated to calculate coefficients for a new application, e.g. for simple design methods as in *Watson (1998), Schneekluth and Bertram (1998), Bertram (2012)*. This procedure requires specification of not the main input parameters, but also the type of functional relation between input and output parameters. Most often in the past, simple linear relations (or even worse just constants) have been chosen. Designers plotted data and by visual inspection sometimes chose also simple polynomial relations. Higher-order polynomials have the unfortunate tendency to introduce unphysical oscillations.

This approach is cumbersome and unsuitable for many nonlinear relations. Unsatisfactory approximations in conventional regression analyses stem mainly from the inappropriate choice of inherent function used in statistics. In the language of Germans and mathematicians, we fail from the 'ansatz'. Wouldn't it be nice to have some mathematical way of mimicking the curve we would instinctively draw through such data sets, ignoring implausible outliers and following the trends our eye sees, something flexible yet smooth and free of inappropriate oscillations? For the naval architect, this is old hat. We have approximated arbitrary point sets for centuries, Fig.2), using first flexible thin beams (splines), Fig.3, and later using aptly named spline curves, which do not oscillate and form smooth curves and surfaces, see e.g. *Veelo (2004)*.

The machine learning community prefers other functions, such as sigmoid functions, Fig.4. Combining many of these, we have similar basic qualities of flexible approximation and avoiding oscillations.

Fig.3: Rembrandt painting of shipbuilder using smooth curves to describe ship lines | Fig.4: Traditional splines for ship design, source: TU Berlin

$$f(x) = \frac{1}{1 + e^{-\beta x}}$$
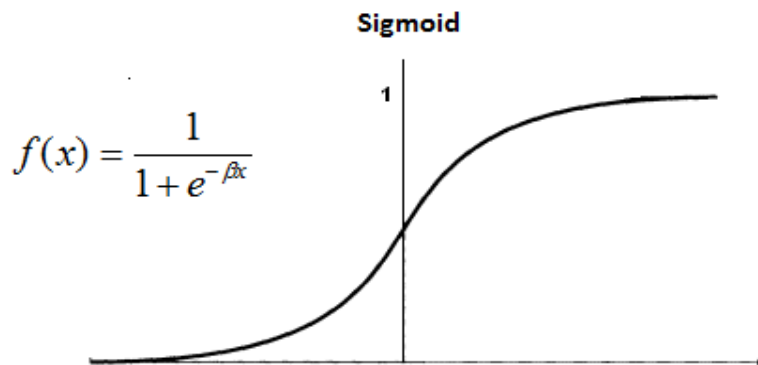
Fig.4: Sigmoid function (typically $\beta = 1$ in our applications)

2. Artificial Neural Nets for functional approximation

Artificial Neural Networks (ANNs) offer a more versatile and user-friendly approach to system identification, *Mesbahi (2003)*, https://en.wikipedia.org/wiki/Artificial_neural_network. ANNs can generally represent the mapping of multi-dimensional input/output data sets, i.e. an arbitrary number of input variables x_i and output variable y_i. An ANN structure consists of several layers; each layer consists of several nodes. In the example in Fig.5, we have the input layer, the output layer, and one hidden layer.
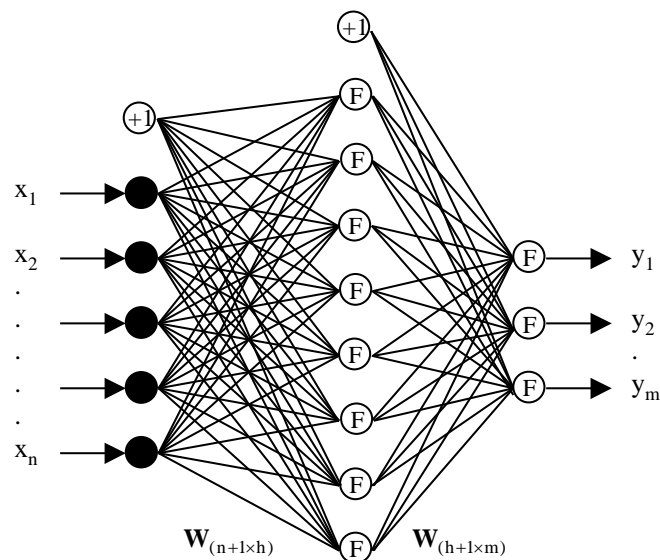
Fig.5: General structure of an Artificial Neural Network

The ANN is "trained" on data sets. This training process results in mathematical relationship output variables y_i and input variables x_i, e.g. of the form (for a single-input, single-output ANN):

$$y = c_0 + c_1 \cdot \text{sig} [b_0 + b_1 \cdot \text{sig}(a_{10} + a_{11} \cdot x_1 + a_{12} \cdot x_{2+\ldots}) + b_2 \cdot \text{sig}(a_{20} + a_{21} \cdot x_1 + a_{22} \cdot x_{2+\ldots}) + \ldots]$$

Here, sig denotes the sigmoid function. After sufficient training, adjusted values for the coefficients a, b, and c are derived and the non-linear relationship is determined. Now the ANN can very rapidly determine values y_i for given values x_i. For numerical reasons, it is advisable to normalize input and output values between 0 and 1:

$$\text{Normalised value} = (\text{Real value - Min. Value})/(\text{Max. value - Min. value})$$

"Deep Learning", https://en.wikipedia.org/wiki/Deep_learning, is a more recent buzz word used when neural nets with two or more hidden layers are used. Having an additional layer means that the transfer function (e.g. the sigmoid function) is calling in itself a transfer function. This adds more flexibility in approximating functions, but requires also more data for training to be successful.

ANNs are a powerful tool in numerical statistics for many applications, and particularly in our context for empirical formulas used in conceptual ship design or formal optimization applications, when fast and moderately accurate estimates are needed. They are not a magic bullet; they cannot perform miracles. ANNs reach their limitations in several cases, *Bertram (2022), Colle and Morobé (2022)*:

- random or quasi-random processes
- scarce data sets
- extrapolation far beyond the data set used in the system identification

3. Application to harbor tugs

The starting point of each ANN analysis is a database. In our case, the database was developed using tug designs of Kölln/Jacoby consulting engineers in Hamburg, enriched by additional data supplied by Hitzler shipyard, Schottel, and Voith Hydro. 58 tugs of different size, age, and propulsion systems retrieved from paper files to feed the database.

For the ANN analyses, between 70% and 80% of the datasets were used for training the ANN; the rest was set aside for validation. The accuracy of the ANN predictions was presented by calculating the correlation between the real and predicted outputs.

Key input parameters are design speed V in [kn], bollard pull t in [t] and length L_{pp} in [m]. The non-metric units of knots and tons (for forces) are used, as these are the customary units in the tug design community.

Key output parameters are mass displacement Δ in [t] and engine power P in [kW]. If L_{pp} is not known in early design (as it depends in turn typically on installed power), it may be estimated based on required bollard pull t and propulsion type:

- Schottel: $L_{pp} = (60.513 \cdot t - 40.278)^{0.1560}/0.1269$
- Voith-Schneider: $L_{pp} = (72.103 \cdot t - 8.0)^{0.2244}/0.1996$
- Conventional: $L_{pp} = 7.272 \cdot t^{0.4063}$

To make the results accessible for the wider community, we extracted the internal representation from the ANN software to derive the following explicit and programmable formulas, *Bertram and Mesbahi (2000)*:

$$\Delta = 26 + 886 \cdot \text{sig}[-4.36 \cdot \text{sig}(-0.1093 \cdot t - 0.6485 \cdot V + 14.1646) - 3.08 \cdot \text{sig}(-0.0579 \cdot t - 0.6912 \cdot V + 7.402) + 3.6]$$

$$P = 1060+3354 \cdot \text{sig}(1.23-6.44 \cdot \text{sig}(0.08652 \cdot L_{pp}-0.3171 \cdot t-3.84 \cdot V+60.4709)$$
$$+2.97 \cdot \text{sig}(0.8539 \cdot L_{pp}+0.2307 \cdot t-0.484 \cdot V-23.07)$$
$$-5.98 \cdot \text{sig}(0.2596 \cdot L_{pp}+0.0856 \cdot t+0.51 \cdot V-17.577)$$
$$+2.61 \cdot \text{sig}(0.2857 \cdot L_{pp}+0.7132 \cdot t+0.476 \cdot V-25.7645))$$

After training the neural network on the data subset for training, predicted results were compared with real values from the data subset for validation. Agreement was good, e.g. for the power prediction, Fig.6, with a correlation coefficient of 0.9945.
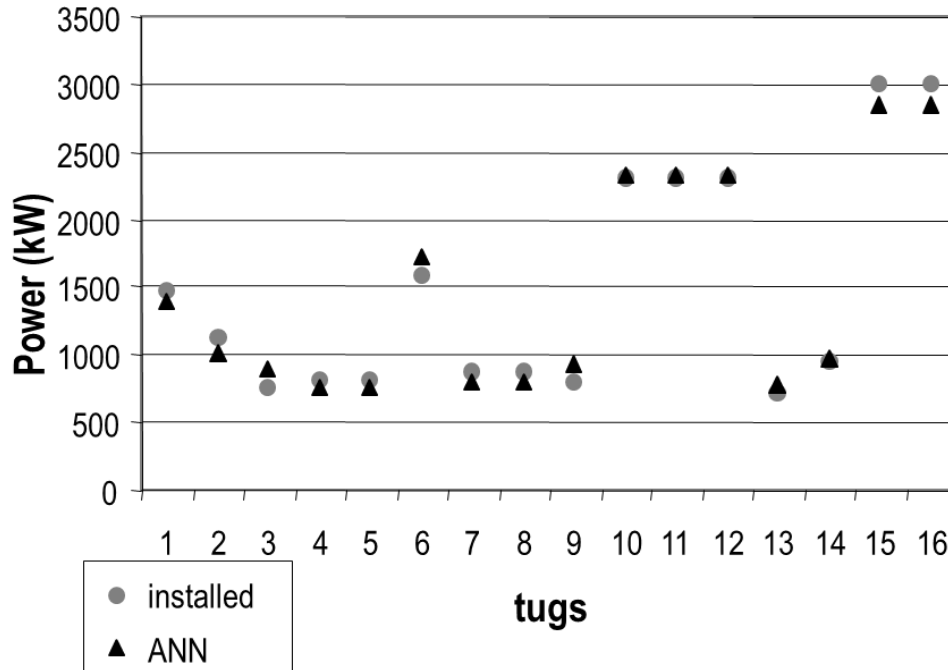
Fig.6: Comparison of ANN predicted and installed power in validation data set

4. Conclusion

Artificial neural nets are a powerful tool to derive empirical design formulas. They require a sufficiently large data set; this can be a challenge in some applications in ship design, namely for unconventional ship types. Training process and application are straight-forward in comparison.

Acknowledgements

References

ALLAN, R.G. (2003), *Tugs and towboats,* Ch.48 Ship Design and Construction (Ed. T. Lamb), SNAME

BENTIN, M.; BERTRAM, V. (2000), *Entwurfsgrundlagen für Hafenschleppern*, Handbuch der Werften, Hansa-Verlag

BERTRAM, V. (2012), *Practical Ship Hydrodynamics,* Butterworth & Heinemann

BERTRAM, V. (2022), *Capabilities and Limits of Machine Learning*, 7th HullPIC Conf., Tullamore, pp.16-23, http://data.hullpic.info/HullPIC2022_Tullamore.pdf

BERTRAM, V.; MESBAHI, E. (2000), *Anwendungen Adaptiver Neuronaler Netze im Schiffsentwurf/ Adaptive Neural Network Applications in Ship Design,* Jahrbuch der Schiffbautechnischen Gesellschaft, Springer

BERTRAM, V.; BENTIN, M. (2001), *Tugs,* 36th WEGEMT Summer School, http://www.wegemt.com/wp-content/uploads/2019/04/36th_WEGEMT_Summer_School_on_Manoeuvering_and_Manoeuvering_Devices.pdf

COLLE, C.; MOROBÉ, C. (2022), *Saving AI from its Own Hype: Getting Real about the Benefits and Challenges of Machine Learning for Ship Performance Modelling Aimed at Operational Optimizations*, 7th HullPIC Conf., Tullamore, pp.198-206, http://data.hullpic.info/HullPIC2022_Tullamore.pdf

MESBAHI, E. (2003), *Artificial neural networks – Fundamentals,* 39th WEGEMT School OPTIMISTIC – Optimization in Marine Design, pp.191-216, http://www.wegemt.com/wp-content/uploads/2019/04/39th_WEGEMT_Summer_School_on_Optimistic_Optimization_in_Marine_Design.pdf

MESBAHI, E.; BERTRAM, V. (2000), *Empirical design formulae using artificial neural networks,* 1st COMPIT Conf., Potsdam, pp.292-301, http://data.hiper-conf.info/compit2000_potsdam.pdf

SCHNEEKLUTH, H.; BERTRAM, V. (1998), *Ship Design for Efficiency and Economy*, Butterworth & Heinemann

WATSON, D.G.M. (1998), *Practical Ship Design*, Elsevier

VEELO, B. (2004), *Variations of Shape in Industrial Geometric Models*, PhD thesis, NTNU, Trondheim, https://www.sarc.nl/publications/variations-of-shape-in-industrial-geometric-models/

Keeping EEDI and CII in CHEK through Intelligent Ultrasonic Biofouling Protection

Xavier Mayorga, HASYTEC electronics, Schönkirchen/Germany, x.mayorga@hasytec.com
Jan Kelling, HASYTEC electronics, Schönkirchen/Germany, j.kelling@hasytec.com

Abstract

This paper describes our contributions to the EU R&D project CHEK in progress. The project's larger context is decarbonization of shipping through innovative technologies, where ultrasonic antifouling technology is the specific contribution of HASYTEC to increase energy efficiency in operation and bring down the Carbon Intensity Indicator (CII). The application cases in CHEK are a cruise vessel and a bulk carrier. Progress in the energy efficiency of ultrasonic biofilm prevention is due to application of Artificial Intelligence (AI) in parameter settings of transducers. Each transducer is AI-enabled to adapt its parameter settings (frequency and intensity level) to optimize effectiveness in biofilm protection.

1. Introduction

IMO, www.imo.org, has the ambition to halve GHG emissions by 2050 and to completely decarbonize shipping "as soon as possible" within this century. The initial IMO Greenhouse Gas strategy will be revised in 2023, including these goals. IMO is following a two-tier approach to implement decarbonization measures, focusing first on short-term energy efficiency improving measures, before embarking on more comprehensive medium-term and long-term measures that will include alternative low-carbon/no-carbon fuels, *Bertram (2021)*.

Current measures addressing GHG emissions include three mandatory requirements:

- The Energy Efficiency Design Index (EEDI) for newbuildings mandating successive improvement in design performance of 30% compared to the average of ships built 1999-2009.
- The Ship Energy Efficiency Management Plan (SEEMP) for all ships above 400 GT in operation, making a continuous energy efficiency improvement management plan mandatory, although not stating explicit requirements to content, scope and implementation.
- The Fuel Oil Consumption Data Collection System (DCS) mandating annual reporting of CO_2 emissions for all ships above 5000 GT.

At MEPC 76, in 2021, three additional measures were adopted, affecting all existing cargo and cruise ships after 2023:

- The Energy Efficiency Design Index for Existing Ships (EEXI), essentially making requirements equivalent to EEDI Phase 2 or 3 mandatory to all existing ships.
- A mandatory Carbon Intensity Indicator (CII) and rating scheme for all cargo and cruise ships above 5000 GT. Poor CII ratings will lead to mandatory requirements for corrective action plans to improve the CII. The criteria for CII ratings will get progressively stricter by 1% per year for 2020-2022, followed by 2% per year for 2023-2026.
- SEEMP requirements were made stricter (Enhanced SEEMP) to include mandatory content, such as an implementation plan on how to achieve the CII targets.

These new requirements for existing ships will increase the focus on energy efficiency measures both in design/retrofit and operation. For the operational measures, improved hull management is widely seen as one of the most important measures, with potential gains in the order of magnitude of 10%.

2. EU R&R Project CHEK

2.1. Overview

The R&D project CHEK (de<u>C</u>arbonising s<u>H</u>ipping by <u>E</u>nabling <u>K</u>ey technology symbiosis on real vessel concept designs) has as a goal to reduce CO_2 emissions in global shipping. The focus is on the combined application of advanced key technologies in shipbuilding. The CHEK project is supported by the European Union with a total of 10 million Euro from the Horizon 2020 funding program, https://ec.europa.eu/programmes/horizon2020/en/home. The Horizon 2020 program is the biggest EU research & innovation program ever, with nearly € 80 billion of funding over 7 years. Its aim is combining European research and innovation to achieve excellent science, industrial leadership and tackling societal challenges.

2.2. Project goals

The CHEK project proposes to reach zero-emission shipping by disrupting the way ships are designed and operated today. The project will develop and demonstrate two bespoke vessel designs – a wind energy optimised Kamsarmax bulk carrier and a hydrogen powered cruise ship, Fig.1 – equipped with an interdisciplinary combination of innovative technologies working in symbiosis to reduce greenhouse gas emissions by 99%, achieve at least 50% energy savings and reduce black carbon emissions by over 95%. The innovative energy-saving technologies include the use of wind energy, batteries, heat recovery, hydrogen as a fuel, air lubrication and ultrasound anti-fouling.

Rather than "stacking" novel technologies onto existing vessel designs, the consortium is proposing to develop a unique Future-Proof Vessel (FPV) Design Platform to ensure maximised symbiosis between the novel technologies proposed and taking into consideration the vessels' real operational profiles (rather than just sea-trial performance). The FPV Platform will also serve as a basis for replicating the CHEK approach towards other vessel types such as tankers, container ships, general cargo ships and ferries. These jointly cover over 93% of the global shipping tonnage and are responsible for 85% of global GHG emissions from shipping.
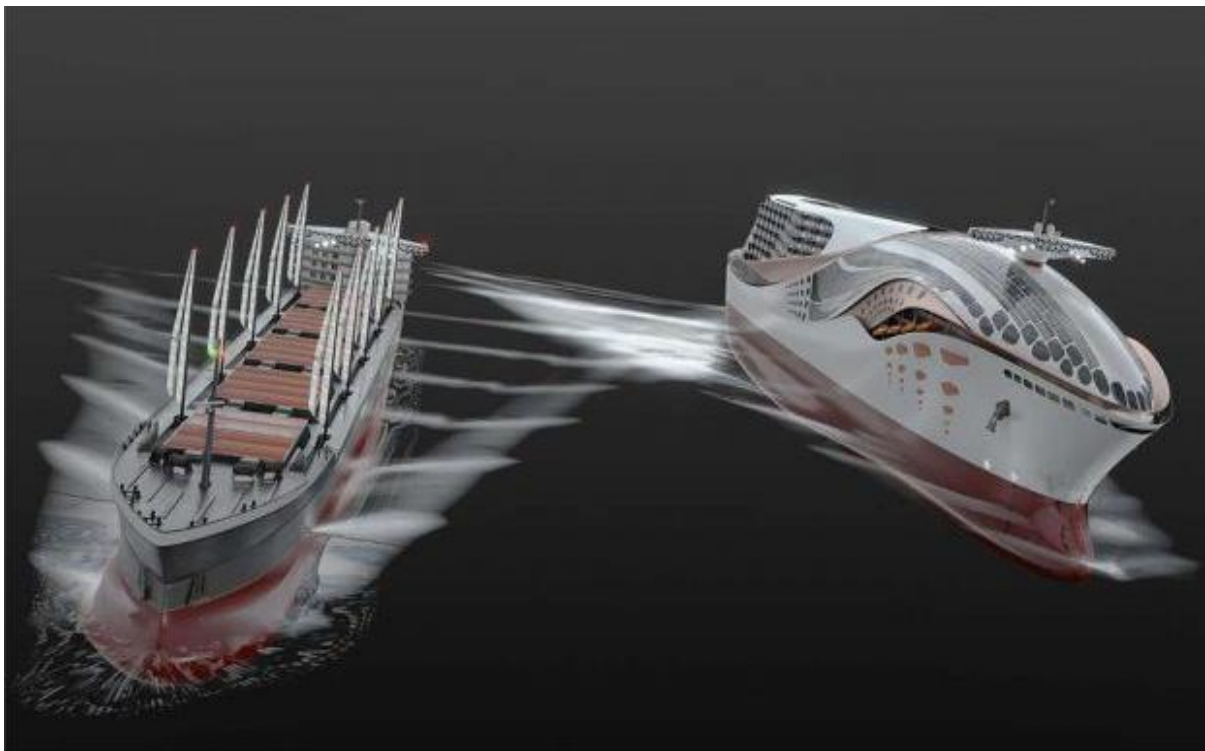
Fig.1: Application cases: Bulk carrier and cruise ship, source: Wärtsilä

In order to achieve real-world impact and the decarbonisation of the global shipping fleet, the consortium will undertake an analysis of framework conditions influencing long-distance shipping today (including infrastructure availability) and propose solutions to ensure the proposed vessel designs can and will be deployed in reality. A Foresight Exercise will simulate the deployment of the CHEK innovations on the global shipping fleet with the aim of reaching the IMO's goal of halving shipping emissions by 2050 and contributing to turning Europe into the first carbon-neutral continent by 2050 (as stipulated by the European Green Deal).

2.3. Application cases and applied technologies

The project aims to combine a variety of innovative technologies to achieve its goals, Fig.2:

- New energy technologies
  - Fixed wing sails
  - Fuel-cell ready hydrogen engine
- Operational technologies and practices
  - Automated vessel routing/sailing
  - Cruise vessel itinerary optimization
- Propulsion/Power supply technologies
  - Fuel-flexible gas engine incl. over-the-air software updates
  - Scalable power plant
  - Hybrid energy management
  - Waste heat recovery
  - Waste-to-power
- Drag reduction technologies
  - Gate rudder
  - Air lubrication
  - Ultrasound antifouling
  - Ship hull optimization
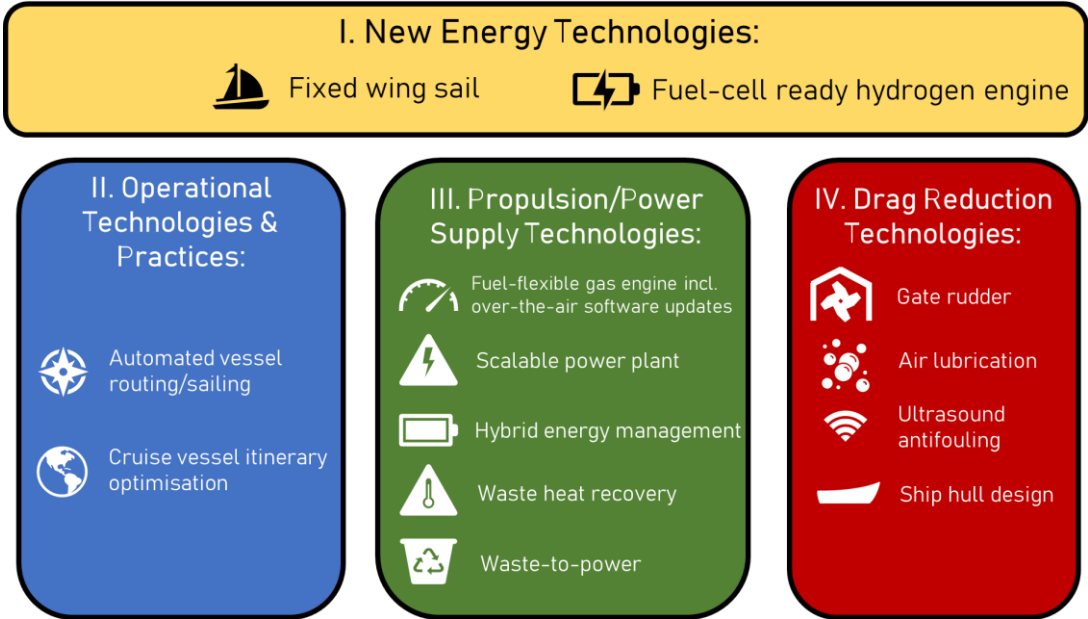
Fig.2: Technological synergy for emission savings

The effectiveness and saving potential of the various options depend on various factors, including ship types and associated typical operational patterns. Within CHEK, two very different ship types are considered, namely a bulk carrier and a cruise vessel. Fig.3 gives the selected measures for the bulk carrier, and Fig.4 for the cruise vessel.
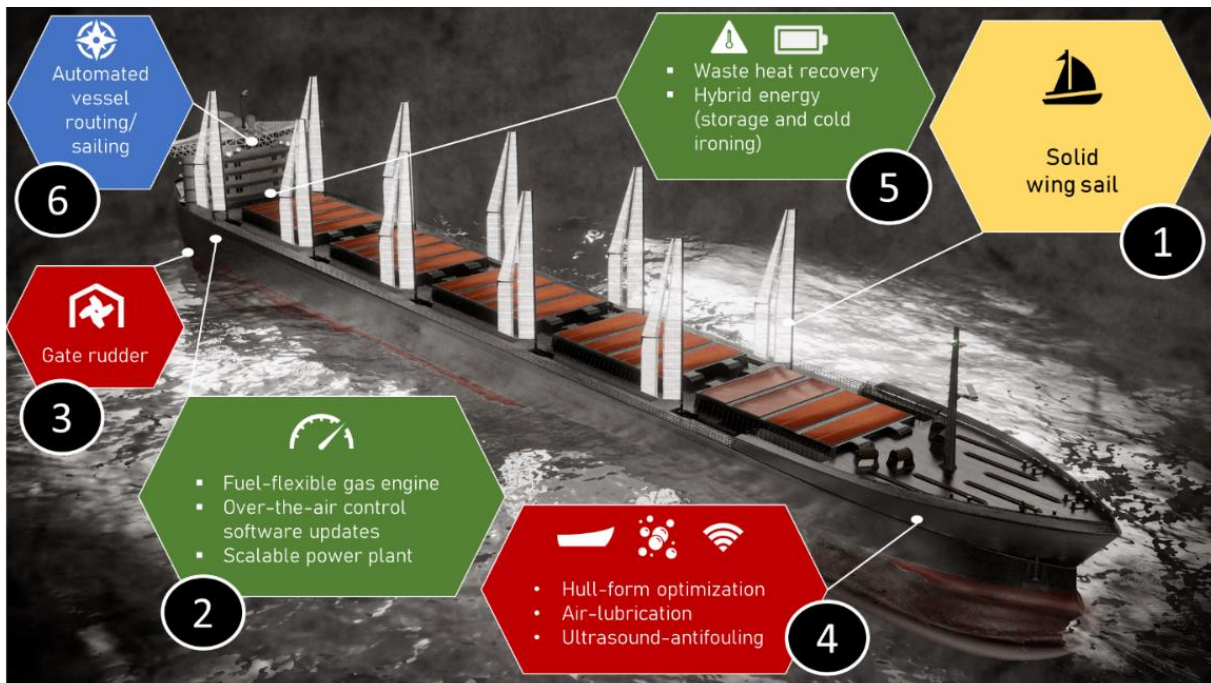
Fig.3: Emission saving technologies envisioned for bulk carrier
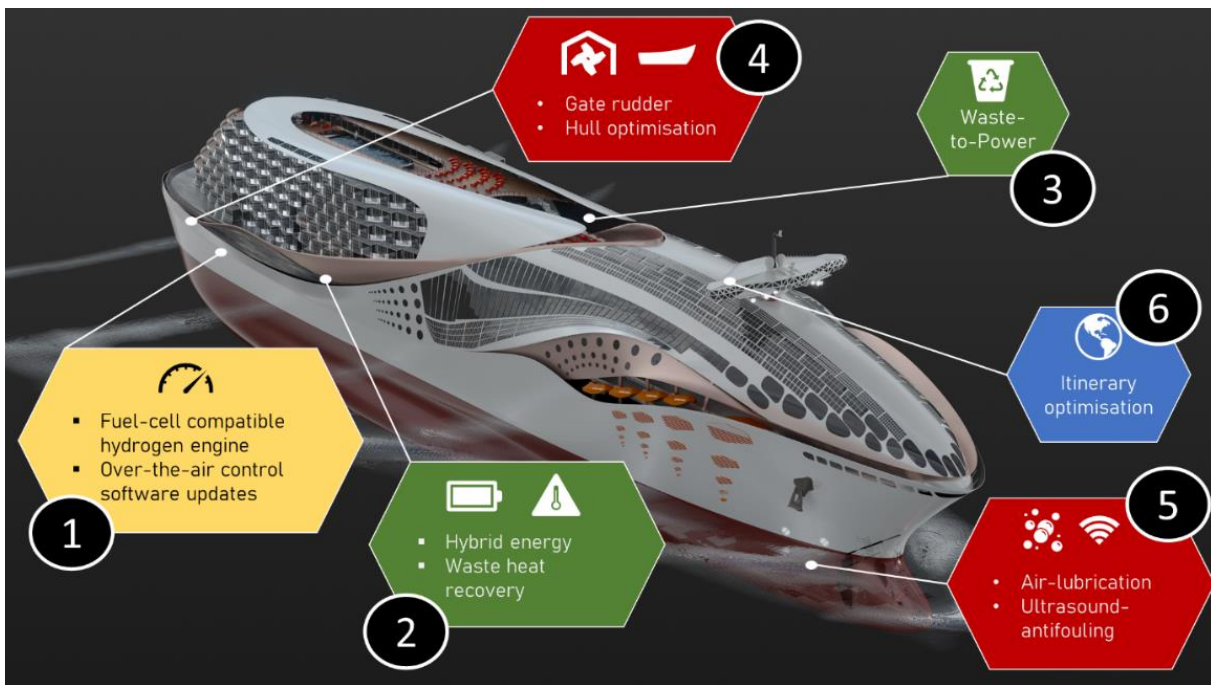
Fig.4: Emission saving technologies envisioned for cruise vessel

Figs.5 and 6 compares the expected CO_2 emissions to a baseline design, where the bars are normalized to 100% for the baseline design, for bulk carrier and cruise vessel, respectively. The selected measures lead to an expected decrease in CO2 emissions of 40% for the bulk carrier and 50% for the cruise vessel.
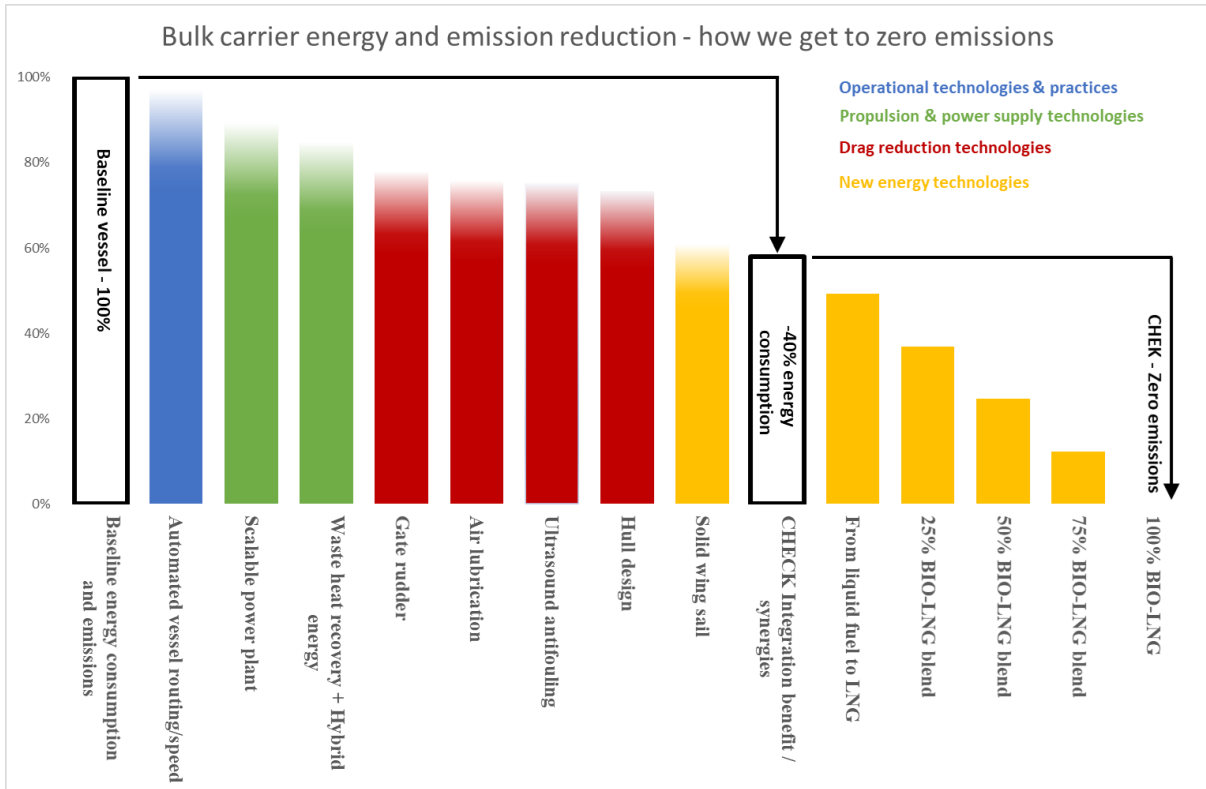
Fig.5: Expected emissions compared to baseline design for bulk carrier
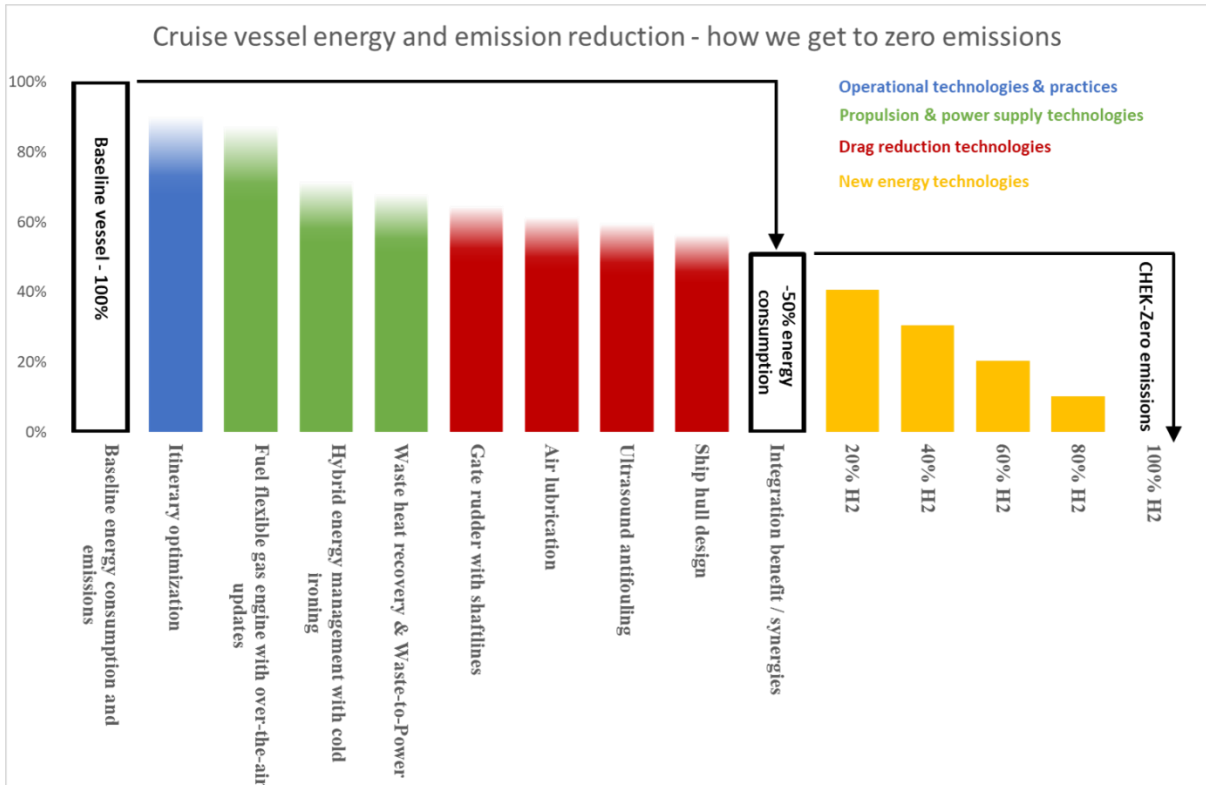
Fig.6: Expected emissions compared to baseline design for cruise vessel

3. Intelligent Dynamic Biofilm Protection

3.1. Short introduction to Artificial Intelligence

This chapter is closely based on *Bertram (2022a,b)*. Further recommended reading includes *Colle and Morobé (2022)*, on applications of machine learning for ship hull management.

Artificial Neural Networks (ANNs) are a key technology of machine learning, which in turn is a key technology of Artificial Intelligence (AI). ANNs offer a more versatile and user-friendly approach to system identification, *Mesbahi (2003)*, https://en.wikipedia.org/wiki/Artificial_neural_network.

ANNs can generally represent the mapping of multi-dimensional input/output data sets, i.e. an arbitrary number of input variables x_i and output variable y_i. An ANN structure consists of several layers; each layer consists of several nodes. In the example in Fig.7, we have the input layer, the output layer, and one hidden layer.
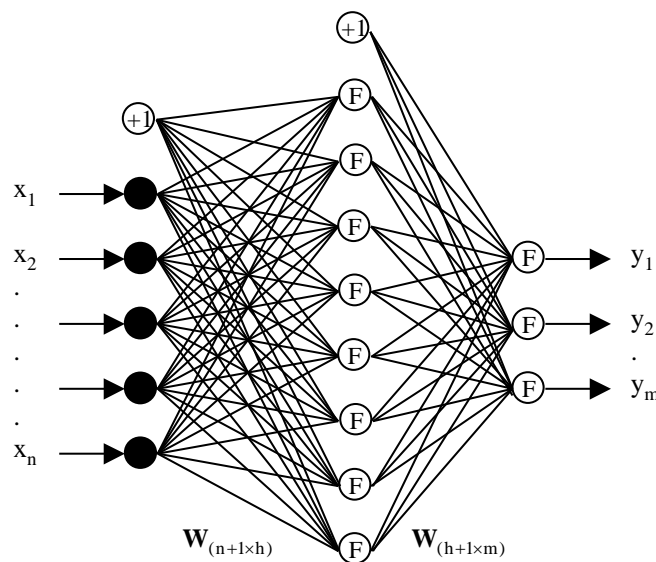
Fig.7: General structure of an Artificial Neural Network

The ANN is "trained" on data sets. This training process results in mathematical relationship output variables y_i and input variables x_i. After sufficient training, adjusted values for the coefficients are derived and the non-linear relationship is determined. Now the ANN can very rapidly determine values y_i for any given values x_i.

"Deep Learning", https://en.wikipedia.org/wiki/Deep_learning, denotes neural nets with two or more hidden layers. This adds more flexibility in approximating functions, but requires also more data for training to be successful.

3.2. Ultrasonic biofouling protection in CHEK

In relation to the AFS convention, *IMO (2001)*, the EU Regulation No. 528/2012 details restrictions on the marketing and use of biocide containing products. As an example, almost no copper-based active substances will get permission to be used in the future. This leaves essentially two options:

- taking the risk of using less effective antifouling systems which leads to higher costs for maintenance and repair as well as to higher fuel expenses
- looking for alternatives to replace the traditionally used antifouling systems

Ultrasonic systems are such an alternative and are increasingly adopted by various segments of shipping. Ideally, such ultrasonic systems inhibit the chain of fouling development at the beginning, namely the biofilm.

3.3. Hasytec's DBPi solution

Biofilms are formed when bacteria adhere to a solid surface, and is a prerequisite for later, more developed and harmful fouling stages, *Kelling (2017)*. Addressing biofouling already at the biofilm stage avoids numerous issues with macrofouling, such as the complete capture of removed fouling in cleaning operations to avoid the spread of Aquatic Invasive Species.

Older ultrasound methods followed the idea of getting rid of hard growth which had already attached. Using hard cavitation, this might work in certain situations but may also damage the vessel's steel or coating itself. Consequently, this approach was not accepted by the market. Low-powered ultrasound (avoiding cavitation) destroys the cell structures in biofilm, thus the prerequisite for higher stages of fouling, such as barnacles, shells, and algae. Unlike some coating solutions, ultrasonic antifouling solution are also 100% effective at zero speed, e.g. in longer stays in port or at mooring. Ultrasonic antifouling solutions have enjoyed exponentially growing market acceptance in shipping over the last 5 years. For details, see e.g. *Kelling (2017), Kelling and Mayorga (2020)*.

Fig.8 shows the effectiveness for a smaller workboat, *Kelling (2017)*. Within the CHEK project, the effectiveness of large-scale installations for hull and internal equipment of large commercial ships shall be demonstrated. The effectiveness of these installations shall be increased significantly harnessing the power of Artificial Intelligence.

Fig.8: Tugboat without (top) and with (bottom) ultrasonic antifouling protection

Dynamic Biofilm Protection Intelligent® (DBPi) is the next generation of the multiple award winning Dynamic Biofilm Protection® of HASYTEC, *Kelling and Mayorga (2020)*. DBPi prevents marine growth, biofouling and biocorrosion on all liquid carrying surfaces even more efficiently and at the same follows the current and future demands of the shipping industry.

The underlying process is unique, and the first time AI has been applied to ultrasonic biofouling protection. Each single transducer, Fig.9, measures its own environment at the installation spot, considering all influencing ambient parameters, such as temperature, material and thickness of substrate material attached to, viscosity and temperature of water. Using Artificial Intelligence (namely a trained neural net), the optimum combination of frequency and intensity level is then set. Each transducer adapts itself to the permanently changing conditions, based on the measured parameters.

Fig.9: Transducers   Fig.10: Modular control unit

The integrated USB port allows easy installation of software updates. In addition, all relevant data of the system can be analyzed, driving further development of the DBPi keeping pace with the latest state of the art during the lifetime of the ship. The new hardware design provides the opportunity to upgrade each system to up to 8 transducers, with a maximum cable length of 50 m to each system.

DBPi is the first ultrasonic antifouling technology with type approval by a classification society (Lloyd's Register).

4. Outlook

The CHEK project started in June 2021 and has a planned duration of 36 months. During this time, concept designs will be developed, and performance monitoring will validate expected energy savings of installed devices. The DBPi technology will be installed on various ships, the CHEK project ship type candidates and other customer projects ships. In parallel, work continues on the AI technology inside.

Project progress and insight gained, with particular focus on the ultrasonic antifouling technology, will be disseminated in suitable conferences like this one.

Acknowledgements

References

BERTRAM, V. (2021), *Fuel Options for Decarbonizing Shipping*, 13th HIPER Symp., Tullamore, pp.12-20, http://data.hiper-conf.info/Hiper2021_Tullamore.pdf

BERTRAM, V. (2022), *Capabilities and Limits of Machine Learning,* 7th HullPIC Conf., Tullamore, pp.16-23, http://data.hullpic.info/HullPIC2022_Tullamore.pdf

COLLE, C.; MOROBE, C. (2022), *Saving AI from its Own Hype: Getting Real about the Benefits and Challenges of Machine Learning for Ship Performance Modelling Aimed at Operational Optimizations*, 7th HullPIC Conf., Tullamore pp.198-206,   http://data.hullpic.info/HullPIC2022_Tullamore.pdf

IMO (2001), *International Convention on the Control of Harmful Anti-Fouling Systems on Ships*, Int. Mar. Org., London

KELLING, J.; MAYORGA, X. (2020), *Dynamic Biofouling Protection*, 5th HullPIC Conf., Hamburg, pp.184-187, http://data.hullpic.info/HullPIC2020_Hamburg.pdf

KELLING, J.; (2017), *Ultrasonic Technology for Biocide-Free Antifouling*, 11th HIPER Symp., Zevenwacht, pp.70-76, http://data.hiper-conf.info/Hiper2017_Zevenwacht.pdf

MESBAHI, E. (2003), *Artificial neural networks – Fundamentals,* 39th WEGEMT School OPTIMIS-TIC – Optimization in Marine Design, pp.191-216, http://www.wegemt.com/wp-content/uploads/2019/04/39th_WEGEMT_Summer_School_on_Optimistic_Optimization_in_Marine_Design.pdf

SILBERSCHMIDT, N.; TASKER, D.; PAPPAS, T.; JOHANNESSON, J. (2016), *Silverstream® System – Air Lubrication Performance Verification and Design Development*, 10th HIPER Symp., Cortona, pp.236-246, http://data.hiper-conf.info/Hiper2016_Cortona.pdf

Appendix I: CHEK project partners

The CHEK project partners are:

- University of Vaasa (UV), http://www.uwasa.fi/, is a business-oriented, multidisciplinary, and international university.

- Wärtsilä, www.wartsila.com, is a provider of ship machinery, propulsion and manoeuvring solutions, supplying engines and generating sets, reduction gears, propulsion equipment, control systems, and sealing solutions for all types of vessels and offshore applications.

- Cargill Ocean Transportation, https://www.cargill.com/transportation/cargill-ocean-transportation, is a freight-trading business that provides bulk shipping services to customers across the globe.

- MSC Cruises, www.msccruises.com, is a global cruise line, which is part of the Cruises Division of MSC Group, the privately held Swiss-based shipping and logistics conglomerate.

- Lloyd's Register EMEA (LR), www.lr.org, is part of the Lloyd's Register Group, a global independent risk management and safety assurance organisation that works to enhance safety and improve the performance of assets and systems at sea, on land and in the air.

- World Maritime University (WMU), www.wmu.se, was established in 1983 by the International Maritime Organization (IMO).

- Silverstream Technologies, https://www.silverstream-tech.com/, was established in 2010 and the company specialises in Air Lubrication Technology, Silberschmidt et al. (2016), which is designed to reduce the frictional impact between the flat bottom of the ship hull and water.

- HASYTEC Electronics GmbH, https://www.hasytec.de/, is market leader in ultrasound based antifouling technology.

- Deltamarin, https://deltamarin.com/, is a ship engineering and design company.

- Climeon AB, https://climeon.com/, has well proven technology to convert waste heat to clean power.

- BAR Technologies, https://www.bartechnologies.uk/, have used its in-house tool ShipSEAT to design and optimise their own patented and trademarked wind propulsion system called WindWings, https://www.bartechnologies.uk/project/windwings/.

Application of Virtual Reality Tools in Ship Design

Kenneth Goh, Knud E. Hansen, Perth/Australia, KEG@knudehansen.com

Abstract

This paper reviews the importance of correct visualisation in the design process and limitations of CAD for design review and collaboration. The benefits and requirements that can lead to successful outcomes using Virtual Reality (VR) technology for ship design are discussed. The investigation focuses on implementation and use of Stirling Labs' ShipSpace™ VR visualisation and collaboration tool. Experience gained from using ShipSpace™ in various stages of the ship design process is discussed as is some of the barriers to implementing such ground-breaking technology.

1. Background

Goh and Spencer (2018a,b) investigated the varying ability of people to visualise a ship design by only reading drawings that show views, elevations, and sections. Goh and Spencer conclude that design and problem solving is much better if people can see the design in natural way instead of applying cognitive load to imagining the design. In the following section, the limitations of CAD systems with screen displays for understanding complex 3D models like a ship are described and why the recent advent and application of consumer VR hardware is such a powerful visualisation and communication medium for design and engineering.

1.1. Limitations of 3D CAD as a Visualisation Tool

With the increasing power of digital computing in the last decades, the ability to create more realistic digital virtual representations of the real world and design has developed tremendously. From using computers as a simple drafting tool for traditional 2D drawings, to the ability to created accurate 3D geometrically accurate forms that can be viewed from any perspective, Fig.1, CAD replaced the traditional drawing board in less than a decade.

Fig.1: Computer-generated image of design project based on CAD model

There are dozens of modelling and engineering CAD programs that can create realistic 3D objects and complex virtual environments such as a ship, complete with internal details. While these CAD systems are still needed to create the 3D models and environments, CAD systems with a normal screen display and mouse and keyboard interface cannot themselves be considered as VR and have significant limitations that prevent them from be a useful design communication and collaboration platform.

- Navigation in 3D

  The change between designing in two dimensions to designing in three is quite profound. In 2D design, the concept of up, down, left and right is well established and many of our paper and computer-based tools such as the computer desktop and mouse all are optimised for two-dimensional navigation. Even the computer monitor is a 2D display device. When working in three dimensions, using traditional tools designed for two dimensions becomes clumsy and time consuming. Simply navigating around a three-dimensional environment can be difficult. New devices such a 3D mouse can help, but still required a new skill and a high cognitive load to operate. The difficulty of working in a 3D virtual environment is often reported as a barrier for expanding its use in engineering design.

- Observation in 3D

  The normal method of rendering a three-dimensional environment onto a two-dimensional display monitor is akin to looking at a picture or through a window into another world. This can make understanding the scale and size of objects in complex environments such as a ship's engine room very difficult. When using a CAD system with a screen display the field-of-view (FOV) is generally limited to 30-45° horizontally compared to human eye-sight which has a FOV of about 180°. Projecting a 3D image onto flat 2D screens distorts the view and limits the useful FOV that can be displayed. If the user changes the zoom or FOV, this alters the 3D image and how it needs to be interpreted. As with traditional pictures of objects or environments like landscapes, images on a computer screen need some understanding of the context since the picture is normally smaller than how it would look in reality. There is also no possibility to use human stereoscopic vision when using computer monitors to help understand size and distances.

- Rendering Limitations

  A complete 3D virtual model of a ship with all its internal and external details included is an enormous amount of data, even for modern computing hardware. Since CAD software is optimised for fast editing, it often takes a large amount of time to open a scene or update the image when the virtual camera is moved. This makes CAD systems poor at displaying the fast-changing images and other graphical nuances needed to create the illusion of motion for VR.

1.2. What Is Virtual Reality?

Virtual Reality provides a computer-generated visual experience that tricks your mind into reacting as if you are in a real physical environment, even though you are just seeing a digital virtual construct.

Key aspects of achieving this immersion include:

- Immersive vision – Wide field-of-view, you do not feel you are looking through a window or camera.
- Stereoscopic vision - Both eyes to gauge size and distance as you do in the real world.
- Vision tracking - The view is coordinated with your head movement without noticeable lag.
- Graphical stability - The visual display is smooth, without jerkiness, stutter or drop-out.
- Real world concepts – Notion of up and down is preserved, simulated gravity constraining you onto a surface, etc.
- Interactive - You can interact with the virtual environment.

1.3. Implementing Virtual Reality

Theatre-type single large screen front projection is often used when many people need to view the virtual world. A three-dimensional effect is sometimes provided using shutter or polarised glasses, Fig.2 and Fig.3. This is often proclaimed as VR; however, it is the least immersive because the field-

of-view is limited and cannot be controlled by individual observers. While this form cannot be considered proper VR, it is included so the reader can understand the limitations of the technique.

With theatre projection the perspective is only correct for a single observer position. It is also not possible to understand the size of objects because there are multiple scaling factors such as the size of the screen and distance of the screen to the observer. The technique also usually induces a high degree of motion nausea among the observers because of navigation in the virtual world is controlled by a third person and the aforementioned inaccuracies of the projection. All other observers are 'along for the ride' and quickly leads to motion nausea. Typically, 10-15 mins is people's threshold, or even less if motion is frequent. This makes theatre type VR very limiting as a design collaboration tool.

Fig.2: 3D movie with polarized glasses, source: Wikipedia

Fig.3: 4D visualization hall, *Gaspar et al. (2009)*

Projection caves and domes are also used provide a VR-like experience, but they are very expensive to set up and have significant limitations. In particular, objects in the virtual environment that are close to the observer cannot be displayed or approached as they are removed from the image projection when they 'enter' the cave or dome. This make them particularly unsuitable for human factor engineering which is primarily interested in direct human interaction with the environment. In addition, the view in a cave or dome is correct only for a singular position. If the observer inside the cave or dome only rotates their head the perspective may be correct, however if the user translates their head by leaning from one side to the other or squatting down, the view the observer sees will no longer be accurate. This also means that design collaboration by having multiple observers inside the cave or dome is made more difficult by inaccurate visuals.

Table I: Comparison of Virtual Reality options

	Space required	**Equip. cost**	**360° view**	**Close objects**	**View accuracy**	**Wear -able**	**Motion nausea**
Theatre	Medium	Medium	No	Yes	Low	Glasses	High
Cave & Domes	High	High	Yes	No	Medium	Glasses	Medium
HMD	Low	Medium	Yes	Yes	High	HMD	Low

Virtual Reality is currently best achieved with a Head Mounted Display (HMD), highly accurate positional tracking system and computer software that updates the display as the user moves with sufficient fidelity that the user sustains the illusion that they are immersed in the virtual environment displayed. The high precision tracking of HMDs allows the observer to study objects in VR up close and peer around or under objects. With a HMD the observers perspective of the virtual environment will always be correct regardless of where the objects are or where the observer is looking.

Many early adopters of VR using theatre and cave projection have a poor impression of VR due to the aforementioned limitations of such systems. Regardless of the benefits of HMD type VR, poor software implementation can lead to inadequate graphics performance with stuttering and laggy image display. Many people have been discouraged to use VR as a design tool due to experiencing poor VR implementations.

As with many things new, there is a general lack of understanding of VR technology. People incorrectly identify the HMD as the 'magic' hardware that creates the virtual worlds. What they fail to understand is that the HMD is essentially a dumb display device. Some believe that they can just plug the HMD into any CAD machine and get VR. A powerful computer and well written software are needed to create the 3D graphics at a speed fast enough to sustain the VR illusion. The display for each eye needs to be refreshed at 90 frames per second and the time lag between moving your head and the image updating to match needs to be less than 11 milliseconds.

While the graphical load can be carefully optimised when making a VR game or a training simulation to keep the display fluent, such manual attention would be both time consuming, *Lindenau and Bertram (2003),* and could remove important details from the 3D model. Both are limitations to using VR as a design collaboration tool. For VR to be useful as design tool the ShipSpace™ application must be able to handle massive amounts of 3D information and be clever enough to perform graphical optimisations automatically and to keep the display fluent without losing any detail.

2. Virtual Reality as a Design Tool

The key benefits of VR as a design tool are:

- Most realistic way to experience an unbuilt design without using any physical constructs
- No need to be able to interpret a drawing
- No need to imagine, everyone sees the correct picture
- Reduced abstraction and therefore reduced cognitive load
- Cognition can be applied more productively, ie. solving the problem or improving the design.
- Realistic sense of scale and arrangement
- Sight lines can be checked
- Work areas can be checked
- People can collaborate on the design together even though they may be in different locations
- No need to travel to discuss leads to more frequent communication on design issues
- Experts can more easily add value to the design process

The limitations are:

- Requires a 3D model, can be expensive if not already created in the design process
- Realistic tactile interaction with the virtual environment is limited
- Navigation can be unrealistic (teleporting)
- Poor implementation can cause motion nausea and migraine
- Some people don't like using HMDs, uncomfortable, vanity etc.

Many aspects of ship design can benefit from better communication and collaboration of ideas. The use of VR for human factor engineering and design reviews is particularly useful. Some applications of VR using ShipSpace that have demonstrated to be useful for ship design include:

- Arrangements
  There are many spaces within a ship that demand careful arrangement in the concept design stage. Spaces such as the bridge, operations rooms, galley and messing spaces all require a high level of teamwork and can be tested in ShipSpace™ to ensure optimal functionality. Other spaces, such as engine rooms can be so densely packed with equipment and services, that access for maintenance and removal paths are often compromised. VR can be used to quickly check dimensions, potential interferences and serviceability. Arrangement of mooring equipment, especially with the increasing use of enclosed mooring spaces, can also benefit from using VR for optimisation and validation.

- Sight lines
Sight lines can be accurately investigated using virtual reality, allowing ergonomic and effectiveness optimisation. Traditionally, full-size mock-ups have been used to check arrangement of equipment in the bridge. Such physical constructions, normally inside a large building/warehouse, reveal nothing about the ability to see another vessel sailing in formation, checking visibility while sailing into ports or viewing activities on open deck areas. These aspects can easily be modelled and better checked within a virtual reality environment.

- Launch & Recovery
Small boat and helicopter operations require a high degree of co-ordination and are inherently dangerous for personnel involved. Visibility between various control stations is paramount and can be optimised in a VR environment against ergonomic, technical and other requirements.

ShipSpace™ is a design visualisation and collaboration tool developed by Stirling Labs for use in the maritime and naval design process. ShipSpace™ reads normal CAD files directly and displays the 3D model in virtual reality, complete with all of the detail at very high fidelity. Special techniques are used to maintain rendering latency of less than 11 ms so that immersion is maintained, and surfaces and light are treated carefully to create a strong sensation of presence. ShipSpace™ provides a range of sophisticated tools to interrogate the model in various ways, such as reading metadata, Fig.4, "x-ray vision", controlling object layer visibility, measuring distances, Fig.5, and many others. The tool enables up to 64 users to collaborate in the same virtual space.
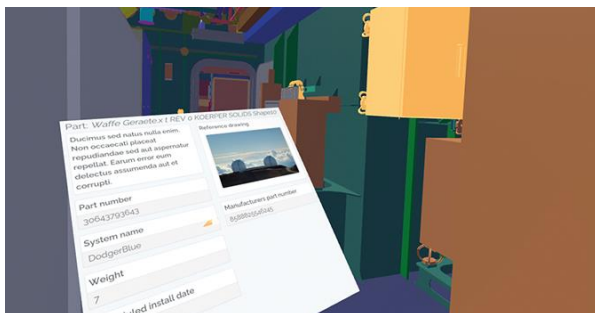
Fig.4: ShipSpace™ reading metadata

Fig.5: ShipSpace™ measuring distances

3. Virtual Reality in the Ship Design Process

3.1. Sales

The purpose of using VR for sales should not be underestimated. In projects past, it is often a single well executed artist impression or a scale model, Fig.6 (left), that has been the driving vision for a new project be it a ship, aircraft, or building, such is the power of visualisation. This inspiration is needed to garner support and ultimately funding for any undertaking of significance such as a new ship. As noted above, the use of computer-based 3D models, Fig.6 (right), has largely replaced the traditional work of artists and model makers.

Fig.6: Scale models (left) have been largely replaced by 3D computer generated images (right)

Typically, any existing 3D models built for exterior renders can be viewed in VR using ShipSpace. Often some additional interior rooms of interest such as the bridge will also be modelled to provide a more interesting experience for the viewer. These models are accurate in layout and arrangement but lack any proper engineering details such as the structural elements, piping and so forth. Even equipment arrangements such as navigation consoles and furnishings will be notional as opposed to accurate or final. The idea of the sales model is to give an overall impression of the vessel with realistic details without the details being fully resolved at that stage. This is also a fundamental aspect of the concept design which will be discussed next.

The use of VR for sales has been the easiest and most natural implementation of this new technology. Users are almost always keen to experience the design in VR. Initially this is partly due to the novelty of using VR, which is still only a few percent of the general population. However, users are then overwhelmingly astounded by the realism of the experience. In most cases, new users are in a state of disbelief. The visual accuracy of the ShipSpace™ VR experience is so compelling that their brain is being fooled. New users often reach out for handrails that they see in VR when approaching the side of a deck, or duck under low overhead objects. This demonstrates that the level of realism provided by the ShipSpace™ VR tool is so convincing that the amygdala, the small part of the brain that provides survival instincts, is over-powering the front cortex, the large part of the brain responsible for reasoning and higher cognitive functions.

3.2. Concept Design

While the 3D models built for sales use are based on the concept design, implementing VR in the actual process of developing the concept design is a different matter. Developing a concept design requires people with good visualisation and imagination skills because they are creating something new. Convincing these people that they need VR tools to help with their concept design can be challenging. The common objection to using VR for concept design is the time-consuming need to create a 3D model in the first place.

The concept design phase can be a very fluid process with arrangements, superstructures, and hull forms changing constantly. Good concept designers have a very high level of ship knowledge and are highly adapt at understanding how various design changes will affect other aspects of the design. Currently the methods and tools for creating 3D models can be too time consuming to be useful for concept design. Compounding the problem is that the concept design is generally developed by individuals whose core competency does not include construction of 3D models. This is changing, however; particularly younger designers are recognising the benefits of VR and subsequently are more willing to create the 3D models necessary.

Knud E. Hansen has also experienced good use of 3D models and VR in developing concepts in validation of designs. For example, utilisation of hull spaces where waterlines change rapidly in the fore and aft ship can be evaluated in VR, once the hull stability model has been developed. Sightlines from the bridge to working deck areas can be quickly validated or tweaked once the 3D exhibition model has been developed. This tends to come later in the tender and contract phase of the project, when it is important to check carefully aspects of the design.

3.3. Basic Design

In the basic design phase of a vessel, the general arrangement of the vessel is agreed, and the most important aspects of the ship design are the development of the structure of the vessel and arrangement of main machinery spaces. In this phase, structure and equipment need to come together in a convolution of either connection or avoidance of one another. Equipment such as engines and shaftlines need to marry to structural foundations while having sufficient clearance for access and maintenance. Piping and ductwork need to snake through girders and deck penetrations to be sure the design can be made to work when it comes to the detail design. Many of the experience-based dimensioning and space estimations need to be verified in the basic design.

In this phase of the project, the benefits of the ShipSpace™ VR tool are obvious. As the structural model is being developed in 3D, equipment can be easily added to the model, Fig.7. Naval architects and engineers then can experience the developing design in VR to better resolve interface and clearance issues. Arranging equipment and reticulating piping in an engine room is a complex three-dimensional puzzle. The benefit of using VR is that it is much easier to use your intuition since you are experiencing the design as if it was already built. The advantage of naturally changing your viewpoint in ShipSpace™ VR by moving your body and head as you would in real life makes evaluating the design much easier, quicker, and more thorough. Users appreciate that everything they see is correct in scale and perspective.
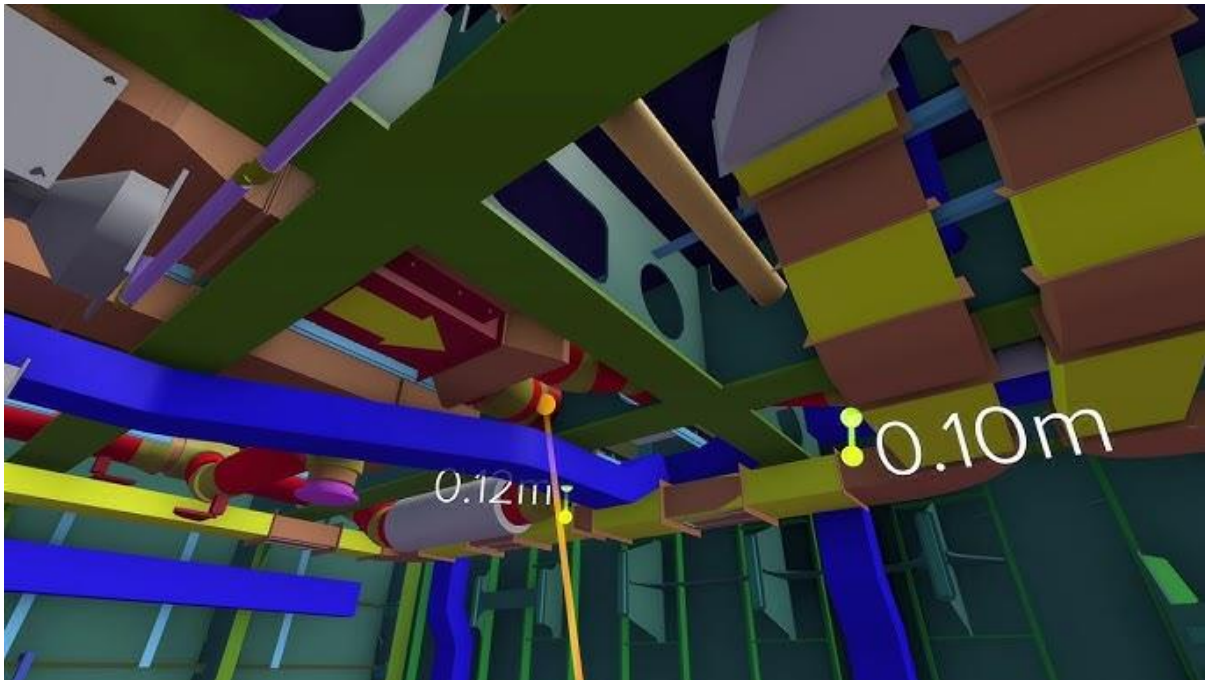
Fig.7: ShipSpace™ allows easy addition of equipment to the structural model

It is often commented by people who have used ShipSpace™ and gone back to using a computer monitor for viewing a 3D model, that it feels like they are just looking through a camera or window. It is not possible to understand the size and scale of the 3D model on a monitor. The control of the viewpoint is also unnatural and can quickly induce nausea, especially on larger screens.

Class Societies are moving increasingly towards using 3D models in the approval process, e.g. *Son et al. (2022)*. The use of VR tools and the natural way the design can be understood and communicated can only aid the process. Furthermore, the ShipSpace™ VR system enables up to 64 simultaneous users in the same VR session. As a designer, being able to collaborate with Class experts inside the 3D model, as if it was already built, will lead to faster and easier resolution of many design issues. We look forward to an opportunity to trial such a system with Class.

3.4. Detail Design

One of the great benefits of using VR tools in the detail design phase is the ability to find and resolve clashes. Typically, during the detail design process, many people are involved with developing the piping and cabling routes from schematic or single-line drawings. A preliminary space reserve or 'space grab' is often modelled by experienced designers as a first step before detail designers follow or trace over with the final pipe spool design complete with joining flanges, valves, filters, and other elements that could be in the pipeline.

Despite the initial space reserve planning, invariably clashes (interference between two or more objects that could not exist in the real world), occur in the detail design process that need to be resolved

or deconflicted, Fig.8. Furthermore, even if there are no clashes, the design must be checked for 'buildability' by experienced production personnel and possibly modified to ensure that it is possible to construct and install.
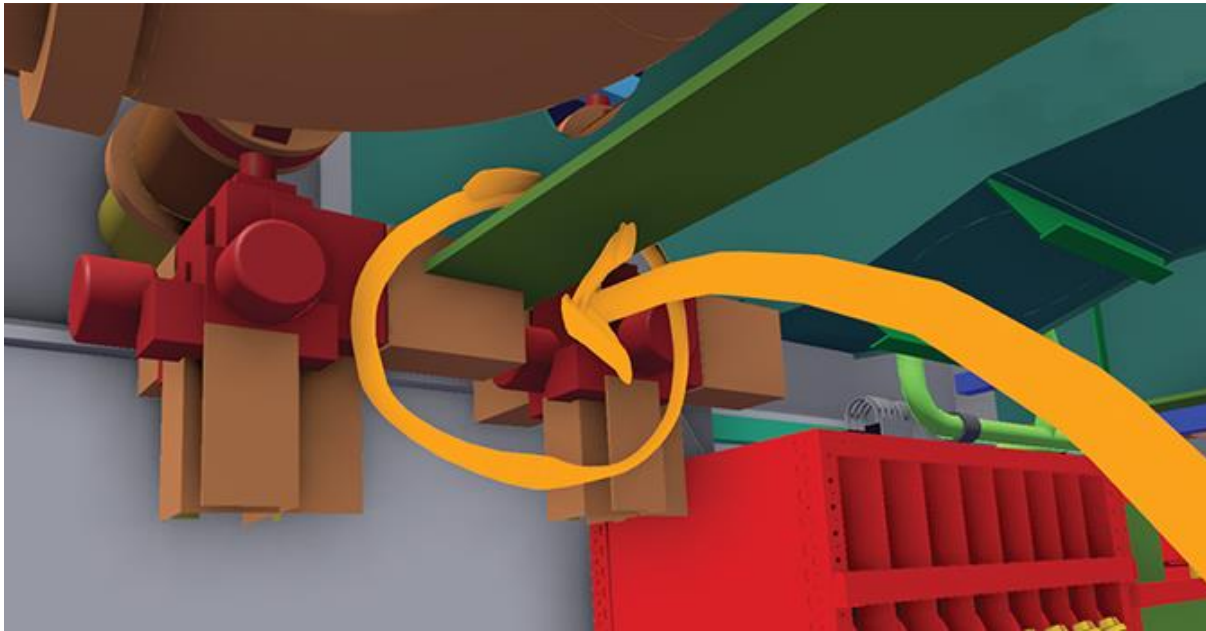
Fig.8: Use of the paintbrush tool allows marking up proposals, changes and/or corrections directly in the design

The current method of checking for clashes and buildability is to use a CAD system or 3D model viewing application on a screen display. Most CAD software has built-in clash detection; however, such checking can often be flawed because many correct instances are flagged as clashes. There is also no capacity to check for buildability, such as the situation where there is no clash, but insufficient space has been allowed for installation or disassembly.

I haves experienced on many occasions finding significant clashes while examining a model using the ShipSpace™ VR tool and having great difficulty finding the same clashes using a traditional CAD system and a screen display. I suggest that a VR Head Mounted Display (HMD) is much better than a screen simply because users are able to take in so much more of the environment at any given time. When using a CAD system and screen display the field-of-view (FOV) is limited to 30-45° horizontally. A consumer VR HMD has a FOV of typically 110°. This amounts to 5 to 10 times more viewable area when considering a 2:1 horizontal to vertical FOV ratio.

The natural way in which the HMD user changes their viewpoint, by moving their head and body like in the real world, also seems to allow much faster and effective interrogation of the digital environment compared to the typical hand operated mouse interface of a CAD and screen display system.

In my observation, one barrier to using VR in detail design is actually the shipyard. Once in contract with the Owner, the last thing the shipyard wants is any change to the detailed design. Using VR tools that provide the Owner with better understanding of the design increases opportunities for Owners to make changes which is not in the interest of many shipyards whose primary concern is staying on schedule. Changes, regardless of variation costs, will always put pressure on the schedule. Some shipyards only begrudgingly provide Owners access to the 3D model for the same reasons or delay access until it becomes difficult to make any changes to the design because the module is already in production.

Another issue is that multiple types of 3D models are used throughout the design process. There is sales and concept model, a FEM model, a detail design model etc. Each type of model is suited to a

different stage of development. For example, for concept design the 3D model must be very easy and fast to construct and modify. However, for detail design the 3D model must be configured to work with the other production systems in the yard, such as the parts database and plate cutting machines. If the yard has been contracted to develop the design from the concept stage this could be less of problem.

4. Conclusion

Good spatial skills and high cognitive loads are required to imagine and interpret drawings into mental images that are useful for solving design problems or optimising solutions. The notion of virtual reality, its benefits for design and the requirements to effectively deliver a VR experience were presented. VR removes the need to use cognitive load for visualisation and imagination and allows users to apply their thinking to solving design problems. Subject matter experts who may not have good visualisation skills can more easily contribute to the vessel design.

A number of case examples demonstrate how naval architects, engineers, designers, and operators are using the ShipSpace™ VR tool to assist in many phases of the design process. Although the overall benefits of VR are not in question, there are barriers and resistance to using VR tools similar to the introduction of any revolutionary new technology.

References

GASPAR, H.M.; TANIGUCHI, D.; RUOCCO, P.; NISHIMOTO, K. (2009), *A real-time 3d post-processor for a numerical model-basin simulator,* 8th COMPIT Conf., Budapest, pp.512-524, http://data.hiper-conf.info/compit2009_budapest.pdf

GOH, K.; SPENCER, R.J. (2018a), *Virtual Reality for Design of New Warship Concepts*, RINA Warship Conf.: Future Surface Vessels, London

GOH, K.; SPENCER, R.J. (2018b), *Virtual Reality for Human Factor Engineering*, RINA Human Factors Conf., London

LINDENAU, O.; BERTRAM, V. (2003), *The making of a VRML model for an SES with streamlines and pressure distribution*, 2nd COMPIT Conf., Hamburg, pp.5-14, http://data.hiper-conf.info/compit2003_hamburg.pdf

SON, M.J.; SEPPÄLÄ, T.; MERIKANTO, J.; AAE, O.; ASTRUP, O.C. (2022), *Utilization of OCX as part of 3D model based approval in ship design process,* 21st COMPIT Conf., Pontignano, pp.258-272, http://data.hiper-conf.info/compit2022_pontignano.pdf

Metal Foams – Ready for Shipbuilding?

Thomas Hipke, Fraunhofer Institute for Machine Tools and Forming Technology,
Chemnitz/Germany, thomas.hipke@iwu.fraunhofer.de

Abstract

The paper presents the development of metal foam for the powder metallurgical route. The overview will cover some highlights in research and development, in manufacturing and the application side. In the last years some new real applications have been coming up in the fields of automotive, railway, ship building, machine tools and for design purposes. But the numbers of parts manufactured to date is relatively low. The main reasons are the high processing costs. In shipbuilding, the paper will show some interesting projects from "Bioship" to "Watertruck". In these projects, metal foam sandwiches (SAS) bring a great lightweight reduction potential, in some cases up to 25% in same cases.

1. Introduction

The Fraunhofer Institute for Machine Tools and Forming Technology (IWU) is an institution of the Fraunhofer-Gesellschaft zur Förderung der angewandten Forschung e.V., founded in 1991. The Fraunhofer IWU is a research and development partner of industry. In this way, innovative solutions can be created for continuous process chains from components to assemblies to complex machine systems. Lightweight structures and the use of new materials play an essential role.

Lightweight materials, especially aluminum foams and fiber-reinforced plastic composites (FRP), are the focus of the research work of the Fraunhofer IWU's "Functionally Integrated Lightweight Construction" department. The department is home to the three working groups "Metal Foam", "Battery Systems" and "Pultrusion".

In collaboration with steel, aluminium foam is perfectly suited for lightweight design – in particular as sandwich structure with cover sheets, Fig.1. Such sandwiches are highly versatile and convince due to their excellent properties.

Fig.1: Example of a steel-aluminium foam-steel sandwiches with overall thickness of 35 mm (3/29/3) (left) and different samples (right)

These properties make them also ideal for selective applications in shipbuilding industry:

- high bending stiffness with low weight,
- effective shielding against electromagnetic waves,
- fire resistance,
- acoustic insulation,
- energy absorption, and
- vibration reduction.

2. Projects relevant for shipbuilding

Fraunhofer IWU has extensive experience in the development and manufacture of lightweight materials and assemblies. Knowledge on the subject of lightweight construction in shipbuilding was acquired primarily in three major joint projects:

- MESCHLAS - Joining of large metal foam sandwiches in ship structures using laser welding
  - The main area of application for the new developments is highly stressed ship structures and ship structural components, such as engine foundations, rudder structures, or safety doors. In conjunction with laser welding technology, which is already well established in shipbuilding, it is possible to produce large lightweight structures, such as those commonly used in shipbuilding, in a rational and economical manner.
  - BMBF-joint project
  - Duration: 01.12.2009 – 31.05.2012

- ULIVES - Ultralight Materials for Ice Going Cargo Vessels
  - Transfer of innovative lightweight construction concepts to the internals and superstructure of a ship and development of approaches for significant mass savings. Consideration of new material concepts, such as aluminum foam with aluminum cover sheets and PUR foam with GFRP deck layers.
  - The aim of the project was to drastically reduce the ship's mass. Implemented lightweight design concepts enabled an increase in payload and thus in transport efficiency. In the long term, benefits can be achieved for both shipyard and ship owners.
  - MARTEC – Maritime Technologien as ERA-NET, Project sponsor Jülich
  - Duration: 01.04.2009 – 30.06.2012

- WATERTRUCK
  - Transfer of innovative lightweight construction technologies to cargo ship 'Watertruck', which can self-discharge due to on-board crane.
  - BMWi-joint project
  - Duration: 01.12.2015 – 31.05.2019

2.1. MESCHLAS

MeschLaS was basically about producing large sandwich composites and joining them with laser welding. Here, TKMS Blohm + Voss Nordseewerke GmbH and the Laserzentrum Hannover e.V. joined forces. The aim was to develop a lightweight construction method for highly stressed ship structures and ship structural components such as engine foundations or rudder structures by producing large steel-aluminum foam sandwiches. As a result of the project, the demonstrators "gear foundation" and "rudder structure" were produced on a scale of 1:1, Figs.2 and 3.

2.2. ULIVES

The aim of Ulives was to reduce the ship's mass and increase transport efficiency through innovative lightweight design concepts for the internals and superstructure of a ship using new material concepts. It was to be implemented on a transport ship for wood chips in Finnish domestic transport, Fig.4.
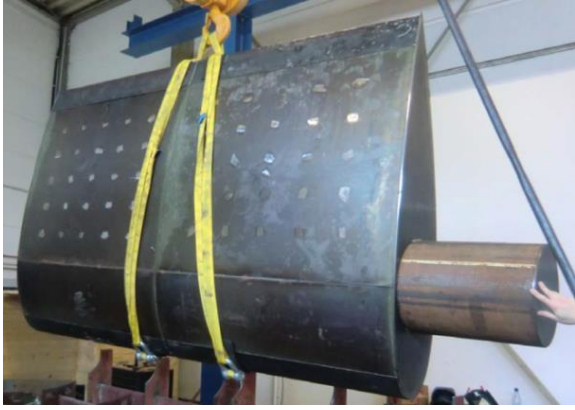
Fig.2: Project demonstrator "Rudder",
22% mass reduction

Fig.3: Project demonstrator "gearbox foundation",
20% mass reduction
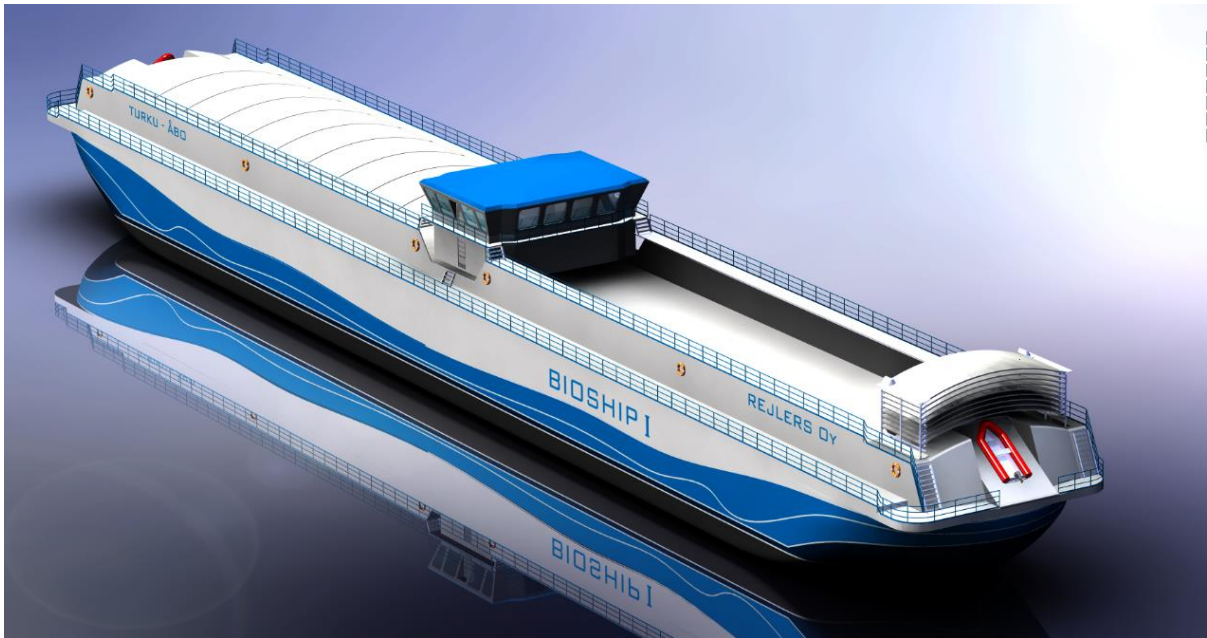
Fig.4: Vision of Laffcomp Oy's first barge to be made entirely of metal foam, "Bioship I"

Fig 5: Demonstrator, scale 1:4., full view (left) and detail (right)

Proof of feasibility was provided by a single segment with original dimensions of 5 m x 7 m x 10 m (length x width x height), which was built to a scale of 1:4, Fig.5. The hull below the waterline was conventionally designed with 10 mm thick ship's steel due to the required ice-going ability. Sandwiches of steel-aluminum foam steel (SAS) were used for the stabilizing longitudinal and transverse frames inside the ship.

2.3. WATERTRUCK

The long name of the project is "Lightweight inland vessel for container transport with the ship's own handling system for loading and unloading without port infrastructure". The project highlights the particular challenge of building a ship with a crane that is nevertheless lighter than the before.

The R&D objectives of the joint project resulted from the conditions of container inland waterway transport, such as the low draught, limited passage heights and economic minimum loads, as well as from the just-in-time requirements of container handling.

The realization of the project objectives required the fundamental development and investigation of innovative super-lightweight structures for a flat-bottomed inland container ship with utilization of the ship's hold for container cargo as well as a lightweight, on-board handling system and the ship stabilization system necessary for its operation to ensure economic performance while accommodating considerable additional functions and resulting loads.

Based on the functional requirements for the WATERTRUCK ship and the results of the analysis of potential areas of application, a container barge (ship type Johann Welker) with a length of 85 m, a width of 9.5 m, a maximum draught of ~2.5 m and a deadweight of ~440 t was developed. This has a 61.3 m long and 7.7 m wide hold and thus a container loading capacity of 90 TEU or 45 FEU, Fig.6.
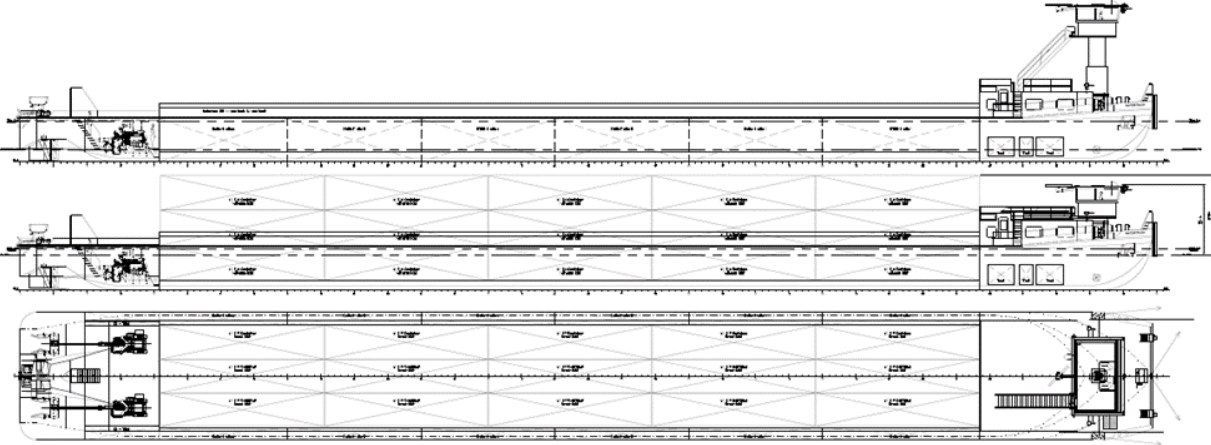
Fig.6.: WATERTRUCK concept with crane – ship type Johann Welker (class IV)

In order to reduce the weight of the ship's structure, various lightweight measures were investigated with regard to their applicability and effectiveness. As a result of the investigations, a lightweight hybrid design of the ship's hull was developed using innovative sandwich materials (steel-aluminum foam sandwiches), Fig.7. These are used in the ship's inner hull, i.e. in the hold floor and hold side areas, and their significantly higher bending strengths enable stiffening components such as stringers to be reduced, resulting in significant reductions in material and manufacturing costs. Overall, it was possible to achieve a weight reduction of ~22% compared with a steel structure and thus create the basis for absorbing the loads resulting from the on-board handling system.

Feasibility of production and the realization of the functional requirements were successfully demonstrated in the course of demonstrator production and testing, Fig.8.
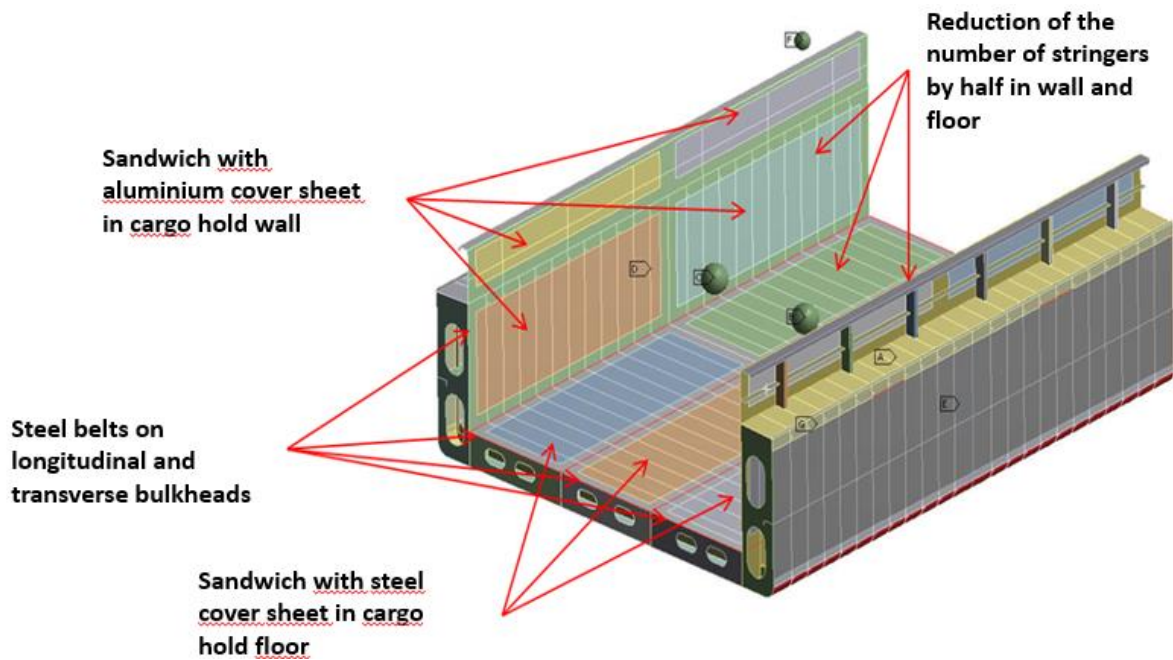
Fig.7: Lightweight construction measures to reduce the weight of the WATERTRUCK hull

Fig.8: Demonstrator section to prove technical feasibility of concept

3. Conclusion

Several projects have demonstrated that the weight reduction in ship structure of 20-27% can be achieved using metal-aluminium foam-metal sandwich panels. The advantages are a lower draught and/or a higher payload by the saved mass.

However, these sandwich panels are also more expensive than normal steel. An economic efficiency calculation is therefore always advisable before starting the project, looking at lifecycle costs of the ship.

References

HIPKE, T.; LANGE, G.; POSS, R. (2007), *Taschenbuch für Aluminiumschäume*, Aluminium-Verlag

KRÄUSEL, V.; THÜMMLER, R.; KAUFMANN, P. (2007), *Entwicklung großformatiger Stahl-Aluminiumschaum-Sandwichelemente und Stahlblech-Hüllelemente für den Einsatz in temporären Bauwerken*, 3. Landshuter Leichtbau-Colloquium, Landshut, pp.225-238

On the Determination of the Relative Wave Direction based on Measured Ship Responses using Deep Multi-Task Learning

Malte Mittendorf, Technical University of Denmark, Kgs. Lyngby/Denmark, mamit@dtu.dk
Ulrik Dam Nielsen, Technical University of Denmark, Kgs. Lyngby/Denmark, udni@dtu.dk
Harry B. Bingham, Technical University of Denmark, Kgs. Lyngby/Denmark, hbbi@dtu.dk
Gaute Storhaug, DNV, Høvik/Norway, gaute.storhaug@dnv.com

Abstract

In the present study, a Panamax container vessel sailing in the Northern Atlantic is taken as a case study. Deep neural networks are trained on results of cross-spectral analysis of 6-DOF accelerations to predict significant wave height, peak period, and relative wave direction, which were initially derived from measurements of an X-band wave radar. Both an Inception network and a residual network are compared. Overall, it is found that the vector decomposition of the relative wave heading shows superior prediction accuracy in contrast to other methods from state-of-the-art literature. Several possible extensions of the presented methodology are pointed out.

1. Introduction

Real-time monitoring of the ambient wave environment is indispensable for safe and intelligent ship navigation, in order to mitigate maritime accidents, such as container losses, and enhance the energy efficiency of ship operation simultaneously. As a result, research efforts have been invested in the realm of ship-based sea state estimation, i.e. exploiting the wave buoy analogy. The concept allows the mathematical inverse mapping from measured ship responses to the governing wave energy density spectrum. The fundamentals of the wave buoy analogy are described in detail in *Nielsen (2018).* Most past methods rely on ship motion transfer functions or RAOs (Response Amplitude Operators). *Nielsen (2017)* provides an extensive review of methods for *model-based* onboard sea state estimation. However, the presented algorithms are greatly dependent on both the reliability and, obviously, the availability of accurate transfer functions. The degree of accuracy may be improved by correction methodologies, as described in *Nielsen et al. (2021),* i.e. calibration of RAOs according to in-service motion and wave hindcast data. Still, detailed hull shape information is scarce in ship operation and hence the number of studies pertaining to machine learning (ML) based sea state estimation has been increasing over the last couple of years. One clear advantage of ML driven studies is their independence of RAOs, i.e. they are *not* model-based.

Irrespective of the approach, the estimation of the relative wave heading β needs special attention, due to (1) the circular ambiguity, (2) the fact that β is a function of phase differences of the individual responses and (3) that an asymmetric response has to be considered, in order to distinguish between port and starboard wave directions, *Nielsen (2006)*. *Åvist and Pyörre (2013)* employ non-parametric regression methods, i.e. MARS (Multivariate Adaptive Regression Splines), and a random forest regressor for the prediction of significant wave height and encountered wave direction based on features obtained from spectral analysis of actual in-service data from a container ship. Their study showed sufficient accuracy for significant wave height; however, the predictions of the relative encounter direction showed large scatter and uncertainty. *Mak and Düz (2019)* trained deep neural networks on 2.5 minute time sequences of motion recordings obtained on a frigate-type vessel and wave parameters measured by a X-band radar. In their work, they apply the hyperbolic tangent (*tanh*) function as the activation function of intermediate (hidden) layers and the output layer. In general, they come to similar conclusions as *Åvist and Pyörre (2013)*, i.e. the prediction of the relative wave heading β is of higher complexity than correctly estimating the content and distribution of energy in the wave spectrum characterized by, say, H_s (content) and T_p (distribution). In an extension, *Düz et al. (2019)* applied transfer learning for sea state estimation, i.e. they pre-trained an initial model on simulated data and retrained it on actual in-service measurement data. *Mittendorf et al. (2022b)* provide approaches in both the time and frequency domain, based on simulated data of a container vessel in unimodal and

unidirectional sea states. The frequency domain model is trained on spectral moments of the auto cross response spectra as well as the peak spectral ordinates and the corresponding peak frequencies obtained from the off-diagonal cross response spectra. In doing so, the phase interactions are preserved in the frequency domain, as the cross-correlation of the individual ship responses is determined. Overall, the time domain models showed higher accuracy in case of the wave heading in contrast to the model based on spectral moments, but at higher computational cost. The time domain approach is based on raw heave, pitch and roll time series and the residual network stood out in terms of accuracy. In case of the relative wave heading, no dedicated transformation has been applied. *Kawai et al. (2021)* provide also a study using simulated data for the prediction of multiple parameters of an Ochi-Hubble type spectrum, i.e. for possible application in multi-modal sea states. The key aspect of their work is the use of sequences of spectral ordinates from cross-spectral analysis as input to a convolutional neural network. Moreover, the encountered wave heading was decomposed into its vector components, i.e. *sin(β)* and *cos(β)*.

From the presented literature, it stands out that different approaches towards the accurate determination of the encountered wave heading have been studied, but no rigorous comparison has been made until now. Thus, the goal of the present paper is to investigate the effect of several treatments of the relative wave heading on the prediction accuracy of all three sea state parameters. Both *Mittendorf et al. (2022b)* and *Kawai et al. (2021)* employ multi-output-regressors and, thus, the prediction of all three targets, i.e. H_s, T_p and $β$, is interrelated, which reflects also the underlying physics. The presented ML-driven system identification approach is carried out in the frequency domain using 25 min. samples of 6-DOF acceleration data and based on multi-task learning.

2. Data processing

In this section, the case ship is introduced, and the filtering techniques are presented. The data acquisition as well as its preprocessing is described in a detailed manner in *Mittendorf et al. (2022a)*. The case ship of the present work is a Panamax container vessel, which was built in 1998 and has a capacity of 2800 TEU. The data acquisition period took place between August 2007 and March 2009. Its main particulars are presented in Table I and the recorded GPS position is depicted in Fig.1.

Table I: Main particulars of the case study, cf. *Storhaug et al. (2007)*

Dimension	Unit	Magnitude
L_{pp}	[m]	232.0
B	[m]	32.2
T	[m]	10.78
C_B	[-]	0.685

In view of Fig.1, it is appreciated that the vessel traded in the Northern Atlantic between Western Europe and Canada in the investigated period. Moreover, the effect of seamanship as well as weather routing stands out, as multiple routes deviate from the shortest path, e.g. in one particular case the ship sails around the British islands to avoid severe weather conditions. In addition, uncertainties related to the vessel's position are observed in Fig.1 in the region of the St. Lawrence River and Newfoundland. *Ikonomakis et al. (2022)* elaborate on possible errors in the GPS positions of vessels and suggest several correction methods. It is evident that the vessel frequently sails in restricted and coastal areas. In order, to filter for shallow water influence and possible refraction from the coastline, the dataset has been filtered according to geographic thresholds imposed at -55 and -5 degrees of longitude. Moreover, we filter for forward speeds U<5kts, in order to disregard samples possibly influenced by maneuvering. It is stressed that U corresponds to SOG (Speed Over Ground) as the ship speed has been determined by GPS data.
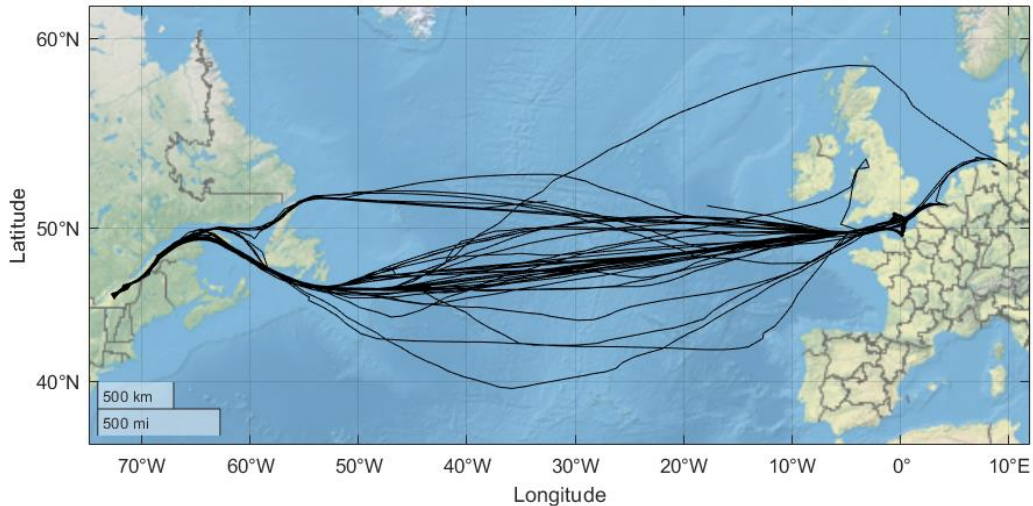
Fig.1: Display of the GPS position history of the midsize container vessel in 1.5 years

Ocean waves are completely characterized by a directional spectral density function $E(\omega,\mu)$. It is noted that E is dependent on the angular wave frequency $\omega=2\pi f$ [rad/s] and the direction of single waves μ [rad]. The container vessel was equipped with an X-band wave radar manufactured by Miros. The so-called Wavex (Wave Extractor) wave radar provides samples of E in a 30 min interval based on one minute sample periods. In this work, we parameterize the information contained in E using the methodology described in *Longuet-Higgins et al. (1963)*. The result of the analysis are three parameters: H_S, T_p and β. The corresponding histograms – including U – are presented in the following figure.
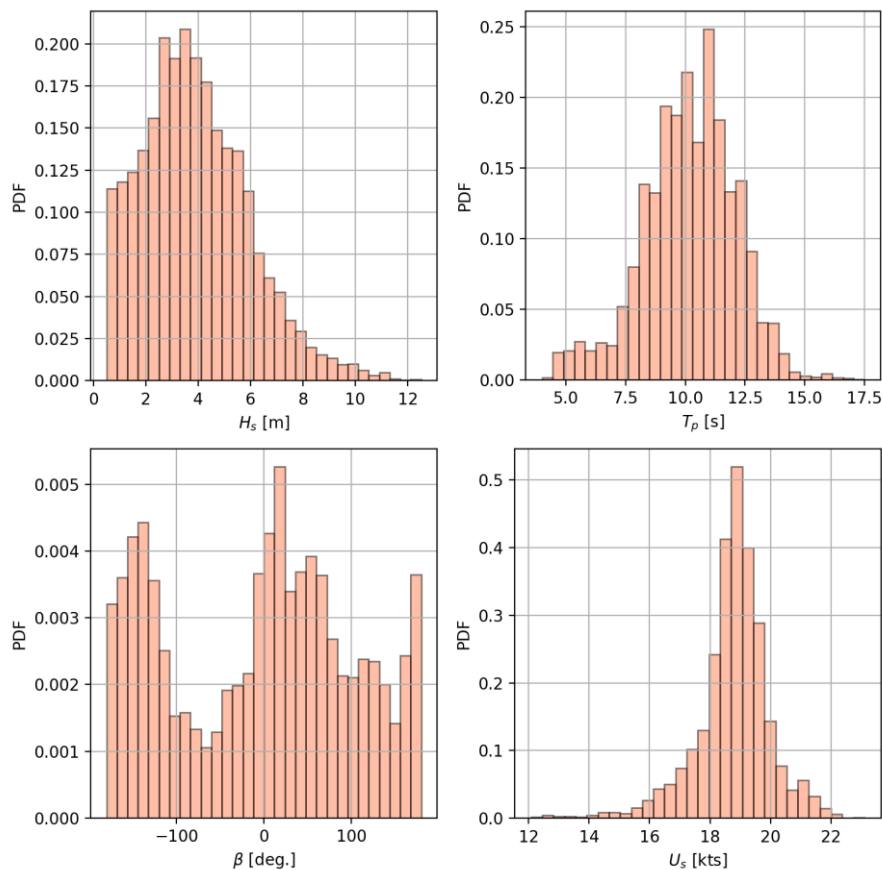
Fig.2: Distributions of the encountered significant wave height, peak period, relative wave direction and forward speed (upper left to lower right)

As can be seen in Fig.2, the container vessel encountered severe sea states in the Northern Atlantic and the H_s histogram follows – as expected – an exponential distribution. Moreover, it appears that samples $H_s<0.5$ have been filtered due to reduced accuracy of wave radars in this regime and due to the negligible vessel response in very low sea states. In addition, it is visible that the case ship underwent harsh sea states in spite of weather routing and seamanship. The peak period T_p shows a symmetrical distribution and is centered around 10s. Often, the Northern Atlantic characterized by winds coming from a westerly direction. This can clearly be seen in the multimodal distribution of the relative wave heading β. It is noted that |180| deg. indicates head waves, whereas 0 deg. stands for following waves. The ship experiences predominantly head and following waves due to alternating easterly and westerly passages. As a side note, the reported accuracy of the wave radar for all wave parameters is in the range of ±10%, *Miros (2017)*. The advance speed U of the case study is centered around 19kts and both the voluntary and involuntary speed loss due to wave impact may be reasons for the stochastic distribution of the advance speed.

The vessel's motion response has been recorded by an MRU (Motion Response Unit) located 78.5m forward of the aft perpendicular (AP), 11.7m above base line (BL), and at the centerline (CL). The MRU was installed in a socket filtering noise in the range of 50-100Hz resulting from thrusters, pumps and other machinery. In a few cases, samples with unrealistic impulses had to be filtered manually. The raw acceleration data was measured in 20Hz, but has been resampled to 5Hz and stored in 25 min. samples for all 6-DOF. The procedure of synchronizing wave radar and MRU data as well as filtering leads finally to 4779 valid samples. According to sensitivity studies in *Mittendorf et al. (2022a)*, 25 min. sequences of 6-DOF accelerations were processed by cross-spectral analysis. This leads to an $N \times N$ complex-valued matrix, where N is the number of the considered DOF. It is stressed that only one side of the off-diagonals are taken into account, as the matrix is complex conjugate symmetric. Ultimately, a matrix of shape 36×64 is fed into the model as input. Thereby, it is understood that 64 discrete spectral ordinates are extracted from 6 real-valued auto cross response spectra and 15 complex-valued cross response spectra, from which the imaginary and real parts were treated separately. As a side note, the wave radar provides data at time t_{radar} and we chose the starting point $t_1 = t_{radar} - 25$min in case of the acceleration data for consistency reasons. Moreover, due to the exponential distribution, the significant wave height has been transformed by the logarithm before normalization in order to force a more symmetrical shape onto the distribution. Both input and targets were normalized, since neural networks are not scale-invariant. Lastly, the dataset is split into training and validation set, where the latter makes up 20% of the total. In the paper of *Mittendorf et al. (2022a)*, the spectral approach was compared to a time domain approach using 5 min. time series samples and it turned out that the former methodology is characterized by higher computational efficiency, accuracy and robustness.

3. Methodology

Machine Learning is increasingly applied in general ship hydrodynamic problems including the field of sea state estimation. In theory, artificial neural networks are inspired by the underlying principles of dendrites in mammalian brains, *Goodfellow et al. (2016)*. The mathematical learning algorithms are employed as universal function estimators, because stacking of affine functions, i.e. matrix operations, and non-linearities, i.e. activation functions, lead in theory to the universal approximation theorem. A traditional neural network comprises three layers: An input and output layer as well as a hidden layer and is therefore considered as a composite function. In the last couple of years, deep neural networks (DNN) – neural networks with more than one hidden layer – have emerged in the machine-learning field achieving impressive performance in a vast variety of tasks.

Mitchel (1997) defines machine learning as the following: "A computer program is said to learn from *experience* E with respect to some class of *tasks* T and *performance measure* P , if its performance at tasks in T , as measured by P, improves with experience E." In order to turn this abstract definition into a more tangible one, the problem at hand is used for clarification: The task T is considered as a multidimensional regression problem. In other words, the learning algorithm – here a deep neural network – is asked to approximate the function $f: \mathbb{R}_n \rightarrow \mathbb{R}$ and the output consists of multiple continuous variables. The supervised machine-learning algorithm experiences E, a dataset, where an

input tensor *X* is associated with a known output vector *Y*. The employed performance measure P is specific to the task T and in this case, the mean squared error (*MSE*) is applied as loss function. Multi-Task Learning (MTL) is considered as parallel transfer learning and has been initiated by *Caruana (1997)*. In the case of MTL, each output is considered as a *separate task*. Hence, each task has its own fully connected hidden layer(s) and output layer. In the present models, two hidden layers with 100 and 50 neurons make up each of these separate estimators. The different output branches share the same input and feature processing architecture, hence a hard parameter sharing approach is taken, which reduces the danger of overfitting immensely according to *Ruder (2017)*. The overall concept of the chosen MTL strategy is depicted in Fig.3. *Mittendorf et al. (2022a)* showed empirically that the MTL approach outperforms procedures using a single output vector. It is stressed that all output layers are activated by the linear activation function – as it is typical for regression. The global loss function is calculated as the sum of the local loss functions from all three branches.
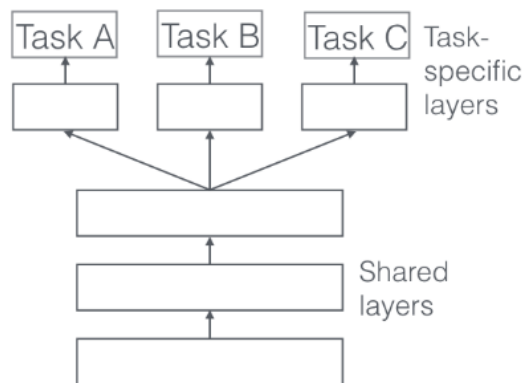

Fig.3: Concept of hard parameter sharing according to *Ruder (2017)*

The focus of the present paper is solely on Deep Learning (DL) architectures due to their capability of handling high dimensional input tensors and their ability of implicit feature construction, i.e. generating meaningful data *themselves*. Other advantages of deep architectures over traditional machine learning algorithms include better scalability as well as increased generalization capability by transfer and multi-task learning. One key problem has been most influential on the development of methods and architectures in deep learning: The occurrence of vanishing/exploding gradients during training. Very broadly speaking, the performance of DNNs is a function of the number of hidden layers. However, with an increasing number of layers, the risk of vanishing gradients rises. The trainable parameters of a DNN are free variables under backpropagation in a gradient-based optimization problem of an arbitrary loss function. With more hidden layers, however, the magnitude of the gradient, i.e. the influence on parameter updating, reduces. This is mainly attributed to "legacy" activation functions, such as the *tanh* or sigmoid functions, since they force the input into a narrow number space and thus a huge change in the input leads to a small one in the output. With an increasing number of hidden layers, the magnitude of the gradient vanishes. The activation function Rectified Linear Unit (ReLU = max(0, x)) not only decreases the chance of vanishing gradients, but also speeds up the training process, as it is faster to differentiate. Batch normalization as well as advanced architectures, such residual networks by *He et al. (2016)* were proposed for mitigating the occurrence of vanishing gradients. Additional to the vanishing problem, the increased computational effort for training as well as the proclivity of overfitting on small datasets are other drawbacks of deep learning. The theoretical intricacies of deep learning are provided in *Goodfellow et al. (2016)*.

In this paper, the residual network as well as the Inception model proposed by *Szegedy et al. (2017)* are applied and use one-dimensional convolutional layers, as they are best suited for sequential data. The model architectures as well as the concept of convolutional layers are outlined in the following. It is noted that batch normalization is applied after each layer and before the ReLU function. Moreover, the individual outputs are activated by the linear function, except in case of the *tanh* approach – taken from *Mak and Düz (2019)* – where just the β branch is activated by *tanh*. The underlying idea is that the prediction of the relative wave heading is bounded between 0 and 1, which makes sense in case of a

normalized heading angle, but does not acknowledge the circular ambiguity. Furthermore, the method by *Åvist and Pyörre (2013)* works without any transformation of the relative wave heading and *Kawai et al. (2021)* decomposes *β* into sine and cosine components. These three approaches will be compared in terms of accuracy in the present paper.

3.1. Convolutional layers

The recent success of deep learning is mainly credited to novel layer types, such as convolutional layers. *Krizhevsky et al. (2012)* laid the foundation for convolutional neural networks (CNN) and this special model type was originally aimed at image processing. The model utilizes spatially shared weights followed by a pooling or subsampling procedure. Formally, a convolution takes a multidimensional array *x* as input, modifies it by the kernel *w*, another multidimensional array, whose parameters are adapted according to the training algorithm. The output of this layer type is often referred to as feature map *s* and the convolution operation is denoted as an asterisk.

$$s(z) = (x * w)(z) = \sum_a x(a)w(z-a) \tag{1}$$

As can be inferred by Eq. (1), *a* filters are applied and the index *z* takes integer values. Note that in this paper only sequential convolutional layers are of interest, i.e. convolutions along one axis (Conv1D). The following subsampling procedure is seen as feature extraction and is primarily used to reduce the size of the tensor resulting from the convolutional layer. The herein applied average pooling layer selects an average value from each region of the feature map and places it in the corresponding place in the output.

3.2. Residual network

He et al. (2016) proposed the Residual Network (ResNet) and its block-wise architecture draws inspiration from the pyramidal cells of the cerebral cortex. The feedforward ResNet consists of multiple residual blocks, which are bypassed by identity mappings or skip connections allowing for very deep models without vanishing gradients. The structure of the present residual block is made out of three convolutional layers with 8, 4 and 2 kernels, respectively. Whereas, the output of the block is the sum of the last layer's output and the input matrix gated through the skip connection activated by ReLU. The overall model comprises 4 blocks with filters of size 32, 64, 64 and 64, respectively. The tail part of the residual network has an average pooling layer and a fully connected layer with 50 neurons. For detailed information pertaining to implementation and theoretical background consult the paper by *He et al. (2016)*.

3.3. Inception network

The Inception architecture went through multiple iterations and we make use of the version proposed in *Szegedy et al. (2017)*. The Inception-v4 has also a block-wise structure building upon the novel Inception module. The module (and thus the network) is named after the science fiction movie by Christopher Nolan. The reason is the common premise of embedding networks within networks at different scales (or dreams within dreams in case of the movie). In general, CNN benefit from feature extraction at different scales (i.e. with a varying filter size), which has resemblance to the working principles of the visual cortex within the human brain. The module is made out of three parts: (1) The bottleneck part is located prior to the computationally intensive parallel convolutional layers and thus improves computational efficiency. (2) The second part consists of three parallel convolutional layers with kernel sizes of 16, 8 and 4, respectively. (3) The third element is the skip connection and comprises a max pooling and an additional bottleneck layer. Finally, the two gates are concatenated and it is stressed that the Inception architecture has also an outer residual skip connections bypassing entire Inception modules. The herein used model has a constant filter size of 16 and 8 inception modules in total with individual residual connections. *Szegedy et al. (2017)* provide additional information regarding Inception networks.

3.4. Training setup

In the present work, the programming language Python 3.6 is used and the deep learning framework is TensorFlow 2.6 as proposed by *Abadi et al. (2015)*. For GPU parallelization of the computations, CUDA (Compute Unified Device Architecture) was employed. The computations of the training procedures were carried out using a GPU node of the DTU computing center equipped with two Nvidia© Volta-100 GPUs, each with 16GB of memory (RAM) and multiple Intel© Xeon© Gold 6126 CPU with 2.60 GHz. Moreover, the Adam optimizer is employed as training algorithm. The optimizer uses the exponential moving average of the gradient and scales the learning rate, i.e. the step size, according to the squared gradient. The chosen batch size is 64, and the initial learning rate is set to 10^{-3}. *Mak and Düz (2019)* suggest that 5-fold cross validation with shuffled samples leads to increased performance in a sea state estimation task. It is stressed that several callbacks were implemented for alleviating the risk of overfitting.

4. Results and discussion

In the following section, the obtained results will be presented and discussed. Initially, we define the used accuracy metric – the root mean squared error (RMSE) – in Eq. (2). It is noted that $\hat{y}_i$ indicates the model approximation, whereas y_i denotes the data obtained from Wavex (or the "ground truth").

$$\text{RMSE} = \sqrt{\frac{1}{N}\sum_{i=1}^{N}\left(y_i - \hat{y}_i\right)^2} \tag{2}$$

The RMSE penalizes variance and outliers to a larger extent than, e.g. the mean absolute error. Due to the circular ambiguity in case of the relative wave direction, the absolute values of β are considered when calculating the RMSE. The results for the validation and training dataset are presented in Tables II and III, respectively. The model assessment will be carried out exclusively based on the performance on the validation set and the results of the training set are only included for the sake of completeness.

Table II: RMSE of the predictions based on the validation set

Target	(a) Åvist and Pyörre (2013)		(b) Mak and Düz (2019)		(c) Kawai et al. (2021)	
	Inception	ResNet	Inception	ResNet	Inception	ResNet
β	20.54	21.54	20.11	23.27	**10.50**	12.34
H_s	0.942	0.895	0.996	0.946	**0.927**	0.932
T_p	0.884	0.900	0.956	0.928	**0.878**	0.881

Table III: RMSE of the predictions based on the training set

Target	(a) Åvist and Pyörre (2013)		(b) Mak and Düz (2019)		(c) Kawai et al. (2021)	
	Inception	ResNet	Inception	ResNet	Inception	ResNet
β	8.933	11.66	12.64	12.33	**4.910**	5.106
H_s	0.448	0.435	0.614	0.487	0.425	**0.413**
T_p	0.452	0.431	0.568	0.486	**0.381**	0.393

Initially, it can be seen in Table II that the decomposition by *Kawai et al. (2021)* yields the lowest error and other sea state parameters are predicted with higher accuracy as well in comparison to the other methods. Moreover, it turns out that the Inception network provides higher accuracy than the ResNet, which may be due to the increased model capacity, i.e. number of trainable parameters. The *tanh* activation function (*Mak and Düz (2019)*) leads to even lower accuracy than the linear activation function, i.e. no dedicated transformation as presented in *Åvist and Pyörre (2013)*. *Goodfellow et al. (2016)* state that the *tanh* function is usually better suited than the sigmoid function, but ReLU is still considered as standard practice as activation function of *hidden* layers in a deep learning context due to the vanishing gradient problem. In general, the linear activation function of the output layer is considered best practice in case of regression problems.

In Fig.4, the predictions of all three separate Inception models are presented according to Table II. It stands out that (a) and (b) are characterized by larger scatter in the proximity of |180| deg. due to the circular ambiguity. However, there are minor outliers in the whole range of relative wave headings and it appears that the approach itself is subject to several uncertainty sources. In addition, the prediction accuracy of H_s and T_p is depicted for the Inception model trained on the vector components of β in Fig. 5. In view of Fig.5 it is stated that the overall estimation methodology provides satisfactory results on the validation set. Several reasons for inaccuracies and uncertainties are discussed in the following part.
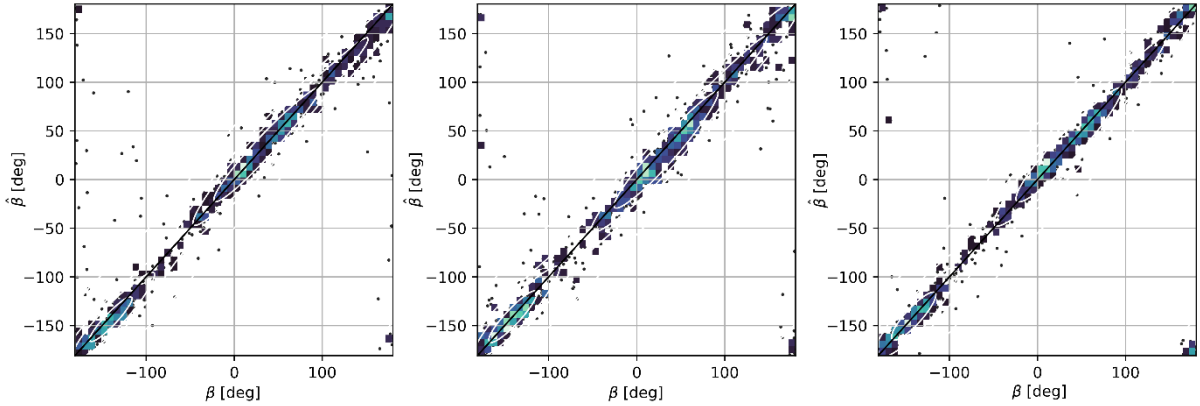

Fig.4: Correlation plots for the (a) linear, (b) *tanh* activation function and (c) vector decomposition of β based on the validation set. The plots are combinations of scatter, 2D histogram and KDE plot.
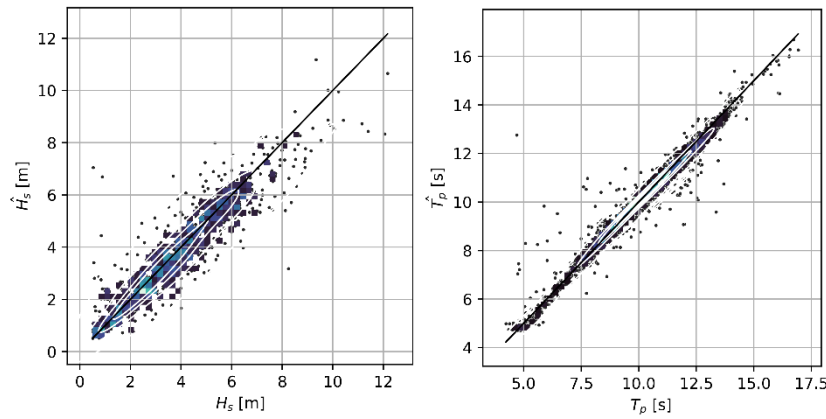

Fig.5: Correlation plots for significant wave height and peak period according to the (c) Inception model

For instance, draft and trim have not been recorded during the data acquisition period. Even though *Storhaug et al. (2007)* report that the typical transit draft is around 9.5m and the transit trim is in the range of 0.5 to 1.0m. However, it is interesting that the models are able to establish the abstract inverse mapping between ship response and sea state parameters without any information of, e.g. loading condition or even forward speed. Additionally, the wave radar data itself is subject to error. As it has been stated in Sec. 2, the accuracy of the used wave radar is in the range of ±10%, *Miros (2017)*. Moreover, it is very likely that parts of the data are influenced by reduced accuracy due to precipitation. Additionally, the "mean" sea state parameters are predicted when, in fact, they lose their physical meaning in case of multimodal seaways – the encounter wave direction in particular. Therefore, it is envisioned to estimate the inputs to a multimodal Ochi Hubble type spectrum, as shown in *Kawai et al. (2021)*. Lastly, it is evident that the presented method is negatively influenced by unbalanced data. This stands out in Fig.5, in which reduced accuracy (high variance and bias) can be seen in case of $H_s > 8$m and $T_p < 7.5$s. Ultimately, this observation reveals a clear drawback of machine learning in general: It is not well suited for extreme (or possibly unseen) events. The other key disadvantage is the data greediness of deep learning. Thus, it is thought that a hybrid approach of traditional model-based methods, relying on RAOs, and machine learning has strong potential. From a machine learning perspective, model-based methods, as presented in *Nielsen (2006)*, are considered as *self-supervised* and do not

require any labeled data. In addition, the approach itself could arguably be seen as <u>physics-informed</u> due to the use of RAOs. Furthermore, transfer learning as described in *Düz et al. (2019)* seems worthwhile for the possible application to a different vessel or in case of an additional wave data source, e.g. hindcast data. For industry adoption, a reliable estimate of uncertainty is of high relevance and therefore it is thought that the presented methodology could be extended not only towards explainable artificial intelligence (XAI), but also towards uncertainty quantification. In case of the latter, probabilistic deep learning and quantile regression, seem to enable an uncertainty-aware methodology for sea state identification. As shown by *Mittendorf et al. (2022c)*, the optimization of quantile loss functions allows establishing reliable uncertainty bounds in an efficient and straightforward manner.

5. Conclusion and future work

In this paper, a machine learning driven sea state identification approach has been presented. The focus of the work was on the prediction of the relative wave direction and associated preprocessing methodologies. It has been found that the vector decomposition into the sine and cosine components yields the highest accuracy, as the circular ambiguity is circumvented. It is thought that estimation procedures, like the presented one, are applicable for enhancing digital representations of ships, e.g. for monitoring the accumulation of fouling or even fatigue damage. Sea state estimation also facilitates on-board decision support for, e.g. determining the probability of parametric rolling or propeller ventilation. Moreover, it is seen as a stepping-stone on the way towards autonomous shipping. It is an interesting aspect for future work to pursue a data fusion approach for the calibration of the wave radar data by monitoring the experienced ship motions, as presented by *Thornhill and Stredulinsky (2012)*. In addition, the *non-parametric* estimation of the spectrum, i.e. providing the entire directional spectrum, seems worthwhile in a machine learning context. For instance, *Scholcz and Mak (2020)* use a convolutional encoder-decoder network, whereas *Han et al. (2022)* employ a generative adversarial network for non-parametric sea state estimation.

Acknowledgements

References

ABADI, M.; AGARWAL, A.; BARHAM, P.; BREVDO, E.; CHEN, Z.F.; CITRO, C.; CORRADO, G.S.; DAVIS, A.; DEAN, J.; DEVIN, M.; GHEMAWAT, S.; GOODFELLOW, I.; HARP, A.; IRVING, G.; ISARD, M.; JIA, Y.Q.; JOZEFOWICZ, R.; KAISER, L.; KUDLUR, M.; LEVENBERG, J.; MANE, D.; MONGA, R.; MOORE, S.; MURRAY, D.; OLAH, C.; SCHUSTER, M.; SHLENS, J.; STEINER, B.; SUTSKEVER, I.; TALWAR, K.;TUCKER, P.; VANHOUCKE, V.; VASUDEVAN, V.; VIEGAS, F.;VINYALS, O.; WARDEN, P.; WATTENBERG, M.; WICKE, M.; YU, Y.; ZHENG, X.Q. (2015), *TensorFlow: Large-scale machine learning on heterogeneous systems,* TensorFlow, http://download. tensorflow.org/paper/whitepaper2015.pdf

ÅVIST, P.; PYÖRRE, J. (2013), *Modeling the Impact of Significant Wave Height and Wave Vector using an On-board Attitude Sensor Network*, 12th COMPIT Conf., Cortona, pp.283-292, http://data.hiper-conf.info/compit2013_cortona.pdf

CARUANA, R. (1997), *Multi-task learning*, Machine Learning 28 pp. 41-75

DÜZ, B.; MAK, B.; HAGEMAN, R.; GRASSO, N. (2019), *Real Time Estimation of Local Wave Characteristics From Ship Motions Using Artificial Neural Networks,* 14th PRADS Conf., Yokohama

GOODFELLOW, I.; BENGIO, Y.; COURVILLE, A. (2016), *Deep Learning,* The MIT Press, Cambridge

HAN, P.; LI, G.; SKJONG, S.; ZHANG, H. (2022), *Directional wave spectrum estimation with ship motion responses using adversarial networks,* Marine Structures 83, No. 103159

HE, K.; ZHANG, X.; REN, S.; SUN, J. (2016), *Deep residual learning for image recognition,* IEEE Conf. Computer Vision and Pattern Recognition (CVPR), pp.770-778

IKONOMAKIS, A.; NIELSEN, U.D.; HOLST, K.K.; DIETZ, J.; GALEAZZI, R. (2022), *Validation and correction of auto-logged position measurements,* Communications in Transportation Research 2, No. 100051

KAWAI, T.; KAWAMURA, Y.; OKADA, T.; MITSUYUKI, T.; CHEN, X. (2021), *Sea state estimation using monitoring data by convolutional neural network,* J. Marine Science and Technology 26, pp.947-962

KRIZHEVSKY, A.; SUTSKEVER, I.; HINTON, G.E. (2012), *Imagenet classification with deep convolutional neural networks,* NIPS 2012, pp.1106-1114

LONGUET-HIGGINS, M.S.; CARTWRIGHT, D.E.; SMITH, N.D. (1963), *Observations of the directional spectrum of sea waves using the motions of a floating buoy,* Ocean Wave Spectra, pp.111-136

MAK, B.; DÜZ, B. (2019), *Ship as a Wave Buoy – Estimating Relative Wave Direction from In-Service Ship Motion Measurements using Machine Learning,* 38th Int. Conf. on Ocean, Offshore & Arctic Engineering (OMAE), Glasgow

MIROS (2017), *Wavex® v5.6 - The X-band radar-based wave and current monitoring system,* www.miros-group.com

MITCHELL, T.M. (1997), *Machine Learning,* McGraw-Hill, New York

MITTENDORF, M.; NIELSEN, U.D.; BINGHAM, H.B.; STORHAUG, G. (2022a), *Sea State Identification using Machine Learning - A Comparative Study based on In-service Data from a Container Vessel,* Marine Structures 85, No. 103274, https://doi.org/10.1016/j.marstruc.2022.103274

MITTENDORF, M.; NIELSEN, U.D.; BINGHAM, H.B. (2022b), *The Prediction of Sea State Parameters by Deep Learning Techniques using Ship Motion Data,* 7th World Maritime Technology Conf. (WMTC), Copenhagen

MITTENDORF, M.; NIELSEN, U.D.; BINGHAM, H.B.; LIU, S. (2022c), *Towards the Uncertainty Quantification of Semi-empirical Formulas Applied to the Added Resistance on Ships in Arbitrary Heading,* Ocean Engineering 251, No. 111040

NIELSEN, U.D. (2006), *Estimation of on-site directional wave spectra from measured ship responses.* Marine Structures 19, pp.33-69

NIELSEN, U.D. (2017), *A concise account of techniques available for shipboard sea state estimation.* Ocean Eng. 129 pp. 352-362

NIELSEN, U.D. (2018), *Sea state estimation based on measurements of wave-induced ship responses.* Dr. Techn. thesis, DTU Mechanical Engineering, Lyngby

NIELSEN, U.D.; MOUNET, R.E.G.; BRODTKORB, A.H. (2021), *Tuning of transfer functions for analysis of wave-ship interactions,* Marine Structures 79, No. 103029

RUDER, S. (2017), *An overview of multi-task learning in deep neural networks,* arXiv:1706.05098v1

SCHOLCZ, T.P.; MAK, B. (2020), *Ship as a wave buoy – estimating full directional wave spectra from in-service ship motion measurements using deep learning,* 39th Int. Conf. on Ocean, Offshore and Arctic Engineering (OMAE), Fort Lauderdale

STORHAUG, G.; MOE, E.; PIEDRAS LOPES, T.A. (2007), *Whipping Measurements Onboard a Midsize Container Vessel Operating in the North Atlantic,* Marintec China, Shanghai

SZEGEDY, C.; IOFFE, S.; VANHOUCKE, V.; ALEMI, A.A. (2017), *Inception-v4, inception-resnet and the impact of residual connections on learning,* 31st AAAI Conference on Artificial Intelligence pp.4278-4284

THORNHILL, D.C.; STREDULINSKY, E.M. (2012), *Ship Motion and Wave Radar Data Fusion for Shipboard Wave Measurement,* J. Ship Research 55/2, pp.73–85

Innovative E-Powered Asymmetrical Coastal Icebreaker Design

Thomas DeNucci, U.S. Coast Guard, New London/USA, thomas.w.denucci@uscga.edu
Dianna Garfield, U.S. Coast Guard, New London/USA, dianna.d.garfield@uscga.edu
Walter Gnaan III, U.S. Coast Guard, Honolulu/USA, walter.n.gnaan@uscg.mil
Richard Gordon, U.S. Coast Guard, New Haven/USA, richardgordonn@gmail.com
Joseph Zingarella, U.S. Coast Guard, Portsmouth/USA, joseph.m.zingarella@uscg.mil
Daniel Brahan, U.S. Coast Guard, New London/USA, daniel.j.brahan@uscga.edu

Abstract

This paper describes the concept design of an innovative asymmetrical icebreaker with an integrated propulsion system. The primary advantages of the asymmetrical hull form are icebreaking efficiency and maneuverability. At an angle of attack ~38°, the vessel can break ice at a width comparable to its length rather than its beam. Additionally, the maneuverability of the asymmetrical hull is exceptional due to its ability to break ice at a range of angles of attack. Consequently, this hull form is a promising choice for icebreaking missions involving channel clearing, direct assistance, and escort functions. The hull form trade-offs, general arrangements, weight prediction, tow-tank testing results and powering of this design will be presented as well as its seakeeping and operability. Challenges pertaining to stability modeling (asymmetrical geometry) and resistance prediction will also be discussed.

1. Introduction

The U.S. Coast Guard (USCG) is the only federal agency with the authority to provide icebreaking services. As directed by 14 U.S.C. 2 and Executive Order 7521, the USCG is mandated to support navigation by keeping channels and harbors open according to the demands of commerce. Although this role of icebreaking typically occurs on U.S. inland waterways and the Great Lakes, the recent rate of Arctic ice melt presents new areas of responsibility for this mission. As Arctic ice continues to decrease and waterways become more navigable, the demand for icebreaking services including channel clearing, search and rescue, and vessel assistance will only increase.

Under the National Infrastructure Protection Plan, the U.S. Coast Guard must achieve a 90% open sea way for all 'Tier One' shipping lanes on the Great Lakes, *United States Coast Guard (2018)*. 33 CFR 2.36(a) defines 'Tier One' shipping lanes as all connecting waterways of the Marine Transportation System (MTS) or other navigable waterways deemed the highest priority due to geographical location or commercial importance to the public. Natural resources, such as iron ore, coal, steel, and limestone as well as farm produce are among the primary commodities transported on this waterway system. This commerce accounts for $45.6 billion in annual economic activity, supports 328,500 jobs and facilitates the movement of over 253 million tons of goods and products annually on the Great Lakes, https://www.marinedelivers.com/economic-impacts-marine-shipping/. Losing availability of the MTS for even one day could cost the economy millions of dollars and further strain an already fraught logistical structure.

The Great Lakes are typically frozen between late November and late March. In severe years, ice can remain in some areas until early May. The extent of ice coverage and thickness varies with the severity of winter weather. Shoreline and island communities rely on icebreakers to clear ice to prevent flooding and allow ferries to operate to provide supplies and passengers. Maritime commerce relies on icebreakers to clear channels and free vessels which become trapped in ice, *United States Coast Guard (2016)*. Historical records show that the Coast Guard cannot maintain the 90% open sea way requirement on the Great Lakes in the event of a severe winter – suggesting the need for additional icebreaking capability.

1.1. Current Great Lakes icebreaking Fleet

The current fleet of U.S. Coast Guard assets capable of performing this mission on the Great Lakes is deficient. The primary assets are the 140-foot (43 m) WTGB icebreaking tugs, which were commissioned between 1978 and 1980. These vessels, shown in Fig.1, have now exceeded their intended thirty-year service life and require undue maintenance to remain operational, *United States Coast Guard (2016)*. Other operational limitations of the 140-foot WTGB fleet include its limited non-icebreaking mission capability during summer months and its restricted ability to transit across the Great Lakes due to excessive topside icing and insufficient fuel capacity. Although its recent Service Life Extension Program added approximately 15 years to the expected service life, the USCG expects the asset will need to be replaced by 2030, *United States Coast Guard (2016)*. Current operational forecasting indicates that the USCG would need approximately five additional 140-foot WTGBs along with an additional medium icebreaker to meet the current demand for statutory icebreaker requirements on the Great Lakes.

Fig.1: U.S. Coast Guard 140-foot WTGB Icebreaking Tug (left) and Medium Icebreaker (right)

The USCG also maintains a 73 m (240 ft) multi-purpose medium icebreaker, 'USCGC MACKINAW', on the Great Lakes which completes both the icebreaking and Aids to Navigation (AToN) missions. Since 'USCGC MACKINAW' is much larger than the 140-ft WTGB, and the only vessel in its class, it is both costlier to maintain and can only service the deeper waters of the Great Lakes.

1.2. Design Requirements

To increase the icebreaking capability and the area of operations in the Great Lakes, a new asset is required. The vessel should resolve the limitations of the 140-foot WTGB, while adding the capability to conduct AToN operations during the summer months at a capacity that meets or exceeds that of the 175-foot USCG Coastal Buoy Tender. The design must also have a relatively shallow draft, so that it can operate on inland rives and transit through the locks of the Great Lakes. Additionally, increasing the range and endurance of the current Great Lake ice breaking fleet is important. While a fuel level of 70% or more maximizes the icebreaking capabilities of the 140-foot WTGB, a fuel level less than 50% dramatically reduces its ability to break ice, reducing both its endurance and effectiveness. Therefore, it is critical to mitigate the effects of changes in displacement, i.e., fuel consumption, on icebreaking capability.

2. Market Research

A similar ships analysis reviewed a selection of 18 vessels ranging from the USCG Bay Class, USCG Keeper Class coastal buoy tender, harbor tugs, light and medium icebreakers, and several other types of vessels. The most important characteristic across these vessels was their ability to perform icebreaking. Three other objectives in this analysis were a length overall of 40 – 45 m (130 – 150 ft), a draft of 3.7 – 5.5 m (12 – 18 ft) and the capability to perform the AToN mission. The similar ships analysis revealed a wide range of vessel types available to complete both the icebreaking and AToN mission.

Using the icebreaking capability as the primary driver, Table I shows the target principal characteristics resulting from parametric analysis.

Table I: Principal Characteristics determined from Similar Ships Analysis

Target Principal Characteristics		
Characteristic	Value	Methodology
Power	10,000 BHP	Regression
Displacement	1,250 LT	Regression
LWL	45 m	Regression
B	13.7 m	Regression
Draft	4.6 m	Regression
C_b	0.43	Calculation
F_r	0.31	Calculation
Underwater Volume	1,239 m^3	Regression
Speed (max)	12.4 kts	Calculation

3. Hull Geometry

After consulting the primary requirements, estimated principal characteristics from the similar ships analysis (Table I) and U.S. Coast Guard guidance on icebreaker hull forms, *Keionin et al. (1991),* three primary hull forms were designed for further analysis and consideration: a dual-acting hull form, an open water hull form with an optimized icebreaking bow and an asymmetrical or oblique hull form.

3.1. Hull Form Variants

The most important parameters for ice resistance are the beam and the stem angle, *Riska (2010).* A large beam causes more resistance and thus narrower ships, with a large length to beam is the result ratio (especially if there is a draft limitation). For an icebreaker however, a small beam is not ideal, as escorted ships desire as wide a channel as possible. As a point of reference, the beam of a typical large icebreaker is approximately 28 m (90 ft).

Smaller icebreaking designs rely on bending forces to fracture ice rather than crushing forces to break ice. As such, modern icebreakers tend to have smaller stem angles to induce larger bending forces (while keeping the horizontal force component smaller), 20 to 25-degrees being common in ships. The stem shape is also rounded to decrease ice crushing at the stem.

The first design considered was a dual-acting icebreaking hull. It is unique because it has two bows. The forward bow is optimized for open water transit and light icebreaking (moving ahead); conversely, the stern is optimized to break heavy ice (moving astern). In this manner, the vessel achieves superior ice breaking performance without sacrificing open water efficiency. Additionally, this hull form has improved seakeeping performance over traditional icebreaker hulls due to the geometry of its open water bow. It has a rounded hull shape with a stem angle in the 45+ degree range and flare angles in the 40° to 45° range. The dual-acting hull is illustrated in Fig.2.
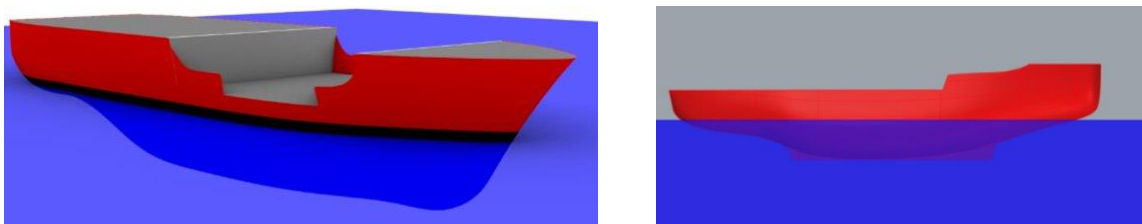

Fig.2: Dual-Acting Hull Design (left) and Optimized Open Water Icebreaking Hull Design (right)

The second hull form is an open water hull form fitted with an optimized icebreaking bow. The bow was created by lofting lines of the USCGC Polar Star; the concavity associated with a typical 'white bow' was reduced to improve open water performance. The cylindrical bow shape, ending with a tight rounded shoulder eliminates ice crushing at its shoulders. The hull has a 20° stem angle and very mild 15° flare. A forefoot was also added under the bow to stop the icebreaker from rising onto ice and losing stability. The open water hull with an optimized bow is also illustrated in Fig.2.

The last hull designed was an asymmetrical or oblique icebreaking hull. As the name implies, the vessel is asymmetrical along its centreline; the starboard side of the vessel is specifically designed to break ice at oblique angles of attack from 0° (going ahead) to 180° (going astern). At a 38° angle of attack, this 30.5 m vessel can break a 46 m channel in one pass – a width any vessel transiting the Great Lakes – St. Lawrence Seaway can pass through unhindered. The stem angle as well as the bilge angles on the starboard (icebreaking) side are 48°. The vessel has no flare and very mild (5-degree) tumblehome to assist with AToN operations. Only 7% of the hull has complex curvature, aiding in producibility, and by extension, reduction in cost. Fig.3 shows an illustration of the asymmetrical icebreaker design.
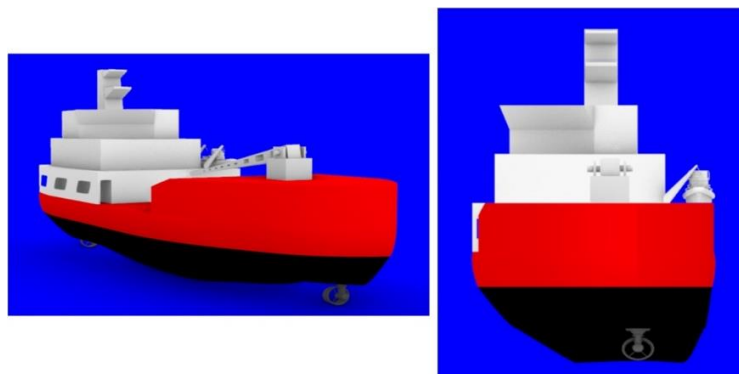

Fig.3: Asymmetrical or oblique Icebreaker Hull Design (bow out)

After conducting an initial hydrostatic stability analysis using General Hydrostatics Software (GHS) and open water resistance calculation using both NavCad and Computational Fluid Dynamics (CFD) for each hull form, a final hull form was selected for further development.

3.2. Hull Down Select Process and Rationale

The open water hull form with an optimized icebreaking bow was eliminated from further consideration due to its relatively lower block coefficient and rounded bilges. Further consideration of this geometry indicated that this hull would be particularly susceptible to rolling. This is disadvantageous during AToN operations, when a comparatively stable working deck would be necessary for both work efficiency and Coast Guard personnel safety. Furthermore, the trends in newer icebreakers vary differently in bow and overall body shapes drastically with considerably less emphasis on open-water efficiency underway, *Hovilainen et al.* (2014). As a result, this hull was eliminated from further consideration first.

Choosing between the dual-acting hull and asymmetrical hull was more challenging. Both hulls were modern, and each had its own unique design features. The dual-acting hull substantially improves sea-keeping by incorporating two separate bows on the same ship. The forward bow reduces the effects of slamming and green water on the weather decks with its higher stem, buttock, and flare angles. Conversely, the stern shape of the vessel with its shallow stem and buttock angles, and lower flare angles, does not significantly impact the seakeeping characteristics of the vessel. When going astern to break ice, friction reducing effects are recorded due to the 'flushing effects' of prop wash which can reduce the friction on the hull breaking ice by up to 50% in some cases, *Hovilainen et al.* (2014). Coupled with an icebreaking stern and azimuthing propulsion, which has the highest flushing and ice milling benefits, the dual acting hull can acquire significant icebreaking capabilities.

An oblique hull improves upon an icebreaker's capacity to break larger channels and significantly improves maneuverability by being geometrically asymmetric along the centreline of the vessel. Although seakeeping performance is not quite as good as the dual-acting hull, the benefits of this hull form are considerable. As noted previously, oblique hull can break a channel width comparable to its length instead of its beam. In addition, the variable angle of attack also provides this hull form with exceptional maneuverability. Because the 140-foot WTGB spends 75% of winter operational time performing direct assistance and preventative icebreaking, this capability would be unmatched. Fig.4 illustrates the exceptional maneuverability of the oblique icebreaker at various angles of attack. The ability to operate safely near other vessels, even those with azimuthing propulsion, can simply not be achieved by other icebreakers.
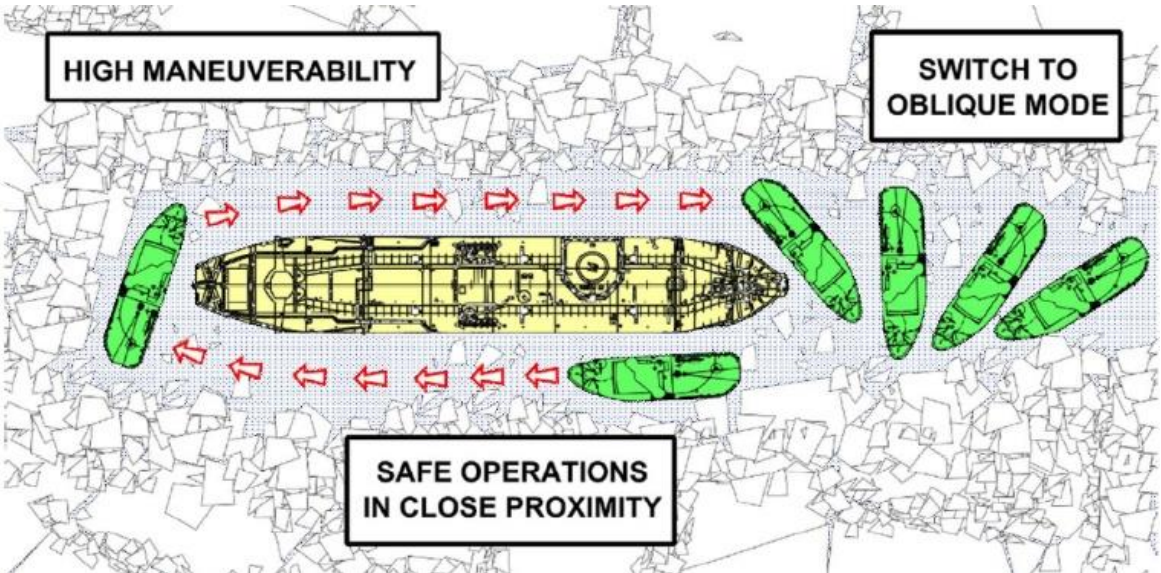

Fig.4: High manoeuvrability of oblique hulls in close quarters.

Ultimately, the asymmetrical hull best met the requirements and most closely aligned with the similar ship characteristics identified in Table I. Once this candidate hull form was selected, two important modifications were made to the vessel. First, the 4th weather deck provided excessive volume and was eliminated from the design. Second, the area of the buoy deck size was reduced from 186 m^2 to 124 m^2 to match, not exceed, the AToN capacity of the U.S. Coast Guard 175-foot Coastal Buoy Tender. The resulting outboard profile is displayed in Fig.5. In later revisions of the hull, the underwater volume was further refined to reduce resistance and the curvature on starboard side was faired to improve icebreaking. A perspective view of the final design appears as Appendix A and a rendered body plan appears as Appendix B.

Principal Characteristics	
Length	45.7 m
Beam	14.3 m
Draft	4.72 m
Displacement	1,560 LT
Brake Power	13,500 HP
Max Speed	12 kts
Icebreaking Capability	55.9 cm plate ice @ 8 kts ahead
	50.8 cm plate ice @ 3 kts and 38° angle of attack

Fig.5: Asymmetrical Icebreaker Hull

4. General Arrangements

4.1. Bulkheads and Decks

Bulkhead placement was prescribed by the *U.S. Navy Design Practices and Criteria DPC-079-1 (2016)*. DPC-079-1 requires the use of a two-compartment flooding standard, meaning that any two adjacent compartments must be able to flood without submerging a margin line placed 76 mm (3 in) below the deck edge. The minimum bulkhead spacing prescribed by the regulations was set at 4.25 m (14 ft). A forward collision bulkhead was placed in accordance with *U.S. Design Data Sheet DDS-079-1 (2003)*, which required the bulkhead be placed in the vessel at a distance approximately 5% of the LBP aft of the forward perpendicular –1.94 m (6.36 ft) in this case. Since an oblique hull will likely make way both forward and astern, an additional aft collision bulkhead was placed at 3.1 m (10.2 ft) forward of the aft perpendicular. Bulkhead spacing was manually varied in GHS to achieve the two-compartment standard; the resulting bulkhead configuration used ten bulkheads to create eleven compartments. Each compartment passed the two-compartment floodable length standard at 0.95 compartment permeability; machinery spaces passed at 0.85 compartment permeability.

Compartments were arranged with careful consideration of mission specific requirements, progressive design, and habitability. All General Arrangements meet the ABS Habitability Guide and the USCG Technical Standard 640, *U.S. Coast Guard (2014)*. The vessel has a total of 4 decks spaced 3 m (10 ft) apart, except for the distance between the 2nd deck and the main deck, which is spaced 4.6 m (15 ft) apart to accommodate the engine room, generator room, and other auxiliary machinery spaces.

4.2. Deck Layout

All engineering spaces were placed on the second deck including the engine room, generator room, auxiliary room, as well as both the forward and aft thruster rooms. The engine room is a separate compartment from the generator room to increase the survivability of the ship. Also included on this deck are two four-person berthing areas, a cargo hold, a reverse osmosis system, workshops, and potable water tanks.

The main deck of the vessel accommodates the AToN gear and includes a 124 m^2 buoy deck with chain stoppers, a 1.8 m by 1.8 m cargo hatch, a buoy chain handling system, and an AToN workshop. Aft of the buoy deck is the main deck superstructure, which includes berthing spaces, the galley and mess deck (seats 30). Dry and frozen food storage is also placed on this level.

The 01 deck houses the command staterooms as well as two four-person staterooms. The emergency generator space was also placed on the 01 deck to achieve physical separation from other engineering spaces. The small boat and dual point davit system was placed on the port side of the 01 deck. The AToN crane is located on the forward part of the 01 deck. The crane's pedestal extends all the way down to the 2nd deck to mitigate the stress from operational loads.

The bridge is located on the 02 deck. The bridge has 360-degree visibility except for a small portion on the port side where the exhaust stack is located. There are three helm stations on the bridge: one for normal forward operation, one for astern icebreaking, and one for oblique icebreaking. The forward starboard portion of the bridge is angled to allow good visibility while conducting oblique icebreaking operations.

5. Power Estimation

Bare hull resistance estimations were derived from NavCad regression models based on the asymmetrical hull form. The 'Roach' regression model was chosen as the primary source of the bare hull power prediction while 'Holtrop' was used to model appendage resistance based on an equivalent increase in effective wetted surface. Since azmuthing drives do not have traditional shafting, the propulsor units were modeled through strut bossing length, diameter, root and tip chords and as well as span of chords

in NavCad. Wind resistance was predicted by assuming the area of the hull and superstructure which was exposed above the waterline while moving in a forward direction. The 'Taylor' prediction method for wind resistance, based on tanker, cargo ship and passenger liner models which was a best estimate for wind resistance. The resulting regression analysis predicted an effective horsepower requirement of 1,098 hp (808 kW). Fig.6 shows results of the regression-based 'Roach' and 'Anderson' power prediction models.

Icebreaking resistance was predicted using the Canadian Icebreaking method, *Spencer (1992)*. The hull was modeled using the most extreme ice breaking condition – icebreaking at a 38-degree angle of attack. The predicted effective horsepower to break 55.9 cm (22 in) of plate ice at 8 knots ahead using the round bilge formulation was 1,265 hp (930 kW) while the hard-chine formulation required 1,393 hp (1024 kW).
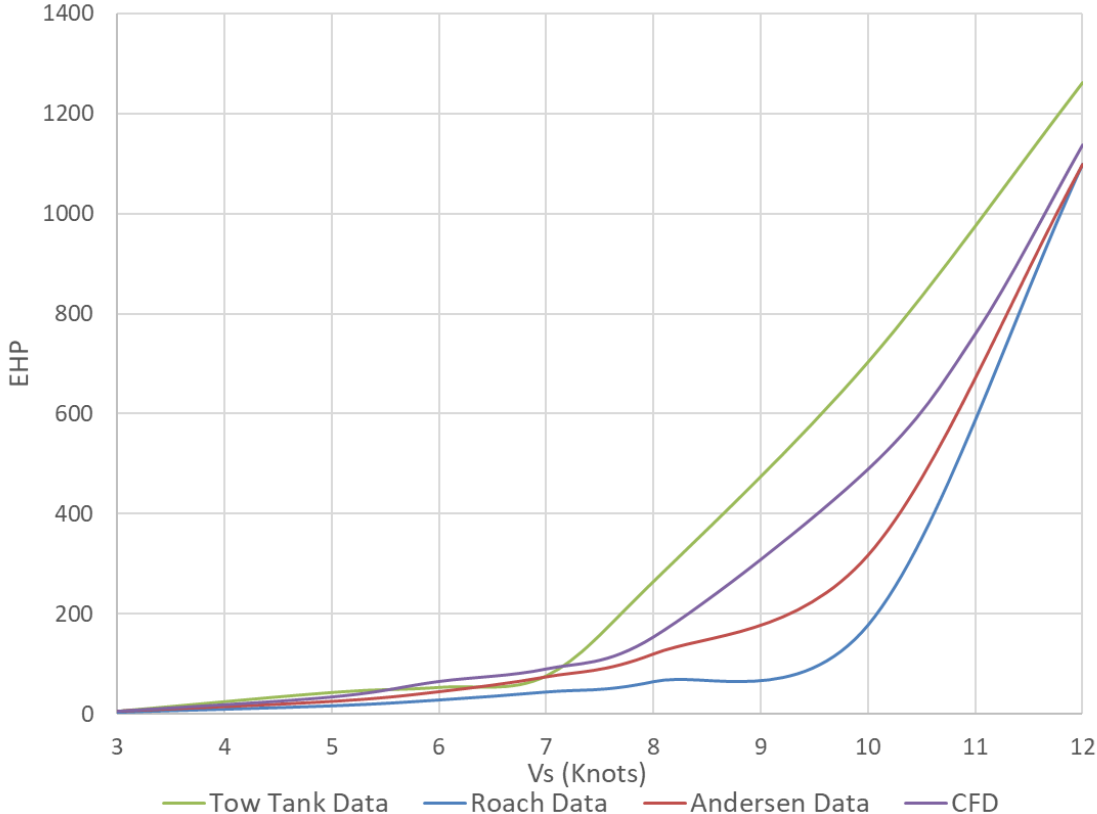

Fig.6: Power prediction using regression analysis, CFD, and tank testing

5.1. Tow Tank and CFD Validation

To validate NavCad power predictions a 1:30 scale model of the vessel was tested in the U.S. Coast Guard Academy's tow tank. Model testing visibly showed a larger bow wave on the starboard side which would indicate a much greater pressure than the port side. These two regions of high and low pressure indicate that the natural tendency of the hull while tracking straight will be to turn to port and be more susceptible to yaw motions. The results from the tow tank testing showed that the bare hull resistance of the vessel is, on average, higher than the NavCad predicted resistances (1,262 hp or 929 kW). Tow tank results also show that wave making resistance overcomes frictional resistance at lower speeds than predicted. To investigate these differences, a CFD resistance analysis was also performed on the final hull form. Results from this analysis show increased resistance between 8 and 11 knots relative to the regression models, but not as high as the tow tank testing. The NavCad and CFD resistance results are also shown in Fig.6 and the wave pattern of the hull at 12 knots is shown as Fig.7.
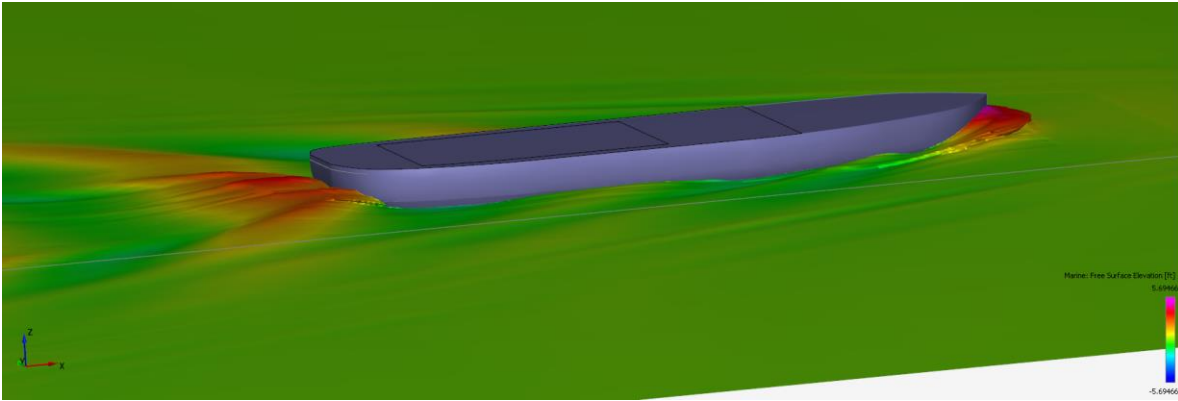
Fig.7: Asymmetrical icebreaking hull at 12 knots (ahead)

5.2. Brake Horsepower

To calculate brake horsepower, propulsion efficiencies were applied to the effective horsepower predictions. To be conservative, the hard-chine formulation effective horsepower (1,393 hp or 1024 kW) was used to predict brake horsepower. Efficiencies used for a diesel electric propulsion plant and L-drive propulsion unit are hull open water, relative rotative, shaft, electrical motor, electrical transmission, and generator efficiency. Using NavCaD, an optimized propeller was developed based on the predicted operational profile of the oblique vessel breaking ice at a 38° angle of attack through 50.8 cm (20 in) of ice. The result of this optimization was the selection of the 4-blade Kaplan 19A Kc (P/D = 1.0) ducted propeller with an open water efficiency range of 0.165 to 0.49 depending on the operational condition. A list of propulsion efficiencies used to determine brake horsepower is displayed in Table II.

Table II: Propulsion Efficiencies

Estimated Efficiencies	
Hull	0.93
Relative Rotative	0.99
38° angle of attack @ 3kts in 50.8 cm of plate ice	0.165
Average open water condition	0.49
Shaft	0.99
Electric Motor	0.96
Electrical Transmission	0.99
Generator	0.96

The maximum brake power requirement for the vessel occurred at a 38-degree angle of attack while breaking 50.8 cm (20 in) of plate ice at 3 knots resulting in a power requirement of 10,152 hp (7467 KW).

5.3. Prime Mover Selection

The main constraint that drove the prime mover selection was the length of the main engine room. Initial analysis of stability and floodable length curves limited the distance between engine room bulkheads to be only 6.0 m (20 ft) feet apart. Consequently, the vessel is outfitted with three Fairbanks Morse Colt Pielstick PA6B STC generator sets. The generator sets provide enough power for all operational conditions including transit, ice breaking (ahead) and ice breaking at a 38-degree angle of attack. To account for growth, each of the generator sets was sized at 85% of the manufacturers' continuous rating.

5.4. Electrical Loads

The required electrical loads were determined by categorizing equipment by using the Ship's Work Breakdown Structure (SWBS) and identifying the connected loads of the required equipment in each

category. Using ratiocination, electric loads from CGC MACKINAW's electric plant load analysis (EPLA) were used to estimate the connected load for each piece of equipment. Once connected loads were determined, they were multiplied by loading factors which provide best estimates of the operating loads recommended in *U.S. Navy Design Data Sheet DDS-310-1 (2012)*, Design Data Sheet for Electric Power Load Analysis for Surface Ships.

Because the vessel was designed with an Integrated Power System (IPS) in mind, propulsion generators and smaller, service generators, can be utilized to share loads. In all operating conditions except shore and anchor, the vessel is making way, and therefore, has propulsive needs that require at least one propulsion generator for the large electric demands of the propulsion system. Because the main engines have excess of power available, they can satisfy other electrical demands during summer and winter operating conditions.

In order to run efficiently at shore and anchor conditions, and provide redundancy to the power system, service generators were selected. The largest load generated in these two conditions occur during a summer anchor condition when a demand of 567.4 kW (including a 15% margin) is required. Since IEEE Std 45-2002, 7.4.2, Selection and Sizing of Generators mandates that power be always produced by a singular genset (with another on standby) to service the essential and habitable loads, the MTU MG10V2000M41B (579 kW) was selected. While having some of the most efficient specific fuel consumption, the genset is also the most compact and power dense of four different generator sets considered. The emergency diesel generator selected was the Wartsila 12V14 (1,005 kW). It was selected because it reached the target emergency generator MCR of 946 kW.

A line diagram of the electrical propulsion system is illustrated in Fig.8. The power system was designed to be both flexible and redundant – to supply power in a variety of paths in a variety of operating conditions. The layout of the switchboards and AC Buses was designed in such a manner that any number of main gensets can power both the entire propulsive and auxiliary electrical system. This is an integral part of the IPS. Additionally, The EDG is linked with an Automatic Bus Transfer (ABT) switch. In the event of power loss, electricity can be quickly restored to critical components.
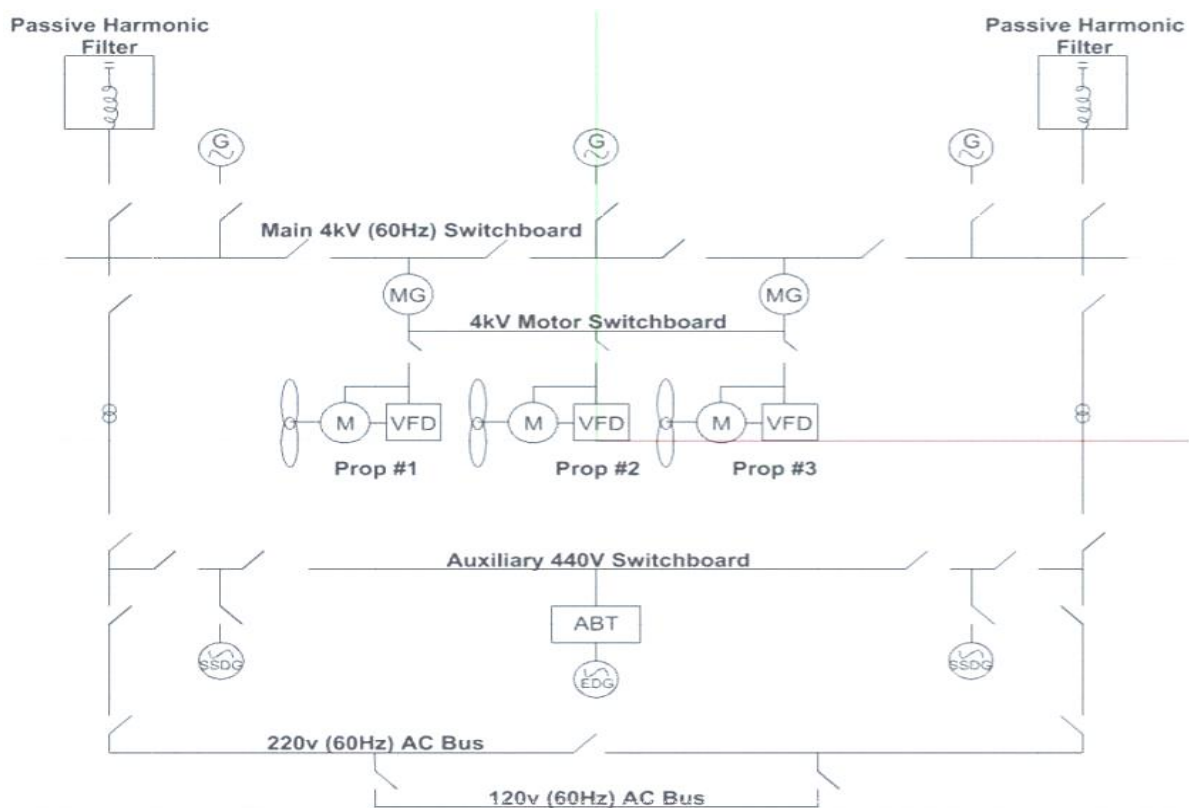

Fig.8: Integrated Power System diagram

6. Weight Estimate

Before commencing an initial weight estimate, full load and light ship conditions were defined. These conditions were assumed to represent the best-and-worst-case stability scenarios for the vessel. The fully loaded condition represents a fully crewed vessel departing for sea while the lightship condition describes the vessel with no variable loads.

The initial weight estimation was performed using ratiocination, *Straubiner, et al. (1983)*. Ratiocination utilizes the ratios between a parent hull's characteristics and the new vessel's characteristics as a scale factor. The ratios between the lengths, depths, shaft powers or other characteristics are multiplied by the parent vessels weight to determine the new weight and KG of the vessel. The parent hull weights for this vessel were the U.S. Coast Guard 140-foot WTGB (Fig.1) and U.S. Coast Guard WLM Coastal Buoy Tender. Because the oblique hull design would be the first-in-class design, generous acquisition margins (10% weight – 6% KG) and service life margins (12% weight – 6% KG) were applied to the weight estimate. Table III shows the results of SWBS-based weight estimation and Table IV shows the resulting displacement and KG.

Table III: Weight Estimation using ratiocination, *Straubiner, et al. (1983)*

SWBS	Weight (LT)	KG (m)	Moment (LT· m)	LCG (m)	Moment (LT· m)
100	545.5	6.3	3,436.7	23.7	12,928.4
200	179.2	5.8	1,039.4	27.6	4,945.9
300	25.5	5.2	132.6	33.7	859.4
400	6.5	10.7	69.6	29.6	192.4
500	197.6	3.3	652.1	12.0	2,371.2
600	123.5	6.2	765.7	24.6	3,038.1
700	0.6	7.6	4.6	26.5	15.9
Full Load	154.8	2.3	356.0	22.0	3,405.6
Total	**1,233.2**		**6,456.5**		**27,756.8**

Table IV: Full load displacement and center of gravity

	Displacement (LT)	KG (m)
Full Load	1,233	5.2
Full Load w/ Margins	1,519	5.9

7. Stability

An intact and damage stability analysis was performed on the vessel in accordance with the regulations in DPC-079-1, *US Navy Design Practices and Criteria for U.S. Navy Surface Ship Stability and Reserve Buoyancy DPC-079-1, (2016).* The asymmetrical geometry of the oblique icebreaker requires each side of the hull to be considered independently of the other during both the intact and damage stability analysis.

7.1. Intact Stability

A righting arm analysis, shown in Fig.9, shows that the initial stability of both the port and starboard side are approximately the same. However, Fig.9 also shows that starboard (icebreaking) side of the vessel has substantially more righting energy than the port side. Therefore, the portside of the vessel is the source of all limiting maximum KG curves. This distinction is important. Although GHS analysis was run on both sides to verify the maximum KG condition, the port side was responsible for every limiting maximum KG due to having the least amount of righting energy.
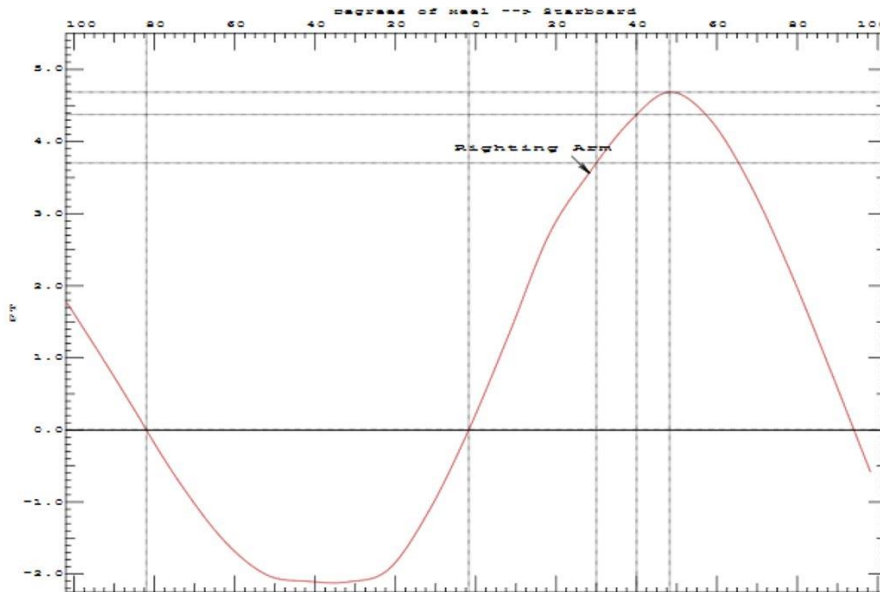
Fig.9: Righting arm curve of the asymmetrical icebreaker

Intact stability was evaluated at six different conditions as prescribed by DPC-079-1:

1. Beam winds with rolling (80 knot wind)
2. Beam winds with icing (45 knot wind, ship assumed to be heeled 25 degrees)
3. High Speed turn at 12 knots (160 m radius)
4. Passenger crowding (20 passengers with average weight of 84 kilograms)
5. Weight over the side (9 tons @ 19 m off centerline of ship)
6. Towline pull (criteria specified by regulations)

The vessel passed all criteria at the full load with margin condition described in Table IV.

7.2. Damage Stability

Damage stability criteria is specified in DPC-079-1. Stability is considered satisfactory if:

a. The initial angle of heel after damage does not exceed 15 degrees
b. The reserve of dynamic stability shall not be less than 1.40 times the energy imparted to the ship by rough seas with beam winds
c. The value of the maximum righting arm minus the value of the wind heeling arm at the same angle of heel shall be greater than 0.076 m
d. After damage, the margin line at the side shall not be submerged at the static angle of list

For this analysis, the vessel was analyzed in a worst-case scenario, i.e., a minimum operating loading condition with buoys lashed down to the deck and a wind velocity of 31 knots. The longitudinal extent of damage was defined as two consecutive adjacent subdivisions. Seven adjacent-compartment damaged cases were analyzed using GHS; every scenario passed all limits in accordance with the regulations. The largest trim experienced by the vessel was when the two forward compartments were flooded, resulting in a 4.08-degree trim by the bow and draft of 7.4 m, Fig.10.

Damage to both the engine room and auxiliary room is considered the worst-case damaged stability case for two reasons. First, the margin with which the design passes the DPC-079 criteria is the smallest with this damage. Second, the compartments which are damaged are critical areas (engine room and auxiliary room) and rendered inaccessible. Despite this – the ship is still operational - the IPS directs the service generators to absorb the additional load on the system.

CG - Draft: 24.23 @ 0.00   Trim: fwd 4.08 deg.   Heel: port 4.83 deg.

| Tanks					
	8 BALLAST1P.S	16 DUBBOT2.S	24 GREYWTR.S	32 ETSHOP.S	40 ENGINERM.S
1 FOREPEAK.S	9 FUELTK1.S	17 FUELTK3.S	25 BALLAST5S.S	33 FIREPMP.S	41 AUXRM.S
2 AFTPEAKC.S	10 BALLAST2P.S	18 SERVICETK1.S	26 BALLAST5P.S	34 EMSHOP.S	42 GENRM.S
3 AFTPEAKP.S	11 BALLAST2S.S	19 SERVICETK2.S	27 AFTVOID.S	35 FWDBERTHING.S	43 AFTTHRUST.S
4 AFTPEAKS.S	12 DUBBOT1.S	20 BALLAST4P.S	28 POTABLEWTR1.S	36 CARGOHOLD.S	
5 FWDBALLAST.S	13 FUELTK2.S	21 BALLAST4S.S	29 POTABLEWTR2.S	37 POTEQUIPRM.S	
6 BALLAST1C.S	14 BALLAST3P.S	22 DUBBOT3.S	30 BOWTHRUST.S	38 AFTBERTHING.S	
7 BALLAST1S.S	15 BALLAST3S.S	23 SEWAGE.S	31 CRANERM.S	39 ECC.S	

Fig.10: Damage stability analysis illustrating maximum trim condition

8. Seakeeping

Seakeeping and operability were analyzed in GHS. Input to these analyses include the vessel radii of gyration, wave characteristics, and critical points. Critical points, or points of interest, were defined throughout the ship for GHS to recognize the root location for the evaluation of seakeeping. Fig.11 shows 12 critical points defined on the vessel.
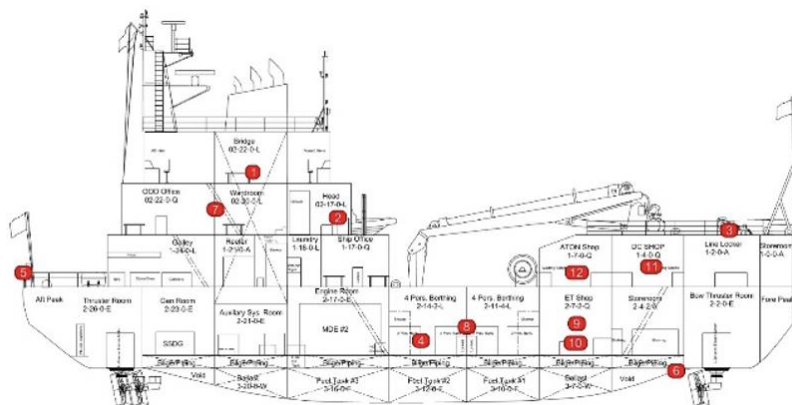
Fig.11: Critical points defining 'key' location on the vessel

8.1. Wave Characteristics

The Great Lakes-St. Lawrence seaway spans over vast areas of water. To accurately capture wave characteristics, significant wave height and period were collected from nine NOAA buoys spanning nearly three decades (1970 – 2000). Using statistical methods, the average the significant wave height and wave period of the 75th percentile of recorded data was 1.42 m (4.66 ft) and 4.15 sec respectively. Fig.12 shows the asymmetrical hull in this sea state at a speed of 8 knots.
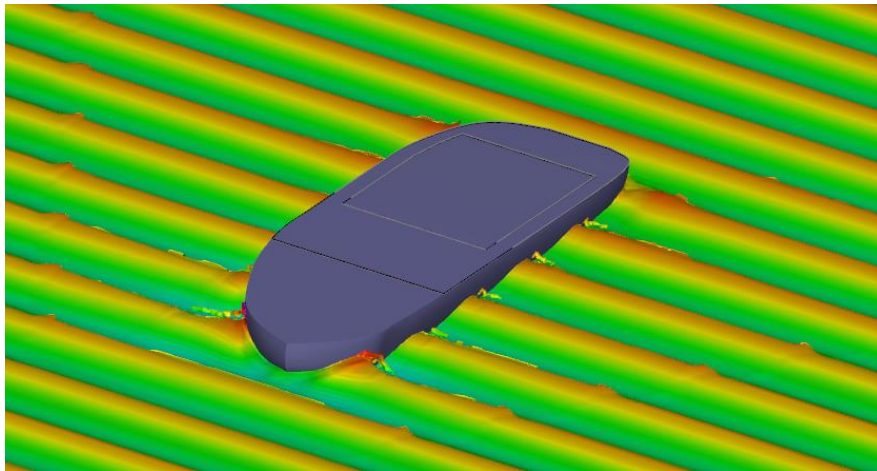

Fig.12: Asymmetrical hull in 75th percentile Great Lakes seas

8.2. Seakeeping Criteria

Seakeeping analyses were performed for transit and small boat operations. Criteria for both operations were guided by criteria from *U.S. Coast Guard Engineering Logistics Center (2008)* and are shown in Table V. Transit operations were evaluated at 8 knots while small boat operations, dependent on the dynamics of ship motion, ship speed, and the significant characteristics of the waves, was evaluated at speeds of 0, 3.5, and 8 kts.

Table V: Seakeeping Criteria

Criteria	Transit Mission	Small Boat Operations
Roll	<4°	<4°
Pitch	<1.5°	<1.5°
$\ddot{z}$ @ pilothouse	<0.2g	<0.2g
$\ddot{y}$ @ pilothouse	<0.1g	<0.2g
Deck Wetness (foredeck)	<30 occ/hr	--
Slamming (station 3)	<20 occ/hr	--
Sway @ stern	--	<1.5m

8.3. Seakeeping Results

The vessel passes every criterion with the exception roll criteria in both the transit and small boat operability conditions when the seas off the port beam (8-degree roll). Since this is the only combination of relative heading and seas where excessive roll occurs, it can be mitigated by simply changing course and/or reducing speed in the sea state and the vessel with fall within acceptable parameters. Additionally, passive roll dampeners such as bilge keels might also be included in future iterations of this design to eliminate excessive roll. The benefit of this device is two-fold because it can also help to provide a stable working platform in AToN operations too.

8.4. Seakeeping Effects due Asymmetrical Hull

The three main motions that affect crew operability and comfort tend to be roll, pitch, and heave accelerations. Fig.12 illustrates the maximum roll acceleration in port beam seas ($8.25°/s^2$) at 0 knots. Beam seas off the starboard beam produced significantly reduced roll acceleration. This is a direct characteristic of the asymmetry of the hull.
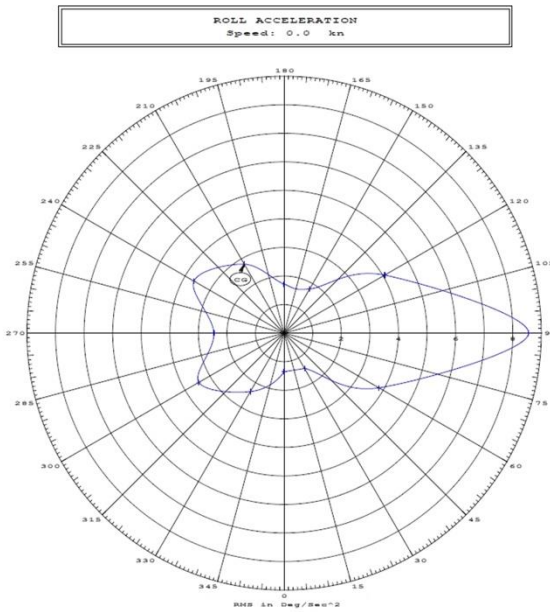

Fig.12: Maximum Roll Acceleration
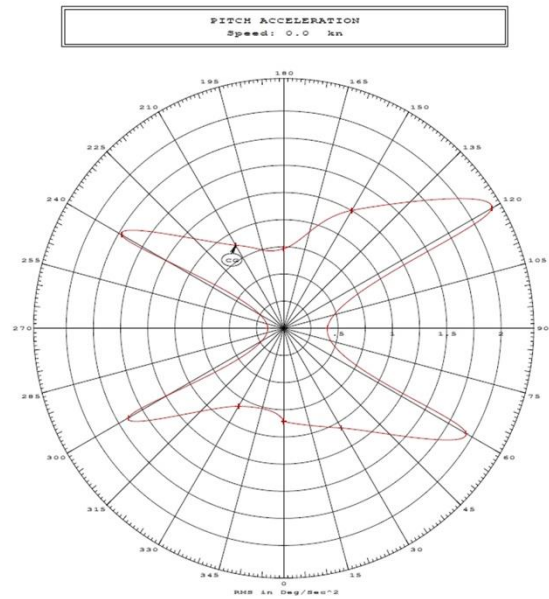
Fig.13: Maximum Pitch Acceleration

Maximum pitch accelerations, Fig.13, show reduced pitching in beam seas and maximum pitching in quartering seas. The asymmetry of the oblique hull has only a minor effect on the range of pitch accelerations as well. The relative heave acceleration polar plot is one of the only generated figures in the seakeeping report that is symmetrical about the y-axis. Heave acceleration is negligible forward of the beam regardless of the sea's direction. The maximum relative heave is observed in following seas.
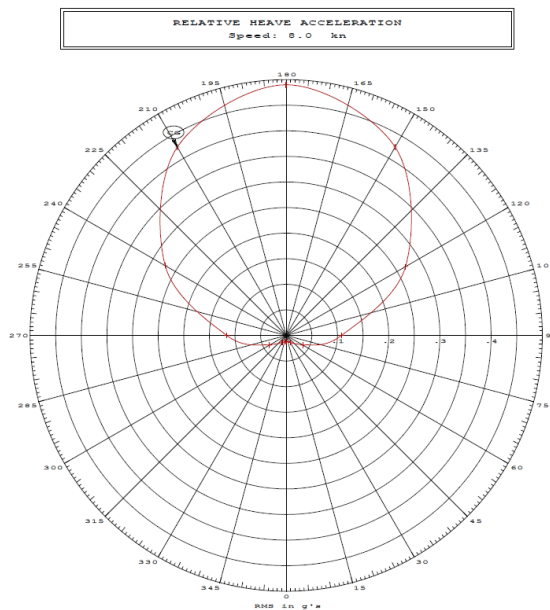

Fig.14: Maximum Relative Heave Acceleration Polar Plot

120

Analyses were also performed for Motion Sickness Incidence (MSI). MSI, is a quantitative measure of the incidence of seasickness in a population exposed to vertical motions during an established exposure period. MSI is returned as a value, between 0 and 100, that represents the percentage of the population expected to become seasick. MSI was analyzed at eight critical points including the pilothouse, engineering control, berthing areas, and workshops. No location experienced MSI more than 13% from any relative wave angle in a one-hour period.

9. Conclusion

An asymmetrical icebreaker with AToN capability offers a promising alternative to conventional icebreaking designs in the Great Lakes. This design employs an oblique icebreaking technique which allows it to break a 46 m wide channel of 50.4 cm of plate ice at 3 knots. This allows the vessel to clear a channel wide enough for any vessel operating in the Great Lakes in one singular pass. With azimuthing propulsors controlled through an integrated propulsion system, the vessel is extremely maneuverable and offers a flexible and efficient power management system. The asset is smaller and more effective than current Coast Guard icebreakers with comparable capabilities, and has the potential to greatly improve the operational footprint of the Coast Guard on the Great Lakes and in the navigable Arctic.

References

HOVILAINEN, M; UUSKALLIO, A.; ROMU, T. (2014), *Next Generation to Break the Ice -The Oblique Icebreaker*, OTC Arctic Technology Conference, Houston

KEINONEN, A.; BROWN, R.; REVILL, C.; BAYLY I. (1991), *Icebreaker Performance Predictions*, SNAME Trans. 99, pp. 221-248.

KEINONEN, A.; MARTIN, E; BERROW, J; BROWN, J.; REVILL, C.; SMITH, N. (2010), *Icebreaker Vessel Technologies for USCGC Missions*, Technical Document Number HSCG40-08-P-60591

RISKA, K. (2010), *Design of Ice Breaking Ships*, Cold Regions Science and Marine Technology 1, pp.1-43

SPENCER, D. (1992), *A standard method for the conduct and analysis of ice resistance model tests*, 23rd ATTC Symposium, pp.301-307

SPENCER, D.; JONES, S. (2001), *Model Scale/Full Scale Correlation in Open Water and Ice for Canadian Coast Guard R-Class Icebreakers*, J. Ship Research 45/4, pp.249-261

STRAUBINGER, E; CURRAN, W.; FIGURA, V. (1983), *Fundamentals of Naval Surface Ship Weight Estimating*, Naval Engineers J. 95/3, pp.127-144

U.S. COAST GUARD (2016), *Coast Guard Great Lakes Icebreaking Mission Analysis*, Fiscal Year 2016 Report to Congress

U.S. COAST GUARD (2018), *Maritime Commerce Strategic Outlook*, U.S. Coast Guard

U.S. COAST GUARD (2014), *Living and Berthing Spaces*, Naval Engineering Technical Standard 640

U.S. NAVY DESIGN DATA SHEET DDS-079-1 (2003), *Stability and Buoyancy of U.S. Naval Ships*, DDS-079-1

U.S. NAVY DESIGN DATA SHEET DDS-310-1 (2012), *Electric Power Load Analysis for Surface Ships*, DDS-310-1

U. S. NAVY DESIGN PRACTICES AND CRITERIA DPC-079-1 (2016), *Design Practices and Criteria for U.S. Navy Surface Ship Stability and Reserve Buoyancy*, DPC-079-1
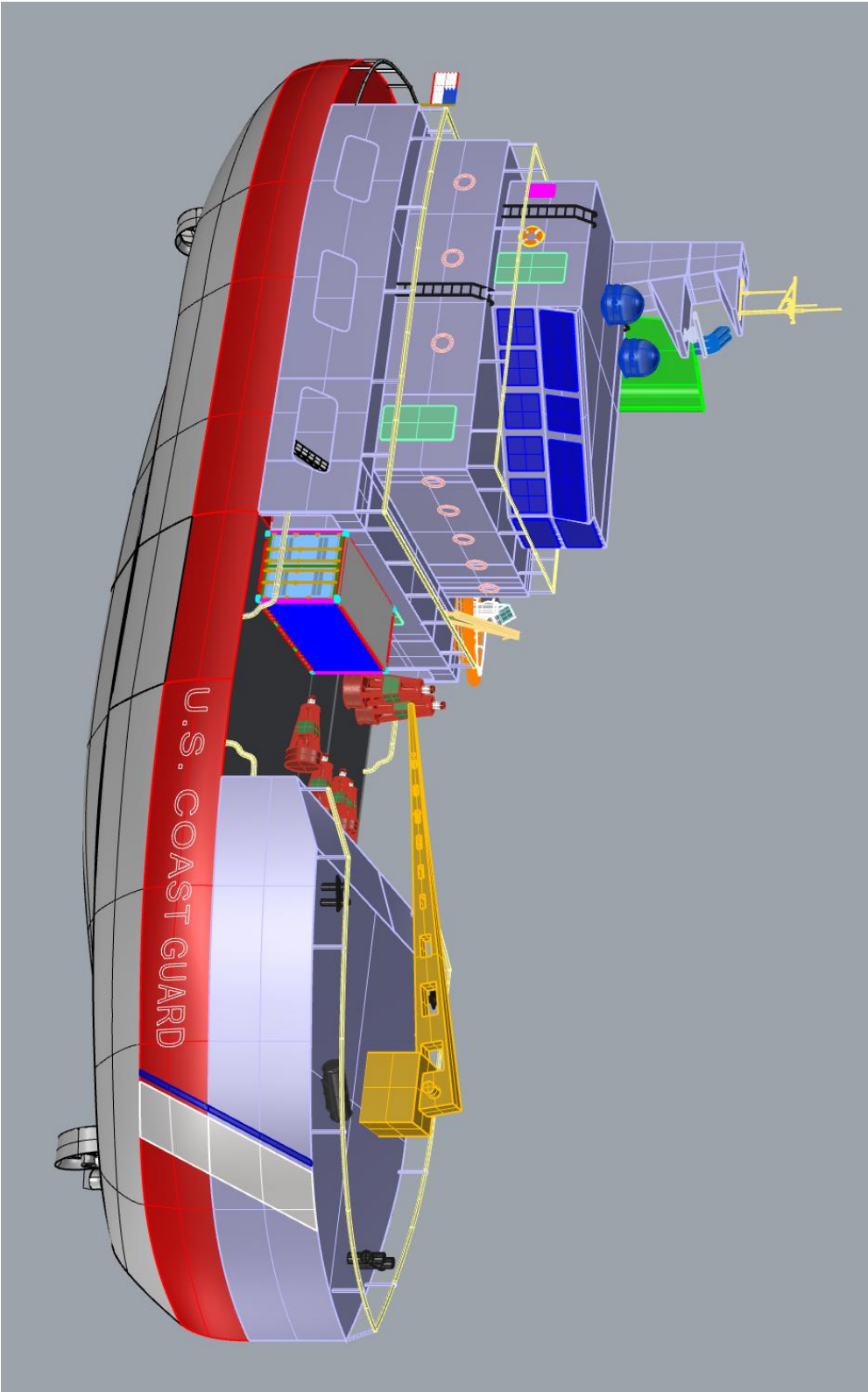
Appendix A

Appendix B

Current Status of Maritime Batteries and Future Outlook

Syb ten Cate Hoedemaker, Maritime Battery Forum, Rotterdam/Netherlands,
director@maritimebatteryforum.com

Abstract

The Maritime Battery Forum keeps track of the development of battery powered vessels in its Ship Register. This paper describes the development of maritime batteries over the past decades divided in 3 different periods. The number and type of vessels powered by batteries, as well as the size and type of the installed batteries are discussed. Current trends are evaluated and projected to create an outlook for the coming decades.

1. Introduction

Battery powered boats have been around since the 19th century, but it is not until the last 15 years that batteries started to claim a more important role within the maritime industry. In 2014 the Maritime Battery Forum (MBF) was founded with the goal to promote batteries in the maritime industry by sharing knowledge and information. The MBF, in collaboration with DNV, maintains a Ship Register to keep track of the development of battery powered ships, https://www.maritimebatteryforum.com/ship-register. This study describes an analysis of the battery powered ships in the MBF Ship Register, divided in three main periods.

First the early years of battery powered ships between 1998 and 2013 are discussed. Then the industry saw a significant change with the delivery of the full electric ferry "Ampere", leading to the second generation of battery powered ships between 2014 and 2018. The current period between 2019 and 2022 is described as the current generation of battery powered ships, where a wider range of vessel types is being electrified and battery systems are increasing in size significantly. This is followed by a general overview of the development of the global fleet of battery powered ships up to 2022.

One specific country stands out when it comes to battery powered ships, Norway. The key factors for success in Norway are discussed, followed by a calculation of the future demand of maritime batteries up to 2050, based on the trends identified between 2008 and 2022. The current growth is projected to match the global marine decarbonization goals, and it is seen that a further increase in effort is required by the maritime industry to achieve the IMO goals of an overall reduction in emissions of 50% by 2050, compared to 2008.

This study is based on the data from the MBF Ship Register. This is considered as the most complete database of battery powered ships available, however, there can be specific ships missing in this database. Future updates of the Ship Register might change the conclusions in revisions of this paper.

2. The early years (1998-2013)

The oldest battery powered vessel in the MBF Ship Register is "Le passeur", a 10 m long ferry built in 1998 in La Rochelle, France, with an installed battery capacity of 20 kWh. In the period between 1998 and 2010 several other battery-powered ferries were built in France, with batteries ranging from 20 up to 130 kWh. These ferries used Lead-acid or Nickel-Cadmium batteries as energy source.

The first ship mentioned in the MBF Ship Register using a Lithium-ion battery system as energy storage system was the sailing yacht "Ethereal" built by Royal Huisman in the Netherlands in 2008. This 58 m long sailing yacht used a 500 kWh battery system in a hybrid propulsion system. From 2010 several car/passengers ferries and private submarines followed with battery systems between 40 kWh and 1446 kWh of installed capacity. In Canada a research vessel was retrofitted with a battery system in 2011. In 2013 the first hybrid tugs started sailing with a battery capacity ranging from 117 kWh up to 546 kWh.

74% of the battery installations on board of ships between 1998 and 2013 were on newbuild vessels, the other 26% were retrofits. The majority (48%) of the battery powered ships delivered in this period were pure electric, 37% of the vessels were hybrid and 15% of the battery powered vessels were plug-in hybrid, Fig.1.
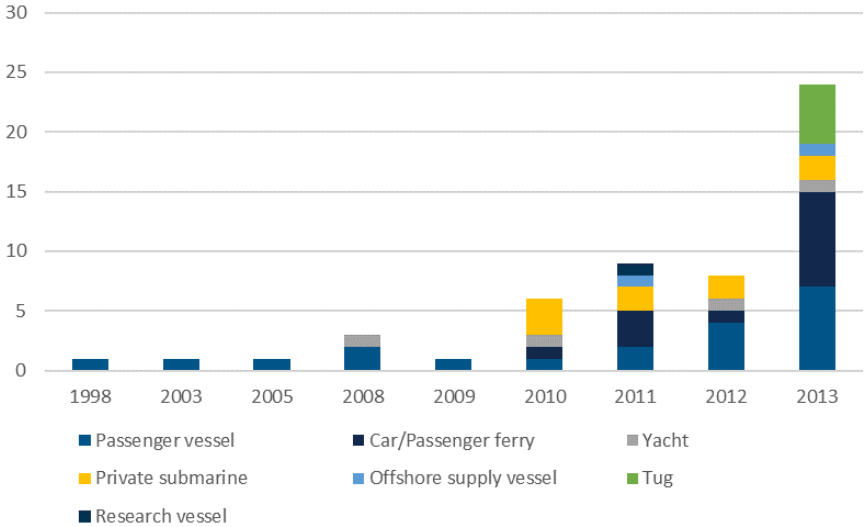

Fig.1: Types of ships with batteries installed between 1998 and 2013

The earliest battery powered ships used Nickel-Cadmium and Lead-acid types of batteries, Fig.2. In 2008 the first Lithium-ion battery system was installed on board a ship. For pure electric ships, only powered by batteries, Lead-acid and Nickel-Cadmium batteries were the preferred choice until 2011, and Lithium-ion batteries were predominantly used in hybrid propulsion systems.

From 2011 more ships started using Lithium-ion batteries, first mainly of the NCA type, but quickly LFP and specially NMC types of Lithium-ion batteries became more popular than NCA, mainly due to the higher fire risks related to NCA batteries.
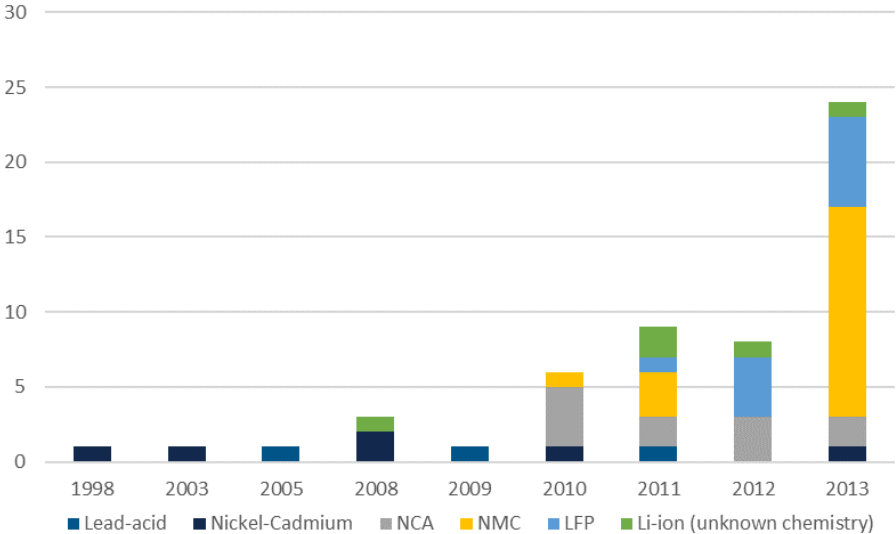

Fig.2: Types of battery chemistries installed between 1998 and 2013

The installed battery capacity for the oldest vessels in the Ship Register was only 20 kWh, but this soon started to increase with an average installed capacity of 253 kWh in 2008, 479 kWh in 2011 and 567 kWh in 2013. Due to the limited number of battery powered vessels in those years, the average installed battery capacity per year fluctuated significantly due to specific battery installations. The majority of

the battery powered vessels between 1998 and 2013 were below 30 m in length. Pure electric vessels did not exceed 20 m in length.
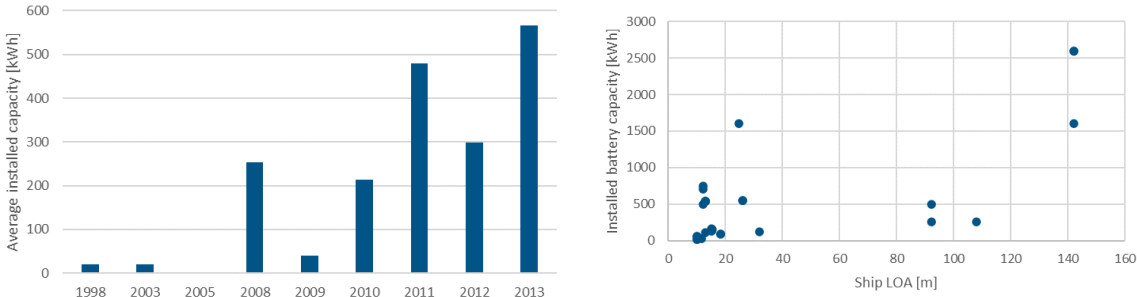

Fig.3: Average battery capacity installed per ship (left) and over ship length (right) in kWh between 1998 and 2013

3. The Ampere age (2014-2018)

In 2014 the first pure electric car/passenger ferry "Ampere" was delivered in Norway. With 1860 kWh of installed battery capacity, it was the start of a new age of full electric ships, and a good example of the possibilities for batteries in the maritime industry. Although in 2014 and 2015 the number of battery powered ships delivered was less compared to 2013 (Fig.4), and the average installed battery capacity was smaller as well (Fig.6), the different types of vessels using batteries for propulsion started expanding further. First, several workboats and different types of vessels for the fishing and fish farming industry were electrified. Followed by a variety of cargo vessels such as general cargo ships, RoRo cargo ships, bulk carriers, and Oil/chemical tankers, as well as a patrol vessel. The number of battery powered offshore supply vessels, yachts, tugs and research vessels continued to increase as well.

63% of the battery installations on board of ships between 2014 and 2018 were on newbuild vessels, the other 37% were retrofits. The majority (58%) of the battery powered ships delivered in this period had a battery integrated in a hybrid propulsion system, 17% of the vessels were plug-in hybrid and 25% of the battery powered vessels were pure electric. Compared to the period between 1998 and 2013 we see an increase in retrofits and an increase in popularity of both hybrid and plug-in hybrid propulsion systems.
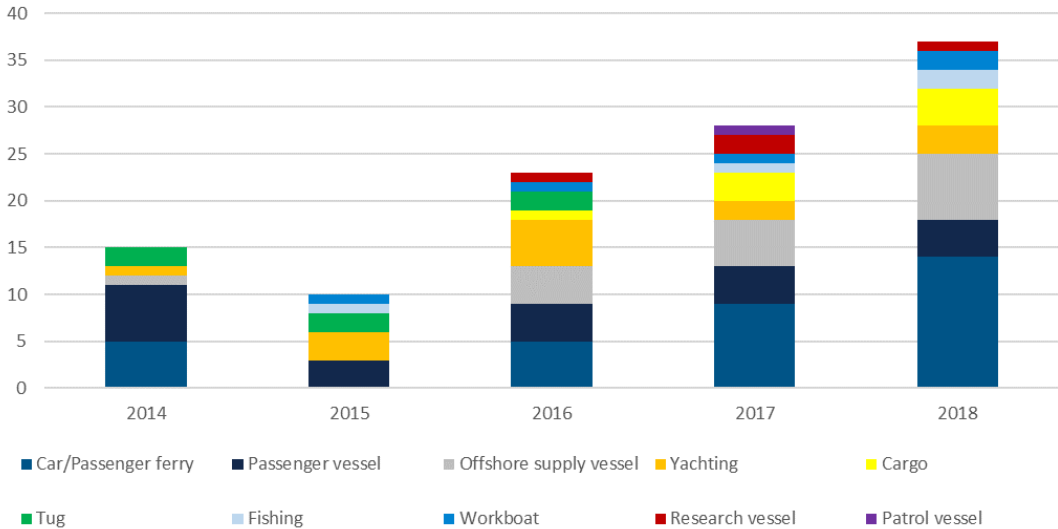

Fig.4: Types of ships with batteries installed between 2014 and 2018

Except for one ferry powered by a Lead-acid battery in 2014 and two Nickel-Cadmium powered ferries in 2016, Lithium-ion batteries showed their potential for electrification of ships. LFP and NCA were

126

used in some cases, as well as LTO sporadically, but the majority of the vessels were powered by NMC batteries. Of the vessels delivered in 2018, 97% used NMC batteries.
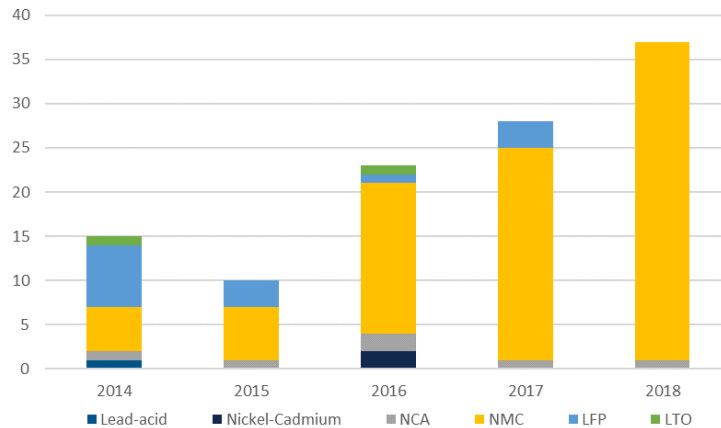

Fig.5: Types of battery chemistries installed between 2014 and 2018

Between 2010 and 2016 the average installed battery capacity per vessel varied between 200 kWh and 570 kWh, with no clear increase until 2017. The largest installed battery in 2013 was 2600 kWh, by 2018 this was 4160 kWh. On a year-by-year basis the average installed battery capacity fluctuates significantly, but an overall increase in battery size is shown to be the trend.
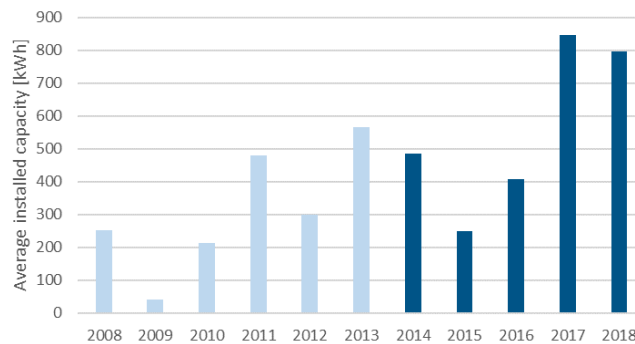

Fig.6: Average battery capacity installed per ship 2008-2018

There is no clear link between ship length and installed battery capacity, or between the installed propulsion power and the battery capacity, as can be seen in Fig.7. This can be explained by the large variety of applications for batteries on board of ships, as well as the varying operational profiles of ships. Batteries can be used for electric propulsion, but also for applications such as peak shaving, spinning reserve, or load leveling, which combined with the specific operational profile of the vessel, will have different requirements for the battery system size.
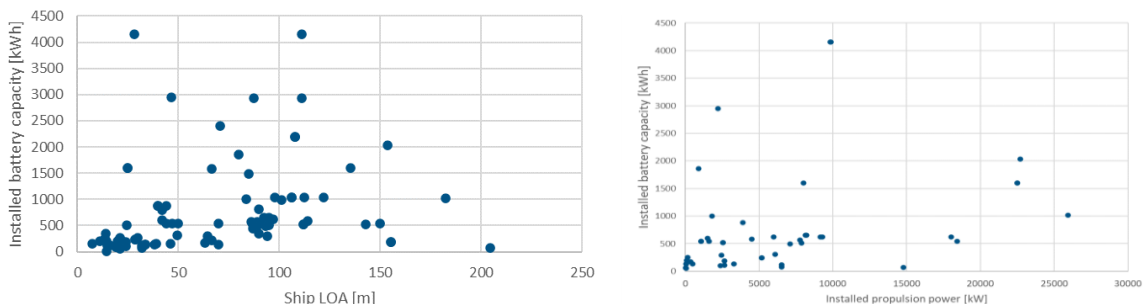

Fig.7: Battery capacity compared to ship length [m] and propulsion power [kW] (2014-2018)

4. Current generation of battery powered ships (2019-2022)

Over the last 4 years the diversification of types of ships with batteries has continued. Offshore supply vessels continued to gain a position as one of the most popular types of ships for battery installations, but an impressive growth is shown for cargo ships and ships in the fishing/fish farming industry. The category cargo vessels contains bulk carriers, container vessels, tankers, and general cargo vessels. The category fishing contains amongst fishing vessels also fish farm support vessels and fish carriers. Two categories that started to increase in size over the last two years are cruise vessels and vessels for the offshore wind industry. In 2021 there is a clear dip in the number of delivered battery powered vessels.

75% of the battery installations on board of ships between 2019 and 2022 were newbuild vessels, the other 25% were retrofits. The majority (53%) of the battery powered ships delivered in this period had a battery integrated in a hybrid propulsion system, 26% of the vessels were plug-in hybrid and 21% of the battery powered vessels were pure electric. Compared to the period before 2019 we see an increase in the percentage of newbuilds and an increase in popularity of plug-in hybrid propulsion systems.
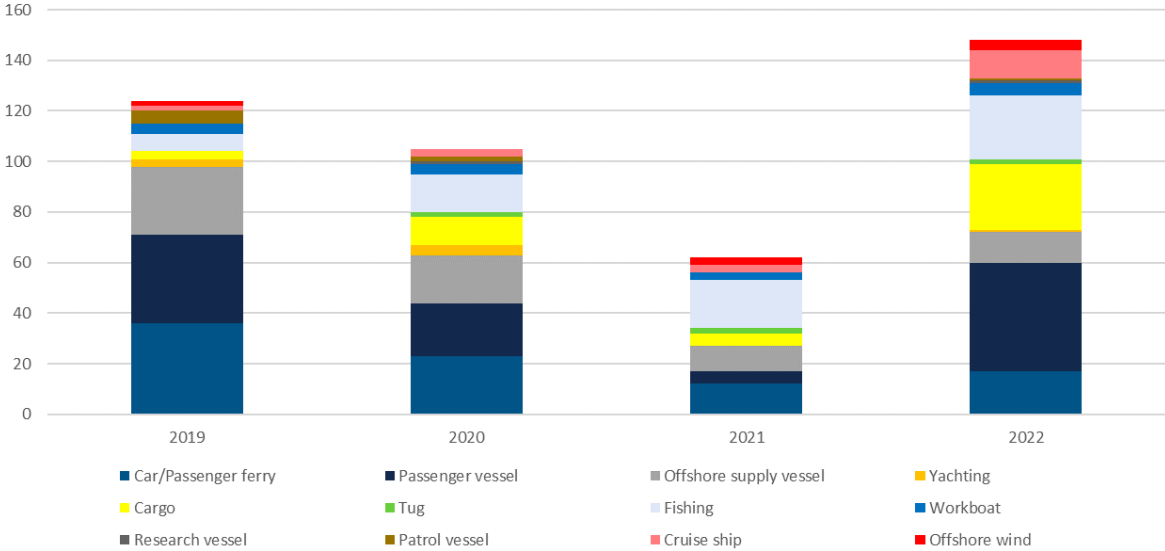

Fig.8: Types of ships with batteries installed between 2019 and 2022

As can be seen in Fig.9, NMC has taken the position as preferred Lithium-ion chemistry for maritime battery systems. Although LFP remains the choice for some of the vessels in France and China, there has not been a significant increase in the use of LFP battery systems, as is the case for the automotive industry. In the maritime industry it seems like LTO batteries are lining up to challenge NMC batteries.
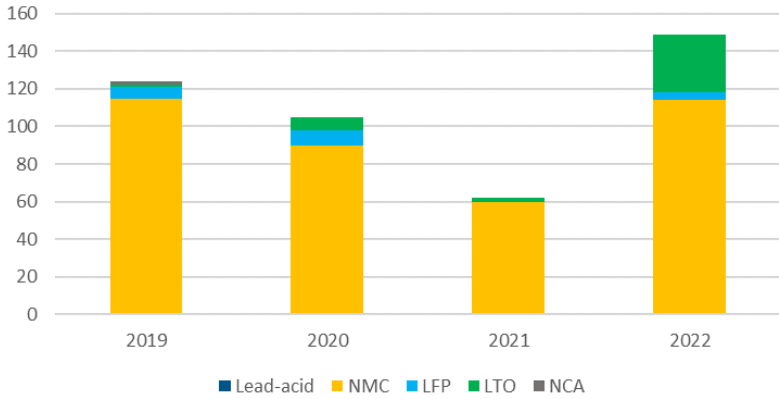

Fig.9: Types of battery chemistries installed between 2019 and 2022

128

The average installed capacity per ship continued to increase over the last four years to an average of approximately 1.2 MWh per ship. The largest installed battery in 2013 was 2.6 MWh, and in 2018 it was 4.2 MWh. By 2022 the largest installed battery system on board of a ship is 10 MWh.
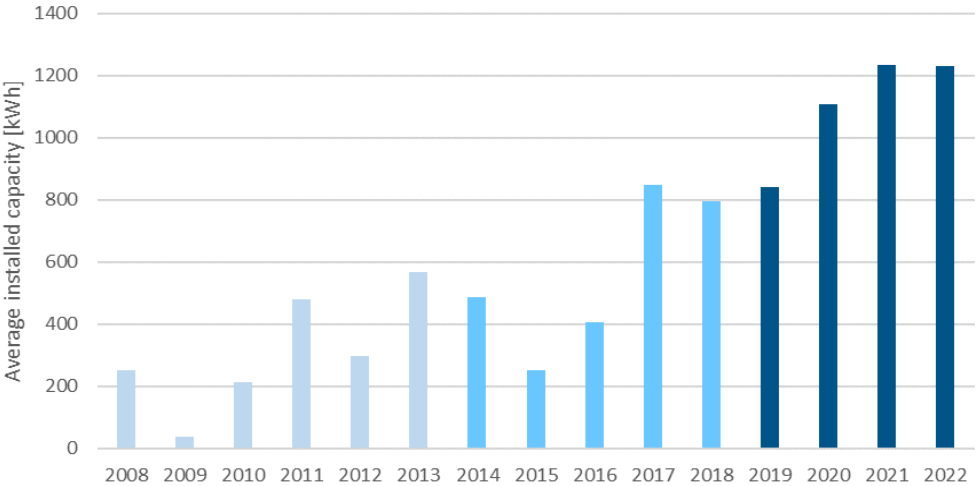

Fig.10: Average battery capacity installed per ship 2008-2022

5. Summary of battery powered ships until 2022

The average installed battery capacity per year is shown in Fig.11. Here it can be seen that a significant increase in installed battery capacity happened in 2019, and after a small decrease in 2021, the installed capacity in 2022 has increase significantly again to a total of approximately 180 MWh. Note that this paper is written in July 2022 and although many of the vessels under construction are taken into account in the ship register, the total installed battery capacity in 2022 is expected to increase.
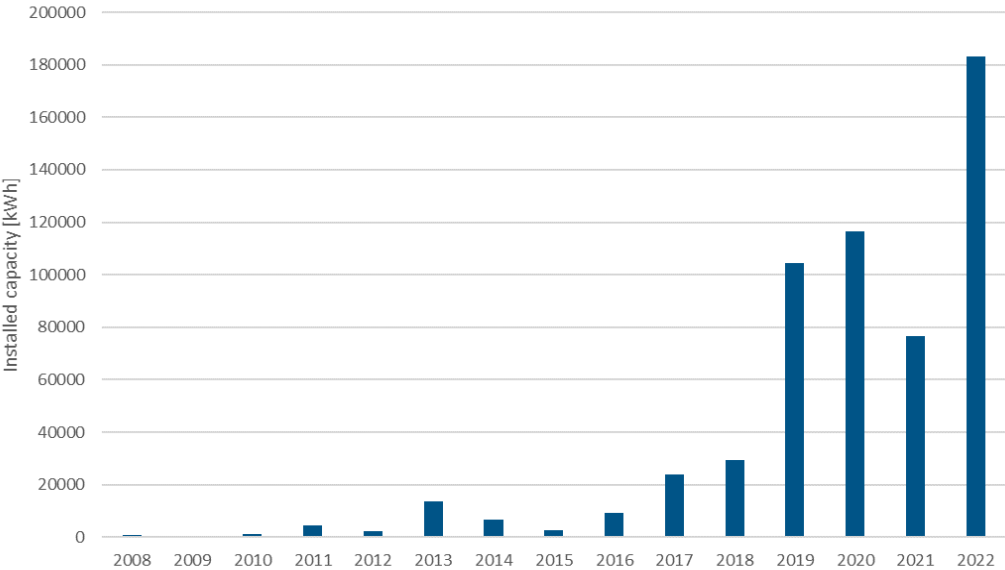

Fig.11: Total installed battery capacity per year in kWh (2008-2022)

Fig.12 shows the average installed capacity of the different ship types over the complete period between 1998 and 2022. The vessels with the largest battery systems installed are container vessels, Ro-Ro cargo ships, cruise ships and RoPax vessels.
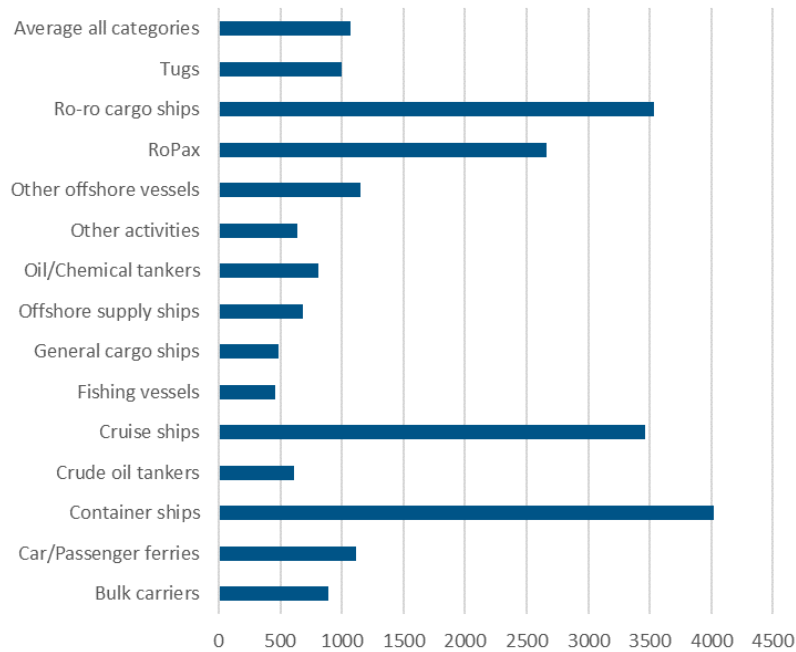
Fig.12: Average installed battery capacity per ship type
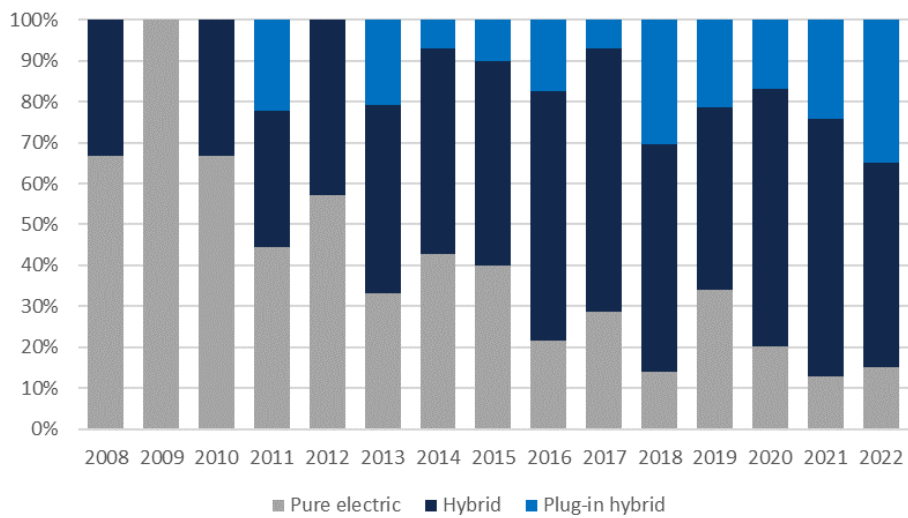
Fig.13: Types of electric propulsion configuration
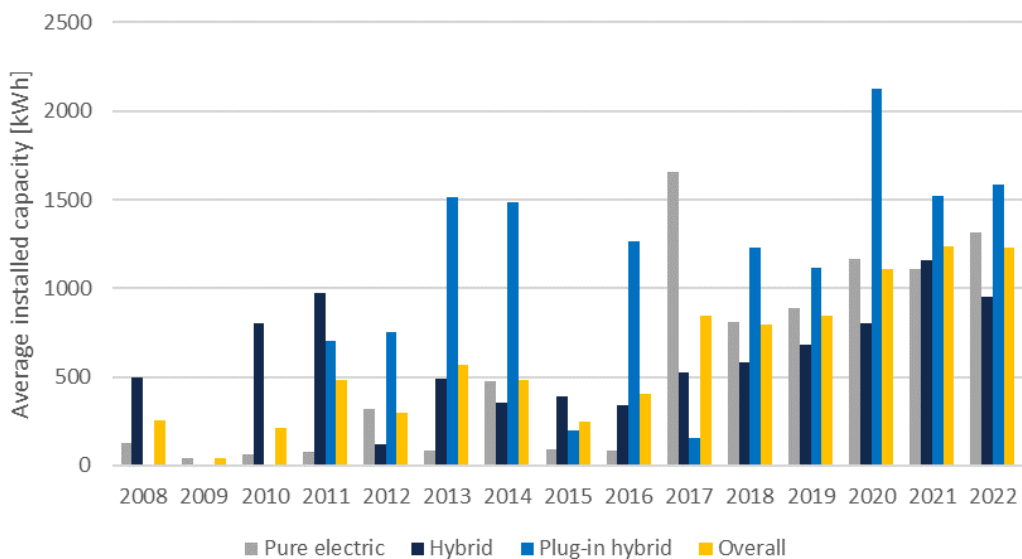
Fig.14: Average installed capacity for different configurations

The electric propulsion configuration of battery powered ships is divided in 3 types in the Ship Register: Pure electric, Hybrid, and Plug-in hybrid. Fig.13 shows the percentages of the types of configuration of the fleet of battery powered vessels per year. Pure electric ships was the largest group from 2008 until 2012. From 2012 the hybrid configurations took over as most popular configuration for battery powered ships, and it is still the most common configuration. However, there is an increase in plug-in hybrid vessels, which already outnumber the pure electric vessels and are approaching the same numbers as hybrid vessels. With a larger availability of shore power and standardization of charging systems, it is expected that plug-in hybrid vessels will gain more in number compared to hybrid vessels as well.

Since 2018 the average installed capacity on plug-in hybrid vessels has been the largest compared to pure electric and hybrid vessels. Except for 2021, the average installed capacity on board of pure electric vessels since 2018 has been larger compared to hybrid vessels, Fig.14.

6. The accelerated adoption of batteries in Norway

There is one specific area that stands out with the total number of battery powered ships, Norway. Almost half of all the battery powered ships are operating in Norway. 25% of the battery powered ships operate throughout the rest of Europe, 14% in Asia, 8% in the Americas (mainly North America), and 4% of the battery powered ships operate globally.
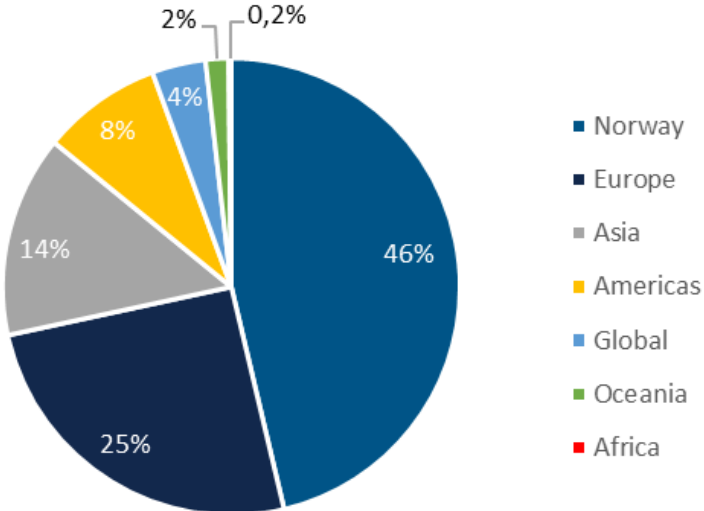


Fig.15: Area of operations of battery powered ships
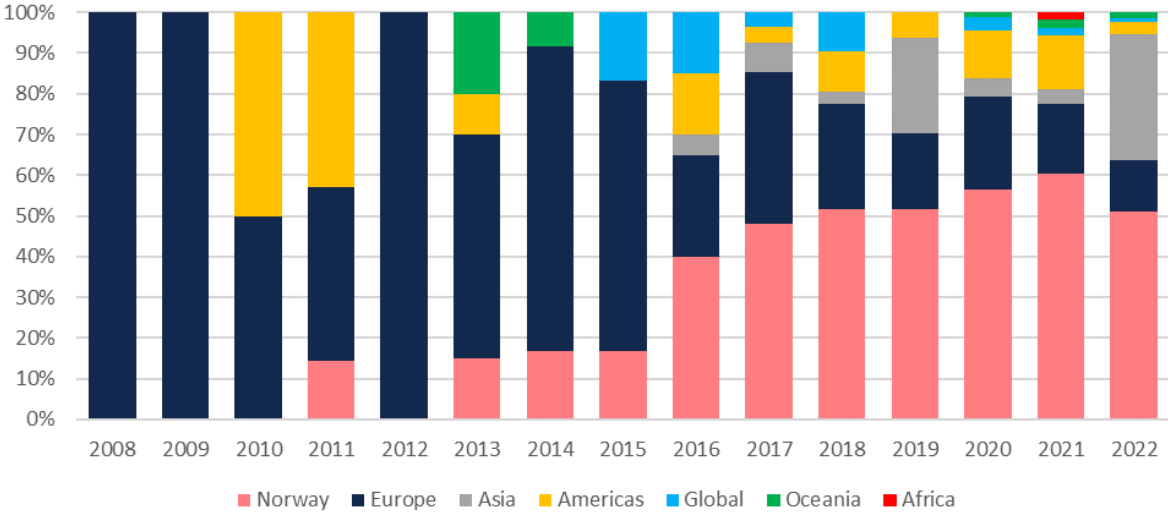
Fig.16: Area of operations of battery powered ships delivered per year

Fig.16 shows how the area of operation of battery powered ships delivered per year has changed between 2008 and 2022. Europe started first with the adoption of battery powered vessels, followed by North America. In 2011 the first Norwegian battery powered vessel went in operation. From 2013 until 2021 the market share of battery powered vessels for Norway increased every year. In 2022 for the first time the market share decreased slightly. The market share of (the rest of) Europe and North America decreased over the years. In 2019 and 2022 there has been a large increase in battery powered vessels in Asia.

Rostad Sæther (2021) identified four key factors for the success of electrification of Norwegian ferries:

1. Norway has a ferry innovation system characterized by a culture of close collaboration, mutual trust, and information-sharing. This made it possible to overcome potential initial resistance to electrification and for the maritime sector to pull in one direction.
2. The Norwegian state acted entrepreneurially, by moving beyond merely being a de-risker through playing an active role in market creation and transformation through public agencies and support schemes.
3. A lack of resistance from vested interests. The maritime sector constitutes a politically influential potential brake. It is important that there are no losers in the energy transition, as losers can make it go slower.
4. The transition was accelerated by a shock, namely the 2014 oil price crash, which inflicted empty order books on a maritime sector overly dependent on orders from the petroleum sector, providing an incentive to find new markets.

These key factors can also be transferred to match the local conditions in other parts of the world and can support the accelerated energy transition within the maritime industry on a global scale in a more general approach. Companies should focus more on collaboration, trusting partners, and sharing information, instead of competing for being the first to offer the best zero emission solution. Governments should play a more active role in market creation and transformation. Tender specifications should be made with technology development in mind, as battery technology is improving so fast that there is a fear of locking in solutions that might soon be obsolete. The parties relying on the traditional technology in ship propulsion should be motivated to become a part of the solution by transitioning to new technologies. The final part of the equation is a shock to accelerate the transition. This shock can also be considered as something created by governments, e.g. taxation of pollution, in combination with incentives on decarbonizing solutions.

Interesting to mention is that the incentives for battery powered ships in Norway, provided through Enova. Where applicants can apply for funding for infrastructure expenses for up to a maximum of 40% of the cost. Has been discontinued on 1 October 2021, as battery electrification has established itself as an economically feasible and suitable solution for zero- and low-emission ships, *Enova (2021)*.

6. Effect of global decarbonization goals on maritime battery demand

The initial GHG strategy by the IMO envisages a reduction of CO2 emissions compared to 2008 of at least 40% by 2030 and pursuing efforts towards 70% by 2050, and that total annual GHG emissions from international shipping should be reduced by at least 50% by 2050 compared to 2008, *IMO (2022)*. This will not all be realized with installing batteries on board of ships only.

Alternative fuels like hydrogen, methanol and ammonia will play a crucial role in this as well. As the world is transitioning to different energy sources and fuels, the costs for these new technologies will be higher compared to the current situation. Therefore, there will be a stronger focus on energy efficiency and fuel reduction.

Batteries have proven over the last decade that they are very well capable of improving energy efficiency and reducing the fuel used on board of ships, *NN (2022)*. Hydrogen Fuel cells are for most

applications dependent on a battery to handle the peak power demands and therefore it is expected that the future of ship propulsion will lay in hybrid propulsion systems, where batteries will play an important role to support the selected type of alternative fuel system.
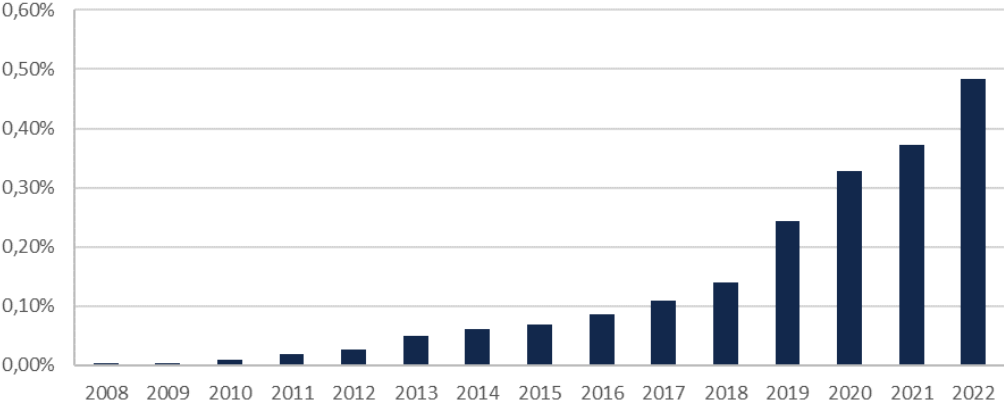

Fig.17: Percentage of global merchant fleet with batteries on board

Fig.17 shows the percentage of ships in the global merchant fleet that have batteries installed on board, based on the statistics of the global merchant fleet by *EMSA (2020).* The increase in fleet percentage with batteries is fitted with a 3rd order polynomial trendline to estimate the increase in battery demand from now until 2050. These statistics show an average annual growth of 1,94% of the global merchant fleet between 2008 and 2020. This growth is assumed to applicable to the global merchant fleet up to 2050.

The increase of battery powered ships as percentage of the global merchant fleet is used to estimate the increase of battery powered ships up to 2050, based on the growth between 2008 and 2022, Fig.18. If the increase in adoption of maritime batteries continues to develop as it did between 2008 and 2022, it is calculated that by 2050 18.2% of the global merchant fleet, approximately 38.959 vessels will have batteries installed on board.

Assuming that by 2050 the goal is to reduce overall emissions by 50% compared to 2008, and the expectation that vessels with alternative fuels will need batteries as well, this is considered to be an underestimation of the growth in demand for maritime batteries. A significant growth in battery installations will be needed to reach the global decarbonization goals for the maritime industry by 2050.
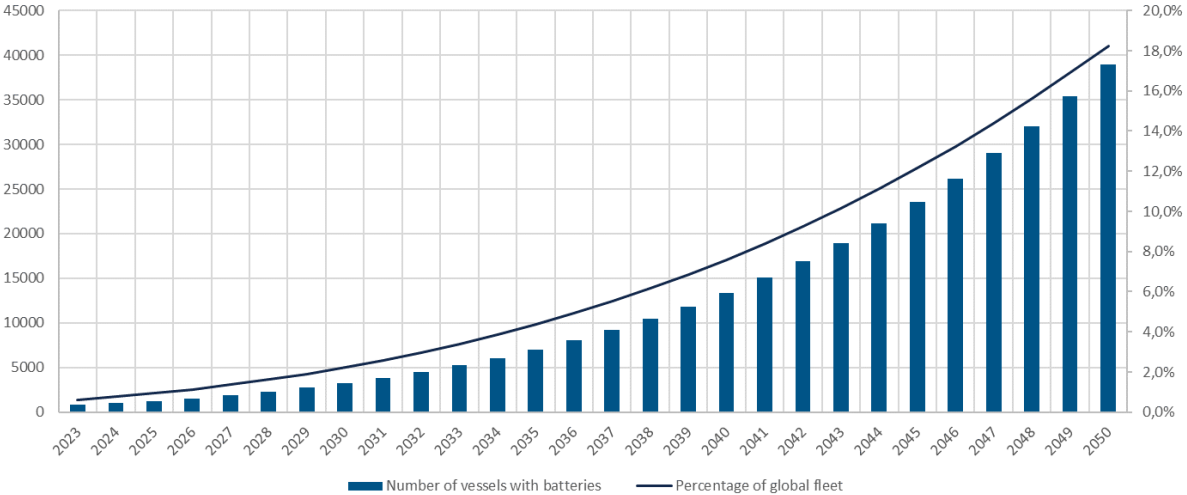

Fig.18: Increase in battery powered ships globally up to 2050 based on growth between 2008-2022 (conservative)

A calculation is made for the expected global demand of maritime battery systems based on the increase in number of battery powered ships, Fig.18, and assuming a linear growth of the average installed battery capacity per ship based on the batteries installed between 2008 and 2022 as shown in Fig.14.

This linear assumed growth in average installed battery capacity will result in an average installed battery capacity of 1778 kWh per ship in 2030 and 3343 kWh per ship in 2050. As shown in Fig.19, by 2030 the annual global demand for maritime batteries will be 916 MWh, by 2040 it will be 3950 MWh, and by 2050 it will be 11955 MWh. An average annual increase in battery demand 16% is calculated between 2023 and 2050 assuming the market will follow the same trends in growth of fleet size and battery size compared to the growth between 2008 and 2022.

As mentioned, this is not expected to be sufficient to reach the global marine decarbonization goals by 2050 and therefore the demand for batteries will be pushed even further up due to these goals.
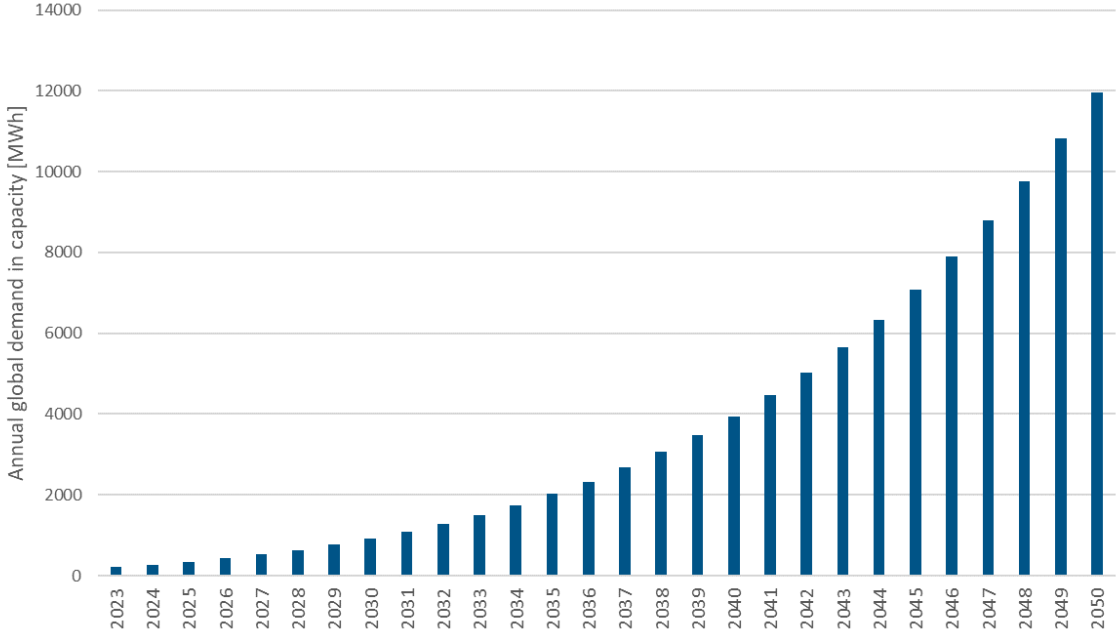
Fig.19: Global annual demand for maritime batteries based on growth trends between 2008-2022 (conservative)

7. Conclusions

Batteries have seen a promising uptake on a global level in the maritime industry. All types of vessels can potentially benefit from installing a battery system on board, when applied for the right reasons. Initially there was a strong focus on pure electric vessels. Soon the advantages of hybrid propulsion systems for other types of vessels were discovered. With the increase in availability of charging stations and standardization, the number of plug-in hybrid vessels will continue to grow, significantly reducing local emissions and pollution.

The projected estimations in this paper are based on the development of the maritime battery market between 2008 and 2022. Assuming the market will develop at a similar pace, it is expected that 18,2% of the global merchant fleet will have batteries installed by 2050. Assuming that batteries will be part of the solution for the adoption of future fuels like hydrogen, methanol and ammonia the current rate of installing batteries, with an annual growth in installed capacity of 16%, will not be sufficient to comply with the IMO goals of an overall emission reduction of 50% compared to 2008 by 2050.

The four key factors for the success of maritime batteries in electrifying the Norwegian fleet should be adapted to fit the local situation in other regions to increase the global uptake of maritime batteries.

These four key factors are:

- An innovation system characterized by a culture of close collaboration, mutual trust, and information sharing;
- An entrepreneurially acting state;
- A lack of resistance from vested interests;
- A market shock accelerating the transition.

References

EMSA (2020), *The 2020 World Merchant Fleet – Statistics from Equasis*, Technical reports, studies and plans - The world merchant fleet - statistics from Equasis - EMSA - European Maritime Safety Agency (europa.eu)

ENOVA (2021), *Enova avvikler støtten til infrastruktur for offentlige transporttjenester*, https://presse.enova.no/pressreleases/enova-avvikler-stoetten-til-infrastruktur-for-offentlige-transporttjenester-3112353

IMO (2022), Initial IMO GHG strategy, https://www.imo.org/en/MediaCentre/HotTopics/Pages/Reducing-greenhouse-gas-emissions-from-ships.aspx#:~:text=The%20initial%20GHG%20strategy%20envisages,that%20total%20annual%20GHG%20emissions

NN (2022), *Eidesvik – A battery success story,* Workboat365, https://workboat365.com/commercial-marine-news/power-propulsion-news/eidesvik-a-battery-success-story/

ROSTAD SÆTHER, S. (2021), *A green maritime shift: Lessons from the electrification of ferries in Norway*, Energy Research & Social Science 81

Web-based Microservices for Fast Modeling and Easy Collaboration

Simon Hauschulz, FRIENDSHIP SYSTEMS, Potsdam/Germany,
hauschulz@friendship-systems.com
Stefan Harries, FRIENDSHIP SYSTEMS, Potsdam/Germany, harries@friendship-systems.com
Fabian Thies, FRIENDSHIP SYSTEMS, Gothenburg/Sweden, thies@friendship-systems.com
Heinrich von Zadow, FRIENDSHIP SYSTEMS, Potsdam/Germany,
von.zadow@friendship-systems.com

Abstract

Expertise and know-how can be wrapped up in web-based microservices for convenient access and efficient utilization. Building on the frequently used web applications (webApps) for propeller design and generation, the so-called Wageningen webApps developed and hosted by FRIENDSHIP SYSTEMS on the basis of CAESES 5, further microservices have been created in order to support fast modeling and easy collaboration. The paper will give an account of the usage of the Wageningen webApps. It will further discuss a webApp for the parametric modeling of rudders and another webApp for the creation of hull forms from openly available data, either approximating a ship in operation or serving as a starting point for preliminary design. These microservices illustrate how to undertake fast modeling and how to promote easy collaboration, making the expertise of specialists available to a wider community.

1. Introduction

For quite a few years already, data storage in the cloud, co-authoring of documents (e.g., Excel and Word), remote computing, Software-as-a-Service (SaaS) for design and engineering and various other microservices have enjoyed increasing popularity. The global COVID-19 pandemic has further accelerated mobile work and remote collaboration. People are very much used to sharing data via the internet and working together online while not all resources are necessarily located on their own computers or within a company's intranet anymore.

When looking at the definition of microservices on Wikipedia, https://en.wikipedia.org/wiki/Microservices, the following main characteristics shall be highlighted:

- "The goal is that teams can bring their services to life independent of others. Loose coupling reduces all types of dependencies and the complexities around it, as service developers do not need to care about the users of the service…"
- "Communication requirements are reduced. These benefits come at a cost to maintaining the decoupling…"
- "Services are small in size, messaging-enabled, bounded by contexts, autonomously developed, independently deployable…"

Closely related to microservices are web applications, https://en.wikipedia.org/wiki/Web_application:

- "A web application (or web app) is application software that runs in a web browser, unlike software programs that run locally and natively on the operating system (OS) of the device. Web applications are delivered on the World Wide Web to users with an active network connection."

In the context of this paper a web application, called webApp hereafter, is a special microservice that has an easy-to-understand purpose, a clear sequence of steps to be followed, does not require any comprehensive training, and creates added value quickly but within limited scope. See *Harries et al. (2018)* for an elaboration. A webApp is different to a large software system that typically allows solving rather diverse and often very complex tasks, supporting different workflows.

Up until now, the overwhelming majority of large systems of Computer Aided Engineering (CAE), be it for modeling and design (CAD) or for analysis and assessment (CFD and FEA), are installed on dedicated hardware, say an engineering workstation, and need substantial training and expertise. They are run locally or remotely via a virtual private network (VPN) by an employee of the company or the institute that holds a valid license. Access to the system is typically restricted and most licensors exclude third-party usage explicitly. In this sense, the users and the providers of the software are very tightly connected.

Contrary to this, web-based microservices potentially decouple the service provider and the user as they may only have a short-term relationship, i.e., the service provider grants temporary access to a webApp for a certain fee or even for free. This creates new opportunities for both academia and businesses as there are many high-quality codes and expertise which presently are very difficult to access and benefit from. The aim is to enable faster work and easier collaboration, see also *Harries and Abt (2021)*.

Within this paper the Wageningen webApps for propeller design and generation, respectively, developed and hosted by FRIENDSHIP SYSTEMS, shall be discussed with regard to their usage since their introduction in 2018. Furthermore, a new webApp for the modeling of rudders shall be introduced. It is used to explain the method of building and deploying a webApp on the basis of CAESES 5, including an elaboration on the underlying fully-parametric model. Finally, a webApp for the fast generation of hull forms representative of smaller tankers shall be presented. The webApp generates a first level approximation of a bare hull from very little input data, intending to support ship operators and design offices alike. The three microservices combined already enable the user to produce a sophisticated representation of the hydrodynamically relevant components of a ship with very limited resources.

2. Wageningen webApps

2.1. Background

In 2018, FRIENDSHIP SYSTEMS introduced a webApp for the generation of Wageningen B-series propellers. It is accessible via https://www.wageningen-b-series-propeller.com/, *Harries et al. (2018)*. The user is able to create a watertight geometry with just a few input parameters, like the outer diameter of the propeller, the number of blades, the propeller material and general information about the engine, as seen in Fig.1. These input parameters already "determine the other blade details, like skew-back, rake, radial pitch distribution, blade contour, and blade section shapes. Also the hub diameter and contour are described" as explained by *Harries et al. (2018)*. The calculations and the modelling are run in the background and within seconds the user can download the propeller geometry as a STEP or STL file.
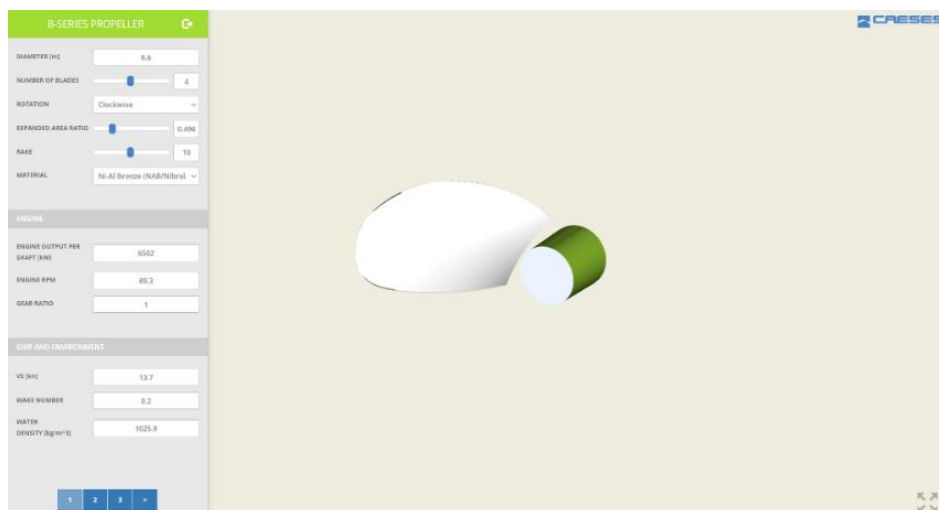

Fig.1: Modeling of a standard propeller via the Wageningen webApp called 'design tool'

A second webApp for the Wageningen B-series is also made available, the 'geometry tool'. The 'geometry tool' is meant for users that already know the values of their blade parameters. They have options to enter the pitch-diameter ratio, expanded area ratio and the rake angle. They can also enter thickness settings for leading and trailing edge and at the root and tip of the blade.

Neither the 'design tool' nor the 'geometry tool' are meant to replace a proper propeller design and optimization process but rather have other valid use cases such as quickly getting estimates for thrust, torque and efficiency and generating a stock propeller for CFD.

2.2. Public use over the years

In April 2021, FRIENDSHIP SYSTEMS started to collect data on the use of the Wageningen webApps. As depicted in Fig.2, the design and the geometry tool are both regularly used.
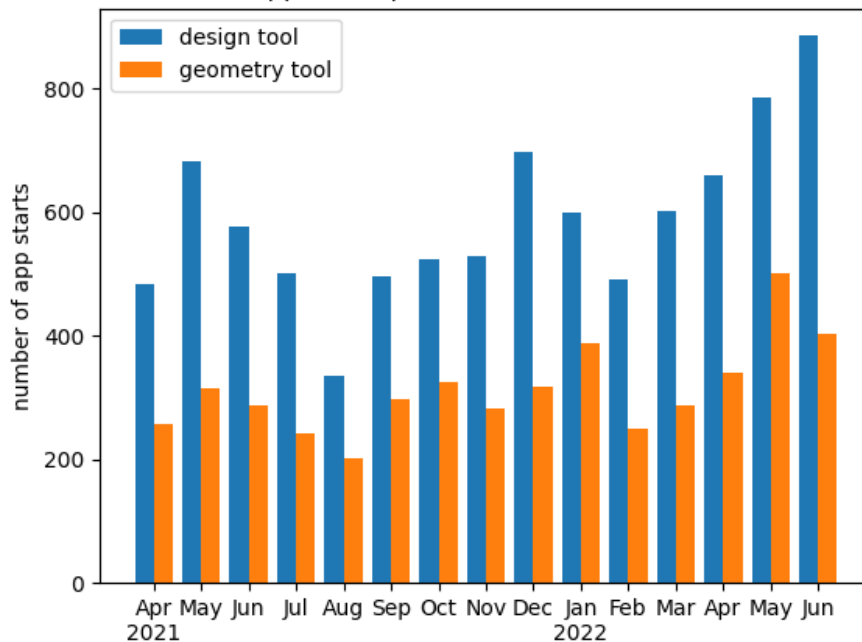

Fig.2: Number of App starts per month of the Wageningen webApps

Over a period of 15 months the design tool webApp was started more than 8800 times and the webApp for the geometry tool more than 4600 times. These numbers clearly show that web-based microservices offer added value.

3. Rudder webApp

The rudder webApp is accessible via https://www.friendship-systems.com/products/web-apps/show/app/shiprudder. It allows the fast and easy generation of spade and semi-balanced rudders which can then be downloaded as a STL file.

3.1. Underlying parametric model

As in all parametric models a focus should not only be put on high functionality but also on robustness of the model. This holds especially true for parametric models which will be used for webApps. In general, a webApp user does not know the underlying parametric model and therefore does not know if a certain input will lead to failures in the generated geometry. So, adapting the parametric model to the use case of a webApp is beneficial, meaning to think pro-actively about solutions which intercept incorrect usage. Furthermore, a robust parametric yet-flexible model allows the user to switch between two rudder types, a spade rudder and a semi-balanced rudder, with just one click, Fig.3.

Fig.3: Rudders generated within the webApp

The first step of the rudder modelling is the selection of a profile. Two standard profiles are provided, namely the NACA 0010 and the HSVA MP73-20 profile. The NACA 4DS (four digit series) being built-in in CAESES. The data for the HSVA profile was taken from *Bertram (2012)*. Both profiles are normalized to chord length and scaled to a thickness of 0.1 for easier modelling in later stages.

In the next step, the contours of the rudder from both the side and the front are defined via three curves. One for the leading edge from the side, one for the trailing edge from the side and only one for the front view, assuming symmetry. The three curves consist of a linear top part and a lower part which is a B-spline curve with three points, as shown in Fig.4.
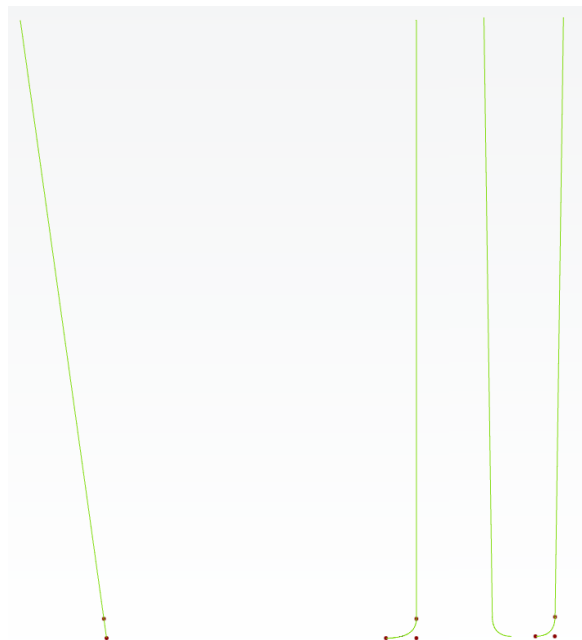

Fig.4.: Rudder contour from the side and the front

The last point of the B-spline can be moved in longitudinal direction (x-direction) via a design variable which will thereby change the shape of the contour at the bottom. This can be done independently for all three curves. If the so-called roundness design variable has the value zero, the B-spline is a straight line and for the value one, it has the maximum permissible roundness with the curves still not intersecting. There is also the option to change the z-position of the first point of the B-splines to give even more control over the bottom shape. This can be done only simultaneously for all three curves.

For the side view, the considered parameters are the rudder height, chord length at the top and the bottom, the roundness at the bottom at the front and back and the sweep angle. For the front view, the parameters are the rudder height, the ratio of thickness to chord length and the roundness at the bottom.

These two views now hold most pieces of the information needed for the creation of the rudder surface. The surface is generated via a CAESES Feature Definition. The feature extracts the information about the chord length from the side view and about the thickness from the front view in discrete steps in vertical direction (z-direction). On every z-position the profile initially chosen will be scaled according to the local information taken from the contours, Fig.4, and then a so-called Meta Surface (see Meta Surface: An Introduction › CAESES) is lofted across all these profiles. The resulting smooth surface will be converted into a closed BRep, i.e. a watertight geometry. From this, the spade rudder would already be available.

The spade rudder is used as a basis to build the other rudder type that is available in the webApp, the semi-balanced rudder.

For the creation of the skeg and the movable rudder part three sections are needed. The profile at the top of the rudder and two sections with z-positions chosen by the user, Fig.5.

In a next step, the profiles are cut and depending on which part they are used for either closed with a line or a semicircle. All the necessary surfaces are created based on these new curves. The resulting parts are shown in Fig.6.

Fig.5: Initial modelling steps for the semi-balanced rudder
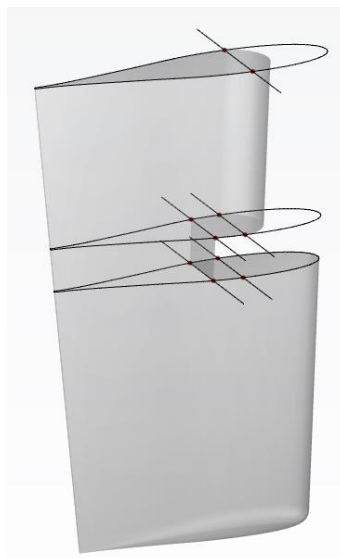
Fig.6: The parts of the semi-balanced rudder
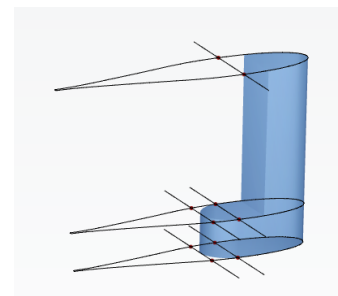
Finally, a bulb can be added to the rudder. Two types are implemented. A Costa bulb and a short bulb which is flush with the propeller hub. The profile for the costa bulb is a NACA 4DS profile. For the short bulb the first 25 percent of the NACA 4DS profile are trimmed. The longitudinal and vertical position (x- and z-position) of the bulb can be controlled. The x-position is measured from the tip of the top profile. For the z-position, the rudder type is taken into account to prevent the generation of infeasible geometries. Therefore, the normalized parameter for the vertical position results in different absolute values depending on the chosen rudder type. The bulb and the rudder are finally joined via a Boolean operation (union).

In addition, there is also an option for a headbox which is shaped according to the top profile of the rudder and does not allow any variances. This could be improved in a next-generation webApp or be provided via a separate webApp.

140

Furthermore, the parametric model allows extending the functionality of the webApp in the future. Some of the possible ideas are:

- support different shapes of the leading edge (not just linear ones)
- implement energy saving devices such as x-shape and z-shape rudders
- provide additional profile definitions or give the user the option to upload their own profiles

3.2. Set-up of a webApp via CAESES 5.1

There are two ways to generate a webApp out of a parametric model. First, the faster and simpler way, by just clicking on the 'create template' button when a scope is selected, see Fig.7. This will create a webApp page and will automatically generate all the necessary elements from the data in the selected scope. This can serve as a convenient baseline for further adaptations.
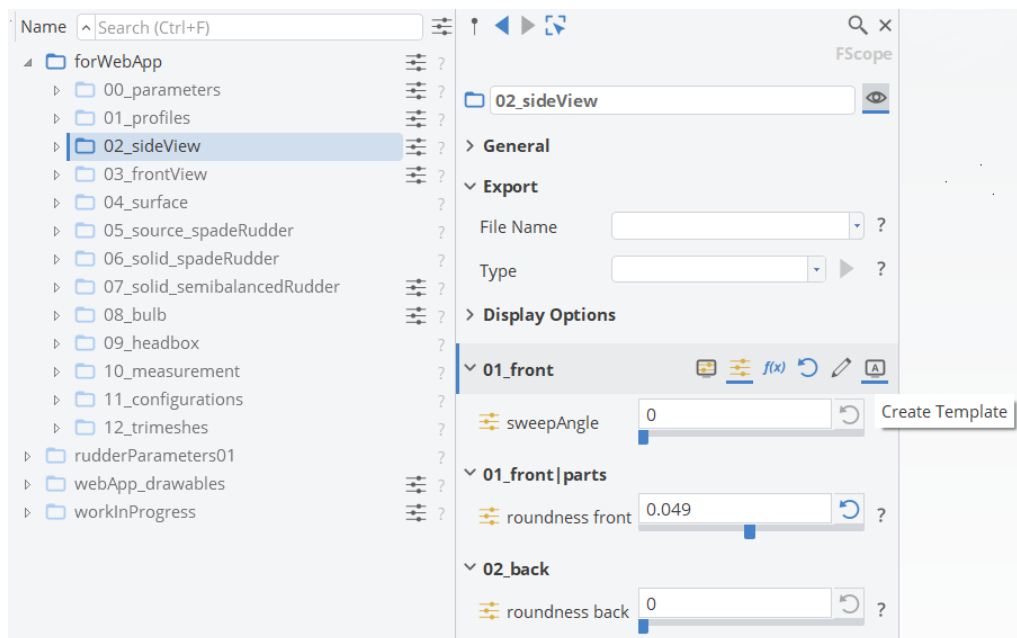

Fig.7: Create a webApp page with one click

Alternatively, an app may be built from scratch by a more experienced user. The rudder webApp was built that way. To show the different functionalities that can be implemented in a webApp in CAESES 5.1, the fourth page of the rudder webApp will be discussed by means of an example.

WebApps in CAESES consist of Web App Pages. On these pages, it is defined what objects, e.g. curves or BReps, are displayed in the central window and what controls are given for the webApp user, Fig.8. Right now, there are four control categories: buttons, misc, options and value fields.

For example, the first control in Fig.9 is a 'String-Options' selected from 'options', Fig.10. This control generates a drop-down list. The strings in this list are connected to the values of a design variable. So in this case, when "spade" is selected, as in Fig.9, the design variable "selectRudderType" will be set to 1. When the user chooses "semi-balanced" the design variable will be set to 2.

All the other controls are set up quite similarly to the 'String-Options', Fig.10. Which of them are the most useful, depends on the purpose of the webApp.

Note that this control is not directly responsible for changing the displayed rudder geometry but just changes the value of a design variable. That there actually is a change of the geometry is the result of a Feature which has the design variable as input and depending on an if-condition, either gives the spade or the semi-balanced rudder as an output.
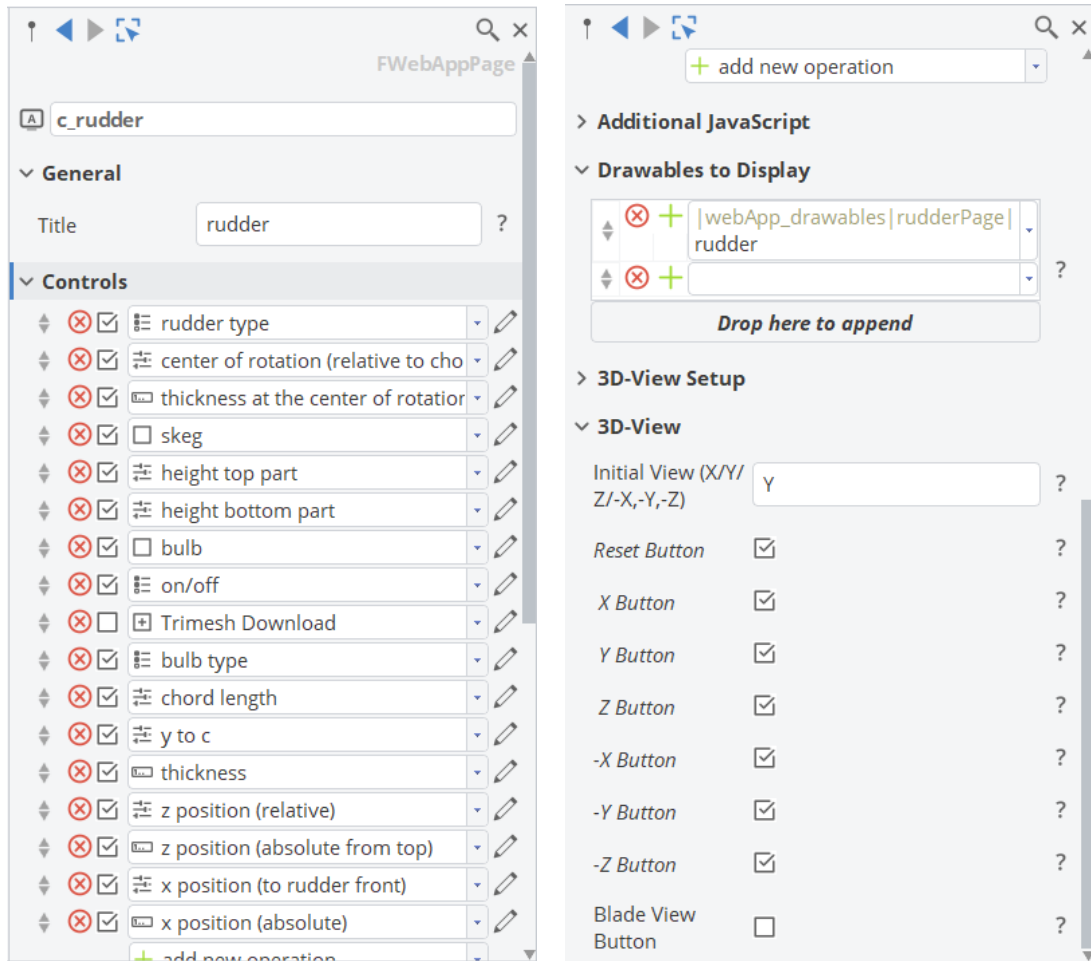
Fig.8: Object Editor of a webApp page within CAESES 5.1; here page 4 of the rudder webApp
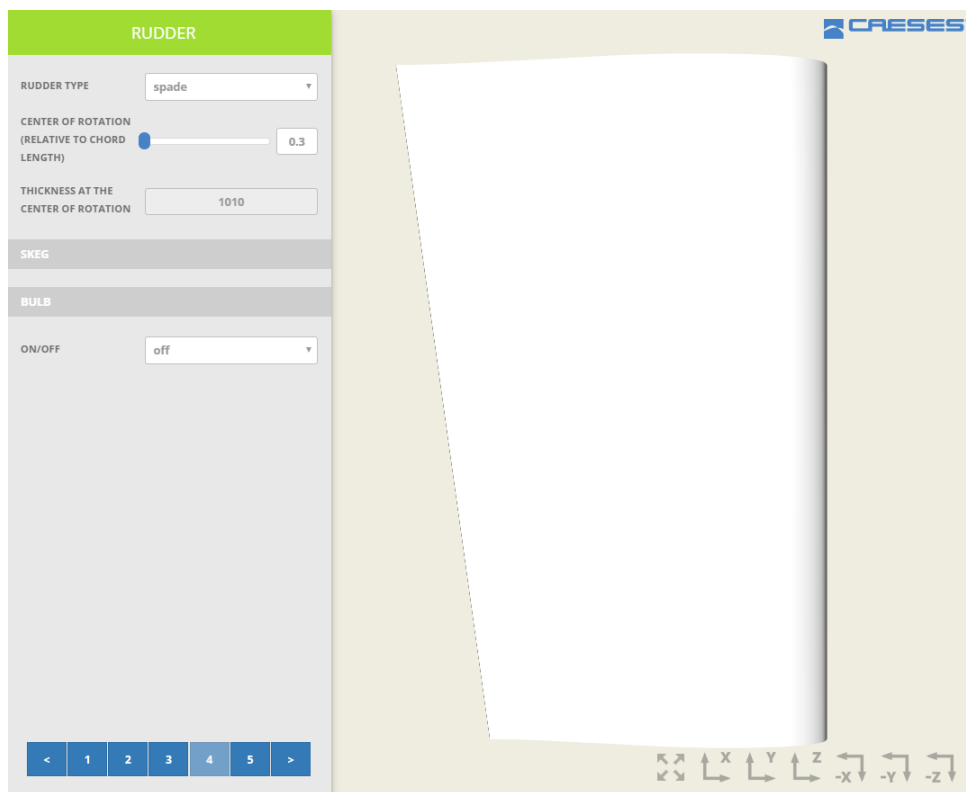
Fig.9: Final view of page 4 of the rudder webApp (no bulb selected)
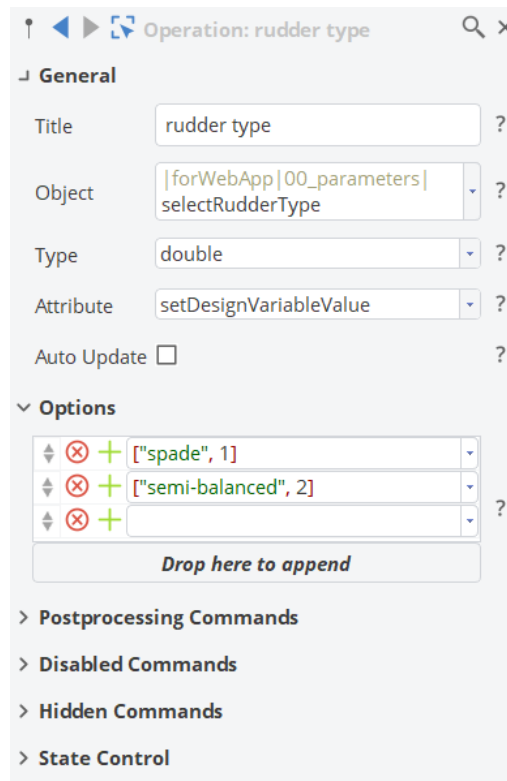
Fig.10: Control 'String-Options'
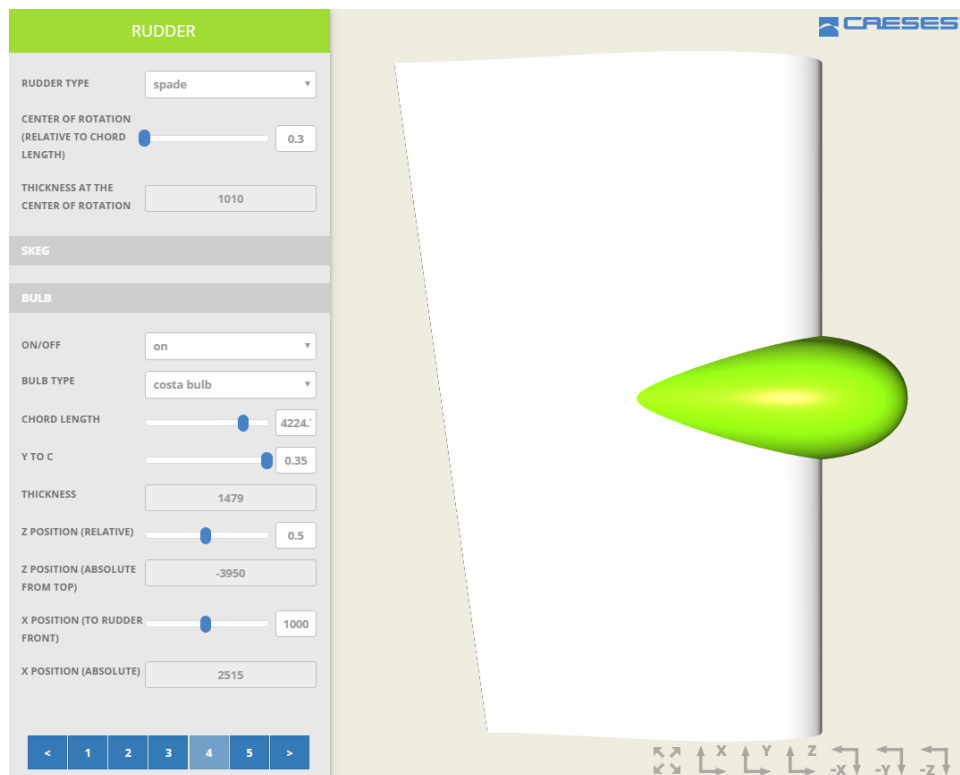
Fig.11: Final view of page 4 of the rudder webApp (Costa bulb selected)

For better usability of a webApp, it may be convenient to not show some of the controls when they change objects that are not displayed at the moment. On webApp page four this is the case for the "skeg" and the "bulb" section. Fig.11 shows the string-option "ON/Off" set to "on" and now controls are displayed that define the shape and position of the bulb. This is achieved with a Boolean condition in the 'Hidden Commands' tab, presented in Fig.10, which hides the control when true.

3.3. Deployment

Two main use cases are to be considered when it comes to deployment of a webApp. A certain service may be provided internally, e.g., to provide quick access to complex projects for colleagues that might just need a condensed output and limited flexibility to build on. In other cases, it might be desirable to give access to an external user base. Commercial tools and services will most often ask for the latter except for those that underly restrictive data policies and should therefore be hosted locally. The technicalities are similar in both cases but cannot be described and structured in exact procedures and processes due to the various requirements and characteristics of different applications and hardware configurations.

To start with, we will consider the case of local deployment. Any time CAESES is running on a computer it will offer a web interface which is available over a certain port. A user can therefore access CAESES through this port and operate the program through the network. The front-end layout, as seen by the user in a web browser, is defined through a set of XML files, one for each page of the application, that define the available functionalities such as in- and output values, views, file uploads and downloads, etc. and is fully responsive to allow requests from various devices such as mobile phones, tablets and workstations. Whether this type of connection is established locally, on one and the same machine, or within an intranet, does not make any difference. In this simple case, deployment is already accomplished just by running an instance of the software and project file, along with a set of XML files for the configuration of the front-end and sharing the local port with other users.

Once a webApp shall be made available to the public and a potentially larger user base, a few other administrative tasks need attention. The efficient utilization of available hardware capacities is one of the main concerns when it comes to scaling up. Wrapping applications such as CAESES (along with the project files needed for a certain app) into so-called containers provides a reliable and efficient means of hosting a service and encapsulating it to ensure data confidentiality. A proxy server implementation can distribute the various parallel CAESES sessions to a container orchestration tool which takes care of container deployment, management and scaling for efficient load balancing. Using Docker technology, a set-up as described has been established by FRIENDSHIP SYSTEMS, *Harries et al. (2018),* and is also what is used for the deployment of the webApps presented in this paper.

4. Hull webApp

The hull webApp is accessible via https://www.friendship-systems.com/products/web-apps/show/app/levelonehull. It provides a reasonable approximation, a so-called level 1 hull, for small tankers. The generated geometry can be downloaded as a STL file.

4.1. Parametric model for a level 1 hull

The underlying parametric model for the hull webApp is a model for a so-called level 1 hull as introduced in *Harries et al. (2022)*, which is used for the creation of hull forms of small tankers. It only requires a few, often publicly available, input parameters like the design speed, length over beam ratio, beam-over-draft ratio, the block coefficient and the longitudinal centre of buoyancy, Fig.12, along with the length of the ship.

4.2. Use cases

The hull webApp is targeting two use cases, namely

- remodeling of an existing geometry and
- generation of a baseline for preliminary design.

An example for the first use case is that someone, e.g. a shipping company, is interested in chartering an existing ship but the only information they receive easily and beforehand are the main dimensions.
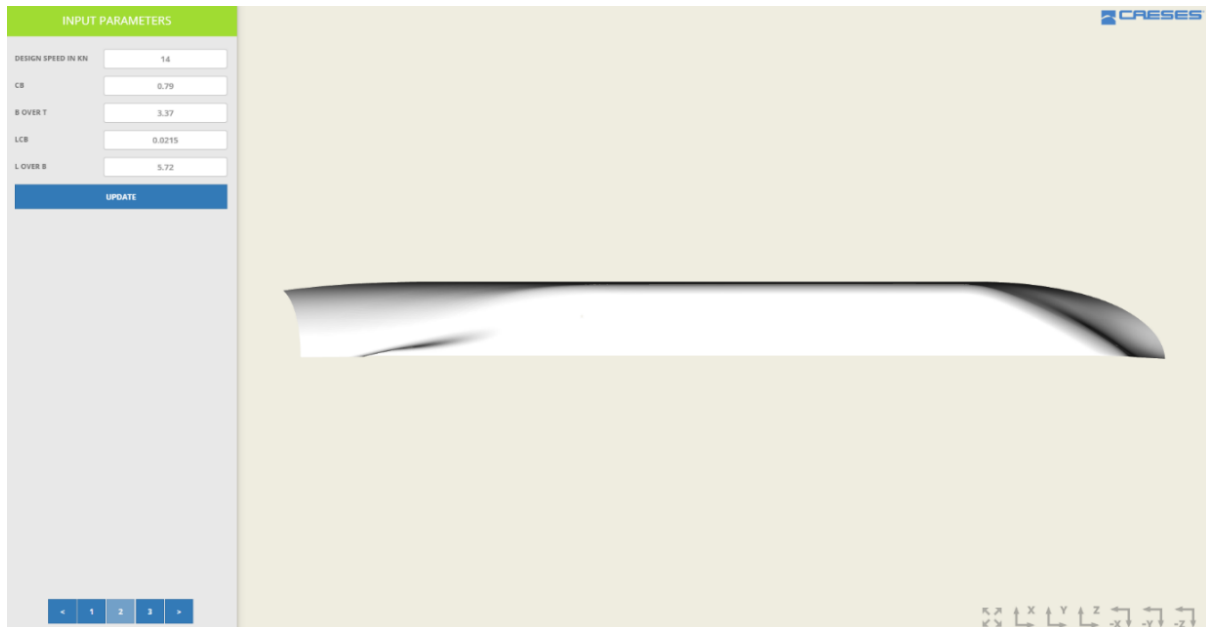
Fig.12: Input page of the hull webApp

Then the webApp can help to get a model that is a reasonable approximation of that ship, so that they can run some simulations to see if the ship is suitable for the intended service.

The other use case is that the webApp enables naval architects to generate a watertight geometry within minutes in a development stage where there will be changes of the dimensions anyway and it is not necessary to invest a lot of resources into a more sophisticated model.

5. Combining microservices

As shown in *Harries et al. (2022)* for the remodeling of a chemical tanker, the CB Adriatic owned by Carl Büttner Shipmanagement, as undertaken within the German R&D project MariData, https://maridata.org, the webApps can be readily combined. With quite limited data, either publicly available or estimated via a naval architect's educated guesses, a pretty good representation can be realized within minutes, Fig.13.
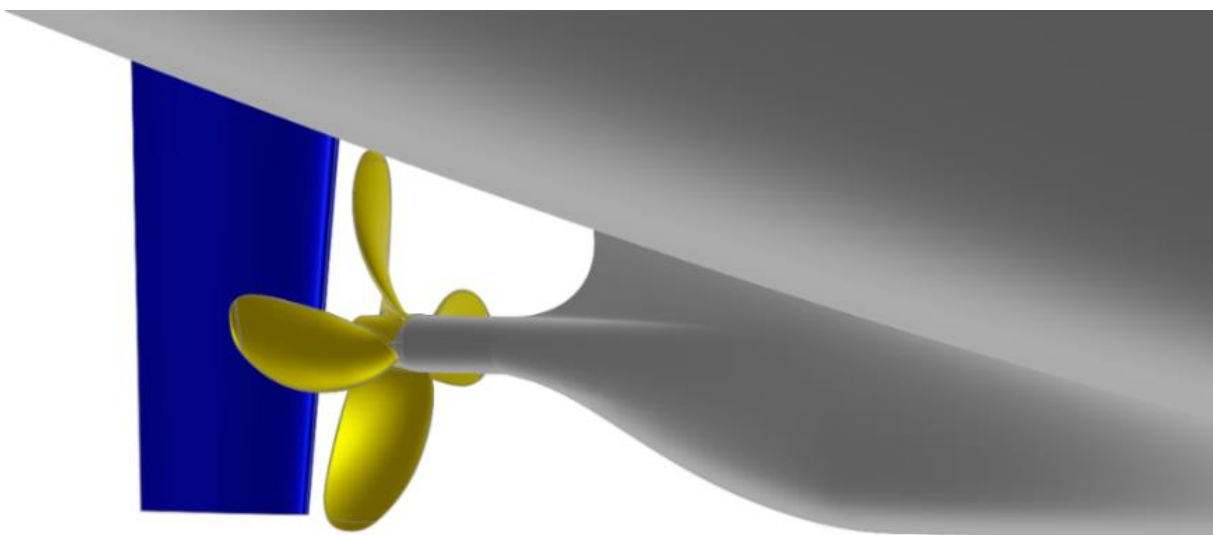

Fig.13: Level 1 remodeling for aftship, propeller (Wageningen) and rudder (as needed for CFD)

Nevertheless, the level 1 geometry differs still quite a bit from the original geometry. One of the main differences is for example the asymmetric aftship which cannot be recreated at this level. But CFD simulations have shown that for this hull the speed-power curves at scantling draft are very similar for the original and the remodeled level 1 hull, see *Harries et al. (2022)*. However, there a deviations between the speed-power curves at ballast draft. These results should be treated carefully and cannot be readily transferred to other hulls. There is the possibility that a level 1 hull performs better or worse, or just differently for other tanker hull shapes. Still, the level 1 hull is a good first approximation that can be generated quickly and conveniently.

6. Conclusions and outlook

The generation and deployment of web-based microservices has been presented, enabling webApps of limited yet very powerful functionality. The three webApps discussed cover hull form generation, rudder modeling and propeller design. All three tasks typically require lots of expertise and experience when undertaken in a CAE system. By deliberately sacrificing functionality and details, high-quality results can still be produced within seconds to minutes. This is because expert knowledge has been built into the webApps.

The purpose of webApps is neither to replace CAE systems nor to suggest that detailed design and sophisticated simulations would not be needed. Rather, the idea is to complement large CAE systems with their particular ecosystems and high-end engineering tasks with fast modeling within an environment of ready access easy collaboration. WebApps are meant to get good starting points and educated guesses.

With the feedback of users, the described webApps will be most likely modified for an even better user experience and extended in functionality with some ideas already outlined for the rudder webApp in section 3.1.

The public deployment of webApps comes with the usual difficulties of security, confidentiality and resource management but has been proven manageable with existing available container technology over the last years of successful hosting for a number of webApps by FRIENDSHIP SYSTEMS. It is, however, still a customized solution requiring expert knowledge to set up and maintain. The development of user-friendly solutions to streamline set-up, deployment and maintenance is therefore considered an interesting field of R&D for the future.

The authors would like to encourage that more webApps are offered by many different providers, steadily creating the critical mass for a marketplace in which many different microservices are available.

References

BERTRAM, V (2012), *Practial Ship Hydrodynamics*, Elsevier

HARRIES, S.; LORENTZ, K.; PALLUCH, J.; PRAEFKE, E. (2018), *Appification of Propeller Model-*

ing and Design via CAESES, 17th COMPIT Conf., Pavone, pp.292-307, http://data.hiper-conf.info/compit2018_pavone.pdf

HARRIES, S.; ABT, C. (2021), *Integration of Tools for Application Case Studies*, Papanikolaou, A. (Ed.), A Holistic Approach to Ship Design – Vol. 2: Application Case Studies, Springer

HARRIES, S.; MARZI, J.; GATCHELL, S.; THIES, F.; HAUSCHULZ, S. (2022), *Comparing Hydrodynamics of Original and Remodeled Hull Forms and Appendages for Digital Twins*, 21st COMPIT Conf., Pontignano, pp.169-186, http://data.hiper-conf.info/compit2022_pontignano.pdf

A Case Study for a Zero-Emission, Fuel-Cell driven Dry Cargo Vessel

Jogchum Bruinsma, Nedstack Fuel Cell Technology bv, Arnhem/The Netherlands
jogchum.bruinsma@nedstack.com
Cas Kluiters, HZ University of Applied Sciences, Vlissingen/The Netherlands

Abstract

The emission of greenhouse gasses (GHG) has grown to be a major subject in shipping. As answer, the maritime industry is looking for zero-emission transport options. This paper presents a concept study for a feasible retrofit for a deep-sea dry cargo vessel, using LT-PEM fuel cell technology and LH2. The power demand is determined using basic information and information from the automatic identification system. Both are used as input for the Holtrop-Mennen method which provides a good estimation of the propulsion power demand.

1. Introduction

The shipping industry is considered to be a hard-to-abate sector, indicating emission reduction of large ocean-going vessels, as well as inland shipping is not going to be easy. Nevertheless, a lot of effort is invested in alternative fuels to allow vessels to reduce or even omit their emissions. Low temperature PEM fuel cell systems are considered one of the promising and feasible technologies to remove emissions from shipping. Current demonstrators are mainly focusing on either auxiliary power for seagoing ships or full propulsion power for inland navigation vessels. However, as multi-MW fuel cell systems have already been built before and cryogenic storage of hydrogen is common in other sectors, hydrogen and fuel cell systems also present a feasible alternative for propulsion power in deep sea shipping.

1.1. PEM fuel cell technology

As a conventional diesel generator, a Proton Exchange Membrane Fuel Cell (PEMFC) converts the chemical energy of the fuel into electrical energy. The major difference with an Internal Combustion Engine (ICE) is that a fuel cell converts the fuel directly in electrical energy, whereas the ICE converts the chemical energy in mechanical energy and in electrical energy using a generator.

A fuel cell will produce energy and heat as long as there is fuel supplied. The main components of a fuel cell are the anode, cathode, electrolyte, and the external electrical circuit. Fig.1 shows the overall electro-chemical reactions which takes place in a PEM fuel cell. The hydrogen is split into positively charged protons and negatively charged electrons by using a catalyst at the anode. The electrons flow through an external electric circuit to the cathode side of the fuel cell. The energy created in the external circuit is then used to power the load. At the cathode, the protons and electrons react with oxygen and produce water (H_2O).
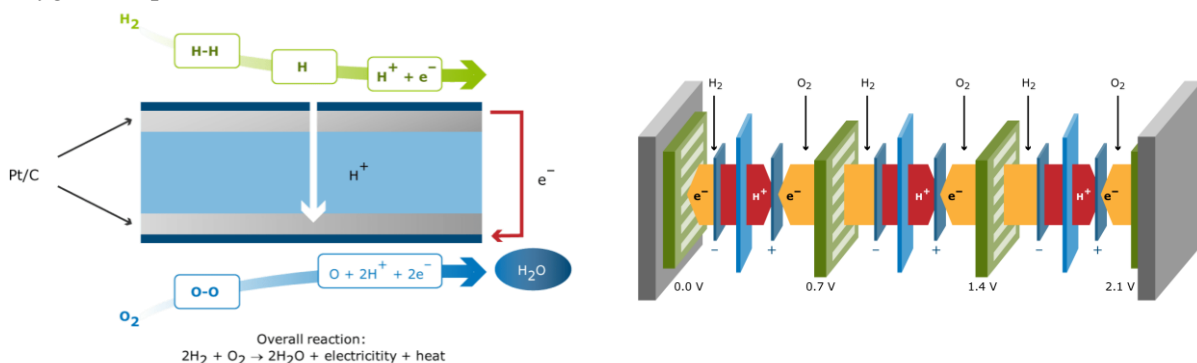

Fig.1: Fuel cell working principle

1.2. Vessel characteristics

The 'Falcon Triumph', Fig.2, Table I, is a deep-sea cargo vessel built for transporting bulk cargo, sailing worldwide. The vessel was built in 2017 by Jinling Shipyard in China. The vessel has its own cargo handling equipment like cranes.

Table I: 'Falcon Triumph' specifications (Jinling Shipyard , 2016)

Length overall	199.90 m
Length PP	194.50 m
Breadth	32.26 m
Depth	18.50 m
Design draft	11.30 m
Main engine	MAN B&W
Engine output	8050 kW
Service speed	14.3 kn

Fig.2: 'Falcon Triumph'

2. Power demand estimation

For most ships, a detailed power demand based on time is not available. Nonetheless, there are other ways to the calculate and determine the required power for a certain ship at a certain speed. When the required propulsion power is known, a new power system based on fuel cell system can be designed. This study used the Holtrop-Mennen method, together with data from the ships load balance to calculate the estimated power demand.

2.1. Holtrop-Mennen method

The Holtrop-Mennen method was developed by J. Holtrop and G.G.J. Mennen in 1982 at TU Delft. The method is designed to estimate resistance and powering of displacement of ships. The method uses a regression analysis of data from scale models, as well as some data from sea trials.
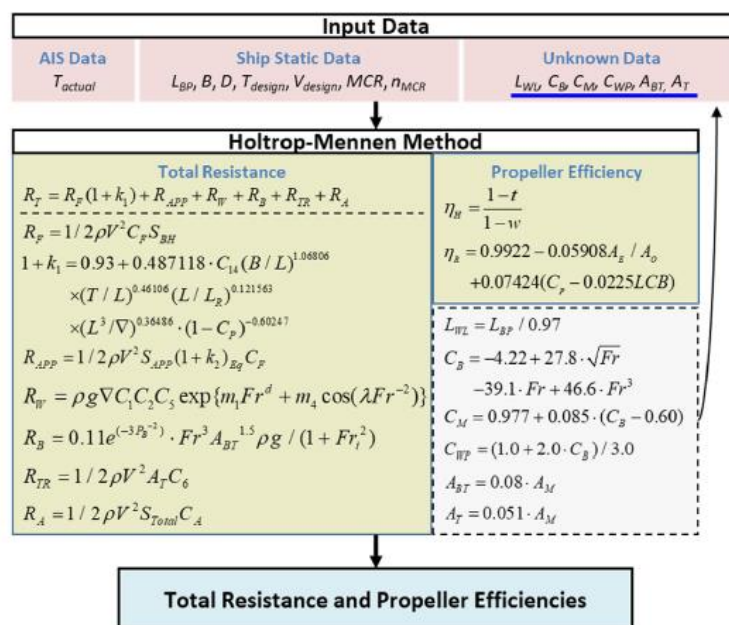

Fig.3: Holtrop-Mennen method, *Kim et al. (2020)*

For this study, the application of the Holtrop-Mennen method by *Kim et al. (2020)* was used. The input data for the Holtrop-Mennen method consists of the static data of the vessel and some operational data from the AIS service. Examples of this operational data are the draft, average speed and voyage length. The method is presented in the Fig.3.

2.2. Fuel to propeller efficiencies

The resistance of a vessel is representative for the power being delivered by the engine. Between the resistance and power output of the engine, energy is lost at multiple occasions due to lower efficiencies in drive train components like propulsive and the transmission efficiency. The propulsive efficiency is composed of the hull efficiency, the open water efficiency and the relative rotative efficiency. The transmission efficiency is made up by the shaft and gearbox efficiency. This is illustrated by the efficiency model from *Klein Woud and Stapersma (2002),* presented in Fig.4.
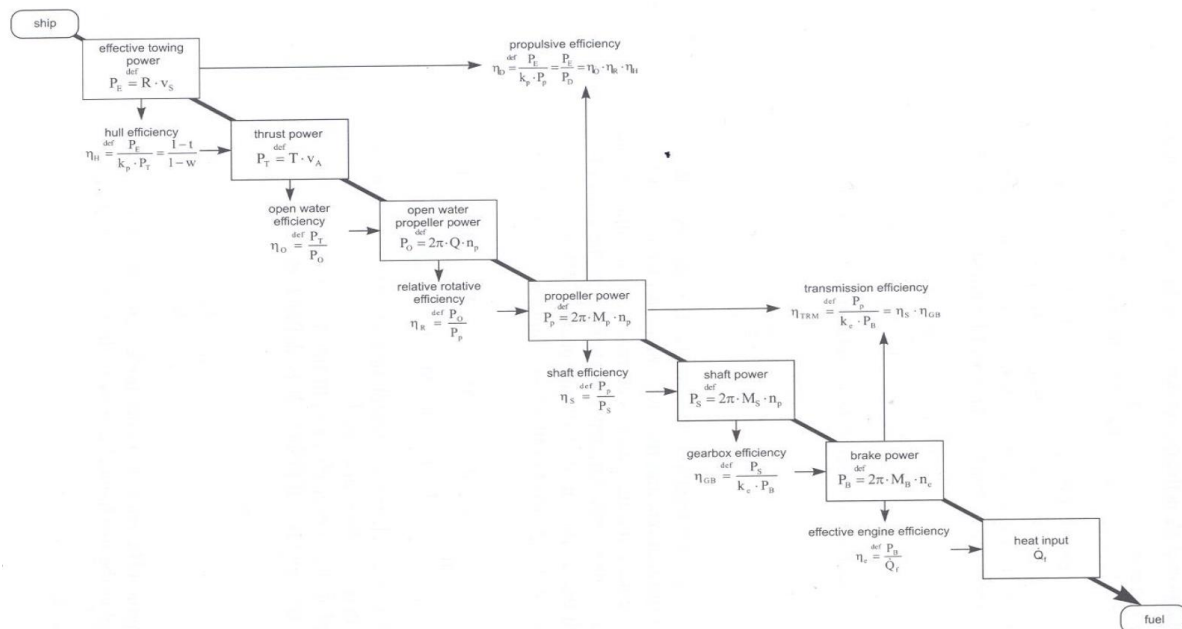

Fig.4: From effective power to fuel power, *Klein Woud & Stapersma (2002)*

2.3. Auxiliary load

The auxiliary load of a ship represents all electric consumers, like engine room pumps, lighting and for instance deck equipment. For this study, the auxiliary load is derived from the new build power calculations of the Falcon Triumph. In Table II, the load from different categories of consumers while in port is presented. The load in port does not include the use of the cargo handling equipment and is therefore suitable to represent the auxiliary load during sailing.

Table II: Auxiliary load

Category	Power (kW)
Lighting	125
Machinery	90
Air conditioning	40
Galley	30
Engine room fans	5
Workshop	5
Total	**290**

With the fuel cell system, some additional systems may be introduced in the fuel cell balance of plant and hydrogen storage systems. However, at the same time, similar systems for the existing diesel engines are removed. In addition, the waste heat of the fuel cell system can also be used to reduce the power demand for heating the accommodation, cargo holds and the warm water system on board. Furthermore, the fuel cell cooling water systems could be used to evaporate the cryogenic hydrogen. Ultimately, heat pumps can be used to create cold-water systems for air-conditioning, utilizing the heat retracted during the regasification process of liquid hydrogen.

2.5. Implementation

From www.MarineTraffic.com, the information of 22 voyages in one year was retrieved and used to calculate the average velocity based on departure and arrival time and voyage distance. In addition, the voyage draft was also logged and could therefore be used with the parameters found on the general arrangement in the Holtrop-Mennen method to calculate the resistance and therefore the propulsive power. With the propulsive power, drive train efficiencies and auxiliary load, the total average power demand was calculated per trip. To compensate for variations in power due to sea conditions, an additional sea margin of 15% is included. The total power is therefore defined as:

$$Total\ power = \left(\frac{(Rt * v)}{Propulsive\ efficiency * 0.85} \right) + Auxilary\ load$$

The average power demand of all 22 voyages is presented in Fig.5.
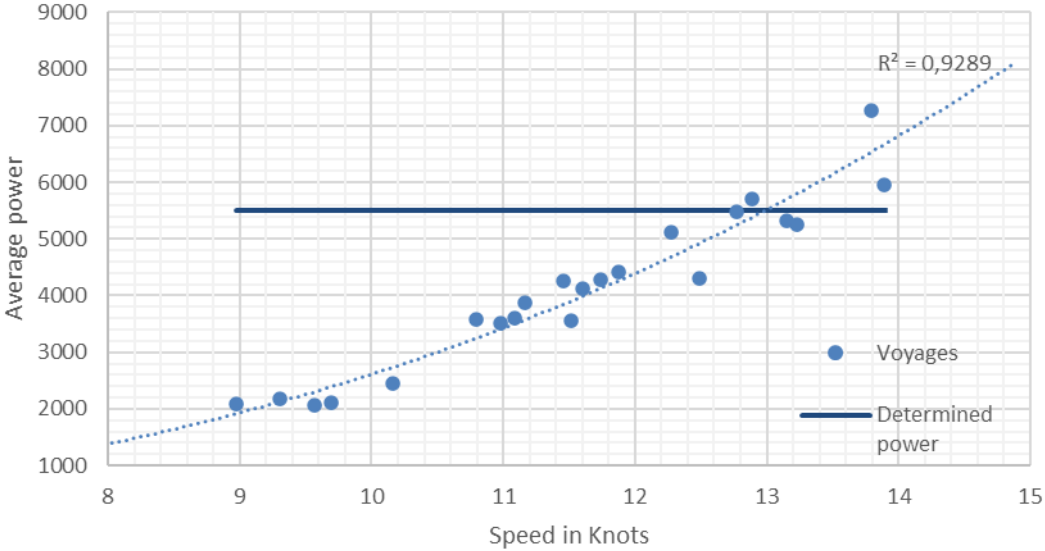
Fig.5: Power demand vs. speed based on AIS data

Based on average speed and average power demand, the design power was determined at 5500 kW propulsion power. At this design power almost 90% of the voyages would have been achieved, which is deemed to be sufficient. At the design power a maximum speed of 13 kn can be maintained. It also implies that the design speed of 14.6 kn would no longer be possible, but given today's trend on slow steaming, this is not considered to be vital.

2.4 Power distribution system

The output from a fuel cell is a variable DC voltage related to the fuel cell current. To create a stable grid, either AC or DC, power conversion and distribution is required. The power conversion and distribution system introduces some additional energy losses, which needs to be compensated by the fuel cell system. The total efficiency of the power system is estimated at 93.5%. The fuel cell systems should therefore be capable of providing approximately 5900 kW.

For this concept study, the fuel cell power installations from Nedstack fuel cell technology are considered. The largest commercially available system today, the PEMGEN© MT-FCPI-500 is capable of delivering 550 kW electric output power and end-of-life. The system is slightly oversized to compensate for internal losses and performance degradation over time. To supply the required power demand, a total of 12 fuel cell systems is distributed over two bus-ties. The fuel cell systems are connected to DC/AC inverters and double-stock transformers, to feed into a 6900 VAC distribution grid and keeping harmonics within acceptable limits. A single line representation of the concept power distribution system is shown in Fig.6.
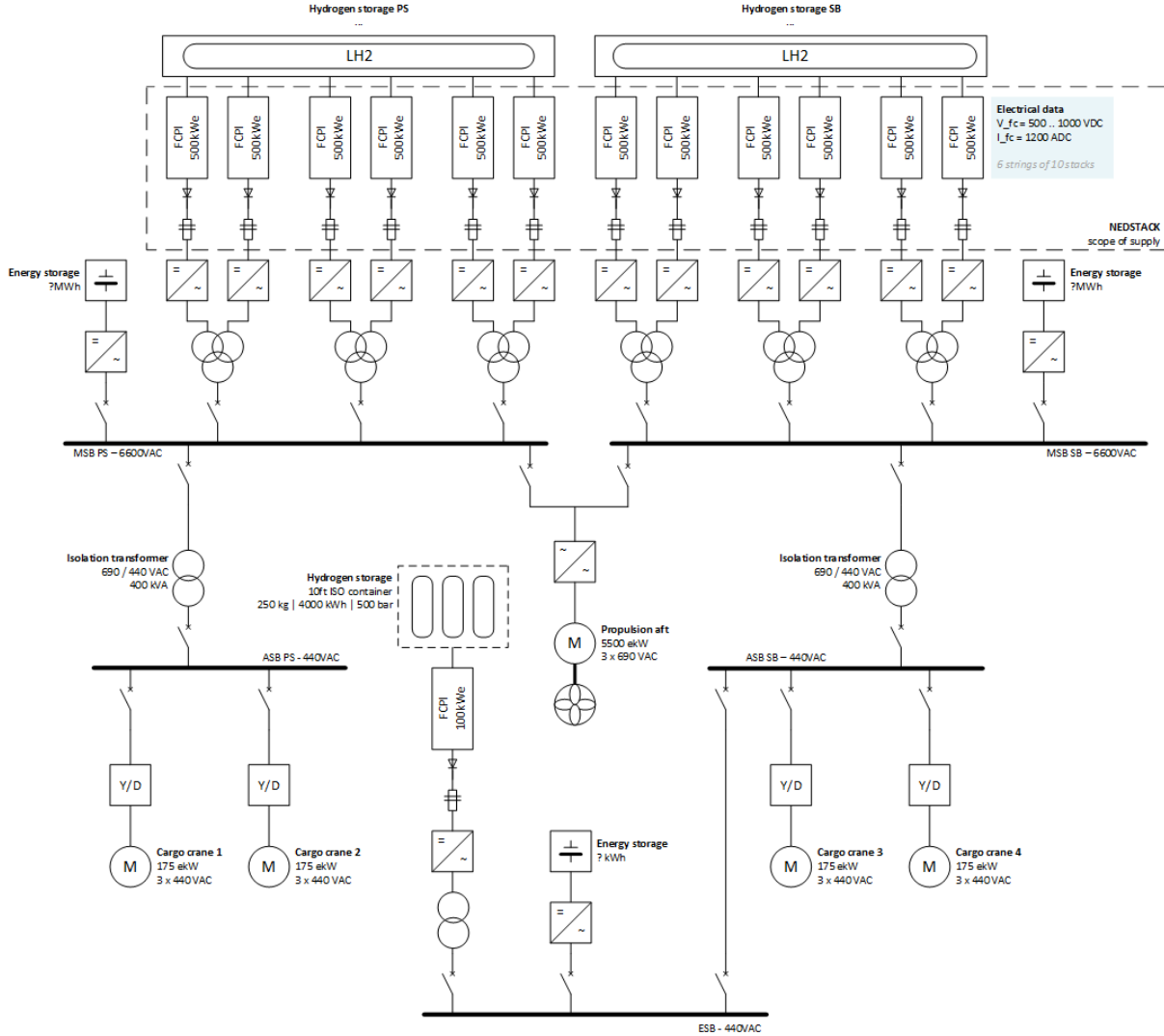

Fig.6: Concept power distribution single line diagram

2.6. Validation

For one of the trips, actual fuel consumption of the 'Falcon Triumph' and logbooks were received from the shipowner and compared to the calculated power based on the AIS data. The fuel consumption, together with the engine efficiency results in an estimation of the used power. The fuel consumption of the specific voyage 287.8 t of heavy fuel oil. The specific energy of the fuel was derived from the fuel quality report and was 42.43 MJ/kg. The efficiency of the main engine was assumed to be 49%, resulting in an actual average power of 4373 kW.

The vessels log also shows propeller rpm and the calculated speed, based on fixed pitch. The log shows that the speed-over-ground (SOG) and speed-through-water (STW) are similar to those retrieved from the AIS data. However, the power required to maintain either SOG or STW is

significantly less when compared with actual fuel consumption. The difference can be explained by the fact that both SOG and STW do not represent actual wind and current conditions. As the shaft speed is a result of the reference speed, issued by the operator, it gives a better representation of the actual power which is consumed. If the propeller rotations are used for the Holtrop-Mennen method, the calculated power is within 5% of the actual power based on fuel consumption and engine efficiency estimates.

Table III: Comparison AIS data with ships log using Holtrop-Mennen method

	SOG	STW	RPM	Ship log
Speed [kn]	9.6	10.6	12.3	9.6
Power [kW]	2070	2742	4179	4373
Deviation [%]	56	37	4	-

Table III shows the difference between the propulsive power demand based on the various speed measurements. The table shows a large difference of 56% when taking speed-over-ground and 37% for speed-through-water into account for the estimation of propulsive power. When instead the actual propeller shaft rotations are used to calculate the representative speed, the difference between the HM calculation and power estimated based on fuel consumptions is 4%. This difference is considered to be reasonable and acceptable.

5. Energy storage

As the main fuel is no longer heavy fuel oil, but as the energy is provided by hydrogen, alternative storage tanks are applicable. To make a fair comparison to the actual capabilities of the ship, only the current heavy fuel oil tanks and exhaust casing behind the accommodation were considered for hydrogen storage. In this way, no significant changes were made to the stability of the vessel and no commercial space was sacrificed.

5.1. Cryogenic hydrogen storage

The amount of hydrogen that needs to be stored will be significant. Therefore the energy density of the fuel and storage needs to be as high as possible. Only technology which is available today on a commercial scale is considered in this study. Given the high quantity of hydrogen, compressed storage is not considered feasible. Therefore cryogenic storage of hydrogen is used in this study. The liquid hydrogen tanks have replaced the heavy fuel oil tanks, including all of the required insulation. The total amount of LH2 that could be stored in these locations was 134 t.

5.2. Range

With the determined power and design speed, the actual hydrogen consumption can be estimated. The hydrogen consumption of the MT-FPCI-500 fuel cell systems, assuming operation in parallel at equal load, is approximately 400 kg/h. At 5500 kW propulsive power, the speed was determined at 13 kn. With a total amount of hydrogen stored on board of 134 t, the vessel range is determined.

$$vessel\ range = \frac{total\ H2}{H2\ consumption} * vessel\ speed$$
$$vessel\ range = \frac{134000}{400} * 13 = 4355\ nm$$

Based on the AIS date, the average trip length of 2091 nm. Therefore, the total range of the vessel is sufficient to cover the average trip. Actually, the amount of hydrogen storage covers 90% of all trips, for many it would be sufficient for a round trip. For reference, the amount of energy that can be stored in hydrogen is approximately 15% when compared to the energy stored in HFO for the same volume.

5.3. Boil-off

To prevent pressure rise in the storage tanks due to LH2 evaporation, hydrogen will be boiled off when the tanks are not being used. The boil-off is assumed to be around 1% per day. At maximum fill rate, the boil-off would be 1340 kg/day, which would be consumed in less than 3.5 hours while sailing. In port the power consumption is much lower, the amount of boil-off gas is larger than the actual consumption of approximately 500 kg/day. However, low pressure extraction methods can be used to reliquefy the remaining boil-off gas, omitting venting of hydrogen.

6. Conclusion

For a technical feasibility study on a zero-emission retrofit deep sea dry-cargo vessels, the operational profile of the vessel regarding the sailing profile and the performance on board was examined. The total power delivered by the ME on board was determined with the Holtrop-Mennen method for a year of voyage data. With this method, a power demand including sea margin and auxiliary load was calculated, indicating that for 90% of the voyages 5500 kW propulsive power was sufficient, limiting the ships design speed to 13 kn. AIS data showed an average trip length of 2091 nm, which could be rounded with the amount of stored hydrogen.

Nevertheless, generally available AIS data might give a first insight into the power and range requirements. They may come short as it lacks actual weather and current information. On the other hand, using propeller RPM information from ships logs, as input for the Holtrop-Mennen method, results in realistic data to estimate propulsive power and could be a well-funded basis for initial system design, without the need for advanced data acquisition systems.

The maximum amount of hydrogen stored in cryogenic form was 134 t, resulting in a range of 4355 nm, when continuously sailing at 13 kn. This was deemed an acceptable profile and range, as the 'Falcon Triumph' is a bulk carrier which does not require a high speed for cargo transportation. Therefore, a retrofit with LT-PEM fuel cells and liquid hydrogen storage is feasible.

Acknowledgements

References

KIM, S.H.; ROH, M.I.; OH, M,.J.; PARK, S.W.; KIM, I.I. (2020), *Estimation of ship operational efficiency from AIS data using big data technology,* Int. J. Naval Architecture and Ocean Engineering, pp.440-454, https://www.sciencedirect.com/science/article/pii/S2092678220300091

KLEIN WOUD, H.; STAPERSMA, D. (2002), *Design of Propulsion and Electric Power Generation Systems*, IMarEST, London

SH2IPDRIVE - Sustainable Hydrogen Integrated Propulsion Drives

Jogchum Bruinsma, Nedstack Fuel Cell Technology, Arnhem/The Netherlands,
jogchum.bruinsma@nedstack.com

Abstract

SH2IPDRIVE's main objective is to develop reliable, safe, standardized, scalable and cost-effective solutions for zero-emission propulsion and energy systems for hydrogen-based ships. The project is conducting new research into the development of safe applicable technologies for hydrogen in four different forms. Another important pillar is the increase in scale of fuel cells. The developments at the level of technological components and subsystems are (modularly) integrated and validated, and then elaborated in five validated concept designs, representative of different types of ships that are important for the Dutch economy.

1. Introduction

A Dutch project consortium called SH2IPDRIVE (Sustainable Hydrogen Integrated Propulsion Drives) has been awarded a €24.2m subsidy from the R&D Mobility Fund in the Netherlands. Consisting of 25 companies and knowledge institutions from within the maritime sector, the consortium aims to accelerate the uptake of hydrogen as a marine fuel by working collaboratively on innovation projects. With a total project fund of €34m, the consortium will be able to carry out extensive research and development into an array of hydrogen applications. SH2IPDRIVE aims to lay the foundation for a strong maritime hydrogen economy in the Netherlands. The project will cover the full scope of hydrogen research and development and has been separated into nine different work packages including: bunker and storage systems, hydrogen carriers, fuel cells, data collection and system validation, system integration, modular testing, ship design and safety. The project will also conduct research into the development of safe technologies that utilize compressed hydrogen gas, liquid hydrogen, and hydrogen bound to carriers such as liquid organic hydrogen carriers and borohydrides. Fuel cell systems with a greater power density and a longer lifespan will also be explored. The development of technological components and subsystems will be validated in five concept designs to represent a range of ship types that are viewed as important for the Dutch shipping industry. These include inland shipping new construction, inland shipping retrofit, coastal/shortsea shipping, passenger vessels and specialist ships.

2. Background

The outbreak of the corona crisis has had a disruptive effect on (international) trade flows, which has also greatly affected the Dutch maritime sector. Combined with the uncertain economic outlook, this leads to a reduced willingness to invest in new ships. As a result, Dutch maritime suppliers are insufficiently encouraged to invest in the development of new technologies.

At the same time, there are important developments to give priority to making the maritime sector more sustainable, enabling the TRL of hydrogen technology for maritime applications to be significantly increased in the short term. Examples are the introduction of the Energy Efficiency Existing Ship Index (EEXI) and the European Commission's intention to include shipping in the emissions trading system. Due to the long service life of ships, there is a great risk that part of the current fleet will no longer be able to operate (stranded assets). The measures force ship owners to invest seriously in measures in the field of CO_2 reduction in the short to medium term: in retrofitting existing ships or in new construction.

The Dutch maritime sector has the ambition to make a major contribution to the global climate transition. Investing in innovation to accelerate the transition to zero-emission shipping is a top priority to maintain a strong international position and counter the COVID-19-related economic

downturn. In the Dutch maritime sector, hydrogen and methanol are considered the most promising alternative energy carriers. This research project focuses on the maritime application of hydrogen in fuel cells. This is a completely emission-free and silent conversion, in which no greenhouse gases, no NO_x and no particulate matter is released. With the Dutch and European zero-emission targets, it is expected that hydrogen will become an important energy carrier in the medium term.

In the Sustainable H2 Integrated Propulsion Drives (SH2IPDRIVE) project, companies and knowledge institutions are working together on a broad and ambitious innovation project to accelerate the introduction of hydrogen as an alternative energy carrier. Although the focus is primarily on the maritime sector, the technology can also facilitate the introduction of hydrogen in other (mobility) sectors. Hydrogen is an energy carrier that can be produced completely carbon-neutral by means of green electricity. By electrochemically converting hydrogen into a fuel cell, power can be generated on board to drive ships completely emission-free. SH2IPDRIVE lays the foundation for a strong maritime hydrogen economy in the Netherlands, gaining a leading position in Europe and the world.

SH2IPDRIVE is explicitly in line with the objectives formulated in the Maritime Master Plan, which sets out the ambition to make the Netherlands a world leader in the field of sustainable shipbuilding and shipping, including by putting at least thirty emission-free ships into service by 2030. An important pillar of this ambition is the development of technology for the application of alternative energy carriers, for example within the theme 'hydrogen energy and propulsion systems.' It states: 'the aim of this theme is to develop proven and scalable propulsion and energy systems for hydrogen and the related (innovation) ecosystem for realistic maritime usage profiles.'

SH2IPDRIVE gives substance to this ambition and thus makes an important contribution to the social challenge of making the maritime sector highly sustainable.

3. Project description

SH2IPDRIVE's main objective is to develop reliable, safe, standardized, scalable and cost-effective solutions for zero-emission propulsion and energy systems for hydrogen-based ships. The project focuses on the development of hydrogen technologies in four different forms:

- Compressed hydrogen storage
- Liquid or cryogenic hydrogen storage
- Liquid Organic Hydrogen Carries
- Borohydrides.

Another important pillar is research into new fuel cell systems with a higher power. The developments at the level of technological components and subsystems are (modularly) integrated and validated, and elaborated in 5 validated concept designs, representative of different types of ships:

- inland navigation (retrofit),
- inland navigation (new construction),
- short sea shipping,
- passenger ship and
- specialist vessel.

3.1. Partners

The consortium is made up of 25 partners, 22 of whom apply for subsidies: sixteen technology-driven companies (of which fourteen are SMEs) from the maritime sector and six leading knowledge institutions. These 22 partners are listed in Table I.

Table I: List of funded partners

Future Proof Shipping	H2 Circular Fuel
Technical University Delft	H2FUEL Cascade
Nedstack Fuel Cell Technology	Royal Roos
Maritiem Research Instituut Nederland	Solid Hydrogen
Koedood Dieselservice	University of Amsterdam
C.V. Scheepvaartonderneming Van Dam	Voyex
Holland Shipyards	Encontech
TNO	Technical University Eindhoven
Van Halteren Technologies Boxtel (Bosch Rexroth)	University Twente
Cryovat Internationaal	Rivermaas
H2Storage	IHC Holland

In addition, the following organizations will participate in-kind:

- Shell
- Concordia Damen
- Defence Material Organisation

These organizations have signed a Statement of Support and have also co-signed the cooperation agreement. Finally, the 14 parties listed in Table II have indicated their support the objectives of SH2IPDRIVE:

Table II: Supporting parties

|	
Anthony Veder	InnovationQuarter
Boomsma Shipping	Panteia
Cornelis Vrolijk	Port of Rotterdam
Deal Drechtsteden	PTC
European Hydrogen Alliance	Province of Zuid-Holland
Heerema	SDS (Heuvelmangroep)
OSD-IMT	Vertom
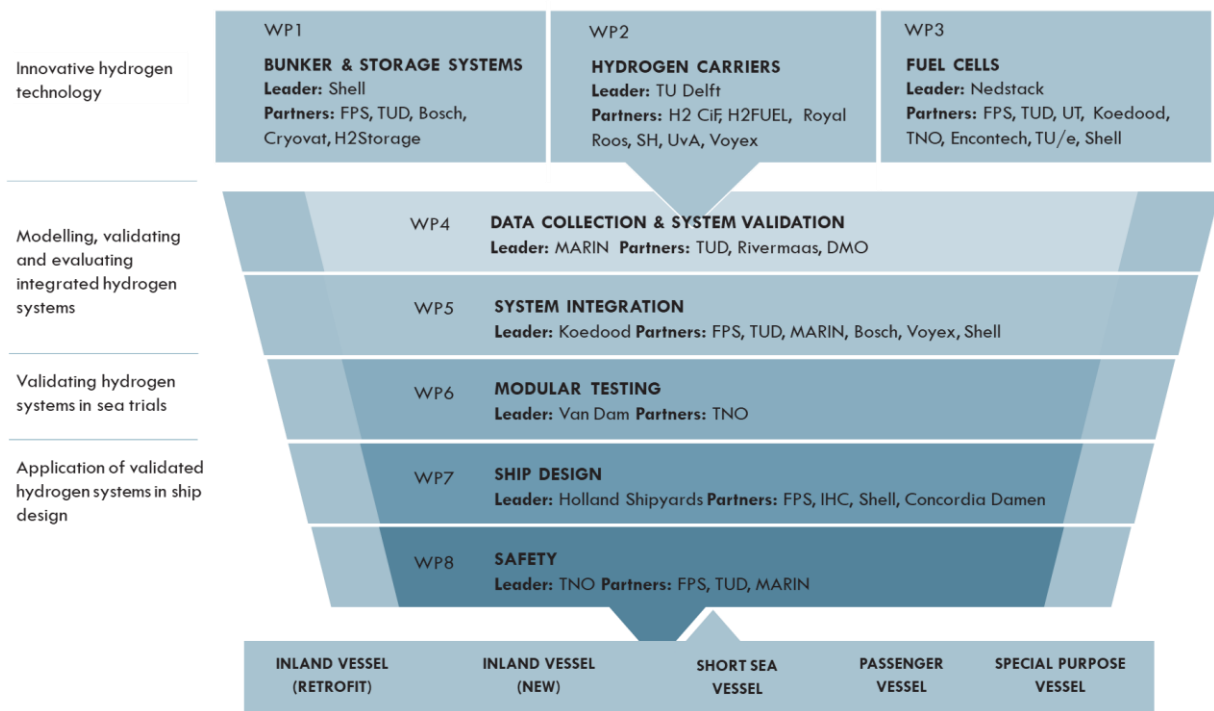
Fig.1: Work package structure

4. Work packages

The project has been divided into 8 different work packages, all focusing on a specific part of hydrogen fuel-cell based ships. Fig.1 depicts the work package structure.

4.1. WP1 – Bunkering and storage systems

Bunkering and storage techniques for hydrogen have not yet been sufficiently developed to be applied in the maritime sector. The main problems are an insufficient volumetric energy density, which lacks to create adequate operational autonomy and the safety risks are not yet fully known. This ambitious work package should lead to both the first standardized maritime CH_2 container based on type 4 composite fuel tank at 700 bar and the first LH_2 maritime storage tank in Europe. Research is also being carried out for the bunkering and storage techniques and handling methods for solid hydrogen.

4.2. WP2 – Hydrogen carriers

In this work package research is conducted into different types of experimental hydrogen carriers. This creates solutions with a much greater volumetric energy density and potentially fewer safety risks than with CH_2 and LH_2. The prospects of hydrogen carriers are promising, but the technology is far from reaching a mature stage. Specifically, liquid organic hydrogen carriers (LOHC) and different types of Borohydrides (BH) are used; the most promising solution is elaborated in detail and validated on a laboratory scale and in test setups.

4.3. WP3 – Fuel cells

In the transition to sustainable shipping, fuel cells provide a zero-emission solution for the generation of electrical power and heat. This work package is aimed at research into fuel cells with a higher power density and higher power. Low pressure fuel cells are efficient and suitable for application with different hydrogen carriers. The current technology for Proton exchange membrane (PEM) fuel cells is further developed to provide a reliable and robust alternative to conventional marine power generation systems. Furthermore, the work package will research fuel cell aging mechanisms and develop mathematical models. In addition, the utilization of low temperature waste heat is further explored as are high temperature fuel cells, specifically solid oxide fuel cells (SOFC).

4.4. WP4 – Data collection and system validation

Data collection on ships is still in its infancy, but adequate and reliable data is essential to achieve good emission-free designs of hydrogen systems. This work package focuses on ways in which data can be collected quickly and efficiently, how this data can be translated into functional requirements of hydrogen systems and how physical models of the hydrogen powertrain and engine room can be validated and calibrated on the basis of operational data from ships. In addition, digital twins of the hydrogen propulsion and energy installation are developed to contribute to improved design and improved operation through decision support. This work package provides the operational profiles for the system integration of hydrogen systems for different ship types in WP5 and also takes care of the validation of the systems developed in WP3. This is also important input for the ship design of hydrogen ships in WP6 and WP7.

4.5. WP5 – System integration

In order to actually get innovative systems on board, a smart integration of components is essential. In this work package, the dynamic behaviour of complex Power Propulsion Energy (PPE) systems is modelled and validated. By using validated models, different control and control techniques are investigated and different concepts will be optimized. This will lead to more efficient powertrains and control methods. Furthermore, in this work package, results from WP 1-3 are modelled to analyse the integration of these systems into a PPE. In this way, insight is gained into the integration of these

systems with batteries, the electric motor and smart heat integration. Finally, a Power Management System (PMS) is tested to investigate whether SOFC is feasible in shipping. Given the high efficiency (up to 80%) that an SOFC can achieve, this is a promising addition to the spectrum of alternative solutions.

4.6. WP6 – Modular testing

Tests will be carried out in laboratory setups, virtual environments and test setups on land. For some technologies, it is necessary to also perform tests on a moving maritime platform and gain insight into the technological performance in an operational environment. In the laboratory, it is extremely challenging to reliably investigate the effects of movements, vibrations, shocks and a salt laden air environment on integrated systems. These tests are modular in nature and are kept as small-scale as possible; the aim is to carry out temporary tests with a small fuel cell with a power of up to 100kW. A floating platform in coastal shipping is chosen, specifically the short sea cargo vessel MS "Ankie", because it can be tested under different MetOcean conditions.

4.7. WP7 – Ship design

The application of hydrogen will have a huge impact on ship design and basic design, as well as crew training, maintenance and the nature and frequency of bunkering. This work package will remove these uncertainties and will focus on inland shipping, passenger ships and specialist workboats. Activities aimed at short sea shipping are carried out in WP6. In WP7, the technological developments from all the work packages described above and the work package 'Safety and certification' described below are taken into account.

4.8. WP8 – Safety and certification

For the broad application of hydrogen in the maritime sector, it is necessary to control the safety risks of hydrogen. The necessary measures in the maritime domain are still partly unknown for the integrated system. As a result, insufficient or excessively strict requirements can be imposed on the systems. This work package is therefore aimed at research into the safety of bunkering, storing and distributing hydrogen on board, with the aim of demonstrating equivalent safety compared to conventional fuels. To ensure regulatory integration, this work package will involve collaboration with classification societies (American Bureau of Shipping, Bureau Veritas, DNV, Lloyd's Register and RINA) and authorities.

5. Expected results

The SH2IPDRIVE project started in November 2021 and has a total duration of 4 years. The project is expected to deliver a variety of results, related to their individual work packages:

1. Feasibility studies, handling procedures and concept designs of both compressed and liquified hydrogen storage containers. Business case and benchmark studies comparing different hydrogen storage technologies.
2. Development of LOHC and BH as hydrogen carriers, including hydrogen extraction and hydrogen regeneration on scale. Integration studies of hydrogen carriers in ships systems.
3. New generation of LT-PEM fuel cell stacks and systems, as studies into next generation high temperature fuel cells. Modelling and digital tools for implementation, monitoring and design of fuel cell systems. Technology development of low-temperature heat utilization improving both efficiency of LT and HT fuel cell systems.
4. Generic operational profiles and load profiles of typical energy consumers on board. Measuring methods for simple data collection and analysis on board. Validated models for drive train simulation.
5. New insights for system optimization and control strategies. Conceptual PPE models for selected ship types and an advanced PMS for maritime SOFC solutions.

6. Test program for modular hydrogen systems at sea and related results. Blueprint for hydrogen based short-sea vessel.
7. Scalable, standardized, and modular design of propulsion drive train and future engine rooms. Blueprints for retrofitted and new built inland navigation ships, passenger ships, and specialized ships.
8. Safety studies and characteristics for hydrogen storage and fuel cell systems. Risk assessments for the selected ship types and experimental results to validate technical gaps. Methods and tools to quantify risks and consequences of hazardous hydrogen related events.

Acknowledgements

Levelling the Playing Field: A Numerical Platform for the Fair Comparison of Wind Propulsion Systems

Frederik C. Gerhardt, SSPA Sweden AB, Gothenburg/Sweden, fge@sspa.se
Sofia Werner, SSPA Sweden AB, Gothenburg/Sweden
Da-Qing Li, SSPA Sweden AB, Gothenburg/Sweden
Karolina Malmek, SSPA Sweden AB, Gothenburg/Sweden

Abstract

Wind propulsion systems (WPS) are major investments and the decision to install them requires careful consideration of many complex questions. One of the recurring and challenging issues for ship owners is the choice of a suitable WPS for a specific ship and a specific operational pattern. Today most WPS providers offer on-demand case studies, but obviously the underlying performance prediction methodologies differ from provider to provider. This makes comparing different technologies from competing suppliers next to impossible. In this paper we present a numerical platform to compare different WPS of different makes, sizes, and costs in a fair way. The fundamental idea is to use aerodynamic WPS datasets that are independently verified by SSPA through wind tunnel test, sea trials or extensive CFD. This is combined with a hydrodynamic dataset from SSPAs database of tank tests. The same performance prediction method, identical routes and weather statistics are then used to determine Key Performance Indicators and financial metrics of the competing wind propulsion technologies. The purpose is to provide guidance for shipowners at the early concept stage of a vessel and help them select a system that suits their particular requirements.

1. Introduction

Due to the many advantages of Diesel propulsion and the availability of cheap oil, interest in commercial sailing vessels has been non-exiting for most of the 20th century. But the climate crisis has changed this.

In 2018 international shipping accounted for around 2.89% of globally produced CO_2 emissions. Forecasts about a future increase range from 90% to 130% by 2050 compared to the baseline year of 2008. Such projections have placed the topic of decarbonising shipping on the forefront of the global policy making agenda. The International Maritime Organizations (IMO) reached a milestone agreement in April 2018: In alignment with the emission-reduction goals set out in the United Nation's 2015 Paris Agreement, IMO agreed to cut greenhouse gas emissions by at least 50% by 2050 and CO_2 emissions per transport work by at least 40% by 2030 and 70% by 2050 compared to the 2008 level.

To achieve such goals the international community is currently examining various measures and actions to enhance the energy efficiency of the maritime transport sector, *Chou et al. (2020)*.

Bouman et al. (2017) studied the CO_2 reduction potential of a large number of improvement measures and concluded that wind propulsion systems (WPS) are among the more promising ways to reduce emissions. As opposed to many other technologies WPS are also marked-ready and available for installation.

Several WPS concepts are currently being developed and re-discovered. These modern technologies have little in common with the canvas sails of old and range from "Flettner rotors" over kites and suction wings to rigid sails that resemble vertical aircraft wings, *Chou et al. (2020)*.

Modern wind propulsions systems can be grouped into seven main categories, *IWSA (2021)*:

1. Soft Sails: Traditional cloth & modern adaptions
2. Hard Sails: Wingsails with & without flaps

3.   Rotor Sails: Based on the "Magnus"-effect
4.   Suction Wings: Wing with boundary layer suction to increase maximum lift
5.   Kite Sails: Flown off the bow to assist propulsion
6.   Turbines: Wind turbines to generate electrical energy
7.   Hull Form: Redesign of ship's hulls to capture the wind and generate thrust

All of these systems have their specific strengths and weaknesses which need to be considered when selecting a WPS for a specific case. To help shipowners and other stakeholders make informed decisions, we developed a systematic, scientific methodology to compare and assess different WPS at the early concept stage of a vessel. This methodology and the related software tool "SEAMAN Winds" take technical performance questions, the trading routes of the vessel, and financial and risk aspects into account and are intended to help making the "business case", see also *Gerhardt et al. (2021)*.

In the current paper, SEAMAN Winds is used to highlight some of the challenges and pitfalls of comparing and selecting WPS. A first case study looks at a general cargo ship engaged in tramp trade and shows that commonly used Key-Performance-Indicators (KPIs) like "relative fuel savings" [% rel. no WPS] or "savings per mile" [kg/Nm] strongly depend on speed, route, loading condition, etc. This makes it impossible to rank competing WPS, unless exactly the same ship, route, operational profile, and analysis methods are used.

Before this background, the second study then looks at the case of a RoPax ferry in liner trade. SEAMAN Winds is employed to compare two competing WPS in a fair way: A rotor sail and a rigid wingsail with boundary layer suction ("suction wing"). The two systems have different performance characteristics and also vary in investment and operational costs. The case study assesses the economics of the two systems by looking at Payback Time (PBT) and Net Present Value (NPV).

2. Assessment methodology

A detailed description of the assessment methodology behind SEAMAN Winds has been given by *Gerhardt et al. (2021)*. Below follows just a summary of the key features and modelling assumptions.

2.1. Overview

Fig.1 illustrates the structure of SEAMAN Winds. The program consists of four modules that look at ship performance, voyage & routing, financial & environmental, and risk aspects respectively. The general approach is similar to methods developed elsewhere, e.g., *Tillig (2020),* https://blueroute. application.marin.nl/, *BAR Technologies (2021),* but differs in the following respects:

- Hull and propeller modelling build on SSPA's large database of experimental and CFD results, as a complement to the usual empirical methods.
- The method has been used successfully in a number of projects while working as partner or consultant to ship owners and designers. Fig.2 shows some examples. SEAMAN Winds thus has a commercial rather than an academic or research focus.
- An important feature that sets SEAMAN Winds apart from many other programs, and particularly the proprietary tools used by WPS manufactures, is that all aerodynamic datasets have been independently verified by SSPA, either through wind tunnel test, *Marimon et al. (2022)*, sea trials, *Werner et al. (2021,2022),* or extensive CFD, *Li et al. (2012)*.
- Power and fuel saving predictions have been correlated to sea trial results, *Werner et al. (2021)*.
- SEAMAN Winds uses the same modelling approach to evaluate different WPS. This provides customers with decision support material that evaluates competing WPS in a fair way.
- Once the business case for a particular WPS has been made and as the ship design process progresses, the input to the analysis model can gradually be refined. Database values can e.g., be replaced with ship specific CFD or model test results.

162
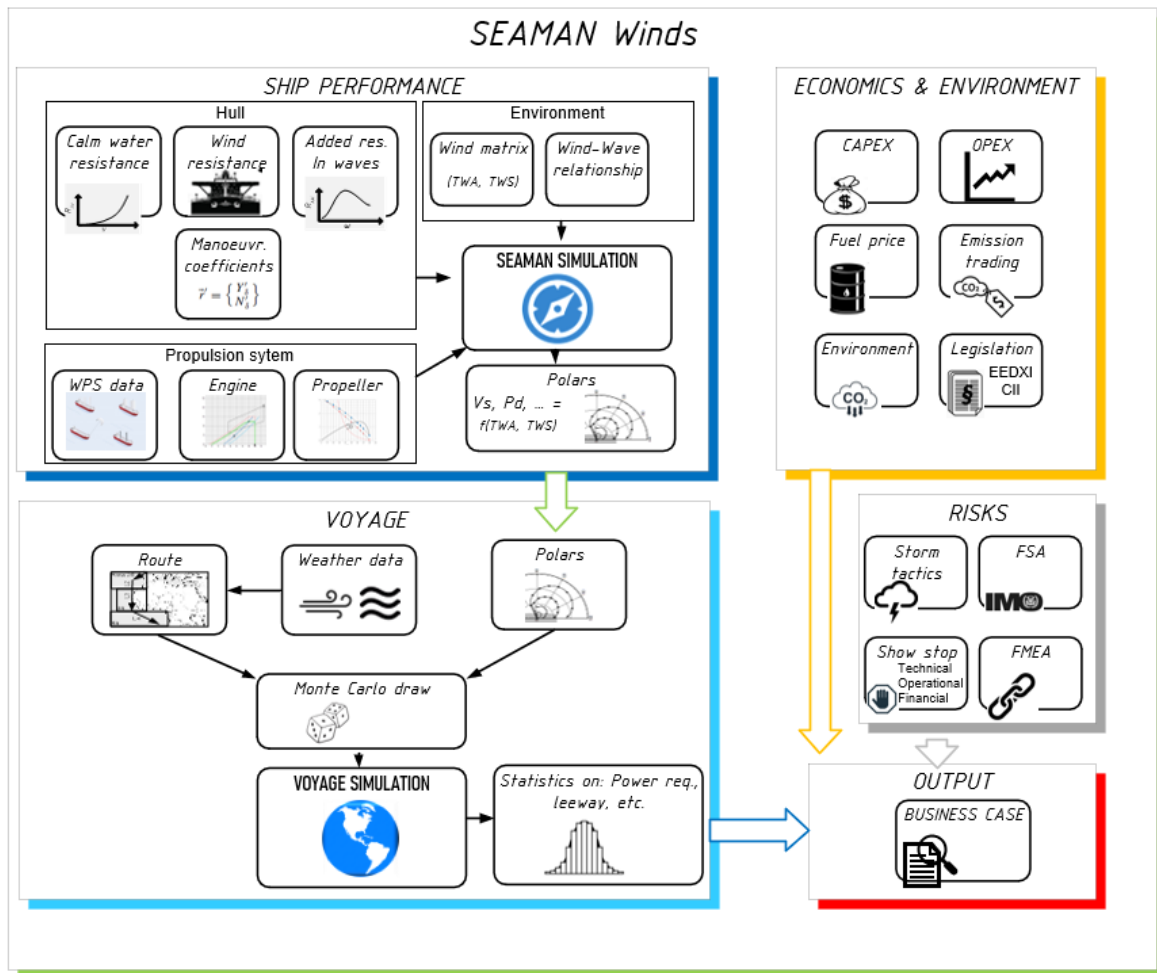
Fig.1: Block diagram illustrating the methodology behind SEAMAN Winds

Fig.2: Recent wind ship projects in which SEAMAN Winds has been used

2.2. Ship performance module

At the core of the 'ship performance' module from Fig.1 is a power prediction based on the modified ITTC-1978 approach described in *Gerhardt and Kjellberg (2017)*. The prediction is carried out in SSPA's inhouse software-suite SEAMAN and balances hull and sail forces in a minimum of 4 DOF (surge, sway, roll, yaw), https://www.sspa.se/tools-and-methods/seaman-simulations, *Olsson et al. (2020)*.

Input to the simulations is a large matrix of true wind angle (TWA) and true wind speeds (TWS) combinations. For each of these, SEAMAN carries out a performance prediction and returns a vector with parameters like: Sail forces, ship speed, required shaft power, propeller rpm, leeway angle, rudder angle, heel etc. This output is stored in the format of 'polars' for further analysis in the 'voyage

simulation' module. More detailed information on modelling the individual force components can be found in *Gerhardt et al. (2021)*. An example output from the ship performance module can be found in the second case study at the end of this paper.

2.3. Voyage simulation module

As illustrated on the lower left-hand side of Fig.1, the output of the SEAMAN simulations from the ship performance module is analysed in the voyage module where information about the intended trading route is combined with weather statistics and the SEAMAN polars.

More specifically, the route is divided into a number of legs. For each of these, a discrete joint weather distribution for true wind speeds (TWS) and true wind angles (TWA) is aggregated based on wind data from the ERA5 reanalysis dataset available at the Copernicus Climate Data Store, https://cds.climate.copernicus.eu/#!/home.

To keep the computational effort within reasonable limits, a Monte Carlo simulation is then performed according to the following steps:

1. For each of the typically $100 \cdot 10^3$ iterations in the Monte Carlo simulation
   a. For each leg on the route
      i. Find the course over ground and distance that the ship will travel on this leg
      ii. Draw a sample weather condition from the discrete, joint weather distribution. The sample is randomly chosen based on its probability of occurrence, i.e. a weather condition with 2% probability of occurring has a 2% probability of being sampled.
      iii. Evaluate ship performance for this specific weather condition using the performance polar curves from SEAMAN, linearly interpolating where necessary.
   b. Aggregate the results for the entire route based on the sub-results from each leg.
2. Combine the aggregate route results from all iterations into probability distributions

The output from the voyage module thus consists of a set of probability density functions, one for each parameter that was 'sent into' the Monte Carlo simulation. Typically sail forces, ship speed, required shaft power, propeller rpm, leeway angle, rudder angle, heel, etc. This data can be analysed to answer questions like:

- What will the average power savings on this route be?
- What is the 95% confidence interval of achieving a power saving of 5%?
- What is the probability of exceeding sail forces of X Newtons or rudder angles of Y° while trying to stay on course?

2.4. Economics & environmental module

The 'economics and environmental module' of SEAMAN Winds looks at investment costs (CAPEX) and maintenance costs (OPEX) for wind propulsion systems and compares these to power (and fuel) savings from the voyage simulations.

The module also uses the information from the voyage simulations to analyse the effect of the WPS on CO_2 emissions and regulatory parameters like EEDI, EEXI or CII.

Based on such calculations, financial information on e.g., the payback time for the installation of a WPS or the effect of measures like 'carbon trading' can be derived.

Inside the economics and environmental module WPS costs can be modelled in different ways. Either in a generic way and based on open-source data, *Gerhardt et al. (2021),* or, perhaps more usefully, based on figures quoted by specific WPS providers.

2.5. Risk module

A unique feature of SEAMAN Winds is the option to assess risks associated with installing a WPS. Such risks fall into the categories 'technical', 'operational', and 'financial'. They range from mechanical failure of the WPS over crew training and recruitment issues to the consequences of a year with very little wind, compare *Gerhardt et al. (2021)*.

3. Case studies

SEAMAN Winds will now be used to highlight some of the challenges and pitfalls of comparing and selecting wind propulsion technologies. Two case studies are presented, first, a tramp ship trading in the Baltic and North Sea, and secondly a RoPax Ferry on a regular Germany-Denmark schedule.

3.1. Example 1: Bulk carrier

The bulker 'm/v Annika Braren', Fig.3, owned by Rörd Braren Bereederungs-GmbH & Co. KG, (L=84.95 m, B=15 m, dwt=5035 t, IMO 9849148) operates mainly in the North Sea region and the Baltic. In 2021, a 3 m x 18 m "Eco Flettner" rotor with top and bottom endplates was installed at the forecastle. The rotor is driven by an electric motor and the rotation speed is set automatically, based on the measured apparent wind speed. The anemometer is positioned in the top of the signal mast over the bridge. The ship has a ducted, controllable pitch propeller.

As part of the EU Interreg North Sea Region project "WASP", SSPA carried out sea trials onboard the vessel and analysed the results, *Werner et al. (2022)*. The following two sections briefly describe how SEAMAN Winds was used to analyse the sea trails and discuss the key findings.

Fig.3: 'Annika Braren' with Flettner rotor

3.1.1. Trial analysis and verified aerodynamic model

To assess the performance of the rotor sail, dedicated sea trials of a few hours' duration were caried out in late September 2021. Trials were conducted north of the island of Gotland in the Baltic and true wind speeds varied in between 9-12 m/s with waves of 0.7-1.5 m significant height.

As described by *Werner et al. (2022)* data from the trials were then analysed in SEAMAN Winds to derive a number of Key-Performance-Indicators (KPIs).

Fig.4 illustrates different aerodynamic datasets that can be used for the analysis of rotor sails. Shown are lift and drag as function of rotor spin ratio SR= n πD/U_∞. The figure compares manufacturer data (from Eco Flettner, *Vahs (2019)*) to SSPA's URANSE calculations and other sources from the literature. As can be seen SSPA calculations and manufacturer data agree reasonably well with SSPA predicting higher lift and higher drag at spin ratios below 4. The most likely reason for this is that the SSPA-URANSE calculations were conducted at full-scale Reynolds numbers $\mathcal{O}(10^6)$ whereas manufacturer data are i.a. based on wind tunnel data at Re $\mathcal{O}(10^4 - 10^5)$. As discussed by *Li et al. (2012)* this affects vortex formation and aerodynamic coefficients. The comparison illustrates that there can be a large spread between datasets from different sources and highlights the importance of backing up experimental results with full scale data.

Numbers shown are for an isolated rotor in homogenous/rectangular inflow and ignore interaction with the ship hull. This interaction is usually significant and therefore the aerodynamic lift and drag forces need to be corrected using sea trial results, when available, or SSPA's inhouse hull interaction model. This model is based on CFD studies and sea trial results from other ships.

Other types of wind propulsion technologies like rigid wingsails or suction wings can also be modelled in SEAMAN Winds and are treated in a similar way. In case of multiple devices on the ship, mutual interaction between the propulsors is accounted for, compare *Gerhardt et al. (2021)* and *Marimon et al. (2022)*.
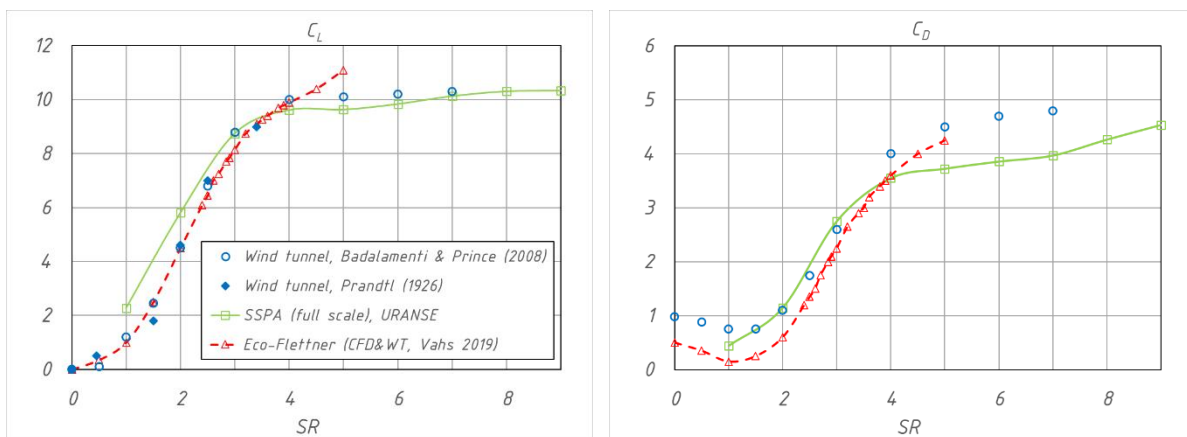
Fig.4: Lift and drag coefficients for single Flettner rotors as function of spin ratio. All equipped with end discs (D_{disc}=2 D_{rotor}, except Prandtl where D_{disc}=3.5 D_{rotor}). Homogeneous inflow, Re,$_{experimental}$ < 100 000. Aspect ratios 5<AR<6.

3.1.2. Results and Key-Performance-Indicators

The performance of wind-powered ships can be expressed in number of ways, e.g. percentage power reduction over a year, bunker or CO_2 savings per year, change in EEDI, power reduction at beam wind, etc. Following the work carried out in the EU WASP project, *Werner et al. (2022),* we here present the Key Performance Indicators (KPIs) "bunker saving per nautical mile" [kg/Nm] and "percentage savings relative to no WPS".

Fig.5 shows the first KPI for a number of different routes and loading conditions. Values were derived by executing the voyage simulation with and without the wind propulsor and comparing the average power requirement, keeping the ship speed constant. This represents the average value of letting the ship sail the route 100 000 times in randomly chosen weather conditions based on weather statistics from the full year of 2019. Some days the weather will be favourable with large power savings, some days it will be adverse.

The large variation from 1.1 kg/Nm (route ① "inbound") to 0.35 kg/Nm (route ④ "outbound") can be explained by the prevailing wind directions in the operational areas. The ship encounters favourable winds from Sunderland to Karlshamn, with dominating wind from aft of the beam, which is very suitable for the rotor performance profile. Whereas the west-southwest route Karlshamn-Vlissingen via Kiel, is not good for a wind-assisted ship.
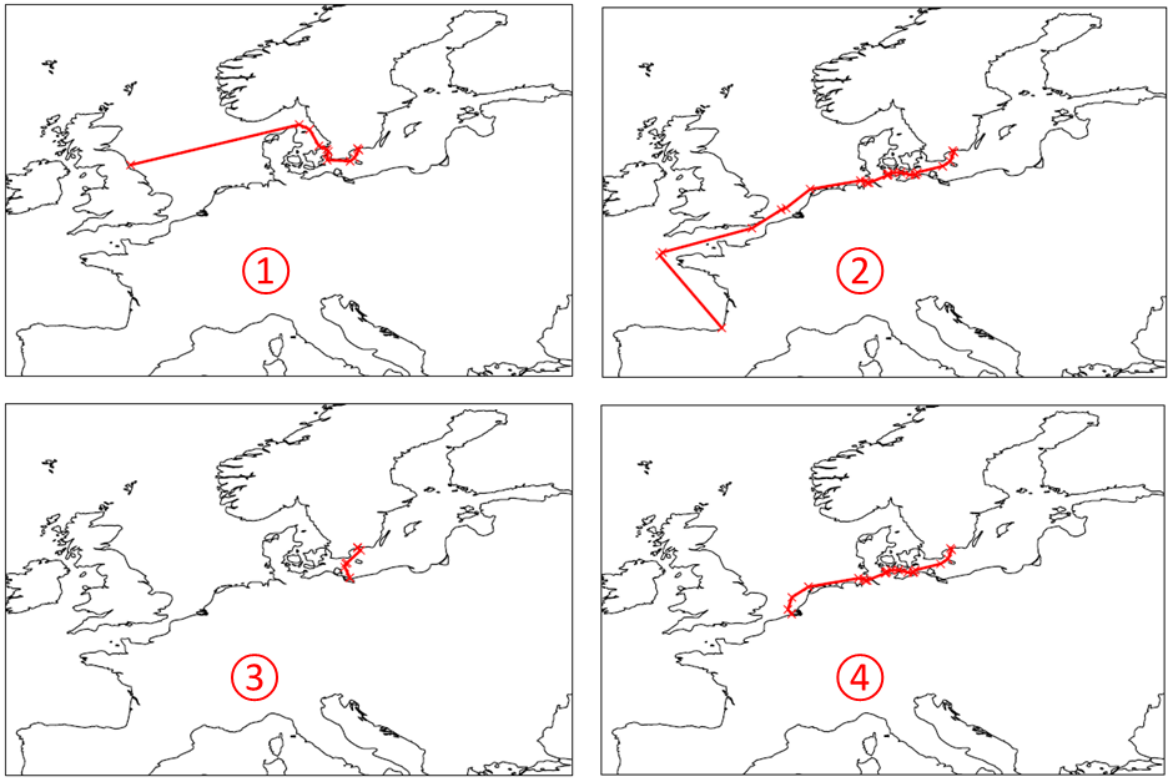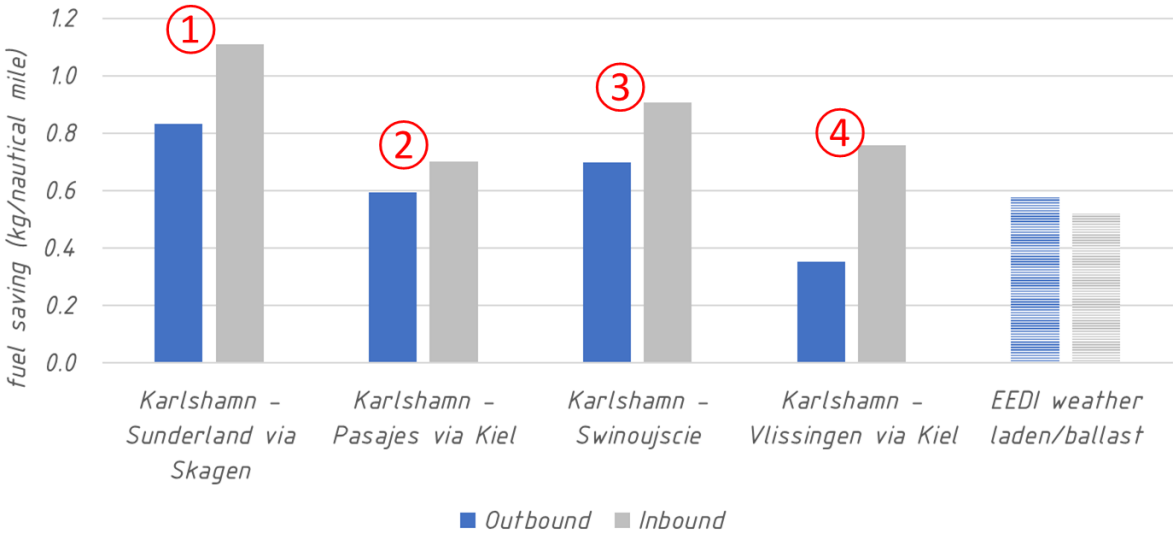

Fig.5: Fuel saving predictions for typical routes of 'Annika Braren'; ship speed 11.5 knots

As Fig.6 illustrates the KPI "relative fuel savings" is very speed dependent and varies by almost a factor of two when decreasing speed from 13 to 10 knots.

In summary, the KPIs are route and speed dependent. This makes it is difficult to rank competing WPS, unless exactly the same ship, route, operational profile and analysis methods are used. This is problematic for ship owners and other stakeholders looking to invest into wind propulsion technology because the on-demand case studies that WPS providers offer are based on prediction methodologies

167

and assumptions that differ from provider to provider. This makes comparing different technologies from competing suppliers next to impossible.

Before this background, the next case study uses SEAMAN Winds to allow a direct and fair comparison of two competing WPS.
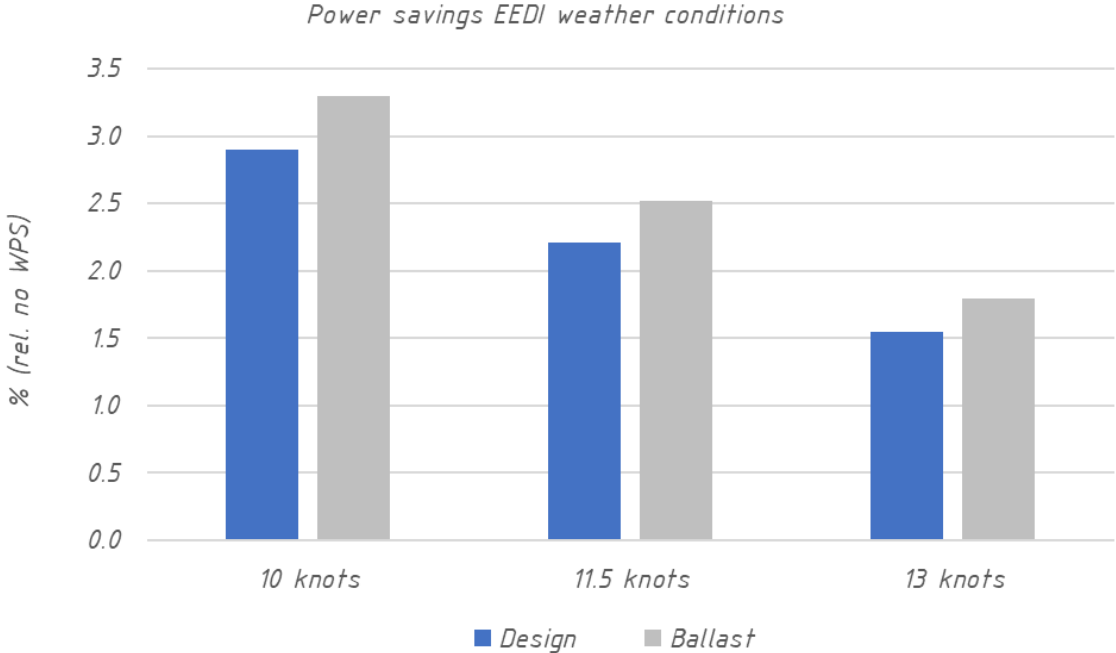
Fig.6: Relative fuel savings for 'Annika Braren', variation with ship speed; EEDI weather conditions

3.2. Example 2: RoPax Ferry

The second case studied is the RoPax ferry 'm/v Copenhagen', operated by Scandlines between Gedser in Denmark and Rostock in Germany. The vessel (L=156.45 m, B=24.6 m, IMO 9587867) was equipped with a 5 m x 30 m Norsepower rotor sail with an endplate. The WPS is positioned longitudinally near mid-ship, 17.2 m above design water line, Fig.7. See *Gerhardt et al. (2021)* for more details.

Fig.7: 'Copenhagen' with Flettner rotor (source: Scandlines)

168

As for the 'Annika Braren', the rotor is driven by an electric motor and the rotation speed is set automatically, based on the measured apparent wind speed. The anemometer is positioned in the top of the signal mast over the bridge. The ship has two azimuth thrusters and a centre propeller with controllable pitch.

SSPA carried out sea trials for this vessel also, and results are presented and discussed in *Werner et al. (2021,2022)*.

3.1.1. WPS configurations and parameters

To demonstrate how SEAMAN Winds works, we here study the additional, and purely hypothetical, case of installing a rigid wingsail with boundary layer suction ("a suction wing") on the 'Copenhagen', Table I.

Table I: Input parameters used for case study

Case	Actual	Hypothetical
WPS	**Rotor (R)**	**Suction Wing (SW)**
Principle of operation	Magnus Effect	High lift wing profile, boundary layer suction to delay stall
Dimensions	30 m x 5 m	24.8 m x 6.13 m
Area S	150 m^2	152 m^2
Aspect ratio AR	6	4
System	Non-tilting rotor	Folded on deck in head winds + in port
WPS power	Electric motor: P_{max}= 100 kW	Fan motor: P_{max}= 80kW
CAPEX	800 000 €	650 000 €
OPEX	3% Capex/a. 2% increase annualy	
WPS life span	25 years, rest value zero	
Ship main engine	2 x 4500 kW Specific fuel oil consumption: SFOC=200g/kWh	
Fuel	VLSFO; Specific CO_2 emmissions 3.11 kg CO_2/kg fuel	
Route	Gedser-Rostock-Gedser; 5 return journeys per day	
Operation	350 days per year	

The rotor performance model is similar to the one discussed in the first case study. The aerodynamic performance of the suction wing is modelled using a combination of 2D CFD simulations and lifting line theory to model three dimensional effects. This approach is similar to the one used *Malmek et al. (2020)* to model rigid wingsails but in the present case URANSE simulations are carried out to determine the 2D characteristics of the wing sections as function of the amount of boundary layer suction. Figures 8 shows 2D streamline plots from the CFD studies. Fig.9 summarises 3D lift and drag values and compares them to wind tunnel data from *Charrier et al. (1985)*. More details of modelling the suction wing can be found in *Gohde (2022)*.
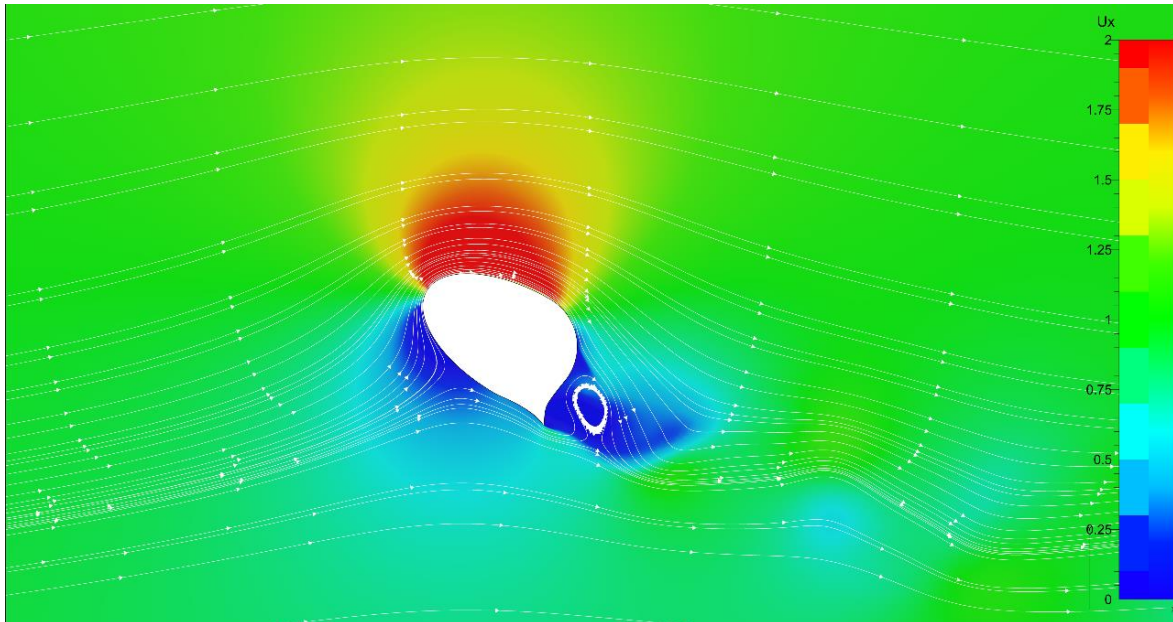
Fig.8: Streamlines around suction wing profile from 2D-URANSE
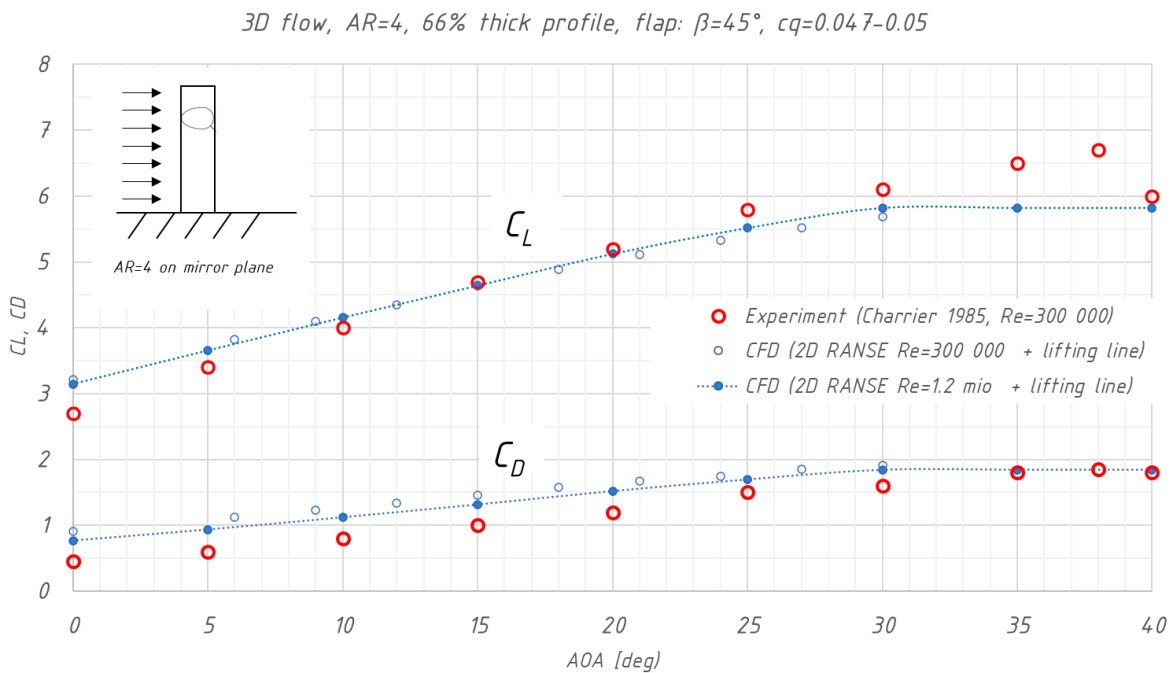
Fig.9: 3D lift and drag values for suction wing. Aspect ratio 4, suction coefficient $c_q \approx 0.05$

3.1.2. Results and the business case

Fig.10 compares power savings for the two systems as function of true wind speed (TWS) and true wind angle (TWA). Shown are net-savings i.e. the power to spin the rotor and the suction power have been removed from the gross-savings. It can be observed:

- For very low true wind angles ($TWA<\approx 20°$) power savings for the rotor are negative. This reflects the drag of the idling rotor in headwind, which in this example cannot be tilted. The suction wing, however, can be folded down onto deck and shows a different behaviour.
- With C_L values of up to 10 the rotor is more powerful than the suction wing ($C_{Lmax} \approx 6$). This leads to larger fuel savings under comparable wind conditions

170

- Under optimal conditions power savings for rotor and suction wing can reach up to 28% and 20% respectively.
- For a ship speed of 16 kts the optimal wind directions for the rotor are slightly aft of the beam (*TWA*≈100°) whereas the corresponding angle for the suction wing is *TWA*≈90°.
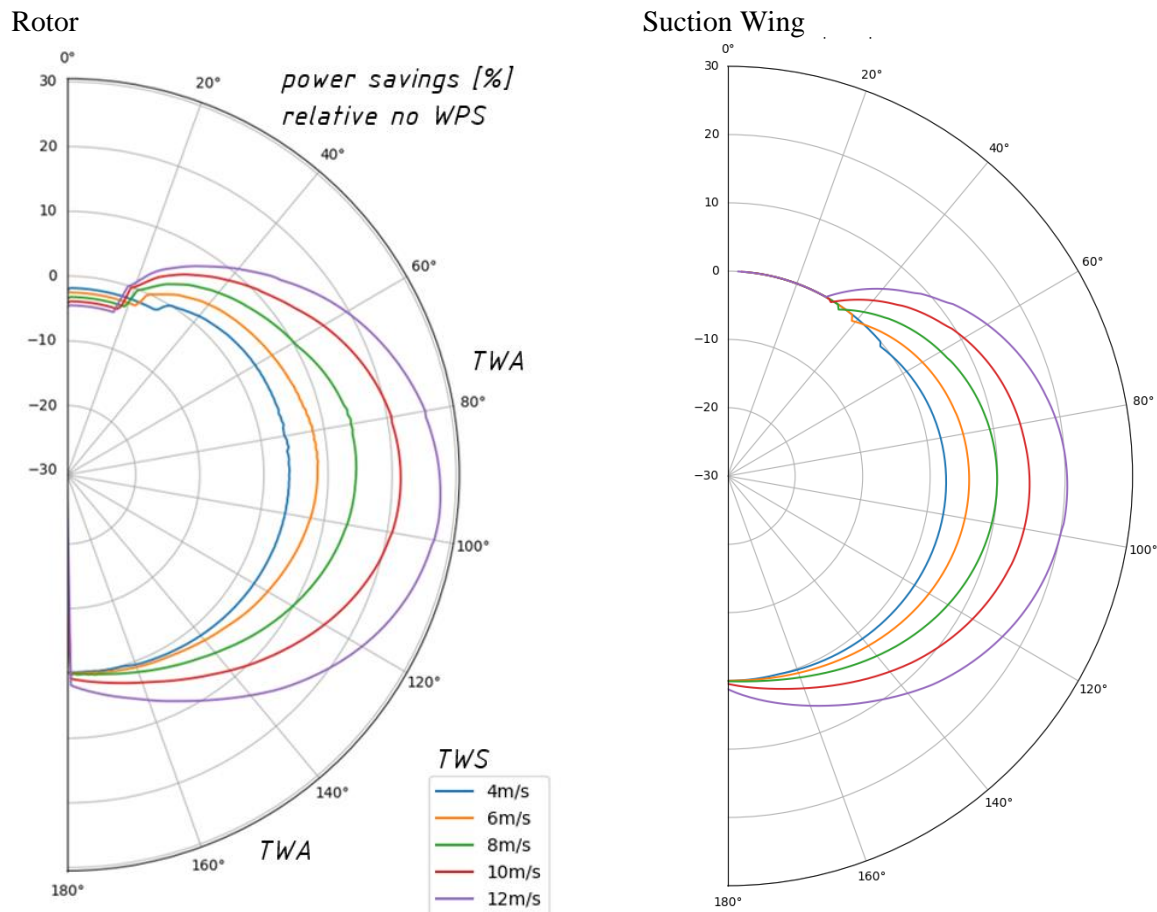
Fig.10: Net-power savings relative to no-WPS case. Fixed ship speed 16 kn.

As the vessel will experience different wind and wave conditions over time, the power for a constant service speed will differ from journey to journey. These effects are evaluated in the voyage module of SEAMAN Winds, which returns statistical information on power savings, CO_2 reductions and other parameters, *Gerhardt et al. (2021)*. Averaged over a typical year, the power savings for the rotor and the suction wing become 3.9% and 2.5% respectively, Table II. This already takes the electrical power required to operate the two WPS into account.

An economic analysis of the two competing WPS crucially depends on bunker prices and their future developments. For the sake of this paper the three bunker scenarios illustrated in Fig.11 were used. Table II summarises the resulting annual fuel savings etc.

Figs.12 and 13 finally illustrate typical output from the economics and environmental module. The numbers and plots serve to illustrate how SEAMAN Winds works. They are based on the discussions with WPS providers and our own estimates and do not represent actual costs or how Scandlines operates the vessel.

As shown in Fig.12 and Table II, payback time (PBT) for the rotor ranges from about 2 to 10 years depending on bunker price scenario. PBTs for the suction wing are larger and vary between 2.5 and 13 years.

Table II: Example results from SEAMAN Winds analysis

WPS	Rotor (R)	Suction Wing (SW)
Power savings	3.9 % annualy	2.5 % annualy
Energy saved	1 240 MWh/a	800 MWh/a
Bunker savings	248 t/a	160 t/a
CO_2 savings	771 t/a	498 t/a
Payback time for bunker scenar.③/②/①	2/3.5/9.75 years	2.5/4.3/13 years

Such simple PBT calculations do not account for the "time value of money", this is problematic because WPS (and ships in general) are long term investments. A common metric to assess such investments is the Net Present Value (NPV) which expresses the current total value of a future stream of payments in "todays money". To determine the NPV each cash inflow/outflow R_t is discounted back to its present value (PV).

$$PV_t = \frac{R_t}{(1 + i)^t}$$

R_t is the net cash flow at time t and i is the "discount rate" i.e. the rate of return that could be earned on an alternative investment. All PV_t are then summed up to yield the NPV:

$$NPV = \sum_{t=0}^{T} \frac{R_t}{(1 + i)^t}$$

With R_0 =-CAPEX as the initial investment during the first year and T as the total number of years over which the investment is evaluated.

Fig.13 shows the NPVs for the rotor and suction wing as function of the discount rate and for $T = 25$ years. Also shown in the figure is a range of discount rates commonly used to assess investments. This range is based on Weighted Average Cost of Capital (WACC) for a number of shipping companies and ship operators. It can be noticed that in this particular case:

- The rotor (with higher CAPEX and OPEX and larger savings) has an edge over the suction wing. This illustrates that the profitability of such long-term investments is determined by fuel saving, not CAPEX.
- The "gap" between rotor and suction wing narrows with increasing discount rate. This is because in these cases the value of larger savings in the distance future decreases and initial investment costs (lower for the suction wing) get relatively more important.
- The incentive to invest into any of the WPS is low for bunker prices of around 500$/t (scenario ①) This is because the NPV is close to zero for industry-typical discount rates from 4% to 8%.
- For the other two bunker price scenarios, the picture changes drastically: For a discount rate of 8% and bunker scenario ② the rotor has a NPV of 2.7 million Dollars. The corresponding value for the suction wing is 1.6 million. This corresponds to a return of 3.4 Dollar per invested Dollar for the rotor and 2.4 Dollar/Dollar for the suction wing.
- In the extreme case of scenario ③ and a with discount rate of 4% the NPVs of rotor and wing increase to 9.1 and 5.7 million Dollars (11.4 and 8.7 Dollar/Dollar invested) respectively.

Remember that such an economic analysis depends on operational parameters and the trading route. The above results apply only to the Gedser-Rostock route, where the predominant wind direction is from abeam. Such conditions favour a rotor sail. The generalised conclusion that rotors "are better" than suctions wings is not admissible!

Using the SEAMAN Winds interface, the analysis can now be carried out for other scenarios, such as another route, ship speed, bunker price development or alternative WPS's.
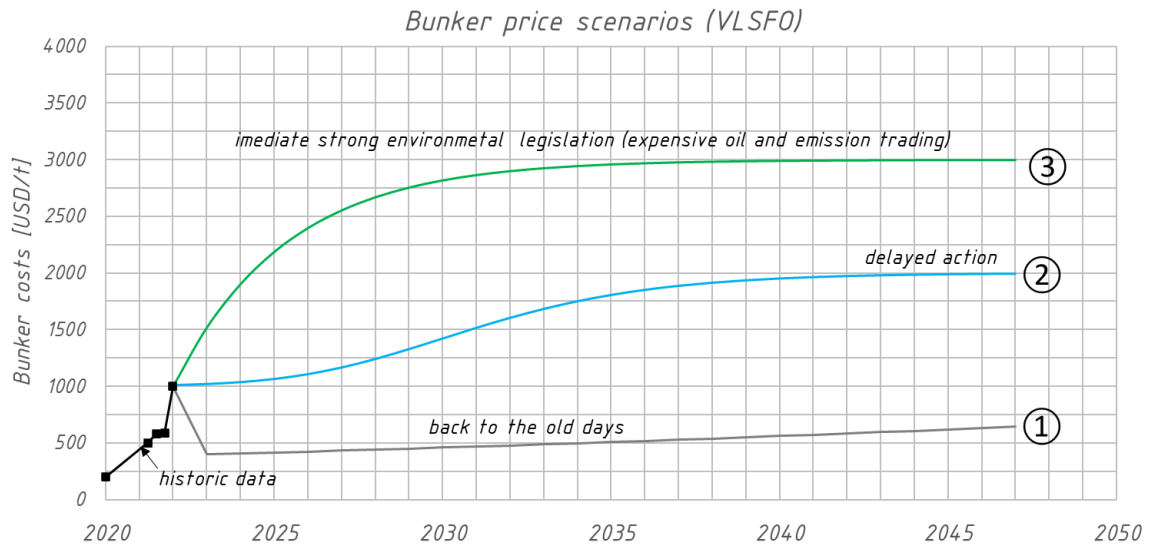
Fig.11: Bunker price scenarios (historic data up to July 2022)
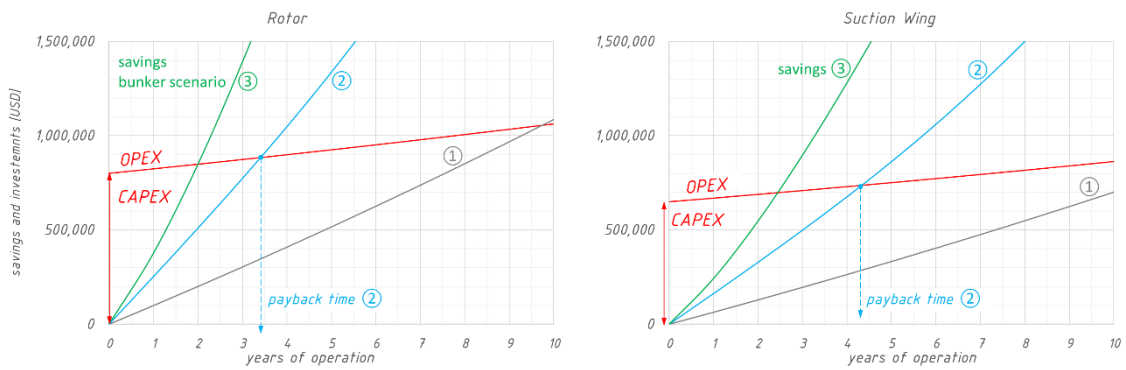
Fig.12: Payback time of the two WPS for three bunker price scenarios
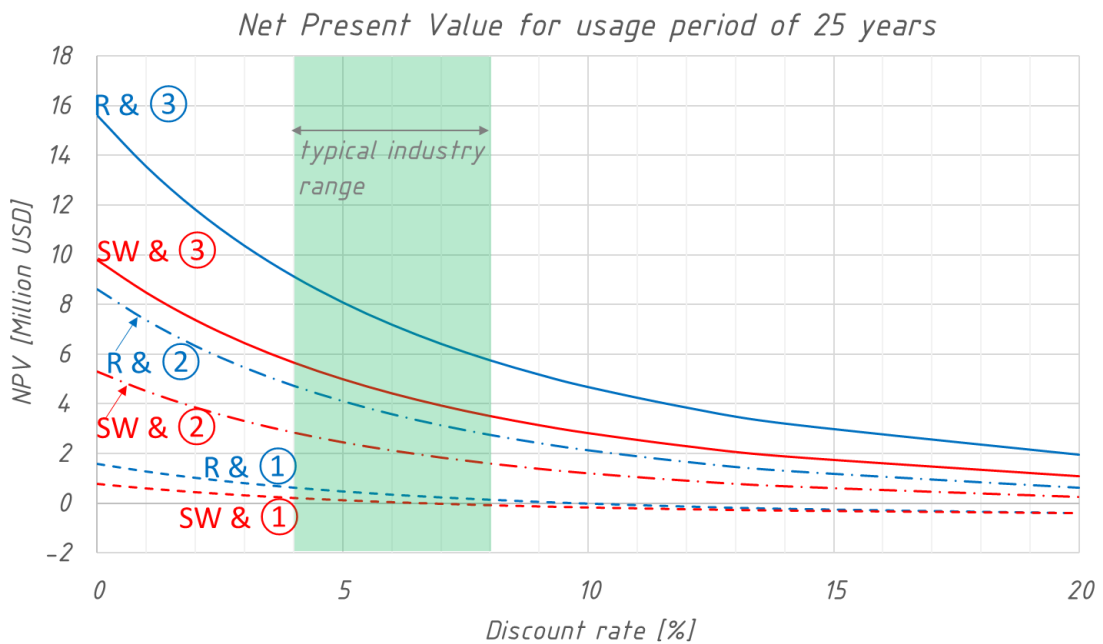

Fig.13: Net present value for rotor (R) and suction wing (SW)

4. Conclusions

Wind propulsion systems (WPS) are a viable way to reduce CO_2 emissions from shipping. Among the key barriers to the market uptake of such systems are high investment costs combined with uncertainty around how effective WPS are in real life, what financial risks they entail, and how to select between competing systems.

We have presented here a systematic, scientific methodology to address these issues. Based on this methodology a software called SEAMAN Winds was developed. This tool can provide guidance for shipowners and other stakeholders and help them select a system that suits their particular requirements.

Unique features include:

- The tool provides an independent third-party assessment of predictions made by WPS manufacturers.
- Hull and propeller modelling is based on SSPA's large database of experimental and CFD results.
- All aerodynamic datasets describing WPS performance are independently verified by SSPA. Either through wind tunnel test, sea trials or extensive CFD.
- The tool uses the same modelling approach to evaluate different WPS. This provides decision support material that evaluates competing WPS in a fair way.
- Once the business case for a particular WPS has been made, and as the ship design process progresses, the input to the analysis model can gradually be refined with increasingly complex and accurate simulation input.

Two case studies show how:

- Commonly used key performance indicators like "relative fuel savings" or "fuel savings per mile" depend on ship speed and route. This makes it is difficult to rank competing WPS, unless exactly the same ship, route, operational profile and analysis methods are used.
- SEAMAN Winds can be used for a fair comparison of competing WPS
- What kind of decision support material can be produced. It is calculated, how many tons of CO_2 can be avoided each year and how "payback times" and "net present values" of a rotor sail and a suction wing are affected by different parameters including bunker price developments.

Acknowledgements

References

BAR TECHNOLOGIES (2021), *Ship System Efficiency Analysis Toolset*, https://www.bartechnologies.uk/project/shipseat/

BADALMENTI, C.; PRINCE, S.A. (2008), *The Effects of Endplates on a Rotating Cylinder in Crossflow,* 26th AIAA Applied Aerodynamics Conf., Honolulu

BOUMAN, E.; LINDSTAD, E.; RIALLAND, A.; STRØMMAN, A. (2017), *State-of-the-art technologies, measures, and potential for reducing GHG emissions from shipping – A review*, Transportation Research Part D: Transport and Environment 52, Part A

CHARRIER, B.; CONSTANS, J.; COUSTEAU, J.Y.; DAIF, A.; MALAVARD, L.; QUINIO, J.L. (1985), *Fondation Cousteau and windship propulsion 1980-1985. System Cousteau-Pechiney*, J. Wind Engineering and Industrial Aerodynamics 20, pp.39-60

174

CHOU, T.; KOSMAS, V.; RENKEN, K.; ACCIARO, M. (2020), *New Wind Propulsion Technology - A Literature Review of Recent Adoptions*, Interreg North Sea Europe Wind Assisted Ship Propulsion (WASP) report D 5.B

GERHARDT, F.C.; KJELLBERG, M. (2017), *Determining the EEDI weather factor fw*, Influence of EEDI on Ship Design & Operation, RINA

GERHARDT, F.C.; WERNER, S.; HÖRTEBORN, A.; LUNDBÄCK, O.; NISBET, J.; OLSSON, T. (2021), *Horses for Courses: How to select the 'right' wind propulsion system and how to make the business case*, RINA Conf. Wind Propulsion, London

GOHDE, S. (2022), *Energetic and economic saving potential of various wind propulsion systems on ships. A comparative study*, MSc thesis, Berliner Hochschule für Technik, Berlin

IWSA (2021), *Technology and Design*, International Windship Association, https://www.wind-ship.org/en/technology-design/

MALMEK, K.; DHOMÉ, U.; LARSSON, L.; WERNER, S.; RINGSBERG, J.; FINNSGÅRD, C. (2020), *Comparison of two rapid numerical methods for predicting the performance of multiple rigid wing-sails*, 5th Int. Conf. Innovation in High Performance Sailing Yachts and Sail-Assisted Ship Propulsion, Gothenburg

LI, D.-Q.; LEER-ANDERSEN, M.; ALLENSTRÖM, B. (2012), *Performance and vortex formation of Flettner Rotors at high Reynolds numbers*, 29th Symp. Naval Hydrodynamics, Gothenburg

MARIMON GIOVANNETTI, L.; DHOMÉ, U.; MALMEK, K.; PERSSON, A.; WIELGOSZ, C. (2022), *Multi-wing sail interaction effects*, 24th Chesapeake Sailing Yacht Symp.

OLSSON, F.; MARIMON GIOVANNETTI, L.; WERNER, S.; FINNSGÅRD, C. (2020), *A Performance Depowering Investigation for Wind Powered Cargo Ships Along a Route*, InnovSail Conf., Gothenburg

PRANDTL, L. (1926), *Application of the "Magnus Effect" to the Wind Propulsion of Ships*, NACA TM 367

TILLIG; F. (2020), *Simulation model of a ship's energy performance and transportation costs*, PhD thesis, Chalmers University of Technology, Gothenburg

VAHS, M. (2019), *Retrofitting of Flettner rotors – results from sea trials of the general cargo ship "Fehn Pollux"*, RINA Conf. Wind Propulsion, London

WERNER, S.; NISBET, J.; HÖRTEBORN, A.; NIELSEN, R. (2021), *Speed Trial Verification for a Wind Assisted Ship*, RINA Conf. Wind Propulsion, London

WERNER, S.; NISBET, J.; OLSSON, F. (2022), *Sea Trial Methodology for Wind Assisted Ships*, 7th Hull Performance & Insight Conf. (HullPIC), Tullamore, pp.124-140, data.hullpic.info/HullPIC2022_Tullamore.pdf

Quantifying the Effect of Green Technologies on Ship Performance using Operational Data – Design of Experiments and Data Collection

Josef Camilleri, Silverstream Technologies, London/UK, josef.camilleri@silverstream-tech.com
David Connolly, Silverstream Technologies, London/UK, david.connolly@silverstream-tech.com
Adam Sobey, University of Southampton, Southampton/UK, ajs502@soton.ac.uk
Dominic Hudson, University of Southampton, Southampton/UK, dominic@soton.ac.uk

Abstract

This paper explores experimental designs to efficiently collect data when quantifying the effect of green technologies on ship performance. The ISO 19030 standard, Short-Term Interruption and Machine Learning are compared with the aim of finding a technology agnostic approach that can accurately quantify performance in any given set of ship operational and environmental conditions. Using operational data from a ship equipped with the Silverstream air lubrication system we highlight the benefits and shortcomings of each approach. It is shown that having datasets that accurately reflect the ground truth in any ship operational and environmental condition and not just the typical cases is key and can be achieved through careful design of experiments.

1. Green technologies for ship performance enhancement

Technologies that improve ship efficiency remain of critical importance to achieving the industry's decarbonisation goals. 'Consuming less' is a mantra that requires a careful balancing of demands. Unfortunately, the marine sector is notoriously conservative in terms of investment since decisions typically impact the full lifecycle of the vessel. Accurate quantification of the effect of green technologies on ship performance is therefore crucial to unlocking substantial, long-term investment.

Ships operate in a complex and stochastic environment where factors such as wind, waves, currents, and temperature cannot be controlled but can have a significant influence on ship performance. In addition, the introduction of green technologies further complicates the problem as their nonlinear behaviour, influenced by environmental and operational factors, prevents the true savings they offer from being fully understood or compared. Traditional approaches based on scaled model tests are expensive and often involve scaling difficulties which can lead to inaccuracies. Modelling approaches, such as Computational Fluid Dynamics, can produce more accurate and reliable results but to model the problem in its full complexity requires prohibitive computational expense.

Recently an alternative has become popular through analysis of operational data gathered from ships in-service and while there are benefits in accuracy and computational cost, this approach is not without challenges. In particular,

1. to quantify the effect of green technologies on ship performance, the preferred approach would be to compare data with and without the technology and with any other variables that may exert some effect on the response (ship operational or environmental variables) held constant. However, as ships operate in non-stationary environments, whether it is due to a temporal or a spatial change, holding all factors of influence constant is a significant challenge.
2. If the technology is not well characterised and the full set of factors that influence the response is not known, there can be confounding variables causing spurious associations.
3. The relationships between variables are generally complex and nonlinear, while the data is noisy and with heavy tailed distributions. Techniques that can model these complex relationships are required.

To tackle these challenges, the industry has largely focused on developing methods for filtering and correcting the observed data, with a larger focus on the analysis of these datasets. However, there is a more limited literature that determines fair and cost-effective datasets which match the expected mean

during operation. Typically, data is gathered by passively monitoring the ship as it operates without any interventions, which means that large datasets collected over long periods of time are required to obtain an accurate representation of the fundamental relationships which generated the dataset, the ground truth, *Dalheim and Steen (2020), Bui and Perera (2021)*. Starting with a dataset that accurately represents the behavior of a ship in operation and that is large enough to ensure that the regression fits to the ground truth is vital to compare "green" shipping technologies fairly and accurately.

This paper therefore explores three experimental approaches for quantifying the effect of green technologies on ship performance: the ISO 19030 standard, and two approaches currently under development at Silverstream Technologies, Short Term Interruption and Machine Learning, with a particular focus on the design of experiment and data collection. The objective is to find a technology agnostic approach that can accurately quantify the effect of green technologies on ship performance in any given set of ship operational and environmental conditions. The methods are applied to a dataset collected from a ship equipped with the Silverstream Air Lubrication system to investigate their benefits and shortcomings.

2. Silverstream® System

The Silverstream® System is an air lubrication system that improves the performance and operational efficiency of ships by reducing the frictional resistance between the water and ship's flat of bottom. The system consists of a set of air release units (ARUs) positioned forward on the hull bottom and connected to a set of compressors that provide a constant supply of air to create a stable air-water interface along the hull bottom. As the ship moves through the water, the velocity difference across the air-water interface causes air to shear, creating a uniform carpet of small bubbles that is captured in the boundary layer reducing frictional resistance, Fig.1. For a ship operating in constant speed mode, this reduction in frictional resistance translates into a reduction in shaft power and an increase in ship speed, Fig.2. The optimal compressors' output airflow that maximizes the power balance equation varies with the environmental and ship operational conditions and is derived from a combination of controlled test results and operational data.

Fig.1: Ship hull bottom coated with air bubbles released from the Air Release Units (ARUs)

The data used in this study are from a large ship equipped with the Silverstream® System collected over an intermittent 6-month period. The dataset contains 3,002,675 datapoints and the sampling period is 5 s. The variables considered in this study include shaft speed, shaft power, speed through water, draught, trim, rudder angle, air lubrication system power, wind speed, wind direction and sea water temperature, Fig.5.
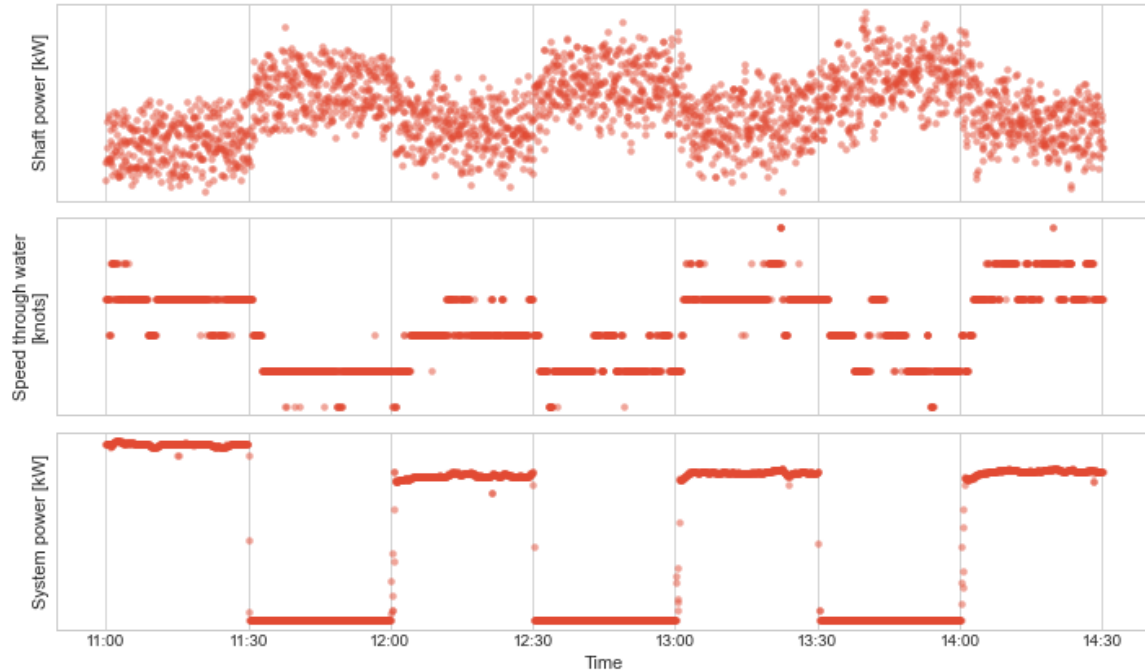
Fig.2: Example time series of shaft power (top), ship speed through water (middle) and air lubrication system power (bottom)

3. Experimental design

3.1. Ship equipped with green technology

The idealised procedure to designing and analysing experiments is to define the hypothesis and objectives; select the response variable(s) of interest; identify and classify the variables that have an influence on the response(s); choose the experimental design; perform the experiment; and finally, analyse the measured data. The experimental objectives are set based on the questions that need to be addressed and experiments are typically performed to characterise, optimise, or verify the problem. Variables that have an influence on the response(s) of interest can be classified into,

- independent – variables that are changed in the experimental study to explore their effects
- Controlled – variables that are held constant in the experiment
- Uncontrolled – variables that cannot be controlled but can be measured and treated as a covariate

The choice of experimental design involves consideration of sample size, selection of suitable run order and determination of whether blocking or other randomisation restrictions are involved, *Montgomery (2017)*.

In this study, this idealised framework for designing experiments is used to guide the exploration and evaluation of the designs considered, ISO 19030, Short Term Interruption and Machine Learning. The hypothesis of the experiment is that green technologies improve the energy efficiency of ships, by reducing the shaft power which can lead to increases in ship speed. The relational graph in Fig.3 illustrates the variables that are considered to have an influence on the response variables, shaft power and ship speed, and the relationships between these variables. The graph is determined from the available literature on air lubrication systems and from experience through operations. The independent variable is the compressors' output airflow and, typically, ship operational variables are controlled and environmental variables uncontrolled.
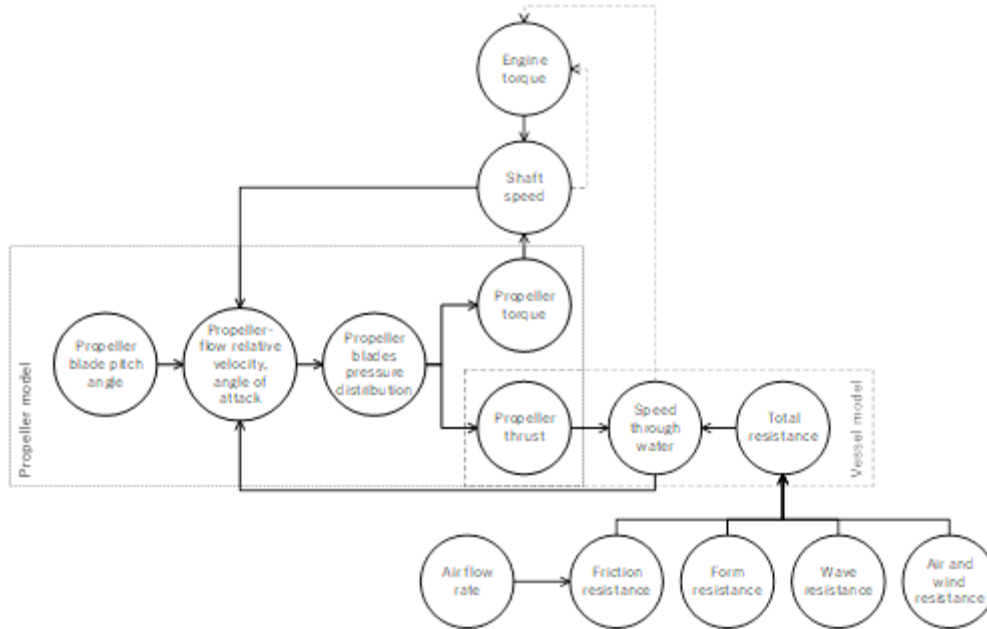
Fig.3: Relational graph of a ship equipped with air lubrication system; the broken arrows represent control signals for the ship in constant speed or constant rpm mode. The graph only includes the main variables of interest for brevity.

3.2. ISO 19030

ISO 19030 (2016) is intended for measuring changes in ship specific hull and propeller performance for maintenance, repair and retrofit activities. In this paper we explore whether the method, in its original form, can also be used to quantify the change in ship performance due to introduction of green technologies. ISO 19030 measures the change in hull and propeller performance by comparing data collected over two periods, reference and evaluation, with the independent variable value set to s_{off} and s_{opt}, respectively where s_{off} is system not in operation and s_{opt} is the optimal setting. The reference and evaluation datasets can be collected either in one long cycles as per the standard or, given the technology is active, in multiple short cycles by changing the independent variable level from s_{opt} to s_{off} for X hours every Y hours. The latter approach is preferred to cancel out the effect of long-term factors such as hull fouling or damage. The ship is operated as normal whilst gathering data and given that environmental variables cannot be controlled, the set of controlled variables is empty for this design. The standard specifies the reference and evaluation periods to both be a minimum of 3 months.

Table I: ISO 19030 filtering and correction steps

	Type	Criteria/ method
Filters	Missing	Missing data for one or more variables
	Outliers (see ISO 19030-2 Annex I)	Chauvenet's criterion not satisfied.
	Erroneous	Non-physical data for one or more variables
	Invalid (see ISO 19030-2 Annex I)	Standard deviation of shaft speed, ship speed and rudder angle > criteria Difference in port and starboard shaft power and speed > criteria
	Reference conditions (see ISO 19030-2 Section 6.3.2)	Sea water temperature < 2 °C Wind speed > BF4 Ship speed < 10knots Absolute difference between speed over ground and speed through water > 1 knot
Corrections	Wind	See ISO 19030-2 Annex G.

The collected data is filtered and corrected such that the reference and evaluation datasets are comparable in terms of the distribution of environmental and ship operational conditions. The dataset is first split into consecutive non-overlapping 10 minutes blocks and for each block, the mean, standard deviation, and probability of occurrence, Chauvenet's criterion, are calculated. Blocks that do not satisfy any of the criteria given in Table I are removed. The true wind speed and direction are calculated from the measured relative quantities and the shaft power is corrected for wind resistance using coefficients from wind tunnel tests.

The change in hull performance between these reference and evaluation periods is defined in terms of power performance values (PPVs) and indicators (PPIs). The PPVs are calculated as the relative difference between the measured corrected delivered power and the expected delivered power, read from a speed-power reference curve at the measured speed through water. In this study the reference curve is generated from the same dataset gathered during in-service operation, the reference dataset, following the procedure for expected speed calculation in ISO 19030-3 Section 5.4.2. The Power law function $P = aV^b$ where P is the power, V ship speed and a, b are unknown constants to be calibrated from the data, is fitted to the data using non-linear least squares. Finally, the power performance indicator is calculated as the change in average power increase in the reference period and the average power increase in the evaluation period.

3.3. Short Term Interruption

The Short-Term Interruption method compares data from immediately before and after the independent variable level is changed, the interruption, to quantify the effect of the technology on ship performance. The experiment involves changing the independent variable level from s_{opt} to s_{off} for A hours every B hours, leading to N changes over the test period, whilst keeping the ship operational variables constant. The period length A is chosen to be long enough to allow the vessel to reach steady state, which depends on the size of the ship, but not too long to increase the chances of comparable environmental conditions in the before and after datasets. The design allows for both system characterization, by repeating the experiment in different ship operational and environmental conditions, and optimisation by repeating the experiment with the independent variable level, s, set to a range of different values from the set, $\{x \in \mathbb{R} \,|s_{min} \leq x \leq s_{max}\}$, and finding the setting s_{opt} that results in maximum ship performance enhancement; s_{min} and s_{max} are the minimum and maximum physical limits of the system.

In Short Term Interruption data filtering is only limited to data points that contain nulls, erroneous data, or outliers. The interruption points are found by convolving the independent variable signal with a unit step signal and searching for the peaks and corresponding times in the convolved signal, Ramesh et al. (1995). The gross power, net power and a score are calculated for each interruption point. The gross power is the sum of the change in shaft power and power equivalent to the change in speed through water, read from the speed-power reference curve. The net power is the gross power with the change in power consumed by the technology subtracted. The score measures how constant the controlled and uncontrolled variables are during the interruption and is used to rank the interruptions. It is calculated as the sum over the controlled and uncontrolled variables of the intersection between and the normalized variance of the before and after histograms. Its possible value ranges between 0, meaning that the controlled and uncontrolled variables remain constant during an interruption and thus their effect on the relationship between the independent and dependent variables is minimal, to 1, no overlap between the distributions and maximum variation.

3.4. Machine Learning

Machine Learning is fundamentally different from ISO 19030 and Short-Term Interruption in that a set of fitted statistical models are used to drive both data collection and performance quantification, Fig.4. In Machine Learning, data is collected in two phases, the exploration phase followed by the guided phase. In phase one, the independent variable level is set to a random value, s, from the set $\{x \in \mathbb{R} \,|\, x =$

$0 \text{ or } s_{min} \leq x \leq s_{max}\}$ every M hours, leading to N repetitions. Randomization is used to balance out the effects of uncontrollable factors and prevent bias in the dataset, whilst M is kept short to increase diversity in the data. The ship is to operate as normal and the number of M-hour blocks, N, is chosen based on the environmental conditions typically encountered and ship operational profile.

Fig.4: Machine Learning, the first iteration is the exploration phase, and any subsequent iteration of the process is the guided phase

The data collected in the exploration phase is explored and cleaned, and an ensemble of feed forward neural networks, Table II, is fitted to random samples from the data. The key to good ensembles is to have diverse ensemble members such that the predictions made by each ensemble member are independent and uncorrelated. In this study, models are fitted to random samples from the dataset and trained using different sets of hyperparameter values to help generate diversity.

The trained models are then queried to identify any areas in the data where the models disagree. The variance of the models at randomly chosen points is taken as the measure of the level of model disagreement and points of relatively higher variance are those at which more data is needed for correct modelling, the guided phase. Data collected in the guided phase is added to the original dataset and the process is repeated until the model variance drops below a given threshold. The advantage of allowing the model to choose data from which it learns is that it reduces the quantity of data required to a minimum without impacting model performance. The output from this process is a set of accurate models that can be used to characterise, optimise, and validate the system. More specifically, the optimal system power setting can be found for any given set of ship operational and environmental conditions by generating predictions with the models for different settings in the range of independent variable values and selecting the setting that maximises the power balance equation.

Table II: Neural networks hyperparameters

Hyperparameter	Value or set
Random sample size (fraction of data points)	{0.3, 1.0}
Layers	{2, 3, 4}
Neurons	{50, 100, 200}
Activation function	SELU
Optimiser	Nadam, learning rate 0.001
Loss function	Mean absolute error
Batch size	{32, 64}

4. Preliminary evaluation of designs

The experimental designs, summarised in Table III, are applied to a dataset gathered from a ship equipped with the Silverstream air lubrication system, to explore their benefits and shortcomings. The available operational dataset was collected by passively monitoring the ship as it operates with the air lubrication system either in normal operation, OFF or Short-Term Interruption mode but does not contain any Machine Learning data.

Table III: Classification of variables and experimental designs for the air lubrication system example

	ISO 19030	Short Term Interruption	Machine Learning
Objective	Verification	Characterisation, optimisation, verification	Characterisation, optimisation, verification
Independent variable	Airflow rate		
Dependent variable(s)	{Shaft power}	{Shaft power, ship speed}	{Shaft power}
Controlled variables	{}	{Ship operational}	{}
Uncontrolled variables	{Ship operational, environmental}	{Environmental}	{Ship operational, environmental}
Independent variable settings	Verification - $s \in \{s_{off}, s_{opt}\}$	Characterisation or verification - $s \in \{s_{off}, s_{opt}\}$ Optimisation $s \in \{x \in \mathbb{R} \mid s_{min} \le x \le s_{max}\}$	Characterisation, optimisation, and verification - $s_{explore} \in \{x \in \mathbb{R} \mid x = 0 \text{ or } s_{min} \le x \le s_{max}\}$, s_{guided} – see text.

4.1 ISO 19030

ISO 19030 attempts to summarise the change in ship performance with a single number, the power performance indicator, by filtering and correcting the observed data to deal with the real-world complexities that affect ships in operation. In our example, ~75% of the dataset is removed, Table IV and Fig.5, despite the expense in collecting that data and the likelihood that smaller datasets won't match to the expected mean. The external validity of the experiment, the extent to which the results are generalizable to the real world, is sacrificed for internal validity, the extent to which the results are accurate reflections of what was measured. The performance indicators are only valid for calm, controlled conditions which are not representative of much of a ships' operational profile.

Table IV: Number of samples remaining after sequential filtering steps

Raw dataset	3,002,675
After removing nulls, erroneous datapoints and outliers	2,458,798
After removing invalid data	1,619,842 (14,937 10-min blocks)
After removing data that does not fulfill reference conditions	689,430 (6,377 10-min blocks)
Reference	83,956 (772 10-min blocks)
Evaluation	605,474 (5,605 10-min blocks)

The reference and evaluation speed-power curves and distributions of Power Performance Values are shown in Fig.6. The speed-power curves are extracted from the data and a single curve covering all loading conditions is extracted per dataset as the ranges of draught and trim values are relatively narrow. The positive effect of the technology on ship performance can be observed from the speed-power curves where the evaluation curve is below the reference curve for all speeds. It can also be observed that the filtered datasets contain regions of sparse data, particularly at the tails of the ship speed range that do not necessarily approximate the ground truth and as nonlinear least squares attempts to fit a model that minimises the sum of the distances between the observed data and fitted model, this can create misleading speed-power curves and thus PPVs and PPIs. Future work will look at evaluating the sensitivity to data sparsity of model fit.
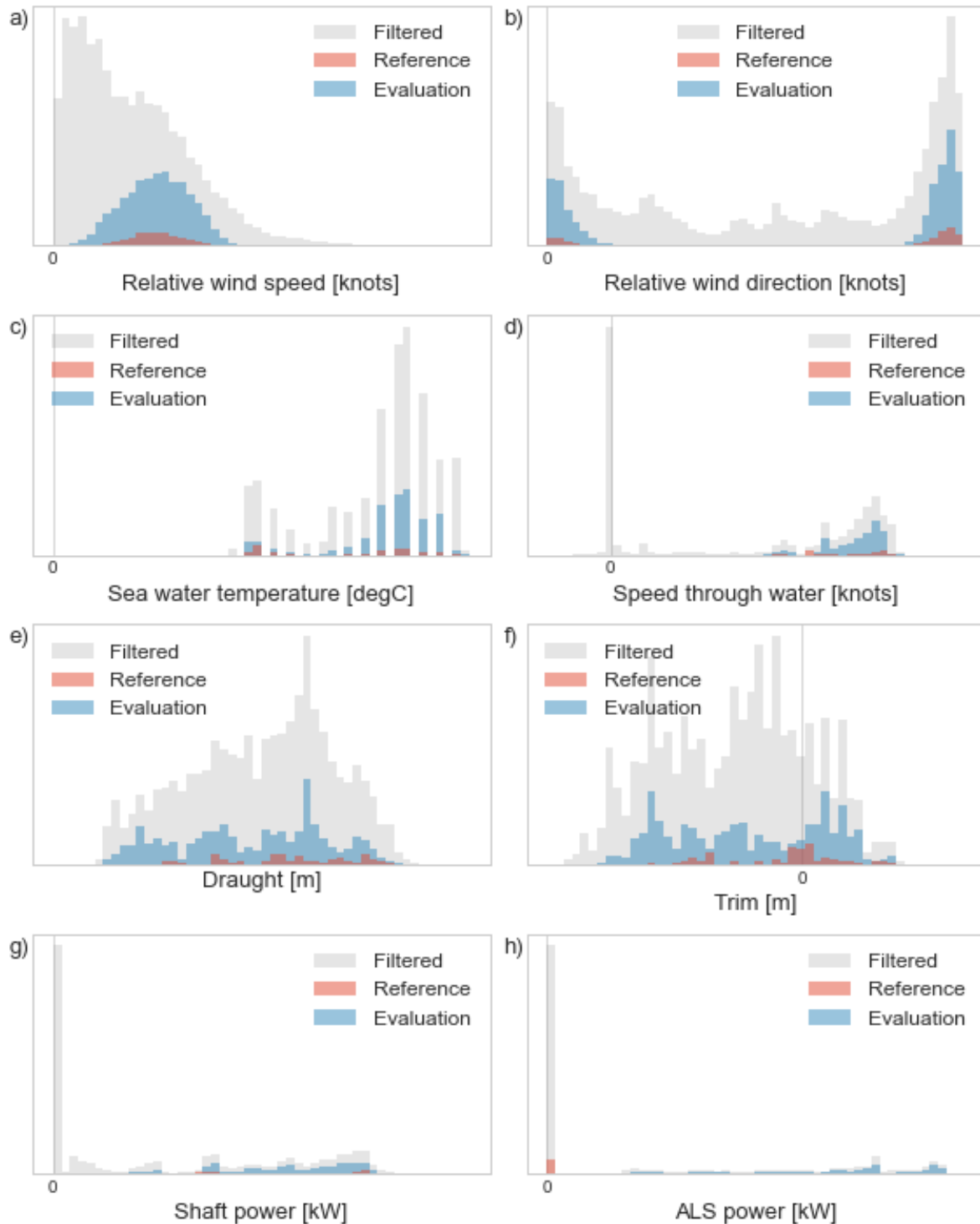
Fig.5: Distributions of relative wind speed (a), relative wind direction (b), sea water temperature (c), speed through water (d), draught (e), trim (f), shaft power (g) and ALS power (h) for the filtered, reference and evaluation datasets.

The distributions of Power Performance Values have a relatively wide range, even after filtering and correcting the data, suggesting that a larger dataset is required to find the true mean of the distributions and the true performance indicator. The positive effect of the technology can also be observed in the distributions where the reference distribution is to the right of the evaluation distribution.
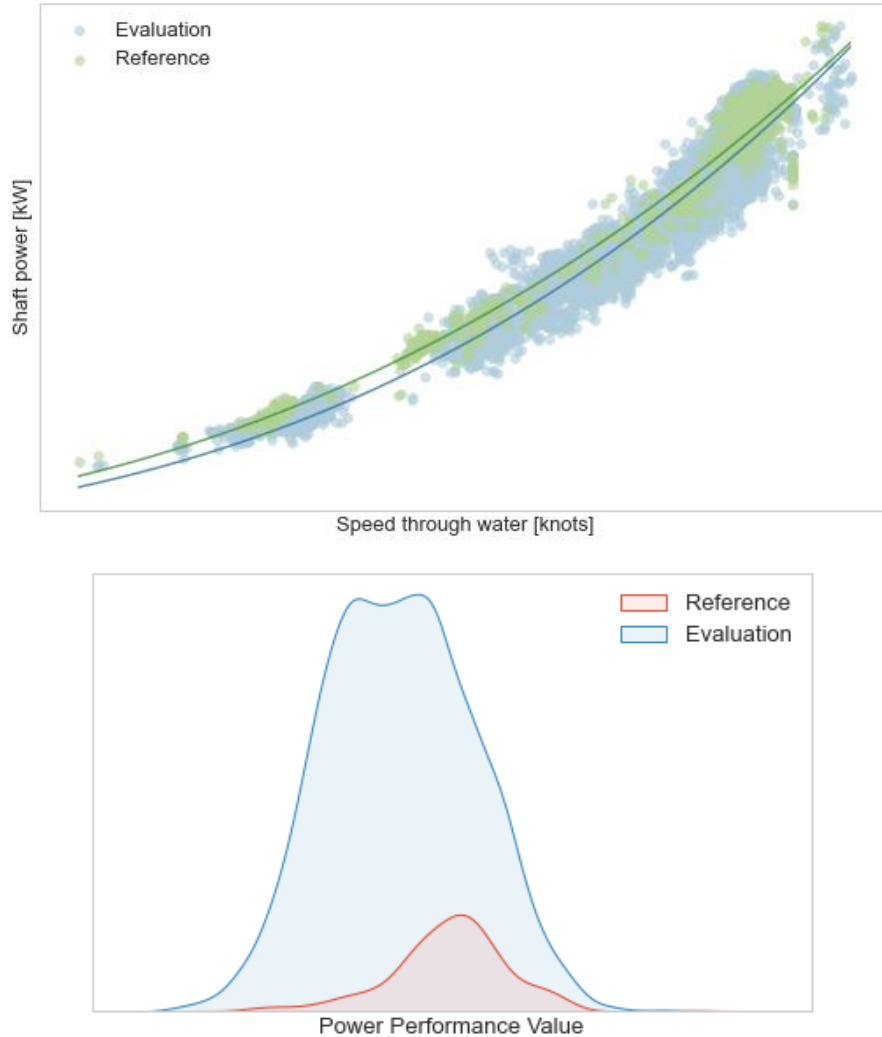
Fig.6: Speed through water to shaft power and power curve fit (top) and distributions of power performance values (PPVs) (bottom) for the reference and evaluation datasets.

4.2 Short-Term Interruption

The distributions of shaft power reduction, power equivalent to the increase in speed through water and net power are shown in Fig.7. The dataset contains 302 interruptions in total, of which 135 have a score higher than the selected threshold value of 0.6 that gives the most stable results. The distributions are largely positive demonstrating that for a ship operating at constant shaft speed, the shaft power drops and ship speed increases as the frictional resistance is reduced from lubricating the hull bottom with air bubbles. However, there is a not insignificant fraction of interruptions with negative equivalent power, meaning that the ship speed drops rather than increases when the system is switched on, which does not support this hypothesis. It is likely there are factors that influence the speed through water, and which are not being controlled for and will be investigated further in future work.

Figs.A-1 and A-2 in Appendix A, are examples of high scoring interruptions where the drop in shaft power when the system is turned can be clearly observed however the increase in speed through water is not always as clear, further suggesting that there are unknown and uncontrolled factors that influence the response. That is, missing nodes or edges in the relational graph in Fig.3. Possible factors that will be evaluated in future work include currents, waves, and dynamic effects, accelerations, or decelerations. The advantage of this approach is that it can provide an accurate measure of the effect of the technology on ship performance with a small dataset, a single interruption, albeit for only the ship operational and environmental conditions at the time of the interruption. To fully characterise the

184

behaviour of the system the experiment needs to be performed in a wide range of ship operational and environmental conditions. However, as the results have shown, the challenge is to identify and control for all the factors that can influence the relationship between the independent and response variables such that the true effect of the independent variable on the response variable(s) can be measured. Fig.A-2 is a good example of this challenge where, despite keeping the ship operational variables constant and the stationary environment, the speed through water signal displays a trend that is caused by some other factor than the independent variable.
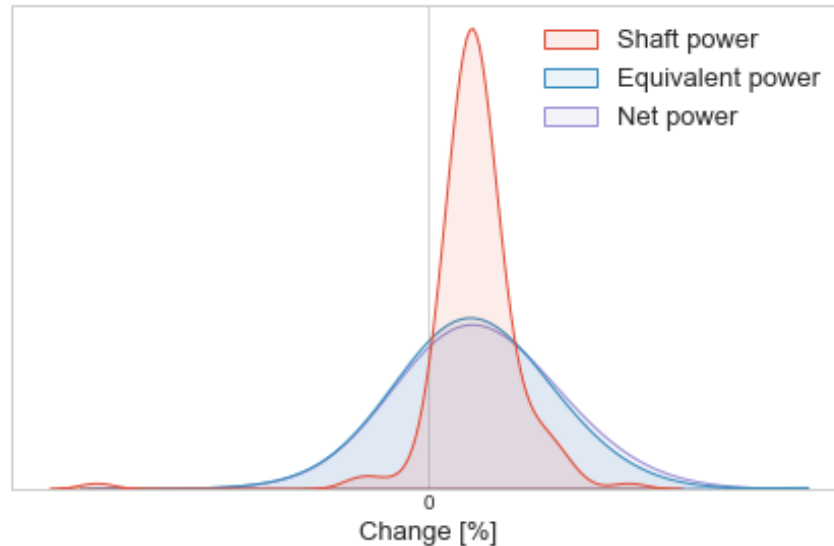
Fig.7: Distributions of shaft power drop, power equivalent to the increase in speed through water and net power

4.3 Machine Learning

Machine Learning is designed to address the highlighted drawbacks with ISO 19030 and Short-Term Interruption. In particular, randomization is used when collecting the data to guard against unknown or uncontrolled factors. Further, the method uses feed forward neural networks to learn the input-output relationships and find generalisable predictive patterns in networks rather than filtering or correcting the data to achieve more homogeneous, noise free, datasets.

Fig.8 shows an example system response plot for a given set of ship operational and environmental conditions. It is produced by generating predictions of the response variable with each model in the ensemble for a range of different independent variable values and keeping all other inputs, the ship operational and environmental variables, constant. System response plots provide insight into the input-output relationships learned by the ensemble and are used for both system characterisation, optimisation, and verification and to better understand the accuracy of the ensemble and guide data collection. In particular,

- the effect of the technology on ship performance in different ship operational and environmental conditions and the influence of individual factors on performance can be characterised by comparing system response plots for the different conditions.
- The optimal system setting is the point on the mean system response plot that maximises the net power.
- The size of the shaded area and the uniformity of the gradient of individual model prediction curves provide an indication of the level of agreement between the models in the ensemble and where more data needs to be collected for correct modelling.
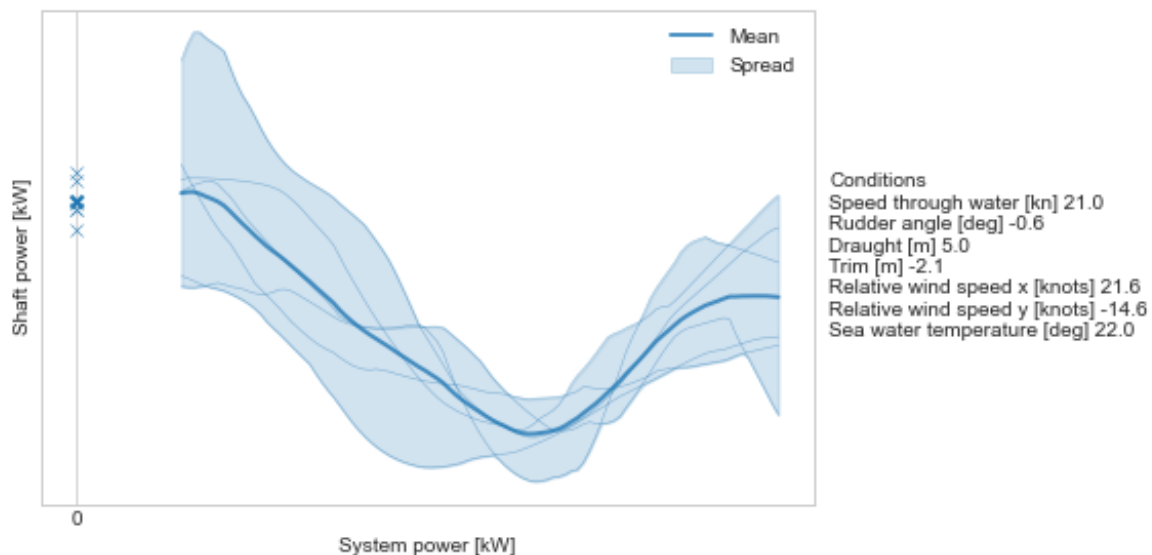
Fig.8: Example system response plot generated by the ensemble of models

5. Conclusions

In this paper we explore three approaches for quantifying the effect of green technologies on ship performance using operational data, the ISO 19030 standard, Short Term Interruption and Machine Learning, with a particular focus on the design of experiment and data collection. We apply the approaches to a dataset gathered on a ship equipped with the Silverstream Air Lubrication System to highlight their benefits and shortcomings.

ISO 19030 is the standard for measuring change in hull performance and although the prescribed methods are intended for measuring the effectiveness of maintenance and retrofit activities, we investigate whether these can be applied to green technology performance quantification. It requires expensive continuous monitoring over several months to collect the reference and evaluation datasets and relies heavily on filtering and correcting the observed data to reduce variability, reducing the dataset size quite significantly and sacrificing the external validity of the results. To enable fair and accurate evaluation and comparison of technologies the dataset needs to be representative of real-world conditions.

The Short-Term Interruption method requires the ship operational variables to be kept constant and the data collected immediately before and after the interruption are compared to increase the chances of constant environmental conditions. The advantage of this approach is that it can provide an accurate and true measure of performance with a small dataset albeit only for the ship operational and environmental conditions at the time of the interruption. To characterise the system fully or find optimal system setting the experiment needs to be performed in different conditions and at different system settings. This approach requires a good level of understanding about the problem, in particular the factors that influence the response variable(s) such that these can be controlled or measured and treated as covariates.

The Machine Learning method uses feed forward neural networks to learn the relationship between the response variable and the independent, controlled, and uncontrolled variables from the gathered data. The models learn a representation of the real-world, a digital twin of the ship and system, and can be used to answer characterisation, optimisation, and verification queries when confident or request more data to be collected. The advantage of this approach is that data collection is minimised without impacting the accuracy of the models.

References

DALHEIM, Ø.Ø.; STEEN, S. (2020), *Preparation of in-service measurement data for ship operation and performance analysis*, Ocean Engineering 212

BUI, K.Q.; PERERA, L.P. (2021), *Advanced data analytics for ship performance monitoring under localized operational conditions*, Ocean Engineering 235

ISO 19030 (2016), *Ships and marine technology: Measurement of changes in hull and propeller performance (ISO Standard No 19030)*, Int. standard Org., Geneva

JAIN, R.; RANGACHAR, K.; BRIAN, G.S. (1995), *Machine Vision*, McGraw-Hill

MONTGOMERY, D.C. (2017), *Design and analysis of experiments*, John Wiley & Sons

Fig. A-1: Example time series of dependent, independent, controlled, and uncontrolled variables for a high scoring interruption. The histograms represent the data in the shaded areas.
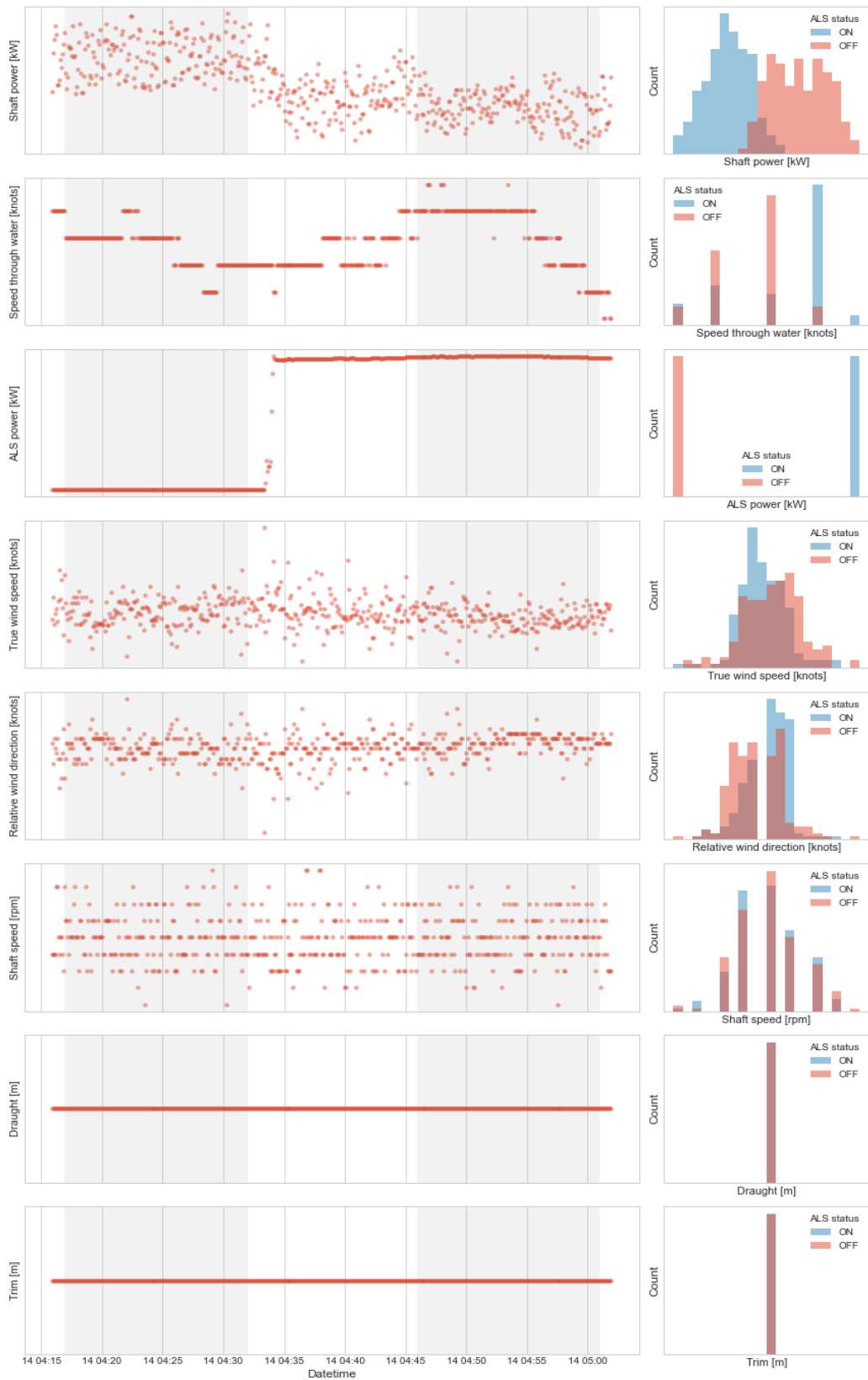
Fig. A-2: Example time series of dependent, independent, controlled, and uncontrolled variables for a high scoring interruption. There appears to be a trend in the speed through water (dependent variable) signal that does not correlate with the system power (independent variable) signals highlighting the challenge with identifying and controlling for all factors.

189

Underwater Hull Cleaning by Laser - Feasibility and Perspectives

Tim Heusinger von Waldegge, Fraunhofer Institute for Manufacturing Technology and Advanced Materials IFAM, Bremen/Germany, tim.heusinger@ifam.fraunhofer.de
Dorothea Stübing, Fraunhofer Institute for Manufacturing Technology and Advanced Materials IFAM, Bremen/Germany, dorothea.stuebing@ifam.fraunhofer.de
Stanislav Zimbelmann, Laser Zentrum Hannover e.V., Hannover/Germany, s.zimbelmann@lzh.de
Benjamin Emde, Laser Zentrum Hannover e.V., Hannover/Germany, b.emde@lzh.de
Jörg Hermsdorf, Laser Zentrum Hannover e.V., Hannover/Germany, j.hermsdorf@lzh.de
Markus Baumann, Laserline GmbH, Mülheim-Kärlich/Germany, markus.baumann@laserline.com

Abstract

The underwater cleaning of ships faces regulatory, environmental, and economic issues. Mechanically abrasive cleaning methods, such as high-pressure water jets and brush cleaning, meet legal and ecological requirements only to a limited extent or under strict constraints. On the other hand, cleaning the underwater hull makes a valuable contribution to minimizing fouling. This in turn prevents the spreading of species and elevated greenhouse gas emissions. The research project "FoulLas" aims to overcome the existing limitations with a novel laser-based cleaning approach. At the Fraunhofer Test Center on the German offshore island of Helgoland, a test facility was set up for this purpose, which irradiates coating samples (commercial SPC, FRC and hard coatings) immersed and fouled under natural conditions, with an infrared- or a blue laser at adjustable intensities. The laser irradiation should neither damage the coating nor cause release of biocides and other substances into the surrounding water. The goal is to lethally damage the fouling organisms so that they detach from the hull at the latest when the ship is underway again. The present paper gives an overview of the current promising status of the project after 2.5 years of development and testing.

1. Introduction

Unwanted biofouling on surfaces in limnic and marine environments has been a significant cost factor for the maritime industry for decades. Especially for shipping even thin layers of slimy biofilm increase the frictional resistance in such a way that more fuel is consumed and thus more harmful greenhouse gases are released into the atmosphere, *Townsin (2003), Schultz et al. (2011), Bressy and Lejars (2014)*. In addition to the economic and climatic consequences, however, an overgrown ship's hull also poses a high risk to sensitive marine habitats because of the spread of potentially invasive species, *Tyrrell and Byers (2007)*, *Fernandes et al. (2016)*. In a time in which many ecosystems are already confronted with species extinction caused by too intensive use of marine resources, habitat destruction, pollution and the consequences of climate change, this factor is becoming even more important and has already prompted countries such as Australia and New Zealand to introduce stringent regulations in biofouling management, *Coutts and Taylor (2004), Hewitt et al. (2011)*.

To effectively minimise these serious consequences of biofouling, fouling-control-coatings are used. Self-Polishing Copolymer (SPC) coatings containing biocides currently dominate the market, *Silva et al. (2019)*. However, they are under increasing regulatory pressure; so intensive research is being carried out into new coating solutions *Dafforn et al. (2011)*. The topic of underwater cleaning of ship hulls has also gained momentum in recent years, *Song and Cui (2020)*. Particularly abrasion-resistant hard coatings, that do not contain biocides, are used for this purpose. However, there are two aspects to be considered when cleaning, which also have a massive impact on the approval process and have so far resulted in the fact that in-water cleaning of ships is still being largely prohibited. Abrasive methods such as brushes and high-pressure water jets remove coating components that accumulate in the sediment. The other is the aspect of species invasion because the cleaning methods could detach invasive species from the hull, which can then colonise new substrates. In addition, larvae can be released. Extraction of removed biofouling does not solve the problem completely, as the filters cannot eliminate everything and therefore a large amount of process water is produced, *Oliveira and Granhag*

(2020). However, in-water cleaning has two decisive advantages. On the one hand, it is possible to efficiently remove biofouling in the early phase and interrupt further biological succession with more frequent cleaning intervals. Secondly, thanks to the continuous development of (semi-)autonomous underwater remotely operated vehicles, the method is significantly cheaper than taking the ship to a dry dock, *FOB (2013)*. Hence, a technology is needed that eliminates the described disadvantages of mechanical cleaning processes. This is where the project FoulLas comes in.

Various studies have already demonstrated the harmful effects of laser radiation on organisms in aquatic environments. The studies focused on the sublethal/lethal effect of different laser radiations (ultraviolet radiation, visible radiation and near-infrared radiation) on microorganisms such as bacteria, cyanobacteria, diatoms and dinoflagellates as well as hard foulers (mainly barnacles), *Nandakumar et al. (2009), Li et al. (2016)*. In many cases, pulsed laser radiation with long irradiation durations was used and primarily a basic effect of the radiation on the organisms was described. Previous approaches focused on the fundamental damage to organisms in aquatic environments, but did not consider a combination of the effectiveness of high-power lasers (area output without affecting the integrity of existing material protection layers (sustainability), which is of particular interest for industrial applications. Compared to UV emitters, lasers have the advantage that they deliver a significantly higher irradiation intensity.
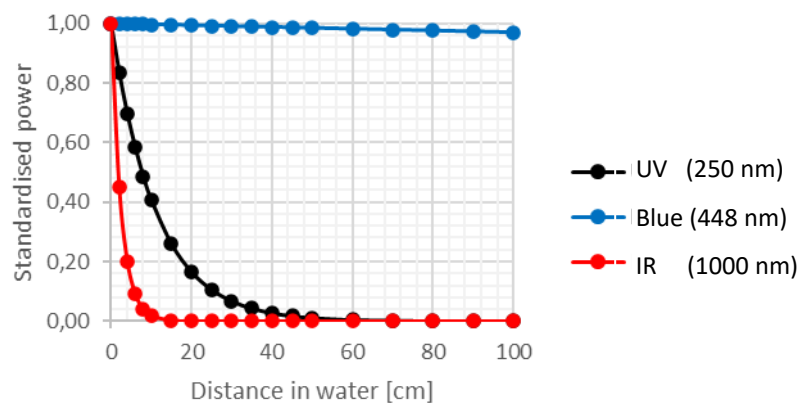
Fig.1: Reduction of laser power depending on the distance in the water [cm] and the wavelength [nm]

Fig.1 illustrates the reduction of the laser power as a function of the distance in the water and the wavelength for UV (250 nm in the range of maximum DNA absorption), blue (approx. 448 nm) and IR radiation (1000 nm). The curves were determined on the basis of the Beer-Lambert law and the absorption coefficients (250 nm 0.09 cm-1 | 470 nm 0.0003 cm-1 | 1000 nm 0.4 cm-1). For UV radiation, it can be seen that the radiation power decreases with increasing distance in the water. However, since the radiation power has a significant influence on the damage to organisms, it is crucial that the distance the radiation travels in the water is not too high. Compared to UV radiation, blue laser radiation therefore has a considerable advantage, as the radiation is only slightly absorbed and attenuated in the water. Thus, even after a long distance in the water, a high radiation power is still available to effectively damage organisms. Fig.1 also shows the course of IR radiation in comparison to UV and blue radiation. Here, the attenuation is much more pronounced, so that industrial use for underwater cleaning would not be expedient.

The industrial use of blue diode lasers is comparatively new, and the power has not yet reached the spheres that IR lasers have. This circumstance is primarily due to the fact that they are significantly more complex to manufacture. Infrared lasers can be built on gallium arsenide (GaAs) semiconductors, on which a dozen layers of atoms are arranged to form the part of the laser that generates light from quantum wells. The substrate can be built free of dislocations and the atoms arranged so that the distance between those forming the bottom and those forming the quantum wells is the same. For blue lasers, however, the best semiconductor is gallium nitride (GaN) crystals, which are much more difficult to produce and require higher pressures and temperatures. A series of further developments led to an ever more progressive reduction of the dislocations and finally provided the breakthrough with the sapphire

surface used today, which is covered with a gallium nitride layer. Quickly, output powers for fibre-coupled diode lasers increased from several hundred watts in early 2018, *Balck et al. (2018)* to 1000 W in 2019, *Baumann et al. (2019)* and even 2000 W in 2020, www.laserline.com. Thus, it was also a declared goal of the consortium partner Laserline GmbH to increase the laser power of the blue laser in this project. In the meantime, it has been possible to develop a 4XX nm diode laser beyond 2 kW of output power, *Baumann et al. (2022)*.

Investigations into the influence of laser radiation at various process parameters on fouling and commercially available coating systems are described and explained below.

2. Biofouling studies and laser test facility on Helgoland

2.1. Coating analysis and biofouling samples

Marine fouling organisms respond differently to heat and drought stress and to disturbances in their osmoregulation. So if you want to assess the influence of a method on the survival rate or, conversely, on the lethality, this requires very good logistics and the shortest possible time intervals between taking the sample from the ecosystem and introducing it into the test environment. Otherwise, artefacts would result. The test facilities of the Fraunhofer IFAM on Helgoland, Fig.2A, and the construction of the laser demonstrator by the Laser Zentrum Hannover (LZH) and Laserline GmbH not far from the test rigs enable this optimised interaction.

In order to be able to carry out market-oriented development work right from the start, the investigations took place on commercial ship coatings of the latest product generation. In addition, the available spectrum of coating technologies was to be included in the test plan. Accordingly, the focus was on self-polishing copolymers (SPC), fouling-release coatings (FRC) and hard coatings. The samples were placed in specially constructed racks, Fig.2B, which were then subjected to static immersion in the North Sea.
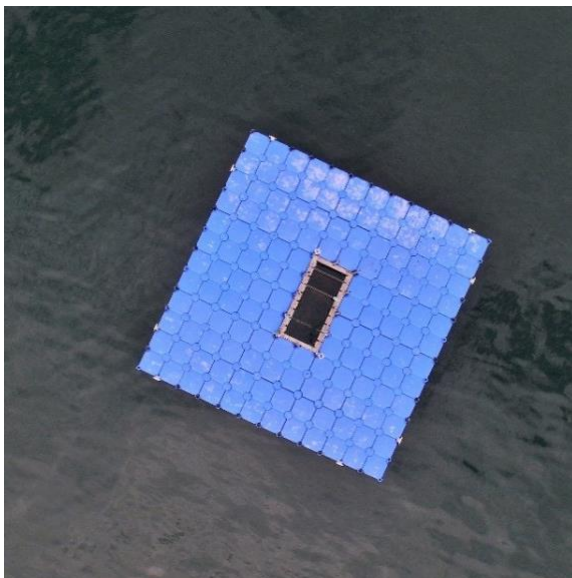
Fig.2: (A) Test rig for static fouling tests by Fraunhofer IFAM on Helgoland

Fig.2: (B) Rack with coated glass slides

2.2. Laser process

Due to different physical parameters and the differences in the maximum available laser power in Watt, the original approach of the laser setup was to test the IR laser in comparison to a blue diode laser.
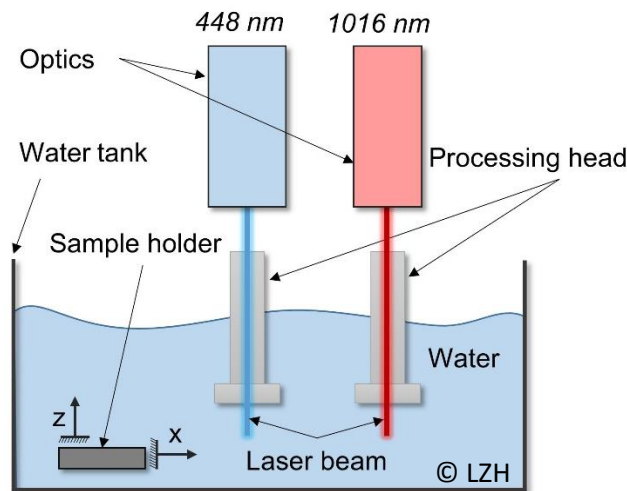
Fig.3: Experimental set-up for the irradiation of the samples

The setup for irradiating the samples consisted of a water tank, a sample holder and two laser optics combined with a processing head was build up from LZH. Fig.3 shows the schematic experimental setup with the individual components. Inside the water tank, filled with natural North Sea seawater, the sample can be moved in z- and x-direction with the help of a sample holder and a two-axis system. Two diode lasers with different wavelengths were used. The infrared diode laser has a maximum power of 3.5 kW and a wavelength of 1016 nm. For the blue diode laser, the maximum power is 1.5 kW at a wavelength of 448 nm. Two zoom optics were used to shape the laser beam and to generate a homogeneous line. Each of the samples was irradiated with only one of the laser sources, the feed rate of the sample holder was not varied and remained at 10 mm/s for all tests. The exceeding of the destruction threshold of a coating was evaluated according to optical criteria on a macroscopic level. Irradiation tests of the fouled samples were carried out in the parameter range below the coating-specific destruction threshold with a maximum possible laser power.

Float glass slides of 76 x 26 mm were used as specimens onto which the coating systems were applied according to the manufacturer's specifications. The same procedure was followed with steel samples (S355) of 100 x 100 mm. In addition to the flat specimens described above, convex and concave geometries were added later in the project to simulate the feasibility of treating more complex structures.

3. Results and Discussion

3.1. Influence of the laser process on the coating

The graphs in Fig.4 illustrate the reflectance properties of SPC and FRC coatings and compare the influence of laser irradiation and paint ageing with the reference condition. The reflective properties of the SPC coating varied strongly depending on the wavelength. In the range of blue laser radiation at 448 nm, the reflection was low. For wavelengths above 470 nm, the reflection of the SPC coating increased significantly. The white FRC coating showed a high reflection rate with a small continuous decrease for increasing wavelengths in the spectral range between 400 nm to 1200 nm. The curves of the laser-irradiated samples, both FRC and SPC systems, showed no change in relation to the respective reference curve. In contrast, the influence of ageing could be observed. Both coating systems showed higher reflectance properties after ageing in the North Sea. In numbers, the average reflection increased for the wavelength range from 600 nm to 1200 nm by 30.02 ± 12.32 % for the SPC system and by 5.32 ± 1.40 % for the FRC system. Irradiation below the destruction threshold had no influence on reflection properties. In addition, the data obtained correlate with those from the destruction threshold measurements and can be used to quantify the ageing of the coatings.
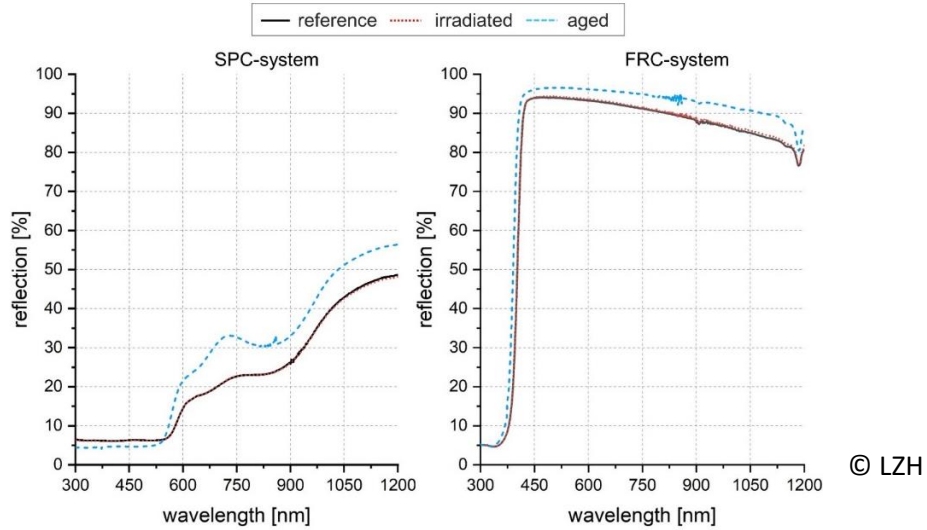
Fig.4: Comparison of the reflection properties of SPC (colour: dark red, left) and FRC (colour: white, right) coatings

In addition to the reflection properties, the coating-specific damage thresholds were also investigated as a function of the laser power in watts. A sample was considered damaged if there were visible indications of a change in the surface colour or blistering. The condition was then verified using microscopic methods.
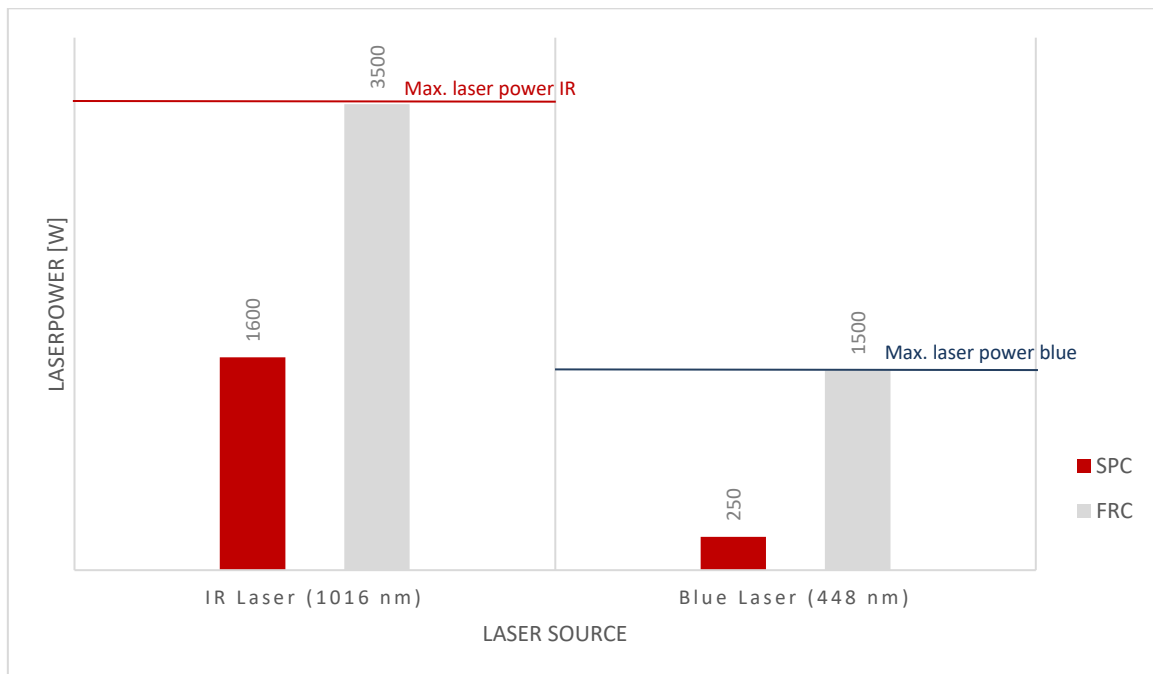
Fig.5: Determined destruction thresholds for the SPC and FRC coating systems with the blue and infrared laser sources

While the destruction threshold of the SPC samples was 1600 W for the infrared wavelength (1016 nm) and 250 W for the blue wavelength (448 nm), the destruction threshold of the FRC samples could not be reached because it is above the maximum laser power of the two laser types. If the influence of the wavelength is considered, clear differences could be detected for the SPC coating. The laser power required to reach the destruction threshold in the blue wavelength range was significantly lower than the laser power required in the infrared wavelength range, Fig.5. However, this does not indicate a fundamental unsuitability for the intended cleaning process, because the laser power used here was clearly above the application-related wattage and only used for determining the damage thresholds.

194

3.2. Investigations into the release of substances through the laser process

Regulatory and ecological aspects regarding the release of biocides through the cleaning of SPC play a decisive role for later usability. To generate findings on this at an early stage, samples of an SPC system in a volume of 50 ml of natural seawater were irradiated with the IR and blue laser respectively. After irradiation, the initial volume was transferred to a 50 ml centrifuge tube. As a reference, 50 ml of natural seawater was taken from the southern harbour of the island of Helgoland and had not previously come into contact with the SPC samples. The tests were intended to provide information on whether laser cleaning leads to the release of copper biocides from the SPC coating. If this were not the case, it would represent an enormous advantage over abrasive cleaning with high-pressure water jets or brushes. With these methods, the process water used is contaminated, there is a release into the environment or, depending on the destination, in-water cleaning is even prohibited altogether.

The thus obtained water samples were analysed by mass spectrometry with inductively coupled plasma (ICPMS: Inductively Coupled Plasma Mass Spectometry). This is a sensitive analysis method for the detection of inorganic elements. At the beginning of the measurement, a high-frequency current of ionised argon is induced and the samples are heated up to 5000 °C to 10000 °C. The high temperature causes the atoms to ionise and a plasma to form. Subsequently, the ions created in the plasma are accelerated towards the mass spectrometer. This is the measuring point where individual elements and isotopes are determined. The detection limit for the majority of the known elements is in the range of ng/l or sub ng/l. Therefore, finest differences are already detectable. The method is thus predestined for trace analysis of heavy metals and is ideally suited for detection of copper in the samples.

The analysis showed a value of less than 0.02 mg/kg for the seawater reference. The process water from the irradiation of the SPC system with the blue laser provided a value of 0.03 mg/kg. In comparison, the value for irradiation with the IR laser was 0.38 mg/kg. The values show a clear difference of more than a factor of 10 between the radiation sources. Different laser powers could be the reason for this discrepancy. The laser power was 900 W for the IR laser and 250 W for the blue laser. These process parameters were based on the previously determined destruction threshold. However, if one goes into further detail and considers the absorption of the IR beam in water and the lower absorption of the blue laser, this is put into perspective. The calculation of the area power before water penetration and under water clarifies this fact. If the power of the IR laser before water penetration is still 1.19 [W/mm²], it is only 0.57 [W/mm²] under water at a working distance (distance between processing head and coating surface) of 2 cm. With the blue laser, on the other hand, the value over the distance travelled before and after water ingress remains almost identical at 0.33 [W/mm²]. The actual difference in area output between the two lasers is therefore only 0.24 [W/mm²] at this point. However, another factor that comes into play is the wavelength-dependent reflection/absorption of the SPC coating. The project results of the reflection and absorption measurements show that the SPC systems absorb significantly more radiation in the blue spectral range than in the infrared range. Consequently, if the wavelength-specific portion of the reflected radiation is subtracted, the values between the IR and blue lasers are approximately comparable. The IR laser delivers a value of 0.34 [W/mm²] compared to the blue laser with 0.31 [W/mm²]. Based on these data, it therefore initially seems unlikely that purely the type of beam source can explain the effect. In principle, however, it should be emphasised that irradiation with the blue laser in particular avoids contamination of the process water with copper. The measured value is almost identical to the comparative value of the untreated control. According to the status, the process therefore fulfils an important aspect for a later regulatory approval. Above all, it appears to be significantly more environmentally friendly than previous invasive cleaning techniques with brushes and high-pressure water jets.

3.3. Lethal damage to the fouling as a result of laser irradiation

The overall objective was to narrow down the process parameters for the two laser sources and to assess the degree of biological damage depending on these parameters for different taxa of the marine biofouling community. For this purpose, different experimental scenarios were created. Even if there was no immediate macroscopic lysis of the biological material, it was possible to check whether and

when this occurred. In addition, the regeneration capacity of certain organisms could also be observed. Above all, an optical colour change of biofilm and higher algae took place. While the biofilm changed its colour from dark green/brownish to light green, red algae lost their original appearance and took on a brownish/green colour after laser irradiation. Red algae were not able to regain their colour or show significant growth within two weeks after laser irradiation. Instead, complete tissue lysis took place during this time. This lysis was also observed for the green alga *Ulva lactuca* during the same period. At the microscopic level, direct cell damage could be seen in *Ulva lactuca,* Fig.6. The non-irradiated comparatively treated reference samples were still vital after the 14 days. These results were achieved with both the IR and blue laser. Consequently, a destructive effect of the laser radiation may be assumed for the higher algae examined. Similarly, lethal effects have been observed in all organisms studied so far (e.g. sea squirts, barnacles, sessile and (partially) mobile crustaceans, hydrozoans and bryozoans). Additional to optical/microscopic methods, microbiological culture techniques were used to investigate post-radiation vitality, which corroborated the findings from optical microscopy. In addition an underwater camera system provided continuous camera data for previously irradiated samples after re-exposure to seawater. This provided continuous and immediate impressions of the real-time development of the biofouling-community, particularly with regard to lysis, regeneration and recolonization.
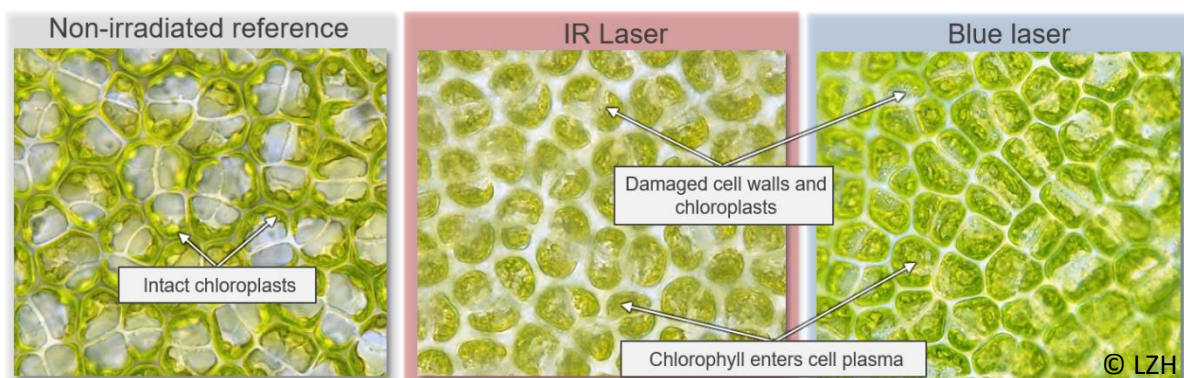
Fig.6: Light microscope image of a green alga *Ulva lactuca* at 60x magnification before (left) and after irradiation with the infrared (middle) and blue laser (right). Damage to the chloroplasts is visible.

3.4. Detachment of damaged organisms after laser irradiation under static and dynamic flow conditions

Previous data showed that the cleaning effect under static conditions took place with a time delay. For this reason, two different states were compared in the further evaluation. The initial state represents the fouled sample surface directly after irradiation (IR 3000 W, blue laser 1400 W) or in the case of the reference, the fouled state without irradiation. The second state shows the samples after four weeks of renewed static immersion in the North Sea. Fig.7 illustrates the comparison using three overgrown FRC samples as examples.

For the evaluation of the cleaning success, it is necessary to be able to simulate the hydrodynamic loads of steaming ship and not to rely exclusively on static test environments. To this aim a flow cell, Fig.8, was used to investigate the biofouling release behaviour depending on the coating system, the laser parameters, the flow velocity and different biofouling communities.

The construction principle and operation parameters correspond to the flow cell described by *Schultz et al.* (2000).
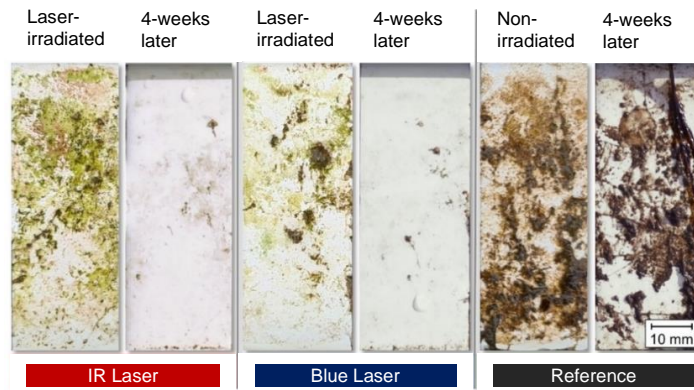
Fig.7: Initial condition as well as condition after renewed 4-week exposure of FRC samples after laser irradiation with IR and blue laser as well as a non-irradiated reference sample
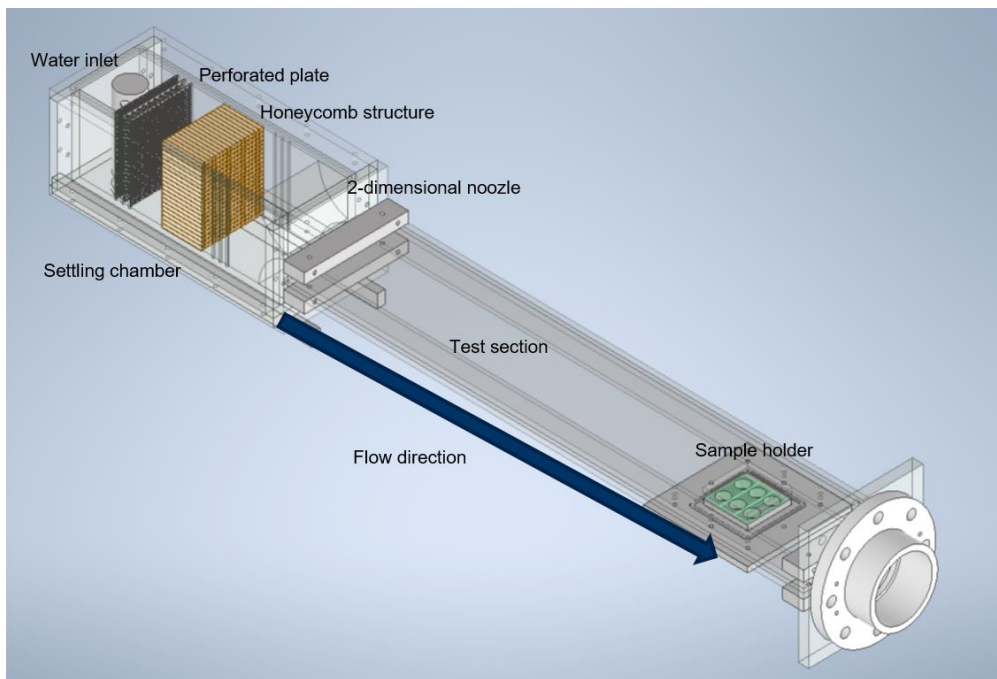
Fig.8: Construction drawing of the IFAM flow cell showing the settling chamber, the test section and the sample holder

To simulate the effect of the water flow, i.e. the movement of a ship, a set of experiments was carried out. In the following experiments, only the blue laser was used. Three slides were irradiated with the blue laser at a power of 1400 W and a feed rate of 30 mm/s and subsequently immersed in the North Sea for 14 days. The results of this irradiation can be seen at the top left of Fig.9. Compared to non-irradiated reference samples (top right), a clear decrease in biofouling could be observed. This means that a cleaning effect was already achieved by a static exposure. After 14 days, the samples were placed in the flow cell and exposed to a water flow of 10 kn for 2 minutes. The laser-irradiated samples were almost completely cleaned (see bottom left in Fig.9). The non-irradiated reference samples (see bottom right in Fig. 9) also showed a decrease in biofouling coverage, but still exhibited considerable residual fouling compared to the samples treated with the laser.

The results showed a time-delayed cleaning effect for soft fouling and but how effective is it against already established hard fouling? Fig.10 illustrates the cleaning results of three FRC samples after irradiation (left) compared to three non-irradiated samples (right). Hard foulers that continued to adhere to the surface are marked in red, although some of the irradiated organisms had suffered lethal damage. Of them, the calcareous exterior structure (rostrum and carina) remained.

197
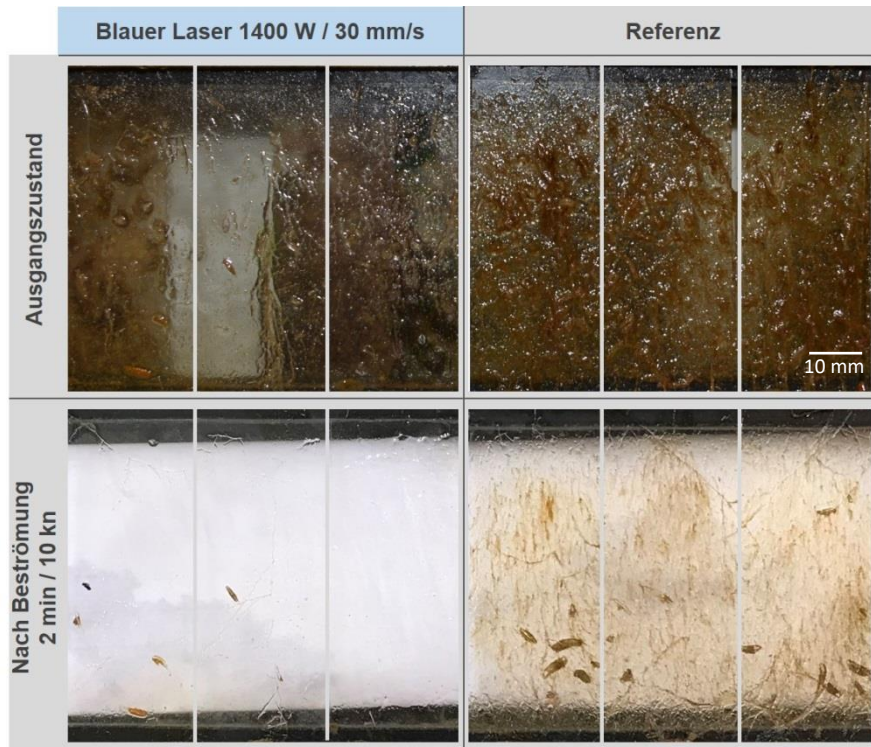
Fig.9: Influence of blue laser irradiation and incident flow for 2 minutes at a flow velocity of 10 kn
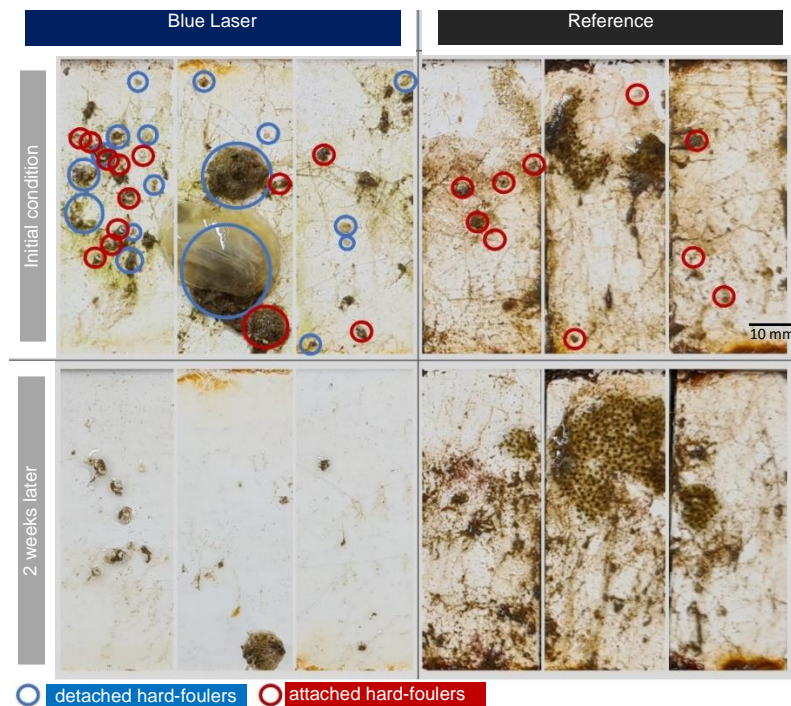
Fig.10: Cleaning results of 3 FRC samples after irradiation (left) compared to 3 non-irradiated samples (right). Hard foulers lethally damaged by irradiation and detached under static immersion conditions in the North Sea are marked in blue. Hard foulers still attached to the surface are marked red, although some of the irradiated organisms were lethally damaged.

6. Conclusions

As part of the project "Fouling removal from maritime surfaces using laser radiation under water - FoulLas", it was shown that biofouling can be damaged by laser radiation under water. In addition to

soft fouling, the laser radiation is also effective against hard fouling, such as barnacles. The damaging effect in these cases was evident from the fact that the organic part of the barnacle was lysed and only the calcareous walls (rostrum and carina) remained intact, which can even detach depending on the substrate. The investigations have shown that the cleaning effect is taking place with a time-lapse of several days in the case of post-treatment static immersion. This scenario simulates a ship that is in port or in the roadstead, where the flow around the ship is significantly less than on a moving ship. It represents the worst-case scenario. The flow cell experiments showed that the detachment of the fouling is intensified by the water current, and ultimately depends on the surface quality of the coating. The contactless laser cleaning method offers the advantage that the fouling-control coating is not removed by the laser radiation, in contrast to abrasive cleaning methods such as high-pressure water jets and brushes. This prevents the release of substances into the environment or the process water. Furthermore, the lethal damage to the fouling organisms counteracts the spread of invasive species.

7. Outlook

Future work shall address the development of an automated/partially autonomous functional demonstrator based on a blue diode direct emitter in combination with a handling system and a laser process control/observation system for use under water. This will make a significant contribution to transferring the process from laboratory scale to practice. Decisive for the next steps towards commercial applicability is the area performance per time, regulatory aspects and the exact evaluation of the cleaning success under dynamic conditions in relation to the resulting savings in fuel and emissions.

Acknowledgments

References

BALCK, A.; BAUMANN, M.; MALCHUS, J.; CHACKO, R.V.; MARFELS, S.; WITTE, U.; DINA-KARAN, S.; OCYLOK, S.; WEINBACH, M.; BACHERT, C.; KÖSTERS, A.; KRAUSE, V.; KÖNIG, H.; LELL, A.; STOJETZ, A.; LÖFFLER, U.; STRAUSS, U. (2018), *700 W blue fiber-coupled diode-laser emitting at 450 nm,* SPIE 10514, High-Power Diode Laser Technology XVI

BAUMANN, M.; BALCK, A.; MALCHUS, J.; CHACKO, R.V.; MARFELS, S.; WITTE, U.; DINAKARAN, D.; OCYLOK, S.; WEINBACH, M.; BACHERT, C.; KÖSTERS, A.; KRAUSE, V.; KÖNIG, H.; LELL, A.; STOJETZ, B.; ALI, M.; STRAUSS, U. (2019), *1000 W blue fiber-coupled diode-laser emitting at 450 nm*, SPIE 10900, High-Power Diode Laser Technology XVII

BRESSY, C.; LEJARS, M. (2014), *Marine fouling: An overview,* J. Ocean Technology 9(4), pp.19-28

COUTTS, A.D.; TAYLOR, M.D. (2004), *A preliminary investigation of biosecurity risks associated with biofouling on merchant vessels in New Zealand*, New Zealand J. Marine and Freshwater Research 38(2), pp.215-229

DAFFORN, K.A.; LEWIS, J.A.; JOHNSTON, E.L. (2011), *Antifouling strategies: history and regulation, ecological impacts and mitigation,* Marine Pollution Bulletin 62(3), pp.453-465

FERNANDES, J.A.; SANTOS, L.; VANCE, T.; FILEMAN, T.; SMITH, D.; BISHOP, J.D.D.; VIARD, F.; QUEIRÓS, A.M.; MERINO, G.; BUISMAN, E.; AUSTEN, M.C. (2016), *Costs and benefits to*

European shipping of ballast-water and hull-fouling treatment: Impacts of native and non-indigenous species, Marine Policy 64, pp.148-155

FOB (2013), *In-Water Hull Cleaning System Cost & Cost Benefits Analysis* (2013), Fisheries Occasional Publication No. 115: Report 2, Department of Fisheries, Western Australia

HEWITT, C.L.; CAMPBELL, M.L.; COUTTS, A.D.M.; DAHLSTROM, A.; VALENTINE, J.; SHIELD, D. (2011), *Species biofouling risk assessment,* Dept. Agriculture, Fisheries and Forestry (DAFF)

LI, T.; BI, Y.; LIU, J.; WU, C. (2016), *Effects of laser irradiation on a bloom forming cyanobacterium Microcystis aeruginosa*, Environ. Sci. Pollut. Res., pp. 20297–306

NANDAKUMAR, K.; OBIKA, H.; SREEKUMARI, K.; UTSUMI, A.; OOIE, T.; YANO, T. (2009), *Laser damage to marine plankton and its application to checking biofouling and invasion by aquatic species: a laboratory study*, Biofouling, pp. 95-98

OLIVERIA, D.R.; GRANHAG, L. (2020), *Ship hull in-water cleaning and its effects on fouling-control coatings,* Biofouling 36(3), pp.332-350

SCHULTZ, M.P.; FINLAY, J.A.; CALLOW, M.E.; CALLOW, J.A. (2000), *A turbulent channel flow apparatus for the determination of the adhesion strength of microfouling organisms*, Biofouling 15(4), pp.243-251

SCHULTZ, M.P.; BENDICK, J.A.; HOLM, E.R.; HERTEL, W.M. (2011), *Economic impact of biofouling on a naval surface ship*, Biofouling 27(1), pp.87-98

SILVA, E.R.; FERREIRA, O.; RAMALHO, P.A.; AZEVEDO, N.F.; BAYÓN, R.; IGARTUA, A.; BORDADO, J.C.; CALHORDA, M.J. *(2019), Eco-friendly non-biocide-release coatings for marine biofouling prevention.* Science of the Total Environment 650, pp.2499-2511

SONG, C.; CUI, W. (2020), *Review of underwater ship hull cleaning technologies*, J. Marine Science and Application 19(3), pp.415-429

TOWNSIN, R.L. (2003), *The ship hull fouling penalty*, Biofouling 19(S1), pp.9-15

TYRELL, M.C.; BYERS, J.E. (2007), *Do artificial substrates favor nonindigenous fouling species over native species?,* J. Experimental Marine Biology and Ecology 342(1), pp.54-60

Stochastic Uncertainty in Fuel-Optimised Ship Routing: How Weather Forecasts Hinder the Carbon Savings from Wind-Assisted Weather Routing

James Mason, University of Manchester, Manchester/UK, james.mason@manchester.ac.uk
Alejandro Gallego-Schmid, University of Manchester, Manchester/UK, alejandro.gallegoschmid@manchester.ac.uk

Abstract

Immediate cuts to shipping emissions are vital to align the sector with the targets of the Paris Agreement. Wind propulsion is one solution that is available to implement in the short term, and combining operations with optimal weather routing can maximise the performance of this novel technology. However, while weather routing theoretically offers synergistic benefits, the detrimental impact of stochastic weather forecasts is unknown. Here, we calculate optimal voyages for a wind-assisted Panamax bulk carrier to show that future novel strategies are essential to mitigate uncertainty and make the technology a viable carbon reduction option for the sector.

1. Introduction

International shipping forms the backbone of global trade and ships emit between 2-3% of global CO_2 emissions annually, *Faber et al. (2020)*. In 2018, the International Maritime Organisation (IMO) laid down a path toward decarbonisation that targets a 50% reduction in CO_2 by 2050 relative to levels in 2008, *IMO (2018).* However, research shows that the sector requires cuts of at least 34% by 2030 relative to 2008 levels to align trajectories with the Paris Agreement goals, with full decarbonisation required by 2050, *Bullock et al. (2022), Traut et al. (2018).* Moreover, with no action, committed emissions from existing shipping infrastructure will consume 135% of a 1.5°C Paris-compatible carbon budget throughout their remaining lifetime, *Bullock et al. (2020).* Stronger action is therefore needed to align emissions trajectories with the Paris Agreement goals, with a particular focus on short-term reductions on existing vessels to complement longer-term decarbonisation efforts.

Wind-assisted weather routing is one retrofit solution that can cut emissions on existing vessels to tackle committed emissions. This technology efficiently routes ships with modern sail technology by guiding them towards areas of the ocean with advantageous wind. Studies show that weather routing can amplify the carbon savings from wind-assisted ships by over 50%, *Mason (2021).* However, while weather routing can theoretically provide benefits to wind-assisted ships, the stochastic uncertainty inherent in weather forecast data has been shown to limit the technology's mitigation potential, *Yoshimura et al. (2016), Rosander and Bloch (2000)*, particularly considering the performance of a wind-assisted ship is more sensitive to wind than for standard ships. Fuel-optimum route calculations can be based on wind forecast data weeks in the future, which can lead to large errors between the predicted weather and the weather realised in practice. No study in the existing wind-assisted shipping literature has successfully explored methods that quantify the scale with which CO_2 savings are reduced when forecast-based optimum routes are assessed relative to the weather experienced by ships in practice.

This paper develops a weather routing method that emulates existing methods within the existing wind-assist literature to calculate the optimum-fuel voyage of a Flettner rotor-assisted ship using weather forecast data available at the start of the ship's journey. This method is advanced by re-tracking the resultant optimum route with historical weather data to quantify the reduction in carbon savings due to uncertain forecast data. The analysis in this paper provides early insights into the first detailed analysis that investigates how standard weather routing methods are impacted by the uncertainty induced by stochastic weather forecast data.

2. Method

2.1. Weather data

This study quantifies how stochastic weather forecast data affects the fuel savings from weather routing when combined with a ship with wind propulsion technology. The weather routing method calculates fuel-optimised shipping routes using weather forecast data available at the start of the ship's voyage, which reflects methods developed in the existing literature. Such optimisation methods that are based on information available only at the start of the voyage are known as a priori optimisation problems, *Manseur et al. (2018)*. Here, the *u*- and *v*- components of wind are obtained from the control forecast of the TIGGE dataset from the European Centre for Medium-Range Weather Forecasts (ECMWF). The dataset contains data with a 1° longitudinal and latitudinal resolution and with a 6-hour time resolution for a total forecast prediction time of 360 hours.

To quantify the accuracy of the optimal route predictions using weather forecast data, termed here as the forecast-optimum, the analysis re-tracks the forecast-optimum voyage with reanalysis data. Reanalysis weather data represents the realised weather and denotes the weather realised by the ship in practice when it travels along its pre-determined forecast-optimum route. The voyage retracked with reanalysis weather data is termed here as the realised-optimum. Reanalysis weather data is obtained from the ERA5 dataset from ECMWF, with a 1° longitudinal and latitudinal resolution and with a 6-hour time resolution. The difference between the forecast-optimum and the realised-optimum provides insight into how stochastic uncertainty in weather forecast data can influence a priori optimal routing decisions for ships with wind propulsion.

2.2. Case study

The analysis here investigates a case study route to quantify the impact of stochastic weather forecast data on existing weather routing methods for wind-assisted ships. Fuel-optimised shipping routes are calculated using the Voyage Optimisation for the International Decarbonisation of Ships (VOIDS) weather routing software developed in *Mason (2021)*. This software uses a grid-based three-dimensional dynamic programming algorithm based on methods developed by *Bellman (1957)* to optimise the route and speed of wind-assisted ships. The fuel savings from combining weather routing with wind propulsion are calculated by comparing a wind-assisted ship on the fuel-optimum route with a standard ship with no wind propulsion travelling on the shortest-distance Great Circle Route (GCR). Furthermore, additional savings from weather routing are calculated by comparing the wind-assisted ship on the fuel-optimum route relative to the GCR.

The analysis investigates weather routing for a wind-assisted Panamax bulk carrier ship with four Flettner rotors installed, each with a height of 35 m and a diameter of 5 m. Performance prediction of the Panamax ship is obtained using software from Blue Wasp Marine. The software calculates performance in four degrees of motion using an advanced aerodynamic and hydrodynamic model, *Bordogna et al. (2019a,b), van der Kolk et al. (2019),* which is validated using experimental data from wind tunnel and towing tank testing. The model includes interaction effects between the rotors and calculates additional resistance from the increased rudder and leeway angles. Operational constraints for rudder and heel angle are set as $\pm 10°$. Additional resistance from waves is calculated using the Gerritsma-Beukelman method, *Gerritsma and Beukelman (1972),* assuming that wave direction coincides with wind direction. Wave height is calculated using a Pierson Moskowitz spectrum, *Pierson and Moskowitz (1964),* which assumes a correlation with wind speeds through the Beaufort scale.

A case study route in the North Atlantic Ocean between the Caribbean (27.0°N, 75.0°W) and the UK (49.0°N, 6.0°W) is investigated, Fig.1. The route is split into stages of 400 km, with a 100 km spacing between grid waypoints that are perpendicular to the direction of motion of the ship. The grid is filtered with Bathymetry data from the General Bathymetric Chart of the Oceans (GEBCO), assuming a ship draught of 14 m. The ship's speed is limited to between 8-13 kn in intervals of 1 kn. Sixty departure

dates are simulated in 2018, with one departure simulated every six days from the first day of each month.
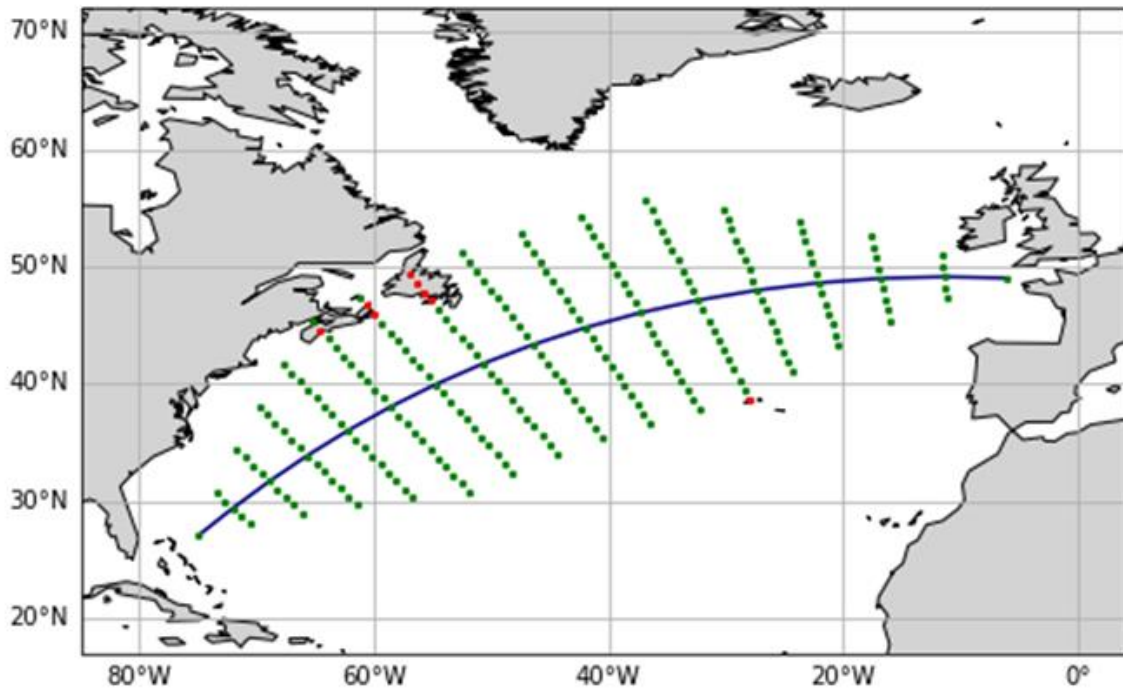
Fig.1: The case study route between the Caribbean and the UK. Red points indicate filtered grid points, while green points form the sailable region. The shortest-distance Great Circle Route (GCR) is shown in blue.

3. Results and discussion

To quantify the stochastic uncertainty in optimum routing for wind-assisted ships, this study calculates the fuel-optimised voyage using a priori forecast data, which uses the weather forecast available at the start of the ship's voyage. The optimum voyage is subsequently retracked with the realised weather to calculate the fuel savings achieved from voyage optimisation technology in practice.

Findings show that the stochastic uncertainty in the initial weather forecast significantly hinders the performance of voyage optimisation technology. Initially, large additional carbon savings calculated using weather forecast data reduce substantially when retracked with the realised weather, decreasing from an annual saving of 32.2% to 20.7%, Fig.2. This reduces below the standard Great Circle Route (GCR) operations, which reduce carbon emissions by 22.0%. The effect is more pronounced in the winter months when carbon savings are typically larger from voyage optimisation due to the presence of strong wind speeds, and a reduction in performance of up to 23.5% is observed (December in Fig.2). This agrees with findings in *Rosander and Bloch (2000)* and suggests that the methods used throughout the literature on wind-assisted voyage optimisation that assume a perfect foresight of weather conditions may produce large inaccuracies when the method is implemented in practice.

These novel results provide useful insight into discussions around ship connectivity at sea. Currently, a large fraction of the global shipping fleet has limited internet connectivity at sea, particularly for long international voyages. Wind-assisted voyage optimisation when used on these ships may therefore rely heavily on weather forecast predictions available at the start of the ship's voyage. For these cases, the early results presented here suggest that the performance of voyage optimisation technology could be significantly hindered by the large uncertainty induced from stochastic weather forecast predictions. More advanced methods, such as an adaptive strategy, are therefore required to increase carbon savings towards the theoretical optimum calculated in previous studies, *Mason (2021), Bentin et al. (2016), Marie et al. (2014).*
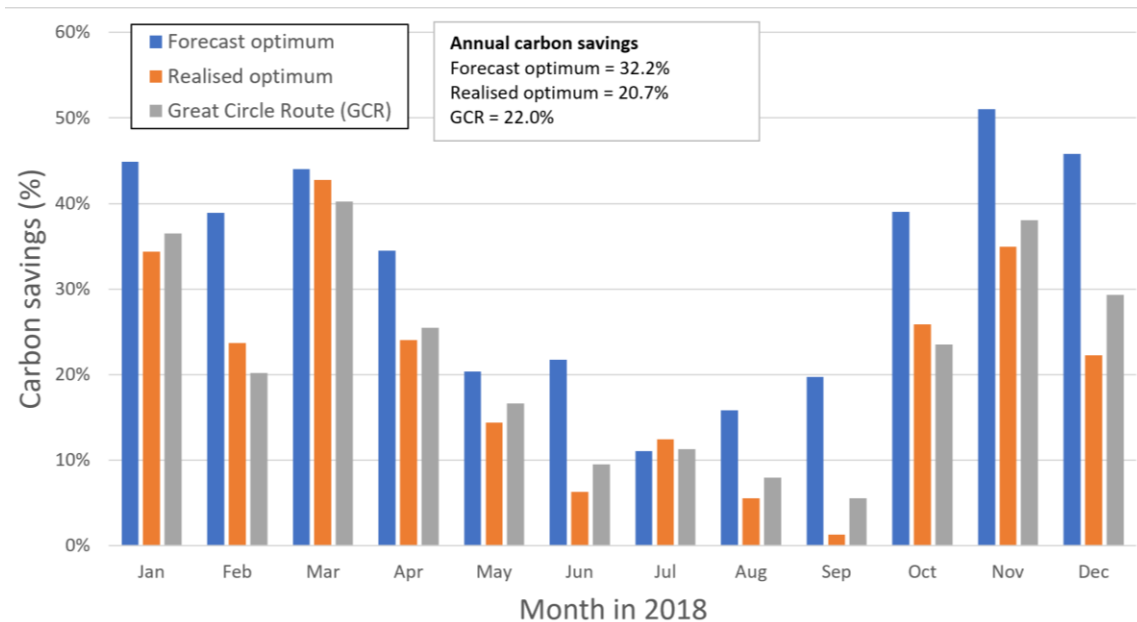
Fig.2: Carbon savings from three cases: 1) voyage optimisation using weather forecast data available at the start of the voyage only (blue), 2) the optimum voyage from case 1 retracked with the realised weather (orange) and 3) on the Great Circle Route (GCR).

4. Future work

The results of this analysis highlight that future novel methods that focus on mitigating the detrimental impact of stochastic weather forecast uncertainty are an essential element in making weather routing technology feasible for wind-assisted ships. Future research should investigate weather routing using an adaptive optimisation strategy, which adapts the optimum routing solution based on information that becomes available along the ship's journey by re-uploading new weather forecast data in regular intervals. Continually updating the optimisation procedure with the latest accurate weather forecast is one method that could reduce the influence of uncertain and stochastic weather forecast inputs.

5. Conclusions

This study provides new insights into the limitations of stochastic weather forecast data when used to estimate optimal voyages for Flettner rotor-assisted ships. By utilising both forecast and historical weather data, we show that calculating a priori optimum voyages using stochastically uncertain weather forecasts removes all benefits from voyage optimisation. Future studies must focus on developing novel methods that mitigate this detrimental effect, such as through an adaptive optimisation strategy. In the face of the imminent climate emergency, maximising the performance of wind propulsion devices using optimisation techniques could prove vital in reducing emissions in the short-term to tackle both cumulative and committed emissions in the global shipping sector.

References

BELLMAN, R. (1957), *Dynamic programming,* Princeton University Press

BENTIN, M.; ZASTRAU, D.; SCHLAAK, M.; FREYE, D.; ELSNER, R.; KOTZUR, S. (2016), *A New Routing Optimization Tool-influence of Wind and Waves on Fuel Consumption of Ships with and without Wind Assisted Ship Propulsion Systems*, Transportation Research Procedia 14, pp.153-162, 10.1016/j.trpro.2016.05.051

BORDOGNA, G.; MUGGIASCA, S.; GIAPPINO, S.; BELLOLI, M.; KEUNING, L.; HUIJSMANS, R.; VEER, A. (2019a), *Experiments on a Flettner rotor at critical and supercritical Reynolds numbers*. J. Wind Engineering and Industrial Aerodynamics 188, pp.19-29

BORDOGNA, G.; MUGGIASCA, S.; GIAPPINO, S.; BELLOLI, M.; KEUNING, J.; HUIJSMANS, R. (2019b), *The effects of the aerodynamic interaction on the performance of two Flettner rotors*, J. Wind Engineering and Industrial Aerodynamics 196

BULLOCK, S.; MASON, J.; LARKIN, A. (2022), *The urgent case for stronger climate targets for international shipping*, Clim. Policy

BULLOCK, S.; MASON, J.; BRODERICK, J.; LARKIN, A. (2020), *Shipping and the Paris climate agreement: a focus on committed emissions*, BMC Energy 2

FABER, J.; HANAYAMA, S.; ZHANG, S.; PEREDA, P.; COMER, B.; HAUERHOF, E.; … YUAN, H. (2020), *Fourth IMO GHG Study*, Int. Maritime Org., London, https://greenvoyage2050.imo.org/wp-content/uploads/2021/07/Fourth-IMO-GHG-Study-2020-Full-report-and-annexes_compressed.pdf

GERRITSMA, J.; BEUKELMAN, W. (1972), *Analysis of the resistance increase in waves of a fast cargo ship*, Int. Shipbuilding Progress 19, pp.285-293

IMO (2018), *Initial IMO Strategy on reduction of GHG emissions from ships*, MEPC.304(72), Int. Maritime Org., London, https://wwwcdn.imo.org/localresources/en/KnowledgeCentre/IndexofIMOResolutions/MEPCDocuments/MEPC.304(72).pdf

MANSEUR, F.; FARHI, N.; NGUYEN VAN PHU; C., HAJ-SALEM, H.; LEBACQUE, J.P. (2020), *Robust routing, its price, and the trade off between routing robustness and travel time reliability in road networks*, European J. Operations Research 285/1, pp.159-171

MARIE, S.; COURTEILLE, E. (2014), *Sail-assisted motor vessels weather routing using a fuzzy logic model*, J. Marine Science and Technology 19, pp.265-279

MASON, J. (2021), *Quantifying voyage optimisation with wind-assisted ship propulsion: a new climate mitigation strategy for shipping*, Doctoral thesis, The University of Manchester

PIERSON, W.; MOSKOWITZ, L. (1964), *A proposed spectral form for fully developed wind seas based on the similarity theory of S. A. Kitaigorodskii*, J. Geophysical Research 69/24, pp.5181-5190

ROSANDER, M.; BLOCH, J.O.V. (2000), *Modern Windships*, Pelmatic Knud E. Hansen, https://www2.mst.dk/udgiv/publications/2000/87-7944-019-3/pdf/87-7944-020-7.pdf

TRAUT, M.; LARKIN, A.; ANDERSON, K.; McGLADE, C.; SHARMINA, M.; SMITH, T. (2018), *CO_2 abatement goals for international shipping*, Clim. Policy 18, pp.1066-1075

VAN DER KOLK, N.; KEUNING, J.; HUIJSMANS, R. (2019), *Part 1: Experimental validation of a RANS-CFD methodology for the hydrodynamics of wind-assisted ships operating at leeway angles*, Ocean Eng. 178, pp.375-387

YOSHIMURA, Y.; OUCHI, K.; WASEDA, T. (2016), *Contributions to EEOI and EEDI by Wind Challenger Ships*, 7th PAAMES and AMEC

Case Studies on Additive Manufacturing for Maritime Applications

Ramesh Babu Govindaraj, DNV, Oslo/Norway, ramesh.babu@dnv.com
Sastry Kandukuri, DNV, Oslo/Norway**,** sastry.kandukuri@dnv.com

Abstract

As the shipbuilding industry increasingly discovers the advantages of Additive Manufacturing (AM), DNV is working closely with industry partners to further expand the range of 3D printed products and prove their safety and functionality. Since 2016, DNV is highly involved in developing the classification rule and standards for maritime and energy industry. From 2018 we are managing a joint industry project, ProGRAM JIP, to produce a guideline formulating the necessary requirements to introduce components made by Additive Manufacturing into the energy and maritime industry. The participants in this industry consortium of twenty-three companies spanned the entire value chain, from end-users and OEMs to service providers, material suppliers and testing companies. This paper presents the consortium's latest findings and overview of certification process.

1. Introduction

Additive Manufacturing technology is making steady advances. While the automotive and aerospace industries, where weight reduction is key to maximizing fuel efficiency and minimizing carbon emissions, have benefitted from AM for a number of years, the maritime sector has only recently begun to explore the opportunities offered by layer-by-layer 3D printing. There are two main fields of interest: establishing a local supply infrastructure for 3D-printed spare parts in major ports to accelerate delivery and exploiting the unique capabilities of AM technology to make parts no other manufacturing process can produce.

As the industry discovers the benefits of Additive Manufacturing compared to casting and forging – such as better control of quality, a more consistent internal structure, innovative shapes, and shorter delivery times – a number of unique projects have been undertaken with DNV's involvement. For example, DNV has issued a verification statement for a ship propeller with a two-metre diameter, made in a Wire Arc Additive Manufacturing (WAAM) process by SY Metal in South Korea. The WAAM process is twice as fast as conventional casting and provides a solution to avoid supply chain bottlenecks; what is more, WAAM-printed parts are generally characterized by higher strength due to a more regular microstructure when compared to castings whose microstructure varies from the surface towards the core, *Govindaraj et al. (2021).* While the fatigue test of the prototype has yet to be carried out, this is a first step towards resolving an issue that is not uncommon for example replacing a ship propeller at short notice after it has been lost at sea. DNV ship classification rule's part 2 Ch 2 has a specific section 14, *DNV (2022),* which gives the requirement for acceptance of additive manufacturing product. First approval of Manufacture was issued to Thyssenkrupp, Germany. The approval process for classification is given in the flow chart in Appendix.

2. JIPs drive the development of rules

DNV's work on Additive Manufacturing continues. DNV had established a flow chart for acceptance of Additive Manufacturing parts in several Joint Industry Project (JIP) consortiums. The Maritime and Energy Systems business areas of DNV are jointly developing new standards. The Singapore Maritime and Port Authority (MPA), which has shown strong interest in promoting AM in the maritime sector, has been involved in a number of AM initiatives. The Global Additive Manufacturing Technology Centre of DNV's Energy Systems in Singapore is supported by the Singapore Economic Development Board (EDB) and focuses on AM research as well as advisory services and industrial certification. DNV Maritime provides class approval services and verifications for ships and offshore structures, which involve a wider scope of requirements, tests, and on-board trials.

The DNV pathway for Additive Manufacturing has made great strides towards making AM a key technology for safety-critical, classed as well as non-class ship parts and components. As more AM materials, processes, manufacturers, and individual part designs receive class approval, ship owners and yards will be able to rely on a growing list of components whose design has been optimized for the intended application, and which feature better, i.e., more regular, material properties and can be made available faster and at a lower cost.

2. ProGRAM JIP - Lighthouse project that demonstrate the power of AM

In 2018, a consortium of twenty-three companies, managed by DNV and Berenschot, started a project, ProGRAM JIP, to produce a guideline formulating requirements necessary to introduce components made by Additive Manufacturing into the oil, gas and maritime industry. The guideline established a practice for qualification and production of parts using two AM technologies: Laser Beam Powder Bed Fusion (PBF-LB), and electric arc-based wire Directed Energy Deposition (DED-arc). The guideline was translated into a standard issued by DNV (DNV ST-B203), *DNV (2021)*.

In May 2020, a group of twenty companies formed a new consortium, ProGRAM JIP Phase II, managed by DNV and supported by Berenschot. The companies participating in Phase II spanned the entire value chain, from end-users and OEMs to service providers, material suppliers and testing companies. The consortium partners included: Saudi Aramco, Equinor, Siemens Energy, Kongsberg Maritime, K-Ferrotech, Voestalpine, Eifeler, Sandvik, Aperam, Imphytek, Intertek, Guaranteed, Addilan, FIT AG – Additive Manufacturing, Group, BMT aerospace, IMI-Critical, ExOne, XDM3D, Howco and NMIS - Strathclyde University.

The goal was to extend standard DNV-ST-B203 with three additional AM technologies: Laser Beam Directed Energy Deposition (DED-LB), Electron Beam Powder Bed Fusion (PBF-EB), and metal Binder Jetting (BJT). As well as focusing on building new parts with these technologies, the consortium also looked at hybrid production, repairing or remanufacturing parts using AM. To this end, using Directed Energy Deposition to build features on an existing substrate was included in the project.

3. Selected Case studies

The project delivered new insights into the capabilities of AM for the production of high-quality spare parts for the energy and maritime industries. The project also showed that hybrid production, as well as conducting repairs with AM, is a realistic, cost-effective, and environmentally friendly manufacturing option. The results from the joint industry project will be incorporated in a new edition of DNV's standard for the Additive Manufacturing of metal parts, DNV-ST-B203, which is due to be published later this year.

Fig.1: Crank disc (Kongsberg Maritime)

Fig.2: Impeller (Equinor)

Fig.1 shows a crank disc produced by DED-arc. This is a component in a controllable pitch propeller. Conventional crank discs are made in forged steel. Reasons for selecting AM were lower cost, shorter lead time, improved sustainability, and improved possibilities for repair.

Fig.2 shows an impeller (part of a centrifugal pump) produced by PBF-EB. Compared to traditional manufacturing (casting), AM was selected to reduce lead time, rerate/customise existing pumps, reduce stock levels, and improve quality.

These application case studies will be discussed in more detail in the following.

3.1. DED-arc: Crank Disc

With regards to the Electric Arc Directed Energy Deposition (DED-arc) process, a dramatic cost reduction was experienced when applying as a hybrid solution to produce a crank disc, Fig.1. Conventional crank discs consist of a disc with a pin on top, manufactured through the forging and machining of often relatively expensive steels or alloy. Additionally, the conventional process is complex and creates waste, which is reflected in the price of the product. When taking a low cost, readily available steel base plate, and using DED-arc to add the critical feature (the pin), the use of high-cost material, and material waste, was reduced.

The main variables to control in the wire and arc DED process are the heat input, the wire feed speed, and the inter-pass cooling temperature, which could be controlled using a pyrometer. This technology was tried in a new build production case and a part repair case. The set-up time for the new part and the repair case were similar, and the execution time and heat treatment were quite similar in both applications.

As a best practice it is recommended that the transition zone between the base material and added feature should be moved outside the high loaded area. Using low-cost, normal-grade steel in the low loaded part, and using high-grade material only in the loaded part delivered by hybrid design, DED-arc technology was capable of manufacturing efficiently and cost effectively, provided that a good metallurgical compatibility exists between the substrate, an AM feature that needs special attention.

3.2. DPBF-EB: Impeller

The experience gained in ProGRAM JIP I, where the same impeller was manufactured using Laser Beam Powder Bed Fusion (PBF-LB), proved to be very useful. Using this experience, first-time-right, cost-effective design and production of the impeller was achieved using PBF-EB, Fig.2.

Regarding the impeller, dimensional tolerances are critical to meet functional tests. After PBF-EB production, a slight warping and some pores were found, leading to small deviations on the openings of the flanges. They had no impact on pump performance but were of a cosmetic nature. All mechanical properties resulting from PBF-EB conformed the requirements in ASTM F3302 standards, despite the high oxygen content in the initial powder material (0.3 wt.%). Hot Isostatic Pressing (HIPing) proved to be the perfect solution to reduce porosity and improve mechanical properties. Another learning was to rethink the set-up of support structures.

Although the part's geometry was quite complex, there were no significant issues with powder removal or part placement in the build. Due to the geometry of the part (the limited key slot openings), the partners elected to use 5-axis machining instead of turning for the final machining of the part.

For the design and production process, it was found that it is practical to build the test specimens and the final parts simultaneously in the same build envelope. In the case of small series, or when slightly adjusting the features of the part, this is considered to be quite convenient for end-users.

4. Conclusions

Furthermore, based on the results of this project, it can be concluded that two AM technologies (wire and arc DED and PBF-EB) are ready to be used for the manufacture of high-quality parts, be they spare parts on demand or production parts. Wire and arc DED also proves to be an excellent option for hybrid production, as well as the repairing or remanufacturing of parts. When looking at wire and arc DED, the project partners observed that this technology can produce high-quality, low-cost spare parts or perform repairs or remanufacturing in a short period of time. This presents a potentially very beneficial business case, with considerable energy savings as compared to conventional manufacturing.

PBF-EB proves to deliver similar or even better quality as compared to conventional manufacturing techniques such as casting. Where it is possible to build more than one part in the same build envelope, PBF-EB delivers lower cost parts while shortening the lead time by at least 10–30%. In our case, the lead time was reduced even further, from twenty-four weeks to just four weeks. PBF-EB, then, is a true competitor to conventional manufacturing and asks for further investigation using new use-cases.

Acknowledgements

References

DNV (2020), *Ship rules for classification, Pt.2 Ch.2. Section 14 - Additive manufacturing*, DNV, Høvik, DNV rules and standards

DNV (2021), *DNV-ST-B203 Additive manufacturing of metallic parts*, Standard, DNV, Høvik, https://www.dnv.com/oilgas/download/dnv-st-b203-additive-manufacturing-of-metallic-parts.html

GOVINDARAJ, R.; JUNGHANS, E.; ANDERSEN, I.; LIM, Y.K.; LINDSTRÖM, P. (2021), *Additive manufactured marine component – Ni Al bronze propeller,* Procedia Structural Integrity 34, pp.20-25, https://www.sciencedirect.com/science/article/pii/S2452321621002808?via%3Dihub

JUNGHANS, E.; GOVINDARAJ, R.B. (2022), *Additive Manufacturing enters the maritime mainstream*, Maritime Impact, DNV, https://www.dnv.com/expert-story/maritime-impact/Additive-Manufacturing-enters-the-maritime-mainstream.html#

KANDUKURI, Y.S.; PONFOORT, O. (2022), *Additive Manufacturing for oil, gas and maritime: An evaluation of capabilities and potential*, Metal Additive Manufacturing magazine 8/2, pp.137-143, https://issuu.com/inovar-communications/docs/metal_am_summer_2022

Appendix – Flow chart

Flow chart:

- **Approval Request** (start)
- **Quality system certified by Third party** — No → Required to have quality system Eg: ISO 9001; Yes ↓
- **Review of AM Technology existing data and feasibility report** — No → Require to have experiance in the technology by means of testing the equipment and printing a product; Yes ↓
- **Qualified Manufacturing Procedure** — No → To be qualified as per DNV-CG-0197 and agreed test plan; Yes ↓
- **Approved feedstock supplier** — No → Feedstock supplier approval DNV-CP-0291; Yes ↓
- **Approved sub-supplier Eg: Post- processing** — No → Sub-supplier approval- DNV-CG-0197 & DNV-CP-0267; Yes ↓
- **Audit to the manufacture based on agreed AoM Test plan** — No → AoM Checklist, Test plan DNV-CP-0267; Yes ↓
- **Approval of Manufacture** — No → AoM documentation and Testing DNV-CP-0267; Yes ↓
- **Approval complete. Publish in Approval finder**

UVC Anti-Fouling Solution –
Design, Experiments and Results of Next Generation Samples

Bart Salters, Philips Electronics, Eindhoven/The Netherlands, Bart.Salters_1@philips.com
Merijn Wijnen, Philips Electronics, Eindhoven/The Netherlands, Merijn.Wijnen@philips.com
Kevin Reynolds, International Paint Ltd, Gateshead/UK, Kevin.Reynolds@akzonobel.com

Abstract

In this paper we present the progress made with our UVC anti-fouling solution. Over the past 2 years, a new generation of tiles has been developed, produced and put to test on various vessels sailing around the world. We describe the details of the latest generation of tiles, including mechanical, optical and electrical aspects. Simulations of the expected results are shown and compared to the actual results of the tests.

1. Introduction

In 2014, Philips started developing a new anti-fouling concept, based on UVC light, *Salters (2014)*. At the highest level, the concept is to completely cover the hull of a ship with a light-emitting layer. UVC light is emitted outwards, which in turn completely prevents fouling from adhering to the hull. Over the years, a wide range of variations on several parameters have been explored; and as a result, many have been optimized.

In several generations of tests, the concept has been explored, *Salters (2016)*. Previously we have reported on a series of tests that were all powered via a wired connection. In 2019, a new generation of wirelessly powered panels was developed – the 4th generation design - with substantially improved characteristics and performance. These tiles have been put to test on a number of ocean faring vessels; and in this paper we will also show the results of these.

Finally, we will provide an outlook towards the future. Currently, the next generation of panels is being designed; and a test at a much larger scale is being planned. This includes an increase in size of about two orders of magnitude, as well as numerous improvements in other aspects.

2. Basic concept and history of previous tile generations

The basic concept of the RunWell technology is based on the idea that UVC light can keep a surface completely clean from biofouling. When emitting light outwards from a surface, biofouling does not have a chance to adhere to a surface at all. As long as the light is being emitted at or above the minimum required level, the surface will stay clean. The light emitting surface is created by embedding UV emitting LEDs in an optically transparent layer, and attaching this layer to the outside of the hull, or to any other submerged surface, Fig.1.
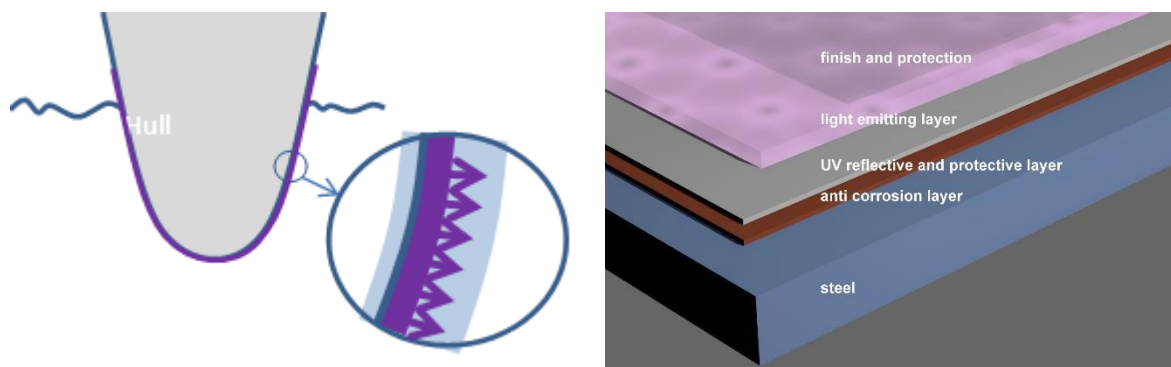
Fig.1: Basic concept of the RunWell technology
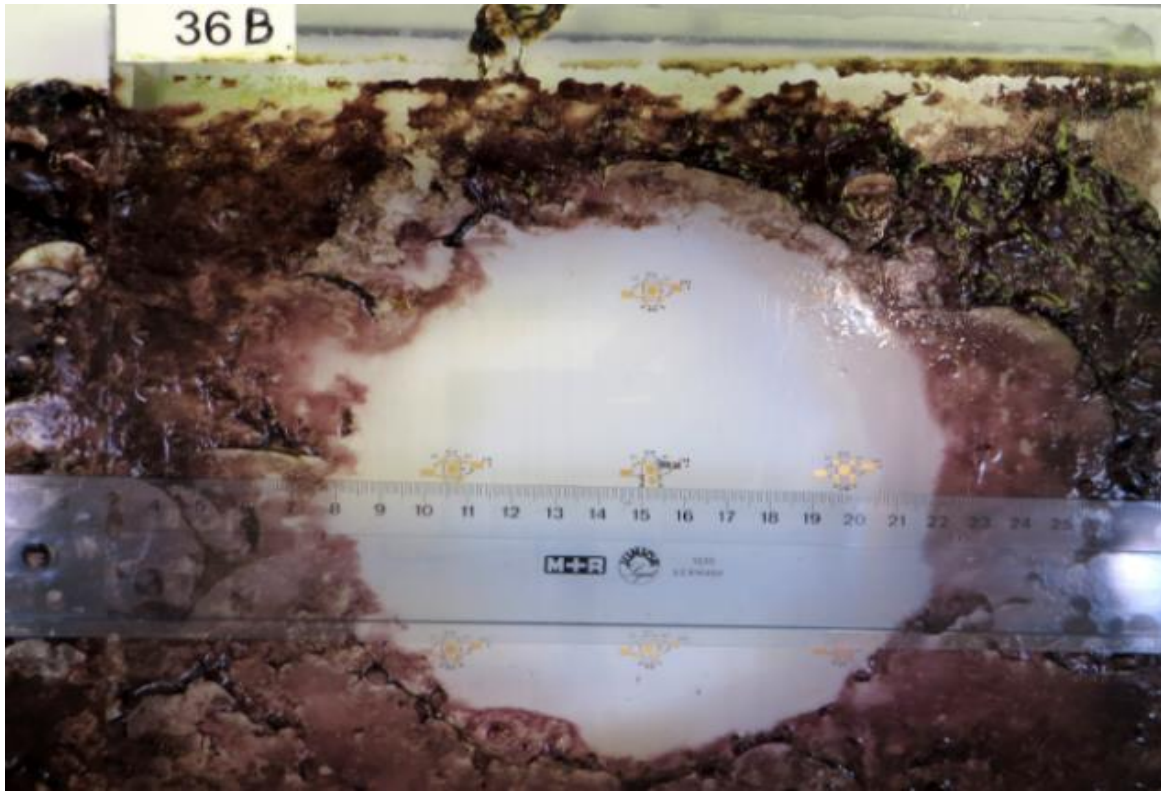
Fig.2: A single 1 mW LED will keep an area of about 110 cm^2 free from biofouling for a prolonged period of time.

The very first samples, made in 2014, *Salters (2014),* show the proof of principle, Fig.2. Although just 1 LED was embedded in a silicone tile, it clearly showed the potential of UVC light. At quite a low power level – a mere 1 mW of UVC light – a significant area could be kept clean for a prolonged time.

(a)

(b)

(c)

(d)
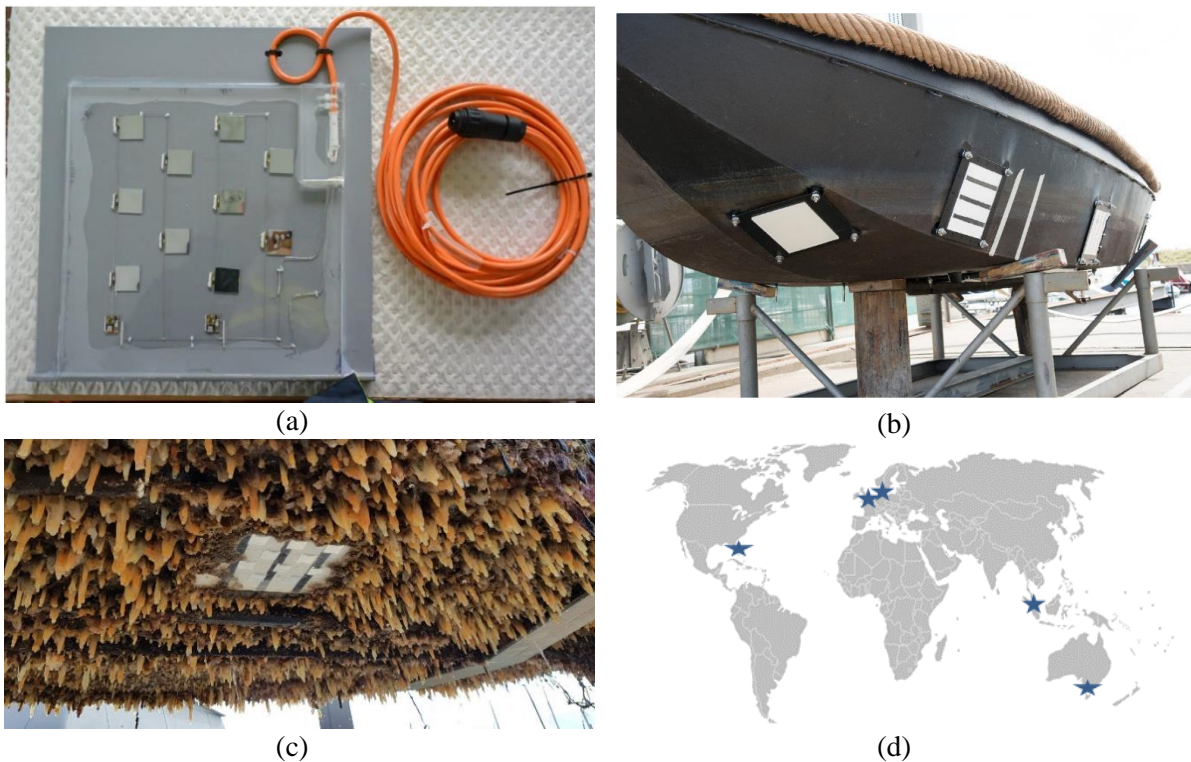
Fig.3: (a) 2nd generation panel with 10 LEDs. (b) Deployed on a small vessel sailing the Dutch North Sea. (c) Results after 12 months in open water. (d) Other test locations around the world.

Following this first result, work has been focused on scaling up to larger sizes and proving the effectiveness in different conditions. This has led to a series of samples and test, which we have reported about in previous presentations as well, *Salters (2016), Jongerius (2016)*. These include larger sizes, different locations around the world, and installations on both static rafts as well as moving vessels, Fig.3.

Following these results, a third generation of panels has been designed; internally known as "Cora". In this phase, a step was made towards ease of manufacturing, as well as an improvement in optical design. One of the main topics to tackle here, is to evenly distribute the light from the LEDs – which are point sources – over the entire surface. Other areas of improvement included the mechanical robustness, and electronic control, Fig.4.
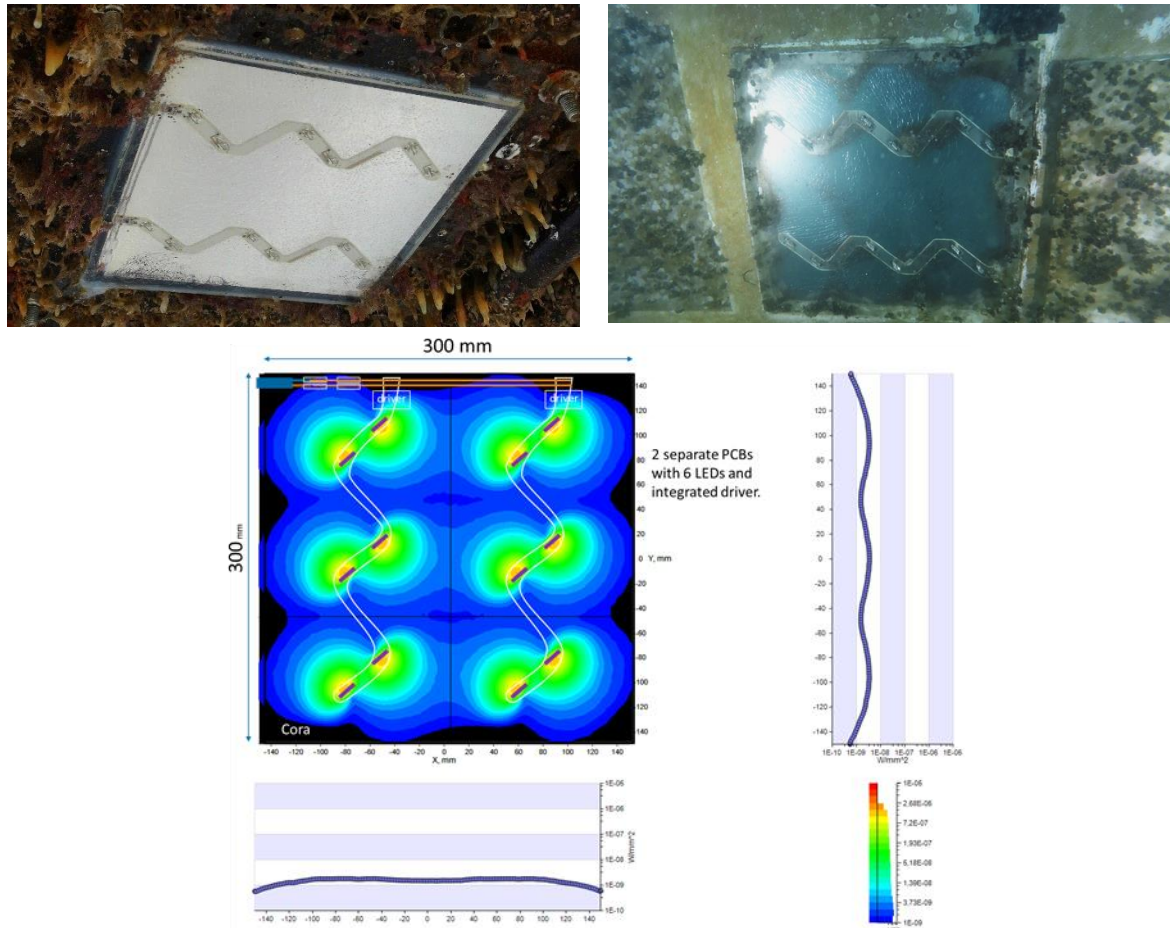
Fig.4: Third-generation panel, shown after 1 and 5 months of deployment. Some fouling is visible on the edge of the panel – closely following predictions from optical simulations. The rest of the panel is completely free from fouling.

In our last publications, right before the corona pandemic hit, we announced a joint development effort between Philips Electronics and AkzoNobel. Together, the 4th generation of panels has been designed, installed, and tested. We are reporting on these results below.

3. Detailed description of 4th generation tiles

In this chapter we will describe the design of the 4th generation (internally known as "Donna"). Compared to the 3rd generation, many aspects have been improved such as the electronic, optical and mechanical design. The goal of this new generation was to develop tiles that demonstrate the practicality and effectiveness of our UVC solution at a larger area, for a longer period of time, on deep sea ocean faring vessels.

These improvements are in the following areas:

- A more refined manufacturing process was used to create the panels: injection molding. Whereas previous samples were made almost entirely by hand, the new generation of tiles is made with injection molding of silicone. This allows for a much larger number of tiles to be produced, in a more reproducible way.

- A new generation of LEDs has been used. Unlike previous LEDs, these emit 'side-ways', parallel to the tile (and thus, the hull of the ship). This allows for a much improved more efficient optical design. Also, with each new generation of LEDs, the lifetime improves substantially. The LEDs in this generation have a specified lifetime of about 10.000 hours (=1 year); after that time the optical output is expected to start diminishing. Although 1 year likely is not enough for commercial applications, this is not a worry; as the commercial and technical outlook for UVC LEDs already at the start of this development phase predicted a further improvement to around 50.000 hours by 2022. As of today, such LEDs are indeed commercially available.

- To emit light, obviously electrical power is needed inside the panels. Up to the 3rd generation design, all panels were powered via a wired connection. A cable would run directly from the power source on board, all the way to (and into) the silicone panels. One of the drawbacks of this is the challenge to make the connection completely watertight. An alternative to a wired connection is wireless power transmission. This is similar to wireless charging of phones or toothbrushes. By embedding a pickup coil inside the panel, power can be transferred into a fully enclosed silicone tile. Thus, water ingress along the cable is no issue anymore.

  The total power required for a panel is now in the order of 10W, which corresponds to 40W/m^2 This includes the power needed for the electronics, the control, and the actual generation of UVC light. With further developments of the LEDs and optimization of the optical and electrical design it is anticipated that power requirements an order of magnitude lower can be achieved.

- A new optical design. A fundamental aspect in the concept of RunWell is to use LEDs – which are point sources – to illuminate a large surface. This implies that the light needs to be spread evenly from those point sources, over the entire surface. By carefully picking the quantity, position and orientation of the LEDs, and matching this to the optical radiation pattern of the LEDs, a better coverage of the surface area is achieved.

- Silicone improvements. The thickness of the silicone panel has been reduced from 10mm, down to 4 mm. This substantially reduces the cost of a panel, as well as the weight. Since this provides less 'space' for the light to travel along the surface, it increases the design challenge even further. Some tradeoffs are needed between efficiency and total power consumption.
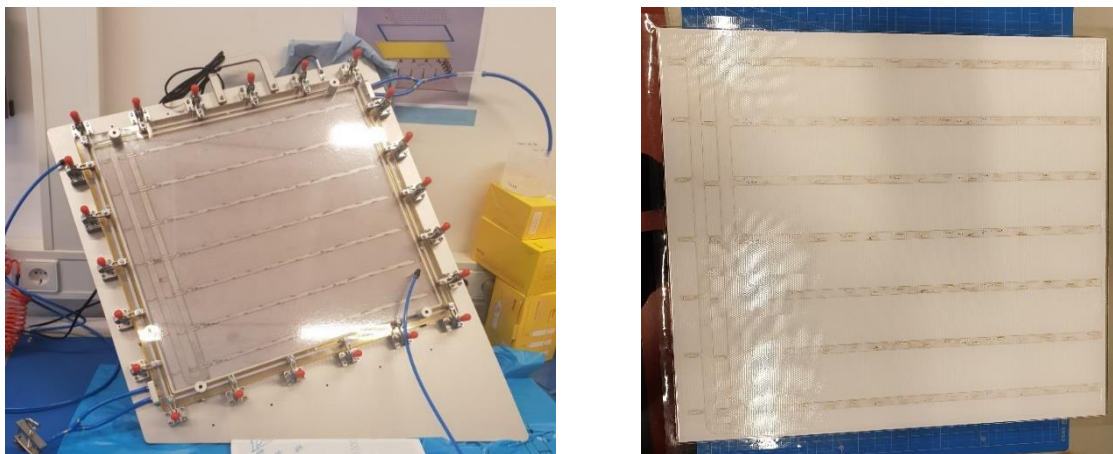
Fig.2: Donna panel in production, during injection molding phase (left), and final result (right).

4. Simulation of results

An important part of the design of our 4th generation panels is the optical performance. After all, getting the right amount of light to every part of the surface is key to keeping the surface clean. For this, we are using a so-called ray-tracing program, LightTools. This software package takes the exact design of the panels as input, including the light sources, material of the tiles, and water on the outside; and calculates the amount of light that will reach every part of the surface.

From previous work, we have established the fact that there is a certain threshold: a level of light that is just enough to keep a surface clean when it is applied continuously. This intensity of light is extremely low – just 1 mW of UVC light per m^2 of surface area, *Salters and Piola (2017)*. Using this as a target for the design process, the design can be optimized to reach that threshold over the entire surface. Parameters that can still be varied are for example:

- The number of LEDs
- The distribution and spacing of LEDs, or alternatively said, the pitch between those LEDs
- The geometry of the design; including the choice of materials, the thickness of individual layers, and the direction the LEDs are pointing in.

Using these variables as input parameters, and the desired intensity as the output target, a new optical design has been created.

4.1. Panel design "Donna".

The panel design that resulted from the simulation activities is shown in Fig.6. The "Donna" panel as shown here is 500x500mm in size, with a thickness of 4mm. A total of 121 LEDs are used, spread out in a carefully calculated pattern over the surface. The LEDs are placed on 7 small PCB (printed circuit boards) strips, as this is a standard production technology. By directing the light in opposite directions for neighboring LEDs, a fairly uniform illumination is achieved. This contributes to an increased efficiency: too little light is not good for obvious reason, but too much light will waste electrical power without achieving any beneficial effect.
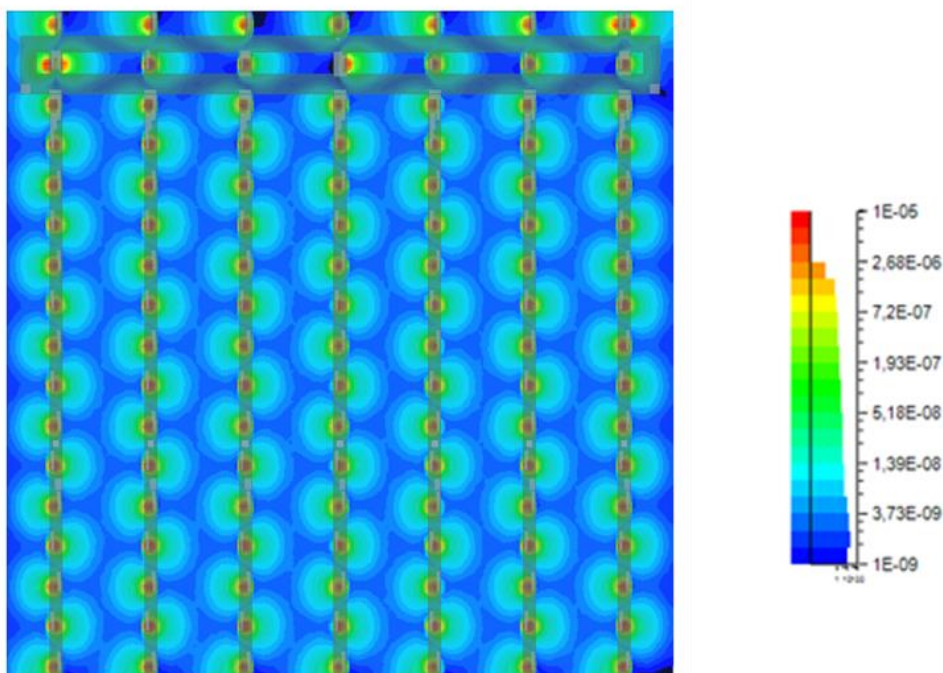
Fig.3: Fourth generation panel, "Donna", with light intensity indicated in W/mm^2

The color coding in Fig.3 is chosen such that the dark blue color indicates an intensity that is just above the threshold, whereas the very small dark areas represent a value that is under the threshold. It can be seen that only a few tiny areas around the edge and corner are predicted to be under the threshold; which in turn means that those areas might still be susceptible to bio fouling.

In other words, the design shown here is predicted to generate sufficient UV light over nearly the entire surface to completely prevent biofouling. Equally important: the predictive value from these simulations also allow us to create larger tiles, different designs, or different shapes; with the knowledge upfront that they will keep a surface clean – without the need for extensive testing.

The final product is shown in Fig.4. Although the LEDs primarily emit UVC light, they also emit a tiny amount of visible light. A long exposure photo will reveal this, when taken in a pitch-dark environment. Note the green optical LED in the upper corner used to indicated that the tile is being powered.

Fig.4: Final Donna tile. The light output matches the simulation quite well.

5. Results

Various panels were installed in different locations. The locations were chosen to test the new design in various circumstances, investigate whether any new or unexpected issues would arise, and collect data from operations over time. Whereas large ships, sailing the world, might be the most realistic test, they also have the drawback of the difficulty of inspections. On the other side, a raft test is likely not subjected to the mechanical and shear forces which will occur on an ocean-going vessel.

5.1. Navy Patrol

This test was performed on a European Navy patrol vessel, Fig.8, sailing the local rivers and coastline. It was in drydock at a convenient moment for installing a panel, and due to its patrol area, it is reasonably accessible for inspection.

This vessel was equipped with a single panel. To power this tile, first the power transmitter coil was glued to the hull. The panel was subsequently glued on top of this power transmitter with the coil in the panel aligned with the coil in the transmitter. Finally, the power transmitter was connected to the ship's main power supply via a cable suitable for permanent water immersion. Also, a reference panel without UVC LEDs was attached. The final situation right before the ship sailed again was as shown in Fig.9.

After 8 months – about 6000 hours of continuous operation – an underwater inspection by divers was performed. Although the water was quite murky, some pictures could be taken, Fig.10.

Fig.8: Navy patrol vessel

Fig.5: Installation of the panel, with a smaller dummy panel to the left of the picture

Several interesting observations were made. First of all, there is a very substantial difference between the active panel, and the reference. As expected, the UVC light has quite an effect: the active panel is substantially free of biofouling. Various details of the panel can be seen clearly, such as the LEDs, the strips of PCB, and the power receiver coil. There are a few tiny exceptions to the clean surface though:

- In the bottom left picture, a small area is seen to be covered in biofouling along the bottom edge. The pattern matches in simulation what happens when a single LED is failing. Hence the conclusion: 1 out of 121 LEDs failed somewhat early.

- Along the left edge in the same picture, a few spots of light fouling can be seen. These match the simulation results as well: along the edge of the panel, the light intensity is expected to be at, or just below, the threshold.
- The same holds for the very top edge, as can be seen in Fig.10(a).

All in all, the panel behaves pretty much as expected. It keeps the surface virtually spotless whenever and wherever the light is being emitted effectively.
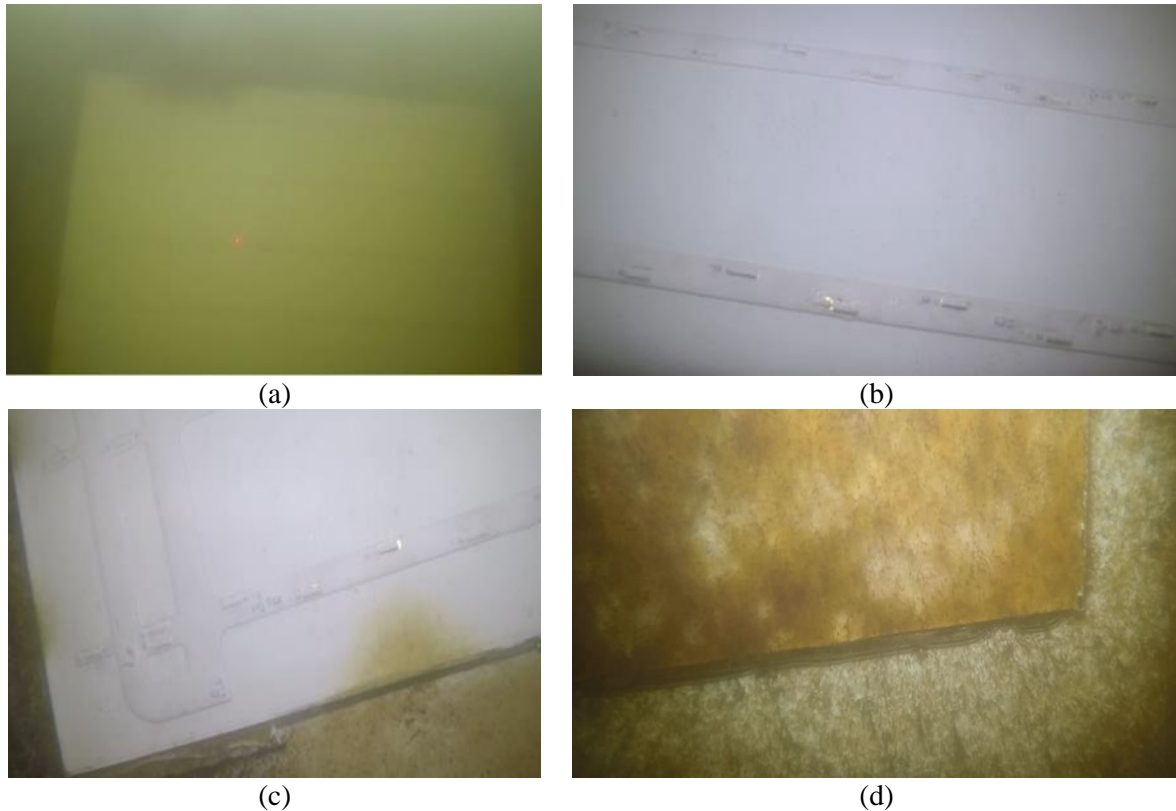
Fig.6: Results from diving inspection. Active panels ((a)-(c)), (d) shows the reference panel.

5.2. Clipper

The second test was on a clipper, used for luxury cruises and adventure trips all over the world, Fig.11. During the trial period it has sailed in and around Holland, and visited the Canary Islands, Caribbean, North America and the Mediterranean during a 2-year world tour. As such, it has encountered a wide variety of conditions. Two panels have been installed on this ship in a side-by-side configuration, again with the tiles placed on top of their power transmitter coils.

(d) shows the results from an underwater inspection, performed by ROV; the vessel has not been back in drydock since the installation of the panels, so this is the only way to obtain results. A number of observations can be made. Despite being at almost double the specified lifetime of the LEDs, most of them still work fine; the panel is almost spotless for most of the surface area. However, along the edge the amount of UVC light has reduced to the point of being insufficient. This is as expected, as the typical failure mode of LED after their designed lifetime is a gradual decrease of light output. In a few other spots on the panel, clear signs of fouling are visible. In these spots, an LED has failed completely. Again, this is to be expected well after the LEDs lifetime. A next generation panel, with LEDs that have a 5+ year life expectancy, is expected to solve this completely.
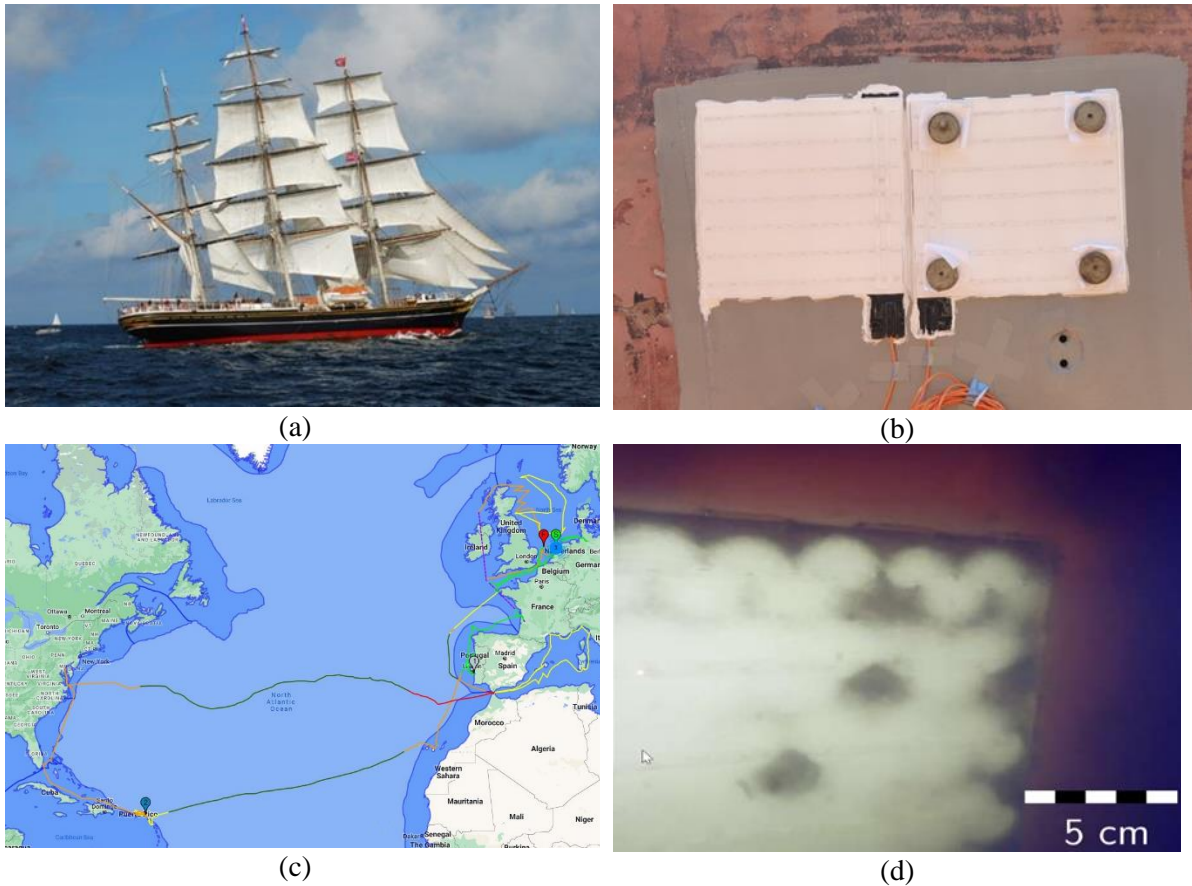
Fig.7: The clipper (a) with 2 newly installed panels (b). Sailing details during the trial period (c). (d) Fouling results after almost 2 years in the water.

5.3. LNG Carrier

The largest vessel to have tiles installed is a commercially owned and operated LNG carrier, onto which two panels were installed. The carrier has been sailing its normal high activity and high-speed schedule all over the world; and at the time of writing, still is in the water.

Fig.8: Tile installation on LNG carrier (left), panel performance after 12 months (right)

Fig.12 (right) shows the results after 12 months in water. Both panels are virtually spotless; the red LEDs indicate minor variations in local voltages; this is used for monitoring the electrical performance.

6. Conclusions and outlook

In this paper, we have presented the details of our 4th generation panel and the results of the tests that

have been done with this design. We have shown that standard production technologies, such as injection molding and standard components on electrical PCBs can be used to manufacture tiles. This allows for cheaper production and more robust tiles.

A close cooperation with suppliers gives us the needed performance for prolonged operations. Regardless of the location – wharf side, small vessel in regional waters or sailing the Pacific and Atlantic Ocean – the results are similar: as long as light is emitted by the LEDs, the surface of the panels stays perfectly clean from biofouling. The robustness of the design is sufficient – no noticeable damage was observed during the tests - and the electrical operation is quite stable.

The various tests ran for considerably longer time than the specified lifetime of the LEDs; only small reductions in light output were seen, matching the results on the panels. In other words, the tiles stay clean except for the expected issues related to lifetime of the LEDs. Substantial technological improvements from the LED manufactures by today's standards already allow lifetimes of up to 50.000 hours; the next generation of panels is expected to reach a 5 year 'perfectly clean' output. With further improvements in optics, LED technology, and material choices, 10 years of lifetime seems quite feasible.

Simultaneously to the tests with active tiles, several other tests have been performed on various aspects. These include the adhesion to the hull, the mechanical strength of the surface, and the exact electrical driving schemes of the wireless power supply to the tiles. Lessons learned from these experiments will be incorporated into the next generation.

In the next steps, which are already underway, we plan on scaling up even further. AkzoNobel and Philips have teamed up with a major shipbuilding group, to make the next step. An area of about 2 orders of magnitude larger – several tens of square meters – will be equipped with RunWell tiles, on a ship in active duty operation. The system will be fully integrated with the ship's systems and is planned to operate for 5 years continuously. Technical improvements will include new LEDs with a much longer lifetime, an optical design that is adapted to also keep the very edge of a panel clean, and a more robust electronic design and operation. Simultaneously, a new production facility is set up to manufacture panels in much larger amounts, at a lower cost and higher throughput speed.

Acknowledgements

References

JONGERIUS, M. (2018), UVC Anti-Fouling Solution: Device Design Simulation and Experimental Verification, 19th Int. Conf. Marine Corrosion and Fouling, Melbourne, http://f.scievent.com/icmcf/19th_ICMCF/Abstracts%20ICMCF%202018.pdf

SALTERS, B. (2014), *Prevention of Bio-Fouling by Using UV-Light Emission Outwards from the Ship Hull*, 17th Int. Conf. Marine Corrosion and Fouling, Singapore, http://f.scievent.com/icmcf/17th_ICMCF/17thICMCF.pdf

SALTERS, B. (2016), *Progress in Phillips Runwell UV-based antifouling technology*, 18th Int. Conf. Marine Corrosion and Fouling, Toulon, http://f.scievent.com/icmcf/18th_ICMCF/20160619-Congess%20Book%2018thICMCF-Toulon.pdf

SALTERS, B.; PIOLA, R. (2017), *UVC Light for Antifouling*, Marine Techn. Society J. 51/2, pp.59-70

Clean Power for the Maritime World

Lars Ravens, eCap Marine, Hamburg/Germany, lra@ecap-marine.com
Frederike Engels, eCap Marine, Hamburg/Germany, fen@ecap-marine.com

Abstract

Clean power generation is one of the biggest challenges for our maritime industry to achieve international agreements and legislations to minimise carbon dioxide emissions in the coming years, thus contribute its share to climate protection. To this end, the shipping industry started seriously considering technical solutions which so far have only been applied on a small scale or on land, extrapolating them to required scale. Whether it is the application of hydrogen, synthetic fuels and such into combustion engines, fuel cells or other energy converters - these alternatives to the conventional solutions so far do not necessarily mean additional challenges. They also open up prospects which were undiscovered previously or not considered interesting, ensure that shipping remains as the most efficient and sustainable solution for worldwide freight transport. This paper deals with the introduction to the most promising alternative fuels nowadays and their possible implementation as power generation systems on board of a 1.4 MW inland water vessel.

1. Introduction

In the ancient marine power supply, for a long period of time, only emission-free energy sources had been used. The earliest evidence of ships was found in Egypt during the 4th millennium BC, *Vance (2022)*. These boats were commonly equipped with sails as well as oars. As the manoeuvring technologies of ships developed, oarsmen are not needed anymore, the traditional sea ships hence evolved. Sailing was the only way of shipping until late 18th century, where the first steamboat was developed in America, *Vance (2022)*. Because of the steam engines poor efficiency that ranges only between 10%-20%, the combustion engine with a better efficiency around 30% was established in the early 1930s, *Vance (2022)*. The emissions were also consequentially reduced by this form of power generation: For the steam engines, 1 kg of coal results in 7.348 kg CO_2 according to its chemical reaction with oxygen (O_2). A conventional combustion of MGO which is being used in shipping nowadays emits approximately 3.3 kg CO_2 per 1 kg of fuel.

In current times of combating climate change, there is an increasing environmental awareness of the 21st century that climate change is greatly caused by human behaviour and the use of fossil fuels for all kinds of industries. A fundamental rethinking of energy sources has to takes place. The UN strives with stricter target setting for climate goals and the IMO adapted its goals to rapidly reduce the total annual Greenhouse gases (GHG) emissions from international shipping via reducing the total annual GHG emissions to at least 50% by 2050 compared to 2008. Possible measures could be speed limitations, or the implementation of new fuels such as biofuels. The IMO encourages also R&D to publish further in-depth studies regarding GHG emissions and to optimize the logistic chain, *IMO (2018)*.

Clean Power for the maritime world needs to be implemented in the shipping industry as fast as possible. Currently available possibilities are rather limited and costly, which brings all parties of the industry into rethinking, to develop alternative and suitable solutions. Only if all suppliers, shipowners, yards, and universities work together, can new technologies be developed and implemented sooner. Nowadays, most people in the maritime world are stuck to the combustion engine, as this energy converter is the most common and reliable option. Fuel cells and batteries in combination with electric motors start a new era of maritime power generation. As also hybrid concepts are further researched and developed in the maritime world and electric motors have a good efficiency of close to 100%, the future of most ships will be the power provision by electric motors. In basic, fuels are a form of energy storage converted on board with the use of a power generator (fuel cells or combustion engine) to electricity, that than will drive the electric motor. In future, the ships will be driven more often by such motors because the ship owner gains a lot more flexibility in the choice of the power generation source.

Consequently, the question that all ship owners need to answer is: Which energy storage will be the most efficient choice to drive the electric motor?

Batteries are already well-developed, enabling energy storage on board of ships and able to be charged from onshore electricity. As electricity is also produced by windmills, solar, coal power, nuclear power, etc., battery systems for storing electricity are quite sophisticated. This paper will relate to raw resources (fuels) used for power generation on ships, as well as investigate into the use of different fuels as alternatives to MGO. The objective of this paper is to evaluate and rank those alternative fuels by taking below aspects into account:

- Sustainability
- Storage possibilities
- Handling on board
- Infrastructure
- Availability
- Efficiency
- Well-To-Wheel emissions

This paper covers the alternative fuels hydrogen, ammonia, methanol, LNG, and biofuels. It describes then a case study, followed by an outlook.

2. Alternative Fuels

Looking up the definition in the encyclopaedia, the term "alternative fuels" considers all fuels except the recognized traditional petroleum fuels. In the shipping industry, the most commonly used fuel is heavy fuel oil (HFO), which is followed by marine diesel oil (MDO) and marine gas oil (MGO). In 2020 the IMO limited the Sulphur emissions to 0.5%, which means that marine fuels (HFO, MDO, MGO) must meet the sulphur level to be compliant or the vessel must use an exhaust gas aftertreatment system, *Senmatic (2022)*.

"Alternative fuels" are all liquid or gaseous substances that can be converted to energy by using power generators, except for the previously mentioned fossil fuels. The available power generators on the market with the best efficiency are fuel cells and internal combustion engines (ICEs). Fuel cells are commonly driven by hydrogen; direct methanol fuel cells can work also with methanol. Furthermore, everything that can be ignited, also can be burned inside a combustion engine. However, this is hard to reach in practice, as the combustion engine needs to be adjusted to the respective fuel. The combustion engines developed so far can burn LNG, biofuels, methanol, and hydrogen. Batteries as another form of alternative power supply can be used for energy storage. Another example, methanol and ammonia that can be reformed to hydrogen. Hydrogen then again can be used in the fuel cell or combustion engine to generate power. Alternative fuels can be flexibly used for any kind of power generation accordingly. For this paper, the previously mentioned five alternative fuels hydrogen, ammonia, methanol, LNG, and biofuels are introduced and compared in this chapter. These are already being considered as alternative fuels in the maritime world. Also, the availability and existing infrastructure of these fuels are already or expected to be soon in place.

2.1. Properties

The alternative fuels are shortly introduced in respect to their availability, infrastructure, handling, and production procedure.

2.1.1. Hydrogen

Hydrogen is in general a gaseous substance with the chemical formula H_2. It can be liquified after cooling down to -253°C, but the storage and transport of the liquid hydrogen involves significant

challenges. Nowadays, gaseous hydrogen is being applied in trucks, busses, and trains as an established system with the usage of fuel cells. Hydrogen filling stations are widely spread across the streets, and more are to come. The volumetric calorific value is low, which means that bigger tanks are needed for the equivalent driving range of a ship.

Table I: Properties of hydrogen

Calorific value	33.33	kWh/kg
Density (gaseous)	0.02	kg/lt
Calorific value per volume	**0.80**	**kWh/lt**
Approx. costs per kg (08/2022)	6.50	€

A big advantage of hydrogen is the emission-free chemical reaction inside fuel cells only adding oxygen with the sole by-product being water. Additionally, fuel cells have the charming property of really low maintenance requirements compared to combustion engines. They also do not require any lubricating oil. The efficiency of fuel cells is between 50% and 55%, much higher than in combustion engines.

Hydrogen can be produced in many ways. As mentioned before, ammonia and methanol can be used in reformers to produce hydrogen. Currently, hydrogen is mostly produced as "grey hydrogen". For the industry, hydrogen is mainly reformed from fossil fuels or biomass. It can also be by-product of oil refining processes. These processes naturally emit a lot of emissions, especially CO_2 emissions. "Blue hydrogen" is a new development that uses Carbon Capture and Storage (CCS), where methane is reformed from natural gas. The by-product of this reaction, carbon, is then captured and stored, *Köllner (2021)*. On the contrary, "green hydrogen" is only generated by using electrolysis with electricity that is converted from sustainable energy source, such as wind, solar, or hydropower energy. Using hydrogen as intermediate energy storage reduces the efficiency compared to the direct use of electricity.

The biggest advantage of hydrogen lies in "green hydrogen" which features the lowest CO_2 emissions and can be considered as sustainable and as emission-free. Hydrogen due to its high flammability will be handled as a high-risk fuel, and experience in handling hydrogen on ships is still lacking. So far, only few regulations in the maritime industry have been published. Those now are being used to certify hydrogen projects based on an IMO guideline, as no official rules have been published yet. Hydrogen is still expensive, because the infrastructure for the use as maritime fuel has not been well established. No hydrogen bunker ships have been built yet, just swappable hydrogen carriers, like containers, are used.

2.1.2. Ammonia

Liquid at 8 bar, ammonia (NH_3) can easily be stored, and the infrastructure is already well established, because ammonia has been widely used for producing fertilizers. With an annual production output rate of 200 million tons, ammonia is one of the top three most-produced chemicals in the world, *Engel (2021)*. The shipping industry is also already familiar with the use of ammonia on ships, transported as cargo and used as refrigerant on board of gas tankers. Ammonia is commonly produced via a catalytic reaction of hydrogen and nitrogen, called the "Haber-Bosch process", *Fricke (2018)*. The initial products of this reaction facilitate producing "green ammonia" by using e.g., wind or solar power plants.

Table II: Properties of ammonia

Calorific value	5.20	kWh/kg
Density (gaseous)	0.68	kg/lt
Calorific value per volume	**3.54**	**kWh/lt**
Approx. costs per kg (08/2022)	0.80	€

Ammonia has approximately 4 times higher volumetric energy density than hydrogen and consequently is highly suitable as an energy storage. Hydrogen can be generated by the usage of reformers and can then be used in fuel cells directly on board of ships, which enables to increase the capacity of hydrogen

immensely, *Engel (2021)*. The combustion inside internal combustion engines was already invented in 1872. Related research still continues, and in the near future both ammonia-powered fuel cells and combustion engines should be commercially available, *Fricke (2018)*.

In the reaction process, ammonia emits no CO_2 and when produced as "green ammonia", this is a renewable resource for nitrogen, water, and oxygen, which can be taken directly from the environment. The drawback of using ammonia is the by-production of the highly effective GHG Nitrous Oxide (N_2O) and nitrogen oxides (NO_x) during the combustion. Thus combustion in a conventional engine requires exhaust gas cleaning. The same issue occurs in the use of fuel cells, where reformers or crackers retransform the ammonia to hydrogen, but the amount of Nitrous Oxide is much lower, *Engel (2021)*. So far, no regulations or guidelines for the use of ammonia by the IMO or any classification society have been published. However, DNV highly recommends future ships to be powered by ammonia by 2050, *DNV (2021)*. Ammonia is also being classified as toxic substance, which might complicate the handling of this fuel and on-board safety regulations. The use of ammonia on board with fuel cells is still subject to research and thus quite expensive, and no reformers have been approved yet for the maritime market.

2.1.3. Methanol

Liquid alkanol methanol (CH_3OH) has been produced mostly from natural gas, but in the future may be produced by gasification of organic materials, synthesis gas, and by a conventional methanol synthesis. This alternative fuel is easy to handle and involves well-established technology, which also eases the classification process. DNV sees the use of methanol in ICEs as the most mature option, being already in commercial use, *DNV (2021)*. Methanol, like ammonia, is a good alternative fuel to store hydrogen, for its high energy density compared to hydrogen and its good storability and infrastructure.

Table III: Properties of methanol

Calorific value	5.47	kWh/kg
Density (gaseous)	0.79	kg/lt
Calorific value per volume	**4.32**	**kWh/lt**
Approx. costs per kg (08/2022)	0.08	€

The biggest drawback of methanol is the emission of CO_2, because it contains carbon. This carbon will always be emitted, no matter which source for production of methanol is chosen. If in the process of methanol production, carbon dioxide from the environment will be used, this will not make this fuel emission-free, but at least climate-neutral for the reaction during the production, *Jendrischik (2020)*. Nonetheless, this alternative fuel has a lot of potential, for its wide range of possible applications in direct methanol fuel cells, fuel cells in combination with reformers, as well as ICEs.

2.1.4. LNG

Liquefied natural gas (LNG) is commonly used as an alternative fuel in the shipping industry, featuring lower emissions compared to the conventional marine fuels. Especially sulphur oxides and particle emissions are close to zero and nitrogen oxide emissions are reduced by 90%, whilst CO_2 emissions are claimed to be reduced by up to 40%, *Podbregar (2022)*. This alternative fuel is thus not emission-free, but already well established in the maritime industry. Class regulations are available and the infrastructure for this type of fuel is well developed. In terms of technology and regulations, LNG has paved the road towards other alternative fuels.

Table IV: Numerical properties of LNG

Calorific value	13.70	kWh/kg
Density (gaseous)	0.45	kg/lt
Calorific value per volume	**6.17**	**kWh/lt**
Approx. costs per kg (08/2022)	3.16	€

LNG must be stored below -161°C. This makes the storage is complicated, expensive, and space consuming. Large fuel tanks are required on-board of ships, reducing cargo space. LNG has also a concern regarding methane slip, which leads to a GHG emission harmful for climate, *Podbregar (2022)*. LNG is overall more climate-friendly than conventional marine fuels, but compared to the previous three fuels, it is more harmful for the environment.

Overall, LNG has nearly the same efficiency to power ICE on ships and in trucks, even slightly better than the conventional ICE. LNG is a fossil fuel, but also can be produced from biogas from waste streams and mud, which reduces the CO_2 footprint significantly, or as synthetic natural gas by methanisation. In this process, captured carbon and green hydrogen are used to produce synthetic methane with similar calorific values like fossil LNG.

2.1.5. Biofuels

The general idea of using biofuels is to replace the common marine fuels by biological alternatives that have similar properties. The formerly used ICEs and fuel tanks can stay in place onboard, and the infrastructure relies on a well-proven system. A charming aspect of biofuel is that it is produced by renewable resources and can be implemented into a fully prepared system of power generation and infrastructure. Biofuels have similar energy density to common fuels. In comparison to all other previously mentioned fuels, biofuel has the highest energy density.

Table V: Numerical properties of biofuels

Calorific value	11.90	kWh/kg
Density (gaseous)	0.89	kg/lt
Calorific value per volume	**10.59**	**kWh/lt**
Approx. costs per kg (08/2022)	1.50	€

Pure biofuels cannot be used in conventional ICEs. Different ignition and injection systems need to be installed, *Baquero (2011)*. So far, only fuel mixtures of biofuel and conventional fuels are used in cars. New ICEs using pure biofuel need to be developed. An advantage of biofuel is that it enables the emission reduction of conventional fuels by up to 60%, *Baquero (2011)*. Retrofit solutions for ships could be easily implemented onboard ships, because of its similarity to common marine fuels and the required infrastructure. For biofuels on ships, certification will be uncomplicated, as rules from handling common fuels can be simply adapted.

2.2. Well-To-Wake comparison

From the economic and ecological point of view, the interesting part in this comparison of possible alternative fuels is the analysis of the effort to produce the fuels, in contrast to the output power. Therefore, the Well-To-Wake numbers considering CO_2 emissions and energy consumption are interpreted in this chapter, Fig.1.

The Well-To-Wake (WTW) climate friendliness of the considered alternatives can vary a lot, Fig.1. High energy consumption producing e.g. "green hydrogen" can be considered as poor in the interest of energy wasting. But if the energy is produced by completely renewable primary energy sources, this waste can be accepted to reduce emissions.

The Well-to-Tank (WTT) numbers, Table VI, show satisfactory CO_2 emission values for blue and green hydrogen as well as ammonia and biofuels. These could be the most promising alternatives relieving the climate change. Considering the WTT energy comparison, blue hydrogen, LNG, and biofuels can be the best alternatives to the conventional marine fuels.
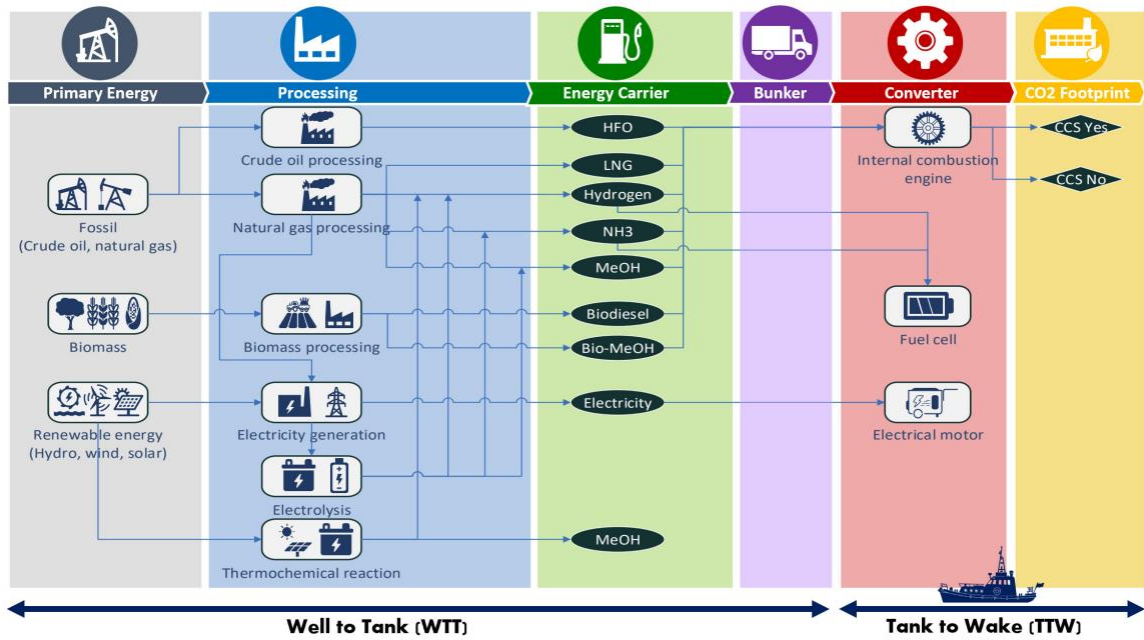
Fig.1: Well-To-Wake (WTW) graphic about fuel pathways. (MeOH: Methanol, CCS: Carbon Capture and Storage, HFO: Heavy Fuel Oil), *Law (2021)*

Table VI: Well-To-Tank (WTT) Analyses (Displayed numbers are partly factual and partly assumed but give a good overview of the magnitude, mostly based on *Law (2021)*; TTW: Tank-To-Wake)

	Convent. Diesel	Hydrogen			Ammonia		Methanol	LNG	Biofuels
		Blue	Grey	Green	Green	Grey			
CO2 emissions [kg CO$_2$/kg fuel]									
WTT	0.7	0.1	10.1	0.1	0.1	1.5	1.7	1.4	0.3
TTW	3.4	0.0	0.0	0.0	0.0	0.0	1.4	1.4	1.2
Sum	**4.3**	**0.1**	**10.1**	**0.1**	**0.1**	**1.5**	**3.1**	**2.8**	**1.5**
Relative Energy									
WTT Energy compared to Diesel (=1.0)	1.0	1.1	42.0	26.8	37.1	8.3	32.5	1.2	0.8
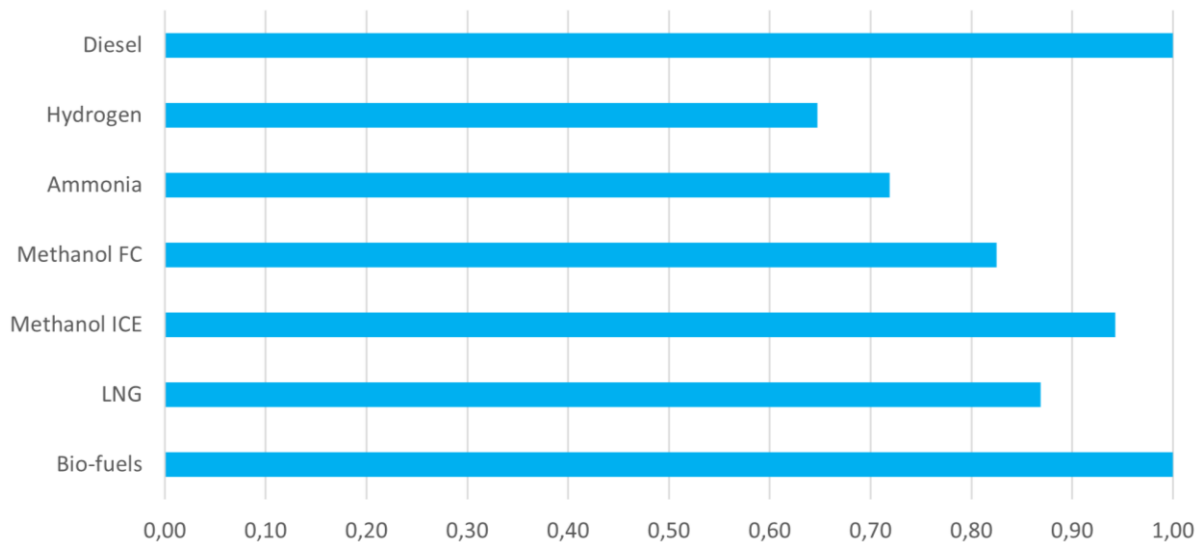
Fig.2: Tank-To-Wheel energy consumption of the alternative fuels to Diesel (=1,00)

The fuel consumption of all alternative fuels can be well compared by calculating the amount of energy [in kWh] required for the specific power generation system to fulfil the power delivery requirement. Fig.2 thus demonstrates a better picture of the efficiency for every alternative being considered, and that can also be referred to as TTW energy comparison.

The following chapter will analyse the fuel consumption (TTW) of an example vessel to set these numbers in relation via the calculation of an example vessel.

3. Case study: Numerical comparison on the retrofit of a 1.4 MW inland water vessel

This chapter shows the analysis of possible retrofit solutions for an inland water vessel with a maximum power of 1.4 MW and a daily energy consumption of 10 MWh. E-Cap Marine conducted a feasibility study for this ship and consequently a detailed power and energy consumption study, used as basis for the following calculations.
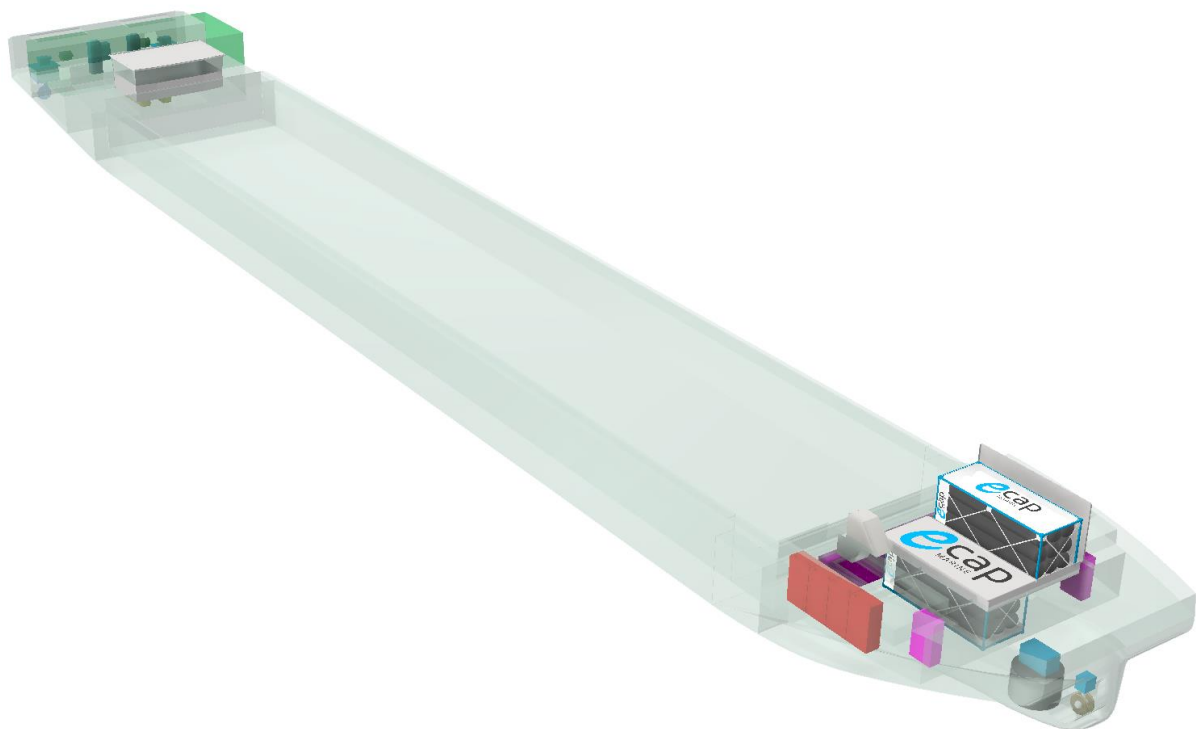
Fig.3: Example inland water vessel with 97.5 m and a capacity of 4000 t copper ore

Important for the comparison of the fuels are the required space and weight compared to Diesel fuel, Table VII. Therefore, the required fuel for one day in kilograms and in litres is compared to the conventional Diesel consumption. Hydrogen is by far the lightest fuel in the comparison, because of its gaseous state of aggregation, while Diesel has the least volume of tank that is needed. Similarly good are only biofuels, which are also a good option because the former Diesel tanks do not need to be replaced. In terms of fuel costs, methanol is the best option due to its high availability.

Additionally, annual costs of CO_2 certificates, that need to be bought in Europe, were added, *Energy Charts (2022).* The costs are increasing rapidly; in 2021 it was only 50€ per ton CO_2 but in 2022 the price nearly doubled. Therefore, the hydrogen variant is the least expensive one. The origin of hydrogen in this context and its previously acquired carbon footprint in production, storage and transport does not matter for the CO_2 certificates to be paid by the ship owner; it is only obligatory to pay for the CO_2 emissions emitted by the ship.

In general, all mentioned fuels would reduce the CO_2 emissions of the considered ship drastically.

Table VII: Case study calculations for alternative fuels ((R: Reformer, FC: Fuel cell, DMFC: Direct Methanol Fuel Cell, Conv.: Conventional); best alternative fuel for the comparing aspect is marked **bold,** per year calculations in italic letters)

	Diesel	Hydrogen	Ammonia	Methanol		LNG	Biofuels
Concept of power generation	ICE	FC	R + FC	R + FC / DMFC	ICE	ICE	ICE
Tanks	Conv.	580 bar gas tank	8 bar tank	Conv.		Cool Tank (-162°C)	Conv.
Efficiency	0.33	**0.51**	0.46	0.40	0.35	0.38	0.33
Required fuel for one day [kg] 10 MWh	*2.546*	***588***	*3.486*	*4.569*	*5.223*	*1.921*	*2.900*
Required fuel for one day [lt] 10 MWh	**1.273**	24.512	5.112	5.769	6.595	4.269	3.169
Required fuel for one year [t] 5000 MWh	*1273*	***294***	*1.743*	*2.284*	*2.612*	*960*	*1450*
Required fuel for one year [m³] 5000 MWh	**1.430**	12.256	2.556	2.884	3.296	2.134	1.585
Fuel costs per kg	1.20€	4.00€	0.80€	**0.40€**		3.16€	1.50€
Fuel costs per year	*1.5 m€*	*1.2 m€*	*1.4 m€*	***0.9 m€***	*1.0 m€*	*3.0 m€*	*2.2 m€*
CO_2 emission factor [kg CO_2/kg fuel]	3.37	**0**	**0**	1.38		1.37	1.35
CO_2 emissions per day [t]	8.583	**0**	**0**	6.282	7.208	2.630	3.910
CO_2 emissions per year [t]	*4292*	***0***	***0***	*3141*	*3590*	*1315*	*1955*
Costs CO_2 certificates GER per year (80€/t CO_2)	343000€	**0€**	**0€**	251000€	287000€	105000€	156000€
Energy consumption per day (TTW) [MWh]	30.303	**19.608**	**21.786**	25.000	28.571	26.316	30.303
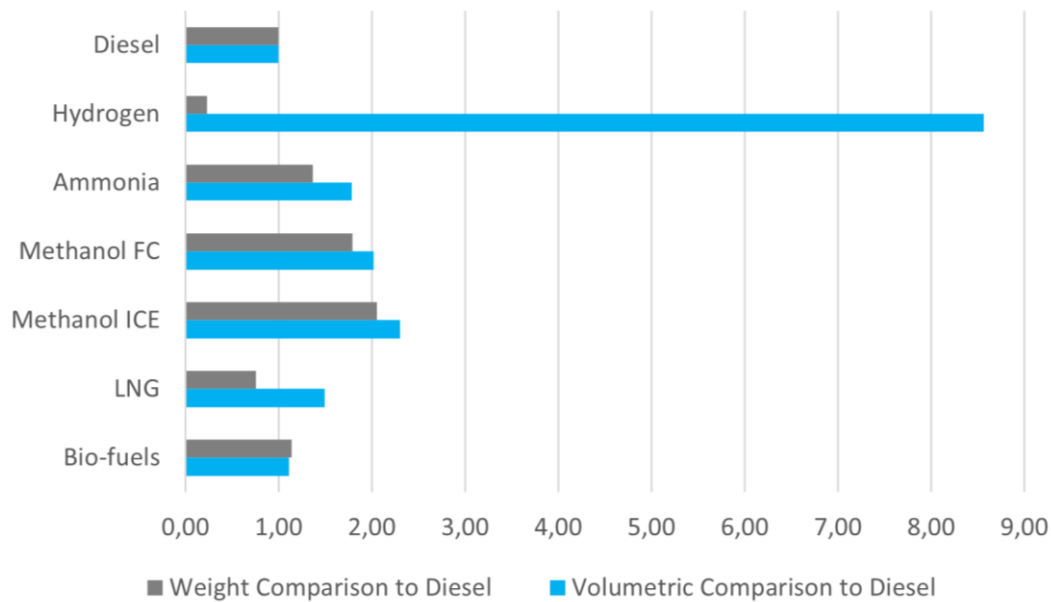
Fig.4: Weight and volume of the alternative fuels to Diesel (=1,00)
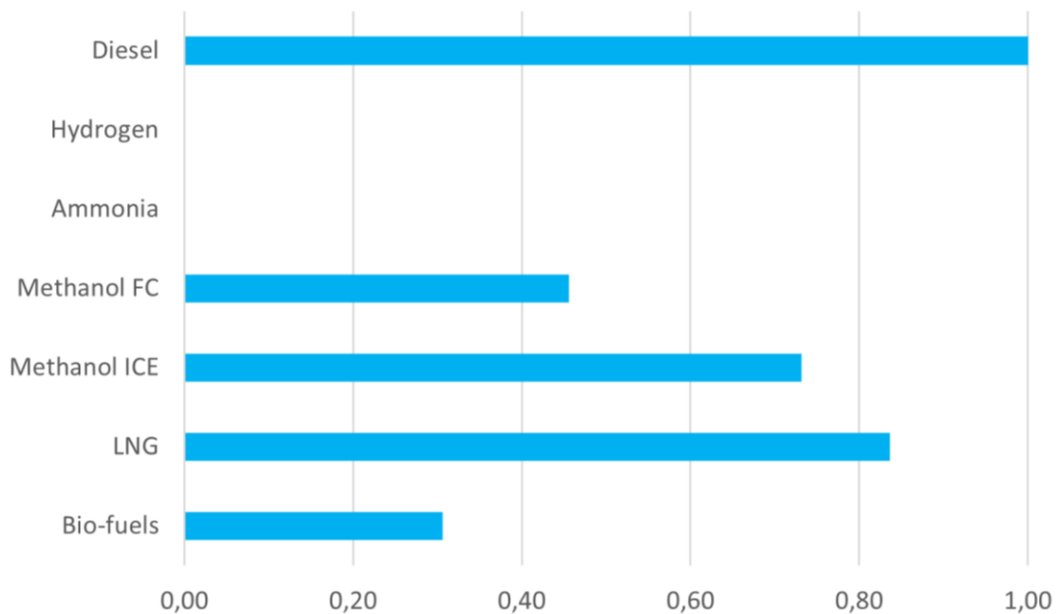
Fig.5: CO_2 emissions of the alternative fuels to Diesel (=1,00)

4. Summary

All alternative fuels have unique advantages and drawbacks compared to the conventional fossil fuels being so popular in shipping for more than 80 years. Alternative fuels have the big advantage to ensure a relatively high efficiency in the ICE while the tank volume is rather small. Considering the tank space requirement, biofuels can be the best option for retrofit solutions. The ICE, which formerly has been used with the marine fuel, needs to be replaced, but the ship and bunkering infrastructure generally remains the same.

LNG would be the best alternative to conventional marine fuels, if the local emissions shall be reduced. However, storage and transportation at -162°C can be a challenge. The tank volume of LNG is generally bigger, due to the cylindric form of the tanks and the cooling system surrounding it. Methane slip is a concern, too, as it may result in LNG being more harmful to climate than conventional fossil fuels.

Evidently, fuel cells driven with hydrogen can achieve locally zero emission. Hydrogen and ammonia are the best possible alternative fuel to avoid CO_2 emissions overall. Hydrogen has a low volumetric calorific value, which means that the tanks for the equivalent amount of fuel need to be much bigger. As hydrogen shall be stored highly compressed, the process of hydrogen fuelling and de-fuelling will be complicated. Also, the infrastructure on board and for bunkering is rarely installed yet and the regulations for hydrogen on board of vessels are still in draft stages. Ammonia faces similar issues, because not much infrastructure is established so far, but ammonia has a much broader availability. It also can be stored more easily, in liquid form at 8 bar. Ammonia and hydrogen can also be recognized as renewable fuels when production is from resources like wind or solar energy, which enables them to be the most environmental-friendly producible alternative fuels.

Methanol is an easy-to-handle fuel and maritime regulations for this have been already set up, as methanol is a common liquid to be carried by tankers or container ships. Methanol can both be used in ICE or fuel cells, even without a reformer by generating power via a methanol direct fuel cell. Methanol has higher space and weight demands for fuel storage than all other alternative fuels. To sum up, Methanol would be the least attractive alternative for the power generation in fuel cells, also due to its high CO_2 emissions in comparison to ammonia and hydrogen. For ICE, methanol can be a good option for the common ICEs, as the CO_2 emissions are quite low in comparison to LNG and conventional marine fuel. Research on methanol ICE is advanced and DNV foresees potential commercial application of methanol ICE already in 2023.
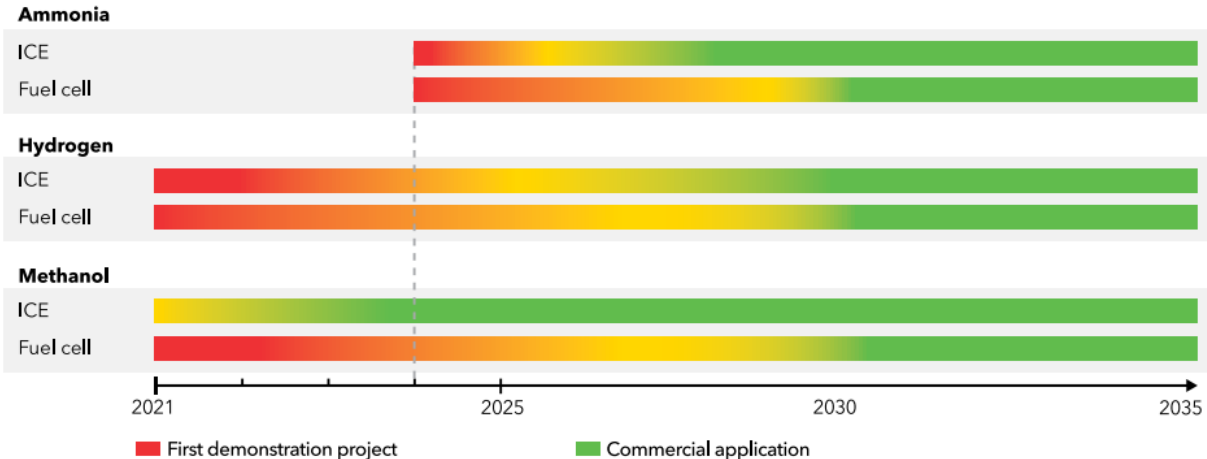
Fig.6: Maritime forecast of technology development, *DNV (2021)*

From the ecological point of view, hydrogen is the best option for emitting no emissions while still generating power for vessels. Ammonia is also promising, but the emission of the GHG Nitrous Oxide results in new climate issues. On the other hand, from the economical point of view, methanol and ammonia are currently by far the cheapest fuels, with yearly fuel costs in the case study even lower than the conventional fossil fuels. However, as CO_2 restrictions are getting stricter, CO_2 certificates will become much more expensive in the years to come.

Acknowledgements

References

BAQUERO, G.; ESTEBAN, B.; RIBA, J.; PUIG, R.; RIUS, A. (2011), *Use of Rapeseed Straight Vegetable Oil as Fuel Produced in Small-Scale Exploitations*, Biofuel's Engineering Process Technology, https://www.intechopen.com/chapters/17477

DNV (2021), *Maritime Forecast to 2050 - Energy Transition Outlook 2021*, DNV, Høvik

DNV (2020), *Ammonia as a marine fuel,* White Paper, DNV, Høvik

ENERGY CHARTS (2022), *Wöchentliche Börsenstrompreise in Deutschland in Woche 31 2022,* https://energy-charts.info/charts/price_average/chart.htm

ENGEL, K.M. (2021), *Ammoniak als Schiffstreibstoff – Unter grünem Dampf*, Spektrum, https://www.spektrum.de/news/ammoniak-als-schiffstreibstoff-unter-gruenem-volldampf/1856677

FRICKE, J. (2018), *Ammoniak – ein idealer Wasserstoff-Speicher - Eine interessante Alternative zum Elektroantrieb?*, Bayern innovativ, https://www.bayern-innovativ.de/de/suchergebnisse/seite/ammoniak-wasserstoffspeicher

IMO (2018), *Adoption of the initial IMO strategy on reduction of GHG emissions from ships and existing IMO activity related to reducing GHG emissions in the shipping sector*, https://unfccc.int/sites/default/files/resource/250_IMO%20submission_Talanoa%20Dialogue_April%202018.pdf

JENDRISCHIK, M. (2020), *Methanol: Energieträger für die dritte industrielle Revolution,* https://www.cleanthinking.de/methanol-energietraeger-fuer-die-dritte-industrielle-revolution/

KÖLLNER, C. (2021), *Woher kommt der Wasserstoff?,* Springer Professional, https://www.springerprofessional.de/betriebsstoffe/verfahrenstechnik/woher-kommt-der-wasserstoff-/17201618

LAW, L. C.; FOSCOLI, B.; MASTORAKOS, E.; EVANS, S. (2021), *A Comparison of Alternative Fuels for Shipping in Terms of Lifecycle Energy and Cost*, Energies 14, 8502, https://doi.org/10.3390/en14248502

PODBREGAR, N. (2022), *Wie „dreckig" ist LNG? - Treibhausgas-Bilanz von Pipelinegas und Flüssiggas im Vergleich,* Scinexx, https://www.scinexx.de/dossierartikel/wie-dreckig-ist-lng/

SENMATIC (2022), *The 5 most relevant marine fuel types,* https://www.senmatic.com/sensors/knowledge/the-5-most-relevant-marine-fuel-types#:~:text=Heavy%20Fuel%20Oil%20(often%20referred,oil%20or%20marine%20gas%20oil

VANCE, J.E. (2022), *History of ships*, Britannica, https://www.britannica.com/technology/ship/History-of-ships

WACHSMUTH, J.; OBERLE, S.; ZUBAIR, A.; KÖPPEL, W., *Wie klimafreundlich ist LNG? - Kurzstudie zur Bewertung der Vorkettenemissionen bei Nutzung von verflüssigtem Erdgas (LNG),* Fraunhofer ISI, https://www.isi.fraunhofer.de/content/dam/isi/dokumente/ccx/2019/2019-05-15_cc_21-2019_roadmap-gas_lng.pdf

Zero-Emission Small High-Speed Craft Conceptual Design using NSGA-II Algorithm for Galapagos Interisland Service

Ruben J. Paredes, **Andrea T. Gaona, Andres N. Toala, José R. Marin-Lopez**, ESPOL Polytechnic University, Guayaquil/Ecuador, [rparedes, atgaona, antoala, jrmarin]@espol.edu.ec
Raju Datla, Stevens Institute of Technology, Hoboken/USA, rdatla@stevens.edu
Joseph W. Pratt, Zero Emission Industries, Alameda/USA, joe@zeroei.com

Abstract

This work aims to assess at conceptual level the technical feasibility of a zero-emission fiberglass reinforced plastic high-speed boat design, with reduced vertical acceleration while also considering boat resistance for interisland service in Galapagos Archipelago. Design variables considered were length, beam, longitudinal position of the center of gravity, and deadrise angle. In addition, constraints considered were dynamic trim angle for porpoising, length-beam ratio, metacentric height, freeboard, and required area for passengers. A multi-objective optimization method was employed along with an open-source planing craft hydrodynamic evaluation framework. First, results show that a reduction in speed is required for existing boats to adopt zero-emission propulsion systems. Later, the impact of including these zero-emission propulsion systems on the main characteristics of the Pareto front solutions is assessed. Finally, a representative non-dominated solution is further evaluated in terms of its energy efficiency and sea performance.

1. Introduction

The development of Zero-Emission solutions in the maritime sector has been fostered by the ambitious GHG reduction goals introduced through mandatory regulations by the International Maritime Organization for all ships of 400 gross tonnage and above, *IMO (2018)*. These solutions use zero-emission propulsion system combining electrical engines with state-of-the-art technologies such as fuel cells, batteries, and supercapacitors in conjunction with the use of zero-carbon fuels such as hydrogen (H_2) and ammonia (NH_3) as main energy sources, *Reusser and Perez Osses (2021)*. In the last years, there have been several feasibility studies demonstrating the commercialization potential of only batteries and fuel cells with either liquid or gaseous hydrogen configurations. The main challenge to achieve a feasible implementation is to find a balance between energy storage requirement and weight availability on board for the propulsion system.

For large capacity vessels, the SF-BREEZE was the first project to demonstrate the technical feasibility of a zero-emission 150 pax commercial ferry that used a fuel cell and liquid hydrogen system to sail at 35 knots, *Pratt and Klebanoff (2016)*. The authors were able to i) reduce the energy consumption to 3110 kWh with a catamaran hull for a 24 nm route, ii) allocate enough fuel cells and hydrogen tanks on board, and iii) proposed to use an energy use index as a feasibility indicator. Afterwards, the same methodology was applied to develop five commercially relevant passenger vessels, *Pratt and Klebanoff (2018)*. In addition, the BB Green project designed a 70 pax boat that used an in-house battery based system using an air-supported monohull to use 400 kWh for a 14 nm route at 30 knots, *NN (2015)*. Recently, the Zero Emission Fast Ferry (ZEFF) project designed 35 knots ferries for three different routes departing from Trondelag, Norway using parametric models, *Fabricius (2019)*. The main dimensions were determined considering two alternatives for their propulsion system: batteries or liquid hydrogen. The ferries required 360, 1370, and 8640 kWh using a hydrophilic trimaran hull for 8.3, 27, and 95 nm routes respectively. In all these examples, the vessels have a per-passenger mile vessel energy use index below 0.75 kWh/pax*nm requiring up to ~50% of its displacement to accommodate the propulsion system.

For small capacity vessels, there are few successful zero-emission implementations for high-speed crafts. For example, the Candela initiative after several iterations was able to design a 30 pax foiled monohull propelled by an only battery system, that can sail at 20 knots requiring 250 kWh with 50 nm

autonomy, *Springer (2021)*. Recently, the Chase Zero prototype, using a fuel cell and gas hydrogen system, performed sea trials that demonstrate that the 6 pax foiled catamaran boat can sail at 30 knots requiring ~1070 kWh with 180 nm autonomy, *NN (2022)*. Although both projects considered foils to reduce the energy requirements, the maximum energy use index still increased to 1.0 kWh/pax*nm and required up to ~70% of the vessel's displacement to accommodate the propulsion system. To the best of authors knowledge, there is not a feasible zero emission small planing monohull proposal so far.

Hence, this work aims to assess at conceptual level the technical feasibility of a zero-emission fiberglass reinforced plastic high-speed boat design, with reduced vertical acceleration while also considering boat resistance for interisland service in Galapagos Archipelago. In a previous work, *Marin Lopez et al. (2021)* applied an optimization process with a weighted combination of drag force and vertical acceleration based on feasible directions approach, *Vanderplaats (2007)*, to calculate main characteristics of these small craft using gasoil outboard engines. Results showed that it was possible to reduce the energy requirements by 4% with an 10% increment in displacement, that would improve the vessel's performance in 1.0-meter waves. However, this optimization algorithm required several combinations of the design variables initial values to check the optimization procedure convergency. *Marin-Lopez et al. (2022)* introduced the effect of flaps to improve the hydrodynamics efficiency of this hull in the multi-objective optimization using a Genetic algorithm to find simultaneously a family of possible solutions, avoiding the need of multiple initial trials for the design variables. The authors demonstrated that it is possible to further reduce the energy requirements by 7% with an 16% increment in displacement. Both works demonstrate that it is possible to reduce the energy use index and to increase the vessel's displacement for planing monohulls, therefore improving the feasibility likelihood of a design using a zero-emission propulsion system.

To achieve the zero-emission goal, battery and hydrogen-based propulsion systems are included in the parametric model used to assess each potential candidate in the optimization procedure. To estimate the Pareto front, the NSGA-II (Non-Dominated Sorting Genetic Algorithm) optimization algorithm, *Deb et al. (2002)*, is chosen considering the complex relations and number of design variables. First, an optimized outboard engine design for service in Galapagos is considered to fit three zero-emission propulsion system alternatives. Later, the impact of including both zero-emission propulsion systems on the main characteristics of the solutions that form the Pareto front is assessed. Finally, a non-dominated solution for each feasible propulsion system is further evaluated in terms of its energy efficiency and sea performance.

2. Methodology

In this work, the Non-dominated Sorting Genetic Algorithm (NSGA-II) is applied for the conceptual design of a planing boat including three zero emission propulsion systems: i) battery only, ii) Liquid H2, and iii) Gas H2, as a multi-objective optimization. This algorithm was proposed by *Deb et al. (2002)* introducing the concept of dominated and non-dominated solutions. The procedure is implemented in a Python script that is linked to the open-source packages "OpenPlaning" developed by *Castro Feliciano (2021)* which implements Savitsky´s method, and to "Pymoo" by *Blank and Deb (2020)*.

The objective functions are total resistance in waves and vertical acceleration of CG. For the resistance, the classical Savitsky formulation is applied, *Savitsky (1964)*, considering the increments due to navigation in waves, *Savitsky and Brown (1976)*, and whisper spray, *Perez and Alonso (2014)*. The vertical acceleration of CG of the boat is related to the motion sickness index, MSI, in the ISO 2631 standard, *ISO (2021)*, and it is used here to judge the improvement in dynamic response in waves. For the vertical acceleration formulations from *Savitsky and Brown (1976)*, based on *Fridsma (1971)* experiments are applied. For the optimization it is applied the NSGA-II algorithm to find simultaneously a family of possible solutions, avoiding the need of multiple initial trials for the design variables.

To achieve the zero-emission goal, battery and hydrogen-based propulsion systems are included in the parametric model used to assess each potential candidate in the optimization procedure. For the hydro-

gen-based or battery-only system, its weight and volume are estimated considering corresponding data-base of commercial proton exchange membrane fuel cell (PEMFC) or marine batteries systems of low C-rate and high C-rate provided by Sandia Laboratories, *Minnehan and Pratt (2017)*.

In the following sections, an optimized outboard engine design for service in Galapagos is considered to fit zero-emission propulsion systems. Later, the impact of including both zero-emission propulsion systems on the main characteristics of the solutions that form the Pareto front is assessed. Finally, a non-dominated solution for each feasible propulsion system is further evaluated in terms of its energy efficiency and sea performance.

2.1. Objective function, design variables and constraints

For the objective functions, resistance, $f_1(x)$, and vertical acceleration of CG, $f_2(x)$, are normalized using f_{1o} and f_{2o} as reference values. The reference values f_{1o} and f_{2o} are estimated considering the main characteristics of boat A as seen on Table III, which is currently operating in Galapagos. The resulting objective function is:

$$Minimize \ \left(\frac{f_1(x)}{f_{1o}}; \frac{f_2(x)}{f_{2o}}\right) \tag{1}$$

Resistance is calculated with semi-empirical formulation developed by *Savitsky (1964)*, which considers frictional, and pressure components. Increment in resistance due to navigation in waves is applied with formulations from *Savitsky and Brown (1976)*, and the contribution of whisper spray is considered with results from *Savitsky et al. (2007)*:

$$f_1(x) = R_{fric} + R_{air} + R_{press} + R_{waves} + R_{wspray} \tag{2}$$

Table I: Design variables and ranges of variation

Variable	Range	Units
Length overall	$9.5 < LOA < 15.0$ (B) $12.0 < LOA < 20.0$ (H2)	meter
Hull beam	$3.2 < B < 5.0$ (Batt) $3.2 < B < 7.0$ (H2)	meter
LCG/LOA	$0.3 < LCG < 0.5$	%LOA
Deadrise angle	$10 < \beta < 30$	deg.

Table II: Constraints and limit values

Parameter	Range	Units	Reference
Possibility of por-poising	$2 < t < t_{Porpoising}$	deg.	*Savitsky (1964)*
Keel wetted length	$L_k < 0.9 * L_{OA}$	m	*Faltinsen (2006)*
Ratio L/B	$3.0 < L/B < 5.0$	-	*Savitsky & Koelbel (1993)*
Vertical position of CG	$0.4 < KG < KG_{DynMom}$	m	Eq (31) *Lewandowski (1998)*
Freeboard	$F_b > F_{b\_min}$	m	Table H.3 *GL (2012)*
Min area for passengers	$A_p > 21.11$	m²	0.56 m² per pax (0.75x0.75) *Marin-Lopez (2007)*
Hull loading	$\frac{A_p}{\nabla^{2/3}} > 5.8$	--	*Blount & Codega (1992)*
Dynamic transverse instability	$\frac{CA_P - LCG}{L_P} > 0.03$	--	

To estimate the vertical acceleration of the boat, the *Savitsky and Koelbel (1993)* formulation is applied. It includes geometric variables of the planning hull, design velocity of 28 knots, trim angle, and significant wave height of 1 m for Sea State 3. The dynamic trim angle results from the calculation of boat resistance with the equilibrium of forces and moments.

The following parameters are taken as design variables: length overall, beam, longitudinal position of CG measured from transom, and deadrise angle. In Table I ranges for each design variable for battery-only and hydrogen-based systems are presented.

For the constraints, aspects like geometry of the hull, static stability, possibility of porpoising, minimum area for passengers, and the influence of forward LCG position on dynamic stability are considered. For the freeboard and required area for passengers, values from actual boats operating in that service are considered; for the maximum value of KG, KG_{DynMom}, to be stabilizing for dynamic transverse reference, *Lewandowski (2004),* is employed. All constraints are implemented as inequalities, see Table II.

2.2. Planing Craft Parametric model

To complete the conceptual design based on the design variables, the following relationships were developed using data from actual boats built with fiberglass reinforced plastic including wooden cores currently operating in Galapagos, *Rodas (2017).* The parametric model implemented to evaluate the planing craft performance is organized in the subsequent modules:

a) Geometric module: From the hull beam B, the depth D is estimated as: $D = (B/2.25), [m]$. The freeboard is estimated $fb = 0.15 + 0.25 * B$, *GL (2019)*. Then, draft T is calculated as the difference between D and fb. Finally, volume, block coefficient, and total weight W_{total} is defined considering the deadrise angle.

Once the beam of the hull, B, and the deadrise angle β have been set up in the optimization scheme, the beam at chine, B_c, is estimated following the geometry of the hull section. For this calculation, the angle of the side of the hull with the vertical has been taken as 15°, following boats currently in operation, Fig.1.
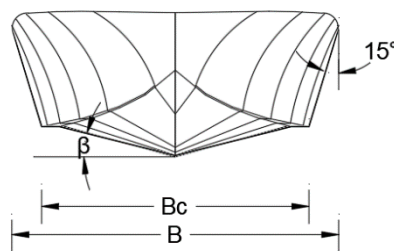
Fig.1: Geometric relationships of the midship section

b) Weight module: Weight of the hull, W_{hull}, is estimated considering the formulation proposed by *Grubisic (2008)* and superstructure is estimated considering a cubic number relationship $W_{sup} = (5.55 * LOA * B)9.8, [N]$, with LOA and B in [m]. Weights of passengers includes crew and baggage loads: $Wpax = pax * 100 * 9.8 [N]$, and consumables considers only fresh water $Wwater = 10lt * pax * 9.8 [N]$. Finally, the weight available for the propulsion system is $W_{disp}=W_{total}-(W_{hull}+W_{sup}+W_{pax}+W_{water})[N]$.

c) Resistance module: Total resistance is evaluated from 2 to 40 knots where displacement, *Holtrop (1984)*, semi-planing, *Savitsky and Brown (1976)*, and planing regime, *Savitsky et al. (2007),* are differentiated as a function of the volumetric Froude number, as shown in Fig.2.

Later, BHP and propulsive energy required (PER) is estimated considering the previously determined operational profile. Finally, acceleration of the CG is evaluated from *Savitsky and Brown (1976),* based on *Fridsma's (1971)* experiments.

d) Required propulsive weight module: The weight of the propulsion system is estimated considering outboard engines, battery only, liquid and gas hydrogen alternatives. For the former alternative, $W_{eng} = (0.4791 * SHP + 437) * 9.8$ [N] if $700 < SHP < 1000$. Similar regressions were obtained considering 2, 3 and 4 engines combinations from a database of 200 to 350 hp available in the local market. Then, fuel consumption, Vol_{fuel} and W_{fuel}, is estimated considering an averaged specific fuel consumption of 0.04 gal/hp-h. Finally, $W_{req} = W_{eng} + W_{fuel}$. The zero emission alternatives are described in the following section.
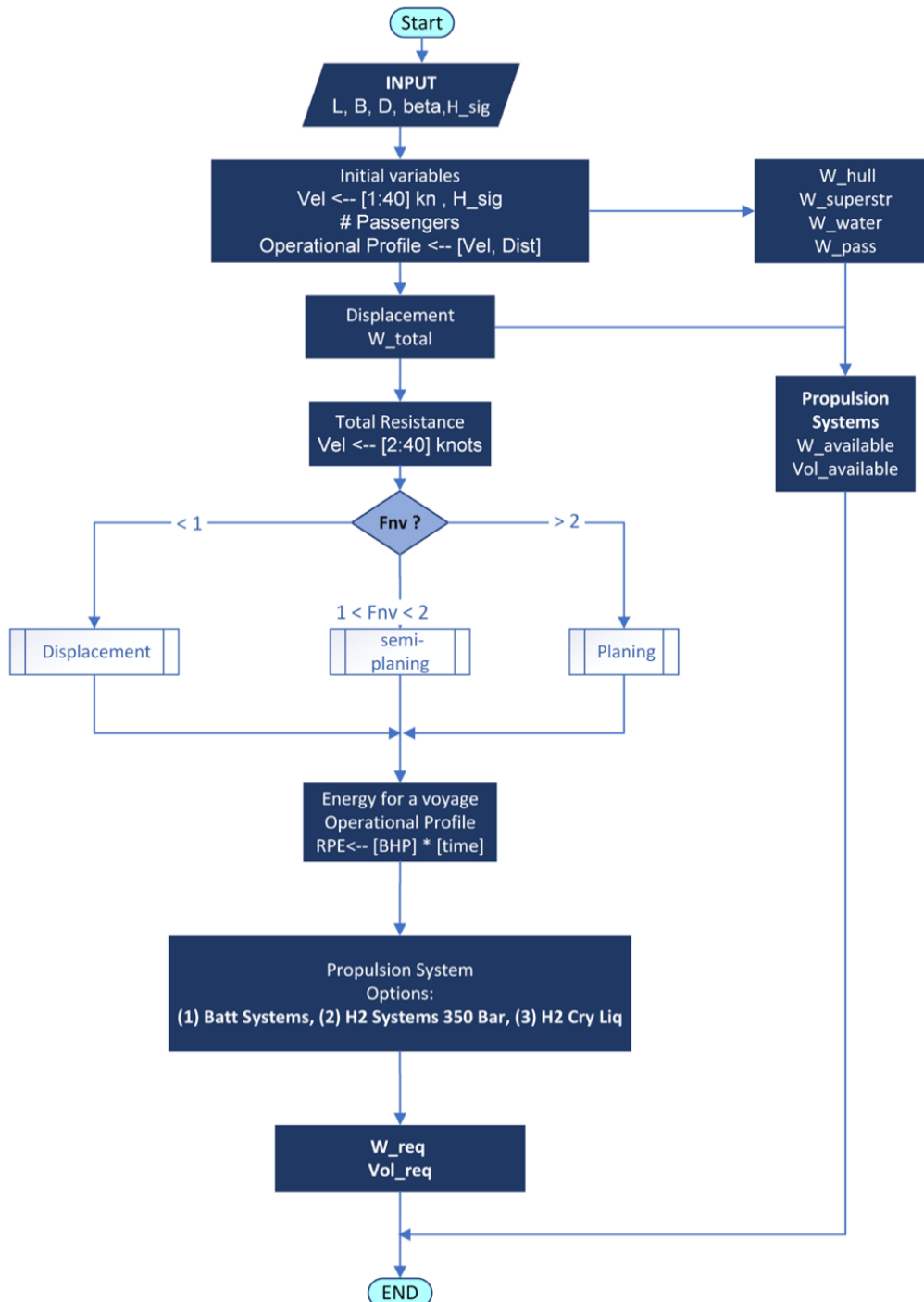
Fig.2: Planing craft parametric model

2.3. Zero-Emission propulsion systems alternatives

Considering previous feasibility studies only three zero emission propulsion systems: i) battery only, ii) Liquid H2, and iii) Gas H2 are considered in the present work. The efficiency of these systems is 45% for the hydrogen-based alternative, and 50% for batteries-only one. Also, weight and volume for each alternative is estimated considering corresponding database of commercial proton exchange membrane fuel cell (PEMFC) or marine batteries systems of low C-rate and high C-rate provided by Sandia Laboratories, *Minnehan and Pratt (2017)*.

2.3.1. Electric engines

Electric engines are used for both battery and hydrogen system. The parametric equations shown in Fig.3 for weight and volume as a function of the required power were approximated using a database of LPMR-type electric motors, https://www.tema.hr/storage/pdf/LPMR_tema.hr.pdf. These series of permanent magnet motors/generators motors were selected for its maximum power-to-volume ratio, very resistant and highly efficient.

a) Specific Power of electric motor   b) Power Density of electric motor
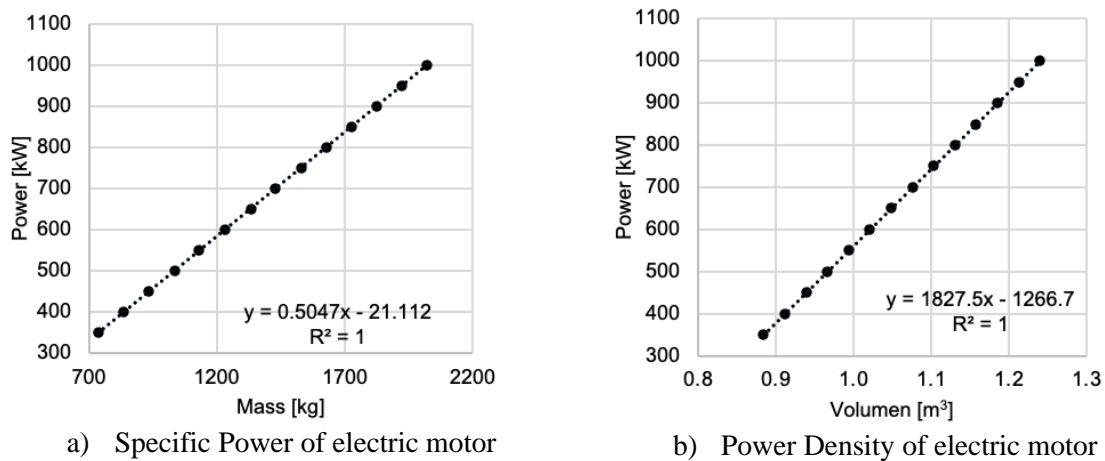
Fig.3: Parametric relationships for weight and volume as a function of power for electric engines

2.3.1. Battery + Electric engine

Fig.4 shows the main components of this propulsion system, namely: batteries, power electronics and electric engines. The power electronics are used to convert the energy stored in the batteries in usable energy for the electric engines.
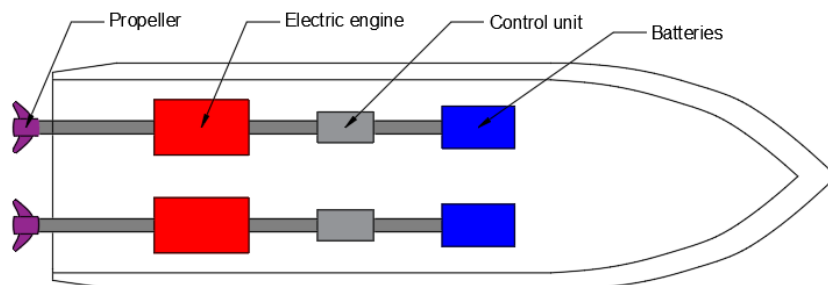
Fig.4: Main components of a Battery + Electric engine propulsion system

Both the specific energy and the energy density for the batteries belonging to the database are shown in Fig.5. The weight and volume of this system is estimated as a function of the required energy including the system efficiency.
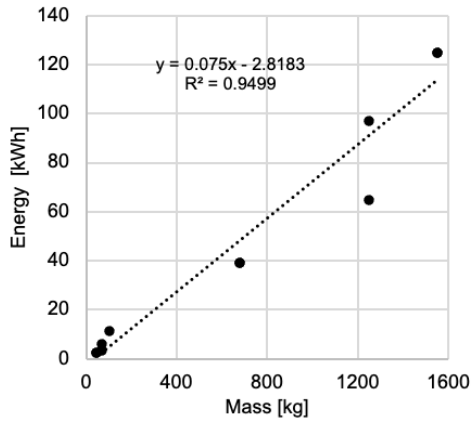
a) Specific Power of batteries	b) Power Density of batteries
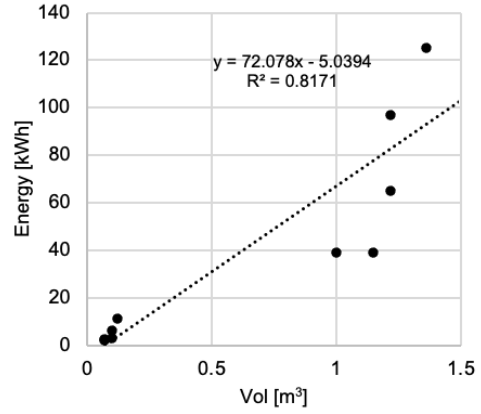
Fig.5: Parametric relationships for weight and volume as a function of Energy for batteries

2.3.2. Gas Hydrogen + Electric engine

Fig.4 shows the main components of this propulsion system, namely: Fuel cells, H2 Tanks, power electronics and electric engines. The commercial proton exchange membrane fuel cell (PEMFC) is considered in this work. Also, H2 is stored in tanks at 5000 psi (350 Bar).
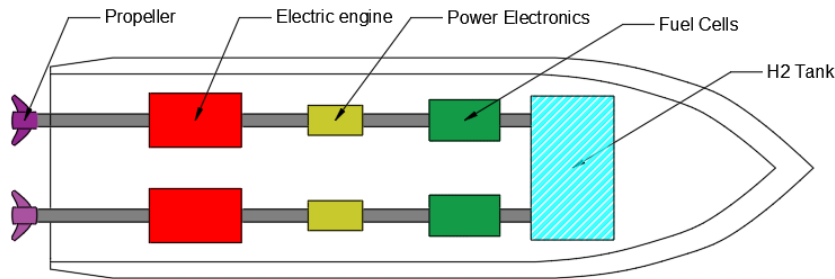
Fig.6: Main components of a Gas hydrogen + Electric engine propulsion system

First, the amount of hydrogen in [kg] is estimated including the system efficiency using Eq.(3):

$$\text{Mass of h2[kg]} = \left(\frac{Energy\ H2}{0.45} * \frac{3.6\ \text{MJ/kWh}}{119.96\ MJ/kg} \right) \tag{3}$$

The gravimetric specification of 17.92 [mass of the empty tank/stored mass of H2] and volumetric 93.7 volume of the tank/stored mass of H2 are used to estimate the weight and volume of the storage tanks. Finally, fuel cells weight and volume are approximated considering the trend lines shown in Fig.7.
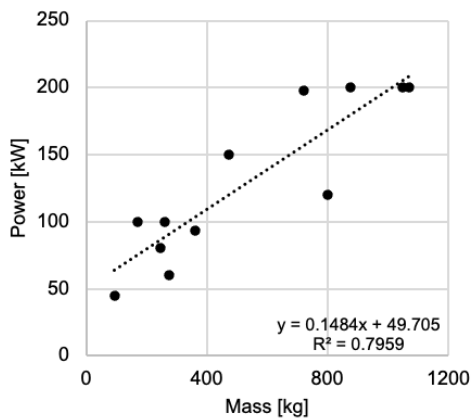
a) Specific Power of fuel cells	b) Power Density of fuel cells
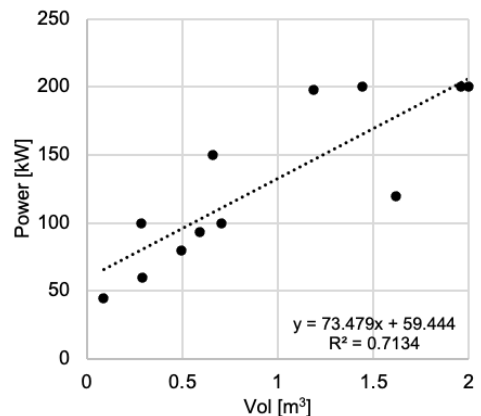
Fig.7: Parametric relationships for weight and volume as a function of power for fuel cells

238

2.3.3. Liquid Hydrogen + Electric engine

Fig.8 shows the main components of this propulsion system, namely: Fuel cells, vaporizers, H2 Tanks, power electronics and electric engines. The main difference with the previous system is the need to vaporize the cryogenic liquid H2 stored in tanks.
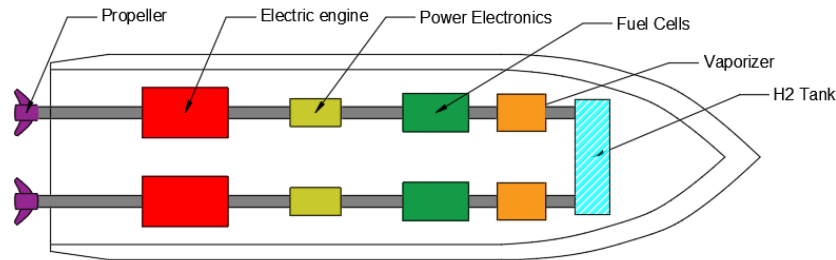
Fig.8: Main components of a liquid hydrogen + Electric engine propulsion system

The gravimetric specification of 8.7 [mass of the empty tank/stored mass of H2] and volumetric 24.8 volume of the tank/stored mass of H2 are used to estimate the weight and volume of the storage tanks.

2.4 Zero-Emission propulsion system adaptation algorithm

Fig.9 shows the algorithm employed to calculate the maximum cruise speed that reduce the energy required to complete the 49 nm route using a zero-emission propulsion system that is lighter and smaller than the available capacity on board. In this process, the vessel defined by the design variables is evaluated using the parametric model described above.
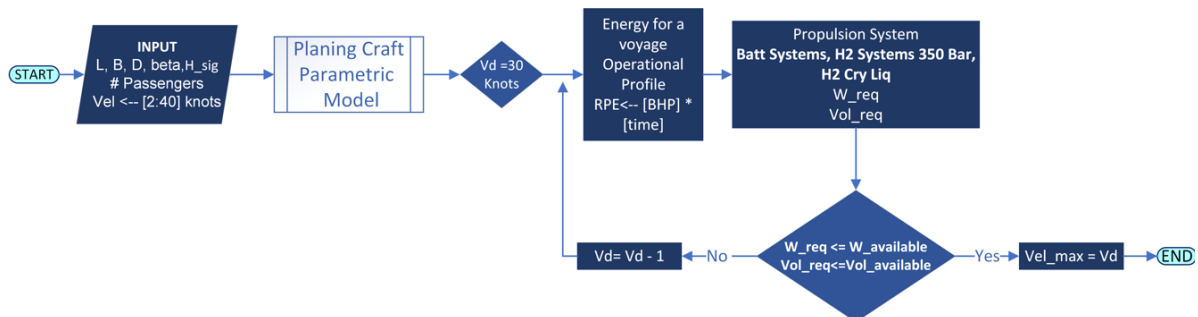
Fig.9: Zero-Emission propulsion system adaptation algorithm

2.4. Optimization algorithm implementation

Fig.10 shows a flow chart of the Python script implementation of the process. The link with the open-source optimization algorithmis performed through the evaluation of the objective function and constrains to identify all the feasible designs.

3. Results

In a multi-objective optimization algorithm, it does not exist a single solution satisfying all requirements of the objective functions. Instead, a set of optimum prospects for the objective functions define a Pareto front, formed by a set of solutions that cannot improve an objective without worsening at least one of the others. In this work the optimal Pareto front for resistance and vertical acceleration of the CG is estimated.
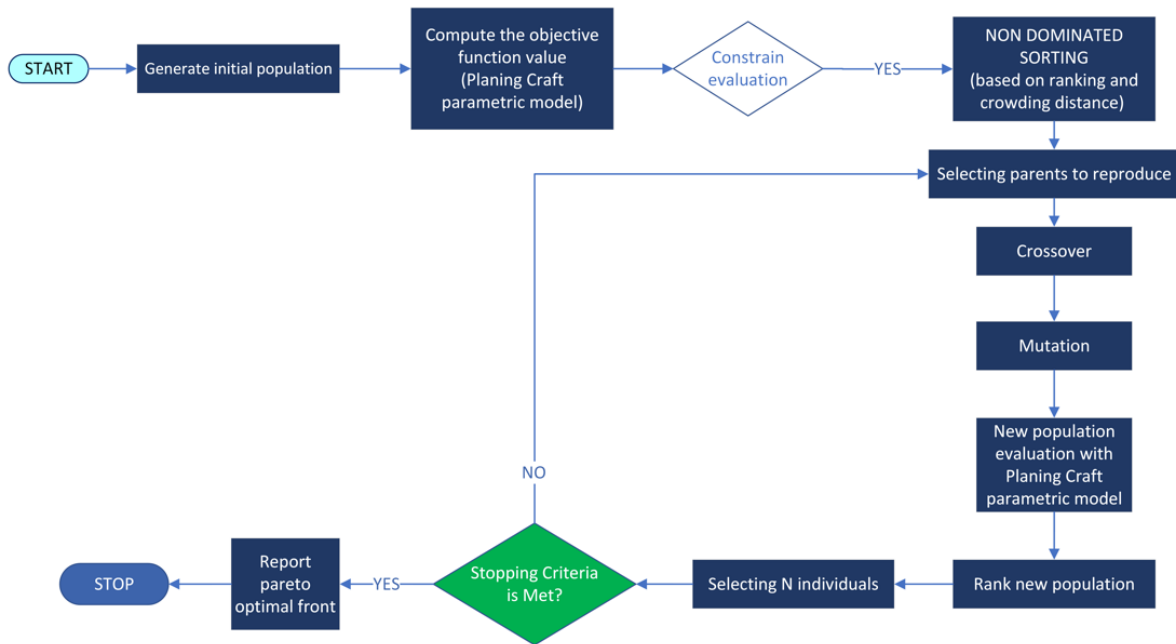
Fig.10: Flow chart for the implementation of the optimization process.

3.1 Adopting Zero-Emission propulsion system

Table III shows the main characteristics of Boat A, that was chosen as a representative boat operating at Galapagos Archipelago. This boat is a gasoil outboard engine monohull that can sail at 28 knots in a 49 nm route in Sea State 3 ($H_{1/3}$ = 1 m) consuming in average 62 gallons of fossil fuel.

Table III: Main characteristics of boats operating in Galapagos

Parameter	Boat A	Boat S	Boat M	Boat Sp
LWL, m	11.01	12.27	12.75	11.88
BxD, m	3.45x1.51	4x1.6	4x1.6	2.61x1.65
T, m	0.45	0.50	0.47	0.51
LCG, m	4.80	5.78	5.82	5.56
Disp., tons	8.26	12.36	8.79	5.92
β, [°]	14	8	14	25
Passengers	28	40	34	33
Installed power, Hp	850	1200	950	500
Total drag, kN	17.95	21.53	20.54	16.15
rms a_{CG}, g	1.14	0.95	0.92	0.76

First, the propulsive energy required to complete a voyage is estimated considering a typical operational profile, as shown in Table IV. The Power for each task is estimated using the resistance module described above.

Table IV: The energy required for a voyage

OPERATION/MANEUVER	V[knots]	t[h]	Distance [nm]	Power [kW]	Energy [kWh]
Fuel maneuver	3	0.08	0.25	0.67	0.06
Transfer to boarding area	5	0.08	0.42	3.07	0.26

240

OPERATION/MANEUVER	V[knots]	t[h]	Distance [nm]	Power [kW]	Energy [kWh]
Passenger boarding	0	0.50	0.00	3.07	1.54
Exit the port	9	0.17	1.50	54.63	9.11
Inter-island navigation	**28**	**1.75**	**49.00**	**553.65**	**968.89**
Entrance to the port	4	0.33	1.33	1.51	0.50
Passenger unloading	0	0.33	0.00	1.51	0.50
Total		3.25	52.50	618.12	**980.86**

The weight available for the propulsion system is W_{disp}=1.56 Tons. In this case: W_{total} = 8.20, W_{hull} = 3.31, W_{sup} = 0.23, W_{pax} = 2.8, and W_{water} = 0.30 [tons]. The volume available of 12.72 m³ is estimated considering under deck, and main deck spaces. The weight and volume required for all three zero-emission propulsion systems alternative is shown in Fig.11 as a function of the inter-island navigation speed. It is evident that the battery-only system is heavier than the weight available onboard. In fact, this system is the heaviest of the three alternatives. On the other hand, both gaseous and liquid hydrogen systems meet the available weight at maximum speeds of 12 and 14 knots respectively.
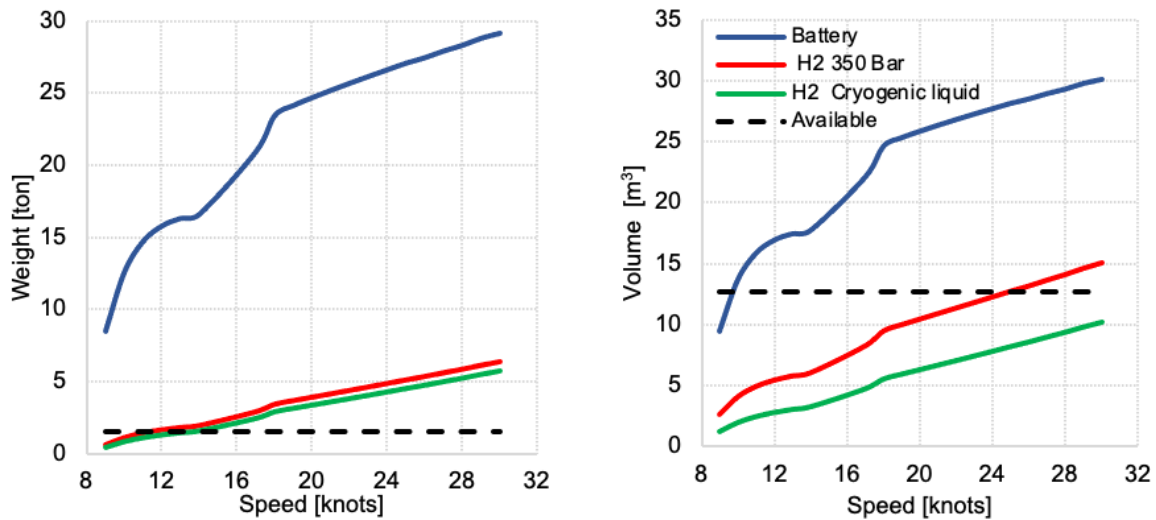
Fig.11: Zero-emission propulsion systems volume (left) and volume (right) requirements

3.2. Fossil fuel Outboard engines

Fig.12 shows the estimated Pareto front for drag and vertical acceleration of CG of a boat using fossil fuel outboard engines. The length and beam converge to 15 and 3.25 m, respectively, along the whole Pareto front. Moreover, deadrise angle is 10° but in the lower edge where increase up to 20°, where vertical accelerations are further reduced by LCG forward variation. Comparing a solution at the middle of the Pareto with the reference values from boat A, the optimization can reduce 10% for the CG vertical acceleration slightly increasing its displacement.
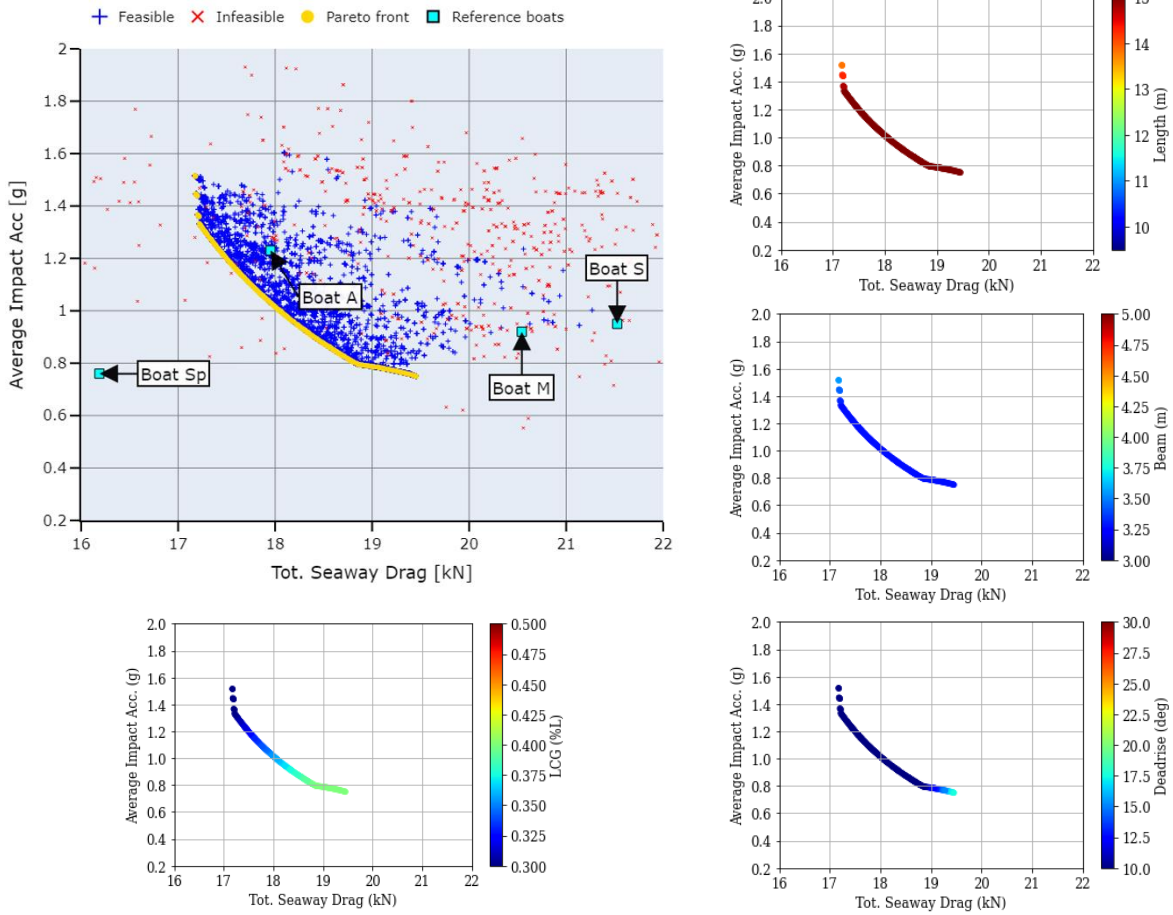
Fig.12: Pareto front and optimal design variables for the conceptual design of Galápagos interisland planning boat using fossil fuel outboard engines

3.3. Gas Hydrogen

Fig.13 shows the estimated Pareto front for drag and vertical acceleration of CG of a boat using gas hydrogen + electric engine system. This Pareto is short and has a slope change that define two branches: vertical and lower one. On the former, length, beam and deadrise converge to 15, 4.7 m and 20°. Here, the decrease in vertical accelerations is related with LCG forward variation. On the latter, only LCG remains constant. Comparing a solution at the middle of the Pareto with the reference values from boat A, the optimization procedure reduces 30% for the CG vertical acceleration but required an 200% increase in beam and displacement to be able to accommodate this propulsion system.
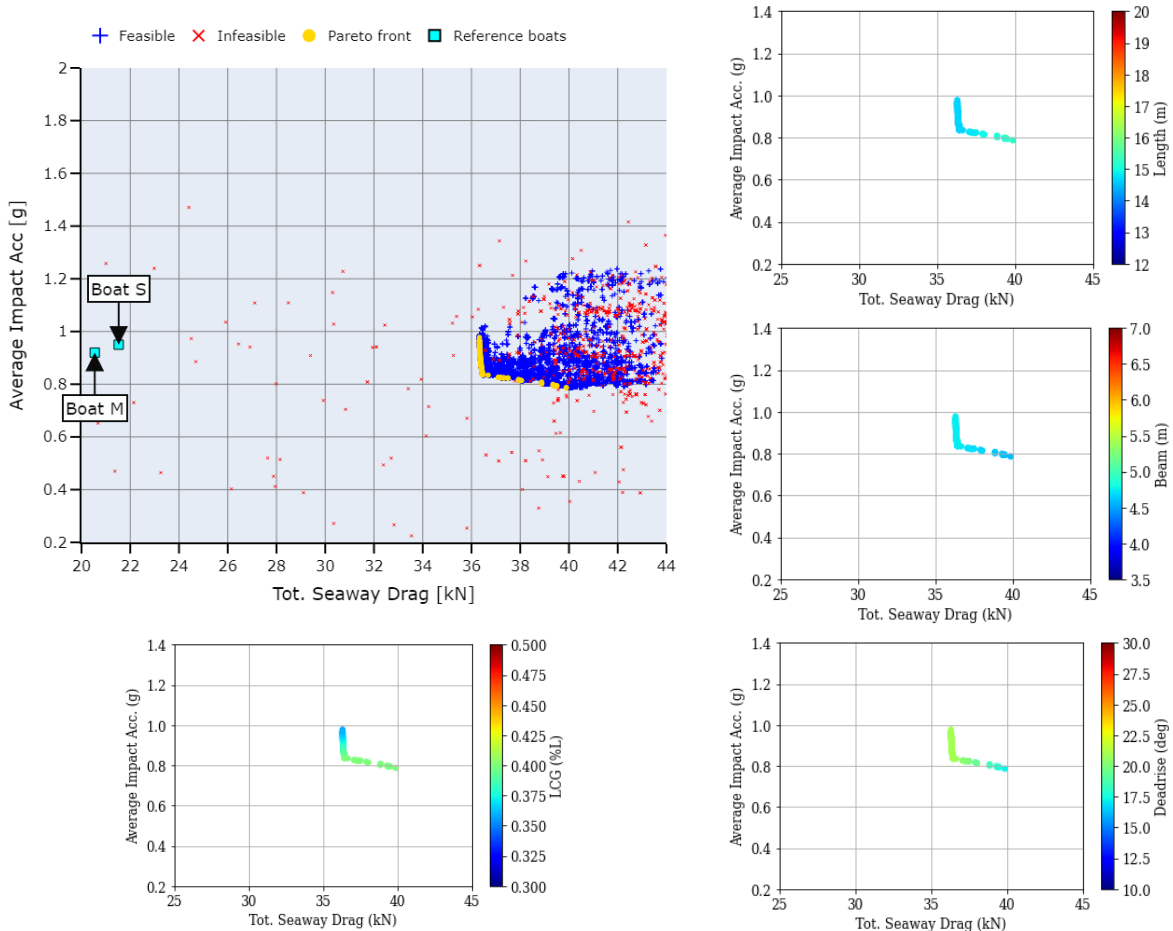
Fig.13: Pareto front and optimal design variables for the conceptual design of Galápagos interisland planning boat using gas hydrogen + electric engine system

3.4. Liquid Hydrogen

Fig.14 shows the estimated Pareto front for drag and vertical acceleration of CG of a boat using liquid hydrogen + electric engine system. Beam converge to 3.8 m along the whole Pareto front. A change from 15 to 19 m increase the total resistance and reduce the vertical acceleration. Besides, when deadrise angle is 20° it is possible to reduce the vertical acceleration by 50% by moving LCG forward. Comparing a solution at the middle of the Pareto with the reference values from boat A, the optimization procedure reduces 50% for the CG vertical acceleration but required an 90% increase in displacement to be able to accommodate the propulsion system.
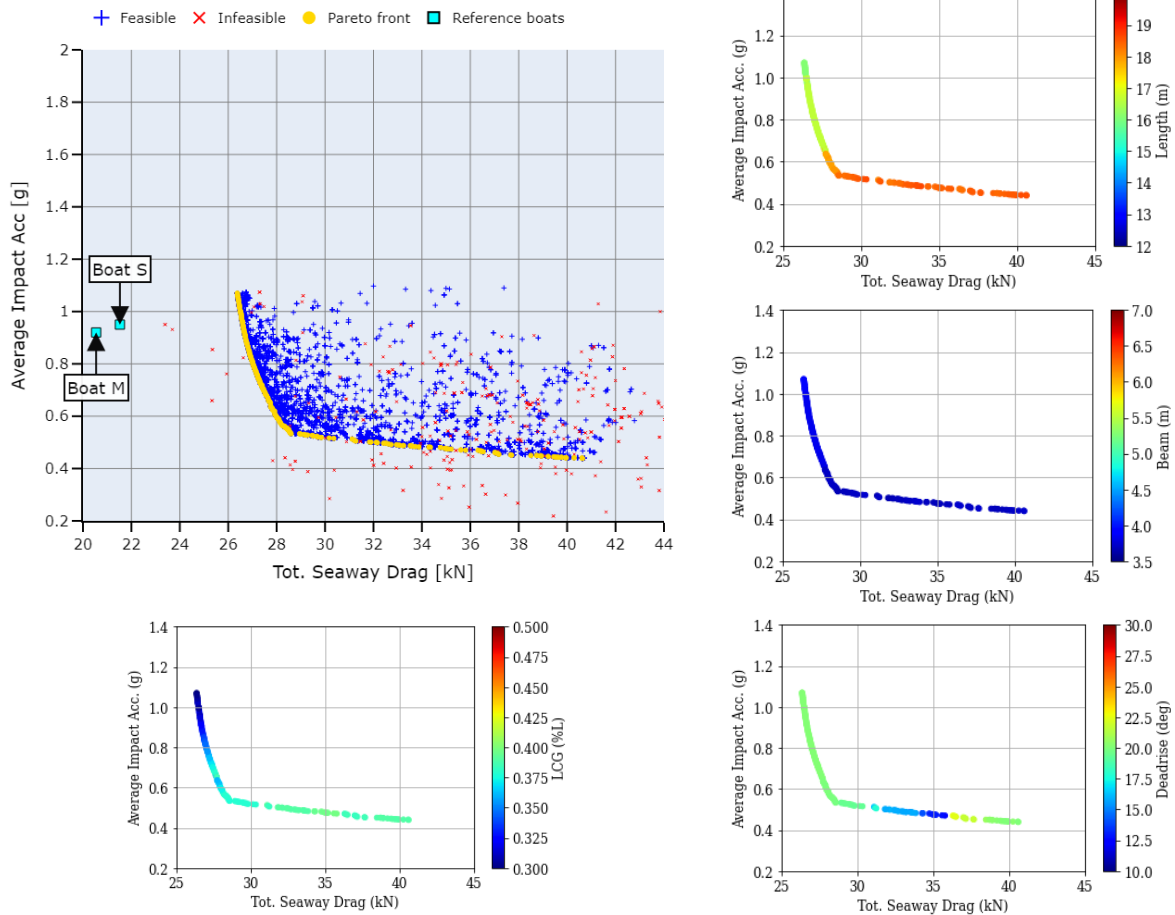
Fig.14: Pareto front and optimal design variables for the conceptual design of Galápagos interisland planning boat using liquid hydrogen + electric engine system.

3.4. Zero-Emission alternatives comparison

Fig.15 compares the Pareto fronts for both zero-emission propulsion system, namely: liquid H2 and gas H2 with fossil fuel outboard engine configuration. The latter alternative demonstrate that one can significantly reduce vertical accelerations without severely increasing the vessel's resistance. On the other hand, gas hydrogen system requires bigger boats that do not reduce vertical accelerations lower than the best fossil fuel option. Furthermore, liquid hydrogen system provides alternatives with wider performance in term of resistance and vertical accelerations. It seems possible to reduce more than 50% vertical accelerations without two folding the total seaway resistance.

Table V shows the main characteristics for optimized planing hulls using i) outboard engines, ii) Boat A using liquid H2, iii) liquid H2, and iv) gas H2. It is shown that it is possible to adopt a zero-emission propulsion system in existing boats, but a reduction in cruise speed is required. The outboard engine design is larger and fuller without increasing its total resistance. In both H2 designs, gas and liquid, the propulsion system requires about 45% of the total displacement and have energy use index between 0.90 and 1.20, that are similar to the Chase Zero prototype.
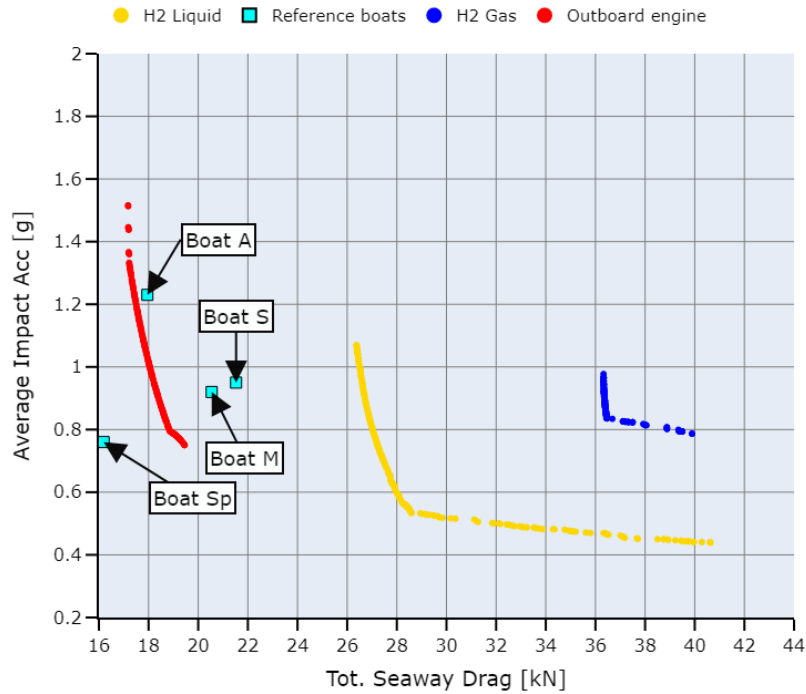
Fig.15: Pareto front comparison for the conceptual design of Galápagos interisland planning boat using zero-emission propulsion systems

Table V: Comparison of optimal boat characteristics at 0.5Rt,0.5Acc using zero-emission systems

Parameter	Boat A *Lopez et al. (2021)*	Zero emission Boat A	Outboard engine	Liquid H2	Gas H2
LOA, m	12.02	12.02	15.00	18.62	15.27
B x D, m	3.45 x 1.51	3.45 x 1.51	3.27 x 1.47	3.84 x 1.70	4.70 x 2.03
T, m	0.45	0.45	0.37	0.59	0.74
Cb	0.45	0.45	0.50	0.39	0.40
LCG, m	4.80	4.80	5.25	7.08	6.11
Disp., tons	8.26	8.26	8.77	15.44	22.56
β, [°]	14	14	10	19	17
Total drag, kN	17.95	8.89	17.98	30.85	37.32
rms a_{CG}, g	1.14	--	1.02	0.51	0.79
V, Knots	28	14	28	28	28
Required fuel	65 gal	41 Kg	64 gal	89.8 kg	112.6 kg
Wprop/Disp	0.19	0.19	0.14	0.46	0.45
Energy use index, kWh/pass*nm	0.71	0.44	0.77	0.94	1.18

4. Conclusions

A multi-objective optimization procedure has been successfully coupled with a parametric model to evaluate the performance of planing hulls operating in Galapagos archipelago at 28 knots including fossil fuel outboard engine, battery-only, gas H2, and liquid H2 propulsion systems. The results for

fossil fuel alternative demonstrate that it is possible to significantly reduce vertical accelerations without severely increasing the vessel's resistance.

A feasible solution requires to reduce energy consumption for a specific operational profile by improving the energy efficiency of the vessel and to choose a zero-emission system light enough to be on board. Results show that it is possible to adopt a zero-emission propulsion system in existing boats operating in Galapagos, but a reduction in cruise speed is required. Feasible alternatives use gas H2 and liquid H2 where the cruise speed will be 12 and 14 knots respectively. In addition, battery-only option is too heavy to be on board.

The same feasible alternatives could be implemented to achieve 28 knots. However, gas hydrogen system requires bigger boats that do not improve vertical accelerations when compared with the best fossil fuel option. Furthermore, liquid hydrogen system provides alternatives with wider performance in term of resistance and vertical accelerations. It seems possible to reduce more than 50% vertical accelerations without two folding the total seaway resistance.

References

BLANK, B.; DEB, J. (2020), *Multi-objective optimization in Python*, IEEE Access

BLOUNT, D.L.; CODEGA, L.T. (1992), *Dynamic Stability of Planing Boats*, Mar. Techn. 29/1, pp.4-12

CASTRO-FELICIANO, E.L. (2021), *OpenPlaning: Open-source Framework for the Hydrodynamic Design of Planing Hulls*, SNAME Int. Conf. Fast Sea Transportation (FAST), Providence

DEB, T.; PRATAP, K.; AGARWAL, A.; MEYARIVAN, S. (2002), *A Fast and Elitist Multiobjective Genetic Algorithm: NSGA-II*, Trans. Evol. Comput. 6/2

FALTINSEN, O.M. (2006), *Hydrodynamics of High-Speed Marine Vehicles*, Cambridge Univ. Press

FABRICIUS, L. (2019), *Sluttrapport Nullutslipps Hurtigbåt Utviklingsprosjekt for Trøndelag Fylkeskommune*, www.lmgmarin.no

FRIDSMA, G. (1971), *A Systematic Study of the Rough-water Performance of Planing Boats (Irregular waves - Part 2)*, Hoboken

GL (2012), *Rules for Classification and Construction I Ship Technology 3 Special Craft 1 High Speed Craft*, www.gl-group.com

GRUBISIC, I. (2008), *Reliability of Weight Prediction in the Small Craft Concept Design*, 6th HIPER Conf., pp.215-226

HOLTROP, J. (1984), A statistical re-analysis of resistance and propulsion data, Int. Shipb. Prog. 31

IMO (2018), *Initial IMO Strategy on Reduction of GHG Emissions from Ships: Annex 11*, Int. Mar. Org., London

ISO (2021), *Mechanical Vibration and Shock - Evaluation of Human Exposure to Whole Body Vibration - ISO 2631-1*, Int. Standard Org., Geneva

LEWANDOWSKI, E. (1998), *The Transverse Dynamic Stability of Hard-chine Planing Craft*, J. Ship & Ocean Technol. 2/1

LEWANDOWSKI, E.M. (2004), *The Dynamics of Marine Craft*, WSPC

MARIN-LOPEZ, J.R. (2007), *Optimization of river planing boats for cargo and passenger transportation*, n/a

MARÍN LÓPEZ, J.R.; VILLAMARÍN, E.G.; MENDOZA, J.I.; PAREDES, R.J.; DATLA, R. (2021), *Conceptual design recommendations to improve seakeeping of small high-speed craft providing interisland transportation in Galápagos*, SNAME Int. Conf. Fast Sea Transportation (FAST), Providence

MARIN-LOPEZ, J.R.; MELENDEZ, J.L.; PAREDES, R.J.; CASTRO-FELICIANO, E.L. (2022), *Optimal conceptual design using NSGA-II algorithm for Galápagos interisland service small craft including flaps*, 20th Int. Conf. Ship & Maritime Research (NAV 2022)

MINNEHAN, J.J.; PRATT, J.W. (2017), *Practical Application Limits of Fuel Cells and Batteries for Zero Emission Vessels*, Sandia Report, pp.1–71

NN (2015), *Battery powered Boats, providing Greening, Resistance reduction, Electric, Efficient and Novelty,* BB GREEN Instrument: Collaborative project, www.bbgreen.info

NN (2022), *Emirates Team New Zealand reach range and speed milestones in 'CHASE ZERO'*, https://emirates-team-new-zealand.americascup.com/en/news/552_EMIRATES-TEAM-NEW-ZEA-LAND-REACH-RANGE-AND-SPEED-MILESTONES-IN-CHASE-ZERO.html

PEREZ, R.; ALONSO, V. (2014), *The ultimate approach for General Arrangement definition*, SNAME Marit. Conv. (SMC), no. M, pp.1–6

PRATT, J.W.; KLEBANOFF, L.E. (2016), *Feasibility of the SF-BREEZE: a Zero-Emission, Hydrogen Fuel Cell, High-Speed Passenger Ferry*, Sandia Report, https://energy.sandia.gov/wp-content/up-loads/SF-BREEZE%20SAND2016-9719.pdf

PRATT, J.W.; KLEBANOFF, L.E. (2018), *Optimization of zero emission hydrogen fuel cell ferry design, with comparisons to the SF-BREEZE,* Sandia Report, https://www.osti.gov/servlets/purl/1513454

REUSSER, C.A.; PÉREZ OSSES, J.R. (2021), *Challenges for Zero-Emissions Ship*, J. Mar. Sci. Eng. 9/1042, p.19, https://www.mdpi.com/2077-1312/9/10/1042/htm

RODAS, H. (2017), *Listado de la flota de naves autorizadas para transporte maritimo de pasaje entre puertos poblados de la provincia de Galapagos*, Guayaquil

SAVITSKY, D. (1964), *Hydrodynamic Design of Planing Hulls*, Mar. Technol. SNAME News 1/1, pp.71–95

SAVITSKY, D.; BROWN, P.W. (1976), *Procedures for hydrodynamic evaluation of planing hulls in smooth and rough water*, Mar. Technol. 13/4, pp.381–400

SAVITSKY, D.; DELORME, M.F.; DATLA, R. (2007), *Inclusion of whisker spray drag in performance prediction method for high-speed planing hulls*, Mar. Technol. SNAME News 44/1, pp.35–56

SAVITSKY, D.; KOELBEL, J.G. (1993), *Seakeeping of hard chine planing hulls*, SNAME T&R Bulletin

SPRINGER, B. (2021), *Candela's High-Performance, Long-Range, Electric-Powered, Hydrofoiling Speedboats Are Going To Revolutionize Boat Travel Just Like Tesla Revolutionized Car Travel*, Forbes

VANDERPLAATS, G.N. (2007), *Multidiscipline Design Optimization*, Vanderplaats Research & Development, Colorado Springs

Appendix
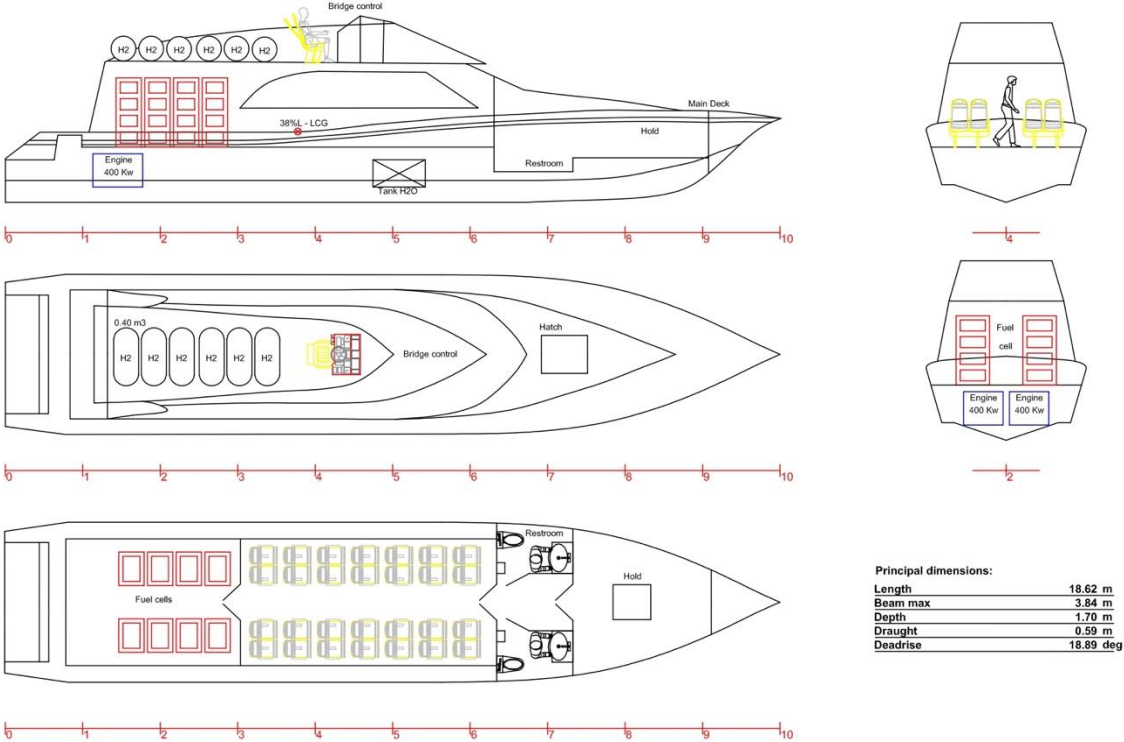
Fig.16: Outboard profile and particulars for the conceptual design of Galápagos interisland planning boat using Liquid H2 + electric engine propulsion systems

The Development of a Battery Hot Swap Prototype for Use on the Autonomous Surface Vehicle SeaML:SeaLion

Vincent E Schneider, Fraunhofer CML, Hamburg/Germany, vincent.schneider@cml.fraunhofer.de
Ching Nok Au, Fraunhofer CML, Hamburg/Germany, ching.nok.au@cml.fraunhofer.de
Akif Budak, Fraunhofer CML, Hamburg/Germany, akif.budak@cml.fraunhofer.de
Johannes Oeffner, Fraunhofer CML, Hamburg/Germany, johannes.oeffner@cml.fraunhofer.de

Abstract

The increasing availability of heavy-duty UAS with autonomous capabilities offers the opportunity of large-scale aerial surveillance of ports and large sea vessels. However, the current battery technology still limits the maximum possible flight time, leading to regular manual replacement of the depleted batteries. In this work removing the human interaction was achieved by developing an automated battery hot-swap station for a DJI M300. This system mounted on the ASV 'SeaLion', enables fully autonomous aerial surveillance of port infrastructure, offering almost continuous drone operation, with minimal downtime of approximately one minute per hour and without any need for human operators.

1. Introduction

The rapid development of Unmanned Aerial Systems (UAS) in the recent decade has led to highly capable and commercially available UAS. Within this work, we will focus entirely on rotary wing UAS, also known as drones. The areas of deployment are ranging from wildlife studies such as bird monitoring, *Sarda-Palomera et al. (2012)*, maritime emissions monitoring, *Mamarikas et al. (2022)*, urban vegetation mapping, *Feng et al. (2015),* or architectural or archaeological studies deploying re-construction of 3D models using photogrammetry, *Remondino et al. (2011)*. Commercial applications range from agriculture to save deer fawn from agriculture-equipment using thermal imaging, *Israel et al. (2011),* to inspection and maintenance of structures with limited access. At mining sites, UAS are used from exploration to reclamation, *Park and Choi* (*2020)*, while in civil engineering difficult to reach structures, such as bridges and their supporting pillars, can be inspected using UAS, *Seo et al. (2018).* Traditionally the inspection of bridges and other high arching infrastructure requires special vehicles equipped with telescopic arms to reach up or down and trained personnel to reach the inspection locations.

Here the deployment of UAS with respective sensory equipment is ideally suited to remove the need of reaching down or up with specialised equipment. Drones can simply take off, approach the structure, and inspect with a given distance and from every angle. Modern systems can even tilt the cameras upwards to gain access to bottom side structures. While a multitude of drone systems exist and custom solutions are offered on the market, within this project a particular UAS system was chosen, and the decision is elaborated shortly. The UAS selected is the DJI Matrice 300 RTK (M300), produced by one of the biggest manufacturers of leisure and professional UAS – DJI. The work presented here is performed within the Horizon 2020 project RAPID (Risk-Aware Autonomous Port Inspection Drones), where the implementation of Beyond Visual Line Of Sight (BVLOS) services for port inspections are developed, *HPA and UWS (2020)*. These services are supported by AI-based obstacle detection and avoidance, a pre-flight risk assessment based on VR simulations and technical as well as legislative U-space integration into a web-based drone control interface. To coordinate and streamline all develop-ments performed within RAPID to reach the aforementioned goals, a widely available, technically robust and performant UAS was needed, hence the M300 was selected.

While UAS solve the problem of accessibility very effectively, they do lack the endurance of other systems due to the nature of hovering in the air – a very energy intensive way of flying. This perceived weakness is an equal strength because detailed inspection, especially when involving AI approaches, need clear image acquisition which is greatly enhanced by slow flying speeds. Nevertheless, UAS flight time is limited by the relation of energy stored in its battery and its own weight. With current Lithium

Polymer batteries being state of the art and their given energy density, flight times of approximately 40 minutes are reasonable to assume.

Flight times of 40 minutes are very suitable for performing inspections, especially when an operator is on site who can quickly exchange drained batteries and continue inspections. But when considering BVLOS applications which span a complete port area with the capability to survey a multitude of bridges, two problems arise. First an operator in close proximity to exchange the depleted batteries is not a given, which means the drone must travel from a launch point to the inspection point and back. Which leads to the second issue being the maximum distance or area a drone can cover. For a M300 with a maximum flight time of 55 minutes and a cruising speed of 20 km/h a theoretical range 19.6 km range is achievable, or a circular area of 9.8 km radius, respectively. When comparing this to the surface area of the ports of Rotterdam and Hamburg – approximated with circles, the ports can be easily covered, Fig.1. Shown in the same figure is the theoretically achievable range when a 40-minute inspection is performed, resulting in a drastic reduction in range.

With these two issues of BVLOS UAS inspection concepts laid out, the need for an approach arises, that can bypass the issue of travelling towards an inspection site without expending the UAS battery power. At the same time, this approach needs to allow for reliable swapping of the batteries to perform extended inspections.
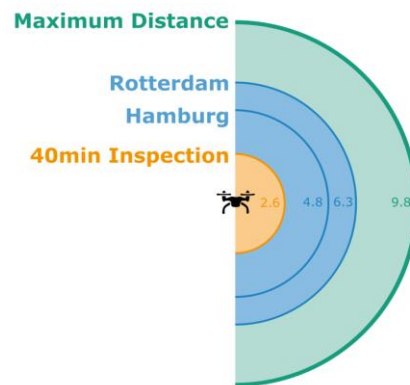
Fig.1: Maximum area a M300 can theoretically cover to reach a target and return (green), approximate area covered by two of Europe's biggest port Rotterdam and Hamburg (blue) and range achievable by a M300 when performing a 40 min inspection (orange).

To answer these two challenges the custom developed Autonomous Surface Vehicle (ASV) SeaML:SeaLion (subsequently called SeaLion) is chosen as a carrier platform for the drone, enabling launching and landing of the drone. Additionally, to increase the maximum inspection time, an automatic battery swapping system is developed and integrated, allowing for a sequenced exchange of the M300's batteries. This sequential exchange yields the advantage of the drone not powering down, allowing for continuous inspection runs and therefore making it a hot swap of batteries.

The aim of this study is to show the design criteria and decision necessary to develop such a waterborne system for a given drone. One specific goal is to not change the UAS nor its batteries to perform the swap, as has been performed in other work *Michini et al. (2011), Lee et al. (2015), Liu et al. (2018)*. This enables the quick exchange of UAS and any model of the M300 can be used within this system. Finally, the integration with the ASV SeaLion will be presented, which elaborates on the challenges of landing and transporting a drone on a free floating and moving target from a hydrostatic point of view.

2. Related works

Recent works relating to battery swap and recharge units have started from the year 2010, *Liu et al. (2018)*. The research has evolved from using a robotic arm to replace the batteries, to create a docking station where drone lands and battery is swapped. *Grlj et al. (2022)* have discussed about the survey

conducted and need for docking stations where batteries of UASs can be swapped automatically. It signifies the necessity of independent technologies for different scenarios depending on the use cases such as fixed docking station, portable docking station, docking stations that can be mounted on ASV, and docking stations on a moving vehicle.

QUADO is one of such prototypes created by *Liu et al. (2018)* where a drone is assisted by infrared LED beacons to land on the docking station. Using the horizontal and vertical motors, battery is swapped. This docking stated is sealed to prevent it from being damaged by external factors such as rain and sunlight. However, this prototype is efficient as a stable and static docking station on ground and can be used for only small drones. Stability and scalability factors make this prototype inefficient to be placed on ASV. Another prototype by *Liu et al. (2018)* is restricted to only docking station with no swapping mechanism available. This prototype has capabilities in assisting drones to land on a moving platform. *Lee et al. (2015)* have presented a design concept for autonomous drone landing and battery swapping but this design concept was just created on paper. There has been no physical prototype created and hence there are no test results available. *Silva et al. (2022)* have presented an inverted docking concept where the quadcopter attaches itself to the ceiling during the battery swapping system.

With the literature survey conducted, there has been no such physical product identified which has capabilities to accurately land drones on a docking station mounted on ASV and efficiently swap the batteries.

3. Materials and methods

Before going into detail about the hardware specifications and design approaches, some general concepts need to be introduced. The routine to land a UAS, position it correctly for a battery swap, swapping the M300 batteries and releasing the vehicle requires two main systems. First, when landed on the landing pad with a given uncertainty in position, the so-called Drone Positioning System (DPS) will locate, centre, and move the UAS towards the second system, the Battery Swap Station (BSS). The purpose of the latter is to swap the two drone batteries sequentially with opening and closing the battery safety lever. The two systems in unity are called Battery Hot Swap System (BHS).

3.1. Morphological study of design specification

To determine the possible subsystems, six essential functions of the BHS are identified as: 1) attachment, 2) detection, 3) positioning, 4) storage, 5) extraction and insertion, and 6) energy-supply. All found solutions for the six elements of the BHS are analysed with respect to their speed and reliability of execution in form of a weighed comparison to yield a quantitative evaluation. Furthermore, a qualitative evaluation with comparison to existing systems is performed for their form factor regarding the ASV size limitations, the total weight of the combined elements as well as mechanical complexity and hence influence on overall system robustness.

3.2. Design and construction of the Battery Hot Swap System

When starting to implement the water-based BHS two vehicles were given as fixed starting points. The former being the ASV SeaLion with its dimensions, fixture points and payload properties, while the latter being the DJI M300 with its respective dimensions, battery parameters (such as weight) and dynamic properties such as landing precision. Starting with the ASV, the modular test platform developed by CML is ideally suited as a carrier platform by its catamaran design, Fig.2. It is 2.2 m in length and 1.5 m in width, has a freely configurable deck, 120 kg payload, and two 4.2 kWh batteries providing 48, 24 and 12 V. With these it can be easily adapted to transport an UAS, incorporate the designed BHS and serve as a launching and landing platform. The implementation onto a ASV defines the challenges of water protection from atop and below, as well as weight and size limitations to incorporate everything on the vessel and leave enough space for the drone to land.

The second essential system is the M300, Fig.3, its parameters such as battery size, insertion height and special features defines the design boundary of the mechanism for opening the battery safety lever (see Chapter 4.2). The UAS has a maximum take-off weight of 9 kg and approximately 45 minutes of flight times. The horizontal hovering precision is limited to plus or minus 0.3 m when relying on visual systems, which influences the minimum size of the landing platform. For the construction of the BHS and all its components, custom solutions had to be designed and manufactured. This is achieved by using Commercial Off-The-Shelf (COTS) components, especially for electronics such as Raspberry Pi, a single-board-computer with digital and analogue input/output pins to control hardware. Furthermore, all mechanical components, such as lead screws are COTS components as well. To manufacture complex and individual solutions such as part to grip the battery or open the battery safety lever on the M300, processes of Additive Manufacturing are deployed, namely the process of Fused Deposition Modelling (FDM).

Fig.2: ASV SeaLion in underwater inspection configuration. The ample deck space incorporates an ROV to perform ship and quay wall inspections. The implement domain (grey box) at the front will remain in the UAS configuration.

Fig.3: M300 equipped with one of the RAPID payloads – ship emission system MESU (Mobile Emission Sensory Unit), developed by CML to measure up to six gaseous emission products.

3.3. Integration and functional testing

After designing and manufacturing the BHS with its two subsystems all components are tested individually and in conjunction. Therefore, the first tests are performed within a controlled laboratory environment to ensure no external influences interfere with the mechanical system and all errors can be understood and fixed. With these tests successfully finished, the integration of BHS with the ASV SeaLion is performed and the combined system put into the water to test the influence of the payload on the hydrodynamic properties of the vessel. Of interest are here the centre of gravity when the UAS is in the extreme positions on the lading platform as well as when moved into the BSS to exchange the batteries. The influence on the centre of gravity is crucial to determine the ships properties with this new payload.

4. Results

4.1. Morphological study of design specification

For the six elemental functions of the BHS up to four mechanical solutions are selected and depicted in Fig.4. All solutions are rated qualitatively, Table I, on a scale from 0 to 10, where 0 is the lowest and 10 the highest score, respectively. The highest scoring systems are highlighted in dark green in Table I and their selection will be described here shortly. For the attachment of the drone's batteries, the chosen solution is predetermined by the design of the M300, which batteries are mounted inside the drone's main body. For the detection if the drone has landed, the nature of the landing being performed and finished by an autopilot yielded the digital communication as the best solution. For positioning the

drone after landing pusher arms scored best due to the ability to cover the complete landing platform with relatively low mechanical complexity. For storage the elevator yielded the smallest footprint on the ASV's surface. For extraction & insertion the spindle drive is chosen for achievable precision and force transmission. The last function is energy supply to guarantee the drone not powering down, which is achieved by relying on the internal energy and changing the batteries sequentially.

Fig.4: Morphological Analysis of possible solutions for the hot-swap mechanism's six elemental functions, chosen solutions coloured green

Table I: Speed and Reliability ratings of the explored solutions of the Morphological Analysis of the hot swap system's six elemental functions, Fig.4, chosen solutions coloured green

Function	Solution and respective speed/ reliability ratings			
Attachment	Underneath 10/5	On top 10/5	Internal 10/10	
Detection	IR sensor 10/8	Communication 10/10	Weight Sensor 5/8	Switch 5/5
Positioning	Drone accuracy 10/3	Guide Rails 10/3	Pusher Arms 6/8	Moving Platform 5/8
Storage	Drum 10/6	Disk 6/8	Elevator 8/8	Sled 8/8
Extraction/Insertion	Rocker Arm 8/5	Spindle Drive 7/10	Belt Drive 10/5	Rack and Pinion 10/6
Energy-Supply	Capacitors in drone 7/9	Capacitors in station 10/7	DC power supply in station 10/7	Internal Batteries 10/10
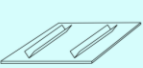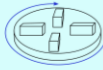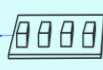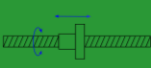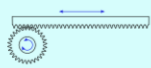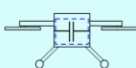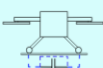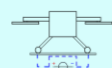
4.2. Design and construction of the Battery Hot-swap System

Adhering to the results of the morphological analysis, the construction process begun with creating a complete CAD-model of the overall BHS consisting of DPS and BSS mounted on the ASV SeaLion. Fig.5 (left), and the subsequent manufacturing of all components and integration and test on the swimming platform, Fig.5 (right). Differences between the two versions become apparent, which arose within the design and construction process, such as water protection of electronical parts as well as the integration of the ship's communication antenna on top of the BSS. While some mechanical features are standard engineering concepts and will not be elaborated in detail, special focus will be laid on the working principles of the DPS and the BSS.
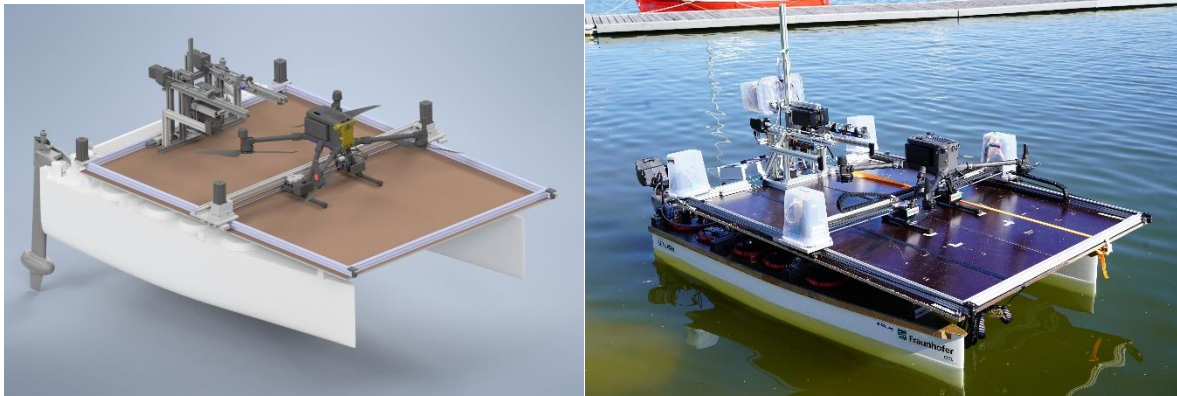
Fig.5: 3D CAD model of BHS on SeaLion (left) and the actual construction (right).

Fig.6: Empty battery slots of M300 with battery safety lever in unlocked (left) and locked (right) position. Clearly visible is the battery contact in the back at the vertical wall and a guiding rail at the bottom of the compartment, on which the battery slides onto.
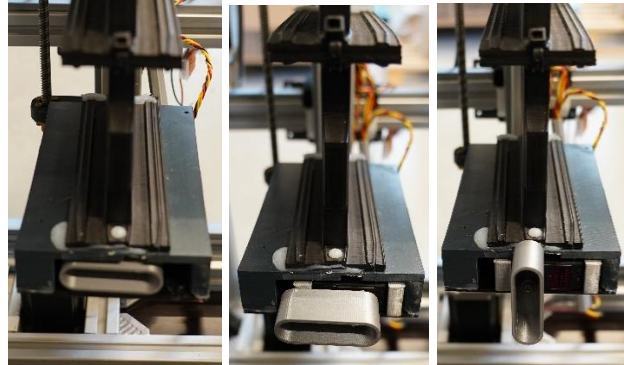
Fig.7: The battery is operated by two servos for longitudinal and rotational movement. When not in use, the Unlocker is retracted (left) into the housing to avoid interferences. To unlock, the part extends (middle) and turns the battery lever to a vertical position (right). After the swapping, the reverse procedure is followed to lock the lever.

With the BSS integrated, the development moved to the Drone Positioning system, which consists of a frame constructed from V-Slot aluminium profile, on which a gantry is mounted with rollers as the systems longitudinal movement axis. The system is depicted in Fig.9, with its frame along the longitudinal axis (1), sleds for longitudinal movement with electronic compartments (2), 8 mm linear shafts for lateral movement (3), U-shaped sliders to detect, catch and secure the drone's legs laterally to position it on the landing platform (4) and the reinforcement and electronics rail of the lateral axis (5). The depicted system represents the realisation of the pusher arm principle selected for positioning. Further features added and not considered in the primary morphological analysis are the U-shaped sliders to catch the drone, which allow to find and centre the UAS and subsequently move it into the BSS and after successful battery swap back to the launching position.

254
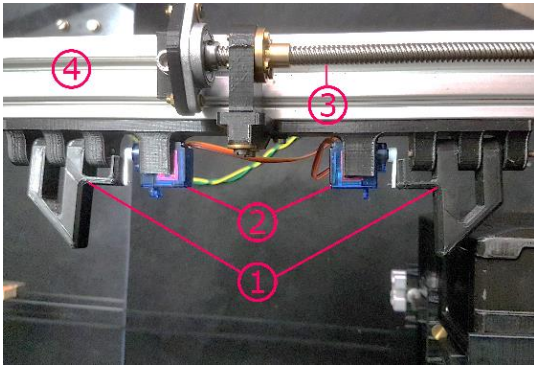
Fig.8: The battery gripper allows securing and moving the M300's batteries without any modifications. The 3D-printed assembly consists of two gripper-jaws (1), each actuated by one servo motor (2). A lead screw realises the horizontal movement of the batteries (3) along an aluminium profile (4) of the BSS.
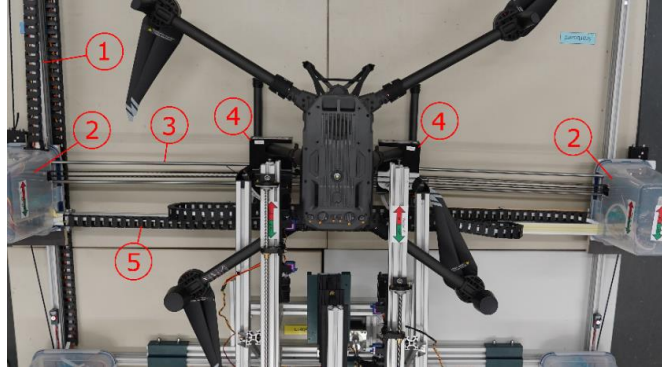

Fig.9: Drone Positioning System consisting of: V-slot profile frame (1), sleds for longitudinal movement with electronic compartments (2), 8 mm linear shafts for lateral movement (3), laterally movable U-shaped sliders to catch drone's legs (4), aluminium profile for reinforcement with drag chains for wiring (5)

4.3. Integration and functional testing

The BHS is set up on a benchtop to test the swapping. Throughout a complete swapping procedure, the BHS goes through the following states: BSS and DPS in ready position and clear for landing, drone landed, Fig.10, drone found, drone centered, Fig.11, drone inside BSS, Fig.12, battery safety lever unlocked, battery one extracted, Fig.13, battery one inserted, battery two extracted, Fig.14, battery two inserted, battery safety lever locked, drone released, and clear for take-off, Fig.15. The functional tests showed the overall routine taking 150 s to perform and allowed for fine tuning the exact positions for tasks such as opening the battery safety lever or having the battery elevator at the correct height to remove and insert batteries.
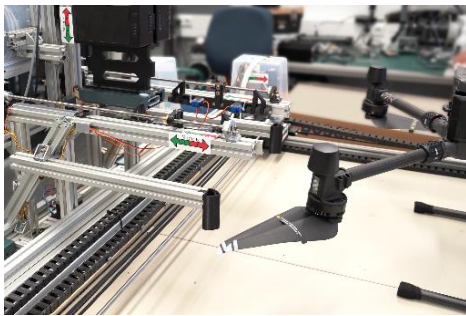
Fig.10: Step 1 - BSS and DPS in ready position, drone has landed
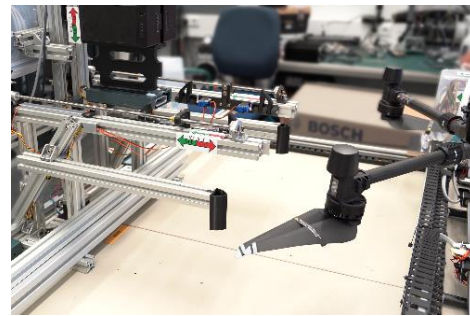
Fig.11: Step 3 - DPS finds drone longitudinally and centers it laterally

Fig.12: Step 4 - DPS positions drone inside the BSS

Fig.13: Step 6 - BSS unlocks battery safety lever and swaps left side battery

Fig.14: Step 8 - BSS swaps right side battery and closes battery safety lever

Fig.15: Step 12 - DPS positions drone on platform in takeoff position

Fig.16: The first setup where the BHS is centered on SeaLion. The landing platform has an inclination of 1.8° before the adjustment.
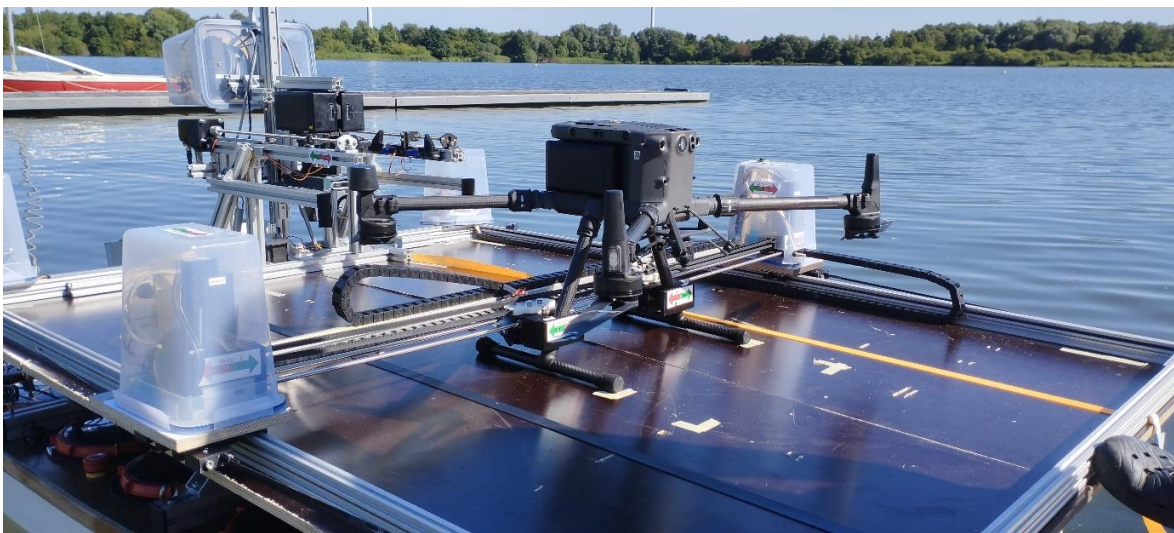
Fig.17 : The integrated system in cruising state. The DPS and UAS is placed near the centre of landing platform to adjust the tilt angle of ASV. The system has a natural frequency of 0.63 Hz about the pitch axis.

To examine the mechanical behavior of the proposed solution, the BHS and DPS is mounted onto the ASV, and the UAS is placed on the landing platform. While the system contains several moving components, their relative positions fall into three main states. At the landed state, the DPS is fully

retracted to maximize landing area and the ASV is stationary. At the cruise state, the drone is held firmly by the sliders while the ASV is in motion. At the swapping state, the ASV is docked and batteries are swapped. Ideally the platform should be level after landing so the UAS does not tend to slide in any directions.

During cruise, the UAS can be moved slightly towards the heck of the ASV to improve hydrodynamic properties such as drag of the vessel. In the test we first centered the BHS on the ASV, Fig.16, put it into the landed state, and adjusted the BHS forwards until the platform is level. Then we set the system to cruise state and finetuned the DPS, so the ASV is slightly tilted backwards, Fig.17. Force is then manually applied to simulate a wavy situation.

5. Discussion

5.1. Morphological study of design specification

With chapters 3.1 and 4.1. explaining the approach end evaluation of the investigated solution for the core functions, a short comparison with the available literature of similar systems is discussed here. The Attachment and Energy Supply of the M300's batteries are considered together due to the nature of the battery integration. The M300 is well engineered considering the battery positioning since it offers easily accessible batteries, which can be removed with one single horizontal motion, thus not requiring additional battery storage solutions. Other works have solved the issue by deploying purposefully built drones, with the batteries mounted to the bottom of the drones for easiest accessibility, *Lee et al. (2015), Michini et al. (2011), Fujii et al. (2013), Liu et al. (2017))*. These systems lack one of the major design requirements of this project, which was to deploy a commercially available drone. Furthermore, the design of the M300 solves another critical design requirement, which is the swapping of batteries without powering the system down. Here the size of the UAS is beneficial, because bigger UAS systems often require more than one battery, allowing for sequential exchange of batteries without a system shutdown. This way no additional modifications must be done to the drone, or the station and complexity can be kept at a minimum, offering optimal reliability and the ability to use an unmodified commercially available drone.

The Detection if the drone has successfully landed is not integrated into the BHS itself, but here another feature of the highly programmable M300 is used. The UAS can communicate its current state to the BHS making detection by direct communication with the drone the fastest and most reliable option. For the Positioning of the UAS, relying on the drones landing precision when in RTK mode, would have been an option. The M300 has a stated horizontal hovering accuracy of 10cm, with a positioning accuracy of 1cm when RTK is enabled, *DJI Official (2022)*. While this precision would be impressive, its achievability would be heavily reliant on surrounding environmental factors such as wind, waves, and the induced movement of the ASV. A system moving the drone into the desired swapping position with sub centimeter precision is required. Other existing swap-systems utilize motors on two horizontal axes, pushing the drone into its final swap position after it has landed, *Fujii et al. (2013)*. While this solution allows for a big discrepancy of the drones intended and actual position and increases the positional accuracy, it introduces increased complexity and requires additional time moving the drone after it has landed. Additionally, this design has relatively high spatial requirements since the positioning system has to be built around the perimeter in which the drone is expected to land. As the intended use case of the M300 in our context is a battery swap surrounded by water, no cutbacks regarding the landing precision can be allowed, since a missed landing will result in a loss of the drone and the attached payload.

For the storage of the batteries, one solution is deploying rotating drums, *Liu et al. (2017), Michini et al. (2011)*, to store the batteries. These systems are advantageous when only one battery is required to power the drone. For the M300, a dual drum system could be used, but would imply the vertical orientation of the drums to rotate individually without interfering with each other, increasing the level of mechanical complexity. The solution of deploying disks to store the batteries can also be found in literature, *Swieringa et al. (2010)*, facing similar limitations for integration with the chosen UAS.

Additionally, the disk-option would be limited in its speed due to its rotational inertia, caused by the large diameter of the disk required. Moving away from rotating approaches, two linear solutions have been considered – moving the batteries vertically with an elevator or horizontally deploying a sled. An elevator is advantageous for several battery storage options, as it can removed batteries from the top, bottom and internal storage. Its biggest drawback is the force needed to hold and elevate the batteries against gravity. The overall speed is considered an advantage since the inertia is lower compared to a rotary system and a single lead screw can be used. Similar to the working principle of the elevator, a sled can be used, which offers the simplest way to exchange batteries on top and underneath the drone, as no movement against gravity is needed. Due to the layout of the M300's arms a single axis horizontal sled cannot be used to access the drone internal battery slots. This option can easily be expanded horizontally to increase its storage capacity, with the drawback of needing a large surface area, which is disadvantageous with the limited surface area available on the ASV. The overall best combination of easiest access, mechanical robustness and smallest footprint is the elevator design, which is used in the presented BHS.

With the UAS in the correct position and the elevator aligned with it, <u>Extraction and Insertion</u> are the last steps needed to perform a successful battery hot swap. *Liu et al. (2018)* use a rocker arm in its station to move the battery from underneath its drone. This solution can remove batteries from atop or below the UAS, but not from an internal storage. While being quick and requiring only a single motion, the design is mechanically complex. Slower but simpler in mechanical design and therefore more reliable is the selected lead screw drive with a gripper unit to move the batteries along one axis. Equally suited for a linear extraction is a belt drive, which can move the gripper faster than a lead screw, but is prone to belt slippage, especially in humid or wet conditions. Another option is the use of a rack and pinion, as done by *Michini et al. (2011)*. A toothed rack is attached to the battery, which interlocks with teeth of the extracting pinion drive. While requiring high positional accuracy between UAS and toothed rack, the needed modification of the battery excludes this solution.

5.2. Design and construction of the Battery Hot-swap System

Starting with the Battery Swap System, the results of the morphological solutions presented in chapter 4.1. and discussed in chapter 5.1 proved to be a successful approach to realize the mechanical integration. With the first completely integrated system a successful battery swap could be performed of both batteries sequentially. Hence the goal of swapping the batteries without powering down the drone is achieved. The chosen approach of using standard Bosch aluminum profiles proved advantageous. Initial instabilities of the basic frame led to inaccuracies in the repeatability of positions but could be removed by adding reinforcing struts to the frame. Also, necessary changes in motor selection to drive the battery grippers required longer lead screws, which were easy to integrate due to a simple exchange of the respective profile sections. All these improvements still left a certain degree of movement within the frame, leading to the necessity of precise fine tuning of the positions for the extractions. This will be addressed in the future by improving the critical joints between the profiles. In a final integration, a custom-built welded frame could increase the rigidity to the best possible levels. Another issue encountered is the mounting of the battery magazine being a single point, giving it an axis of rotation around the aluminum profile on the top of it. This results in the inability to extract batteries from the M300 into the lower chambers of the magazine. The current solution is a series of additional moves to successfully remove the battery. While this approach is working, it requires additional time, which is not ideal. A second mounting point can remove this degree of freedom in the future, making the overall process even faster.

5.3. Integration and functional testing

When testing the BHS in the lab and in combination with the ASV SeaLion, again the successful swapping of both batteries was possible, with the two main systems – the battery safety lever and the battery gripper, performing as intended and opening the batteries, extracting, and inserting them reliably as well as securing the batteries at the end for a secure take off of the drone. With these overall goals successfully achieved, several issues were encountered, that needed addressing. While moving the

M300 using the DPS towards the BSS, pulling on the UAS legs proved more successful than pushing to the geometry of the leg. Unfortunately, several tests showed that the developed locking mechanism to secure the legs while pulling does not work reliably now. Therefore, pushing the drone was chosen for the moment, since inserting the drone into the BSS can be achieved more reliably. The increased force needed can be overcome by the sufficiently strong motors, which have been selected with an adequate safety margin when designing the system. Additionally, the drones' legs are equipped with friction reducing tape to lower the frictional forces when pushing the drone. This tape wears down over time, which increased friction and hence needs regular replacement to not jam the DPS.

Another issue arose with the UAS detection system on the Y-axis within the DPS. Limit switches within this system are triggered when the UAS' legs are touched. These switches are held open using springs, which in combination with friction forces inside the DPS lead to the system not being triggered albeit the legs were touched. The removal of the springs solves this problem but introduces the risk of false positives due to the switches being triggered when the accelerations of the DPS become too fast. Addressing this issue soon is crucial since choppy waters can impose sudden accelerations on the system, leading to false positives and hinder the correct insertion of the UAS into the BSS.

Moving to the functional testing the integration of the BHS with the ASV SeaLion was performed and proved to be successful. The most critical part was proving the calculations of the center of mass are correct, so that the position of the ASV is not tilted too much. Would the ship tilt backwards or forwards too much, this could either results in unwanted sliding of the UAS when landed or when released for take of as well as greatly influencing the hydrodynamic properties of the ASV when moving. With the bow or stern too deep in the water, properties such as maneuverability, acceleration, cruising speed as well as wave resistance could be negatively influenced to a point that driving the ASV autonomously would not be safe anymore. Another issue is the used material for manufacturing the custom parts. The used thermoplastic is called PLA (Polylactic Acid) and is used due to its fast 3D-printing speeds and easy of post processing. Unfortunately, these properties are combined with a relatively low glass temperature of roughly 60°C. With the functional tests on water being performed at 30°C ambient temperature and direct sun exposure, the components started to get soft. Although this issue is critical, the solution is simple and already being fixed. Another thermoplastic called PETG (Polyethylene terephthalate glycol) will be used with much higher glass temperature. Additionally, all components will be printed in white color, further reducing the absorption of heat radiation.

6. Conclusion

The above-mentioned work signifies the importance of integrating ASV and drone docking station with battery swapping capabilities. This approach solves the problem of short flight time of drones while performing inspection and surveys over large areas. The presented battery hot swap system is a novel idea which comprises DPS and BSS. The first integration test conducted have shown a promising result which proves the concept to be feasible. The shortcomings mentioned in the result and discussion will be resolved with further changes to the hardware and validation in upcoming tests on water. A complete test with an UAS autonomously landing on the ASV and performing a successful battery hot swap is planned for late September this year.

Acknowledgements

References

COCCHIONI, F.; MANCINI, A.; LONGHI, S. (2014), *Autonomous navigation, landing and recharge of a quadrotor using artificial vision*, 2014 Int. Conf. Unmanned Aircraft Systems (ICUAS) IEEE

DJI OFFICIAL (2022), M300 RTK - Quick Start Guide V1.4, https://dl.djicdn.com/downloads/matrice-

300/20220311QSG/M300_RTK_Quick_Start_Guide_V1.4.pdf

FENG, Q.; LIU, J.; GONG, J. (2015), *UAS Remote Sensing for Urban Vegetation Mapping Using Random Forest and Texture Analysis*, Remote Sensing 7/1, pp.1074–1094, https://doi.org/10.3390/rs70101074

FUJII, K.; HIGUCHI, K.; REKIMOTO, J. (2013), *Endless Flyer: A Continuous Flying Drone with Automatic Battery Replacement*, IEEE 10th Int. Conf. on Ubiquitous Intelligence and Computing and 10th Int. Conf. on Autonomic and Trusted Computing, pp.216-223

GRLJ, C.G.; KRZNAR, N.; PRANJIĆ, M. (2022), *A Decade of UAS Docking Stations: A Brief Overview of Mobile and Fixed Landing Platforms*, Drones 6/1, pp.17, https://doi.org/10.3390/drones6010017

HPA; UWS (2020), *Project Deliverable D1.2: Use case design specification*, H2020, Risk Aware Port Inspection Drones, https://rapid2020.eu/wp-content/uploads/2022/03/D1.2-Use-case-design-specification.pdf

ISRAEL, M.; EISENBEISS, H.; KUNZ, M.; INGENSAND, H. (2011), *A UAV-based Roe Deer Fawn Detection System*, Int. Archives of Photogrammetry and Remote Sensing XXXVIII-1/C22, pp.51-55

LEE, D.; ZHOU, J.; LIN, W.T. (2015), *Autonomous battery swapping system for quadcopter*, IEEE Int. Conf. Unmanned Aircraft Systems (ICUAS), pp.118-124

LIU, Z.N.; LIU, X.Q.; YANG, L.J.; LEO, D.; ZHAO, H.W. (2018), *An Autonomous Dock and Battery Swapping System for Multirotor UAV*, https://doi.org/10.13140/RG.2.2.19437.90085

MAMARIKAS, S.; MATTHIAS, V.; KARL, M.; FINK, L.; SIMONEN, P.; KESKINEN, J.; DAL MASO, M.; FRIDELL, E.; WINNES, H.; MOLDANOVA, J.; HALLQUIST, Å.M.; MELLQVIST, J.; CONDE, V.; VERBEEK, R.; DUYZER, J.; VAN DINTHER, D.; TIMONEN, H.; JALKANEN, J.P.; SUNDSTRÖM, A.M.; MAJAMÄKI, E.; STYLOGIANNIS, A.; NTZIACHRISTOS, V.; SMYTH, T.; YANG, M.I.; DEAKIN, A.; PROUD, R.; OEFFNER, J., SCHNEIDER, V.E.; BEECKEN, J.; WEIGELT, A.; GRIESEL, S.; SCHOPPMANN, H.; OPPO, S.; ARMENGAUD, A.; D'ANNA, B.; TEMIME-ROUSSEL, B.; KNUDSEN, B.; KNUDSEN, J.; KUOSA, M.; IRJALA, M.; BUCKERS, L.; VAN VLIET, J.; NTZIACHRISTOS, L. (2022), *2.21 Monitoring of ship emissions to enforce environmental regulations - The SCIPPER project*, Transport and Air Pollution (TAP) Conf.

MICHINI, B.; TOKSOZ, T.; REDDING, J.; MICHINI, M.; HOW, J.; VAVRINA, M.; VIAN, J. (2011), *Automated Battery Swap and Recharge to Enable Persistent UAV Missions*, Infotech@Aerospace, pp.1946-9802

PALAFOX, P.; GARZÓN, M.; VALENTE, J.; ROLDÁN, J.J.; BARRIENTOS, A. (2019), *Robust Visual-Aided Autonomous Takeoff, Tracking, and Landing of a Small UAS on a Moving Landing Platform for Life-Long Operation*, Applied Sciences 9/13, pp.2661, https://doi.org/10.3390/app9132661

PARK, S.; CHOI, Y. (2020), *Applications of Unmanned Aerial Vehicles in Mining from Exploration to Reclamation: A Review*, Minerals 10/8, p.663, https://doi.org/10.3390/min10080663

REMONDINO, F.; BARAZZETTI, L.; NEX, F.; SCAIONI, M.; SARAZZI, D. (2011), *UAV photogrammetry for mapping and 3D modelling - current status and future perspectives*, The Int. Archives of the Photogrammetry, Remote Sensing and Spatial Information Sciences XXXVIII-1/C22, pp.25-31, https://www.int-arch-photogramm-remote-sens-spatial-inf-sci.net/XXXVIII-1-C22/25/2011/isprsarchives-XXXVIII-1-C22-25-2011.pdf

SARDÀ-PALOMERA, F.; BOTA, G.; VIÑOLO, C.; PALLARÉS, O.; SAZATORNIL, V.; BRO-TONS, L.; GOMÁRIZ, S.; SARDÀ, F. (2012), *Fine-scale bird monitoring from light unmanned aircraft systems*, Ibis 154/1, pp.177-183

SEO, J.; DUQUE, L.; WACKER, J.P. (2018), *Field Application of UAS-Based Bridge Inspection*, J. Transportation Research Board 2672/12, pp.72-81

SILVA, S.C. de; PHLERNJAI, M.; RIANMORA, S.; RATSAMEE, P. (2022), *Inverted Docking Station: A Conceptual Design for a Battery-Swapping Platform for Quadrotor UASs*, Drones 6/3, pp.56, https://doi.org/10.3390/drones6030056

Analysis of Uncertainties in the Prediction of Fuel Savings from WASP Installations

Fabian Thies, Chalmers University of Technology, Gothenburg, Sweden, tillig@chalmers.se
Jonas W. Ringsberg, Chalmers University of Technology, Gothenburg, Sweden,
jonas.ringsberg@chalmers.se

Abstract

Many ship owners, operators and ship designers tend to put more trust into sophisticated, often CFD based, models for fuel consumption prediction with or without wind-assisted propulsion (WASP). Time consuming and expensive methods are often accurate, but sometimes not required for all parts of a complex system, such as a ship with WASP. Instead, the component imposing the highest uncertainty on the prediction should be modelled with the highest accuracy, while those components causing low uncertainties can be modelled with less sophisticated methods to save computation/analysis time and money. This study analyses the uncertainties from different parts of a WASP ship on the fuel saving prediction. Included components are the sail forces, the sail interaction, the wind speed profile over deck, wind shear, lift to drag and lift coefficients of the hull as well as the rudder forces and the center of lateral resistance of the hull. Further, it is evaluated how the accuracy of the initial power prediction of the ship without sails (including wind and waves) affects the fuel saving prediction. The results of the study provide a guideline on the most important parts of a WASP ship and highlights where sophisticated methods are required. Further, the study evaluates the expected accuracy of the empirical/ analytical fuel consumption/fuel saving prediction model ShipCLEAN developed by the lead author.

1. Introduction

To reduce the risk for shipowners and operators, and to study new possibilities to save fuel, sophisticated models to predict the power and fuel consumption of ships are necessary and became available during the last decade. Especially for the prediction of fuel savings from wind-assisted propulsion, the models must include more than only the forward thrust of sails and propellers, due to the large side forced generated by the sails. The hydro- and aerodynamic interaction effects increased the number of parameters, e.g., lift and drag of the sails, added resistance from drifting, etc, that must be evaluated to predict the fuel savings from wind-assisted propulsion. While methods and tools to predict the calm water resistance and propulsive efficiency of ships are widely existing, methods to predict static drift forces are less common. The use of manoeuvring equations might be tempting but has proven to be not accurate, *Tillig and Ringsberg (2020)*. On the other hand, CFD computations with multiple speeds and drift angles, potentially including the sails, rudder angle, heel angle, etc., are time consuming and not applicable if multiple points of sail shall be researched. Thus, it is crucial to identify the parameters with the biggest influence on the accuracy of the prediction. This study presents a sensitivity study of all parameters describing the aero- and hydrodynamics of a wind-assisted propelled ships to provide the information requested above. Additionally, a randomized variation is performed using the performance prediction model ShipCLEAN to estimate the achievable accuracy with a generic model, i.e., without the use of time-consuming CFD methods.

2. The generic performance prediction model ShipCLEAN

ShipCLEAN is a generic performance prediction model for ships with and without wind-assisted propulsion or for pure wind-propelled ships. During the development of the model, the focus was put to achieve the highest possible accuracy with a very low number of input parameters, i.e. only parameters that are publicly available. The accuracy of the model without wind-assisted propulsion is assessed in *Tillig et al. (2018)*. Besides a classic calm water prediction, ShipCLEAN also includes methods for added resistance in waves, due to shallow water, wind, ice and course and speed correction because of currents. Further, the frictional resistance can easily be modified to capture the effect of fouling. The module for wind propulsion, respects four degrees of freedom, i.e. solves the static

equations for surge, yaw, drift and roll, including a variable rudder angle. All details about the model and the wind propulsion part are presented in *Tillig and Ringsberg (2019,2020), Tillig and Ringsberg (2020)*. An overview over the parts of ShipCLEAN is provided in Fig.1.
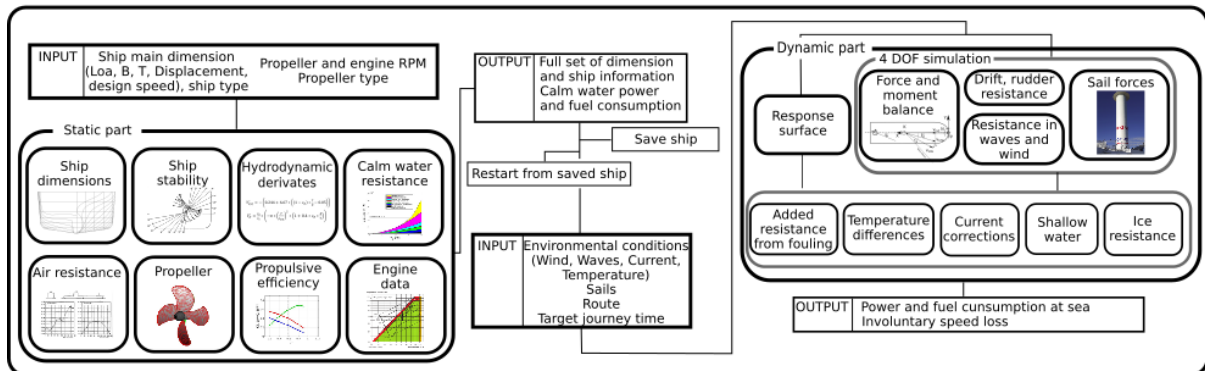

Fig.1: Overview over the ShipCLEAN model

3. The case study vessel

This study uses one of the case study ships of the EU-Interreg project WASP, *Tillig and Ringsberg (2021)*, to study the influence of parameter uncertainty on the prediction accuracy. The ship is a RoPax vessel, equipped with one 30m x 5m Flettner rotor, operating in the Baltic Sea between Germany and Denmark. The main dimensions of the ship are presented in Table I, and a sketch of the ship with the Flettner rotor is presented in Fig.2. Some variation studies using the same case study are presented in *Tillig and Ringsberg (2021)*.

Table I: Main dimensions of the case study vessel

L_{oa}	156.45 m
B	24.80 m
T	5.50 m
Δ	11996 t
Service speed, v_S	16 kn
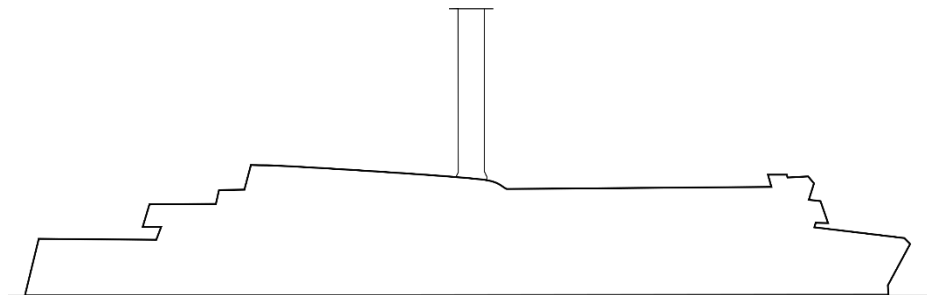
Fig.2: Sketch of the case study vessel with one Flettner Rotor

A polar plot of achievable fuel savings for 16 kn ship speed and 10 and 20 kn true wind speed is presented in Fig.3. The average fuel savings over all evaluated points for the one-rotor ship is 11.9%, which is used as a baseline in the variation study presented in this study.

During the sensitivity study, results for an alternative arrangement with two rotors, situated at 1/3 of L_{pp} and 2/3 of L_{pp} from the bow, is discussed. The polar plot for the two-rotor ship in 10 and 20 kn TWS and 16 kn ship speed is presented in Fig.3. The average fuel savings over all evaluated points for the two-rotor ship is 24.4%, which is used as a baseline in the variation study.
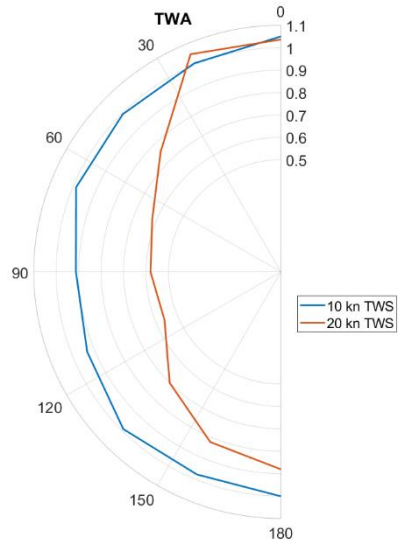
Fig.3: Relative fuel consumption over the true wind angle (TWA) for the case study ship with one Flettner rotor
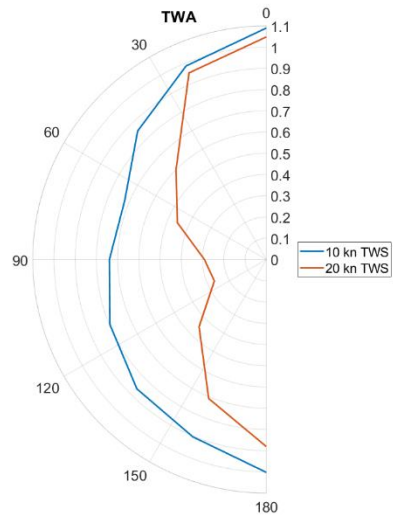
Fig.4: Relative fuel consumption over the true wind angle (TWA) for the case study ship with two Flettner rotors

4. Parameters for the performance prediction of wind-assisted and wind-propelled ships

In contrast to conventional propelled ships (i.e., without sails), where the propeller provides pure longitudinal thrust, sails introduce large side forces. Thus, apart from evaluating the sail forces and aerodynamic interactions, also the hydrodynamic response of the ship, i.e. drifting for side force balance and rudder movement for yaw balance, must be evaluated.

The parameters that must be evaluated can be devised into three groups: (1) parameters of the hydrodynamic response of the ship, (2) parameters to evaluate the sail performance, and (3) parameters describing the aerodynamic influences. All parameters are discussed in the following sections and summarized in Table II.

In addition to the parameters discussed here, the optimization of the sail trim influences the performance of a wind-assisted or wind-propelled ship. However, in this study it is assumed that the sails are always trimmed to the optimum.

264

Table II: Parameters for the performance prediction of WASP

Hull	CLR	Center of lateral resistance of the hull
	c_{D_hull}	Drag coefficient of the drifting hull
	c_{L_hull}	Lift coefficient of the drifting hull
Sails	c_{D_sail}	Drag coefficient of the sail
	c_{L_sail}	Lift coefficient of the sail
Wind	Delta AWA_deck	Change of wind direction due to deck-sail interaction
	Induced speeds	Induced speeds due to sail-sail interaction

4.1. Parameters to evaluate the sail performance

The performance of a sail, whether it is a Flettner rotor, soft sail, wing sail or similar, can be described using the drag and lift coefficients (c_D and c_L). Both usually depend on a trim parameter, e.g. the rpm of a Flettner rotor or the angle of attack of a wing sail. Examples of the drag and lift coefficients for wing sails and Flettner rotors are presented in Fig.5. The lift and drag coefficient influence the total force provided by the sails and the angle of that force to the centerline of the ship.
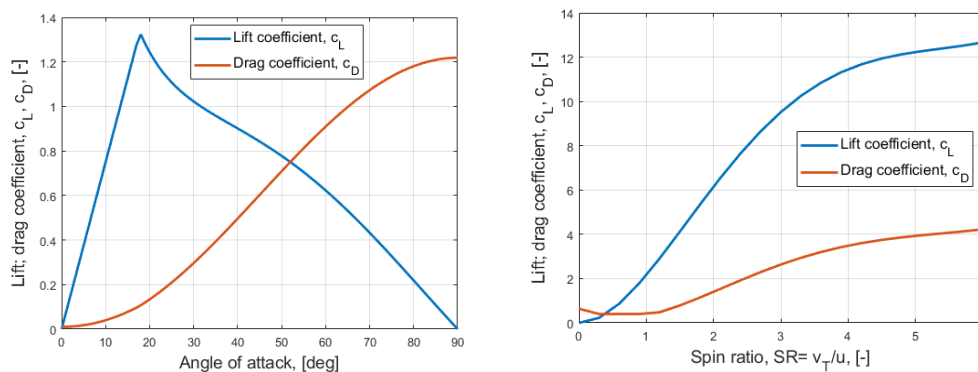
Fig.5: Lift and drag coefficient for a Wing sail (left) and a Flettner rotor (right)

The lift and drag of sails/ rotors can be predicted using CFD, model tests or full-scale measurements.

4.2. Parameters describing the aerodynamic interactions

The sails on a ship are influenced from the ship and its superstructure and from other sails on the ship. Sail-sail and deck-sail interactions are currently research in numerous projects, e.g., *Tillig and Ringsberg (2020), Bordogna (2020), Bordogna et al. (2020), Shoot (2022)*.

Sail-sail interactions are due to induced speeds from the bound and the tip vortices of the sails which change the local apparent wind angle (AWA) and speed (AWS) for other sails, *Tillig and Ringsberg (2020)*. These induced speeds will always be radial to the sail, thus, only the magnitude might be varied.

Special cases of higher influences can be found if sails are placed in the wake of another sail, or of the superstructure. Those cases are limited to a narrow range of wind angles and are neglected in this study.

The deck-sail interaction mainly affects the wind angle (AWA) of the sails due to a distortion of the wind flow over the deck. The wind flow tends to follow the transverse direction of the ship, thus diverting from the original wind angle. In *Schoot (2022)* it is shown that the apparent wind angle is also influenced by the ships deck. In beating conditions (i.e. TWA between 0° and 90°), the AWA was increased by up to 10°, while in downwind conditions, the AWA was decreased by up to 10°.

Combining the influences from other rotors and the influence from the deck, three parameters must be considered, (1) the change of AWA due to deck interaction, as a function of the wind angle which is only applied to the lower part of the sail and is (in ShipCLEAN) linearly decreasing to 0 at 50 m height over the deck, (2) a change of the AWA and the AWS due to sail-sail interaction which can be captured by a single parameter changing the magnitude of the induced speeds, and (3) a change of the wind speed profile.

In ShipCLEAN, the sail-sail interaction is evaluated using a highly simplified Navier-Stokes equation, *Tillig and Ringsberg (2020)*. An example of interactions on a ship with four rotors is presented in Fig.6.
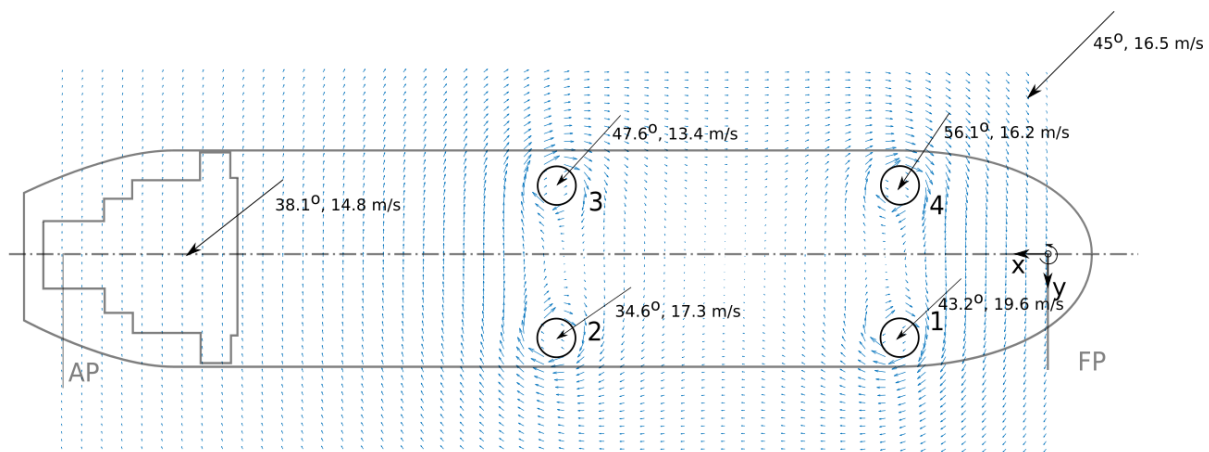
Fig.6: Variation of the local wind speed (AWS) and wind angle (AWA) because of sail-sail interaction effects

As a standard, the peak of (1), i.e. the change in AWA due to deck-sail interaction is 8° in Ship-CLEAN and the change of AWA over TWA is assumed to follow a sinusoidal curve, Fig.7.
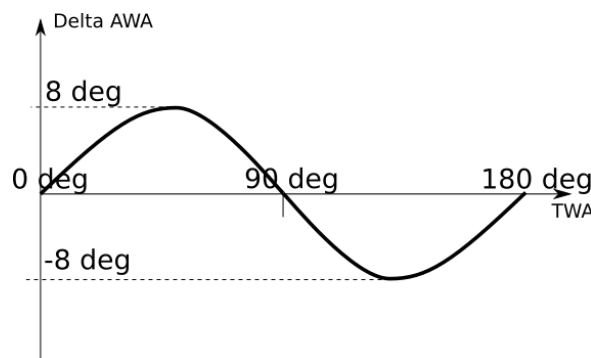
Fig.7: Change of AWA due to deck-sail interaction, over TWA

4.3. Parameters to evaluate hydrodynamic response of the ship

The hydrodynamic response of the ship to the side forces and yaw moments of the sails are a drift to compensate the side forces and a rudder angle to compensate the yaw moment. For the drift, the lift force, i.e. the created side force over the drift angle, and the additional resistance are of interest. As for the sails, those forces are defined using a lift and a drag coefficient. For the yaw moment, the rudder side force and the centre of lateral resistance (CLR), i.e., the longitudinal center of the side force, are of interest. Since the rudder forces are supposed to be well-predicted by common methods, they are not included in this study. While the lift and drag forces are varied by a scaling factor between 0.9 and 1.1, the CLR is moved fore and aft by 10% L_{pp} of the ship.

The calm water resistance and propulsive efficiency surely have a huge impact on the performance of a ship. However, this study focuses on fuel saving on wind-assisted propelled ships. In that case, any

uncertainties in the resistance or propulsive efficiencies would be equal for the ship with and without wind-assisted propulsion, and thus only have neglectable effects on the fuel savings.

5. Sensitivity study

To estimate the impact of variations and uncertainties of the parameters discussed before, a sensitivity study was performed. During that study, each of the parameter was set to 90% and 110% of the baseline value and the resulting fuel savings were estimated. In total 20 environmental conditions were evaluated, true wind angles (TWA) between 0° and 180° with steps of 20° and true wind speeds of 10 and 20 kn. In Table III, the average fuel saving with the different variations are compared as percentual difference to the fuel saving with the baseline values for the ship with one Flettner rotor. The results for the two-rotor ship are presented in Table IV. In both tables, only the results for the variation of one single parameter at the time are presented, i.e., in each row of the table are all but one parameter unchanged. For easier interpretation of the table, the rows are color-coded with green for lowest influence and red for highest influence. However, it must be kept in mind, that the table shows results for a percentual equal variation for all parameters but does not consider the achievable accuracy of each parameter. As an example, a 10% difference in the lift coefficient of a sail is very much, given the multiple and trustable data sources available. On the contrary, a 10% difference of the change in AWA due to deck interaction is less than 1° of the wind angle, and thus very small, given that good data is only available if time expensive CFD computations are performed. More information about the achievable accuracy using a generic model is given in section 6.

Table III: Results of the sensitivity study for the ship with one Flettner Rotor

| | | Difference in average fuel saving to the baseline | |
		-10% from baseline value	+10% from baseline value
Hull	CLR	0.01%	-0.01%
	c_{D_hull}	3.4%	-2.0%
	c_{L_hull}	-1.4%	0.4%
Sails	c_{D_sail}	0.4%	-1.4%
	c_{L_sail}	-15%	16%
Wind	Delta AWA_deck	-3.7%	1.5%
	Induced speeds	0%	0%

Table IV: Results of the sensitivity study for the ship with two Flettner rotors

| | | Difference in average fuel saving to the baseline | |
		-10% from baseline value	+10% from baseline value
Hull	CLR	-0.01%	0.7%
	c_{D_hull}	2.3%	-1.2%
	c_{L_hull}	-2.2%	1.7%
Sails	c_{D_sail}	4.2%	-0.6%
	c_{L_sail}	-11.8%	14.1%
Wind	Delta AWA_deck	-2.3%	1.2%
	Induced speeds	0.2%	-0.3%

Results in Table III and Table IV show that, in general, the variations are smaller for the two-rotor ship. For both ships, the lift coefficient of the sail has the highest impact, followed by the drag coefficient of the drifting hull and the change in apparent wind over the deck, i.e. the deck-sail interaction. The variability of the induced speeds has very small influence on the results, which can be explained by the

fact that the direction of the induced speeds is kept constant and only the magnitude is changed. However, a smaller induced speed might be beneficial for a rotor further aft, but at the same time the positive effect at the forward rotor is reduced as well. Thus, the effects seen in this study are mainly due to changes in the center of effort of the sail force. About the changes in AWA due to deck interaction, it must be kept in mind, that a 10% change of the peak value means that the difference in AWA is maximum 0.8°. This shows the importance of accurate TWA readings for the sail trim and the huge impact of the TWA on the total performance of wind propulsion.

As is further discussed in the following section, the lift and drag coefficients of sails are relatively well predictable, thus their effect will be rather limited. However, the drag coefficient of the hull and the deck-sail interactions are not easily predictable without time expensive CFD computations, mainly due to the lack of reliable data. Thus, those parameters should be seen as the most critical for the accuracy of fuel saving predictions from WASP installations.

6. Achievable accuracy using ShipCLEAN

To evaluate the accuracy of a prediction using ShipCLEAN, a randomized variation using a SOBOL algorithm with 200 variants was performed for the case study vessel. The reason to use a randomized variation instead of a Monte Carlo simulation is, that a lack of data for most parameters makes it impossible to define probability functions. In a randomized variation, the probability is constant over the whole design space of each of the variables/ parameters.

The maximum and minimum boundaries for the individual parameters were defined according to the discussion in *Tillig and Ringsberg (2020)*. Except for the change in AWA due to the interaction with the deck, which was not included in the above study. This parameter is set as a best guess, using the differences between the values in ShipCLEAN and the results shown in *Schoot (2022)*. Note that in this study, the lift coefficient of the hull and the lift to drag ratio of the hull are varied, but not the drag coefficient which is evaluated from cL and cL/cD. This is because only the uncertainties of the lift and the lift to drag ratio were discussed in *Tillig and Ringsberg (2020)*. All parameters with their lower and upper bounds are summarized in Table V.

Table V: Upper and lower bound for the variation study

		Lower bound	Upper bound
Hull	CLR	0.99	1.06
	c_{L_hull}/c_{D_hull}	0.85	1.1
	c_{L_hull}	0.92	1.3
Sails	c_{D_sail}	0.99	1.01
	c_{L_sail}	0.98	1.02
Wind	Delta AWA_deck	0.95	1.2
	Induced speeds	0.9	1.1

The results of the variation studies are presented as histograms in Fig.8 for the one-rotor ship and Fig.9 for the two-rotor ship. The mean value of the difference of the fuel savings was about 1.1% (i.e., about 0.2% fuel saving) for the one-rotor ship and about -1.4% (i.e., about 0.3% fuel saving) for the two-rotor ship. The standard deviations were 2.5% (i.e. about 0.5% fuel saving) for the one-rotor ship and 3.9% (i.e. about 0.9% fuel saving) for the two-rotor ship. For both set-ups the standard deviation is less than 1% in terms of fuel savings, which must be seen as very good, considering that ShipCLEAN is a generic model without the use of CFD. The higher standard deviation for the two-rotor ship originates from the increased importance of the drag of the drifting ship with increased sail power, unfortunately the drift coefficients are also those with the highest prediction uncertainty. Care must thus be taken for ships with large sail areas since the side forces become even more important.
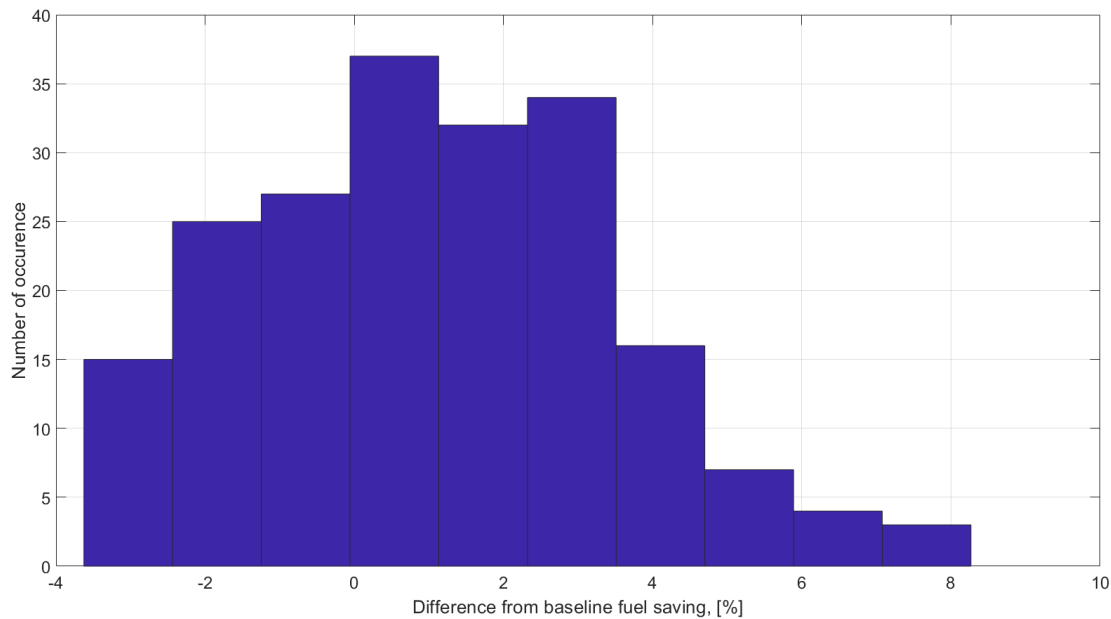
Fig.8: Results of the variation study for the one-rotor ship
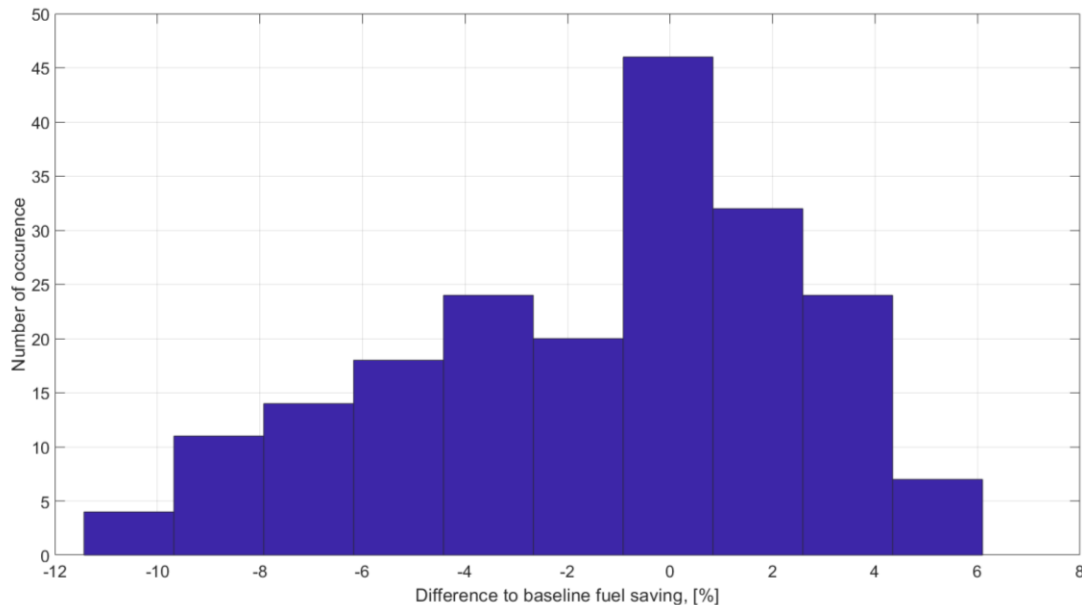
Fig.9: Results of the variation study with the two-rotor ship

7. Summary and conclusions

This study presented an approach to quantify the uncertainties in the fuel savings prediction of WASP installation. A sensitivity study with seven parameters and a variation study using ShipCLEAN were presented. It was shown that the lift coefficient of the sails and the drag coefficient of the drifting hull were the parameters with the highest influence during the sensitivity study. The variation study showed that, despite the high uncertainties in predicting the hydrodynamics of a drifting hull, a generic model like ShipCLEAN can provide very accurate predictions of the fuel savings. It must be concluded, that the higher the installed sail area becomes, the greater the importance of the hydrodynamics of a drifting ship. Thus, it is recommended to use CFD computations for pure sail-propelled or highly sail-assisted vessels. However, for WASP installations as seen today, generic models as ShipCLEAN are sufficient.

The sensitivity study also showed that the predicted fuel saving is very sensitive to changes in the wind angle. Note that instrumentation of ships to accurately measure the wind angle is often missing, faulty

269

or badly calibrated. It could thus be assumed that uncertainties due to inaccurately measured or predicted environmental conditions is much higher than the model uncertainty studies in this paper.

Acknowledgements

References

BORDOGNA, G. (2020), *Aerodynamics of wind-assisted ships*, PhD thesis, Delft University of Technology

BORDOGNA, G.; MUGGUASCA, S.; GIAPPINA, S.; BELLOLI, M.; KEUNING, J.; HUIJSMANS, R. (2020), *The effects of the aerodynamic interaction on the performance of two Flettner rotors*, J. Wind Engineering and Industrial Aerodynamics 119

SCHOOT, J. (2022), *Effective wind modelling for performance prediction, including for EEDI/EEXI,* Presentation at BlueWeek 2022, Rotterdam

TILLIG, F.; RINGSBERG (2019) *A 4 DOF simulation model developed for fuel consumption prediction of ships at sea,* Ships and Offshore Structures 14:sup1, pp.112-120, DOI:10.1080/17445302.2018.1559912

TILLIG, F.; RINGSBERG, J.W. (2020), *Design, operation and analysis of wind-assisted cargo ships,* Ocean Engineering 211, https://research.chalmers.se/publication/517710/file/517710_Fulltext.pdf

TILLIG, F.; RINGSBERG (2021), *Performance prediction and design of wind-assisted propulsion systems,* Int. Conf. Wind Propulsion 2021, pp.43-47

TILLIG, F.; RINGSBERG, J.W.; MAO, W.; RAMNE, B.J. (2018), *Analysis of the reduction of uncertainties in the prediction of ships' fuel consumption – from early design to operation conditions,* Ships and Offshore Structures 13:sup1, pp.13-24, DOI:10.1080/17445302.2018.1425519

Hull Form Optimization for Wind-Powered Ships

Fabian Thies, Chalmers University of Technology, Gothenburg/Sweden, tillig@chalmers.se
Hannes Renzsch, FRIENDSHIP-SYSTEMS, Potsdam/Germany, renzsch@friendship-systems.com

Abstract

The (re-)introduction of sails on commercial ships has drastically changed the requirements on new ship hulls. For traditionally propelled ships, designers aim for a low resistance and high propulsion efficiency, or an optimal trade-off in between those. While a low resistance still is crucial for wind-powered ships, the propulsion efficiency is replaced by the need for high stability, high course keeping ability, combined with a high lift coefficient and a high lift to drag ratio when drifting. All these new requirements arise from the high side forces introduced by the sails, which have to be compensated by the ship hull and the rudder. This study combines a parametric modelling software (CAESES), a CFD software (Shipflow) and a generic fuel consumption prediction model (ShipCLEAN) in an integrated workbench to optimize the hull form of a 45,000 m³ tanker with respect to the new demands for wind-propelled ships. The results of the study highlight the differences in optimization strategies for hull forms for traditionally propelled and wind-powered ships. Further, the difference in performance of a common reference and a hull form designed for wind propulsion are evaluated.

1. Introduction

Society must fight climate change. To do so, we must drastically reduce our carbon emissions. Because of its huge share in global trade, shipping also is one of the main contributors to global greenhouse gas emissions. Consequently, IMO set ambitious goals to drastically reduce such emissions, *IMO (2018).*

Considering the increase of trade since the reference year (2008), the goals become even more ambitious, meaning that shipping has to save ~60% of emissions per cargo mile, considering todays trade levels and the goal to reduce shipping's emissions by 50%. Naturally, such reduction is not achievable by any form of optimization of today's well-designed but traditionally propelled ships, not even by adding alternative propulsion, such as wind-assisted propulsion. Wind-assisted propelled ships can save about 20-30% of fuel and emissions, compared to similar ships with traditionally powered ships, *Tillig and Ringsberg (2020)*, but are far from the necessary 60%. Thus, it is time to introduce zero-emission ships, *Julia et al. (2020).* Together with significant emission reduction of all ships, a significant number of zero-emission ships can make shipping achieve the goals set by IMO. In this study, fully wind-powered ships are researched as one form of zero-emission ships.

However, wind powered ships are complex systems. Not only do they encounter similar, challenging environmental conditions as traditional powered ships, but sails as propulsion also introduce large side forces. Those side forces cause a drift, a heel, and a yaw of the ship, which must be compensated by the ship's hull creating side force, the ships righting moment and the rudder(s). This requires new approaches in both, the hull form design and the performance evaluation. Hull form design must focus on low resistance in a drifting condition, high stability and a good yaw balance. Aside from the added resistances of traditional ships, performance evaluation of wind powered ships has to include advanced sail trim controls of multiple sails, the hydrodynamics of drifting ships, ship stability and aerodynamic interaction effects. Additionally, the performance prediction cannot focus on the power requirements on certain speeds, but must evaluate the achievable speeds at different environmental conditions, i.e. different wind speeds and direction with associated waves.

This study presents an approach to combine multiple CFD computations with the performance prediction model "ShipCLEAN", which also evaluates the aerodynamic effects and sail forces, to form workbench allowing the designer to optimize the hull form of wind propelled ships.

2. The simulation platform

The simulation platform consists of three parts. Firstly, the parametric modeling and optimization software CAESES where the hull model was set up, the optimization was run and the external processes (i.e., the CFD computations and ShipCLEAN) were started. Secondly, the CFD computations which were performed in SHIPFLOW during optimization and in OpenFOAM as a final comparison. Lastly, the performance evaluation while sailing was performed using ShipCLEAN, a generic energy systems model programmed in Matlab, *Tillig and Ringsberg (2020).* While SHIPFLOW is readily coupled to CAESES, Matlab (and thus ShipCLEAN) was coupled using the custom integration provided in CAESES. All processes were controlled by CAESES, where also the results were compiled. A flowchart of the full optimization process is presented in Fig.1.
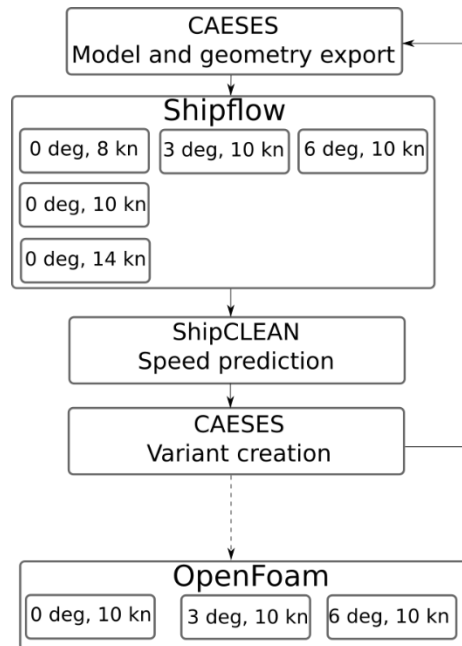
Fig.1: Flowchart of the simulation workbench

2.1. Parametric model in CAESES

The parametric hull model in CAESES built to be a simple and stable model, which adjust the displacement to match the target value. The hull form is controlled by the start and end positions of the flat of side and flat of bottom as well as their areas, the z-position of transom and the sectional fullness along the hull, specified at three points, the parallel midship as bilge fullness, at the transom and 10 m from the forward perpendicular. Additionally, the centroid of the sections at the forward end can be specified. Such model is easy to handle, requires very few parameters, but it lacks some control over details, e.g., the shape of the waterline in the forebody. However, the purpose of this study is to showcase an approach instead of a detailed optimization, thus a stable and fast model was selected.
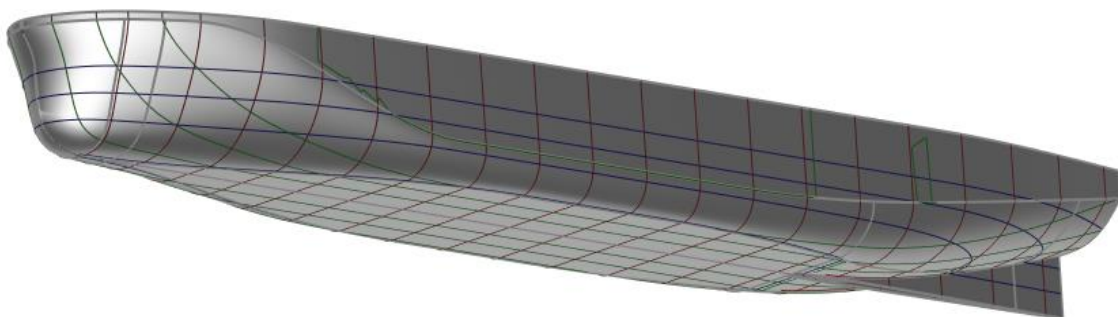
Fig.2: Rendering of the baseline sailing hull

For the wind powered ships, the traditional skeg of the baseline ship presented in *Harries et al. (2022),* was replaced with a straight skeg extending all the way to the transom, Fig 2.

2.2. CFD computations using SHIPFLOW

The CFD software SHIPFLOW is readily coupled to the optimization and modelling workbench CAESES, thus it is convenient to use SHIPFLOW for optimization purposes. Additionally, SHIPFLOW offers sophisticated automatic mesh generation. For stability and to safe time, all computations were run in model scale. For each variant, five computations with drift angles of 0°, 3° and 6° were performed. The condition without a drift was evaluated at three speeds (8, 10 and 14 kn) and the conditions with 3° and 6° were evaluated only at 10 kn.

During optimizations, the main task is to compare different variants, this a reasonable fine mesh was chosen, which still delivered good accuracy. For all computations a grid with about 3.4 million cells were used and all computations were run without symmetry and with a global approach, i.e. viscous computation over the complete hull. The free surface elevation (waves) was computed using potential flow methods. One computation took about 30 minutes on 16 cores; thus one variant was fully evaluated with CFD in about 2.5 hours. Volume of fluid methods which would deliver a more accurate result, would increase the computational time with a factor of 10 and were thus limited to the final computations of the baseline and promising designs using OpenFOAM.

2.3. CFD computations using OpenFoam

To support the optimization results obtained using SHIPFLOW selected cases for relevant geometries were simulated using a highly modified version of OpenFOAM, *Renzsch et al. (2017)*, *Meyer et al (2016)*. Again, to be able to use a validated simulation setup and accelerate turnaround times, the simulations were carried out in model scale. Following cases were computed:

- Baseline, initial sailing design and final hull shape
- Speed: 10 knots
- Drift angles: 0°, 3°, 6°

For the simulations, body-fitted split cartesian meshes with boundary layer refinement were generated using snappyHexMesh. At 0° drift angle this resulted in meshes of ~2.5 million cells, with drift angle of ~5.0 million cells.

The free surface is captured by a volume of fluid approach with appropriate mesh refinement in the free surface region and bespoke differencing schemes to keep a sharp interface between air and water.

2.4. Speed predictions using ShipCLEAN

ShipCLEAN is a generic performance prediction model for ships with or without wind-assisted propulsion or for fully wind-powered ships. During performance prediction, the model respect four degrees of freedom, i.e., it solves the static equations for surge, yaw, heel and drift including the rudder angle for yaw compensation. The methods, accuracy, and theory of ShipCLEAN have been presented in *Tillig and Ringsberg (2018,2019,2020).* An overview of the ShipCLEAN model is provided in Fig.3.

In this study, ShipCLEAN is used to predict the maximum ship speed in full-sailing mode in 22 conditions: true wind angles between 50° and 150°, in steps of 10° and true wind speeds of 10 and 20 kn. For the optimization, the average speed achieved in all of the 22 conditions was used as a target to maximize.
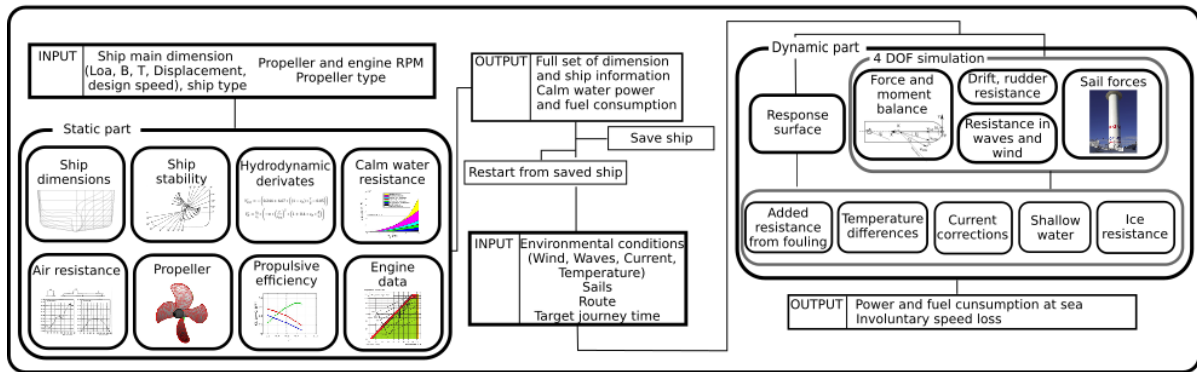
Fig.3: Flowchart of the ShipCLEAN model

3. Baseline vessel

The baseline vessel is the level 1 hull from the MariData project presented in *Harries et al. (2022)*. This hull is a remodelling of an existing tanker, the CB Adriatic, Fig.6, only considering main dimensions and general design features, e.g., a straight stem.

Fig.4: The CB Adriatic, baseline vessel for this study

For this study, the ship was equipped with six Flettner rotors with 5 m diameter of 5 m and 30 m height, Fig.7. Flettner rotors were used since this is the sail type best validated in ShipCLEAN, *Tillig and Ringsberg (2020)*.
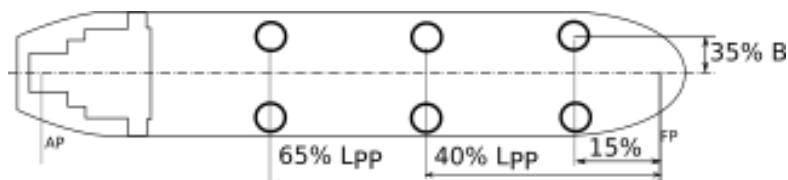
Fig.5: Flettner rotor arrangement for this study

4. Sensitivity study

Prior to the formal optimization, a sensitivity study is performed using ShipCLEAN. In total 5 parameters were varied, and the average and maximum speed achieved in TWS 20 kn and a TWA of 30°, 60°, 90°, 120° and 150° were compared. The varied parameters are the lift and drag coefficient (cL and cD) at 5° drift, the metacentric height, the center of lateral resistance and the total resistance, seen

over the full range of speeds. Each of the parameters were increased and decreased by 20% in a design of experiment using a Sobol algorithm with 100 variants.

Results of the study show that the maximum speed is mainly influenced by the resistance of the ship, Fig.8, not surprisingly since the maximum speed is achieved at a TWA of around 120°-15°, where side forces play a minor role.
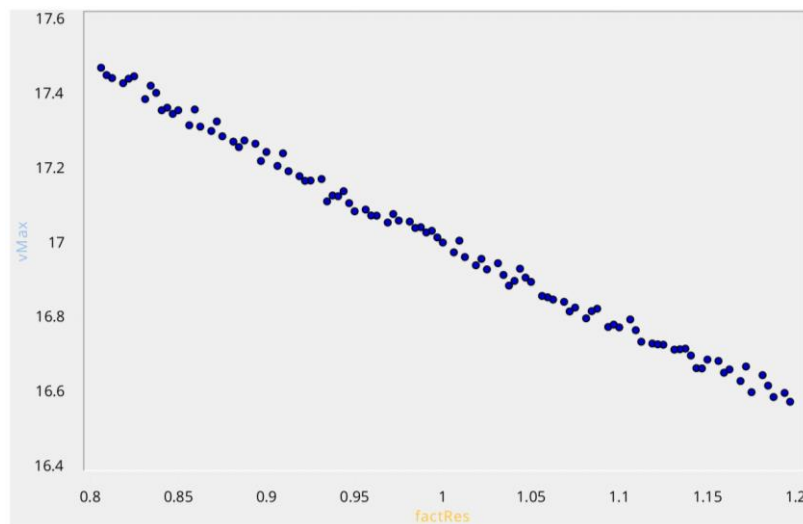
Fig.6: Achievable maximum speed over the relative resistance

Naturally, the resistance also influences the average speed. However, the results show two different levels of achieved average speed. These levels are caused by the fact that some of the ships are able to beat against the wind, i.e., sail at TWA less than 90°, while others are not. The main driver of the effect proved to be the drag coefficient of the hull while drifting, as shown in Fig.9, where the average speed is shown over the drag coefficient on the left and over the lift coefficient on the right. These results show that the absolute value of drift is less important, compared to the induced drag.
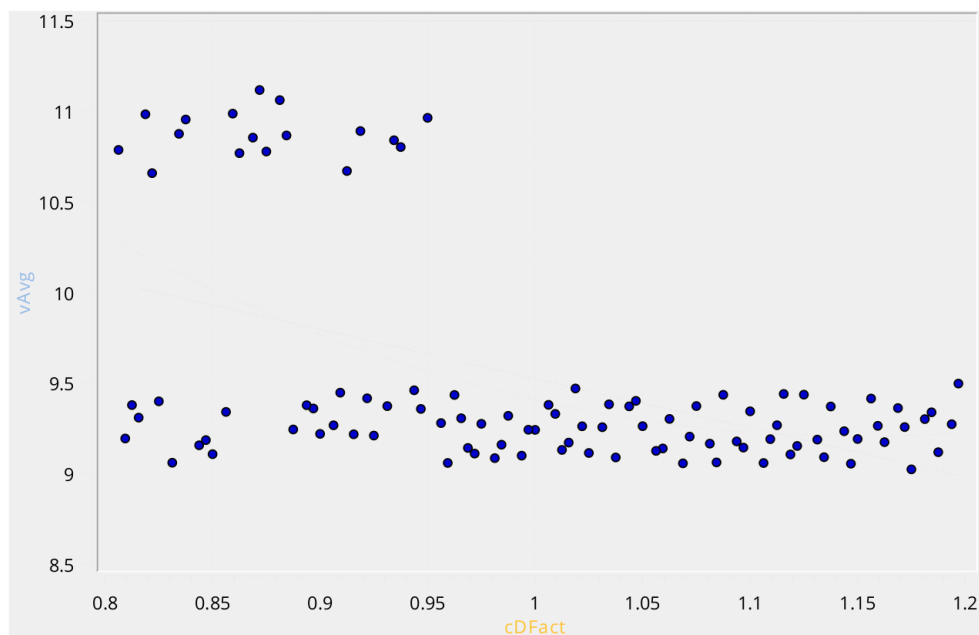
Fig.7: Average speed over the relative drag coefficient at 6° of drift

The KM proved to have no effect on the results, which is due to the high stability of this ship type. Even the CLR didn't have a major effect on the average or the maximum achievable speed.

5. Results and discussion

During variation and short formal optimization, about 150 variants were created. This section presents the hull form, the viscous CFD results and the predicted speeds of three variants, the original hull, the baseline sailing hull and the most promising hull from variations. While the baseline, the baseline sailing hull and the most promising hull (imprSail) were evaluated using OpenFOAM.

5.1 Hull designs

The original (baseline), the baseline sailing (baseSail) and the improved sailing hull (imprSail) are compared in Fig.8, with the baseline hull in black, the baseline sail hull in red and the improved sailing hull in green.
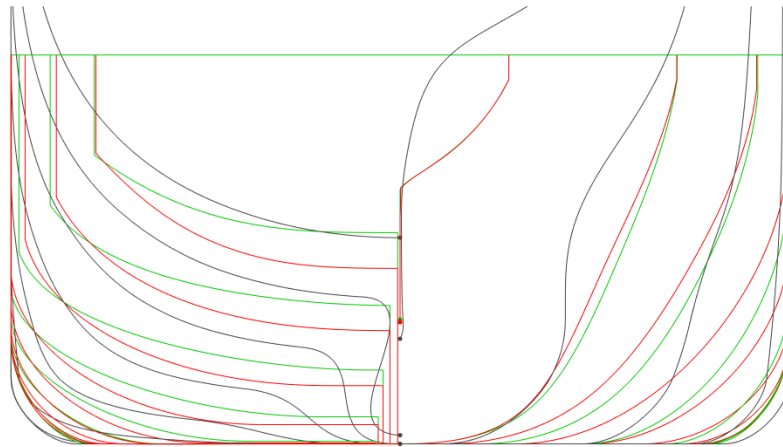
Fig.8: Hull forms of the baseline (black), the baseSail (red) and the imprSail (green) hull

A notable difference is the fuller bow of the sailing hulls, when compared to the baseline. This is mainly due to the parametric model. In between the sailing hulls, the improved variant features a larger bilge radius and a higher transom.

5.2 Viscous flow simulations

Selected hull designs were evaluated using OpenFOAM, namely the baseline, baseSail and an improved variant of baseSail (improSail). As the simulations were run in model scale and all geometries variants are within very narrow brackets of wetted length and wetted surface are the comparison is based on force coefficients and normalized effective draught (coefficients are computed with the wetted surface area).

The value of $\partial c_L/\partial \beta$ given an indication about the effectiveness of the hull to generate side force with increasing leeway angle β. The normalized effective draught t_{Eff} is calculated from the gradient of resistance by side force squared $\frac{\partial R_T}{\partial (F_H^2)}$ by

$$t_{Eff} = \frac{1}{T\sqrt{\frac{\partial R_T}{\partial (F_H^2)}0.5\rho U^2\pi}}$$

It includes all lift-depended contribution to resistance (parasitic profile drag and induced drag) that are usually considered to be proportional to side force squared. Its value gives a good indication about the hull's efficiency as a lifting surface. The results are given in Table I.

Table I: Evaluation of viscous flow simulation results for selected hull variants, relative to the baseline value at 0° drift (c_L relative to the baseline hull at similar drift angle).

Hull	b	c_T / c_{T_0}	c_R / c_{R_0}	c_L / c_{L_0}	$\partial c_L / \partial b$	t_{Eff}
[-]	[deg]	[-]	[-]	[-]	[deg^{-1}]	[-]
Baseline	0	1	1	-	4.368E-04	0.775
	3	1.02	1.12	1		
	6	1.15	1.65	1		
BaseSail	0	1.12	1.55	-	7.523E-04	1.264
	3	1.18	1.82	1.48		
	6	1.31	2.36	1.72		
ImprSail	0	1.05	1.14	0	7.085E-04	0.981
	3					
	6	1.18	1.71	1.62		

From above results it can clearly be seen that the baseline tanker hull – very much optimised for straight line resistance at these speeds – has the lowest drag but is an inefficient lifting surface. Both the gradient of lift by leeway as well as the effective draught are favourable for the hulls optimised for sail assistance. As discussed in Section 2.1, the sailing hull model is not designed for detailed optimization, thus the performance of the baseline model can not be achieved with the sailing hull model.

Figs.9 and 10 show the wave patterns at 6° leeway angle. The difference in resistance as indicated in Table I can clearly be attributed to the significantly different wave patterns generated by these hulls:
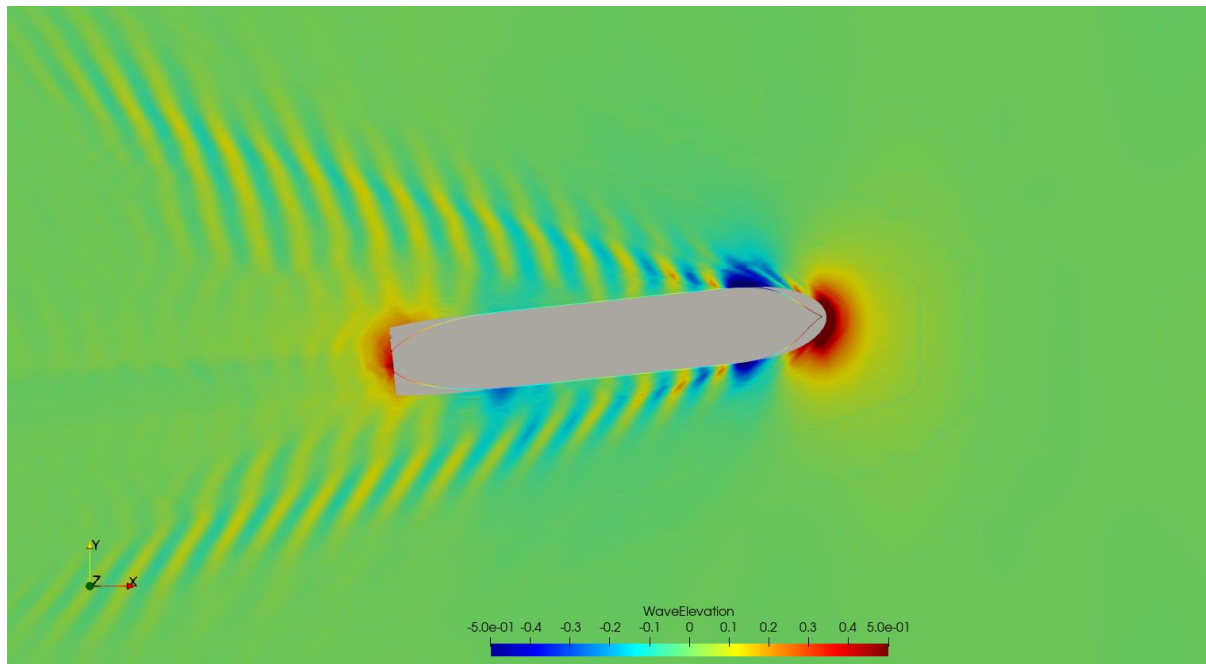
Fig.9: Wave pattern of the baseline hull at 6° leeway

Figs.11 and 12 show the Q-criterion at midships and aft at 6° leeway. The sail-assistance optimised hulls, particularly their skeg, produce a significantly stronger localised vortex, very much explaining the increased sideforce as well as effective draught.
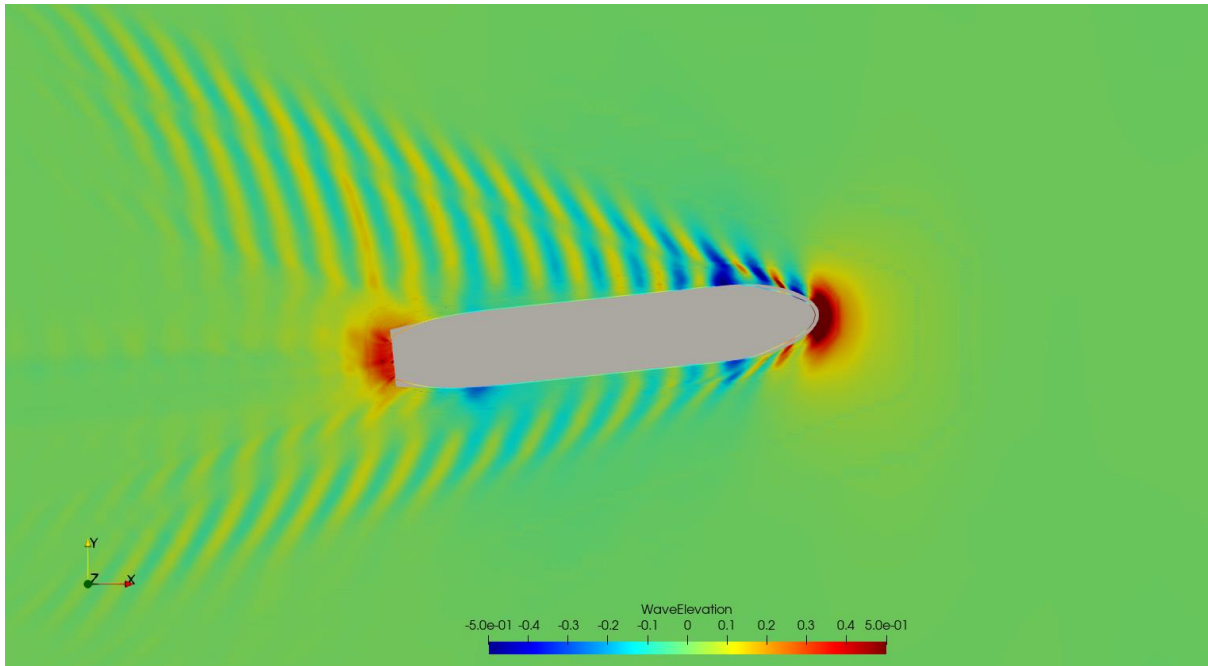
Fig.10: Wave pattern of BaseSail at 6° leeway
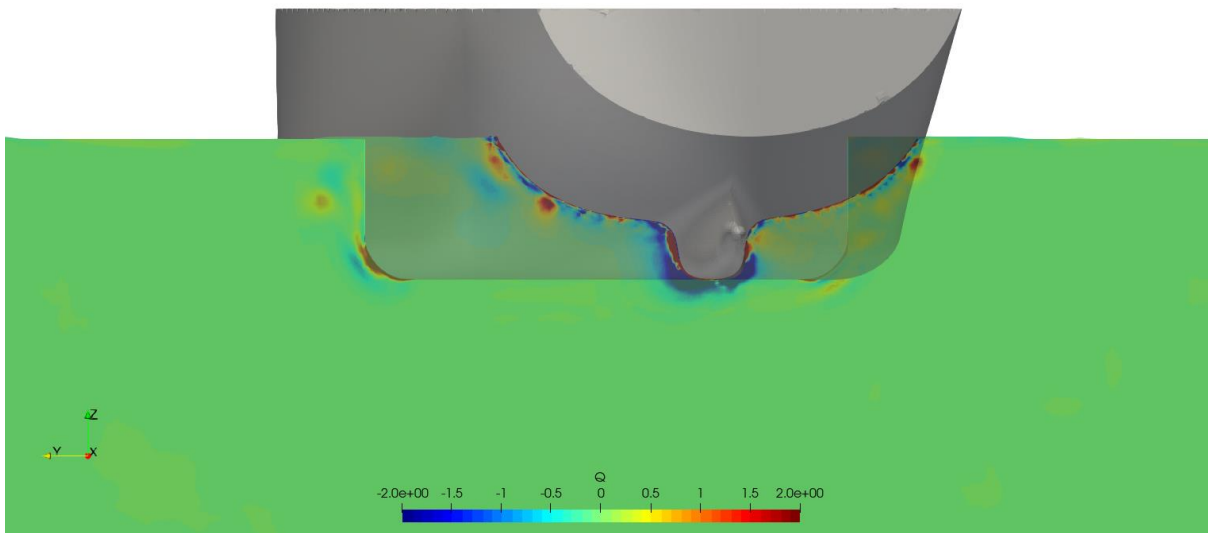
Fig.11: Q-Criterion, baseline hull at 6° leeway
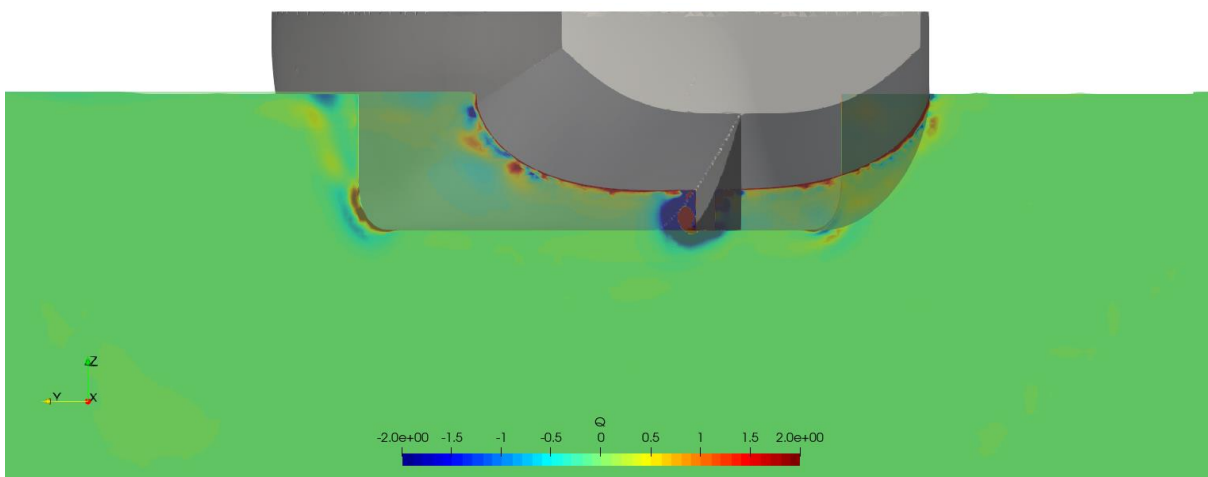
Fig.12: Q-Criterion, BaseSail hull at 6° leeway

278

5.3 Predicted speeds

The predicted speeds for the four variants are summarized in Table II, including the average speeds.

Table II: Predicted speeds of the selected hull variants.

TWA	Achieved speeds [kn]					
[deg]	10 kn true wind speed			20 kn true wind speed		
	Baseline	BaseSail	ImprSail	Baseline	BaseSail	ImprSail
50	0	0	4.19	0	0	0
60	7.92	8.27	8.18	0	0	0
70	9.21	9.34	9.49	0	10.7	10.62
80	10.23	10.24	10.38	12.69	12.68	12.71
90	10.83	10.83	10.90	14.70	14.7	14.72
100	10.95	10.88	10.96	16.00	15.9	15.95
110	10.67	10.59	10.64	16.81	16.63	16.69
120	10.08	10.03	10.02	17.02	16.83	16.89
130	9.37	9.21	9.24	16.63	16.35	16.45
140	8.45	8.30	8.32	15.71	15.5	15.57
150	7.61	7.55	7.57	14.55	14.41	14.68
Average	8.67	8.66	8.83	11.30	12.15	12.38

The results in Table II show rather small differences in the achievable speeds. The baseline hull has the best maximum speed, due to its low resistance. The sailing ship hulls show better performance in beating conditions, i.e., when the side force becomes important.

6. Unconventional hull forms

This study focused on the re-design of an existing tanker for pure wind-propulsion, while maintaining the general characteristics of the hull and a conventional approach to hull design. However, fully sailing ships of the future might require a new thinking, perhaps even re-thinking the old hull form of large sailing cargo ships. On approach could be to form the whole hull like a wing section, thus maximising the lateral area and thus the side force, probably achieving good drag coefficients if the bilge radius is well selected and achieving a low resistance of the hull in general. A sketch of such ship is presented in Fig.13. Unfortunately, the CFD analysis and design improvement of such hull was outside of the scope of the present study.
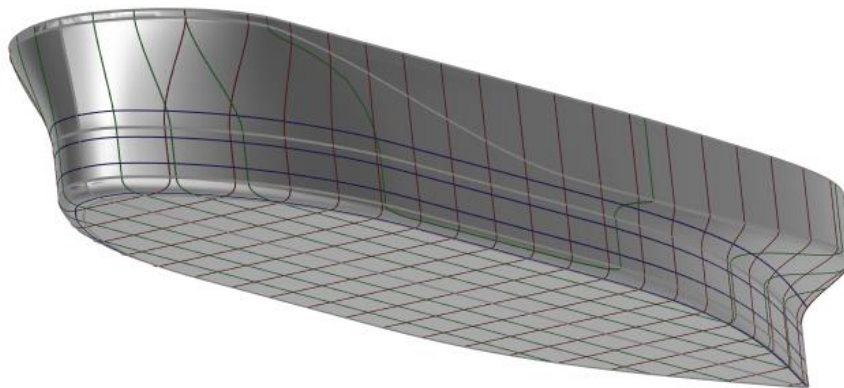

Fig.13: Rendering of an unconventional sailing ship hull.

7. Conclusions

This study presents an approach to optimize the hull form of fully sailing cargo ships. A workbench consisting of a parametric modelling software, a CFD software and a performance prediction model

was created to capture all effects on a sailing vessel and to enable the designer to use the achieved speeds in multiple environmental conditions, or even along a route, as an optimization target.

From a sensitivity study it was concluded that the induced drag due to drifting is the most important parameter in terms of increasing the average speed of a sailing ships. Minimizing the induced drag will enable the ship to sail closer to the wind. In terms of maximum achievable speed, the resistance at no-drift condition was most important. However, the variation also presented that a ship with higher resistance, higher induced and significantly higher lift performs better in terms of average speed and much better in beating conditions. Such "high lift" ship can be a good alternative for routes with large share of upwind sailing.

CFD computations at multiple drift angles showed that the wave pattern can get asymmetrical, causing the increase in drag to be non-linear. Thus, drift angles must be chosen carefully, e.g., the maximum expected/ allowed and one intermediate angle.

The study showed that the design of a sailing cargo ship is complex and requires an integrated approach using parametric modelling, CFD and performance prediction models. However, it can also be concluded that, to simplify and speed up the optimization, some condition might not have to be evaluated. From the sensitivity study and the variation results, one ore two computations at one or two drift angles (larger than 0) can be sufficient. An optimization towards low drag at a drift angle, possibly with a constraint on the lift coefficient, can be much quicker than the method proposed here. However, it must also be concluded, that ships with higher resistance, but lower induced drag and higher lift can achieve higher average speeds, especially because of higher speeds in beating conditions. Thus, a design space exploration, i.e., the randomized variation of variables, should be done with a method as described here, i.e., an integrated approach evaluating the achieved speeds while sailing.

In terms of important design parameters, the bilge height, bilge width and bilge fullness together with the main frame position, i.e., the length of the fore and aft body were most important for the lift and drag coefficients.

Finally, it must be concluded that fully-sailing or heavily wind-assisted cargo ships require a new design approach. Specifically designed sailing ships are better suited than retro-fitted conventional ships.

Acknowledgements

References

JULIA, E.; TILLIG, F., RINGSBERG, J.W. (2020), *Concept Design and Performance Evaluation of a Fossil-Free Operated Cargo Ship with Unlimited Range,* Sustainability 12(16):6609, https://www.mdpi.com/2071-1050/12/16/6609/pdf?version=1597471240

MEYER, J.; RENZSCH, H.; GRAF, K.; SLAWIG, T. (2016), *Advanced CFD-Simulations of free-surface flows around modern sailing yachts using a newly developed OpenFOAM solver*, 22nd Chesapeake Sailing Yacht Symp., Annapolis, pp.161-177

RENZSCH, H.; MEYER, J.; GRAF, K. (2017), *Investigation of modern sailing yachts using a new free-surface RANSE code*, Int. Conf.on Innovation in High Performance Sailing Yachts, Lorient, pp.67-76

TILLIG, F.; RINGSBERG, J.W.; MAO, W., RAMNE, B.J. (2018), *Analysis of the reduction of uncertainties in the prediction of ships' fuel consumption – from early design to operation conditions,* Ships and Offshore Structures, 13:sup1, pp.13-24, doi:10.1080/17445302.2018.1425519

TILLIG, F.; RINGSBERG (2019), *A 4 DOF simulation model developed for fuel consumption prediction of ships at sea,* Ships and Offshore Structures, 14:sup1, pp. 112-120, doi:10.1080/17445302.2018.1559912

TILLIG, F.; RINGSBERG (2020), *Design, operation and analysis of wind-assisted cargo ships,* Ocean Eng. 211, doi:10.1016/j.oceaneng.2020.107603

Innovative Platform for Optimising Renewable Energy Powered Ships

Kenneth Goh, Knud E. Hansen, Perth/Australia, KEG@knudehansen.com

Abstract

This paper presents the concept of a wind-propelled ship, i.e. a ship using wind propulsion as the main source of propulsion. The concept uses a proa form with main hull and outrigger. Due to the unconventional form, much of the design has to follow first-principles methods. The paper explores some of the main technical challenges and economics factors of the proa and introduces the REPAS (Renewable Energy Power Autonomous Ship) concept due to the equal significance of solar power that the platform allows.

1. Introduction

Reducing CO_2 for shipping is a high priority but the small efficiency gains in current internal combustion technology and using wind assisted systems is unlikely to make the significant changes to greenhouse gases that are being sought. KNUD E. HANSEN has been involved with numerous studies and commercial projects involving wind propulsion since 1996. It has been a persistent goal to utilise wind as a primary propulsion system, as opposed to only wind-assisted concepts.

One of the main technical challenges of wind propulsion is that the large sail systems get in the way of cargo stowage and loading operations. In a visionary exploration of future shipping, KNUD E. HANSEN is proposing an unconventional proa hull platform to overcome these cargo issues and that has many further benefits for employing renewable energies. The concept promises true carbon neutral shipping with reduced operational costs.

The proa vessel has a slender main hull and an outrigger hull for stability. When applied to a typical 50,000 DWT Handymax/Supramax cargo vessel, the benefits are intriguing and tantalisingly achievable. This radical departure away from the conventional monohull means the proa vessel falls outside of many Class requirements. Much of the engineering, structure, stability, powering etc, needs to be approached from first principles.

The paper explores some of the main technical challenges and economics of the proa platform in view of future development and studies to verify the benefits and practicality of this radical new vessel.

2. Project Background

Around 1999, KNUD E. HANSEN had developed an impressive concept design for a fully wind powered vessel – The WindShip, *NN (1996), Rosander and Bloch (2000)*. Comprehensive research into the economics and sail technology showed that a wind powered vessel for bulk and liquid cargo was feasible on certain trading routes, but in the year 2000 the additional capital expenditure was not able to be recovered due to very low fuel prices.

The current economic and environmental situation make the WindShip much more attractive. In 2017 an updated 'Windship 2025' concept was proposed that combines the performance of the earlier wing sail rig, a hybrid power system and autonomous operation. A new calculation model was developed to investigate the capital and operational costs and was benchmarked against the previous studies to ensure accuracy. The study demonstrated that very large savings in emissions and the cost of operation are now possible for the Windship within technology that is available today.

From the previous Windship studies, two aspects of efficiency were particularly notable. The first was the relative inefficiency of wind power ships when sailing into the wind. Not only must the Windship tack, meaning a longer sailing distance, but the efficiency of the sailing rig itself is much lower than

other wind directions since less of the lift force contributes to the propulsive effort and the drift forces are much higher. Furthermore, the effectiveness of the abaft sails is reduced considerably due to wind shadowing of the ahead sails.

The other notable aspect was how effective the solar panels were at reducing power requirements. The amount of power that photo voltaic solar panels can generate is slowly increasing, with efficiencies of over 23%, or about 225 W/m^2 now the norm. Would it be possible to install even more solar panels - enough power for significant propulsion such that heading upwind is possible without needing to tack with sail power? Trapeze type structures cantilevered from the main hull are possible, but they would be susceptible to wave damage when rolling in heavy seas provide complications for berthing and loading operations.

A catamaran configuration with the two hulls connected by a wide truss structure supporting the solar panels and sails would have obvious benefits, however the cost of constructing two hulls and supporting cross structure would likely double the cost of the vessel. The cross structure would need to cope with the loads from the other heavy hull as well as the sailing rig. Also, port operations would be greatly complicated by needing to unload and load both hulls.

3. Proa Windship Study

3.1. Proa Windship

Enter the proa – a vessel with a main hull and a smaller side stabilising hull called an amah. A common sailboat type throughout the Pacific for centuries, this highly asymmetrical vessel is known for its speed and stability. This concept is gaining considerable attention, particularly from smaller eco-friendly driven shipping companies targeting high-value bulk cargo such as coffee beans that could benefit from a vessel able to load at small ports. A proa configuration for a large merchant vessel, such as Handymax bulk carrier, would definitely be more expensive to construct than a conventional monohull, but not as much as a catamaran while still having similar advantages, notably:

On a proa, cargo is loaded entirely into the leeward main hull, which is also close to the centre of buoyancy. There will be very little change in righting moment regardless of the cargo load. With a proa, righting moment is provided by the weighted amah and outrigger structure to windward, not buoyancy to leeward. The righting moment remains consistent, meaning stress, scantlings and sail area will also remain consistent between laden and unladen compared to a catamaran. This is conducive to an efficient structure through a widely varying displacement compared to other multi-hulls.

The large space between the main hull and the amah is ideal for locating solar panels and the amah can limit the vessel rolling motions and provide some protection for the solar panels. The proa is designed to always sail with the amah hull to windward. This allows the sailing rig to be located on the windward side of the main hull, moving them out of the way of cargo and loading operations. The interference of the sailing rig with the cargo is one of the main reasons limiting the development of modern ship wind propulsion.

Although the goal is to ultimately have the Proa Windship unmanned, it is expected that a crew will be necessary for longer oceanic voyages, at the time of year 2030, the goal in-service date for the Proa Windship. A crew of eight should be adequate if the vessel is designed for periodic instead of continual maintenance. As per the previous Windship 2025 study, the use of containerised generators, fuel tanks and batteries will significantly reduce the on-board maintenance requirements. So will the use of electric systems instead of hydraulics where possible.

The crew is accommodated in two conning towers, one at each end of the vessel. The vessel can be conned from either tower which solves the problem of masts and sails obstructing visibility. A long internal corridor on the windward side of the main hull connects the towers and also provides access to the various electrical rooms required for the solar power harvesting and controlling the sailing rig.
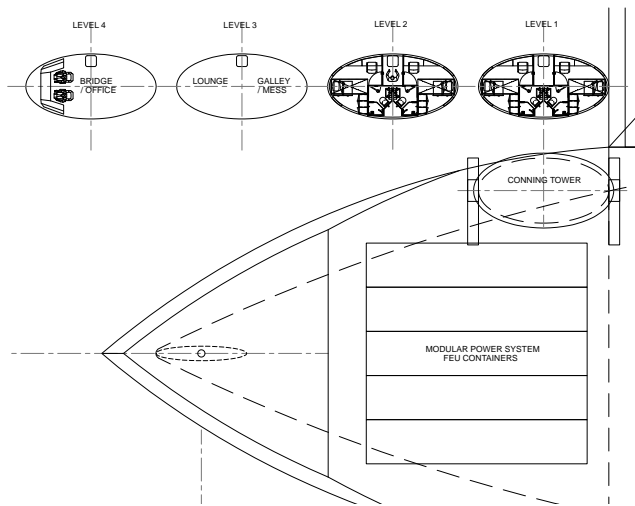
Fig.1: Crewing arrangement
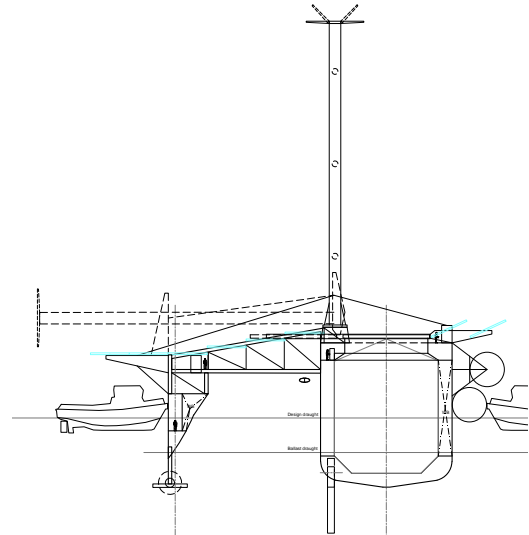

Fig.2: Proa Windship section
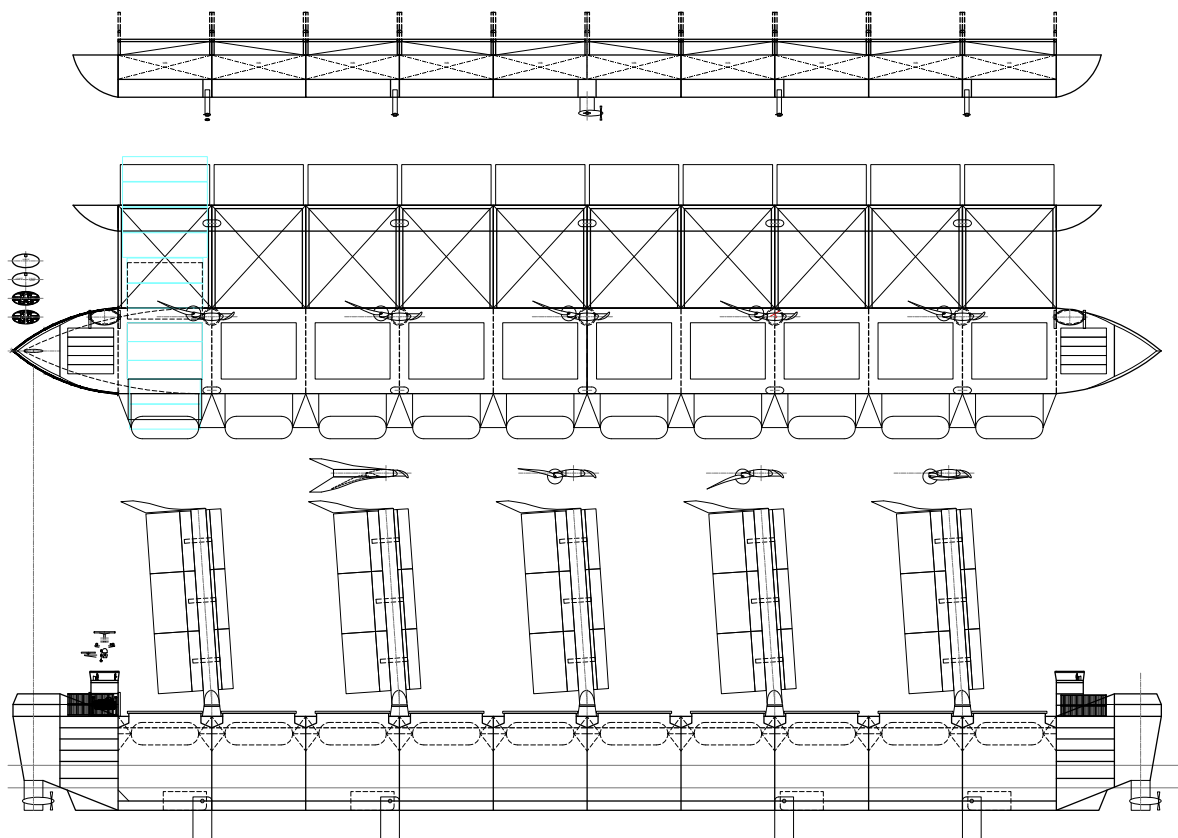
Fig.3: Proa Windship general arrangement

The additional stability afforded by the proa configuration enables the main hull length-to-beam to be increased beyond the normal range of 5-7. The longer hull, 300 m length compared to 225 m, would be less cost effective in terms of steel weight per cargo deadweight, but this is offset by being able to carry more cargo volume. The longer hull can also support a larger solar array to harvest more energy. Another advantage of a longer proa configuration is the greater space available for locating the sailing rig. Masts can be placed at greater spacing to reduce the wind shadowing effect of one mast on another, or more or larger sailing rigs could be installed.

The narrower main hull also means that the cargo is less susceptible to moving when the vessel rolls, which has led to numerous bulker capsizing casualties and loss of life, due to the catastrophic nature and rapid speed of such events.

3.2. Proa Sailing

The proa configuration has some interesting sailing characteristics. Because a proa is designed to sail with the amah always to windward, the vessel does not change tack the same way as a normal sailing craft. Instead, a proa needs to stop with the sails perpendicular to the wind and then reverse direction. This sailing action is called shunting, similar to the way trains can climb steep slopes with the aid of switch-back tracks.

The requirement of a shunting vessel is the need for the vessel to have a symmetrical hull fore and aft like a double-ender ferry. Typically, a double-ender has a lower hydrodynamic efficiency than a similar capacity single ender ferry, however much of this difference is due to a lower propulsion efficiency due to propeller wake-field. This is expected to be less significant for this concept, since a proa will have longer than normal length-to-beam ratio (13 compared to about 7) with finer lines in the bow and stern. Furthermore, the propulsion efficiency of the propeller is less significant since much of the propulsion will come from the sailing rig and the propeller loading can also be lower.
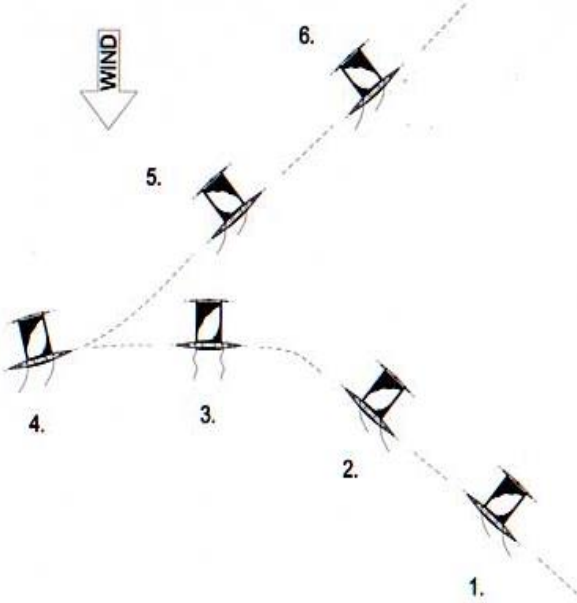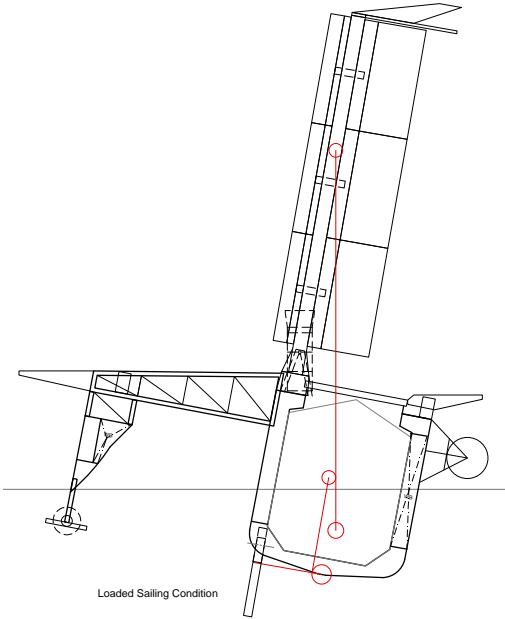
| Fig.4: Proa shunting | Fig.5: Proa sailing heeled at 10° |

To balance the proa, ballast tanks are provided on the leeward side of the main hull and in the amah. When the vessel is in the unloaded condition, the leeward ballast tanks are filled to offset the weight of the amah. When loading cargo, the vessel can discharge the leeward ballast water since the amah buoyancy will take care of the transverse imbalance. However, it is not possible to cover the range of draught with a fixed amah. A variable height amah would work, but incur additional complication and cost. An amah with a raking keel-line to provide different draughts is also possible but or having multiple in a that can change its vertical position above in the vessel will sail heeled to leeward by up to 10° to fly the amah free of the water.

When sailing, ballast water can be used in either the leeward or the amah tanks to balance the wind forces on the sailing rig when flying the amah free of the water. The transfer of ballast water between amah and main hull is not fast enough to cope with wind gusts and resulting variations in the sailing rig over-turning moment. Therefore, T-type control foils are also fitted to the amah to provide rapid response to changing wind forces, with the ballast water used to balance the average sailing forces.

The heeled sailing condition raises some interesting questions. The waterplane area of the heeled main hull will be asymmetrical and will cause the vessel to yaw towards the windward side. If the Proa Windship sails heeled the majority of time, especially at higher speeds, it is logical to shape the hull lines such that the main hull bow and stern create a symmetrical waterplane are when heeled. An asymmetrical main hull will be investigated in a future study. Sailing at a heeled angle will be uncomfortable for the crew, so the conning towers are designed to tilt to keep the accommodations level.

3.3. Proa Structure

The main hull is designed as a full double hull to increase the longitudinal strength and provide for the leeward ballast tanks necessary to balance the amah hull. The windward side of the main hull needs to cope with additional forces from the sailing rig, the amah hull and the retractable keels. Further FEM analysis may show that the double hull could be removed on the windward side of the main hull, but until then the conservative design is implemented.

The high length-to-beam ratio of the main hull falls outside the normal ratio for such bulker vessels as defined by Class. And therefore, many Class structural rules are not applicable for this proa concept. In order to check the structural weight of the main hull, if is necessary to use first principles engineering calculation to check the Still Water Bending Moment (SWBM) for hogging and sagging. This work is on-going and will be reported in a future study.

The structure joining the amah hull to the main hull is designed as a series of trusses connected to the main hull bulkheads to reduce weight. The only purpose of this structure is to support the amah hull and the solar panels. The truss members have an aerodynamic shape to reduce air resistance over the large exposed airflow frontal area.

The truss structure needs to cope with both buoyancy and mass loads from the amah since the amah maybe in the water or free from the surface when it is 'flying'. The wave loads will also be significant, given the heavy weather a wind powered ship is likely to sail in. A basic truss calculation was undertaken to determine the adequacy of the structure and confirm the weight estimate.

The hydro-resistance on the amah is relatively low by comparison to the vertical loads. Therefore, horizontal cross-bracing between the trusses with steel cables is sufficient with the trusses taking the additional compression forces from the cables.

3.4. Proa Stability

The stability of the proa vessel is certainly more complex than a normal mono-hull vessel. As with most stabilised concepts, the amah is designed to have minimum contact with the water. However, the outrigger configuration creates an enormous stability margin from capsizing due to both the buoyancy and weight of the amah acting at a large moment arm. The NAPA stability model showed that even the most extreme forces on the sail rig, the vessel's heel was only affected by less than 5°.

As with most stabilised monohull concepts, the amah is designed to have minimum contact with the water to reduce the resistance created by amah hull. The complication for a merchant vessel is the large draught variation between loaded and unloaded conditions. This is especially the case for bulkers or tankers which have high deadweight to lightweight ratios. Therefore, the Proa Windship is designed to sail heeled leeward to raise the amah out of the water when the vessel is heavily loaded.

Stability of the heeled vessel to windward is well provided by the amah buoyancy should the vessel roll towards the amah. The NAPA stability model showed that the vessel has low stability margin to leeward when sailing heeled. It is proposed that protection from leeward capsizing can be provided by large pneumatic fenders supported off the leeward hull by truss structures. The righting moment of 850,000 kNm would be more than twice of the maximum sail forces. The fenders will also help

balance the rolling moment created by the amah hull during wave encounters. Furthermore, the fenders could also be lowered to protect the hull in berthing.

ID: LC24 : Cargo: Wind 10 Degrees Heel

Floating position:

Draught mean moulded	12.991 m	Dead weight	56462 t	KMt	27.994 m
Thickness of keelplate	0.010 m	Light weight	15682 t	KG Solid	10.905 m
Draught mean (Below keel)	13.001 m	Displacement	72144 t	GM Solid	17.090 m
Draught FP (Below keel)	13.101 m	Seawater S.G.	1.025 t/m3	FS. cor.	0.004 m
Draught AP (Below keel)	12.902 m			KG Fluid	10.909 m
Trim	0.199 m	Heel angle	-10.2 deg	GM Fluid	17.086 m

CARGO　　WATER BALLAST　　FRESH WATER　　Crew Cabin
PROVISION
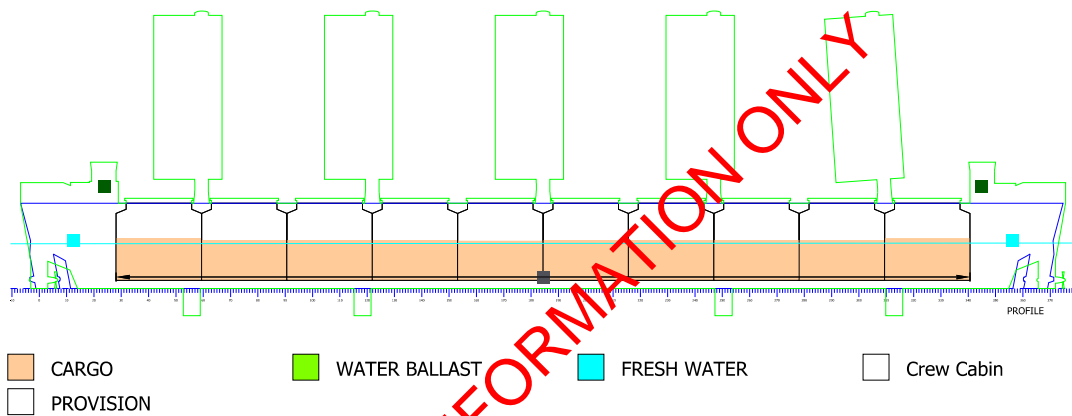
Fig.6: Proa stability max. deadweight with wind and 10° heel
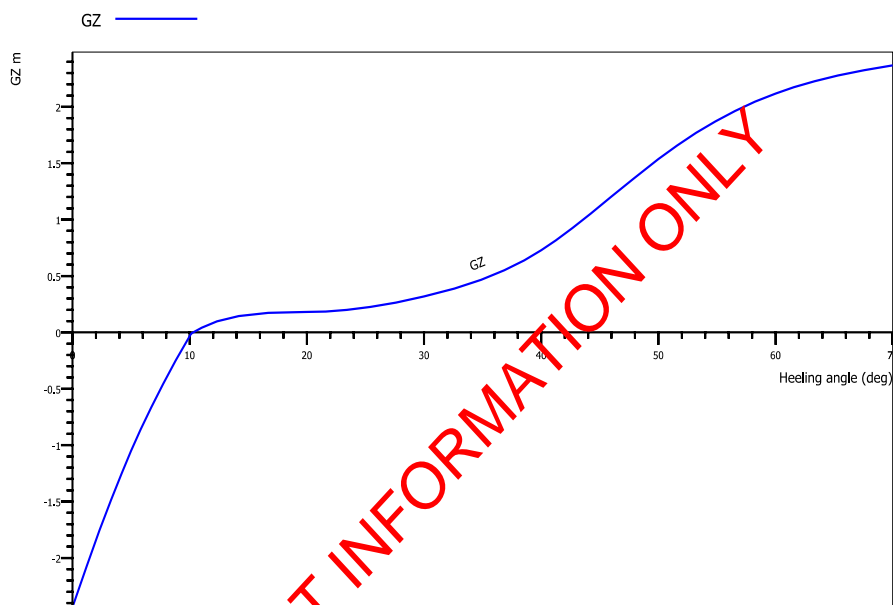
No downflooding within the calculated stability heeling range.

Criteria	TEXT	REQ	ATTV	MINGM	SIDE	STAT
AREA30	Area under GZ curve up to 30 deg.	0.055 mrad	0.063 mrad	17.016	SB	OK
AREA40	Area under GZ curve up to 40 deg.	0.090 mrad	0.149 mrad	16.814	SB	OK
AREA3040	Area under GZ curve between 30 and 40 deg	0.030 mrad	0.086 mrad	16.530	SB	OK
GZ0.2	Max. GZ > 0.2	0.200 m	2.367 m	14.779	SB	OK
MAXGZ25	Max. GZ at an angle > 25 deg.	25.000 deg	70.000 deg	13.970	SB	OK
GM0.15	GM > 0.15 m	0.150 m	17.086 m	0.150	SB	OK

Fig.7: Proa Windship showing unique stability

Current rules do not cater well for the stability of many multi-hull configurations. The NAPA stability model and Class rule requirements for stability only consider static conditions, even when the vessel stability is tested for increasing amounts of roll. What is not considered is the roll second moment of inertia. Regardless of the static stability condition of the proa, for any given roll angle the proa will generally exhibit more stable roll motions than a monohull, since the higher roll moment of inertia results in a lower roll acceleration rate. This is similar to a person extending their arms to help with balancing.

Roll acceleration is particularly important for a wind power vessel, since the sailing rig creates a significant overturning moment, up to 400,000 kNm, and are subjected to sudden increases in force due to wind gusts. The sails are designed to 'give' to reduce gust loads, but a vessel which is less sensitive to roll forces is an obvious benefit for any control system.

In addition to the gust alleviation control by the sails, the Proa Windship has control foils on the amah hull to provide active roll control, similar to anti-roll stabilisers. The combination of the heeling tanks, sail and roll control foils should enable the Proa Windship to safely sail at a heel angle of about 10° with the amah hull flying free of the water surface, with the possibility of reducing resistance and propulsion power.

3.5. Proa Hydrodynamics

The longer main hull of the proa configuration will have a higher frictional resistance due to the lower volumetric and Wetted Surface Area (WSA) to displacement ratio compared to the shorter and wider hulls of similar capacity bulkers. However, the hulls residual resistance comprising of wave-making and eddy currents is expected to be considerably less due to the lower Froude number, about 0.15, of the longer hull and smaller beam.

Due to the unusual hull dimensions of the Proa Windship, semi-empirical calculations and regression formula could not be used for resistance and powering estimations with any certainty of accuracy. Therefore, CFD has been used to compare the Proa Windship with the previous more conventional Windship hull, which is closer in main dimensions to a standard bulk carrier of similar deadweight.
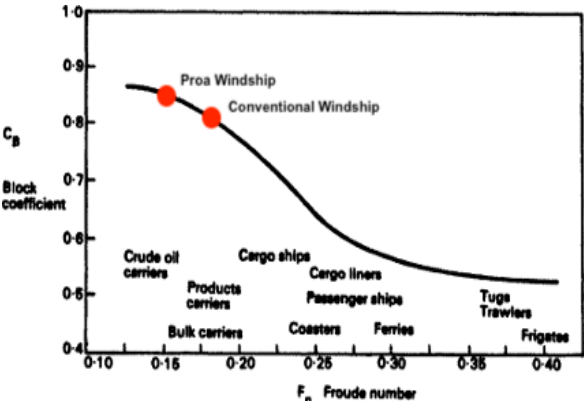

Fig.8: Proa Froude number of main hull   Fig.9: CFD showing multi-hull wave interference
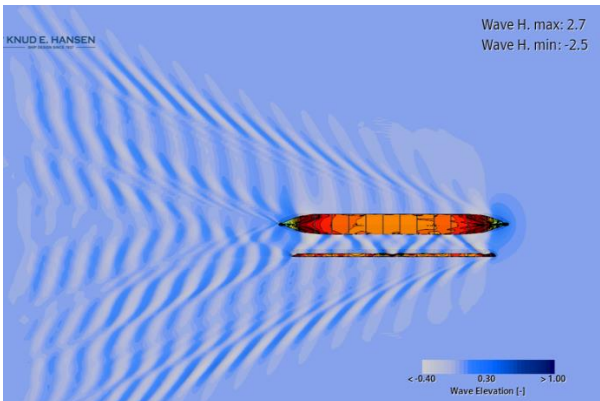
The CFD calculations have been done at ballast and maximum deadweight. The ballast condition was sufficient for propeller immersion. The calculated lightweight of the Proa vessel over the conventional Windship was about 3,000 tons. This was caused by the relative inefficiency of the proa structural configuration compared to a normal configuration. Furthermore, the WSA of the fully loaded proa was higher by about 48% due to the amah hull and high length-to-beam of the main hull. This increased frictional resistance considerably, but at 15 knots the overall resistance between the proa and conventional vessel was very similar due to the lower residual resistance of the longer and narrower proa hull. The effect of wave interference between the main and amah hulls still needs to be investigated.

With a heeled hull the CFD analysis has shown a great potential for reduced powering. At 15 knots and a 5° heel the overall resistance is reduced by 25%. At 10° the amah hull is out of the water, and the resistance is reduced by 60%. Note that these CFD calculations are only preliminary. Although the accuracy of the CFD solver is typically within 2-3% of model tank testing methods, the hull forms have not had any optimisations and trim was also not investigated.

Added resistance in waves is also expected to be reduced considerably with a narrower hull having less frontal area and a longer hull pitching less in heavy seas where a wind powered ship will spend much of its time. Although, this has not been calculated or tested at this time, a reduction of 30% for the added resistance in waves component has been included in the economic calculations for the Proa Windship based on the difference in frontal area. This will be verified in a future seakeeping study.
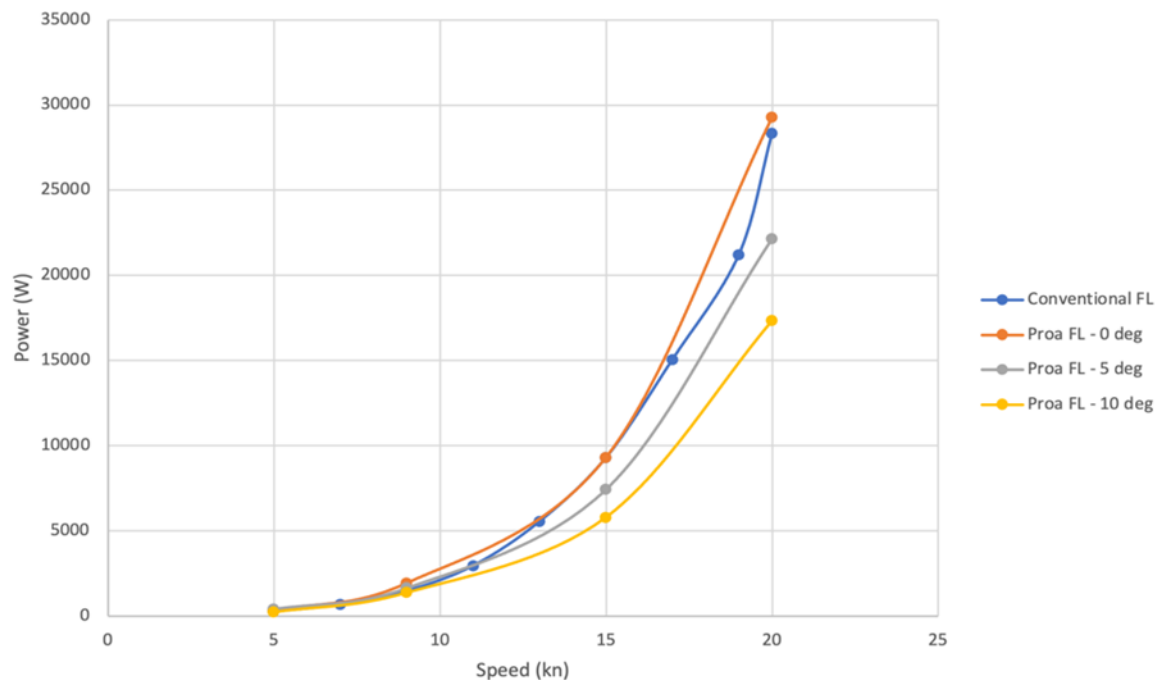
Fig.10: Powering – Full load conventional and proa Windship

WIND VELOCITY	SPECTRUM		SHIP SPEED			
U_{10} /(m/s)	H_s	T_s	10 kn	15kn	20kn	30kn
7.7	2	5.6	0.1 kN	0.0 kN	0.0 kN	0.0 kN
12.1	3	6.7	19.0 kN	12.1 kN	8.3 kN	4.7 kN
15.9	4	7.7	140.5 kN	91.9 kN	63.2 kN	34.2 kN
19.3	5	8.6	386.5 kN	270.3 kN	194.5 kN	104.9 kN

Fig.11: Added resistance in waves – Head seas for conventional Windship

3.6. Sailing Rig

As in the 2017 study, the sailing rig comprises of five wing masts. The wing mast is like an airliner wing during landing. With slats and flaps the sail has a high lift coefficient, of about 3.2. This enables the sail to be much smaller, with only a third of the area compared to a normal sail with a lift coefficient of about 1.0.

The high-lift wing mast provides lift at a wide range of apparent wind directions compared to other high-lift sail types such as Flettner rotors. The disadvantage of this type of high-lift wing sail is the high drag-to-lift ratio making them less efficient than a simple wing in upwind courses. The wing could be designed like an airliner wing to have retractable slats and flaps to reduce drag and improve performance upwind, however this would involve increased mechanisation, cost and maintenance.
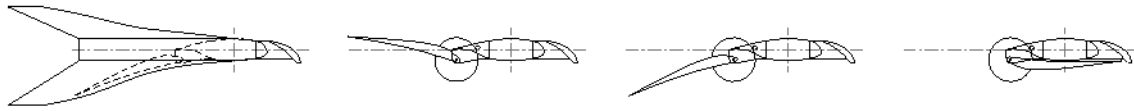
Fig.12: Wing sail section showing winglets, flap position for low drag, high-lift and reefed modes

The wing is comprised of a number of sections that can rotate around the central mast to change the direction of the wing profile, which is necessary when the vessel changes tack. The mechanism can also be used to enable the wing sections to track the sun when wind conditions are too low for effective propulsion.

Each wing section has a slotted slat and a movable flap that can adjust to provide wing twist, and gust alleviation. The flap can also fold forward for reefing in case of wind speeds exceeding the design limit of 50 knots.

The mast is a box structure that also forms the central section of the wing profile. The mast can azimuth to point the wing into the apparent wind and rotates 180° to enable the proa to swap bow to stern when shunting. The entire mast with wing sections can fold down onto the amah hull to:

- Reef the sail rig fully
- Clear traffic & rail bridges
- Prevent damage from cargo loading
- Provide better access for maintenance

A large winglet is installed at the top of each mast to reduce the induced drag from vortex shedding at the end of the wing sail. The winglet comprises of two moveable fins that can fold up or down, depending on the direction the wing profile is facing. One fin is folded onto the wing flap to provide an aerodynamic fence, while the other fin is angled up to reduce the strong vortices at the tip of the wing where low and high pressure streams meet.

The proa configuration allows the sail masts to have greater separation from each other, reducing the loss of lift when the sails are in wind shadow of an upwind mast. These loses can be significant making the sailing rig

3.7. Hydro Propulsion System

The hydro propulsion system is provided by three electric thrusters, each integrated into a steering rudder. One unit at each end of the main hull will provide about 3,000 kW of propulsive power. The third unit is a smaller 1,000 kW unit located amidship of the amah to counter the resistance which otherwise would need to be less efficiently countered by the main hull rudder thrusters. The three thrusters, each being able to azimuth 360° should give the Proa Windship the ability to berth and manoeuvre in and out of ports without tugs, even in moderate wind conditions, further reducing operating costs. The propellers will need to be of a controllable pitch type to work efficiently at different speeds and resistance, since the sailing rig will load and unload the propellers depending on the wind speed and direction.

Since there are two main propellers, the propeller loading can be reduced to increase efficiency. With the power distributed between two propellers, a smaller propeller size is possible. In the ballast condition, this will allow the Proa Windship to run at a reduced draft or without aft trim to keep the propeller submerged, which should also reduce the propulsion power needed.

The Proa Windship will have a symmetrical hull that can sail efficiently in either direction. Studies of the propulsive efficiency of similar double-ender ferries show that the overall propulsive efficiency is much better with only the astern propeller loaded because any accelerated flow created by the ahead propeller creates increased resistance on the forward hull. Therefore, the ahead propeller should be feathered if possible or turned to minimise it's resistance. No optimisation of the hydro powering

system has been performed in this study. For example, it may be better to have each of the main thrusters capable of 4-5 MW. This would increase the abaft propeller loading but reduce the required thrust from the ahead propeller.

As proposed in the previous Windship study, the thrusters can also operate as turbine generators when the vessel speed is favourable. Model testing of the Windship with a conventional hull demonstrates that in a favourable reach (wind from the beam), the bulker vessel could sail at nearly 20 knots in a wind of 15 m/s.

WIND SPEED [M/S]	3	5	7	9	11	13	15	17	19
SHIP'S SPEED [KNOTS]	4.26	7.35	9.90	12.43	14.89	17.32	19.73	22.13	24.51

Fig.13: Windship speed at 100° true wind using only sail propulsion

It is proposed that hydro harvesting is utilised above 15 knots, since the vessel's resistance curve increases steeply above this speed. The efficiency of harvesting will be somewhat lower than the propulsive efficiency since the propeller shall be optimised for propulsion and not as a turbine.

3.8. Solar Power Plant

The amah hull is positioned about 25 m from the main hull to limit the overall beam of the vessel to 50 m. With a maximum draught of about 12 m, the proa vessel should be able to access most trading ports. With a length of 250 m, the area between amah hull and the main hull is 6,850 m². Allowing a conservative 95% solar panel coverage and a panel output of 235 W/m², the peak power output is 1,530 kWe.

A simple folding trapeze structure from the amah will expand the solar collection area by another 3,000 m², adding a further 670 kWe. Solar panels mounted on the large cargo hatches add 700 kWe and a similar trapeze from the hatch extending to leeward, another 600 kWe. The trapeze is mounted to the sliding hatch instead of the main hull to enable the delicate panels to move out of the way during cargo operations. The rigid panel solar peak power totals to about 3,500 kWe.

The rigid structure of the wing sail also provides a perfect host for solar panels and the vertical orientation of the sails will complement the horizontal mounting of the above noted flat panels to even out the solar harvesting throughout the daylight hours. Both side of the wing would be covered by solar panels to maximise harvesting throughout the day. Although the sun cannot be shining on both sides of the sail at once, the side in shade can still generate about 10-25% energy due to light reflection off waves and diffuse lighting.

The curved surfaces of the wing must use flexible solar panels with a lower power capacity of 160 W/m² compared to 235 W/m² for the rigid flat panels. Each of the five wing sails has an area of 1,000 m², resulting in 1,500 kWe with 90% coverage and peak power of about 850 kWe, considering one side will be in shade. During periods of low wind, the wing sail is also able to act as a double-axis solar tracking system.

The resulting total power production of rigid and flexible solar panels is calculated by a mathematical model that takes into account the following factors:

- Date
- Latitude
- Ship heading
- Cloud cover
- Mast azimuth
- Tracking from sails
- Geometry of panels

In addition to the type of solar panels, the harvesting capability of the Proa Windship was divided into different tracking types. The rigid panels mounted to the cargo hatches are fixed in the horizontal plane. The rigid panels in the truss structures have single-axis tracking, with the axis aligned to the vessel's length. When under sail propulsion, the flexible panels on the sail are fixed vertically at the mast azimuth determined by the apparent wind direction. When utilising the sail rig for solar harvesting, the mast and wing sections act like a 2-axis tracker.
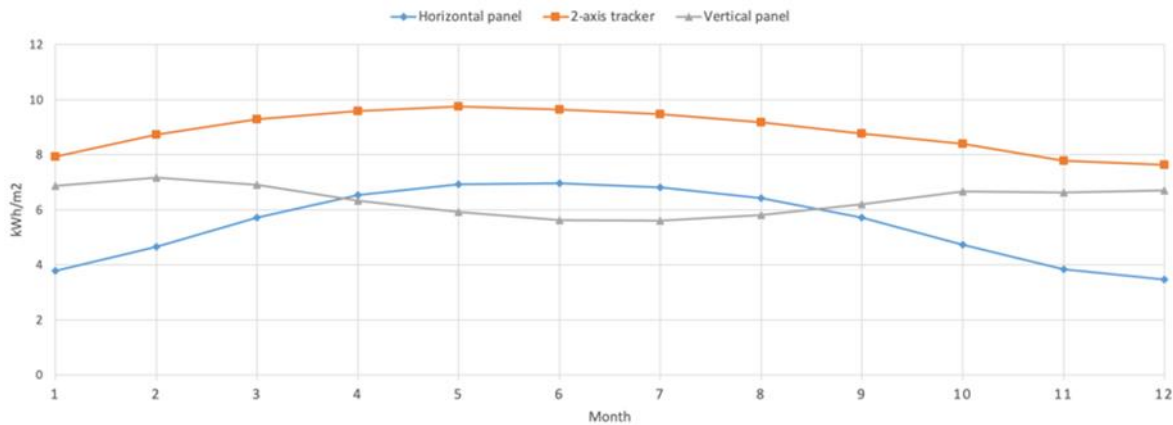
Fig.14: Daily solar irradiation for different PV panel position and tracking (clear sky, 30° N)

The solar calculator showed that on equatorial routes, the average solar power that could be harvested over a day in ideal conditions was nearly 34,000 kWh. This would amount to an average of about 1,350 kW(e) across the entire day and night, allowing for about 5% loss due to converters and some battery charging. This will obviously be much lower in higher and lower latitudes and with effects of the cloud cover. The time of year will also vary the harvesting potential.

The modelling of the solar power across the four various trading routes for August showed that the payback period of the additional cost of the solar power plant is about 4 years in equatorial routes and 6 years in the Atlantic and Pacific routes.

With the proa platform, the solar power is so great, that on many low wind equatorial routes, the power harvested by solar will be more significant than the wind power. Therefore, the Proa Windship project was named the Renewable Energy Powered Autonomous Ship, or REPAS.

3.9. Proa Control Systems

Computer control of the wing masts is necessary to optimise the performance of the whole sailing rig. The sail control system will adjust the wing masts according to the strength and direction of the apparent wind. Gust control through flap alleviation is also critical to ensure the heel angle of the Proa Windship can be maintained in balance while sailing.

The vessel will have a navigation computer for Propulsion Harvesting Automation and Ship Environment Routing (PHASER). The navigation computer, utilising weather forecasting information, will be able to run hundreds of simulations on wind and solar harvesting performance and make decisions on the route and the powering configuration. For example, when heading into the wind, it may be better to head directly into the eye of the wind at a slower speed on solar power, than tack into the wind at a faster speed, but much longer distance. Upwind sailing is not only inefficient in distance covered, but it places the sailing rig under high stress levels for the limited propulsive force that can be extracted.

Another important navigation strategy is whether to sail faster in a strong wind or harvest hydro energy from the propellers to charge batteries and save this energy for when wind or solar is not as strong. There are significant energy loses associated with converting the energy and charging and discharging of the batteries.

4. Conclusions

4.1. Summary

The proa configuration offers the benefits of greater solar harvesting and promises reduced powering requirement at speeds above 10 knots. This is expected to make a wind powered vessel more viable by having a second source of renewable energy for more efficient sailing, particularly on upwind courses.

First principles engineering studies have confirmed the basic viability of the proa configuration for a large merchant vessel, but many technical challenges remain and will need more thorough modelling and investigation. These include the longitudinal structural strength of the main hull and the stability of the vessel particularly when sailing at a heel angle to minimise the amah resistance.

The unusual configuration and physical characteristics of the proa means that many Class rules are not applicable, and will need special consideration with regard to engineering integrity, vessel handling and safety.

4.2. Future Economic Study

In addition to the further technical studies needed, an economic study will be undertaken. As per previous studies, a number of trade routes will be investigated for the performance of the Windship to access the potential cost benefits. In addition to the Atlantic and Pacific routes, two equatorial routes will be added, an east-west route between Singapore and Kuwait, and a north-south route between Australia and China.
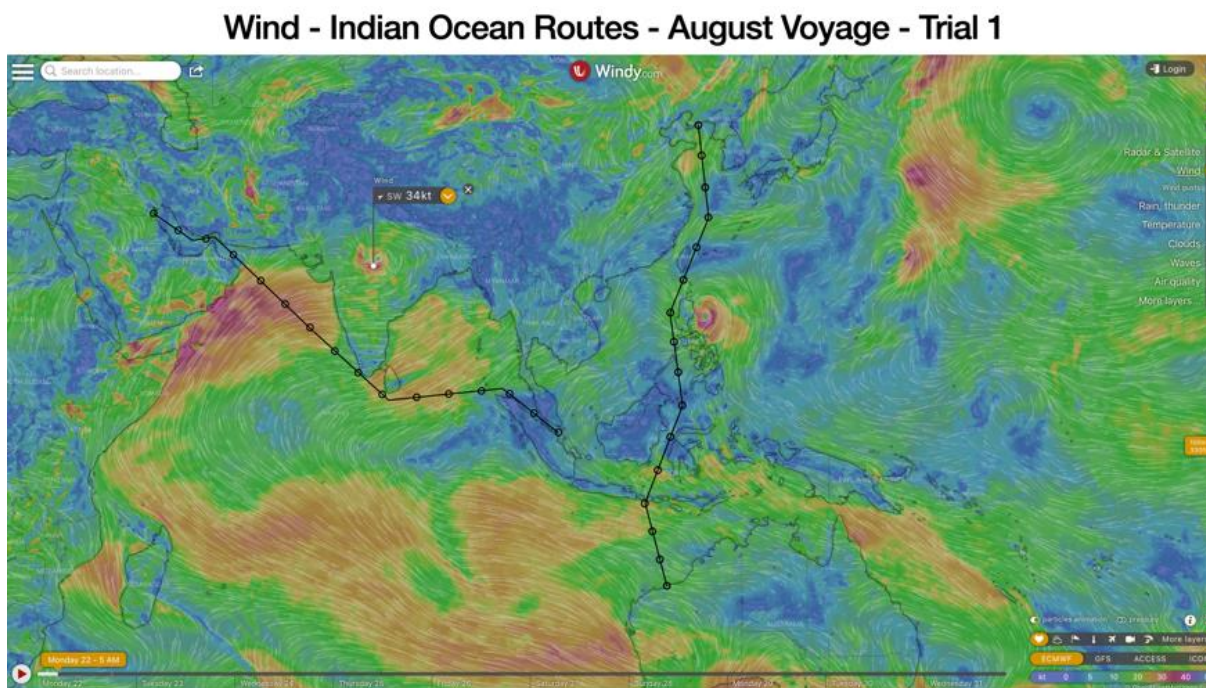
Fig.15: Kuwait Singapore and Australia China trade routes

The calculation spreadsheet will take weather forecasting information from the European Centre for Medium Range Weather Forecast (ECMWF), which is generally considered the most accurate global model, using the excellent Windy.com graphical interface. The spreadsheet is being upgraded to include cloud cover, to aid the solar calculations and wave data to determine the added-resistance-in-waves.

Calculations are being performed for different sailing and harvesting strategies. For example, always tacking into the wind and not tacking to sail the shortest distance. Solar and hydro harvesting strategies will be investigated to determine when the wings should be used as sails or solar trackers.

References

NN (1996), *Modern Wind Ships – Phase 1*, Knud E. Hansen A/S, https://www.osti.gov/etdeweb/servlets/purl/515478

ROSANDER, M.; BLOCH, J.O.V. (2000), *Modern Wind Ships – Phase 2*, Knud E Hansen A/S, https://www2.mst.dk/udgiv/publications/2000/87-7944-019-3/pdf/87-7944-020-7.pdf

Status of Air Lubrication Technology

David Connolly, Silverstream Technologies, London/UK, david.connolly@silverstream-tech.com

Abstract

This paper presents a status update on Silverstream Technologies and its journey in the delivery of green technology to the maritime industry. Silverstream successfully commercialised the Silverstream® System, an air lubrication system (ALS) that deploys a bubble carpet along a ship's hull, thereby reducing the frictional resistance, in turn lowering fuel burn and CO2 emissions. Honest and open communication on the demonstrated savings, in combination with independent third-party verification, has led to exponential company growth and ALS market leader status. Ongoing commitment towards innovation, research and development has further solidified Silverstream's reputation as a thought leader within the industry.

1. Introduction to the Silverstream® System

The environmental footprint of the maritime industry has come under increasing scrutiny in recent years, with the need for the sector to contribute further to the fight against climate change having been clearly identified. Comprehensible ambitions of the International Maritime Organization (IMO) have both been publicised and realised through increasing regulatory pressure (EEXI, EEDI and CII), making the adoption of energy saving technologies ever more compelling. In this light, Silverstream Technologies has developed, patented and commercialised the Silverstream® System, an air lubrication system (ALS) deploying a uniform carpet of air bubbles along a ship's flat bottom to reduce the frictional resistance. As such, the system allows a vessel to reduce its fuel consumption and related emissions. The Silverstream® System is a fuel agnostic energy saving solution. Alternative or transformative fuels are less energy dense and generally more expensive, giving the system a further competitive advantage, as energy savings are achieved independent of the fuel type used.

Over the past decade, Silverstream Technologies has developed its air lubrication technology to allow for a simple installation on both newbuild vessels and retrofits. The straightforward and elegant solution, consisting of four main components, is visualised in Fig.1. A control and automation system, based on ship speed and draught, allows air produced by a set of compressors to be transported via a series of pipes and valves to the Air Release Units (ARUs).
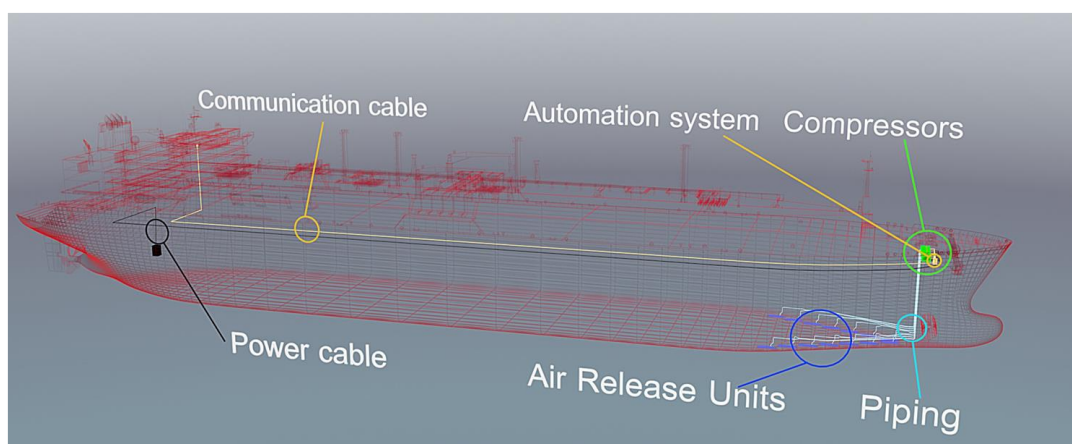
Fig.1: Overview of Silverstream® System layout

Via the patented ARUs, air is introduced into the water through fluid shearing, making the technology unique among air lubrication technology providers. The open air/water interface inside the ARU allows the generation of microbubbles through an effect called the Kelvin-Helmholtz instability. The main advantage of this approach, over 'expulsion' based air lubrication, is found in the high 'quality' of

microbubbles produced and the low energy required to do so. Expulsion based systems depend on high(er) pressure air pressure to 'inject' air into the water, requiring higher amounts of energy as well as disturbing the boundary layer on the ship's hull (the difference between both approaches is illustrated in Fig.2). The airflow to generate the bubble carpet is optimised and controlled based on extensive full-scale testing at HSVA's HYKAT cavitation tunnel to avoid the need for Reynolds scaling. In the experimental work, spanning multiple test campaigns and a speed range of 6 to 18 knots, the relationship between the required airflow and the ship's operating conditions (speed and draft) was established, allowing flexible control and operation of the system.
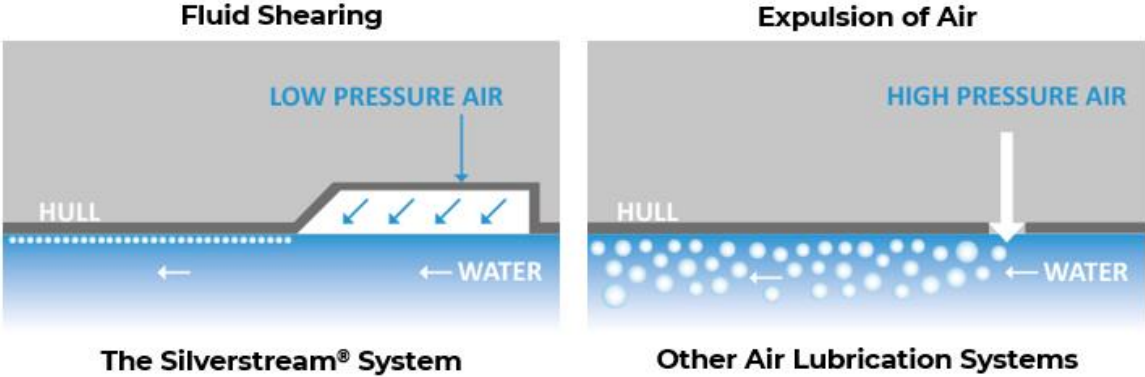
Fig.2: Comparison of air lubrication technologies/concepts

The system's performance manifests itself through an immediate reduction in shaft power combined with an increase in ship speed when the system is switched on, visualised with actual data from recent performance trials in Fig.3. The average net savings achieved by the Silverstream® System range between 5-10% and have independently been verified by various third parties as will be discussed further in the following sections.
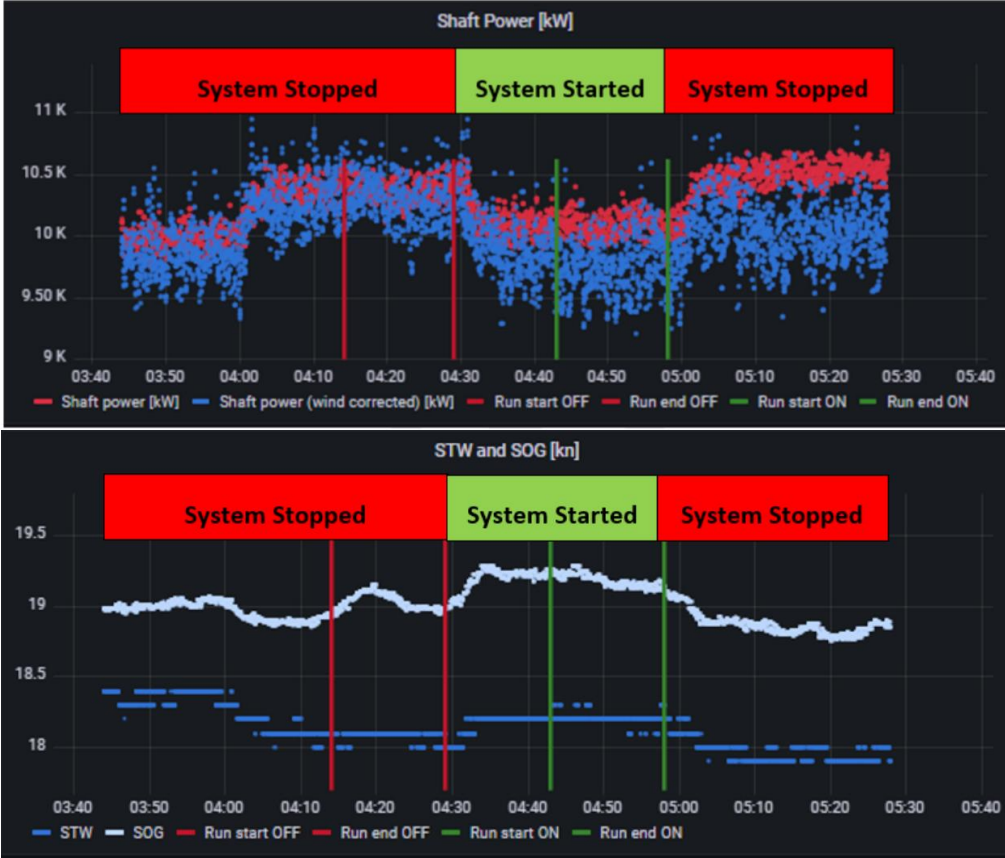
Fig.3: Illustration of system performance manifestation

296

2. Silverstream Technologies, Market Leader in Air Lubrication Systems

Silverstream Technologies has been a pioneer in the air lubrication space for over 10 years. The initial uptake of the technology was driven by 'first movers' like Shell, Carnival, Grimaldi, Vale and MSC, and accelerated by companies embracing a 'close second' strategy. The 'first mover' strategy successfully secured thought leaders in each industry segment (e.g. cruise, tanker, roll-on-roll-off, container, etc.). Additionally, the first movers re-affirmed their trust in both the company and the technology through repeat orders and fleet deals. An overview timeline, visualising Silverstream's journey over the past decade, is found in Fig.3. In the past decade, Silverstream showed that air lubrication technology can be offered beyond the theoretical, protype stage, on a true commercial scale. The timeline in Fig-4 also illustrates how ever-growing regulatory pressure plays an important role in the growth trajectory of the business, and the importance of this aspect is only expected to increase.
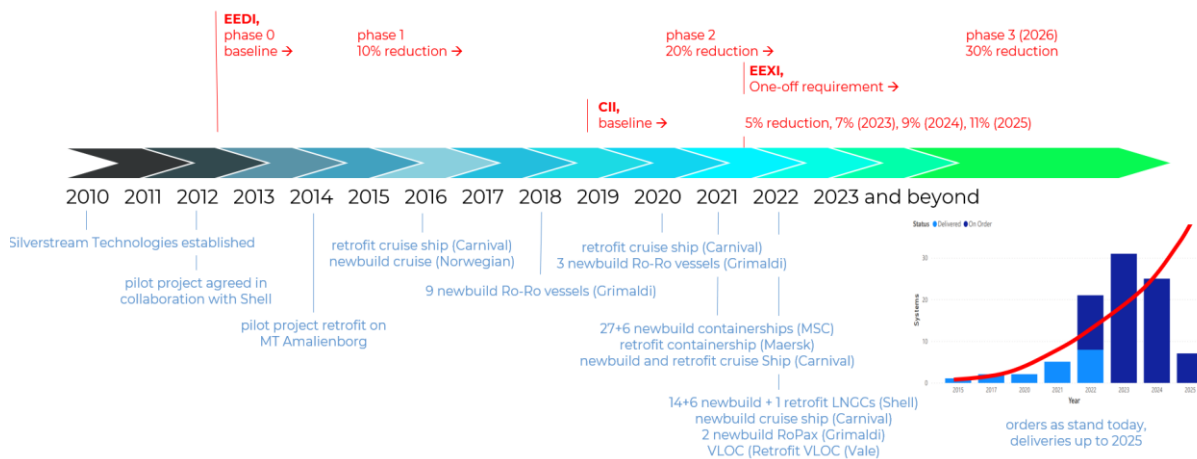
Fig.4: Timeline of Silverstream Technologies orders
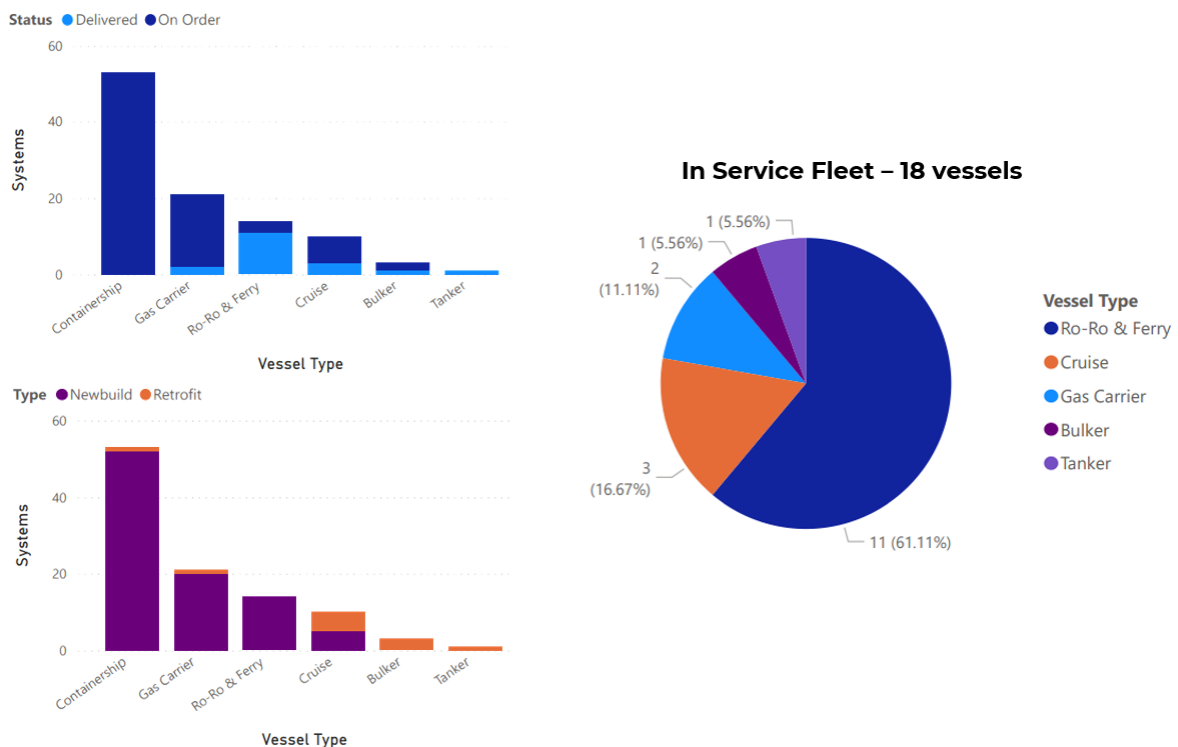
Fig.5: Overview of delivered systems, systems on order and in service systems (for various vessel types / market segments)

297

Since their conception, key to the success of Silverstream and the uptake of the Silverstream® System, has been a clear, open and honest communication strategy. From the prediction of realisable and realistic savings to demonstrating the savings in real world scenarios, Silverstream has always chosen clarity above all else. Through external verification, for example, the customer can be reassured that the savings promised will be the savings delivered. The importance of demonstrating savings is covered in further detail in the next section. The best indicator of the success of the outlined strategy is seen in the exponential growth the company is experiencing, both in terms of the orderbook and the scale-up of the company to deliver the orderbook. A full order roster, illustrated in Fig.5, with systems to be delivered well into 2025, allows for Silverstream to express its ambitions of reporting 500 systems by 2025.

The importance of strategic relationships within the industry to Silverstream's growth journey can hardly be overestimated. Silverstream has always aimed to be a thought leader in the green tech space. As such, working with other thought leaders in the industry allows the company to offer its customers clear expert guidance, bolster innovation, and provide unique insights into implementing energy saving technology in the maritime industry. Through these strategic relationships, Silverstream can solidify its ambitions and reputation as the market leader in air lubrication systems and keep building further on the current momentum, as exemplified by recent repeat business and fleet deals signed across various market segments. Additionally, the strategic relationships provide shipping companies, owners, and operators with confidence in the technology, while agreements with large shipyards and drydocks ensure current and future customers with the assurance that ordered systems can and will be realised in time and on budget. Finally, by engaging in close relationships with well-connected and long-established partners within the industry (e.g. engine and compressor manufacturers), Silverstream can crystalise its image of a young, ambitious, and growing company.

3. Importance of Demonstrated Savings

Lord Kelvin said, 'If you cannot measure it, you cannot improve it', and now more than 100 years later the sentiment still holds great value. Silverstream Technologies has always seen measuring and demonstrating the performance achieved by the air lubrication solution as essential in the further development of the product, as well as in ensuring its wide-spread adoption within shipping. Silverstream has made a commitment to itself, and all stakeholders involved, to continue reporting on the savings achieved across the fleet of vessels equipped with the Silverstream® System (subject to confidentiality obligations to be afforded to the ship owner). Beyond market confidence, a number of aspects warrant the commitment to demonstrate savings:

- Contractual obligations: the contracts with various stakeholders, such as the shipyard, owner, and / or operator can include both short- and long-term obligations with regards to the savings achieved.
- Regulatory compliance: various regulations, such as the Energy Efficiency eXisting ship Index (EEXI), the Energy Efficiency Design Index (EEDI), and the Carbon Intensity Indicator (CII), require reporting of a vessel's performance, environmental footprint, etc. Additionally, the idea of a potential carbon tax on shipping further justifies the need to demonstrate actual vessel performance and savings achieved.
- Market confidence: demonstrated savings inspire customer and market confidence and allow the various parties to gain clear insight into e.g. the return-on-investment potential of the technology, and help in the decision-making process when considering various energy saving technologies.
- Continued product development (IR&D): a world of knowledge can be derived from the system performance measurements and analysis, helping to correlate predicted and real-world performance, understand performance and system behaviour under different conditions, and inspire the further development of the product.

Any new technology, especially in the energy saving device space, needs to prove its ability to deliver on what is promised. Often, this can be hard and cumbersome, however, the Silverstream® System finds

itself at an advantage: the benefit can be established by simply switching the system on and off and measuring the performance difference between both settings. The expected savings are a function of a number of parameters: the ship's frictional resistance, the flat bottom area and percentage of lubrication achieved, the lubrication effectiveness itself, and the energy consumed to achieve the lubrication. Average net savings achieved by the Silverstream® System are to be found in the 5-10% range. The exact savings to be expected will depend on the vessel type/design, the vessel's operational profile, and the chosen system solution, which are all considered in the actual performance estimation process executed for every project. Once the system has been commissioned, various approaches can be considered to demonstrate savings, as will be discussed later. Both internal and external (independent) verification of the savings has been conducted. External organisations, such as RINA, Lloyd's Register, and HSVA have conducted investigations and confirmed reported savings on a number of vessels/ vessel types, as illustrated in Fig.6.
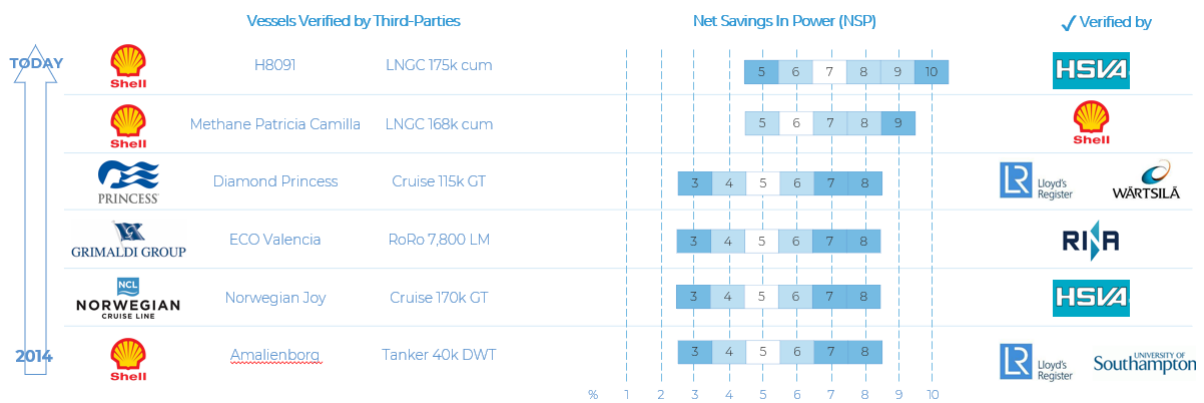
Fig.6: Demonstrated savings as verified by third parties

The performance of the Silverstream® System can be measured by comparing the ship's performance with the system switched on and off. In essence, operation of the system realises a shift of the ship's speed-power curve, lowering the required power to achieve a certain speed as well as increasing the ship's actual speed at a given power. During ship operation, the gross savings achieved can be quantified as the sum of the drop in shaft power measured, summed with the equivalent power derived from the observed increase in ship speed. The net savings are equal to the total of the gross savings after subtraction of the power needed to drive the compressors and achieve the actual air lubrication. Both the shift in speed-power curve and saving calculation method are illustrated in Fig.7.
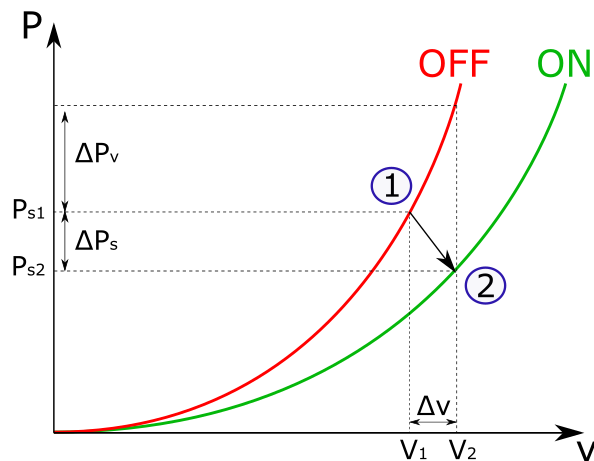
$$\Delta P_{net} = \Delta P_{gross} - \Delta P_{comp} \text{ with } \Delta P_{gross} = \Delta P_s + \Delta P_v$$

Fig.7: Calculation of savings achieved by the Silverstream® System based on speed-power curves (with gross savings ΔP_{gross}, shaft power reduction ΔP_s, equivalent power for increased ship speed ΔP_v, net savings ΔP_{net}, and power consumed by the compressors ΔP_{comp})

Various methodologies are currently employed to measure the ship's performance, and in turn, demonstrate the achieved savings. For first-of-class vessels, the traditional sea trial is often the most logical and chosen approach. During a sea trial, a number of double runs are conducted with the Silverstream® System on and off under constant propulsion conditions (achieving propulsion equilibrium in both conditions, i.e. constant propeller shaft speed, propeller pitch, etc.), and at a constant heading. The on and off results are then corrected for external conditions, according to ITTC/ISO standards, to determine the difference and establish the savings achieved. During actual ship operation, the system's self-test mode can be activated regularly, automatically turning the system on and off for a certain time period; or the more controlled straight-line performance trial protocol can be followed, manually operating the system during a selected voyage or time period. Finally, the collection of data over long periods of time allows to collect data on the ship's performance both with the system on and off, based on which the equivalent speed-power curves can be derived to demonstrate the savings achieved.

4. Commitment to Continued Innovation, Research & Development

Innovation is fundamental to all research and development activities at Silverstream Technologies. The continued efforts of the Innovation, Research & Development (IR&D) team are driven by the need to achieve a deeper understanding of the product (space), but also by the desire to continuously develop and improve the technology further. Focus is placed on benefits that directly impact existing customers by the optimisation of the system performance in a cost-efficient manner, through upgrades and retrofits of, for example, the airflow control system. Deeper understanding of the concept and technology will help Silverstream to remain the air lubrication technology innovator and thought leader. Furthermore, Silverstream aims to develop the technology to have a consequential impact beyond air lubrication, as observed in the potential to reduce underwater radiated noise (URN) or to mitigate cavitation inception. The most important IR&D activity for Silverstream is, and always has been, the full-scale experimental work conducted in the HYKAT facility at HSVA (cavitation tunnel). Since 2011, various test campaigns have been undertaken with the latest campaign (end of 2021) investigating the performance of the system at low speeds, in addition to interaction with coating / anti-fouling solutions, as well as the testing of a novel bubble carpet measurement system. In recent months, the observations made at HSVA have been used to start the development of a Computational Fluid Dynamics model to investigate the technology in closer detail and allow the evaluation of relative design changes and support analysis of critical topics such as the deflector plate (spacing). In the current stage, the initial results have been shown to align with observations made at HSVA, however alignment of the force measurements has proven to be more challenging.

The sensing technology (bubble carpet measurement system) tested at HSVA has since then also been evaluated during trials at sea. The trials confirmed the sensors' abilities to detect the bubble carpet, as well as allowing for the definition of the carpet's density and thickness, including correlation to the observed reduction of the shear force / hull friction. Extended data analysis is currently underway to establish future possibilities for the sensing technology to be included in the control system and / or in the system design process.

The latest campaign at HSVA was made possible through the CHEK project, an EU Horizon 2020 project which focusses on the integration of various technologies to achieve a maximum efficiency impact and reduce emissions of two baseline vessels by 99%. Within the project, Silverstream is integrating the air lubrication system, as such contributing to the emissions reduction target, as well as to objectively reduce the energy consumption of the vessels by 50%.

Further IR&D activities at Silverstream include a Knowledge Transfer Partnership agreement in collaboration with the University of Southampton focused on artificial intelligence and machine learning, *Camilleri et al. (2022)*. Another project, in conjunction with Maersk and Wartsila, works on developing alternative airflow delivery systems in the form of scavenged air (SAALS). Finally, again a follow-up of recent work at HSVA, the interaction of the air lubrication technology with anti-fouling products, such as offered by AkzoNobel and Jotun, has been very compelling. Great potential is believed to be found in the synergy between these products to further achieve optimal ship efficiency

and provide shipowners with a clear competitive edge. The results of these efforts are expected to be presented at various conferences in the near future, as well as published through a range of whitepaper and journal papers.

Silverstream's IR&D roadmap envisions continued thought leadership in the green tech space, extending efforts through both internal and external collaborative projects. Additionally, the aim is to grow university collaborations further and invest in PhD and post-doc projects. Besides academic collaboration, more industry involvement is being sought through the design and engagement in Joint Industry Projects. In general, future projects will expand the focus of the programme beyond upgrades of the current system and push for even further innovation.

5. Conclusions

Silverstream Technologies has successfully developed and commercialised the Silverstream® System, an air lubrication system (ALS) that deploys a uniform carpet of air bubbles along a ship's flat bottom. Through the Kelvin-Helmholtz instability effect, the system's patented Air Release Units (ARUs) deliver an airflow managed by a control and automation system based on the ship speed and draught. The bubble carpet reduces the frictional resistance of the hull and allows a vessel to lower its fuel consumption and related emissions. The fuel-agnostic Silverstream® System helps a ship owner / operator comply with the ever-increasing regulatory pressure aimed at reducing the environmental footprint of the maritime industry.

Over the past 10 years, Silverstream has been a pioneer in the air lubrication space driven by 'first movers' from each industry segment. Silverstream showed that air lubrication technology can be offered beyond the prototype stage, on a true commercial scale. Through a clear and honest communication strategy on the predicted and demonstrated savings, Silverstream assured customers that the savings promised will be the savings delivered. As such, the company has seen exponential growth and is now expressing the realistic ambition to report 500 systems by 2025. Furthermore, Silverstream has shown how strategic relationships, with owners, operators, shipyards, drydocks and established industry partners, help leverage a position as thought leader in the green tech space. By working with other industry thought leaders, Silverstream can offer its customers clear expert guidance, bolster innovation, and provide unique insight into implementing energy saving technology in the maritime industry.

The importance of measuring and demonstrating the performance of the Silverstream® System has been essential in ensuring the further development of the product, as well as achieving its widespread adoption within shipping. An ongoing commitment to demonstrate savings is warranted by contractual obligations, regulatory compliance, market confidence and continued research and development. The average net savings range between 5-10% and have been independently verified during system operation by a number of external third parties, such as Lloyd's Register and HSVA. System performance is manifested by a decrease in the shaft power and an increase of the ship speed, shifting the ship's speed-power curve between system on and off, which can be quantified through a variety of methodologies.

Finally, Silverstream places innovation at the forefront of all research and development activities within the company. Driven by the need for a deeper understanding of the product (space), but also by a clear desire to continuously develop and improve the technology further, continued research and development is undertaken. The activities range from ongoing full-scale experimental work at HSVA, over the use of Computational Fluid Dynamics to evaluate design changes, to the introduction of novel bubble carpet sensing technology. Additionally, various collaborations with universities and industry partners, e.g. investigation of the synergy of air lubrication with anti-fouling technology, are undertaken. Silverstream's IR&D roadmap envisions continued thought leadership in the green tech space, extending efforts through both internal and external collaborative projects in both academia and industry. These promising initiatives are expected to be presented in future at other industry conferences, in whitepapers and in journal publications.

References

CAMILLERI, J.; CONNOLLY, D.; SOBEY, A.; HUDSON, D. (2022), *Quantifying the Effect of Green Technologies on Ship Performance using Operational Data – Design of Experiments and Data Collection*, 14th HIPER Conf., Cortona, pp.81-89, http://data.hiper-conf.info/Hiper2022_Cortona.pdf

Index by Authors

15th Symposium on

High-Performance Marine Vehicles – "Technologies for the Ship of the Future"

Bernried / Germany, 18-20 September 2023

Topics: ultra-efficient & zero-emission ships / EEXI & CII issues / alternative fuels / electric ships advanced designs / shipyard 4.0 / future materials / future use of oceans / blue economy / intelligent & connected ships / future antifouling / biomimetic marine technologies

Organiser: Volker Bertram (volker@vb-conferences.com or volker.bertram@dnv.com)

Advisory Committee:

Catherine Austin	I-tech	**Andrea Coraddu**	TU Delft	**Jiulun Liu**	Wuhan Univ Technology
Carlo Bertorello	Naples University	**Robert Dane**	Ocius	**Kohei Matsuo**	NMRI
Carsten Bullemer	Maritime Data Systems	**Thomas De Nucci**	USCG Academy	**Geir Axel Oftedahl**	Semcon
Emilio Campana	CNR	**Stefan Harries**	Friendship Systems	**Pierre Sames**	DNV
Roy Campe	CMB	**Thomas Hildebrandt**	Numeca	**Noah Silberschmidt**	Silverstream Technologies
Ulrich Bernhardt	DNV	**Jan Kelling**	Hasytec	**Teus van Beek**	Wärtsilä

Venue: The conference will be held at the Kloster Bernried in Bernried/Germany

Format: Papers to the above topics are invited and will be selected by a selection committee.
Proceedings will be electronic pdf version in colour.

Deadlines:

anytime	Optional "early warning" of interest to submit paper
12.6.2023	First round of abstract selection (1/3 of available slots)
12.7.2023	**Second round of abstract selection (remaining 2/3 of slots)**
5.9.2023	Payment due for authors
5.9.2023	Final papers due (50 € surcharge for late submission)

Fees:

600 € / 300 €	regular / PhD student – early registration (by 15.7.2023)
700 € / 350 €	regular / PhD student – late registration

Fees are subject to VAT
Fees include proceedings, lunches and coffee breaks, and conference dinner
Fees apply also to authors

Sponsors: Tutech Innovation – further to be announced

Media Partner: Hansa, Royal Institution of Naval Architects, DNV Maritime Academy

Information: volker@vb-conferences.com